



XXI International Congress

Carpathian Balkan Geological Association
Salzburg (Austria, September 10–13, 2018)

CBGA 2018 – Austria



Franz Neubauer (ed.)

GUIDEBOOK to pre- and post-conference excursions

Berichte der Geologischen Bundesanstalt, 126





XXI International Congress

Carpathian Balkan Geological Association
Salzburg (Austria), September 10 -13, 2018

CBGA 2018 - Austria



XXI International Congress of the Carpathian Balkan Geological Association

Guidebook

to pre- and post-conference excursions

Salzburg, September 10 – 13, 2018



Berichte der Geologischen Bundesanstalt, 126

ISSN 1017-8880

XXI International Congress of the Carpathian Balkan Geological Association – Guidebook to pre- and post-conference excursions

Editor: Franz Neubauer

Recommended citation / Zitiervorschlag

Volume / Gesamtwerk

Neubauer, F. (ed.) (2018): XXI International Congress of the Carpathian Balkan Geological Association – Guidebook to pre- and post-conference excursions, 10–13. September 2018, Salzburg. – Berichte der Geologischen Bundesanstalt, 126, 304 p., Vienna.

Article / Artikel (example / Beispiel):

Raith, J.G., Schmidt, S. & Aupers, K. (2018): Field Trip Pre-EX-5 – Tungsten deposit Felbertal, Salzburg, Austria. – Berichte der Geologischen Bundesanstalt, 126, 7–45, Vienna.

Cover design: Monika Brüggemann-Ledolter (Geologische Bundesanstalt).

Cover picture: View to SW from the CBGA 2018 conference place, the Faculty of Sciences, University of Salzburg, towards the Untersberg Mt. with its north-dipping Middle to Upper Triassic and Upper Jurassic carbonate platform successions at the northern margins of Northern Calcareous Alps (Photograph: F. Neubauer).

Wien, November 2018

Alle Rechte für das In- und Ausland vorbehalten

© Geologische Bundesanstalt, Wien

Technische Redaktion: Christoph Janda

Medieninhaber, Herausgeber und Verleger:

Geologische Bundesanstalt

Neulinggasse 38

1030 Wien

www.geologie.ac.at

Druck: Rieglernik Ges.m.b.H, Piaristengasse 17–19, 1080 Wien

Ziel der „Berichte der Geologischen Bundesanstalt“ ist die Verbreitung wissenschaftlicher Ergebnisse durch die Geologische Bundesanstalt. Die „Berichte der Geologischen Bundesanstalt“ sind im Handel nicht erhältlich.

Preface

The XXI International of the Carpathian-Balkan Geological Association (CBGA 2018) is going to be held at the University of Salzburg between September 10 and 13, 2018. Ca. 330 scientists from ca. 25 countries are registered and will present a high variety of contributions. Geological excursions are an integral part of the conference, presenting new results and overview on present-day knowledge of the geological evolution of the Eastern Alps, particularly of those regions close to the city of Salzburg. There, a number of classical localities of sedimentary geology are well known but many exposures of metamorphic rocks like such in the Tauern Window, too. All these exposures are worth to visit for first-hand insights and to acknowledge the progress of research.

Nearly one hundred years ago, the organization of field trips to study and compare rock successions in the neighbor countries was the basic idea for the foundation of the Carpathian-Balkan Geological Association. This aim and the area of interest widened with time, and the present area in focus of the CBGA is from westernmost Turkey through mountain ranges in southeastern Europe to the Alps.

As organizers of the conference, we gratefully acknowledge the readiness of colleagues from other universities in Austria and abroad as well from the Geological Survey of Austria to prepare field trips and to contribute to the CBGA 2018 Guidebook. Without their help, the entire task would have been impossible.

We also acknowledge the help of the colleagues who read some contributions and Ms. Viktoria Moser for editing all contributions. Furthermore, we gratefully acknowledge the director of the Geological Survey of Austria for allowing the publication of the CBGA 2018 Guidebook in the "Berichte der Geologischen Bundesanstalt", and Mr. Christoph Janda and Mr. Thomas Hofmann for supporting this task.

Salzburg, September 2018

Franz Neubauer

(for organizers of CBGA 2018)

Contents

	Page
Field Trip Pre-EX-5 – Tungsten deposit Felbertal, Salzburg, Austria by JOHANN G. RAITH, STEFFEN SCHMIDT & KARSTEN AUPERS	7
Field Trip Pre-EX-2 – Sedimentary and tectonic processes on a Late Jurassic passive margin and its inversion during Alpine orogeny in the Lofer area by HUGO ORTNER, DIETHARD SANDERS, MICHAELA USTASZEWSKI, MARTIN RITTNER, DAVID MOSNA & SEBASTIAN WOLFGRUBER	47
Field Trip Pre-EX-6 – Paleogene Events in the sedimentary record of outcrops in Salzburg and eastern Bavaria by HANS EGGER & ALFRED UCHMANN	81
Field Trip Post-EX-1 – Transect across the Eastern Alps by FRANZ NEUBAUER & JOHANN GENSER (with contributions by BIANCA HEBERER, ANDREAS ETZEL & OLIVER STAUBER)	137
Field Trip Post-EX-2 – Latest Jurassic to Early Cretaceous evolution in the central Northern Calcareous Alps by OLIVER KRISCHE, JACEK GRABOWSKI, LÁSZLÓ BUJTOR & HANS-JÜRGEN GAWLICK	223
Field Trip Post-EX-5 – Mass transport deposits, geometry, depositional regime and biostratigraphy in a Late Jurassic carbonate-clastic radiolaritic basin fill (Northern Calcareous Alps) by HANS-JÜRGEN GAWLICK, HISASHI SUZUKI & SIGRID MISSONI	259
Field Trip Post-EX-3 – Sediment-landform associations of major glaciations in the North Alpine Foreland by BERNHARD SALCHER, REINHARD STARNBERGER & JOACHIM GOTZ	289

Field Trip Pre-EX-5

Tungsten deposit Felbertal, Salzburg, Austria



JOHANN G. RAITH¹, STEFFEN SCHMIDT², KARSTEN AUPERS²

¹ Department of Applied Geosciences, Montanuniversität Leoben, Peter Tunner Straße 5, 8700 Leoben, Austria.
johann.raith@unileoben.ac.at

² Wolfram Bergbau und Hütten AG, Oberfelben 54, 5730 Mittersill, Austria. s.schmidt@wolfram.at.
k.aupers@wolfram.at

1 Introduction

The Felbertal scheelite deposit in the Eastern Alps is one of the biggest producing tungsten deposits outside China. Wolfram Bergbau- und Hütten AG (WBH) operates the Felbertal scheelite mine since 1975. Current annual production from the underground mine is about 500,000 tonnes of ore grading 0.3 wt.% WO₃; in total about 16 million tonnes of ore have been produced so far.

The deposit is best described as stockwork mineralisation and diffuse dissemination of scheelite in polymetamorphic Early Palaeozoic rocks (mainly metabasites) intruded by Cambrian and Early Carboniferous granitoids. More continuous quartz-rich layers with fine-grained “sheeted” mineralisation parallel to the foliation were also mined in the past. Initially, Felbertal was classified as syngenetic exhalative-sedimentary tungsten deposit genetically related to mafic volcanism but nowadays epigenetic magmatic-hydrothermal models are favoured relating ore formation to Variscan granites. The Felbertal deposit is best interpreted as a poly-metamorphosed granite-related stockwork type tungsten deposit. There is accumulating evidence supporting a genetic relation of tungsten mineralisation with evolved Lower Carboniferous granites.

Key features of the ore deposit will be visited on this field trip. This guide is based on an older field guide (Raith and Schmidt, 2010) and a summary (in German) on Felbertal tungsten deposit available online on the IRIS data base (Weber and al., 2015). New results obtained during a recent project are also integrated (Kozlik, 2015).

2 History

The Felbertal deposit was discovered in 1967, following systematic exploration based on a conceptual model that put the target in connection with a submarine-exhalative “W-Hg-Sb formation” associated with mafic volcanism (Maucher, 1965). Until 1964, scheelite was known in Austria only from the magnesite-scheelite deposit at Tux, Tyrol, from the small gold-scheelite occurrences at Schellgaden, Salzburg and as a rare mineral in Alpine veins. All these occurrences were found by chance. At Tux, scheelite was mined in small quantities as by-product to magnesite intermittently from the 1950s until 1976. There, scheelite occurred in tectonically disrupted metacarbonate layers within low-grade phyllites and black schists of Upper Silurian to Lower Devonian age (Wenger, 1964; Höll and Maucher, 1968; Pirkl, 1986; Raith et al., 1995).

In the mid-1960s, two academic groups started with scheelite prospection in the Eastern Alps in Austria, one from Montanuniversität Leoben, the other from the University of Munich both using panning of stream sediments and subsequent UV lamping. In mountainous terrain, this is a cheap and fast method to determine the approximate location of scheelite occurrences. To identify the accurate position of the outcropping mineralisation requires subsequent night prospection with UV lamps.

Elevated scheelite contents were discovered in various stream sediments in the Upper Pinzgau area of the Hohe Tauern by both groups. The group around Rudolf Höll and Albert Maucher from the University of Munich alone tested some 370 creeks and brooks in the Hohe Tauern area of Salzburg, 153 of which contained scheelite.

On 27 July 1967, the Munich team tested the Felberbach at the junction of the Felber valley with the Salzach valley near Mittersill and discovered an unusually high concentration of scheelite (Höll, 1998). At that time, the UV lamps had much shorter operation periods than nowadays, and only a few additional samples could be tested. This allowed to exclude the Amerbach tributary and the uppermost ranges of Felber valley as source for the anomaly. The last sample was taken close to Tauernhaus Spital, near the entrance of the current underground mine. Here, a very high amount of scheelite detritus was observed, and the first scheelite-bearing boulders were discovered. By 6 August 1967, the ore boulder deposit (slightly dislocated scree in the Eastern Ore Zone) had been discovered and the outcrops of Eastern and Western Ore Zone delineated.

Following the discovery of the Felbertal deposit, mining rights were secured by Metallgesellschaft AG (Frankfurt, Germany) and detailed exploration of the deposit started. After 3000 m of diamond drilling (Fig. 1 b) and 700 m of exploration drifting, WBH was founded in 1975, as a joint venture between Metallgesellschaft AG (Germany), VOEST-Alpine AG (Austria) and Teledyne Wah Chang Corp. (USA). Following several changes in ownership, WBH now belongs to the Swedish Sandvik group.

Mining at the Eastern Ore Zone open pit mine started in 1975 (Figs. 1 c, d), the flotation plant became operational in 1976, and development of the underground mine in the Western Ore Zone commenced in 1977. Right from the beginning the company aimed to become an integrated producer of downstream tungsten products (tungsten carbide and tungsten powder), therefore a refining plant was constructed in the late 1970s at Bergla, Styria, some 320 road-kilometres east of Mittersill.

Due to the harsh climatic conditions, mining in the open pit was seasonal, from May to October only. By 1986, the upper Eastern Ore Zone had been mined out after a production of 2.5 Mt of ore grading 0.6 wt.% WO₃ at a strip ratio (waste / ore) of less than 1.5:1.

The underground mine was developed as modern trackless LHD operation. Initially, the dimensions of the Western Ore Zone were poorly known, and the first objective was underground exploration. Delineated resources increased from 0.9 Mt in 1976 to >9 Mt in 1983. Due to its location close to the Nationalpark Hohe Tauern and in an area of elevated avalanche risk, all auxiliary infrastructure such as change rooms, workshops and offices are located underground. The mining area is connected to the mill site by means of a 3 km long conveyor decline. With exception of the period between February 1993 and June 1995, the mine was continuously in operation.

Triggered by this major discovery, various exploration campaigns covered relevant portions of the Eastern Alps and a number of smaller scheelite occurrences were discovered in the following years (e.g., Neinavaie et al., 1985). However, no further significant economic orebody was discovered, and with the decline of tungsten prices in the early 1980s, these campaigns were largely abandoned.

3 Geological setting

3.1 Pre-Variscan units in the Tauern Window

The Alps formed due to subduction of a Mesozoic ocean and collision of the European and the Adriatic plates in the Cretaceous to Neogene. This collision belt was caused by convergence of the Adriatic continental upper plate and a subducting lower plate including the Mesozoic ocean and the European passive continental margin (Fig. 2, Dal Piaz et al., 2003; Schmid et al., 2004). The core of the collision zone is represented by the Penninic/Austroalpine wedge, a fossil subduction complex, consisting of continental and minor oceanic units thrust on the Molasse foredeep and European foreland. It is part of the Europe-vergent belt separated from the Adria-vergent Southern Alps, (non-metamorphosed thrust-fold-belt and Neogene sediments) by the Periadriatic (Insubric) lineament (Dal Piaz et al., 2003).

In the Eastern Alps the Austroalpine tectonic units are overlying Penninic/Subpenninic and Helvetic units. In the internal zone of the orogen these units are exposed in several tectonic windows, the largest (160 x 40 km) being the Tauern Window (Fig. 2). The three major units in the Tauern Window are: (1) Pre-Variscan basement rocks, (2) Igneous rocks of Variscan age (Zentralgneis, ca. 360–270 Ma), (3) Permian to Mesozoic auto- to allochthonous sequences. They have all been metamorphosed during the Alpine orogeny and form a complex tectonic nappe system (Schmid et al., 2004; Schmid et al., 2013).

Pre-Mesozoic polymetamorphic basement rocks are widely exposed in the central Tauern Window in the *Habach Complex* (Habachserie Frasl, 1958). In the Felbertal area this complex was subdivided (from bottom to top) into the following units overlying a basal amphibolite member (Basisamphibolit) (Höll, 1975; Höll, 1977):

- Basal schist (Basisschieferfolge)
- Volcanic rock sequence (Eruptivgesteinsfolge)
- Phyllites (Habachphyllit)

Later the Volcanic rock sequence was subdivided and renamed into the Lower and Upper magmatic sequence (Kraiger, 1989; Höck et al., 1993). The Upper magmatic sequence is now assigned to the Variscan orogenic cycle (Fig. 3).

3.2 Central Gneisses

During the Variscan orogeny granitoids (Zentralgneis), classified as I-type and to a minor extent as S- and A-type granitoids (Finger and Steyrer, 1988; Finger et al., 1993) intruded these Late Proterozoic to Early Palaeozoic sequences (Fig. 3). They formed due to Variscan collision and amalgamation of northern Gondwana with Laurasia-Avalonia (Eichhorn et al., 2001). In the Tauern Window these igneous rocks were emplaced between the Upper Devonian and the Permian. Most widespread are high-K I-type metagranitoids falling into two age groups: Early (\approx 340 Ma) and Late Carboniferous (\approx 310 Ma) (Eichhorn et al., 2000). S-type granites are rare; the largest one being the Granatspitz gneiss, which forms a km-size dome structure to the SE of Felbertal tungsten deposit (Fig. 3). The age of this metagranitoid is debated: Permian (Eichhorn et al., 2000) vs. Late Carboniferous (314 Ma, Kebede et al., 2005; Kozlik et al., 2016b). Permian granites with A-type affinities are rare and have been related with post-orogenic crustal extension (von Quadt et al., 1999). Some metagranitoids in the Felbertal area such as the Felbertal augengneiss (Figs. 3, 4) or the K1-K3 orthogneiss (K1 Gneis) in the Western Ore Zone were emplaced during the Early Carboniferous (see below).

3.3 Metamorphic events in the Tauern Window

The dominant Barrovian-type regional metamorphism in the Tauern Window is of Young (Neo-) Alpine age (\approx 30-40 Ma, e.g., Grundmann, 1989; Hoinkes et al., 1999; Inger and Cliff, 1994); it reached upper greenschist to lower amphibolite facies conditions. Subduction-related high-pressure metamorphism in the Tauern Window is restricted to the Eclogite zone at the southern margin of the Tauern Window and to the Glockner nappe. For the polymetamorphic rocks at Felbertal P-T conditions of up to 530°C and 5-6 kbar were reported (Thalhammer et al., 1989). Metamorphic temperatures of 600°C were reported from Hintersee about 1 km to the S of the mine (Hoernes and Friedrichsen, 1974).

The extent and timing of pre-Alpine metamorphic events in the Habach Complex and related basement units in the Tauern Window is still debated. First evidence for polyphase metamorphism was provided by Grundmann and Morteani (1982) and P-T conditions of 420°C and 2 kbar were reported by Koller and Richter (1984). A Sm-Nd isochron age of 336 ± 32 Ma for rocks from the Zwölferzug (Fig. 3) provides geochronological evidence for Variscan metamorphism in the Tauern Window (von Quadt, 1992). Re-Os molybdenite ages between \approx 335 to 340 Ma confirm that the dominant metamorphic overprint of the Felbertal deposit is Early Variscan in age (Raith and Stein, 2006).

A Sm-Nd isochron age of 319 ± 34 Ma (Eichhorn et al., 1997) for one of the four scheelite generations (Scheelite 3, see below) was also attributed to Variscan regional metamorphism and so were ages as young as 282 ± 2 Ma (U-Pb dating on titanite, Eichhorn et al., 1995). Recent dating of uraninite inclusions within zircon from the Felbertal mine yielded a surprisingly young age of 268 ± 13 Ma; this age was interpreted as a low-temperature thermal overprint (Finger et al., 2017).

Evidence for a pre-Variscan metamorphic event was recorded from other areas in the Tauern Window. Migmatitic leucosomes with ages of 449 ± 7 Ma (Eichhorn et al., 2001) and 458 ± 11 Ma (Eichhorn et al., 1999b) likely date anatexis related to "Caledonian" high-grade metamorphism. Moreover, von Quadt et al. (1997) reported eclogites of Silurian age (\approx 420 Ma).

4 Geology of Felbertal tungsten deposit

The two main geological units in vicinity of the ore deposit are: (1) Metamorphic rocks of the Habach Complex and Stubach Group.; (2) Metagranitoids and associated metavolcano-sedimentary sequences formed during the Variscan orogeny.

The *Basal amphibolite* (Basisamphibolit, a member of the Stubach Group) is underlying the Habach Complex to the S of the tungsten deposit. It shows MORB characteristics and formed in a back-arc setting (Frisch and Raab, 1987; Ordosch, 2017). Its age is controversial. Based on discordant U-Pb zircon ages (657-486 Ma, von Quadt, 1992) it was regarded as an equivalent of the Habach Complex. In contrast, concordant in-situ U-Pb zircon ages yielded 351-343 Ma (Kebede et al., 2005); this would indicate that the protoliths formed during the Variscan orogenic cycle.

The *Basal schist* (Basisschiefer; synonymous to Biotitporphyroblastenschiefer, Eiser Sequenz) is an up to 500 m thick sequence of metasediments (micaschist, paragneiss, graphitic quartzite) with intercalations of mafic to felsic volcanic rocks formed in a continental island arc (Gilg et al., 1989) or active continental margin setting (Höll and Eichhorn, 2000) (Fig. 4). The Late Devonian maximum sedimentation age indicates that the protoliths of these rocks were deposited during the initial stages of the Variscan orogeny (Kebede et al., 2005).

The *Magmatic sequence* (formerly Volcanic rock sequence, "Eruptivgesteinsfolge", Höll, 1975; Höll, 1977) consists of various meta-igneous and subordinately of metasedimentary rocks and is up to 4500 m thick. Fine-grained amphibolites predominate in the lower part, whereas various amphibolites, orthogneisses, and minor meta-pyroclastics and metasediments are more common in its upper part. This sequence is now subdivided into the Lower magmatic sequence (LMS) and Upper magmatic sequence (UMS, Kraiger, 1989; Höck et al., 1993; Pestal et al., 2009). The LMS includes a meta-ophiolite sequence with metamorphosed ultramafic to mafic igneous rocks; *i.e.*, serpentinite, hornblendite, coarse-grained amphibolite (metagabbro), fine-grained amphibolite (mafic dykes and eruptive flows). The amphibolites are tholeiitic in composition showing MORB affinities (with possible influence of a subduction component) and they formed in a marginal oceanic or back arc basin. The UMS consists of mafic to felsic metaigneous rocks (amphibolite, prasinite, biotite-epidote gneiss, albite gneiss, meta-agglomerate) with intercalations of siliciclastic sediments (micaschist, phyllite). Geochemical data indicate calc-alkaline characteristics and magma generation in a mature arc system, likely in a continental arc. The arc sequence grades into the overlying Habach phyllites, which consist of dark phyllites, micaschists, quartzites with local intercalations of mafic to felsic metavolcanics. The Habach phyllites either formed in an accretionary wedge or an intra-arc/back arc setting (Kupferschmied and Höll, 1994). The stratigraphic assignment to the Late Proterozoic (U. Riphaean-L. Vendian) based on archritarchs (Reitz and Höll, 1988) was not confirmed by U-Pb zircon dating (Kebede et al., 2005).

U-Pb dating and field observations revealed the intrusive nature of some of the orthogneisses in the LMS and UMS, which formerly were all interpreted as felsic metavolcanics. These orthogneisses largely represent I-type granitoids of Cambrian age, which are about 20 million years younger than the fine-grained amphibolites (for details see Höll and Eichhorn, 2000).

5 Ore deposit characteristics

The Felbertal scheelite deposit is situated in the upper ranges of the Felber valley, a tributary of the Salzach, some 10 km south of Mittersill, Austria. It is located in the Hohe Tauern at an outcrop elevation of 1175 to 2200 m. The Felber valley separates the deposit into two sectors, the Eastern and the Western Ore Zone (Fig. 1 a; Fig. 4). The Felbertal scheelite deposit is restricted to the bottom ~400 m of the Magmatic sequence ("Scheelit-führende Serie", Höll, 1975). The host rocks in both ore zones are fine-grained amphibolites (metabasalts) interlayered with coarse-grained amphibolite (Grobkornamphibolit, metagabbro), hornblendite (mafic metacumulate rock?) as well as leucocratic orthogneisses (metagranites, felsic metavolcanics; Fig. 4).

5.1 Eastern Ore Zone

In the Eastern Ore Zone (Ostfeld) hornblendite / coarse-grained amphibolite (Unterer and Oberer Hornblendit-Zyklus) alternate with schists and gneisses. The following succession of rocks has been mapped (Höll, 1975).

- Hangingwall schist
- Upper hornblendite cycle
- Intermediate Schist (Zwischenschiefer)
- Lower hornblendite cycle
- Footwall schist

Thalhammer et al. (1989) distinguished three hornblendite / coarse-grained amphibolite units alternating with fine-grained amphibolite / gneiss units (referred to as metavolcano-sedimentary units); this whole succession is tectonically imbricated. Various gneisses, derived from intermediate to acidic igneous protoliths, form elongate lenticular bodies and layers in the metabasites. A thicker orthogneiss body (Ostfeldgneis) underlies the lowermost hornblendite unit. Whereas in the early days all gneiss intercalations were interpreted as of volcanic origin, this leucocratic orthogneiss has been recognised as intrusive and was dated at 529 ± 17 Ma (Eichhorn et al., 1999a). For some metabasalts a boninitic origin was suggested (Thalhammer, 1987).

The Eastern Ore Zone was mined as an open pit operation between 1975 and 1986 (Figs. 1 c-d). It consisted of a discontinuous (?), elongate and slope-parallel WNW plunging ore body exposed between 880 m and 2240 m altitude; it was mined above 1700 m altitude. Post-glacially dismembered and displaced ores (Obere Erzblockschutthalde) as well as an about 30 m thick in-situ ore body were mined. The mined part of the ore zone in the Eastern Ore Zone was about 1000-1200 m long, less than 200 m wide and max. 30 m thick striking about WNW-ESE and plunging 25 to 55° WSW; i.e., about subparallel to the mountain slope (Fig. 4). Metabasites alternate with various gneisses in the mineralised zone (Fig. 5). High-grade mineralisation (>2 wt.% WO_3 , up to 10 wt.% in individual hand specimens) was hosted by an unusual lens-shaped (900 m x 50 m x up to 8 m) sheeted quartz mass showing fine mm-scale foliation (Quarzitisches Scheelitrezierz, Höll, 1975) mainly composed of fine-grained scheelite and quartz (Figs. 6 a, b).

Elongate scheelite grains in the foliated ore form mm-sized porphyroclasts and are partly recrystallised together with the enclosing quartz matrix (see below). Thus, this ore texture is rather mylonitic – i.e. deformation-related – and not primary sedimentary (Höll et al., 1972) or reflecting banding caused by scheelite-quartz precipitation in fluid over-pressured open cavities (Höll and Eichhorn, 2000).

These foliated scheelite-quartz ores are spatially associated with zones of intense quartz veining forming an about 400 m wide stockwork zone (Fig. 5; 6 c). This stockwork zone was interpreted as a feeder zone underlying the foliated ores (Höll and Eichhorn, 2000). However, drill core loggings from the early days of exploration confirm that this stockwork-like scheelite mineralisation extends laterally as well as into the hanging wall of the foliated scheelite ores (Fig. 5, also see profiles in Höll, 1975). Although the highest tungsten concentrations were found in the foliated ore the whole quartz-veined sequence is mineralised and a ~200 m wide zone within the stockwork zone was also mined (Fig. 5).

Re-Os model ages of molybdenite from the stockwork zone range between 337-343 Ma (Raith and Stein, 2006). In situ-dating of relict scheelite cores (Scheelite 1) from the foliated scheelite ore yielded 335.5 ± 4.6 Ma (Raith et al., 2011). This Early Carboniferous age of scheelite rebut the idea that these ores formed during a Cambrian ore stage, a view repeatedly expressed by researchers from Munich (Eichhorn et al., 1995; Eichhorn et al., 1997; Eichhorn et al., 1999a; Höll and Eichhorn, 2000).

5.2 Western Ore Zone

In the Western Ore Zone (Westfeld) scheelite is only mined in the active underground mine. The mineralised zone (300 x 500 m in cross section) plunges at medium angles to WNW (Fig. 7). It has been mined for more than 850 meters along the plunge direction. In 2018 the deepest level of the mine was at 625 m. The downdip extension of the deposit is unknown. In the early days 8 distinct ore bodies

(labelled K1 to K8) were distinguished and selectively mined. However, with increasing depth some of the ore bodies merge (Fig. 7).

Mineralisation is pervasive and the ore bodies are defined by the actual cut-off grade. Economic grades are commonly found in zones with intense quartz veining (Quartz 1) (Figs. 8 a-c, Figs. 12 c, d, Figs. 13 a, b).

The Western Ore Zone is divided into three major tectonic units (Fig. 9). A barren wedge of Basal schists (Basisschieferschuppe) separates two mineralised wedges each containing several ore bodies (Schmidt, 1988); ore bodies K1 to K4 are located in the upper wedge and K5 to K8 in the lower one. K1 and K3 ores were mined at the contact of the Variscan K1-K3 orthogneiss to the host rocks. The horse-shoe shape (in plan-view) of this gneiss is caused by a large-scale Alpine (?) fold structure with an about SW plunging fold axis. The K1-K3 orthogneiss can be traced to depths of about 950 m in the mine (Fig. 10) though smaller orthogneiss lenses have been discovered at even deeper mine levels more recently. The leucocratic orthogneiss is strongly foliated, especially at its margins (Fig. 11 a). In less deformed parts apophyses and intrusive contacts have been preserved (Fig. 11 d). Elongate to planar lenses and rafts of non-mineralised host rocks occur as deformed xenoliths in the K1-K3 orthogneiss (Fig. 11 a). These observations confirm the intrusive nature of the gneiss protolith. A chemically very similar orthogneiss is exposed in the Eastern Ore Zone (Kozlik and Raith, 2017).

Two ore bodies (K1-K3) of major economic importance were spatially associated with the K1-K3 orthogneiss. They are structurally controlled by NE-SW and E-W trending shear zones, preferentially developed at the margins of the gneiss (Fig. 9) and the host rocks that converge towards deeper levels in the mine. Metre-thick foliated masses of pure quartz are developed at the margins and within the gneiss. The major quartz mass within the K1-K3 orthogneiss has a lens-like morphology and plunges at about 45° to NW/NNW (Schenk, 1990a); it extends to >300 m towards depth and is up to 30 m thick. Main scheelite in the K1-K3 ores (Scheelite 2, see below) forms large up to cm-sized porphyroclasts and is of greyish colour, fatty lustre and yellowish fluorescence. This type of scheelite has been observed in deformed scheelite-quartz veins within the Lower Carboniferous K1-K3 orthogneiss (Figs. 11 b, c) thus excluding a pre-Variscan age of this mineralisation. Locally bluish beryl occurs in these veins (Fig. 11 f).

The K2 ore body includes foliated scheelite-quartz ores, quartz veins and a W-rich breccia (Figs. 12 a, b). Fine-grained scheelite and quartz are strongly re-crystallised defining a mylonitic fabric. Scheelite porphyroclasts (several mm in size, yellowish fluorescent) re-crystallised to fine-grained scheelite (bluish fluorescent) which is aligned in stringers (Fig. 12 b). Elongate to planar xenoliths of metabasites included in the scheelite-quartz masses are scheelite-free. These ores resemble the foliated high-grade scheelite-quartz ores from the Eastern Ore Zone (Figs. 6 a, b). In the upper nowadays inaccessible mine levels the foliated K2 ores were associated with a scheelite-bearing strongly deformed metabreccia. The latter was interpreted as volcanic eruption breccia (Eruptionsbrekzie) and the associated foliated ores as exhalites (Höll and Schenk, 1988; Schenk and Höll, 1989); *i.e.*, as syngenetic ores. An alternative explanation is that these ores are scheelite-quartz mylonites and that the associated breccia could either be of tectonic or of magmatic-hydrothermal origin. The K2' ore body is a set of deformed dm-thick composite quartz veins. Scheelite is concentrated in the marginal parts of the deformed veins. In February 2009 it was exposed at level 775 (Figs. 8 a-c).

An E-W oriented ore body in the immediate hanging wall of the Basisschiefer wedge is referred to as K4. The K4 ores are either alternations of metabasite and gneiss with intense Quartz 1 veining (*e.g.*,

level 1164; Figs. 12 c, d) or shear zones; the latter are exposed in the hangingwall of the Basisschiefer wedge where they form a 30-40 m thick tectonised zone mainly composed of cataclastic biotite-chlorite schists containing tectonic lenses of more competent rocks (e.g., coarse-grained amphibolite).

More recently, the so-called SD-gneiss (scheelite-dotted gneiss) was delineated as separate mineralisation. It is a fine-grained biotite-albite gneiss with dissemination of scheelite largely independent from quartz veining and characteristically intersected by barren xenolithic fragments of mafic (amphibolitic) material (Kozlik, 2015). This gneiss body can be traced from level 1201 to the very bottom of the mine at level 625. Tungsten content increases with depth, with occurrences below level 880 of economic interest. At level 625 the size of the orebody on plan view is about 15 x 90 m.

Ore bodies K5 to K8 are located in the lower ore-bearing wedge in the footwall of the Basisschiefer wedge. In the K5 ore body scheelite occurs often in stockwork like Quartz 1 veins mainly in coarse grained amphibolite, as well as disseminated in the metabasites. In addition, intercalations of metre-thick mineralized orthogneisses were observed on level 1050 and 1065 (Fig. 12 f).

The K6 orebody can be interpreted as an equivalent to the K2 orebody from the hangingwall unit. Emplaced within the intermediate schists in the footwall of the Basisschiefer wedge it has been mined from level 1065 to level 883. The mineralisation is also associated with strongly deformed breccia, surrounded by foliated scheelite-quartz veins.

With increasing importance for the production at Felbertal, K7 is with a strike length of over 250 m the laterally most extensive orebody. At its centre it has a width of about 30 m, while it tapers off to the East and West. The ore is characterised by cm thick quartz veins apparently bedded within the intermediate schist unit. However, the strike of the quartz veins is slightly different compared to the strike of the hornblende schist. The hangingwall contact is marked by a set of brittle cm wide faults that are characterised by an infill of calcite. Other than the remaining orebodies (plunging to WNW), the K7 follows the NW-dip of the main units and thus recedes from the centre of the deposit.

In the K8 area, small but very high-grade mineralisation was recently discovered between levels 940 and 1000 and of lesser grade between 700 and 757. Many different rock types can be observed within these mineralised zones, while scheelite is usually connected to quartz and locally very coarse grained (cm size).

5.3 Scheelite stages and their postulated ages

Initially, three and later four stages (generations) of scheelite were distinguished at Felbertal (Höll et al., 1972; Höll, 1975; Höll et al., 1987; Schenk, 1990b; Schenk and Höll, 1991; Höll and Eichhorn, 2000; Raith and Stein, 2006; Raith and Schmidt, 2010; Kozlik et al., 2016a):

Scheelite 1 is fine-grained (up to 0.4 mm), white with yellowish-white fluorescence and has Mo contents of around 0.3 to 1.8 wt.% (mean 1.1 wt.% Mo) and shows fine-scale oscillatory zoning under cathodoluminescence (CL; Fig. 14 a). It has been reported from the foliated scheelite ores and underlying stockwork mineralisation in the Eastern Ore Zone. In the Western Ore Zone the foliated scheelite-quartz ores from the K2 ore body can be regarded as possible equivalents (Fig. 14 b). It is typically associated with metamorphic scheelite (*Scheelite 3*), which forms via recrystallisation of older scheelite material or overgrowths (Figs. 14 a, b). Chemically, Scheelite 1 is distinguished from the other generations by higher $^{206}\text{Pb}/^{204}\text{Pb}$ and higher U contents reaching up to several tens of ppm U (Höll and Eichhorn, 2000). A Cambrian age has repeatedly been postulated for Scheelite 1 (Eichhorn et al., 1995;

Eichhorn et al., 1999a; Höll and Eichhorn, 2000). An in-situ U-Pb age of scheelite yielded 335.5 ± 4.6 Ma (Raith et al., 2011) and proves the Variscan age of this scheelite stage.

Scheelite 2 is fine- to coarse-grained (up to cm scale), grey with greasy lustre, yellow fluorescent with 0.1 to 1.7 wt.% Mo substitution. It is widespread in the Western Ore Zone and less common in the Eastern Ore Zone. Sometimes growth zoning can be observed in CL (Fig. 14 c). Scheelite 2 often exhibits brittle deformation with micro-fractures filled with Scheelite 3 (Fig. 14 d). Scheelite 2 was originally thought to be of Cambrian age (e.g., Eichhorn et al., 1995) but was later accepted to be of Early Carboniferous age (e.g., Eichhorn et al., 1999a) when it was clear that scheelite-quartz veins with Scheelite 2 crosscut the ≈ 340 Ma K1-K3 orthogneiss (Figs. 11 b, c).

Scheelite 3 commonly occurs as rims and overgrowths or fracture fillings within Scheelite 1 and 2 (Figs. 14 a, b, d, e). It is grey to white with blue fluorescence reflecting its low Mo content. It is often associated with fine-grained molybdenite, which formed from metamorphic breakdown of Mo-bearing Scheelite 1 and 2 (Schenk, 1990b; Raith and Stein, 2006). Under CL it shows much brighter luminescence than Scheelite 1 and 2. Diffuse zoning can be seen in recrystallised Scheelite 3 grains (Fig. 14 f). In foliated ores it is intimately intergrown with Scheelite 1 and aligned in the foliation. The Sm-Nd isochron age of 319 ± 34 Ma of Scheelite 3 is interpreted as the age of metamorphic recrystallisation of older scheelite material during Variscan metamorphism (Eichhorn et al., 1997).

The Sr isotope composition of Scheelite 1-3 is quite radiogenic. The $^{87}\text{Sr}/^{86}\text{Sr}$ ratios of Scheelite 1 range from 0.72078 to 0.76417, of Scheelite 2 from 0.70724 to 0.76832 and of Scheelite 3 from 0.74331 to 0.80689 (Kozlik et al., 2016a).

Scheelite 4 is rare and forms isolated porphyroblasts with white to pale blue fluorescence reflecting its extremely low Mo concentrations. It occurs in Alpine metamorphic quartz veins (Quarz 2, Figs. 13 d-f) and has been interpreted as scheelite mobilised during Alpine regional metamorphism. The Neo-Alpine age of Scheelite 4 is supported by an imprecise Sm-Nd isochron age of 29 ± 17 Ma (Eichhorn et al., 1997).

In summary: The stages 1 to 3 are all of Variscan (Early Carboniferous) age. The age of Scheelite 1 and 2 is not resolvable and both are interpreted as magmatic-hydrothermal scheelites. Stage 3 and 4 formed during the subsequent Variscan and Alpine regional metamorphic overprints of the Felbertal deposit.

6 Petrography, geochemical characterisation and age of the host rocks

This summary is mostly based on the review paper by Höll and Eichhorn (2000) with addition of new data from M. Kozlik's PhD thesis (Kozlik, 2015).

6.1 Fine-grained amphibolite

This is the dominant lithology in the Felbertal scheelite deposit (Figs. 13 a, c). These fine-grained (<0.5 mm) banded and foliated rocks are composed of variable amounts of major calcic amphibole, plagioclase, biotite, garnet and epidote group minerals and minor chlorite, muscovite, carbonate, quartz and opaques. Hornblende prasinites and hornblende schists are also grouped with this lithology. Their protoliths in the Lower magmatic series were interpreted as tholeiitic MOR basalts, those of the Upper magmatic series as calc-alkaline volcanic arc basalts (Höck, 1993). Alternatively a pure volcanic/continental arc setting was proposed for the complete magmatic sequence (Fig. 15 a, Höll and

Eichhorn, 2000). Fine-grained amphibolites show flat REE patterns similar to MORB but are enriched in LIL elements, especially in Rb (Figs. 15 b, c). Zircons from a fine-grained amphibolite yielded a U-Pb SHRIMP age of 547 ± 27 Ma interpreted as the emplacement age (Eichhorn et al., 1999a). These rocks therefore are the oldest dated ones in the Habach Complex.

6.2 Hornblendite and coarse-grained amphibolite

Both rock types are of dark green colour and can be coarse-grained forming up to several m thick layers and lenses emplaced as own units between the fine-grained amphibolites and the Basal schists; i.e. Lower and Upper Hornblendite Cycle. Hornblendite units are usually fine grained but can also be coarse grained (ratio about 70:30). Fine-grained amphibolites also occur as intercalations within them. Hornblendites are predominantly (>75 vol. %) composed of calcic amphiboles (hornblende, actinolite) and minor to accessory biotite, plagioclase, carbonate, epidote group minerals and opaque phases. Very rarely, magmatic clinopyroxene relics of possible cumulate origin are preserved. The associated coarse-grained amphibolites are distinguished by higher plagioclase contents and a very coarse fabric (Figs. 12 e, f). These rocks are high in MgO, Cr, V and low in TiO₂. Similar to the fine-grained amphibolites the hornblendites are characterised by flat to slightly LREE depleted REE patterns and also show enrichment in Rb (Figs. 15 b, c). The hornblendites and coarse-grained amphibolites have been interpreted as metasomatically enriched volcanic arc magmas (e.g., boninites, Thalhammer, 1987). The coarse-grained amphibolites likely are metagabbros A conventional U-Pb zircon upper intercept age of 496 ± 2 Ma from a hornblendite from the Habach Complex was interpreted as the time of the magmatic emplacement (von Quadt, 1992). The coarse-grained amphibolite was dated at 482 ± 5 Ma (Eichhorn et al., 2001).

6.3 Pre-Variscan orthogneisses

Intermediate to felsic orthogneisses occur as several meters thick intercalations throughout the whole magmatic sequence (Figs. 6 d, e). Petrographically, a variety of gneiss types is distinguished including biotite-albite gneiss, epidote-biotite-albite gneiss, hornblende gneiss, muscovite-albite gneiss etc. The gneisses are composed of variable amounts of plagioclase, quartz, biotite, muscovite ± epidote; K-feldspar is only a minor constituent. At the contacts between gneiss and hornblendite biotite- and epidote-richer varieties are developed; these show more intense deformation (Thalhammer, 1987). Their chemical composition indicates that they derived from intermediate to acidic magmas of an Early Palaeozoic arc system; i.e., they show chemical similarities with calc-alkaline I-type volcanic arc granites (Fig. 15 a, Höll and Eichhorn, 2000). Initially, these pre-Variscan gneisses were interpreted as metavolcanics but intrusive contacts and age data rather support a plutonic origin for at least some of them. The leucocratic albite-muscovite gneiss (Ostfeldgneiss; Figs. 6 d, e) underlying the foliated scheelite-quartz ores in the Eastern Ore Zone was dated at 529 ± 17 Ma (Eichhorn et al., 1999a). Orthogneisses in the Western Ore Zone referred to as Older and Younger K2 gneiss are also of intrusive origin. These gneisses are associated with the metabreccia ("eruption breccia"; see above). Gneiss clasts from the breccia were dated at 529 ± 18 Ma, the Younger K2 gneiss yielded an identical age of 529 ± 17 Ma (Eichhorn et al., 1999a).

6.4 Variscan orthogneisses

Variscan metagranitoids are common throughout the Tauern Window. Different types of Zentralgneis have been distinguished in the central Tauern Window based on field relationships, petrography, geochemistry and ages (Finger and Steyrer, 1988; Eichhorn et al., 2000; Kozlik and Raith, 2017).

At Felbertal mine the K1-K3 orthogneiss in the Western Ore Zone testifies to this Variscan magmatic activity. A Rb-Sr whole rock age of 316 ± 10 Ma was the first prove that this granite gneiss is of Carboniferous age (Pestal, 1983). Later Rb-Sr and conventional U-Pb dating on zircons yielded ages of 332 ± 20 Ma and 336 ± 19 Ma, respectively (Eichhorn et al., 1995) which are within the uncertainty of the earlier Rb-Sr age. Recent in-situ U-Pb analyses on zircon of the two varieties of K1-K3 orthogneiss and the associated aplitic gneiss render more precise Early Carboniferous ages between 336-341 Ma (Kozlik et al., 2016b).

The K1-K3 orthogneiss is a medium-grained homogeneous muscovite microcline gneiss containing K-feldspar (microcline), quartz, plagioclase/albite, phengitic mica, biotite and minor epidote-group minerals and garnet (Finger et al., 1985; Kozlik and Raith, 2014; Kozlik and Raith, 2017). Relics of magmatic plagioclase and K-feldspar are sometimes preserved, the other minerals are metamorphic. A biotite-richer dark-coloured and a leucocratic biotite-poor light-coloured variety can be distinguished (Fig. 11 c). In addition, hololeucocratic aplitic gneisses are associated with the K1-K3 orthogneiss (Fig. 11 e). The dark biotite-richer variety is developed towards the peripheral parts of the gneiss body. The intensity of deformation varies within the gneiss, the margins being more prone to intense foliation (Fig. 11 a).

The K1-K3 orthogneiss is characterised by high SiO₂ (70-80 wt.%). The protoliths are metaluminous to peraluminous magnesian monzogranites with calc-alkaline to calcic magma characteristics (Kozlik and Raith, 2017). Chemically it is similar to the Felbertal augengneiss, which is, however, less differentiated. With respect to granite type classification the K1-K3 orthogneiss is ambiguous showing overlapping I- to A-type characteristics (Finger et al., 1985). It has high concentrations of the trace elements Rb, Nb, Ta, Be, Li, Bi, Sn, Cs, Th, Mo and W and shows REE patterns with LREE enrichment, pronounced negative Eu anomalies and flat HREE distribution (Fig. 15 b). Compared to average continental crustal granites the K1-K3 orthogneiss is especially enriched in Cs, Rb, F, U, Nb and Ta (Kozlik and Raith, 2014). Its initial $^{87}\text{Sr}/^{86}\text{Sr}$ values range from 0.704 to 0.708 and the εNd values from -4 to -6 (Höll and Eichhorn, 2000). The initial εHf_t values vary from -7.6 to -4.3 and indicate a Mid-Proterozoic continental crustal source (Kozlik et al., 2016b).

Compared to the other types of Zentralgneis in the central Tauern Window it becomes clear that the K1-K3 orthogneiss in the mine and the associated hololeucocratic aplitic gneiss are the most differentiated granite melts. Extended magmatic differentiation for example explains the systematic decrease in combined Zr/Hf and Nb/Ta ratios (Fig. 17). The closest chemical and genetic (?) relationships exist with the Felbertal augengneiss. Magmatic differentiation, especially fractional crystallisation, seems to be the key process in forming these evolved melts although fractional crystallisation alone cannot explain the relations between the dark and the light-coloured K1-K3 orthogneiss (Kozlik and Raith, 2017).

Chemical data allow a clear distinction of the K1-K3 orthogneiss and the Cambrian orthogneisses (Briegleb et al., 1985; Finger et al., 1985; Höll and Eichhorn, 2000). Whereas the latter can be interpreted as the intermediate to felsic members of arc related magmatism, the K1 protolith is a specialised syn-orogenic (?) granite with unusual trace element composition.

Dykes crosscutting the older gneisses, metabasites and scheelite-bearing quartz veins are exposed in the Western Ore Zone (Figs. 13 c, d). These dykes have been referred to as porphyritic, lamprophyric or dacitic dykes in the literature. Petrographically, they are biotite-albite and muscovite-biotite-plagioclase gneisses. They are important for constraining the relative timing of scheelite mineralisation

because they crosscut scheelite-bearing quartz veins and shear zones containing Scheelite 2 as well as the K1 gneiss but are practically non-mineralised; they only contain traces of remobilised Scheelite 4 formed during Alpine metamorphism. One of these dacitic dykes was dated at 340 ± 5 Ma by Eichhorn (1999a). This age overlaps within the 2 sigma uncertainties with the U-Pb ages of the K1-K3 orthogneiss (Kozlik et al., 2016b), the Re-Os molybdenite ages (Raith and Stein, 2006) and the U-Pb age of Scheelite 1 (Raith et al., 2011) indicating that emplacement of the orthogneiss precursor, tungsten mineralisation, emplacement of the barren dykes and Variscan regional metamorphism occurred during a geologically short time interval during the Hercynian orogeny. The age data are not precise enough to resolve these events.

Combined in-situ U–Pb, Lu–Hf and trace element LA–ICP–MS analyses were performed on zircons from the W mineralized K1–K3 orthogneiss and associated aplite gneiss (Kozlik et al., 2016b). The textural and trace element characteristics suggest the presence of magmatic and hydrothermal zircon (Fig. 18). Magmatic zircons have lower concentrations of W, Nb, U, B and REE+Y and they form euhedral cathodoluminescence (CL) bright cores with distinct oscillatory zoning (zone a). Higher trace element abundances occur in CL-dark zircons with weak oscillatory zoning (zone b) overgrowing the zircon cores and in granular textured zircons restricted to the aplite gneiss and even higher ones in U-rich CL-dark zircons (zone b') lacking any zoning or internal texture (Fig. 18).

7 Mineralogy

Scheelite is the only mineral of economic interest. Fluorite is the most common fluorine mineral associated with scheelite. Calcite is a common gangue mineral next to quartz. It is to be noted that scheelite is the only W carrier. Wolframite and tin minerals like cassiterite are de facto missing. Sulfides and sulfosalts are much more common in the Western Ore Zone.

The following other minerals have been reported from Felbertal tungsten deposit (Weber and al., 2015): Pyrrhotite, pyrite, chalcopyrite, molybdenite, apatite and beryl are quite common; less common are tungstenite-molybdenite solid solutions, marcasite, galena, arsenopyrite, sphalerite, pentlandite, magnetite and hematite. Sulfosalts include galenobismutite, cosalite, bismuthinite, heyrovskeite, lillianite, makovickyite and mummeite, as well as members of the aikinite-bismuthinite series (friedrichite, hammarite, krupkaite, gladite, pekoite) and native bismuth. Very rare minerals are bornite, cobaltite, emplektite, enargite, tetrahedrite, stibnite, „stannite“, tellurides (hessite, joseite-like phases), cassiterite, Nb-Ta minerals (columbite, pyrochlore-group), powellite, wolframite phenakite and chrysoberyl. Recently, cupromakovickyite, cupromakopavonite, felbertalite, kupcikite, cuprobismutite and other members of the aikinite-bismuthinite (aikinite, emilite, lindströmite, paarite, salzburgite) were reported (Werner Paar, personal communication). For some of these new minerals Felbertal tungsten deposit is the type locality.

8 Controversial genetic models

When discovered Felbertal was regarded as the type locality of strata-bound tungsten deposits. The genetic concept of strata-bound and stratiform tungsten deposits goes back to researchers at University of Munich (Maucher, 1965; Höll, 1966; Höll and Maucher, 1968; Höll, 1977). The main postulates of this genetic model were: (a) the co-genetic formation of W with Sb and Hg minerals in ore deposits referred to as the "Sb-W-Hg formation"; (b) the strata-bound character of tungsten

mineralisation often hosted by black schists and genetically related with submarine volcanism; (c) a genetic link of mineralisation with mafic and/or felsic volcanism; (d) time-bound formation of these deposits preferably in the Early Palaeozoic; (e) spatial control of these ore deposits by suture zones, *i.e.* major lineaments at the margins of continents; (f) mobilisation and regeneration of Sb-Hg by subsequent geological processes within these belts.

Scheelite prospecting in the Eastern Alps, based on this then new model, led to the discovery of many scheelite showings including the discovery of Felbertal tungsten deposit (see Introduction, Höll, 1969; Höll, 1971; Höll, 1975; Höll, 1977; Höll, 1998). The main target of mining in the Eastern Ore Zone was the “banded” scheelite-quartz ore (Scheelitreicherz; Figs. 6 a, b) and the associated stockwork ores (Fig. 6 c). The lamination in the former was interpreted as a sedimentary fabric in cherts of exhalative origin (Höll et al., 1972) and was the main argument supporting the syngenetic/syndiagenetic model proposed in those days. According to this model exhalative hydrothermal fluids genetically linked with submarine mafic volcanism precipitated tungsten on or close to the seafloor. Metabreccias associated with the K2 ores in the Western Ore Zone were explained with eruptive volcanism (Höll and Schenk, 1988). Discordant mineralised quartz veins, which did not fit to the syngenetic model, were explained as products of metamorphic mobilisation and the formation of the large scheelite crystals (Scheelite 2) were similarly explained by metamorphic processes.

Another model proposed magmatic pre-concentration (*e.g.*, fractionation of metasomatised mantle melts) of tungsten followed by formation of an economic ore deposit due to intense metamorphic mobilisation of tungsten into quartz veins during polymetamorphism (Thalhammer, 1987; Thalhammer et al., 1989).

All these authors rejected any genetic link to Variscan granites, which were identified in the Western Ore Zone (*i.e.*, K1-K3 orthogneiss) only in the early eighties. After recognition of this gneiss as an intrusive metagranitoid of Carboniferous age (Pestal, 1983; Jahoda, 1984) and its close spatial association with high-grade ores (K1-K3 ore bodies) granite-related genetic models were favoured by a group of researchers (Pestal, 1983; Briegleb et al., 1985; Finger et al., 1985; Trudu and Clark, 1986; Briegleb, 1991; Raith and Stein, 2006).

The epigenetic model was especially propagated by D. Briegleb the former mine geologist at Felbertal. He interpreted the K1 orthogneiss as a highly fractionated residual granitic liquid, which was emplaced along suitable structures during the Variscan orogeny at the base of the older magmatic sequence. Granite-derived hydrothermal fluids formed Quartz 1 veins and associated scheelite mineralisation and caused K-, Rb-, F-, Si- metasomatism. This was succeeded by pre-Alpine deformation and metamorphism causing local remobilisation of scheelite, emplacement of calc-alkaline dykes (porphyrites, lamprophyres). During the Alpine orogeny minor scheelite (Scheelite 4) was remobilised into Alpine quartz veins (Quartz 2).

In the following the epigenetic model and a granitic genetic relationship was also accepted by researchers from Munich (Eichhorn et al., 1999a). However, these authors still argue for a *two-stage* formation of the Felbertal deposit; a first stage of Cambrian (≈ 520 Ma) and a second stage of Lower Carboniferous (≈ 340 Ma) age. Scheelite 1 from the banded ores in the Eastern Ore Zone and the K2 ores in the Western Ore Zone were still claimed to be of Cambrian age whereas the Early Carboniferous age of Scheelite 2 and its genetic link with the K1-K3 orthogneiss has been accepted.

Re-Os dating of molybdenite could only confirm the Variscan event. The model and isochron ages range between 358 and 336 Ma and record several pulses of magmatic hydrothermal and metamorphic molybdenite formation (Fig. 16, Raith and Stein, 2006). These ages confirm the Early Carboniferous age of the K1-K3 ores. Foliated ores from the K2 orebody, regarded as equivalents of the Cambrian "Scheelittreicherz" also yielded Variscan ages and so did molybdenites from the stockwork zone in the Eastern ore field.

The "deathblow" for the syngenetic and the two-stage epigenetic (Cambrian and Early Carboniferous) models comes from in-situ U-Pb dating of Scheelite 1 from the foliated ores in the Eastern Ore Zone. The age of 335.5 ± 4.6 Ma (Raith et al., 2011) obtained for the relict scheelite cores perfectly fits the 336-340 Ma ages of the K1-K3 orthogneiss; hence, a genetic link of W mineralisation to this chemically unusual granite is unavoidable.

In summary, the Felbertal deposit is best interpreted as a poly-metamorphosed granite-related stockwork type tungsten deposit. There is accumulating evidence supporting a genetic relation of tungsten mineralisation with evolved Lower Carboniferous granites.

9 Mining

The Felber valley separates the deposit into an Eastern and a Western Ore Zone (Fig. 1 a). Due to spatial relation between the deposit morphology and the topography, mining of the Eastern Ore Zone was by open pit (Figs. 1 c, d), while the Western zone is mined by underground methods.

The Eastern Zone open pit mine operated from 1975 to 1986. The plunge of the Ore Zone was sub-parallel to the slope of western flank of the Brentling peak (Fig. 1 c). This resulted in a very low strip ratio of 1.5:1 (waste:ore) despite the small lateral extension of the orebody. Mining was undertaken from 1750 m to 2200 m a.s.l. The pit was essentially only a small ravine down-dip along the slope of the mountain (Fig. 1 c). A large portion of the orebody was slightly dislocated by post-glacial slumping and developed as "ore boulder deposit".

Outside of the "ore boulder" area, classical drill and blast open pit mining was applied, with bench heights of 10 m, using electro-hydraulic drill rigs and hydraulic shovels. Transport from the pit to the mill was by dump truck. The entire operation was run by a subcontractor. Due to severe climatic conditions, access to the open pit was restricted to the period from mid-May to October. Highest annual production was achieved in 1980 with 320,000 tonnes. Stockpiling allowed uninterrupted production at the milling facilities.

Total production from the open pit was 2.5 Mt with an average grade of about 0.6 wt.% WO_3 . Following completion of mining, the area was re-cultivated and is now used again as alpine pasture.

Development of the underground mine in the Western Ore Zone started in 1977. The mineralised zone has a section of about 500 by 300 m and a down-plunge extension of more than 850 m, from the outcrop at about 1280 m a.s.l. to the currently deepest exposure at 625 m a.s.l. (Fig. 13). The deposit remains open to depth.

In general, scheelite mineralisation is pervasive, and the ore body definition is largely controlled by the cut-off grade. The mineralised zone is divided by a large fault zone incorporating a slice of sterile schists ("Basisschiererschuppe"; Figs. 8, 9). Within the diffusive mineralisation, up to eight elongated WNW-plunging ore lenses are developed, some of which merge downdip to a single larger ore body.

Due to the location close to the National Park, and to provide adequate shelter in case of high avalanche risk in winter, almost all infrastructure of the mine is located underground (Figs. 19, 20). This includes change rooms, canteen, offices and workshops.

Access from the Felber valley and location of the main infrastructure is on level 1175 m a.s.l. The mine was developed from the onset as trackless operation with diesel powered LDH equipment (Fig. 19 a; Figs. 20 a, b). Standard section of drifts and ramps is around 25 m². By 2018, more than 60 km of drifts and ramps had been developed, but many are not accessible any more. The individual sublevels are connected by means of a spiral ramp, with a 12% inclination, various service and ventilation raises and ore passes.

To assure year-round safe access to the mine and to improve environmental performance, it was decided to connect the mine with the mill by a 3 km adit (Spross, 1984). A crushing plant was erected in a large underground cavern on level 850, comprising screening plant, a jaw crusher for primary crushing and two cone crushers for secondary crushing. A 12 mm-product is delivered by conveyor belt to fine ore bins with some 5000 tonnes capacity close to the portal and then with another set of conveyors to the plant. From 1985 onwards, this system allowed replacing overland truck haulage through the Felber valley.

The first phase of underground mining concerned the ore between mine level (mL) 1175 (then also the haulage level) and the outcrop of the mineralisation at around 1280 mL. Most of the mining was undertaken as open stoping, although all of the stopes have been filled with hydraulic sandfill or paste fill in the meantime.

Subsequently, the ore between the 1175 mL and the feed level of the crusher station (850 mL) was developed in several stages and mined. In the late 1990s, mining advanced below the level of the crusher, which requires intermediate haulage by truck from the active stopes to the run-of-mine ore bin at 910 mL. By the end of 2017, active stoping reached the interval from 650 mL to 675 mL, while development drifting advanced towards 625 mL.

For an underground environment, mined ore grades are fairly low, just below 0.3% WO₃ on average. Thus, large-scale low-cost mining methods have to be employed to allow economic extraction. The mining method for the main orebody is sublevel caving, using 25 m sublevel interval and stope dimensions of up to 40 to 80 by 80 to 100 m with multiple draw points.

Other mining methods currently employed at the Felbertal mine are transversal sublevel stoping, top to bottom over several sublevel intervals, with delayed backfill (normally a mixture of unconsolidated waste rock from underground development and hydraulic sandfill) or longitudinal sublevel stoping bottom to top with smaller sublevel intervals (12-20m). The latter is a variation of cut & fill mining.

Selection of the mining method depends on grade, ground conditions and geometry of the individual ore zones. The rather flat dip (around 45-55°) and increasingly difficult ground conditions in the lower sublevels pose constraints on the flexibility of the mining approach.

Drilling equipment at the Felbertal mine includes two-boom jumbos for drifting (Fig. 19 b) and longhole rigs for ring drilling in the stopes, both, with classic top hammer or hydraulic in-hole hammer. The company also owns a raise bore machine for drilling slots in the stopes and service shafts. Blasting employs emulsion cartridges, loose ANFO explosives, pump emulsion and NONEL detonators.

Mucking and haulage to ore passes or truck loading bays is by 15-tonne scooptrams (Figs. 20 a, b). Mucking from open stopes is undertaken with remote control. Ore produced on the lower sublevels is transported by 30 or 50 tonne ADTs to the ore bin above the crushing plant.

Since 1988, a part of the tailings from the flotation plant is used as hydraulic backfill in the mine (Walser, 1992). This has two advantages: first, decrease of cavities in the underground environment and thus increased stability and lower risk of dilution, and second, reduced storage requirements for tailings on surface. However, loose sandfill will never consolidate, and groundwater circulation poses the risk of washing out the fill. In 2008, the company installed a pastefill plant to produce consolidated fill from tailings and a binder. Fly ash is used as binder, which has economic advantages over cement and adequate technical behaviour.

Annual development comprises 2750 m of drifting, installation of 6000 rock bolts (split sets and cable bolts) and 3000 m³ of shotcrete with steel fibres (Fig. 20 c). Backfill requirements are around 200,000 t per year.

Diamond drilling (Fig. 20 d) and sludge hole drilling is undertaken for exploration and stope definition in the underground environment. The annual diamond drilling volume was around 2500 m until recently, while 5000 m are planned for 2018. Due to geometrical constraints, drilling cannot adequately test the down-plunge continuity of the orebody. A dedicated exploration drift was developed into the hangingwall of the main orebody on level 725, and another one is now planned for level 625.

To allow adequate communication, a leaky feeder underground communication system covers the entire underground development. Mine planning and resource modelling uses state-of-the-art computer programmes providing three-dimensional visualisation.

In total, about 65 persons including maintenance and service personnel are employed in the mine that operates generally on a 5-day / two-shift basis.

10 Beneficiation

To upgrade the low-grade ore a flotation plant was constructed in 1976, directly at the Felbertauern highway, some 1000 m below and (as the crow flies) 3 km north of the open pit (Figs. 21 a, b). The capacity was initially 250,000 tonnes per year (tpa) but was increased to the current capacity of close to 400,000 tpa by the early 1980s. Introduction of sensor-based sorting in around 2010 allowed to further increase the beneficiation capacity to over 500,000 tpa. Crushing facilities are located underground (Fig. 20 e). From the onset, it was only planned to produce low-grade (“non-commercial”) concentrates at the mill, as further upgrading at the Bergla refinery occurs within the same company, and a much higher recovery of tungsten is possible when accepting lower-grade concentrates.

Capacity of the flotation plant is 72 t per hour, with a head grade of around 0.35 wt.% WO₃. The beneficiation circuit briefly comprises of milling by ball mill in closed-circuit to 80% passing 200 µ (seventy mesh), rougher flotation and cleaning stages to produce a concentrate with 30-35% WO₃ at some 86% recovery (Fig. 21 b). The concentrate is dewatered by vacuum drum filter, packed in 1.5-tonne “big bags” and trucked to the refinery in Bergla.

The company is constantly trying to improve the mill performance and undertakes various tests to optimise the flow sheet.

Tailings management in an area of outstanding natural beauty and dense population is a highly sensitive issue. Initially, a small tailings pond was used close to the mill side in the Felber valley which is now inactive. Due to topographic and environmental constraints, additional capacity was then provided in a tailings management facility in the Pinzgau valley near Stuhlfelden, some ten kilometres north of the plant (Fig. 21 c).

Design, construction and operation of the 10 km slurry pipeline were and still are a technical challenge. The tailings are highly abrasive, and a critical minimum velocity of the transport needs to be constantly achieved to avoid sedimentation. An elaborated system of emergency pumps and compressed air containers to operate valves without electricity assures that sedimentation can be avoided in case of power failures. A 4 km tailings pipeline with 200 m head to supply the mine with tailings for backfilling purposes is operated with high pressure pumps.

Since 1983, some 11 Mt of tailings were placed in a number of separate basins at the Stuhlfelden tailings facilities. The tailings itself do not contain any dangerous reagents, and the content of sulphides and heavy metals is low. They are classified as inert non-class A tailings according to the European mine waste regulations. Re-cultivation of the tailings ponds is an ongoing measure, and the older portions of the facilities are now used again as pasture (Fig. 21 c).

The plant includes an assay laboratory employing XRF and AAS techniques and an XRD to determine mineralogical composition of the ore feed. A metallurgical laboratory allows testing for example new flotation reagents. The facilities are also used by Wolfram Bergbau's International Mining Department for project work abroad.

A total of 27 persons are employed at the plant. Other than almost all flotation plants world-wide, the Felbertal facilities are operated discontinuously, for 5.5 days per week only.

11 Acknowledgements

The authors thank Wolfram Bergbau und Hütten AG for making this excursion possible and for logistic and technical support as well as providing data and photos used in this guide book. SEM-CL images were made at Gothenburg University (cooperation with D. Cornell) and by U. Kempe, Bergakademie Freiberg. New data on the K1-K3 orthogneiss were obtained during a joint FFG Bridge project between WBH and Montanuniversität Leoben in 2013-2016. M. Kozlik who did his doctoral thesis in the framework of this project is thanked for providing data used in this publication. In-situ U-Pb age data on scheelite and zircon were analysed in Axel Gerdes laboratory at Goethe Universität Frankfurt on a collaborative basis.



Fig. 1: a. Location of the Eastern Ore Zone (EOZ, open pit) and Western Ore Zone (WOZ, underground) in the Felber Valley; view to $\approx S$. b. Exploration drilling in the open pit area, 1972. c., d. Early mining operation in the open pit (mid-1970s). All photos from WBH archives.

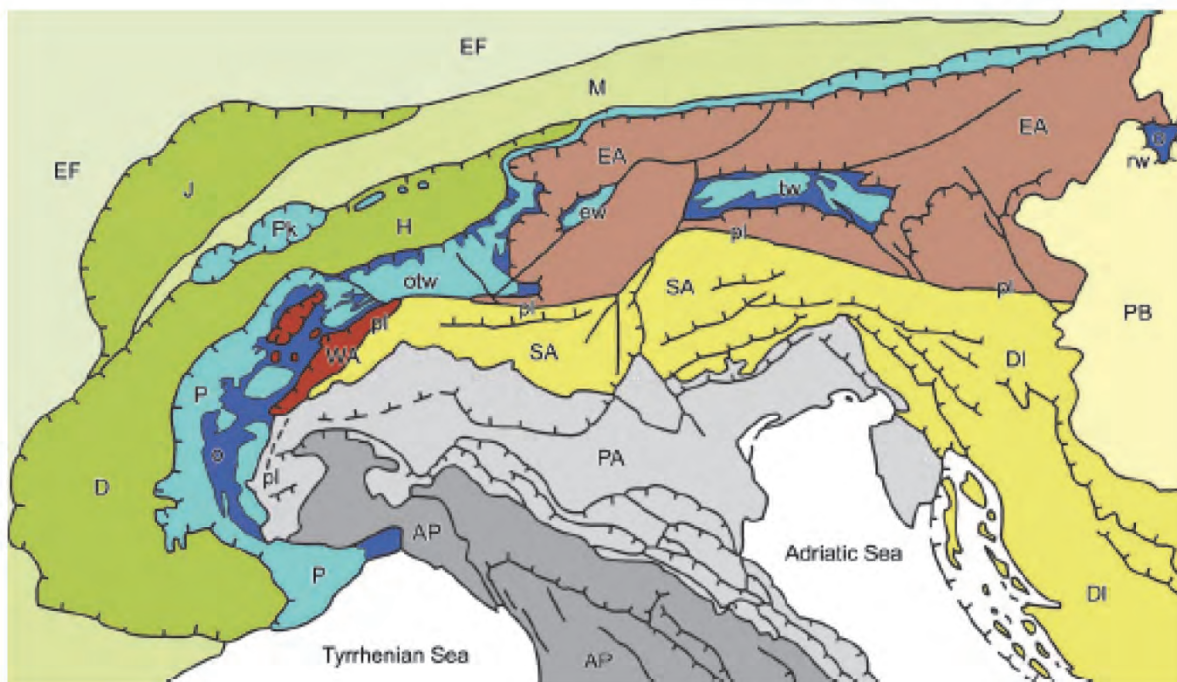


Fig. 2: Tectonic map of the Alps (from Dal Piaz et al., 2003) showing the location of the Tauern Window in the Eastern Alps. (1) Europe-vergent collisional belt: i) Western (WA) and Eastern (EA) Alps; ii) Penninic domain: continental and ophiolitic (o) nappes in the Western Alps and tectonic windows (otw: Ossola-Ticino, ew: Engadine, tw: Tauern, rw: Rechnitz); Pre-Alpine klippen (pk); iii) Helvetic-Dauphinois (H-D) domain; iv) Molasse foredeep (M); v) Jura belt (J). (2) Southern Alps (SA), bounded to the north by the Periadriatic lineament (pl). Pannonian basin (PB), European (EF) and Po Valley-Adriatic (PA) forelands, Dinaric (DI) and Appeninic (AP) thrust-fold belts.

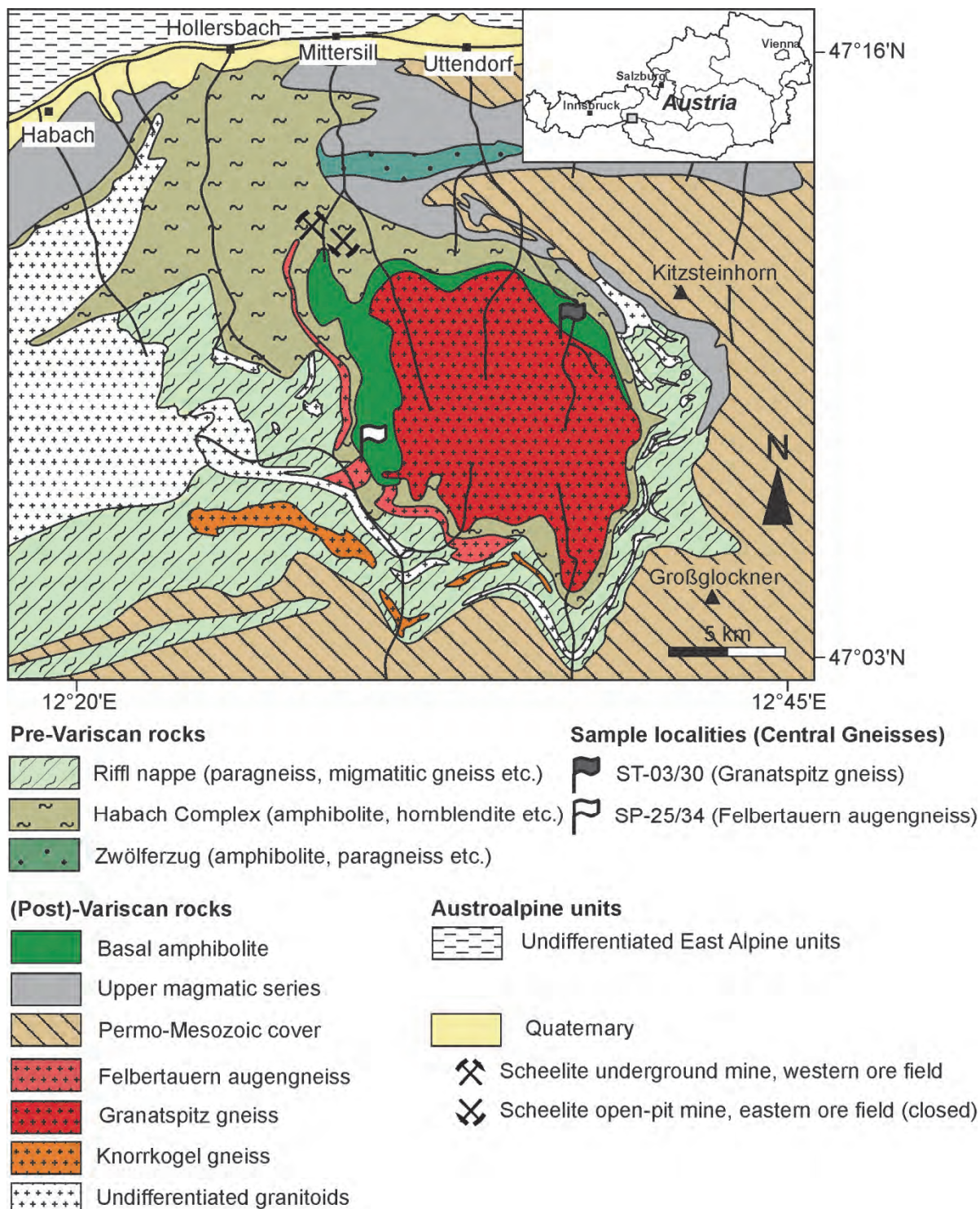
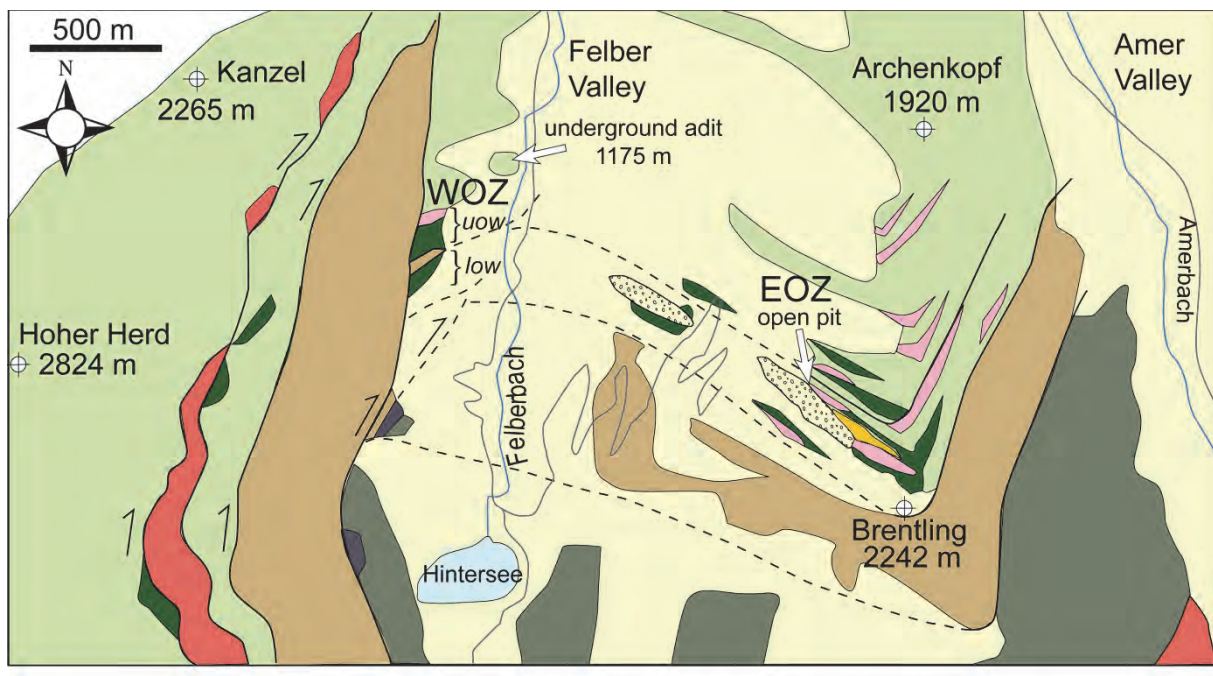


Fig. 3: Geological sketch map of the central part of the Tauern Window (from Kozlik et al., 2016b).



Variscan metagranitoids

	Felbertauern augengneiss		Road
Habach Complex & Stubach Group			
	Scheelite ore, laminated		Lake, river
	Orthogneiss		Alluvium
	Amphibolite, fine-grained		Ore-bearing scree
	Hornblendite; Amphibolite, coarse-grained		<i>uow, low</i> upper & lower ore-bearing wedge
	Basal schist		Alpine thrust faults
	Serpentinite		proven
	Basal amphibolite		concealed, inferred

Fig. 4: Simplified geological map of the area around the Felbertal tungsten deposit (after Höll and Eichhorn, 2000). EOZ Eastern Ore Zone, WOZ Western Ore Zone. Alpine thrust(-slip) faulting caused the stacking of the Basal Amphibolite (Stubach Group) and rocks of the Habach Complex as well as the tectonic imbrication within units of the Habach Complex and the Felbertal scheelite deposit.

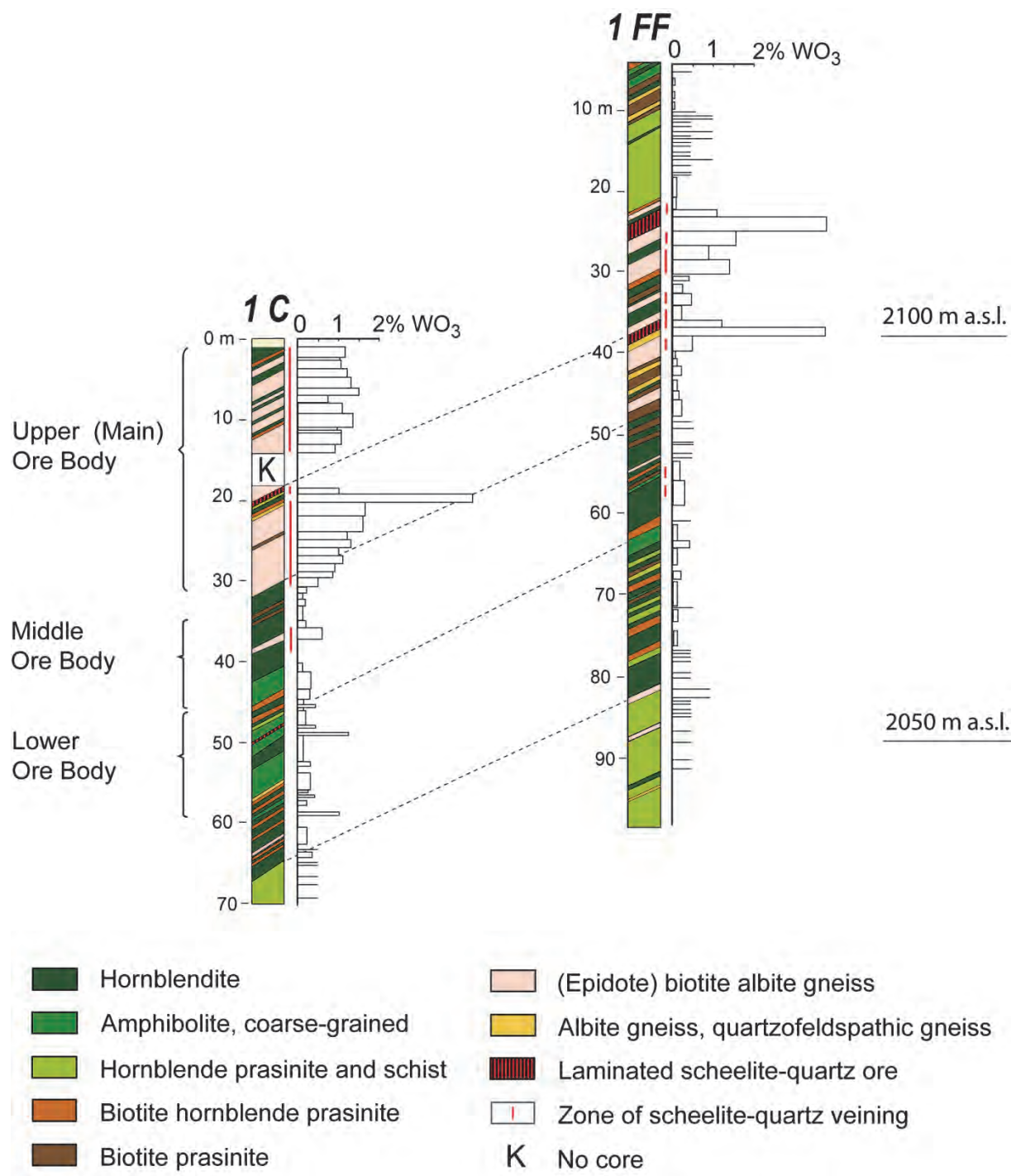


Fig. 5: Drill core logs from exploration drillings 1C and 1FF in the Eastern Ore Zone (based on Höll, 1975). Typically, the whole magmatic sequence composed of alternating layers of hornblendite, various metabasites and gneisses is mineralised. Very high (>2 wt.% WO_3) ore grades occurred in the foliated (laminated) scheelite-quartz ores, though high-grade ore zones (>1 wt.% WO_3) are not restricted to these ores but are also associated with stockwork-like quartz veins (see Fig. 6 c) throughout the whole sequence.

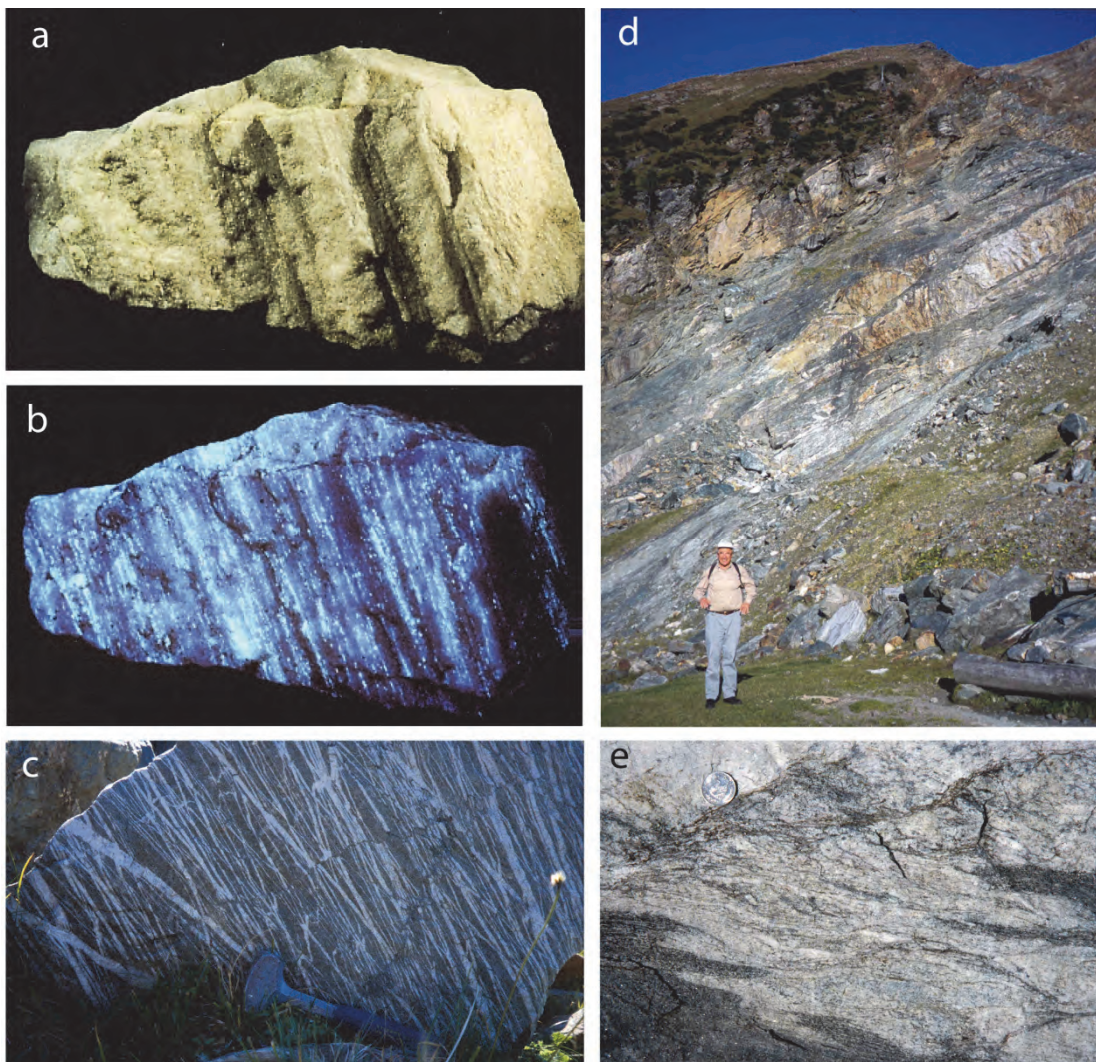


Fig. 6: **a, b.** Foliated high-grade scheelite ore (Quarzitisches Scheelitreicherz) from the Eastern Ore Zone. **b.** in UV light. Photograph from WBH archives. **c.** Stockwork like quartz veins with scheelite in boulder. These stockwork ores were interpreted as the feeder zone of the foliated ores (Höll and Eichhorn, 2000). Boulder from Eastern Ore Zone; photo J.G. Raith, September 1999. **d.** Alternation of ultramafic/mafic and felsic metagneous rocks in the abandoned open pit. The felsic gneisses (Ostfeldgneis) derived from I-type granitic protoliths emplaced at ≈ 520 Ma. The person in the foreground is R. Höll, who discovered the deposit in 1967. Open pit at ≈ 1929 m, Ostfeld; photo J.G. Raith, September 1999. **e.** Tectonically reworked intrusive contact of leucocratic orthogneiss with biotite-rich metabasites. Boulder in open pit at ≈ 1930 m, Ostfeld; photo J.G. Raith, September 1999.

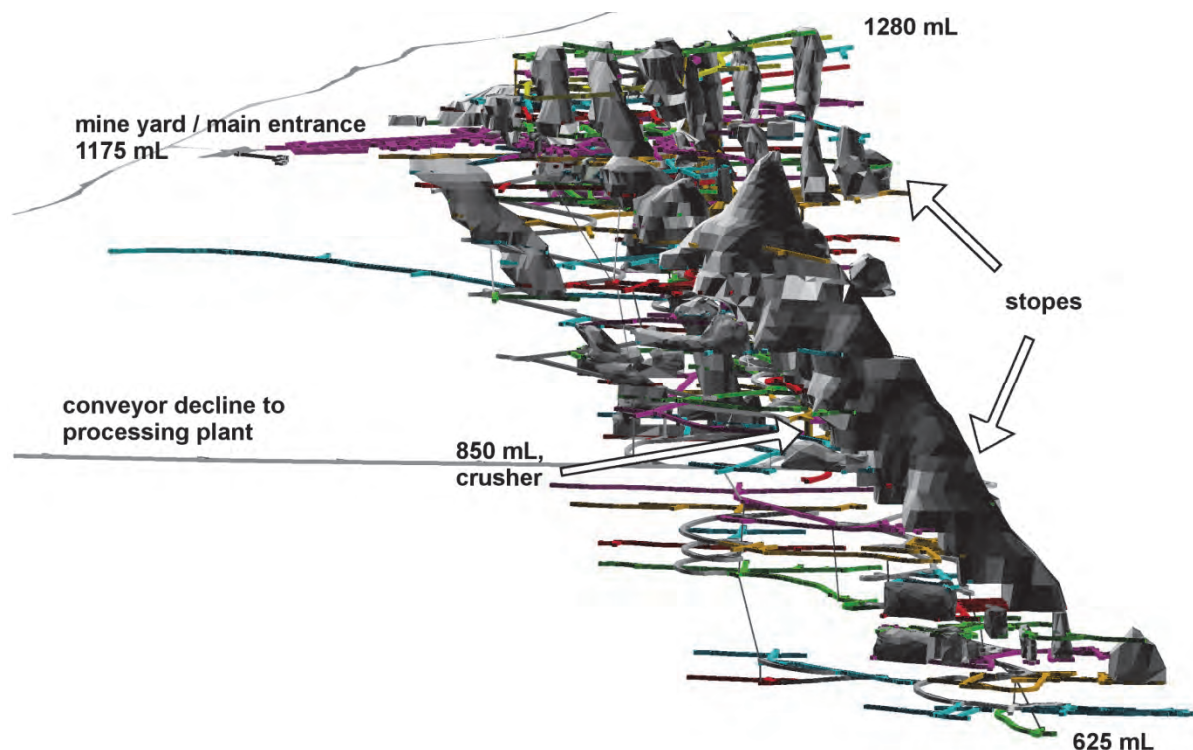


Fig. 7: 3D model of the underground mine in the Western Ore Zone (Westfeld) showing location of the different mining levels and stopes as per August 2018.

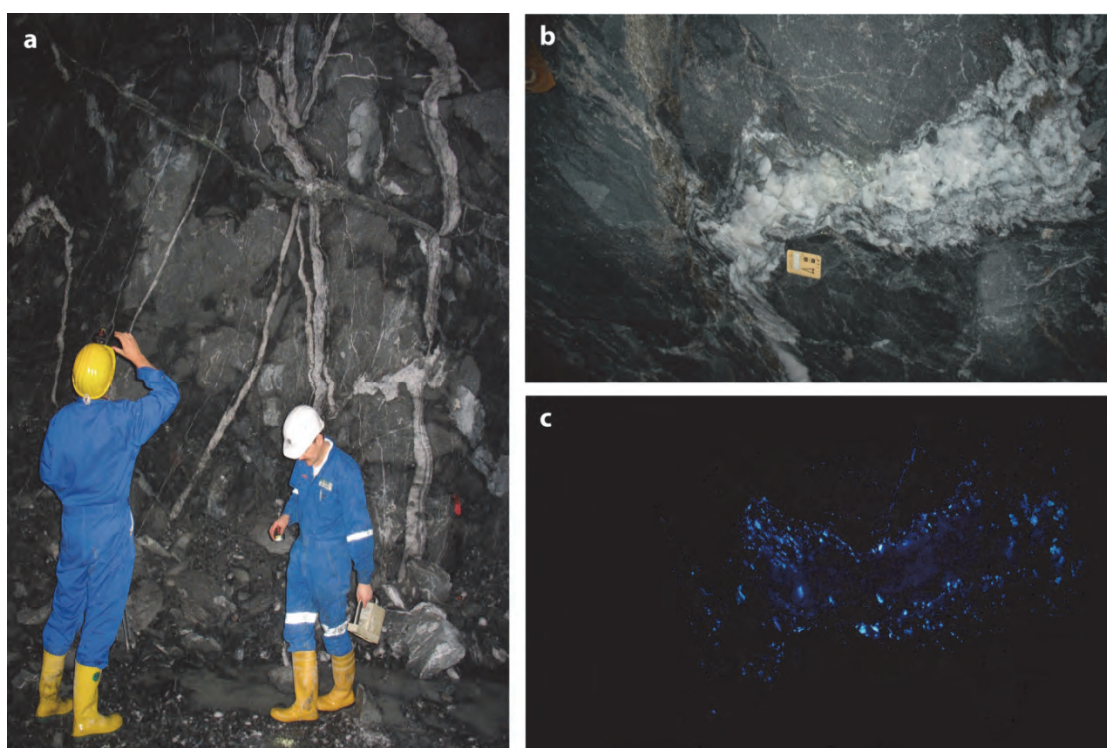


Fig. 8: **a.** Deformed quartz veins in metabasite. K2' orebody, level 775, Westfeld; photo J.G. Raith, February 2009. **b, c.** Deformed quartz-scheelite vein (Quartz 1) in metabasites. Scheelite is concentrated at the vein selvages. Larger scheelite porphyroblasts (Scheelite 2) show yellowish fluorescence in UV light (photo c). K2' orebody, level 775, Westfeld; photo S. Schmidt, February 2009.

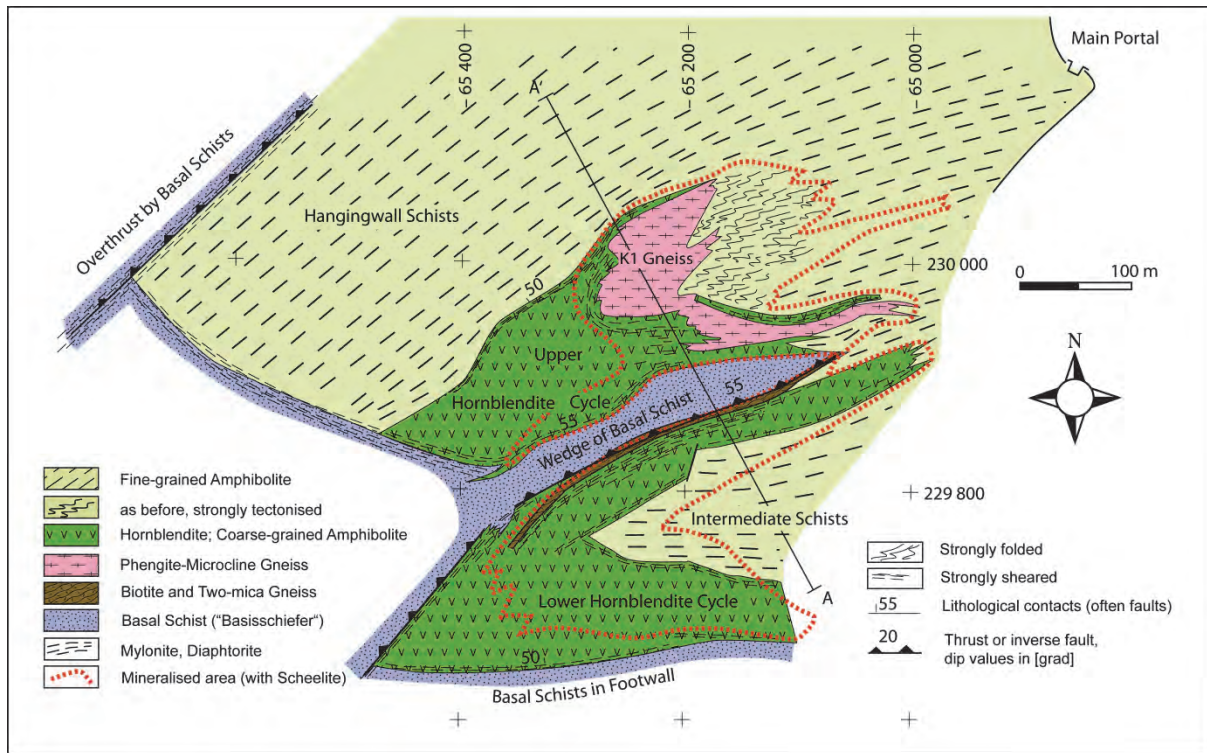


Fig. 9: Geological sketch of level 1175 of the Western Ore Zone showing the two ore-bearing wedges (Lower and Upper Hornblendite Cycle) separated by a barren wedge of Basal Schists (from Schmidt, 1988).

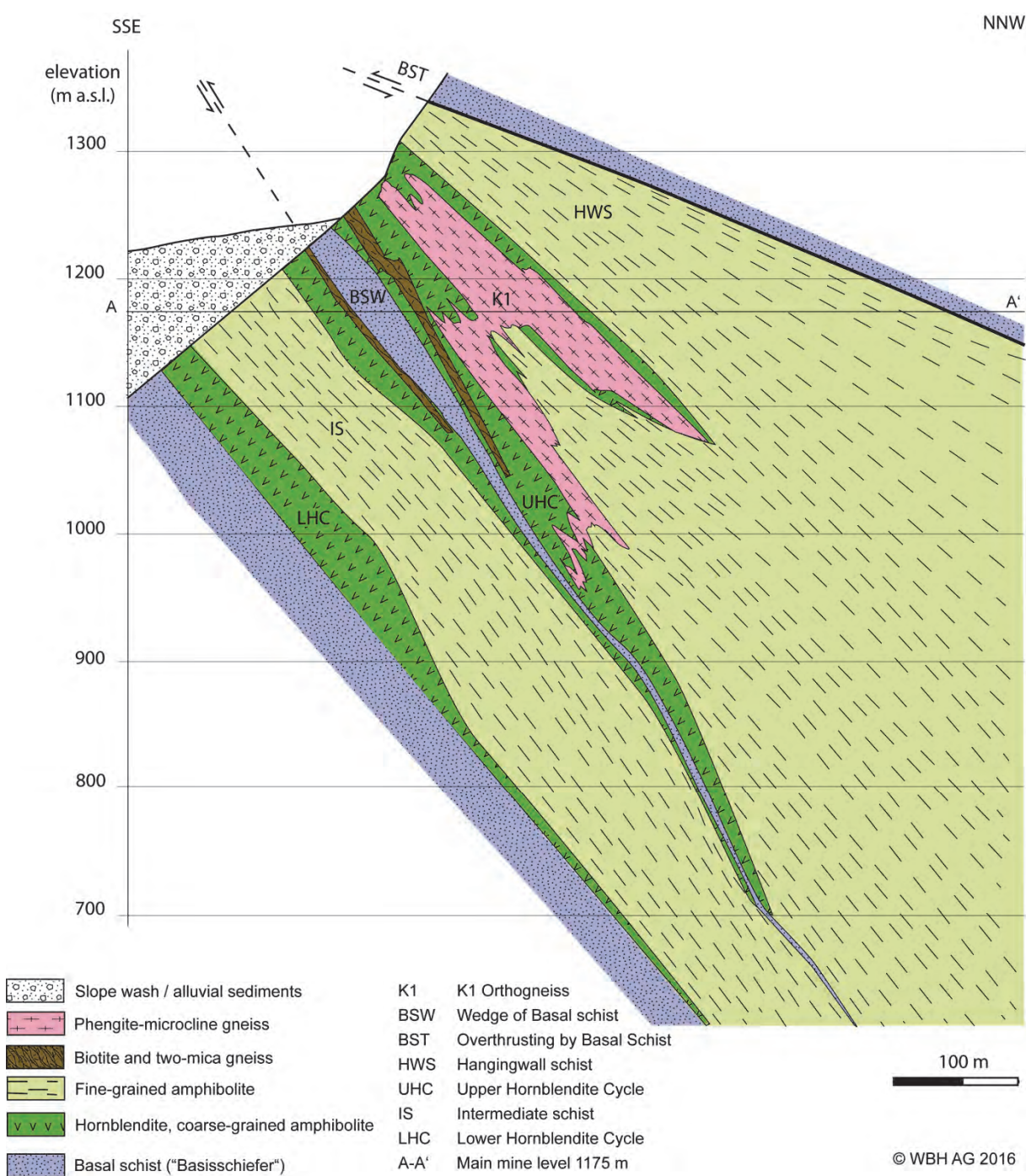


Fig. 10: SSE-NNW profile through the Western Ore Zone; for exact location see A-A' on Fig. 9 (from Schmidt, 1988, updated for deeper mine levels in 2016).

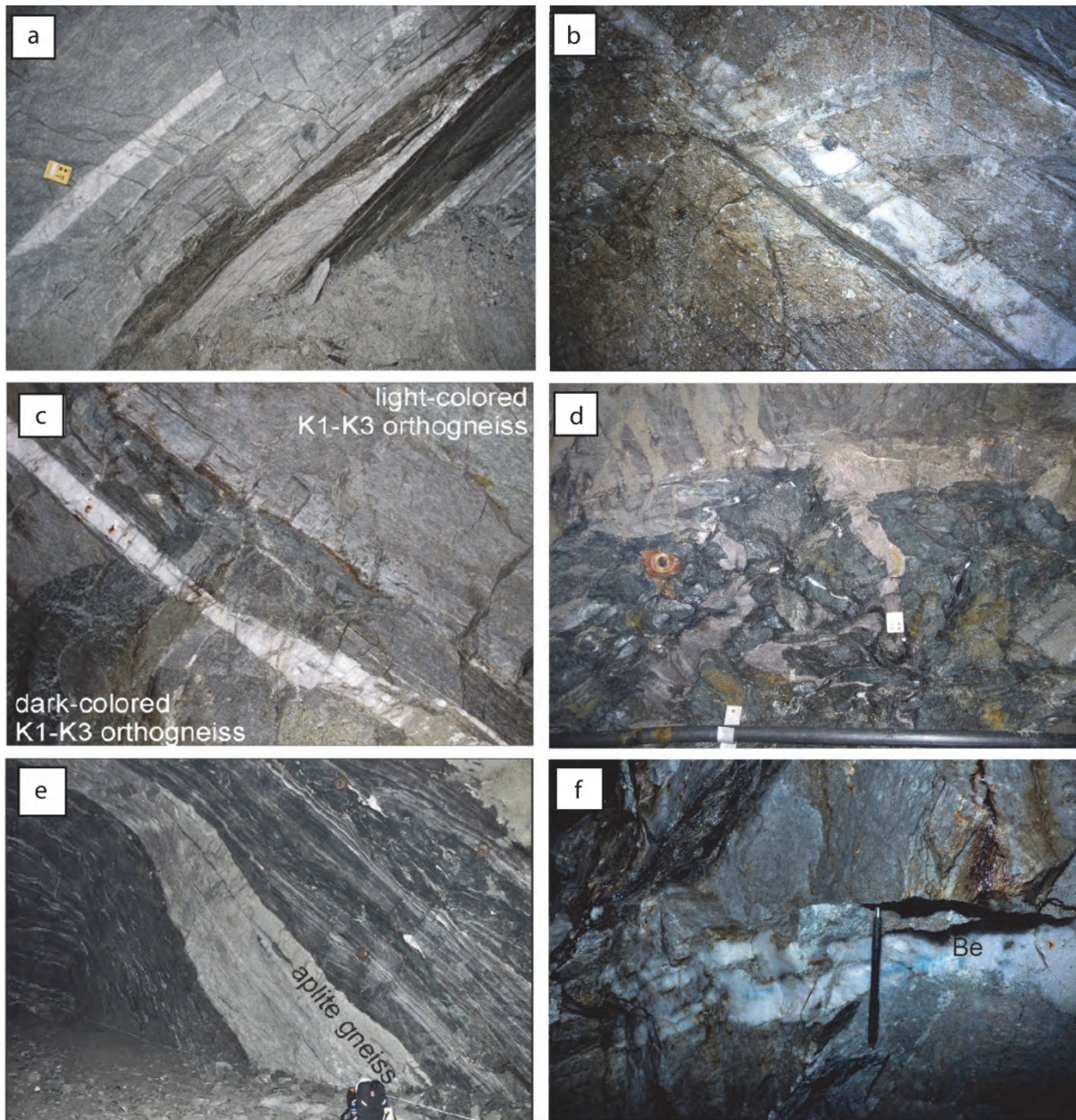


Fig. 11: a. Well-foliated K1-K3 orthogneiss with deformed quartz vein (Quartz 1) and rafts of strongly deformed hornblende-biotite schists. K1' ore body, level 1164; photo J.G. Raith, February 2009. *b.* ~10 cm thick deformed quartz vein containing elongate scheelite (grey, Scheelite 2) in K1-K3 orthogneiss. The mineralised vein crosscuts the Early Carboniferous granite gneiss (336-341 Ma, Kozlik et al., 2016b) but shows penetrative deformation. Upper part of K1 orebody, level 1152; photo J.G. Raith, September 1999. *c.* Sharp contact between dark- and light-coloured K1-K3 orthogneiss varieties. A quartz-scheelite vein (white) crosscuts the gneiss but is aligned in the foliation; level 1164; photo M. Kozlik, 2013. *d.* Folded apophyses of dark-coloured K1-K3 orthogneiss intruding amphibolite; level 1164 m; photo J.G. Raith, February 2013; rectangular scale length ≈8 cm. *e.* Dike of aplite gneiss aligned in dark foliated fine-grained amphibolite; dyke is about 1 m thick; level 940; photo M. Kozlik, 2013. *f.* Quartz-scheelite vein with beryl (Be) crosscutting K1-K3 orthogneiss; level 1164; pen for scale is 12 cm; photo M. Kozlik, 2013.

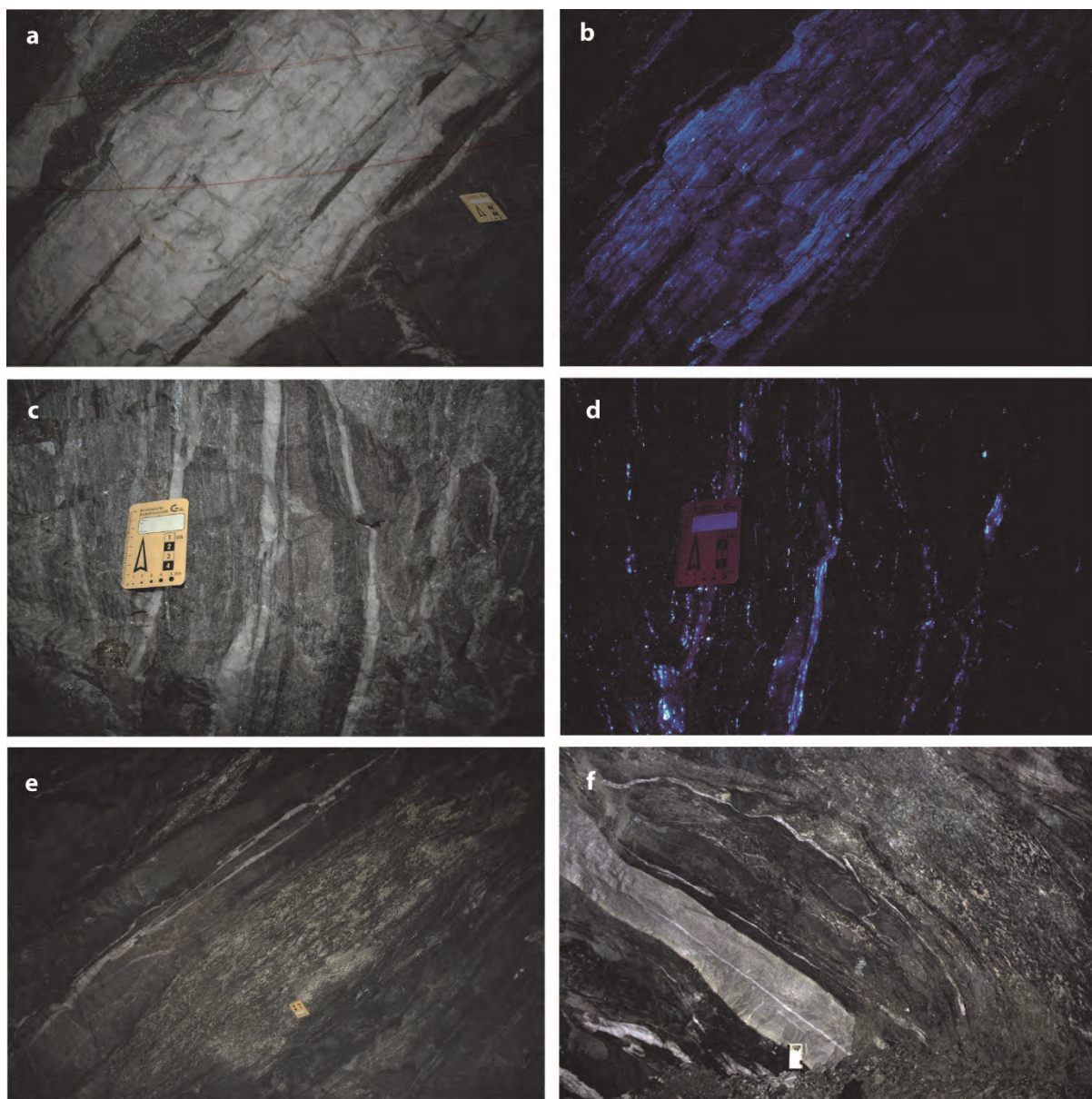


Fig. 12: **a.** Foliated scheelite ore. Note the foliation-parallel thin rafts of darker and scheelite-free/-poor host rocks within the about 1 m thick scheelite-quartz mass. K2 ore body, Level 1000. **b.** in UV light; photos S. Schmidt, February 2009. **c.** Interlayered gneiss (grey) metabasite (greenish) sequence truncated by about foliation-parallel quartz veins (Quartz 1). **d.** in UV light. The higher scheelite concentrations are associated with the quartz veins but minor scheelite is also present as disseminations throughout the host rocks. K4 ore body, level 1164; photos S. Schmidt, February 2009. **e.** Lens of coarse-grained amphibolite (metagabbro), gneiss (brown grey) and hornblendite in phyllonitic biotite-chlorite schist (upper left). K4 ore body immediately in the hanging wall of the Basisschiefer, level 1110; photo J. G. Raith, February 2009. **f.** Intercalation of felsic gneiss in metabasites. A thicker layer of coarse-grained amphibolite is to be seen to the right. This scheelite-bearing quartz veins (Quartz 1) crosscut the gneiss and the metabasites. K5 orebody, level 1050; photo J.G. Raith, February 2009.

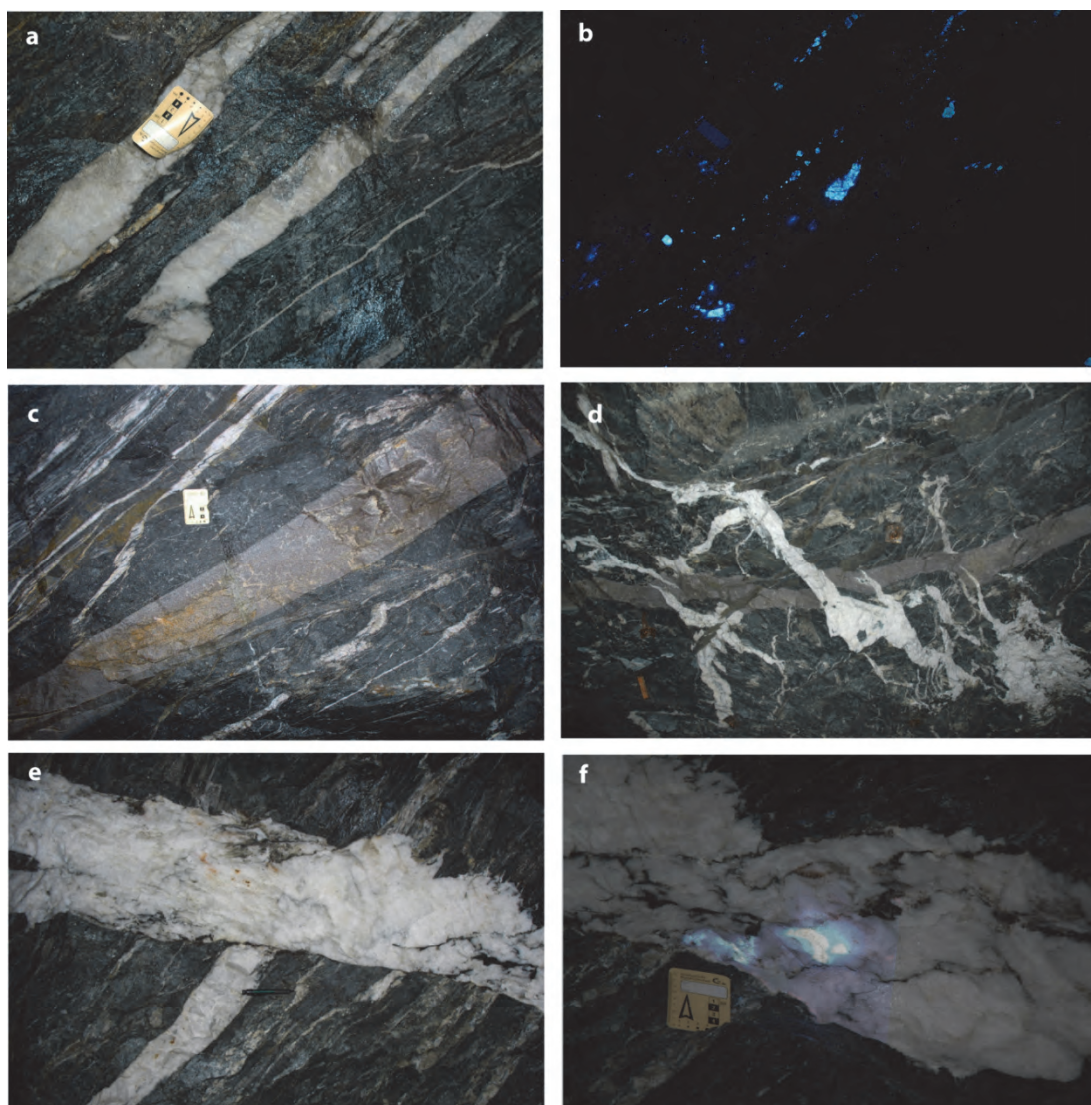


Fig. 13: **a, b.** Two scheelite-bearing quartz veins (Quartz 1) in dark-coloured host rocks (so called "Schwarzerz"). **b.** in UV light. The veins are aligned in the main foliation of fine-grained amphibolite. Scheelite is concentrated in the veins forming larger porphyroclasts (greyish in normal, yellowish fluorescence in UV light; Scheelite 2). Finer-grained re-crystallised scheelite (white, bluish fluorescence, Scheelite 3) is aligned in stringers. Level 1152 hanging wall; photos S. Schmidt, February 2009. **c.** Dyke of ≈ 340 Ma non-mineralised biotite gneiss crosscutting scheelite-bearing quartz veins (Quartz 1) in hornblende schist. In contrast to the schist the dyke is not mineralised (UV photo not shown). Level 1152 hanging wall; photo J.G. Raith, February 2009. **d.** The same biotite gneiss dyke dissected by younger quartz veins (Quartz 2) of Alpine age. Both the dyke and the younger quartz veins postdate scheelite-bearing Quartz 1 veins. Level 1152 hanging wall; photo J.G. Raith, February 2009. **e, f.** Discordant quartz vein (Quartz 2) crosscutting and displacing a scheelite-bearing quartz vein (Quartz 1). Level 1152 hanging wall; photo J.G. Raith, February 2009. **f.** Detail of e. Combined normal and UV light. Up to 5 cm large crystals of scheelite showing bluish-whitish fluorescence (Scheelite 4) in Quartz 2 vein. These younger veins and Scheelite 4 formed due to local remobilisation of quartz and scheelite during Alpine (≈ 30 Ma) regional metamorphism. Level 1152 hanging wall; photo S. Schmidt, February 2009.

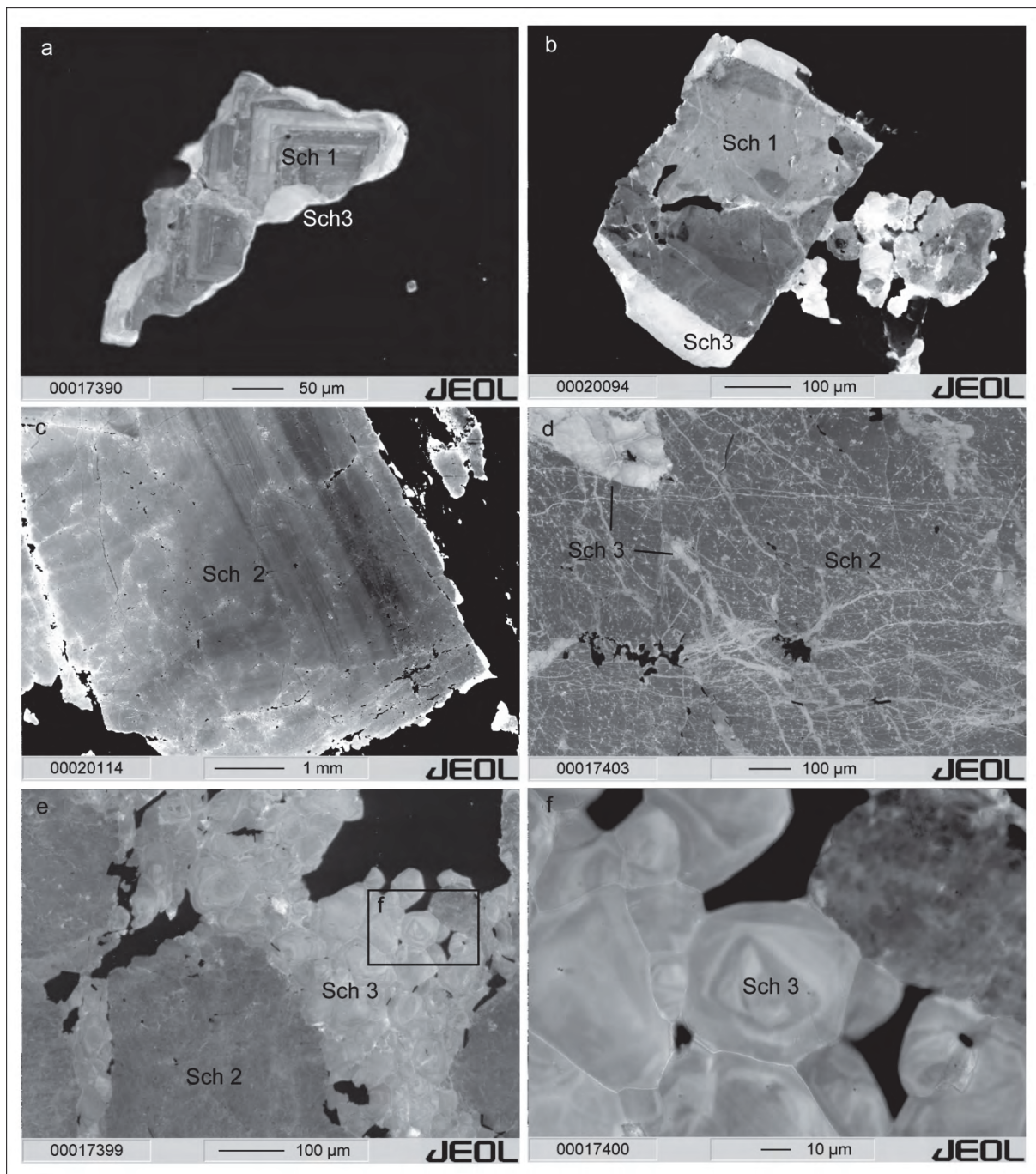


Fig. 14: Cathodoluminescence (CL) micro-images of scheelite from the Felbertal deposit. **a.** Scheelite 1 (Sch1) with fine oscillatory zoning replaced by and overgrown by CL-brighter Scheelite 3 (Sch3); foliated scheelite-quartz ore, Ostfeld. **b.** Scheelite 1 with rim of Scheelite 3; K2 orebody, Westfeld. **c.** Large Scheelite 2 (Sch2) porphyroblast with growth zoning; K1 orebody; Westfeld. **d.** Microfractures in Scheelite 2 filled with CL-brighter scheelite 3. **e.** Recrystallised Scheelite 3 overgrowing and replacing Scheelite 2; K1 orebody, Westfeld. **f.** Detail of e showing diffuse zoning in Scheelite 3.

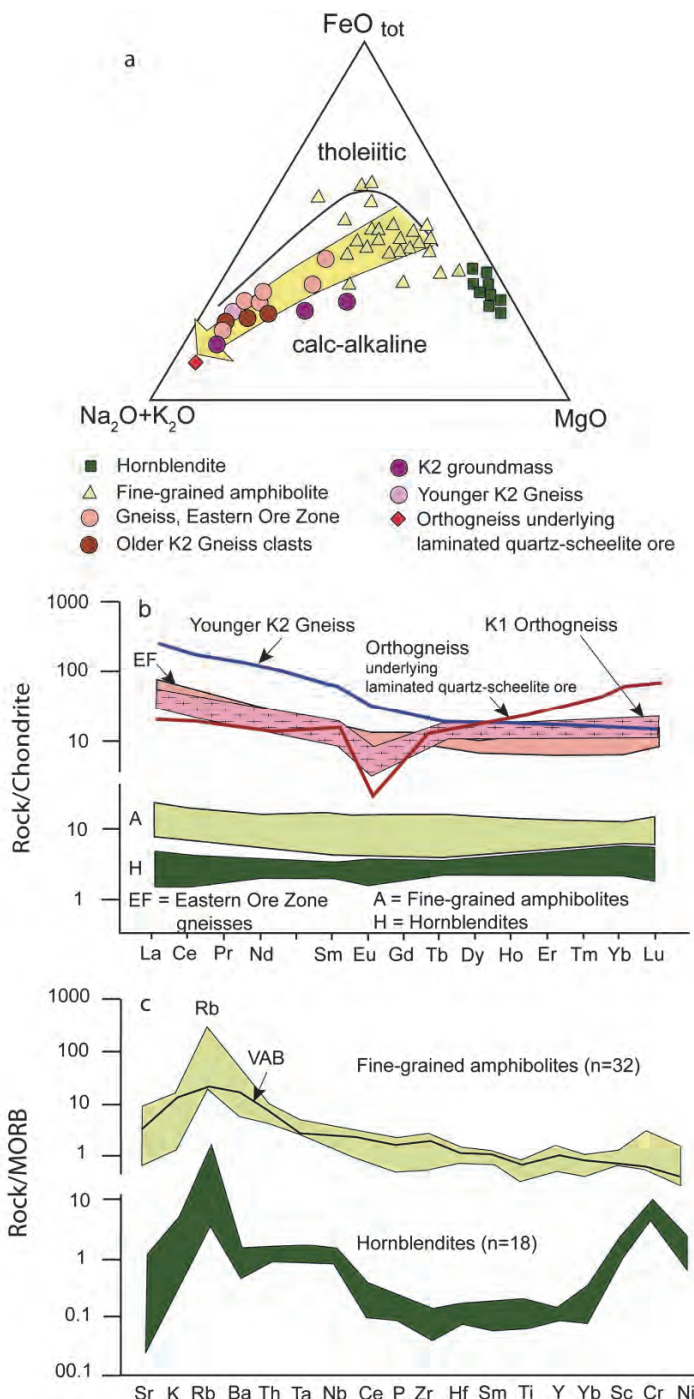


Fig. 15: Diagrams illustrating the chemical composition of rocks of the Habach Complex and the Lower Carboniferous K1-K3 orthogneiss (from Höll and Eichhorn, 2000). a. AMF plot. Most rocks of the Habach Complex follow a calc-alkaline trend typical for arc-related magmatism. A few fine-grained amphibolites from the Lower Magmatic Series are tholeiitic in composition. b. Chondrite-normalised REE patterns. Fine-grained amphibolites (A) and hornblendites (H) show flat REE patterns. Cambrian (Younger K2 Gneiss, EF gneisses from Eastern Ore Zone) and Early Carboniferous (K1-K3) orthogneisses show more evolved LREE enriched patterns. c. MORB-normalised spidergrams for hornblendites and fine-grained amphibolites, the latter showing chemical similarities with volcanic arc basalts (VAB). Both rock types are enriched in LIL elements, especially in Rb, relative to MORB due to fluid-induced alteration related to ore deposit formation.

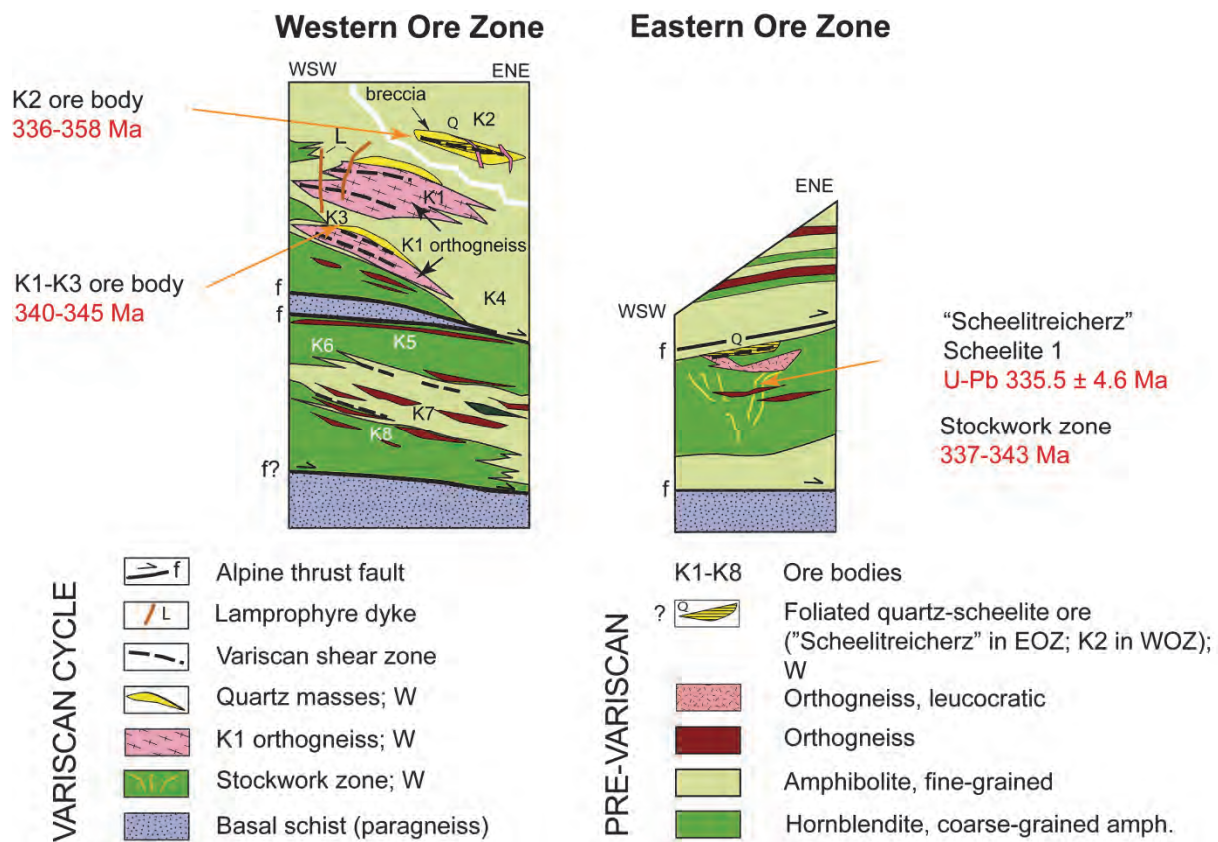


Fig. 16: Schematic sketch of the geology of the Eastern and Western Ore Zones (based on Höll and Eichhorn, 2000). K1 to K8 refer to the different ore bodies (see text). Re-Os molybdenite ages (Raith and Stein, 2006) are shown in red. The U-Pb age of Scheelite 1 is from the Scheelitreichnerz (Raith et al., 2011). All ages are consistent with Variscan ore formation.

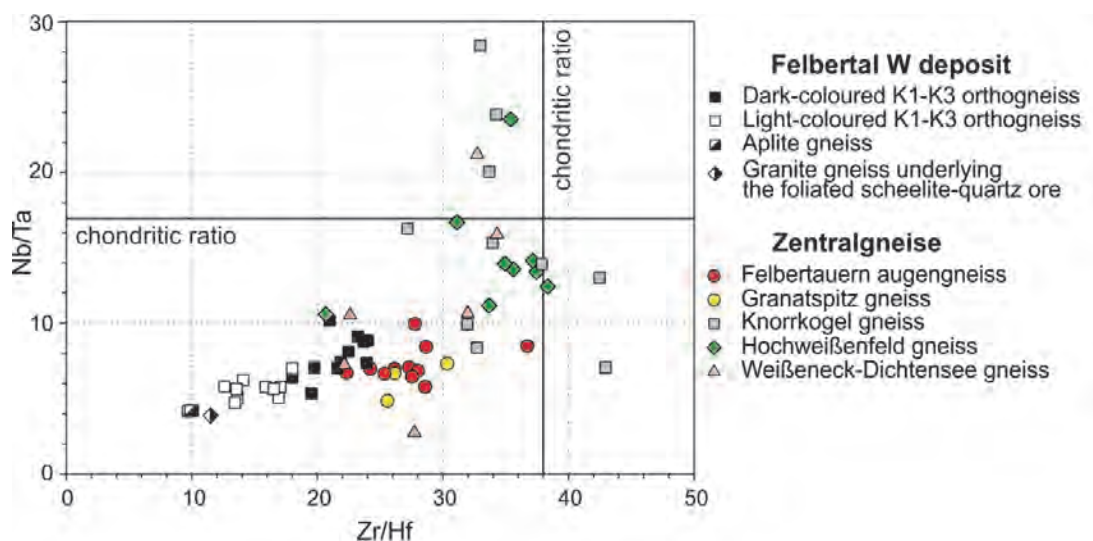


Fig. 17: Diagram of Nb/Ta versus Zr/Hf showing data of Variscan metagranites in the Felbertal tungsten deposit and comparing them to other regional types of Zentralgneis. Decreasing ratios of Nb/Ta and Zr/Hf are interpreted as effects of enhanced magmatic differentiation (from Kozlik et al., 2016b).

Viséan time period

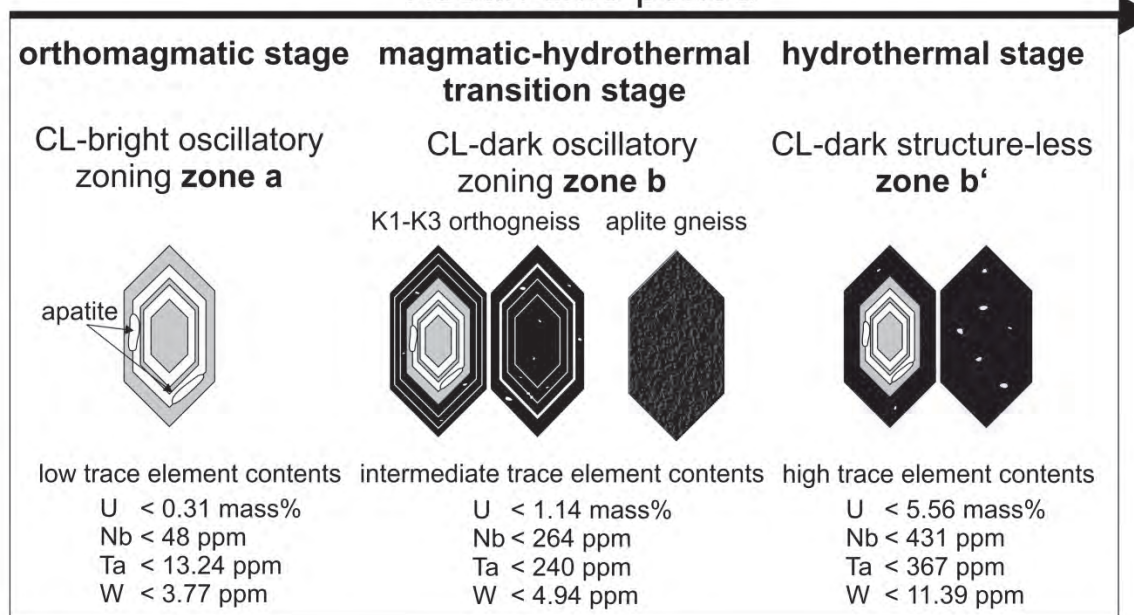


Fig. 18: Model summarizing zircon formation in the K1–K3 orthogneiss during the Early Carboniferous (from Kozlik et al., 2016b).



Fig. 19: **a**. Portal of the Felbertal underground mine. **b**. Drilling with modern computer-controlled two-boom jumbo.



Fig. 20: **a.** Remote-controlled scooptram with 15 tonnes capacity. **b.** Mucking into an ADT truck for underground haulage from the lower sublevels. **c.** Shotcreting of development drifts. **d.** Underground diamond drilling. **e.** Primary jaw crusher in the underground crushing station.

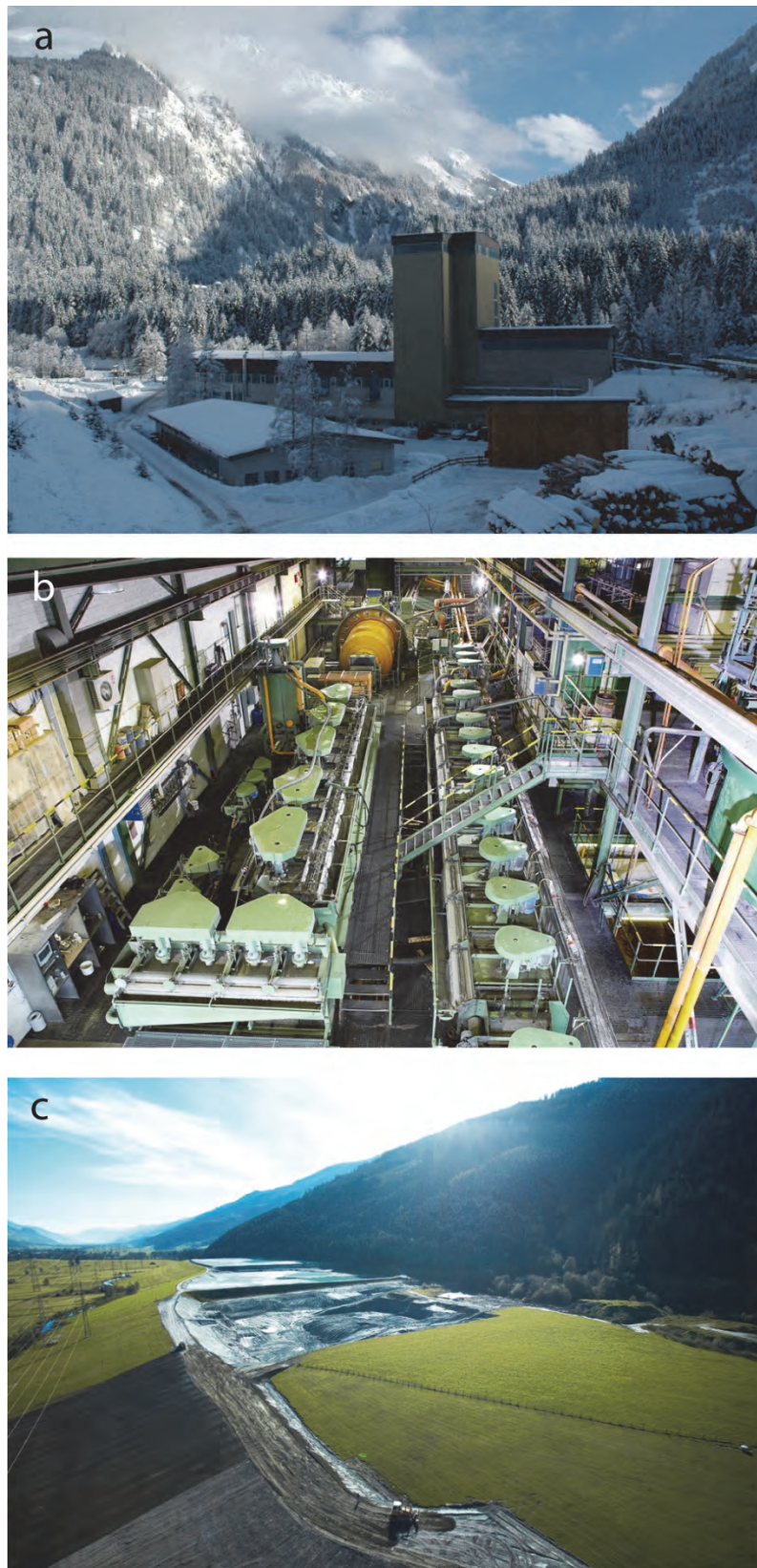


Fig. 21: **a.** Beneficiation plant 3 km north of the mine, directly at the Felbertauern highway. **b.** Overview of milling and flotation circuit. **c.** Tailings management facilities in the Pinzgau valley near Stuhlfelden showing the extent of the re-cultivation measures that occur concurrently with the operation.

References

- Briegleb, D., 1991. Ein epigenetisches Modell der Scheelitlagerstätte Felbertal (Land Salzburg). Berichte der Deutschen Mineralogischen Gesellschaft. Beiheft European Journal of Mineralogy, 3(1), 43.
- Briegleb, D., Finger, F., Kraiger, H., Pestal, G., Steyrer, H.P., 1985. The K1-Gneiss from the Scheelite-mine Felbertal (Hohe Tauern / Austria). Fortschritte der Mineralogie, Beiheft 1, 63: 33.
- Dal Piaz, G.V., Bistacchi, A., Massironi, M., 2003. Geological outline of the Alps. Episodes, 26(3), 175-180.
- Eichhorn, R., Höll, R., Jagoutz, E., Schärer, U., 1997. Dating scheelite stages; a strontium, neodymium, lead approach from the Felbertal tungsten deposit, Central Alps, Austria. *Geochimica et Cosmochimica Acta*, 61(23), 5005-5022.
- Eichhorn, R., Höll, R., Loth, G., Kennedy, A., 1999a. Implications of U-Pb SHRIMP zircon data on the age and evolution of the Felbertal tungsten deposit (Tauern Window, Austria). *International Journal of Earth Sciences*, 88(3), 496-512.
- Eichhorn, R., Loth, G., Höll, R., Finger, F., Schermaier, A., Kennedy, A., 1999b. U-Pb SHRIMP data of pre-Alpine rocks of the Tauern Window (Austria); active margin and back-arc found, but where is the adjacent continental crust? *Terra Nostra*, 99(1), 79-80.
- Eichhorn, R., Loth, G., Höll, R., Finger, F., Schermaier, A., Kennedy, A., 2000. Multistage Variscan magmatism in the central Tauern Window (Austria) unveiled by U/Pb SHRIMP zircon data. *Contributions to Mineralogy and Petrology*, 139(4), 418-435.
- Eichhorn, R., Loth, G., Kennedy, A., 2001. Unravelling the pre-Variscan evolution of the Habach terrane (Tauern Window, Austria) by U-Pb SHRIMP zircon data. *Contributions to Mineralogy and Petrology*, 142, 147-162.
- Eichhorn, R., Schärer, U., Höll, R., 1995. Age and evolution of scheelite-hosting rocks in the Felbertal Deposit (Eastern Alps); U-Pb geochronology of zircon and titanite. *Contributions to Mineralogy and Petrology*, 119(4), 377-386.
- Finger, F., Frasl, G., Haunschmid, B., Lettner, H., Schermaier, A., Quadt von, A., Schindlmaier, A.O., Steyrer, H. P., 1993. The Zentralgneise of the Tauern Window (Eastern Alps), Insight into an intra-Alpine Variscan batholith. In: Neubauer, F., Raumer, J.F. (Eds.), *The Pre-Mesozoic geology in the Alps*. Springer, Berlin, pp. 375-391.
- Finger, F., Kraiger, H., Steyrer, H.P., 1985. Zur Geochemie des K1-Gneises der Scheelitlagerstätte Felbertal (Pinzgau/Salzburg) - ein Vorbericht. *Der Karinthin*, 92, 225-235.
- Finger, F., Steyrer, H.P., 1988. Granite types in the Hohe Tauern (Eastern Alps, Austria) – Some aspects of their correlation to Variscan plate tectonic processes. *Geodinamica Acta*, 2, 75-87.
- Finger, F., Waitzinger, M., Forster, H.J., Kozlik, M., Raith, J.G., 2017. Identification of discrete low-temperature thermal events in polymetamorphic basement rocks using high spatial resolution FE-SEM-EDX U-Th-Pb dating of uraninite microcrystals. *Geology*, 45(11), 991-994.
- Frasl, G., 1958. Zur Seriengliederung der Schieferhülle in den Mittleren Hohen Tauern. *Jahrbuch der Geologischen Bundesanstalt Wien*, 101, 323-472.
- Frisch, W., Raab, D., 1987. Early Paleozoic back-arc and island-arc settings in greenstone sequences of the central Tauern Window (Eastern Alps). *Jahrbuch der Geologischen Bundesanstalt*, 129, 545-566.
- Gilg, H.A., Höll, R., Kupferschmied, M. P., Reitz, E., Stärk, H., Weber-Diefenbach, K., 1989. Die Basisschieferfolger in der Habachformation im Felber- und Amertal (Tauernfenster, Salzburg). *Mitteilungen der Österreichischen Geologischen Gesellschaft*, 81, 65-91.
- Grundmann, G., 1989. Metamorphic evolution of the Habach Formation; a review. *Mitteilungen der österreichischen geologischen Gesellschaft*, 81 (1988), 133-149.
- Grundmann, G., Morteani, G., 1982. Die Geologie des Smaragdvorkommens im Habachtal (Land Salzburg, Österreich). *Archiv für Lagerstättenforschung der Geologischen Bundesanstalt*, 2, 71-107.

- Höck, V., 1993. The Habach-Formation and the Zentralgneis - a key in understanding the Palaeozoic evolution of the Tauern Window (Eastern Alps). In, Raumer, J.F., Neubauer, F. (Eds.), *The Pre-Mesozoic geology in the Alps*. Springer, Berlin (u.a.), pp. 361-374.
- Höck, V., Kraiger, H., Lettner, H., 1993. Oceanic vs. continental origin of the Paleozoic Habach Formation in the vicinity of the Felbertal scheelite deposit (Hohe Tauern, Austria). A geochemical approach. *Abhandlungen der Geologischen Bundesanstalt*, 49, 79-95.
- Hoernes, S., Friedrichsen, H., 1974. Oxygen isotope studies on metamorphic rocks of the Western Tauern area (Austria). *Schweizerische Mineralogische und Petrographische Mitteilungen*, 54, 769-788.
- Hoinkes, G., Koller, F., Rantisch, G., Dachs, E., Hoeck, V., Neubauer, F., Schuster, R. 1999. Alpine metamorphism of the Eastern Alps. *Schweizerische Mineralogische und Petrographische Mitteilungen* 79(1), 155-181.
- Höll, R., 1966. Genese und Altersstellung von Vorkommen der Sb-W-Hg-Formation in der Türkei und auf Chios/Griechenland. *Abhandlungen - Bayerische Akademie der Wissenschaften. Mathematisch-Naturwissenschaftliche Klasse*, 127, 118.
- Höll, R., 1969. Scheelitprospektion und Scheelitvorkommen im Bundesland Salzburg/Österreich. *Chemie der Erde*, 28(3-4), 185-203.
- Höll, R., 1971. Scheelitvorkommen in Österreich. *Erzmetall*, 1971, 273-282.
- Höll, R., 1975. Die Scheelit-Lagerstätte Felbertal und der Vergleich mit anderen Scheelitvorkommen in den Ostalpen. *Abhandlungen Bayrische Akademie der Wissenschaften, Mathematisch-naturwissenschaftliche Klasse*, München, 157 A, 1-114.
- Höll, R., 1977. Early Paleozoic Ore Deposits of the Sb-W-Hg Formation. In: Klemm, D.D., Schneider, H.J. (Eds.), *Time- and Strata-Bound Ore Deposits*. Springer-Verlag, Berlin, Heidelberg, New York, pp. 169-198.
- Höll, R., 1998. Die Entdeckungsgeschichte der Scheelitlagerstätte Felbertal. Unpublished memorandum, Munich, pp. 5.
- Höll, R., Eichhorn, R., 2000. Tungsten mineralization and metamorphic remobilization in the Felbertal scheelite deposit, Central Alps, Austria. *Reviews in Economic Geology*, 11, 233-264.
- Höll, R., Ivanova, G., Grinenko, V., 1987. Sulfur isotope studies of the Felbertal scheelite deposit, Eastern Alps. *Mineralium Deposita*, 22(4), 301-308.
- Höll, R., Maucher, A., 1968. Genese und Alter der Scheelit-Magnesit-Lagerstätte Tux. *Sitzungsberichte Bayerische Akademie der Wissenschaften, Mathematisch Naturwissenschaftliche Klasse*, 1967(1), 1-11.
- Höll, R., Maucher, A., Westenberger, H., 1972. Synsedimentary-diagenetic ore fabrics in the strata- and time-bound scheelite deposits of Kleinarltal and Felbertal in the Eastern Alps. *Mineralium Deposita*, 7(2), 217-226.
- Höll, R., Schenk, P., 1988. Metamorphosed hydrothermal eruption breccia (conglomerate) in the Felbertal scheelite deposit, Eastern Alps, Austria. *Marine Geology*, 84(3-4), 273-282.
- Inger, S., Cliff, R.A., 1994. Timing of metamorphism in the Tauern Window, Eastern Alps; Rb-Sr ages and fabric formation. *Journal of Metamorphic Geology*, 12(5), 695-707.
- Jahoda, R., 1984. Das Westfeld der Scheelitlagerstätte Mittersill (Land Salzburg / Österreich). *Geologie, Petrologie und Vererzung in einem Profil durch die Lagerstätte*. Unveröffentlichte Diplomarbeit Montanuniversität Leoben, Leoben, 150 pp.
- Kebede, T., Klötzli, U., Kosler, J., Sköld, T., 2005. Understanding the pre-Variscan and Variscan basement components of the central Tauern Window, Eastern Alps (Austria): constraints from single zircon U-Pb geochronology. *International Journal of Earth Sciences*, 94(3), 336-353.
- Koller, F., Richter, W., 1984. Die Metarodingite der Habachformation, Hohe Tauern (Österreich). *Tschermaks mineralogische und petrographische Mitteilungen*, 33(1), 49-66.

- Kozlik, M., 2015. Mineralogical, petrological and (isotope) geochemical studies on the Felbertal scheelite deposit, Austria: Development of an epigenetic model for W mineralisation in the context of Variscan magmatism in the Tauern Window. PhD thesis, Montanuniversität Leoben, Leoben, 342 pp.
- Kozlik, M., Gerdes, A., Raith, J.G., 2016a. Strontium isotope systematics of scheelite and apatite from the Felbertal tungsten deposit, Austria – results of in-situ LA-MC-ICP-MS analysis. *Mineralogy and Petrology*, 110, 11-27.
- Kozlik, M., Raith, J.G., 2014. Chemical characteristics of the K1-K3 metagranitoid in the Felbertal scheelite deposit (Austria). *Mitteilungen der Österreichischen Mineralogischen Gesellschaft*, 160, 23-27.
- Kozlik, M., Raith, J.G., 2017. Variscan metagranitoids in the central Tauern Window (Eastern Alps, Austria) and their role in the formation of the Felbertal scheelite deposit. *Lithos*, 278-281, 303-320.
- Kozlik, M., Raith, J.G., Gerdes, A., 2016b. U-Pb, Lu-Hf and trace element characteristics of zircon from the Felbertal scheelite deposit (Austria): New constraints on timing and source of W mineralization. *Chemical Geology*, 421, 112-126.
- Kraiger, H., 1989. Die Habachformation – ein Produkt ozeanischer und kontinentaler Kruste. *Mitteilungen der Österreichischen Geologischen Gesellschaft*, 81 (1988), 47-64.
- Kupferschmied, M.P., Höll, R., 1994. Die geologische Neuaufnahme der Habachmulde und ihre genetischen Implikationen für die Habachgruppe (Tauernfenster/Ostalpen). *Jahrbuch der Geologischen Bundesanstalt*, 137, 139-153.
- Maucher, A., 1965. Die Antimon-Wolfram-Quecksilber Formation und ihre Beziehungen zu Magmatismus und Geotektonik. *Freiberger Forschungshefte*, C 186, 173-187.
- Neinavaie, H., Pfeffer, W., Thalmann, F., 1985. Ergebnisse der geochemischen Prospektion auf Stahlveredler im Bundesgebiet. *Berg- und Hüttenmännische Monatshefte*, 130(4), 111-116.
- Ordosch, A., 2017. W-Sn mineralisation in calc-silicate rocks of the Basal Amphibolite unit at Messelingscharte (Felbertauern area, Austria). Master thesis, Montanuniversität Leoben, Leoben, 188 pp.
- Pestal, G., 1983. Beitrag zur Kenntnis der Geologie in den mittleren Hohen Tauern im Bereich des Amer- und Felbertales. Unpublished doctoral thesis, University of Vienna, Vienna, Austria, 117 pp.
- Pestal, G., Hejl, E., Braunstingl, R. et al., 2009. Geologische Karte von Salzburg 1:200000: Erläuterungen. Verlag der Geologischen Bundesanstalt (GBA), Wien, 162 pp.
- Pirkl, H., 1986. Die Magnesit-Scheelit-Lagerstätte Tux in Tirol. *Mitteilungen der österreichischen geologischen Gesellschaft* 78 (1985), 159-165.
- Raith, J.G., Gerdes, A., Cornell, D.H., 2011. In-situ U-Pb dating of scheelite, constraints on the age and genesis of the Felbertal tungsten deposit. *Goldschmidt Conference Abstracts Mineralogical Magazine*, 75(3), 1690.
- Raith, J.G., Grum, W., Prochaska, W., Frank, W., 1995. Polymetamorphism and polyphase deformation of the strata-bound magnesite-scheelite deposit, Tux-Lanersbach, Eastern Alps, Austria. *Economic Geology*, 90(4), 763-781.
- Raith, J.G., Schmidt, S., 2010. Tungsten deposit Felbertal, Salzburg, Austria. *Acta Mineralogica-Petrographica*, Field guide series, Szeged, 3, 1-24.
- Raith, J.G., Stein, H., 2006. Variscan ore formation and metamorphism at the Felbertal scheelite deposit (Austria): constraining tungsten mineralisation from Re-Os dating of molybdenite. *Contributions to Mineralogy and Petrology*, 152, 505-521.
- Reitz, E., Höll, R., 1988. Jungproterozoische Mikrofossilien aus der Habachformation in den mittleren Hohen Tauern und dem nordostbayerischen Grundgebirge. *Jahrbuch der Geologischen Bundesanstalt*, 131(2), 329-340.
- Schenk, P., 1990a. Lagerstättenkundliche und tektonische Untersuchungen im Westfeld der Scheelitlagerstätte Felbertal/Österreich. Unpublished report, Munich.

- Schenk, P., 1990b. Mikrothermometrische, gefügekundliche und geochemische Untersuchungen zur Genese der Scheelitlagerstätte Felbertal/Ostalpen, Doctoral thesis, University of Munich, Munich, 198 pp.
- Schenk, P., Höll, R., 1989. Metamorphe, hydrothermale Eruptionsbrekzien in der Scheelitlagerstätte Felbertal/Ostalpen (Österreich). Mitteilungen der Österreichischen Geologischen Gesellschaft, 81, 93-107.
- Schenk, P., Höll, R., 1991. Evolution of fluids and metamorphic ore remobilization in the Felbertal scheelite deposit, Eastern Alps. *IOre Geology Reviews*. 6, 425-434.
- Schmid, S.M., Fügenschuh, B., Kissling, E., Schuster, R., 2004. Tectonic map and overall architecture of the Alpine orogen. *Eclogae Geologicae Helvetiae*, 97(1), 93-117.
- Schmid, S.M., Scharf, A., Handy, M.R., Rosenberg, C.L., 2013. The Tauern Window (Eastern Alps, Austria): a new tectonic map, with cross-sections and a tectonometamorphic synthesis. *Swiss Journal of Geosciences*, 106(1), 1-32.
- Schmidt, S., 1988. Geologische Kartierung im Bereich der Scheelitlagerstätte Felbertal, Mittersill / Österreich. Technical Universität Clausthal, Clausthal, Germany, 211 pp.
- Spross, W., 1978. Die Entwicklung des Scheelitbergbaus Mittersill. *Erzmetall*, 31(5), 211-216.
- Spross, W., 1984. Recent developments at the scheelite mine in Mittersill. *Berg- und Hüttenmännische Monatshefte*, 129, 352-360.
- Thalhammer, O., 1987. Boninites as source rock of tungsten mineralization at Mittersill, Austria? *Mineralogy and Petrology*, 37(3-4), 221-242.
- Thalhammer, O.A.R., Stumpf, E.F., Jahoda, R., 1989. The Mittersill scheelite deposit, Austria. *Economic Geology*, 84(5), 1153-1171.
- Trudu, A.G., Clark, A.H., 1986. The Felbertal (Mittersill) scheelite deposit, Austria: A W-Mo-Be vein system related to felsic plutonism, not a submarine-exhalative deposit. *Proceedings of joint working groups 2 and 4, International Geological Correlation Program Project 220*, Canberra, pp. 73-74.
- von Quadt, A., 1992. U-Pb zircon and Sm-Nd geochronology of mafic and ultramafic rocks from the central part of the Tauern Window (Eastern Alps). *Contributions to Mineralogy and Petrology*, 110,, 57-67.
- von Quadt, A., Günther, D., Frischknecht, R., Zimmermann, R., Franz, G., 1997. The evolution of pre-Variscan eclogites of the Tauern Window (Eastern Alps), A Sm/Nd, conventional and ICP-MS zircon U-Pb study. *Schweizerische mineralogische und petrographische Mitteilungen*, 77, 265-279.
- von Quadt, A., Haunschmidt, B., Finger, F., 1999. Mid-Permian A-type plutonism in the eastern Tauern-Window. *Berichte der Deutschen Mineralogischen Gesellschaft*, 11, 185.
- Walser, P., 1992. Praktische Erfahrungen mit dem Spülversatz im Wolframbergbau Mittersill. *Berg- und Hüttenmännische Monatshefte*, 137(2), 63-67.
- Weber, L. et al., 2015. IRIS Interaktives Rohstoff-Informations-System. *Geologische Bundesanstalt*. <https://www.geologie.ac.at/0/webapplikationen/iris-interaktives-rohstoffinformationssystem/>
- Wenger, H., 1964. Die Scheelitlagerstätte Tux. *Radex Rundschau*, 1964(2), 109-132.



Field Trip Pre-EX-2

Sedimentary and tectonic processes on a Late Jurassic passive margin and its inversion during Alpine orogeny in the Lofer area

HUGO ORTNER¹, DIETHARD SANDERS¹, MICHAELA USTASZEWSKI^{1,2}, MARTIN RITTNER^{1,3}, DAVID MOSNA^{1,4} & SEBASTIAN WOLFGRUBER^{1,5}

¹ Institut für Geologie, Universität Innsbruck, Innrain 52, 6020 Innsbruck, Austria. hugo.ortner@uibk.ac.at

² Von-Hase-Weg 15, 07743 Jena, Germany. michaust@gmail.com

³ Tofwerk AG, Uttigenstrasse 22, 3600 Thun, Switzerland. rittner@tofwerk.com

⁴ Amt für Geologie und Baustoffprüfung, Eggentaler Straße 48, 39053 Kardaun, Italy. david.mosna@provinz.bz.it

⁵ Schenker Richter Graf AG, Büttenerhalde 42, 6006 Luzern, Switzerland. sebastian.wolfgruber@fsgeolog.ch

Introduction

The geology of the area around Lofer inspired the Bavarian geologist Felix Hahn to subdivide the Northern Calcareous Alps (NCA) tectonically (HAHN, 1912, 1913b). This subdivision was adopted by, e.g., TOLLMANN (1976b, 1985) and is essentially still in use. The clear relationships between some of the major tectonic units of the NCA is our motivation to do this field trip.

The NCA evolved through several geodynamic stages. In the Triassic, the future NCA formed the southeastern passive margin of Pangea (including present-day Europe) toward the Meliata ocean (e.g., HAAS et al., 1995; STAMPFLI & BOREL, 2002), where a thick succession of carbonates accumulated. Liassic rifting opened the Alpine Tethys ocean and separated the Adriatic plate fragment from the European plate (e.g., HANDY et al., 2010). This created a new continental margin that is well developed in the western part of Adria-derived tectonic units in eastern Switzerland and western Austria (FROITZHEIM & MANATSCHAL, 1996; LAVIER & MANATSCHAL, 2006). In the Late Jurassic, Neotethys oceanic crust had been obducted onto the southeastern margin of the Adriatic plate (SCHMID et al., 2008; SCHMID et al., 2004), however, it is unclear how far this obduction extended into the NCA. During the Cretaceous, the NCA formed as typical foreland fold-and-thrust belt in the external part of the mountain belt that evolved as a consequence of the closure of a part of the Neotethys ocean (e.g., ORTNER et al., 2016). Collision within this belt started during the Early Cretaceous. Probably obduction and collision on one side and rifting and drifting on the other side of the Adriatic plate were kinematically linked by a system of transform faults that crossed the Adriatic plate (TRÜMPY, 1988; WEISSERT & BERNOUILLI, 1985). Closure of the Alpine Tethys and subsequent collision during the Cenozoic caused a second orogenic cycle during which the NCA were passively transported piggy-back into the European foreland. In the late stages of this event, the geometry of the NCA thrust sheets was modified by escape tectonics, when orogenically thickened crust moved east toward the Pannonian basin (RATSCHBACHER et al., 1991; ROSENBERG et al., 2007). The NCA were dissected by NE to ENE-striking subvertical strike-slip faults, some with tens of kilometers offset (DECKER et al., 1994; LINZER et al., 2002; PERESSON & DECKER, 1997) that delimited the eastward moving units against more stable units to the north. However, some of the steep faults near the northern margin of the NCA are rather tear faults related to incorporation and emplacement of

the Helvetic and Subalpine Molasse during oblique convergence between the Alpine wedge and the European foreland (ORTNER et al., 2015).

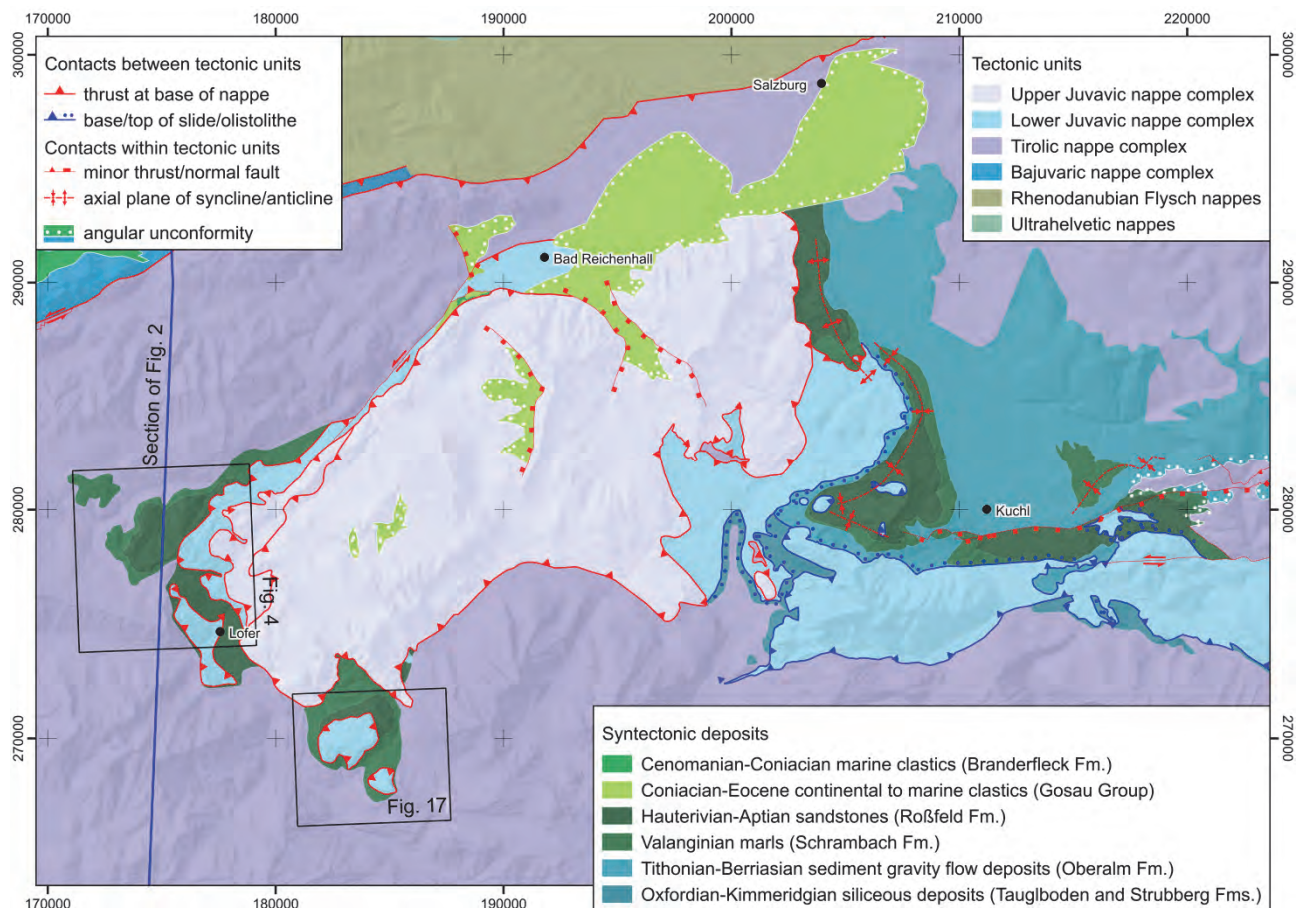


Fig. 1: Tectonic map including syntectonic sediments of the field trip area around Lofer, following the tectonic subdivision of TOLLMANN (1976b). Tectonic boundaries were drawn using also unconformities between tectonic units, which is the case when large olistolithes are emplaced and later covered (ORTNER, 2017b).

As mentioned above, the NCA fold-and-thrust belt formed initially in the late Early Cretaceous. Timing of thrust movements can be deduced from the youngest sediments below a thrusted unit, as shortening was active in a deep-water environment and non-deposition would have left hardgrounds (ORTNER, 2003). Using this argument, two emplacement processes on top of the Tirolic nappe complex can be distinguished: (1) emplacement of the Lower Juvavic unit onto sediments of Oxfordian-Kimmeridgian age (Fig. 1, S and SE of Kuchl), and (2) emplacement of the Lower and Upper Juvavic units onto Aptian deposits (Fig. 1, N and SE of Lofer).

The purpose of this field trip is to showcase several steps of this evolution. During the two days of the field trip we will address following problems:

- The Jurassic sedimentary evolution of the NCA and the relevance of the Upper Jurassic transgression in the Central part of the NCA.
- The controversially discussed Upper Jurassic tectonic evolution of the NCA – Jurassic orogeny within the NCA (e.g., GAWLICK et al., 1999; MISSONI & GAWLICK, 2010) versus passive margin affected by transform faults (FRANK & SCHLAGER, 2006; ORTNER et al., 2008).
- The pattern of young (Miocene) faults that dissects the pre-existing nappe stack

The field trip is led by H. Ortner and D. Sanders. It takes place in an Alpine landscape and is strongly dependent on weather conditions, and changing outcrop conditions. The succession and number of stops may be changed on short notice.

Field Trip

Day 1 - Unkenbachtal: Stops 1 to 4

The Unkenbachtal is the valley of the Unkenbach and a northern tributary of the Saalach. It lies within the northern limb of the Unken syncline (Fig. 2), which is open and roughly ENE-WSW-trending. The Unkenbachtal exposes the complete Jurassic to Cretaceous sedimentary succession of the Staufen-Höllengebirgs thrust sheet of the Tirolic nappe complex, including the Schwarzbergklamm breccia. We will start at the base of the sedimentary succession in the western part of the valley and go into progressively younger sediments toward the outer, eastern end. The main idea of this part of the field trip is to show the Jurassic to Cretaceous succession (Fig. 3).

The Schwarzbergklamm breccia is „chaotic, clast- to matrix-supported and lacks any kind of sorting. The matrix consists of red calcareous micrite. The clasts are angular to sub-angular and consist mainly of Upper Rhaetian limestone, subordinately of Dachstein limestone, marls of the Kössen Formation, red limestones of the Adnet and Klaus Formations and the Ruhpolding Radiolarite. Clast sizes range from a few millimetres to several meters in diameter. Single blocks measure up to 40 meters“ (ORTNER et al., 2008). It attracted the attention of several workers, who gave a wide range of interpretations reaching from tectonic breccias (VORTISCH, 1931) to submarine mass transport deposits (DIERSCHE, 1980; FISCHER, 1965; GARRISON & FISCHER, 1969; VECSEI et al., 1989; WÄCHTER, 1987).

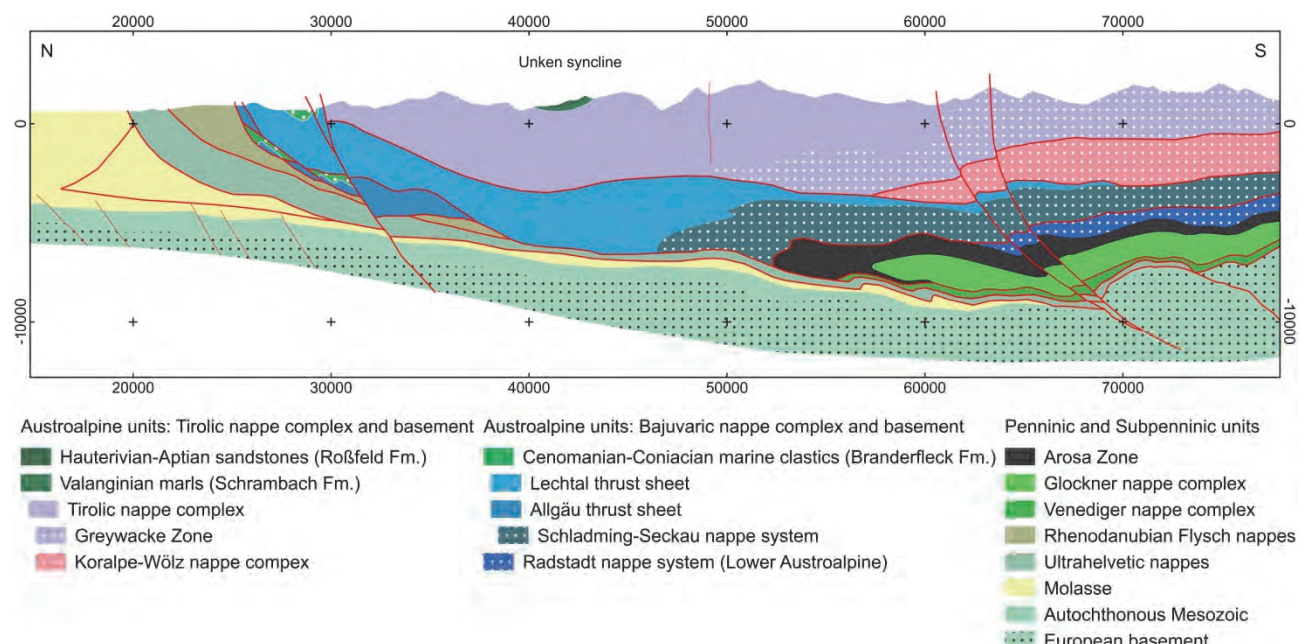


Fig. 2: Regional cross section of the NCA in the field trip area, simplified from BRAUNSTINGL (2005). See Fig. 1 for trace of section. Note the Unken syncline on the center of the section.

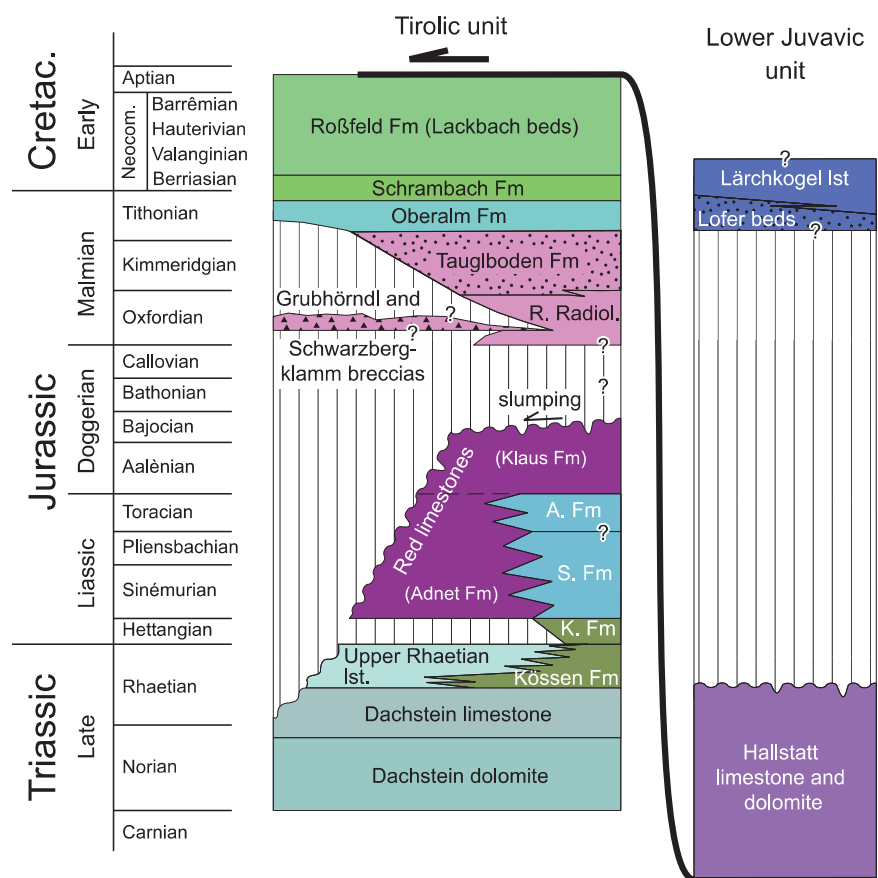


Fig. 3: Chronostratigraphic diagram for the Unken syncline, adapted from ORTNER et al. (2008). K. Fm = Kendlbach Formation, S. Fm = Scheibelberg Formation, A. Fm = Allgäu Formation, R. Radiol. = Ruhpolding Radiolarite, Ist = limestone. Formal and informal subdivisions used in accordance with the Stratigraphic Chart of Austria (PILLER et al., 2004), except “Oberrähkalk”, which is Upper Rhaetian limestone.

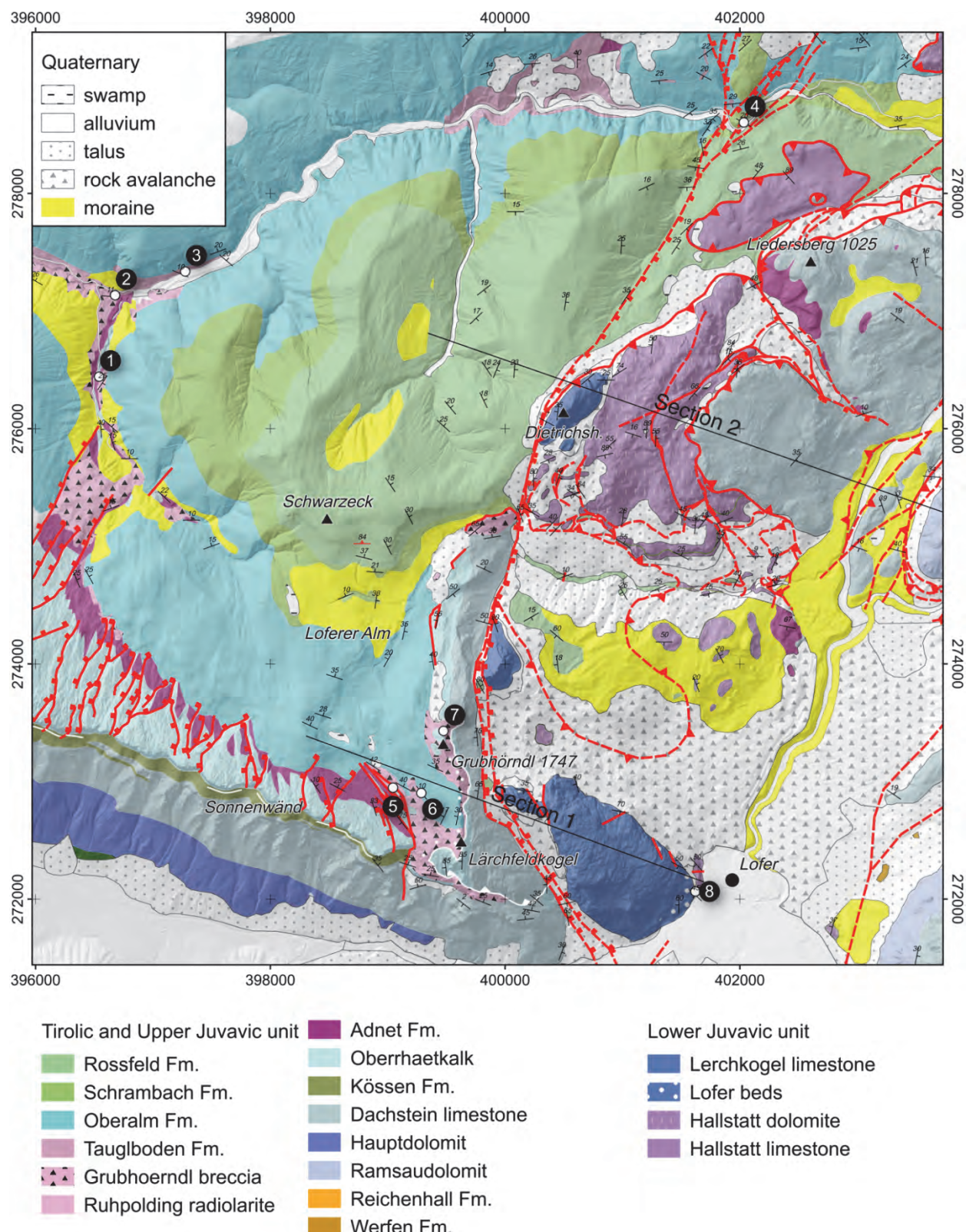


Fig. 4: Geologic map of the Unken syncline and the northwestern part of the Juvavic nappe complex, compiled from LUKESCH (2003) and RITTNER (2006), westernmost part from (HORNSTEINER, 1991). Minor modifications according to (PAVLIK, 2006). We do not follow GAWLICK et al. (2015) regarding the position of the Saalachtal-Westbruch. Numbers 1 – 8 indicate field trip stops of day 1. Sections are shown in Fig. 12. Coordinates: MGI Austria GK M31 shown in Fig. 12. Coordinates: MGI Austria GK M31.

Stop 1. Fußtal near game feeding place

Coordinates: E 12.62285, N 47.62064.

Altitude: 937 m.

At Stop 1 the erosive contact of the Schwarzbergklamm breccia to underlying red limestones of the Klaus Formation is exposed (Fig. 5). Within the breccia, large imbricated clasts can be seen. The red limestones overlie Upper Rhätian limestones in the vicinity of Stop 1.

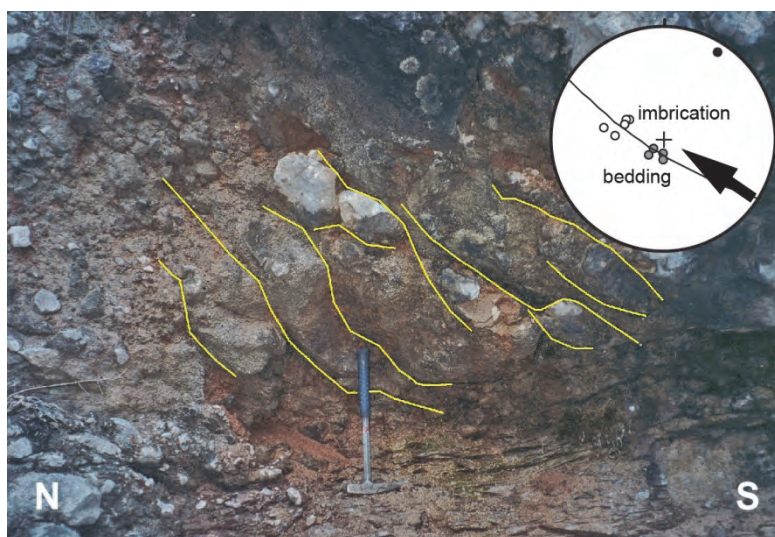


Fig. 5: Field photograph of detail in Stop1. Yellow lines emphasize bases of imbricated clasts near the base of the Schwarzbergklamm breccia. Inset shows poles to bedding (grey circles) and poles to imbricated clasts (white circles), and a common great circle. The asymmetry of the data distribution indicates a local transport direction to the NW (black arrow). Length of hammer for scale is 42 cm.

Stop 2. Schwarzbergklamm

Coordinates: E 12.62261, N 47.63089.

Altitude: 771 m.

The Schwarzbergklamm offers the best outcrops of the Schwarzbergklamm breccia. The gorge is cut into a large block of Upper Rhaetian limestone within the breccia that has a minimum diameter of 40 m. The gorge can be accessed from its downstream end. There, the relationship of the breccia to the underlying deposits can be studied. At the innermost part of the accessible gorge, a part of the breccia underlying the block is in contact with Red limestones (Fig. 6a). The base of the breccia is irregular, and the underlying red limestones are cut by several shear planes cutting upsection into the breccia. The shear planes are seen to root in bedding planes. Bedding parallel shear did cause duplexing within the red limestones, and the topography related to the duplex causes the wavy base of the breccia. The shear planes are not discrete, and a foliation related to shearing is developed. At the time of deformation, neither the Red limestones nor the Schwarzbergklamm breccia were fully lithified. Bedding plane orientations within the duplex indicate a NNW-directed shear direction.

On the southern side of the outer part of the gorge, the breccia is seen between the Red limestones below, and the Ruhpolding radiolarite above, none of the contacts being erosive (Fig. 6b). On the northern side, however, the top of the red limestones cuts downsection and is locally covered by a thin, up to 10 cm thick band of cherts of the Ruhpolding radiolarite, which is in turn covered by the Schwarzbergklamm breccia (Fig. 6c).

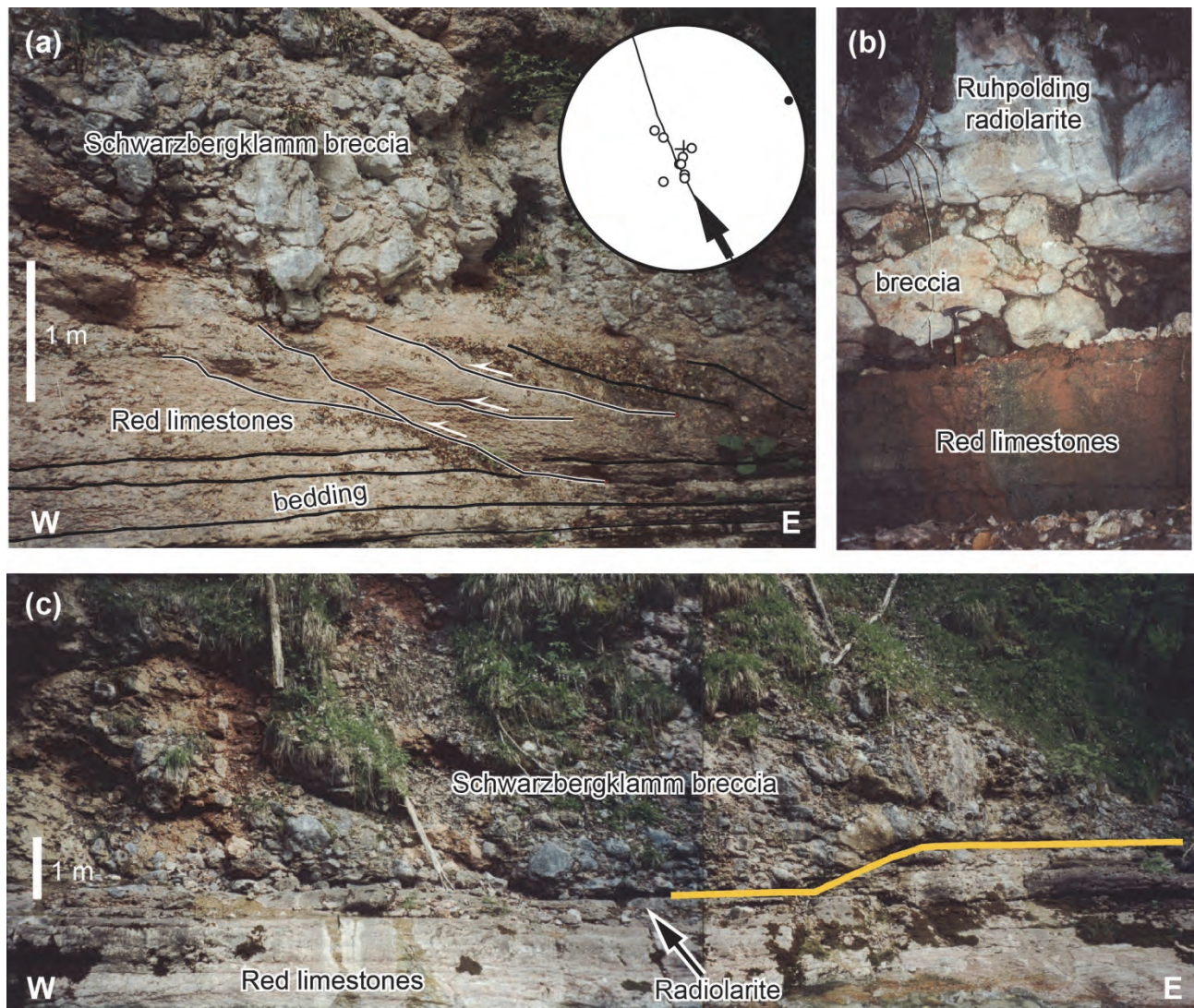


Fig. 6: Field photographs from the Schwarzbergklamm. (a) Shear structures at the base of the Schwarzbergklamm breccia. Inset: Poles to bedding in the Red limestones. The asymmetry and distribution along a great circle segment indicates top to NNW transport of the breccia. (b) At the south side of the outer gorge, the Schwarzbergklamm breccia is intercalated between Red limestones below, and the Ruhpolding radiolarite above. The basal contact is not erosive. (c) At the north side of the outer gorge, the base of the Schwarzbergklamm is lined by a thin discontinuous band of Ruhpolding radiolarite. Yellow line highlights this contact that cuts downsection into the Red limestones.

Based on these observations, the age of deposition of the Schwarzbergklamm breccia can be constrained to be during deposition of the Ruhpolding radiolarite (see Fig. 3). Locally parts of the Red limestones slumped away prior to breccia deposition sometime during the Lower or Middle Jurassic. At the time of deposition of the breccia, the Red limestones were not fully lithified. Emplacement of the breccia did cause bedding-parallel shear of the Red limestones, locally leading to duplexing and deformation of the base of the breccia.

Stop 3. 500 m east of Schwarzbergklamm

Coordinates: E 12.63058, N 47.63227.

Altitude: 745 m.

500 m east of the Geblfußalm, and roughly the same distance downstream from the Schwarzbergklamm gorge, the northern bank of the Unkenbach exposes the contact between the Tauglboden and Oberalm Formations. The Tauglboden Formation develops gradually from the cherts of the Ruhpolding radiolarite by an increase in marl, intercalated with turbidites that redeposit radiolarians, and with some layers rich in lithoclasts (see, e.g., SCHLAGER & SCHLAGER, 1973; VECSEI et al., 1989). In contrast, the Oberalm Formation consists of an alternation of micritic to lutitic limestones with alloclastic limestones („Barmstein limestones“) that transport bioclastic material, and some lithoclastic material into the deep sea (GARRISON & FISCHER, 1969; STEIGER, 1981).

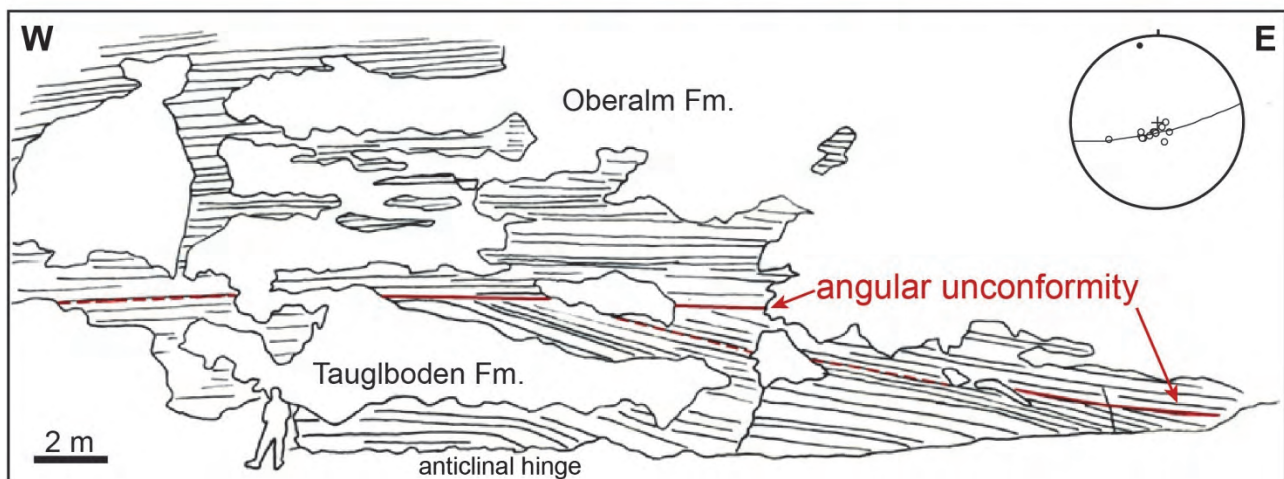
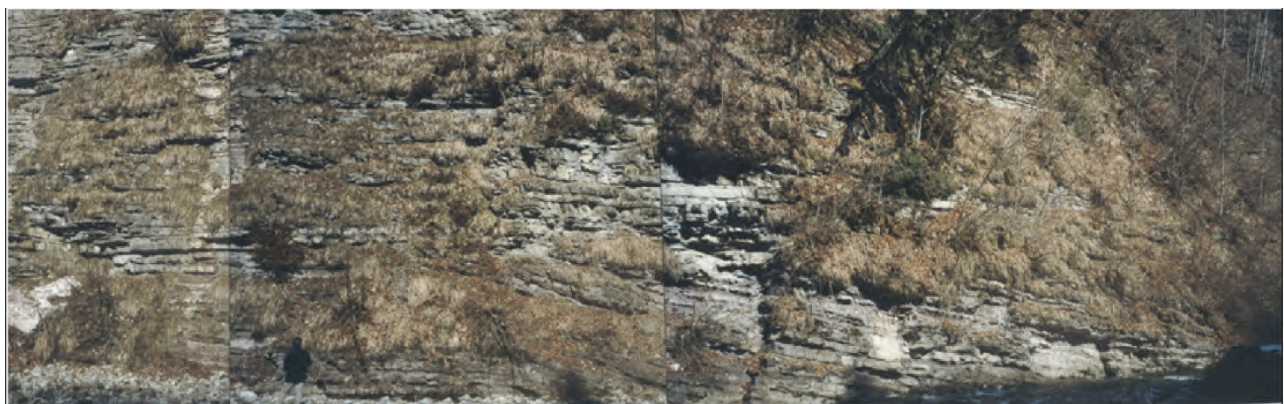


Fig. 7: Angular unconformity between Tauglboden und Oberalm Formations at Stop 3. Within the Tauglboden Formation, the hinge of an anticline is visible, tilting the beds in the eastern limb to the east. There, one or more angular unconformities within the Tauglboden Formation are present, depending on the detail of observation. Inset shows poles to bedding of the tilted beds.

The two sedimentary units are separated by an angular unconformity, increasing in angle from the anticlinal hinge to the east and downsection (Fig. 7). Beds below unconformities are tilted and truncated. Within the Tauglboden Formation, only minor wedging toward the fold hinge is visible, unconformities are related to erosion events that removed part of the sedimentary succession. The principal progressive unconformity, sensu FORD et al. (1997), where all unconformities merge, is the base of the Oberalm Formation. The observed structures are compatible with progressive rollover in the hanging wall of a normal fault.

The geometry observed requires a listric fault rollover. The narrow anticlinal hinge allows to estimate the depth of detachment, which is probably not deeper than a few tens of meters below surface, and this probably within the Red limestones.

Stop 4. Friedlwirt

Coordinates: E 12.69434, N 47.64439.

Altitude: 628 m.

In the outer Unkenbachtal, the Cretaceous part of the sedimentary succession of the Unken syncline is exposed, which includes the youngest part of the Oberalm Formation, the Schrambach and Roßfeld Formations. The base of the Schrambach Formation is characterized by the end of the limestones of the Oberalm Formation, and the onset of a thick marl dominated succession (DARGA & WEIDICH, 1986; RASSER et al., 2003). The transition to the Roßfeld Formation is defined by the first sand rich beds (DECKER et al., 1987), and was described as Lackbach beds in the Unken syncline (DARGA & WEIDICH, 1986).

The Friedlwirt outcrop exposes a very coarse clastic part of the Roßfeld Formation, which is, according to DARGA & WEIDICH (1986), in the upper third of the succession. Rounded to well-rounded components with a diameter up to 15 cm float in a matrix of sandy marl. Most of the components are derived from the NCA, but also phyllites and quartz pebbles are found, and rare ultrabasites (DARGA & WEIDICH, 1986). The sediments are slumped, with slump fold axes in the S to SE and facing to the SW. This may indicate a SW-dipping paleoslope.

Day 1 – Loferer Alm: Stops 5 to 8

At Loferer Alm, the Grubhörndl breccia is exposed. The Grubhörndl breccia was described already at the begin of the 20th century („Buntes Rhät“, Hahn, 1910; „Gosaubreccia“; Ampferer, 1927), but its nature and the connection to the Schwarzbergklamm breccia was only recognized by ORTNER et al. (2008). The most spectacular feature of the Grubhörndl breccia is a mountain-sized olistolite that is wrapped by the breccia on all sides (Fig. 8). Because of its large size, this olistolite controlled the distribution of facies well into the Upper Jurassic.

We cross the Loferer Alm to the south from Haus Schönblick to reach the immediate vicinity of the Grubhörndl, passing a large area where the Oberalm Formation is exposed (Fig. 4).

Stop 5. West of Grubhörndl, eastern side of Urltal

Coordinates: E 12.65622, N 47.59333.

A hardground is exposed between Upper Rhaetian limestones and the Oberalm Formation. As the Grubhörndl breccia is exposed in the surrounding, we suggest that the Upper Rhätian limestone is a large block in the breccia. Nevertheless the hardground documents long time spans of non-deposition on top of the breccia.

Stop 6. Western flank of Grubhörndl, near the end of a dirt road

Coordinates: E 12.65830, N 47.59287.

Altitude: 1535 m.

Here, Barmstein limestones of the Oberalm Formation directly overlie the Grubhörndl breccia. The boundary is a greenish hardground. The Barmstein limestones redeposit lithoclasts, e.g. from the Adnet Formation, and bioclasts, which include crinoids, bivalves, and rare large branched fragments of hydrozoans.

Stop 7. Summit of Grubhörndl

Coordinates: E 12.66105, N 47.59644.

Altitude: 1787 m.

A few meters below the ridge between Lärchfeldkopf and Grubhörndl, the contact between the Upper Rhätian limestone of the mega-olistolith and the Grubhörndl breccia is exposed. Bedding in the olistolith is vertical. The summit of Grubhörndl has a wide view in all directions, and at this point we will discuss some aspects of the geologic evolution of the area.

Toward the west, the view goes over the Waidringer Steinplatte and its famous reef in the Upper Rhaetian limestone. At the ridge toward the Strub valley, the top surface of this limestone has been excavated by erosion. It has an irregular surface (Fig. 4), that is controlled by a system of west-dipping normal faults. The faults cut the limestone into lozenge-shaped pieces that are limited by roughly N- and NNE-striking faults, however, no systematic cross cutting relationships are observed (Fig. 4). The faults are planar, perpendicular to bedding, and only few of them cut across the marls of the Kössen Formation, that underly the Upper Rhätian limestone and separate it from the Dachstein limestone (Figs. 4, 9). Upsection, the faults do offset the Red limestones and the Ruhpolding radiolarites, but they end near the base of the Oberalm Formation.

Therefore, the timing of these normal faults and deposition of the Schwarzbergklamm and Grubhörndl breccias is comparable. The breccias and the normal faults postdate the Red limestones, and predate the Oberalm Formation. As most of the normal faults do not cut down to the Dachstein limestone, the Upper Rhätian limestone must have décolled on top of the Kössen Formation. The faults probably originated as tension joints orthogonal to bedding, and then rotated in a domino style. West-directed transport of the Upper Rhätian limestone was associated with 6-12% stretching (ORTNER et al., 2008). The two conjugate fault sets indicate non-plane strain during joint initiation (e.g., RECHES & DIETERICH, 1983).

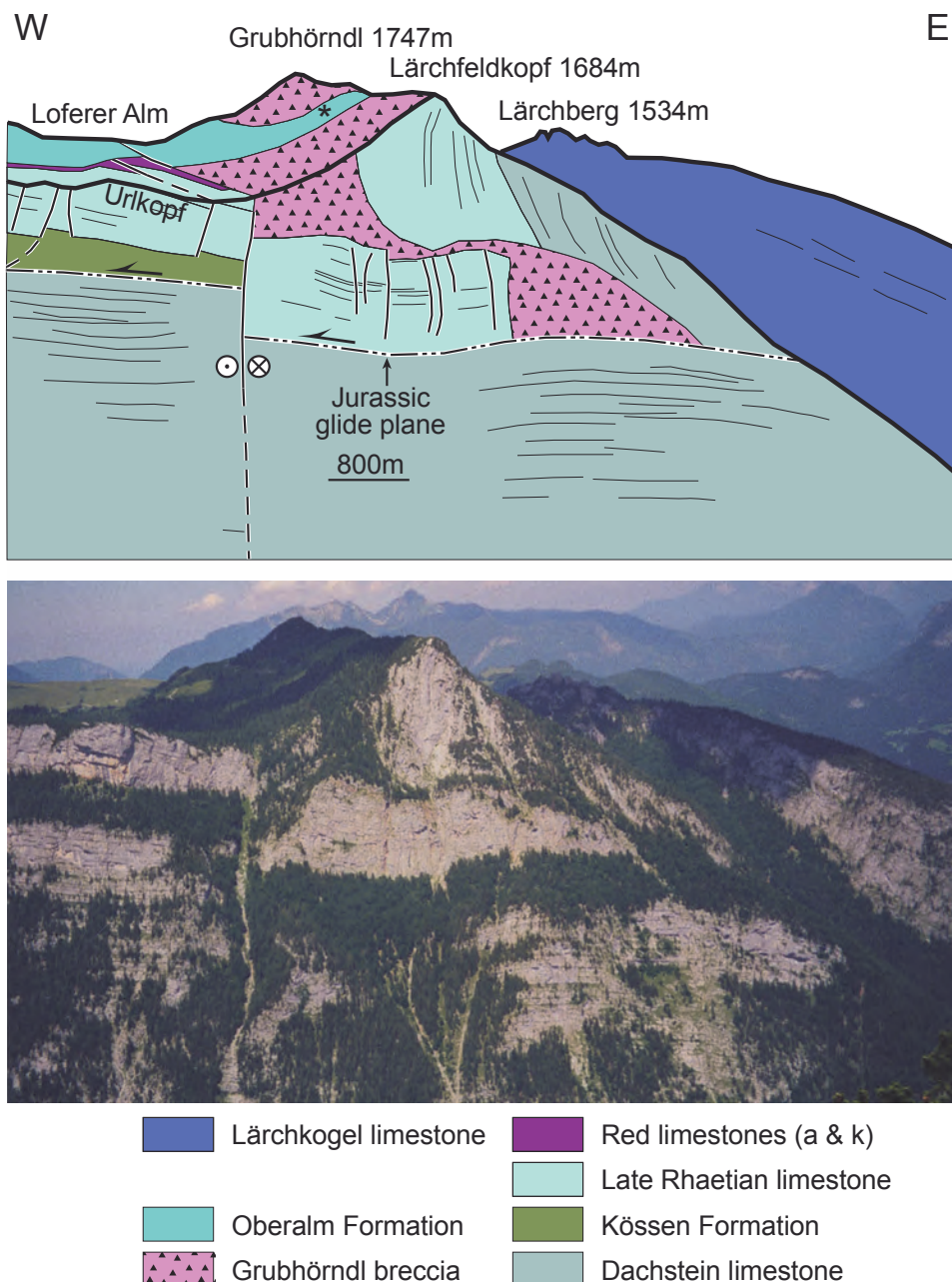


Fig. 8: View of the Loferer Alm and Grubhörndl from the south and its interpretation (adapted from ORTNER et al., 2008). The height of the Lärchfeldkopf olistolith is at least 350 m. The main problem in emplacement models is the angular relationship between the olistolith with vertical bedding and the underlying deposits with subhorizontal bedding.

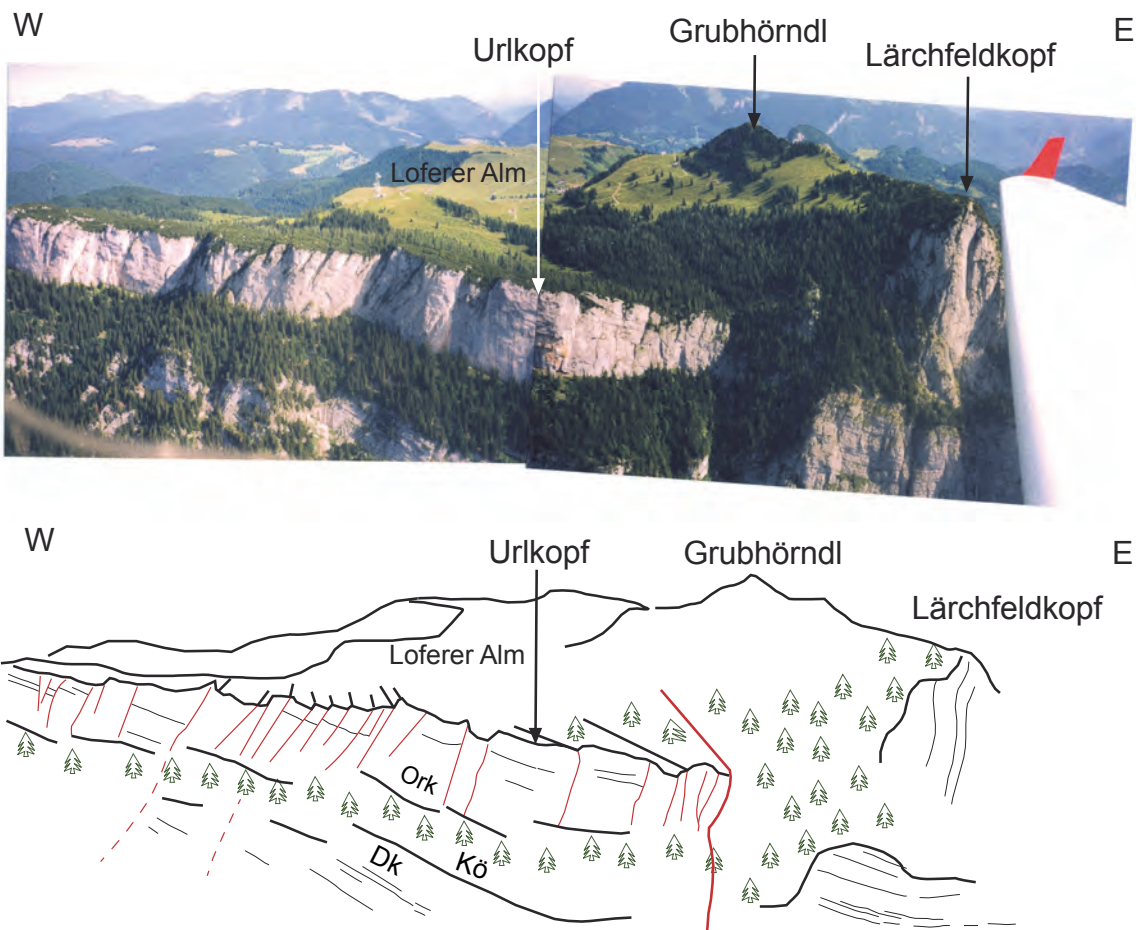
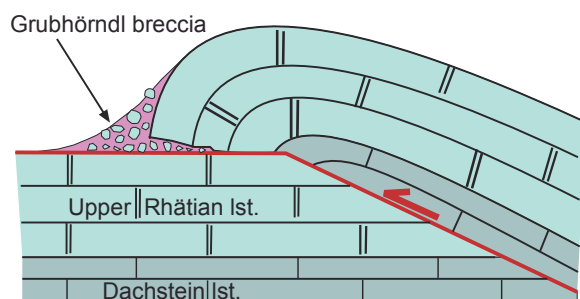


Fig. 9: View of the Sonnenwände from the south. Ork = Upper Rhätian limestone, Kö = Kössen Formation, Dk = Dachstein limestone.

1 Ramp anticline



2 footwall collapse at antithetic normal faults

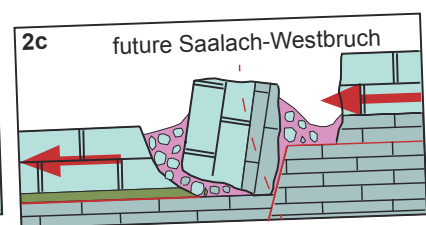
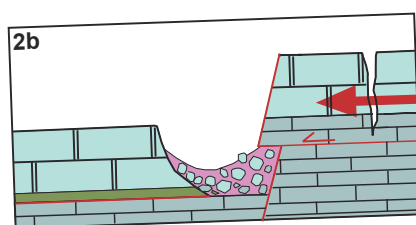
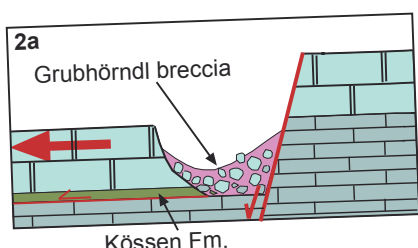
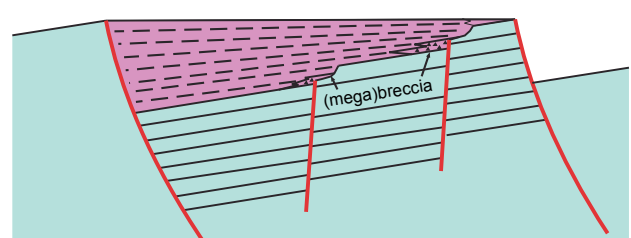


Fig. 10: Emplacement of the Grubhörndl mega-olistolith by 1 – west-directed thrusting, or 2 – tilting of the succession to the west. Sketches are not to scale. See text for discussion.

It is tempting to interpret the inferred normal fault and roll-over of stop 3 (Fig. 7) together with normal faults described here. However, the shallow décollement interpreted there, and the more than 200 m deep décollement in the Kössen Formation preclude a direct connection. Nevertheless, a common driver is probable.

We suggest that the complete sedimentary succession was tilted to the west in the early Late Jurassic (see 2 of Fig. 10 for a sketch). This could have facilitated gliding of the Upper Rhätian limestone, and emplacement of the Grubhöndl megablock. Below and east of the Urlkopf, the Kössen Formation interfingers with the Dachstein limestone, and is already absent below the Lärchfeldkopf (Fig. 8). The end of the Kössen décollement might have detached the Upper Rhätian limestone, thus opening a basin (2a of Fig. 10). A hypothetic antitethic normal fault might have exhumed the top of the Dachstein limestone in the footwall, causing separation of a huge block and bedding parallel sliding east of the normal fault (2b of Fig. 10). Ongoing westward sliding of the Upper Rhätian limestone west of this fault could have opened more space to progressively tilt the block over the exhumed footwall (2c of Fig. 10). We prefer this interpretation over an interpretation as a ramp anticline (1 of Fig. 10) because (1) a thrust of this dimension should be laterally continuous over several kilometers, (2) thrusting is not compatible with the observation of large scale sliding contemporaneous with emplacement of the Grubhöndl block (see above), (3) it would not be possible to redeposit material older than Upper Rhätian limestone, and (4) the base of the block does not show any evidence of thrust related deformation.

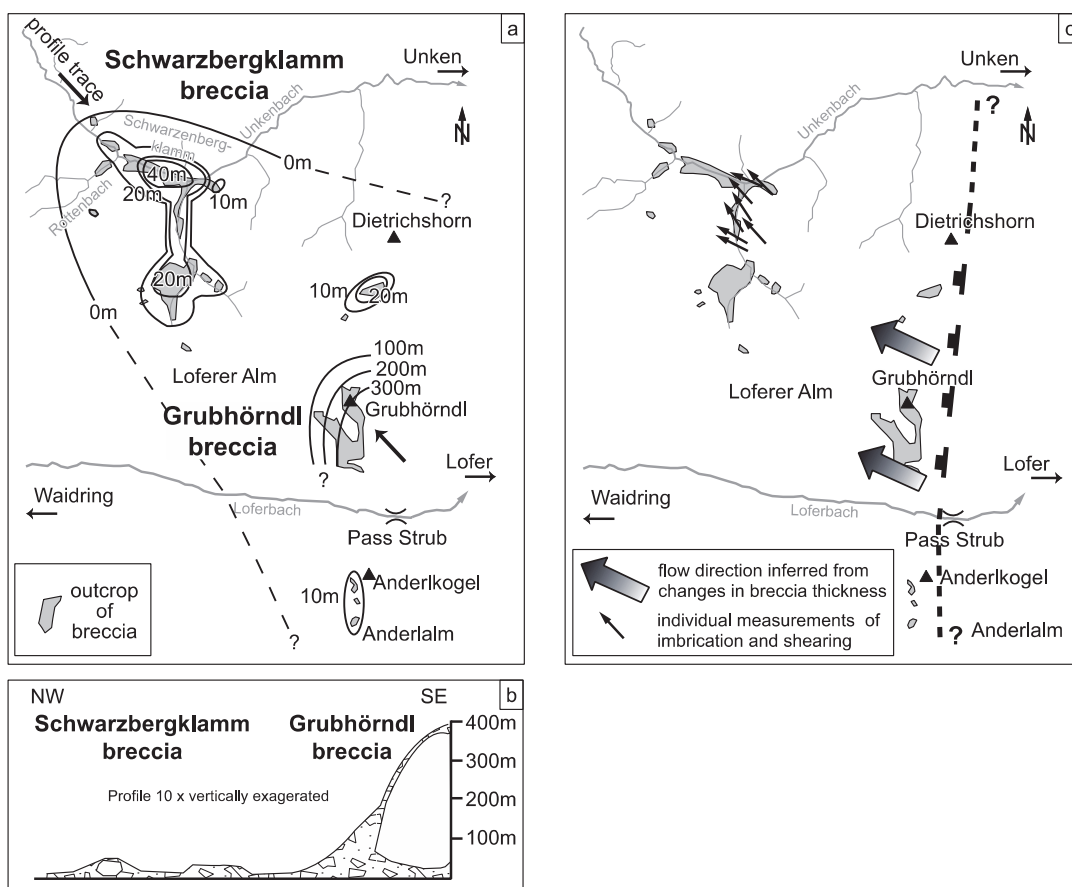


Fig. 11: Thickness distribution of the breccias of the Unken syncline (a, b) and sediment transport directions from imbrication and changes in breccia thickness.

The Grubhörndl block is the only known major Upper Jurassic topographic feature in the area. Most of the block was above the local base level during deposition of the younger part of the Ruhpolding Radiolarite, and the older part of the Oberalm Formation, and a hardground developed on top. The younger part of the Oberalm Formation onlaps the block and the breccia. The delicate hydrozoan fragments found together with other bioclastic material call for a local source. Probably the Grubhörndl olistolithe was originally so big that it had a carbonate platform on its top (ORTNER et al., 2008).

As discussed above, a roughly N-S oriented normal fault is required to facilitate emplacement of the large block. Earlier authors have invoked E-W-striking Jurassic faults to explain the Triassic facies distribution (FISCHER, 1965), Jurassic facies distribution (e.g., PLÖCHINGER, 1953; VECSEI et al., 1989). GAWLICK et al. (1999) suggested Jurassic thrusting at the southern margin of the Osterhorn mountains, and ORTNER (2017a) demonstrated, that thrusting in this area was associated with sinistral wrenching at E-striking faults, using growth strata in the Oberalm Formation. Therefore, we suggest that the breccias of the Unken syncline were most probably sourced at the intersection of two perpendicular fault systems (compare CHANNELL et al., 1992), an E-striking being sinistral, and N-striking normal faults. This could explain the NW- to WNW-directed transport and the consistent thinning of the Grubhörndl and Schwarzbergklamm breccias show away from the block (Fig. 11). E-striking sinistral strike slip faults can probably be interpreted in terms of intracontinental transform faults, linking the opening of the Atlantic ocean with the closure of parts of the Neotethys ocean (SCHMID et al., 2008; SCHMID et al., 2004).

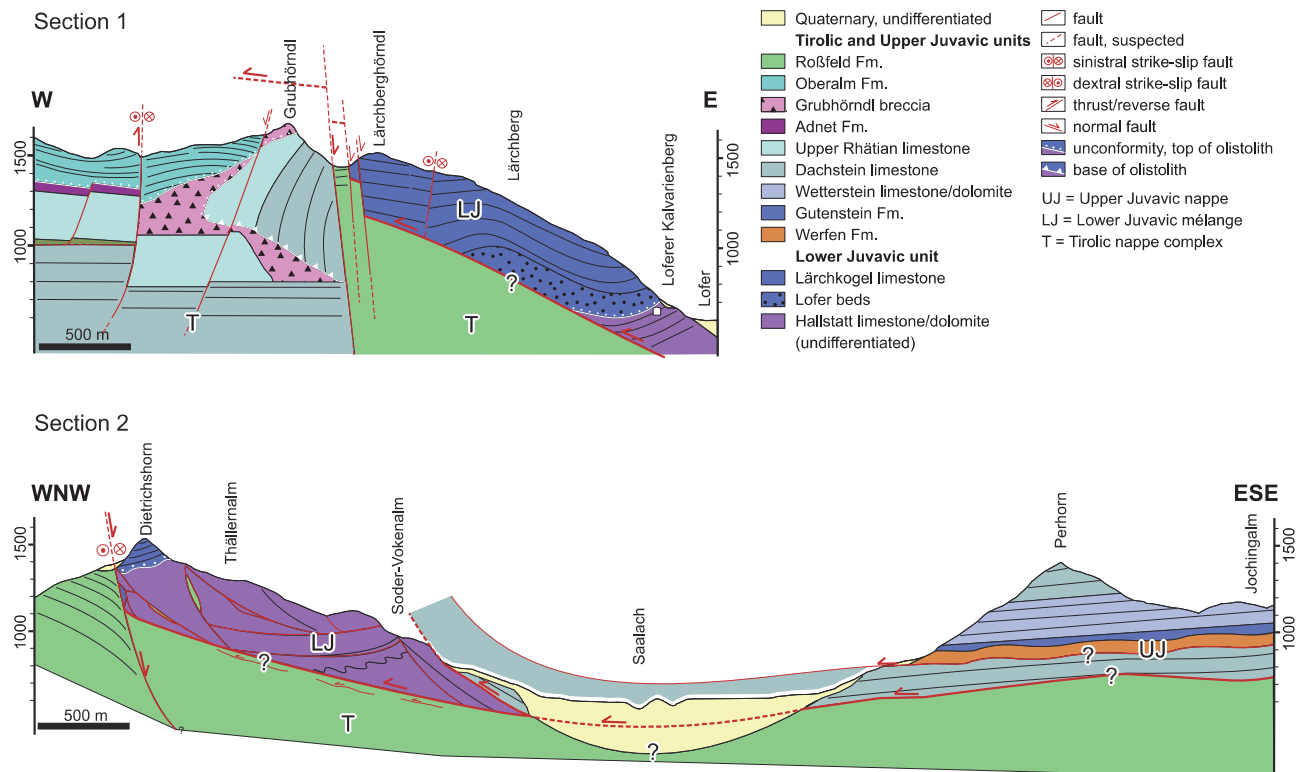


Fig. 12: Cross sections of the Grubhörndl and the Dietrichshorn. Cretaceous nappe boundaries are offset during Miocene faulting. See Fig. 4 for section traces.

Toward the east, the abrupt end of the meadows of the Loferer Alm has geologic reasons, as east and northeast of the Grubhörndl a Miocene fault downthrows the Lower Juvavic against the Tirolic nappe. The view goes across the Gföllhörndl and Lärchberghörndl, in the NE to Dietrichshorn, and below the Saalach valley. These rocky summits are built by the Lerchkogel limestone, which is an Upper Jurassic to Lower Cretaceous carbonate platform, comparable to the Plassen Formation (DARGA & SCHLAGINTWEIT, 1991), unconformably overlying the pelagic limestones and dolomites of the Hallstatt mélange of the Lower Juvavic unit (Figs. 3, 12; LUKESCH, 2003; SANDERS et al., 2007).

An analysis of brittle deformation in the area has shown that six successive paleostress tensors can be distinguished (RITTNER, 2006). These have been interpreted to be related to Cretaceous to Neogene tectonic events, and will be mentioned where appropriate. The normal fault mentioned here has a vertical offset of at least 500 m. Vertical offset diminishes to the north, and sinistral offset increases with the change of fault strike from NNW to N to NE. East of Unken the normal fault is connected to the northernmost branch of the sinistral NE-striking Saalachtal fault. The large-offset normal faulting is related to sinistral transtensive normal faulting during D5 (Fig. 14).

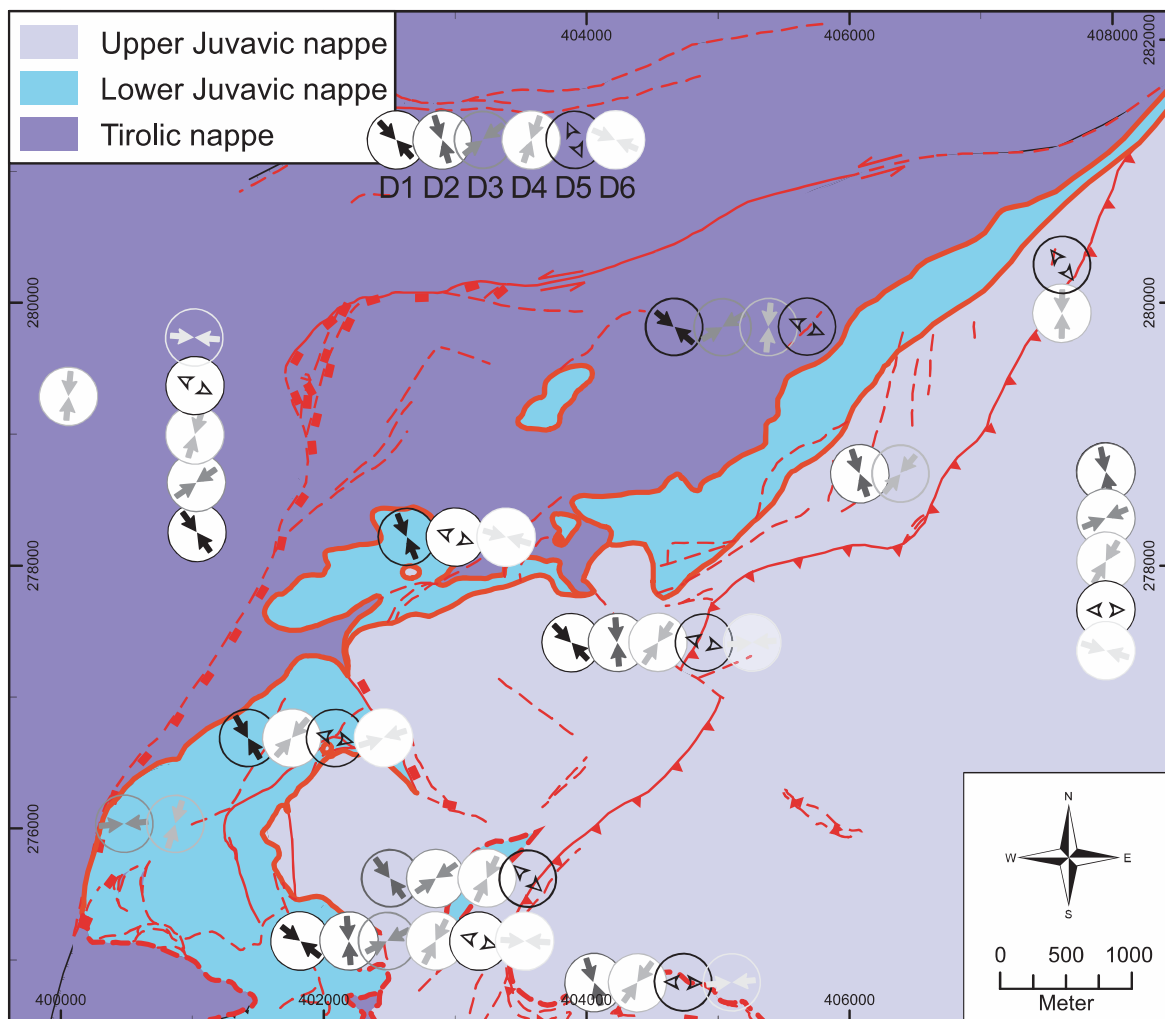


Fig. 13: Measuring stations of brittle faults in the Lofer-Unken area and observed tensors. The point of measurement is given by center of the lowermost symbol, and tensor style can be seen in the example at the top. The stacking pattern of the symbols gives the relative age of the tensors. Open symbols were used for poorly defined tensors. Coordinates: MGI Austria GK M31.

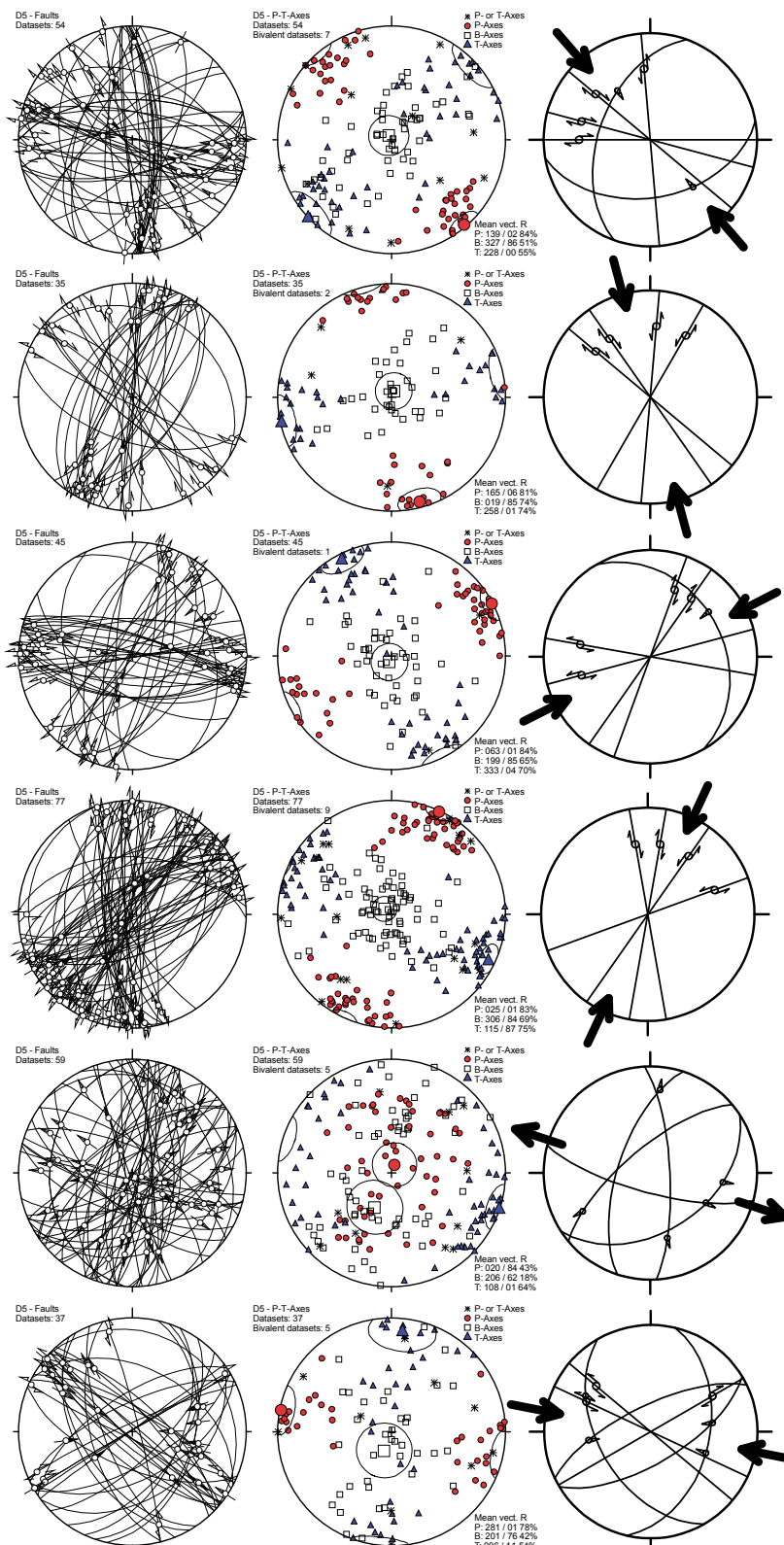


Fig. 14: Brittle faults in the Lofer-Unken area and their tentative interpretation. The diagrams show all faults that have been related to a specific tensor. The left column shows the faults. The middle column gives the P-,T- and B-axes related to the faults, that have been calculated using an angle of 30° between fault plane and P-axis, and the mean vectors of the respective axes with 95% confidence cones. These mean vectors give an estimate of the orientation of the paleostress tensor. The main fault sets observed are shown in the column on the right side.

Stop 8. Loferer Kalvarienberg

Coordinates: E 12.68943, N 47.58576.

Altitude: 650 m.

This stop will demonstrate the Lofer beds and the lowermost part of the Lerchkogel limestone that here discordantly overlies partly dolomitized/silicified Hallstatt limestones (Fig. 15A). The base of the transgressive succession is an interval of clast-supported beachface stylobreccia to conglomerate that consists of clasts of Hallstatt Formation and caliche nodules (Figs. 16A, B). Above, a poorly-exposed backweathering package about 15 m in thickness consists mainly of: (a) medium grey to dark brownish, organic-rich sandy limestones, and (b) organic-rich, brown to blackish marly limestones to marls; both lithologies contain fossils of shallow-marine (and intermittently restricted) environments, such as larger benthic foraminifera (*Anchispirocyclina lusitanica*, *Amijiella amiji*), smaller Textulariina, abundant small gastropods and non-rudist bivalves, and cyanoids. In addition, (c) at least one graded bed ~1 m thick of carbonate-lithic breccia is sharply intercalated; this breccia bed probably had accumulated upon tsunami backflow (Fig. 16C).

In marly limestones of this interval, a large vertebra was found in 2004 by D. Sanders. The vertebra was prepared and lend to the Naturkundemuseum Stuttgart; preliminary inspection by Rainer Schoch suggests that it pertains to a Crocodilian (Fig. 16D). Unfortunately, no further work was done on that vertebra so far. The succession from beachface breccia at the base to organic-rich marls at the top records transgression of a low-energy shore zone over a soil-covered, vegetated land surface that provided input of freshwater as well as of clastic and organic material into a shallow subtidal 'lagoon' seaward of the transgressive fringe (Fig. 15B).

The described interval is overlain by a package ~15 m in thickness of marly to pure limestones with intercalated shell beds of diceratids (*Heterodiceras*) (Fig. 16E). In the shell beds, most of the rudists are embedded toppled and more-or-less fragmented in different stages of taphonomic overprint. The shells are overgrown by other organisms, such as sessile foraminifera, *Milleporidium* (Hydrozoa), serpulids, brachiopods, and *Lithocodium* (Textularina). The co-presence of *Heterodiceras*, *A. lusitanica* and the green alga *Clypeina jurassica* indicates that the Lofer beds here are of latest Tithonian age. Higher up, at Lofer, the lower part of the Lerchkogel Limestone consists of oolithic limestones intercalated with milleporidian biostromes (Fig. 16F). For further details of the described succession it is referred to SANDERS et al. (2007).

Heavy mineral spectra of the Lofer beds are strongly dominated (>50%-99% of total) by apatite, and further characterized by zircon and rutile; tourmaline, staurolite and hornblende are rare. Both the apatite and the zircon show a spectrum of well-rounded to subangular grain shapes. This suggests recycling from pre-existing siliciclastics as well as direct erosion from magmatic rocks. Comparison with literature suggests that the heavy mineral spectrum of the Lofer beds result from a provenance area in which the Alpine Buntsandstein or, more probably, its distal equivalent, the Werfen Formation (Induan-Olenekian), were exposed; in addition, erosion of siliciclastics of the Northern Alpine Raibl beds (Julian-Tuvalian) may have delivered heavy minerals. In the Lofer beds, however, the common presence of subangular apatite with preserved crystal faces requires additional input from erosion of plutonic rocks, consistent with the conclusion derived from the range of grain shapes mentioned before (WOLFGRUBER, 2010).

In the area of Gerhardstein–Hochkranz (Day 2, stops 8-10), the breccias of the Lofer beds contain clasts of mixed siliciclastic-carbonate arenites. These probably were derived from erosion of the Werfen Formation and/or of the Northern Alpine Raibl beds; a derivation from the Alpine Buntsandstein (typically pure quartzites) is considered less probable. A low vitrinite reflectance (0.2-0.5) of coalified plant debris extracted from the Lofer beds indicates peak temperatures of 50-70°C (WOLFGRUBER, 2010).

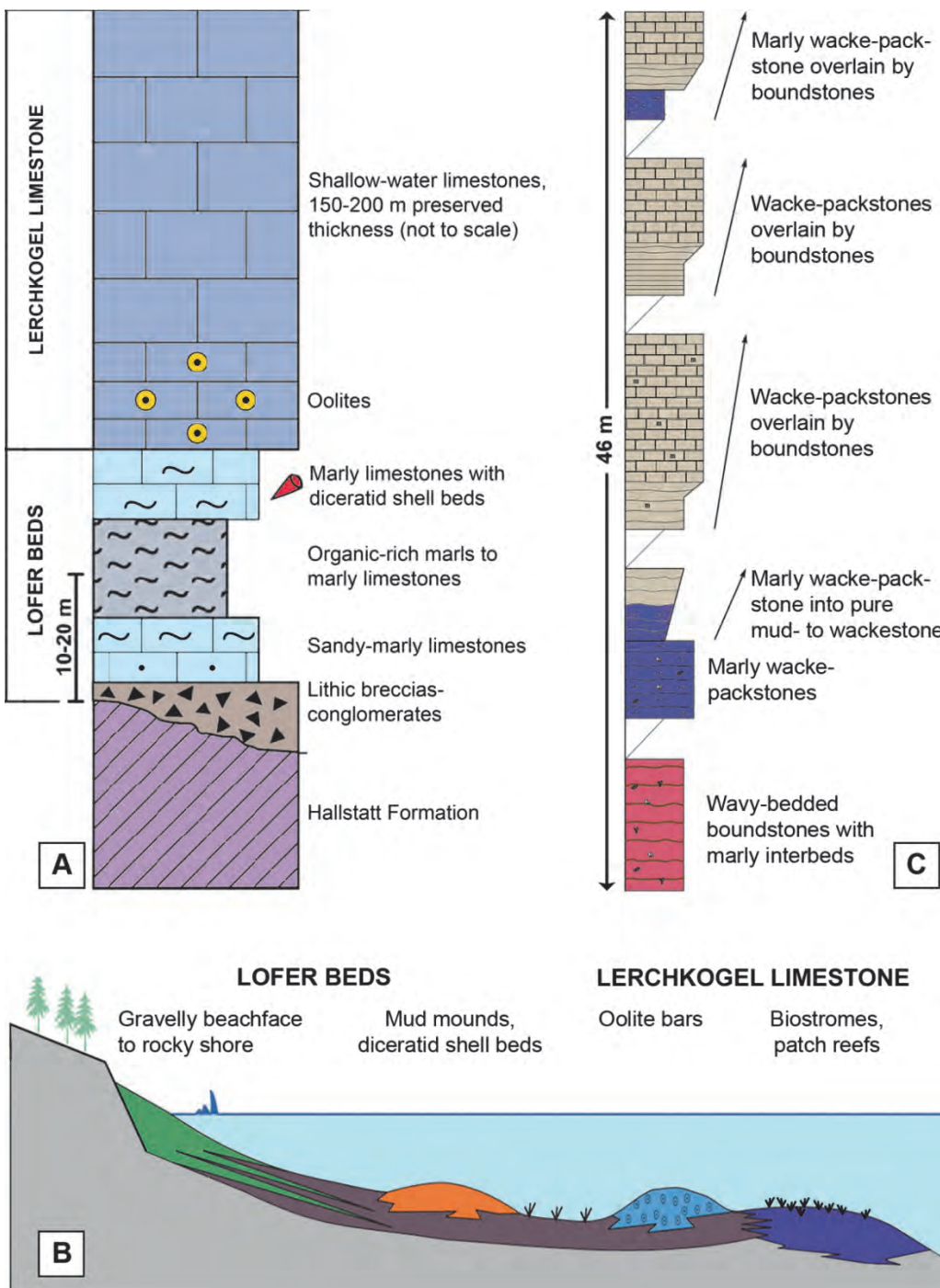


Fig. 15: (A) Generalized section of Lofer beds and Lerchkoegel limestone (SANDERS et al., 2007; modified from FERNECK, 1962). (B) Reconstructed transgressive setting (MOSNA, 2010). (C) Upper part of Litzlkogel section, showing a rhythmic packaging of (marly) wacke-packstones and different types of boundstones (MOSNA, 2010).

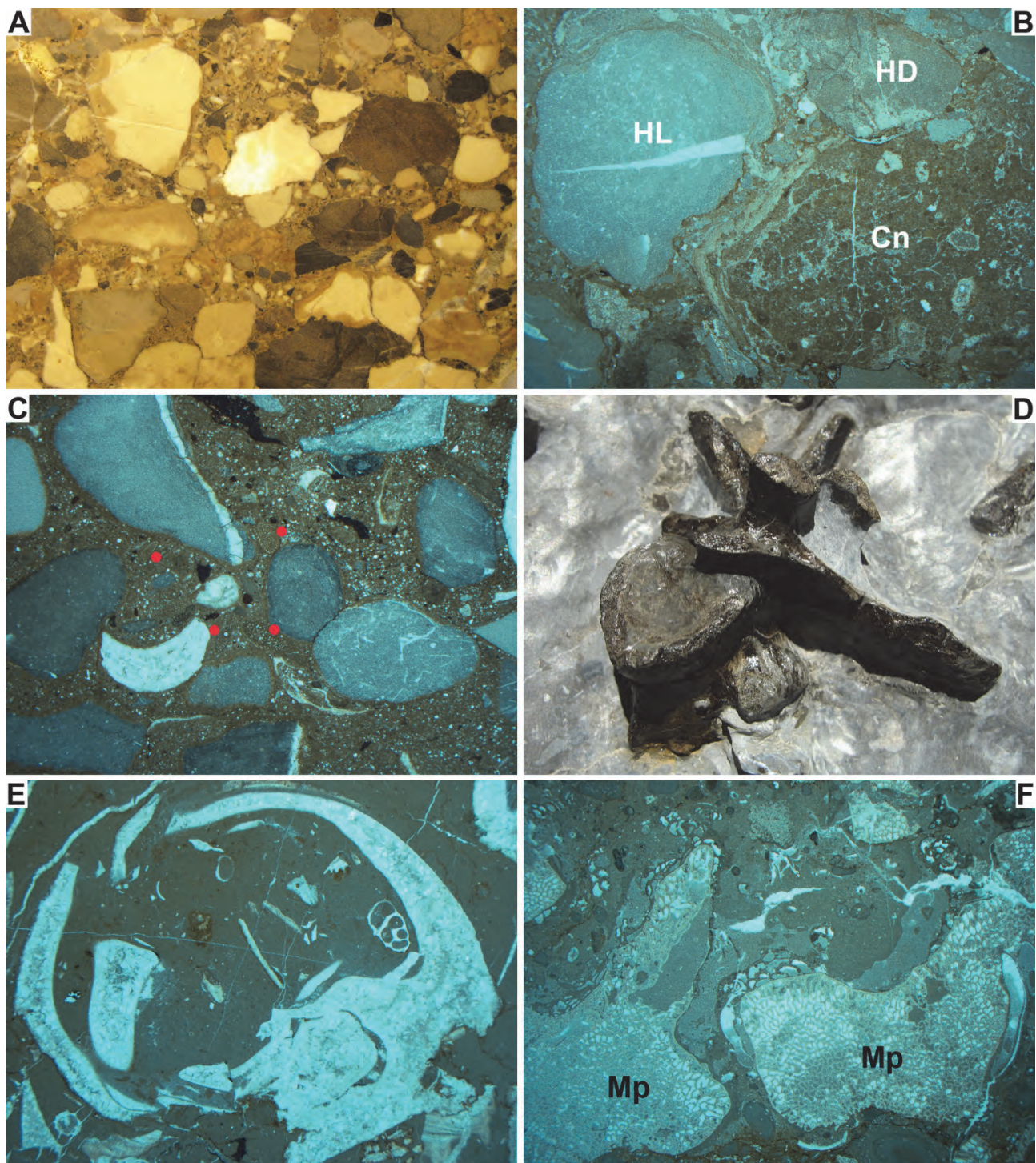


Fig. 16: Lofer beds at Lofer. (A) Polished slab of conglomerate at the base of the Jurassic section. Width: 10 cm. (B) Basal breccia: Clasts of Hallstatt Limestone and -dolomite (HL, HD), and a caliche nodule (Cn). Width: 29 mm. (C) Event bed (probable tsunamiite): Clasts of Hallstatt Formation and plant debris in a matrix of bioclastic wackestone with *Anchispirocyclina lusitanica* (red dots). Width: 22 mm. (D) Reptile vertebra, probably from a Crocodilian, in marly limestones of the Lofer section. Width: ~10 cm. (E) Diceratid rudist from a shell bed. Width: 22 mm. (F) Milleporidium (Mp), overgrown by sessile foraminifera. Width: 29 mm.

Day 2 – Weißbach area: Stops 9 to 14

Southeast of Lofer, the Gerhardstein and Hochkranz klippen of the Lower Juvavic nappe sit on top of a lower Cretaceous synorogenic sedimentary succession (Schrambach and Roßfeld Formations) of the Tirolic nappe complex. The Lerchkogel limestone cliffs of the klippen are widely visible. According to HAHN (1913a), the Gerhardstein has the best exposures of a thrust in the Alps of the state of Salzburg („*die schönsten Überschiebungsaufschlüsse, die in den gesamten Salzburger Alpen zu sehen sind*“), and we showcase one these outcrops at stop 9.

Locally, the transgression of the Lerchkogel limestone directly onto Hallstatt dolomite is mappable (Fig. 17), however, in other places, the Lofer beds are found at the base of the klippen. This suggests that the Late Jurassic „neoautochthonous“ (e.g., MANDL, 2000) succession covered a preexisting topography, and was detached and transported together with the underlying Hallstatt dolomites.

In contrast to the Unken syncline, the Lower and Middle Jurassic of the Tirolic unit is developed in basinal facies. Red limestones of the Adnet Formation are directly overlain by the Allgäu Formation, and the Ruhpolding radiolarite (Fig. 3). We will study this succession at stop 13. Within the Red limestones, huge slide blocks and associated breccias are present (KRAINER et al., 1994). Stop 12 shows the base of such a slide block, deformation at its base and the underlying red limestones.

Stop 9. Base of Gerhardstein Klippe south of Gerhardstein

Coordinates: E 12.75830, N 47.53468.

Altitude: 1250 m.

We follow a dirt road from Stocklaus toward Gerhardstein, passing the Wandbauer hamlet. At stop 9, the basal thrust of the Gerhardstein klippe is exposed in an outcrop along a new dirt road. The footwall are not the Schrambach or Roßfeld Formations of the Tirolic unit, but a slice of the Tirolic unit that has been emplaced on top of another slice of the Lower Juvavic nappe out-of-sequence. Such slices are common at the base of the klippen east of Weißbach, and the largest one is found south of the Hochkranz (SIEWERT, 1973). Most of these slices are part of the Oberalm Formation, only the one at stop 9 has an internal succession of Oberalm Formation, Ruhpolding radiolarite and Schrambach Formation, which is emplaced onto a tectonically deeper slice of Lerchkogel limestone. The outcrop sketches of Figures 18g and h are from the base of this slice, a few tens of meters below stop 9.

The tectonic contact is characterized by penetrative shear bands in the Schrambach marls, and duplexing in the more competent Ruhpolding radiolarites and Oberalm limestones. The contact shows open wavy folding, and the deepest parts being affected by renewed thrusting parallel to foliation that brings the Schrambach marls on top of the Lerchkogel limestone (described as „Verkeilung“ by JACOBSHAGEN & KOCH, 1959). This gives a model for the emplacement of the deepest slice below stop 9.

Local transport directions based on shear band geometry is top to NNE. However, analysis of a larger number of shear bands at the base of the lowermost slice (outcrops a and b of Fig. 18), results in north-directed tectonic transport. Taking into account all measured data from the base of the Gerhardstein and Hochkranz klippen (MOSNA, 2010; WOLFGRUBER, 2010), transport directions vary from top to NW to top to NE. This is in accordance with the observed tensors D1 to D3 of Figures 13 and 14 deduced from the analysis of brittle fault planes. We speculate here that this succession of tensors implies that transport on out-of-sequence thrusts changes progressively from top NW to top NE from base to top as new slices form.

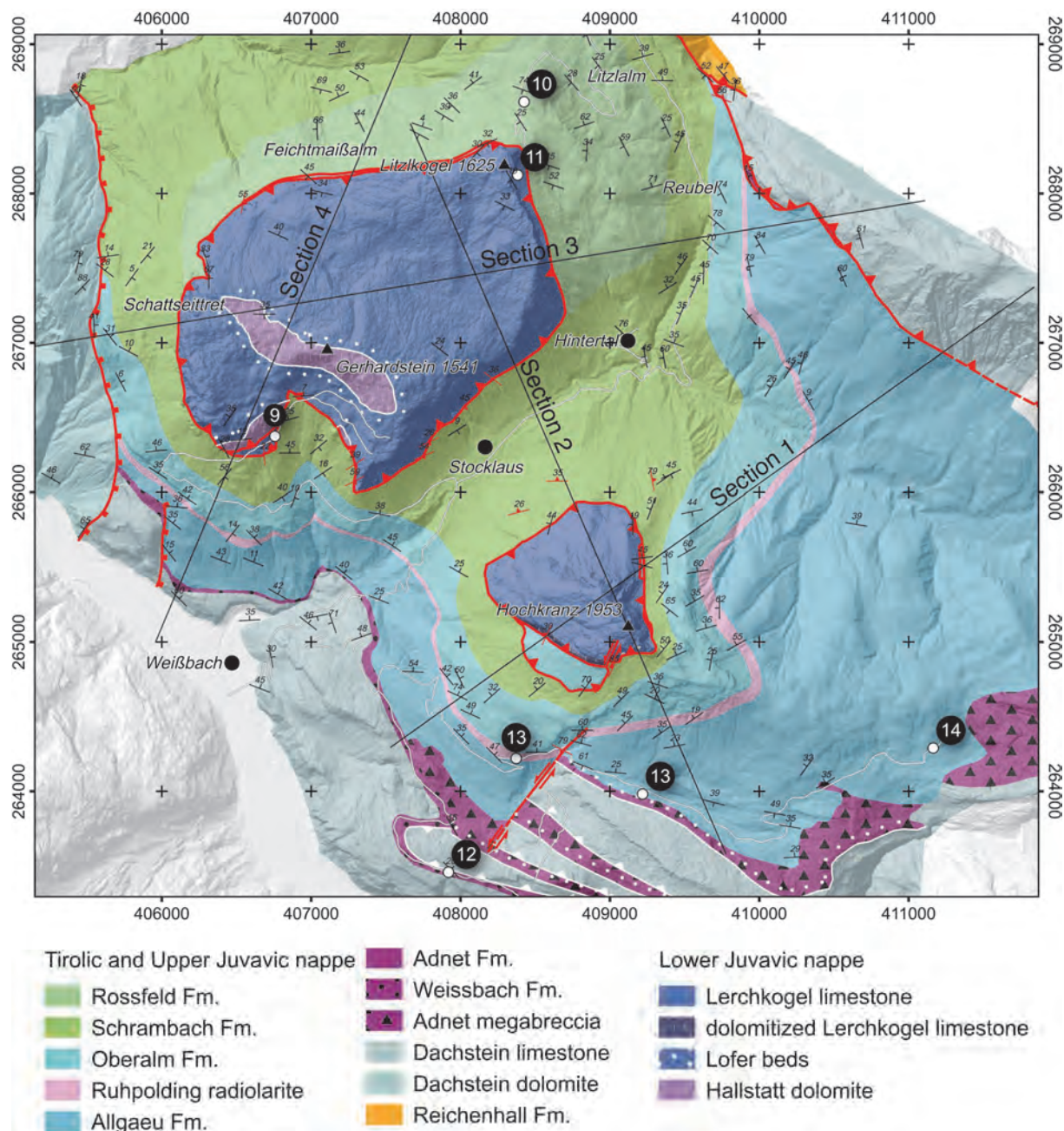


Fig. 17: Tectonic map western end of the Juvavic nappe complex in the Weißbach area, compiled from MOSNA (2010) and WOLFGRUBER (2010). Minor changes according to SIEWERT (1973) and PAVLIK (2006). SSE part redrawn from KRAINER et al. (1994). Numbers 9 – 14 indicate field trip stops of day 2. Sections are shown in Figure 20. Coordinates: MGI Austria GK M31.

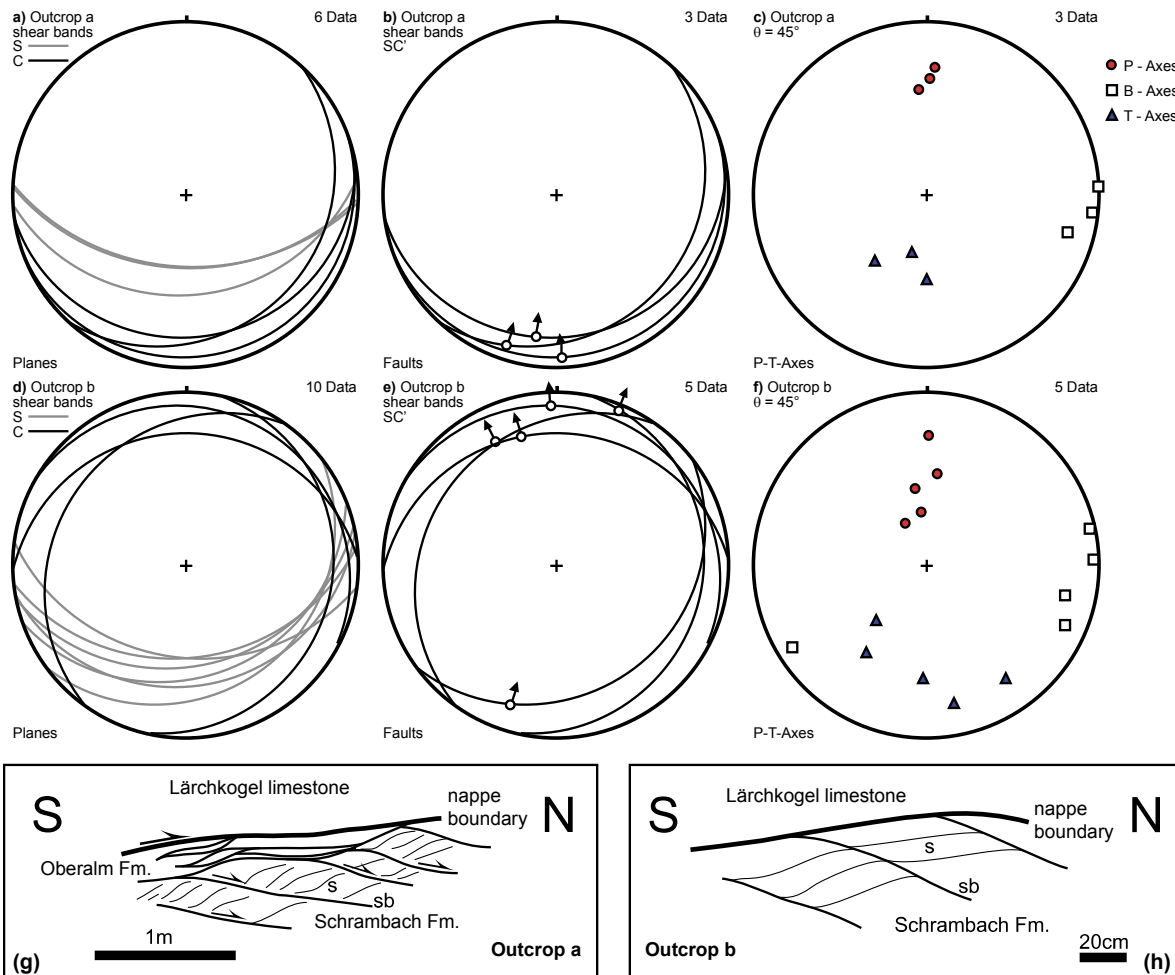


Fig. 18: Structural data from two outcrops at the base of the Gerhardstein klippe in the immediate vicinity of stop 9. Shear bands in Schrambach marls were used to deduce transport directions. a, d) Great circles of s- and c-planes; b, e) Hanging wall movement on C-planes calculated from pairs of S- and C-planes; c, f) Kinematic axes derived from movement on C-planes, using an angle of 45° between C-plane and P-axis. g, h) Sketches of structures at the two outcrops. Note slice of Oberalm Formation between Schrambach Formation of the footwall and Lerchkogel limestone of the hanging wall in (g).

Stop 10. Olistolithe within the Roßfeld Formation at Litzlalm

Coordinates: E 12.77994, N 47.55492.

Altitude: 1420 m.

We go back to Stocklaus, pass the Hirschbichl saddle, continue past the Litzlalm toward Litzlkogel. South of the road to stop 10, olistoliths a few tens of meters in size of limestones are visible that are intercalated into the Rossfeld Formation. These olistoliths will not be visited. They are briefly characterized as cherty spiculitic wacke-packstones with a few inoceramid fragments, small planktic foraminifera and a few grains of quartz, glauconite and phosphorite. The co-presence of small planktic foraminifera with inoceramid fragments suggests that the spiculites accumulated somewhat during the latest Jurassic to early Cretaceous (MOSNA, 2010).

The olistolith that is seen with the excursion was studied along a section 14 m in length. The lower part (2 m) consists of strongly stylolitized, red-coloured lime mudstones to wackestones with radiolarians; this lithology was interpreted as Hallstatt Limestone. The middle part (2 m) contains red to brown

arenites (grainstone and packstone texture) mainly of crinoid ossicles and a few small fragments of rudists and non-rudist bivalves, bryozoans and skeletal sponges. The former matrix of lime mud is selectively replaced by chert, and the interstitial pore space in grainstone texture is filled with megaquartz cement.

The upper 10 m of the section consists of grey wackestones with bioclasts of deep-water and neritic habitats, respectively. Aside of crinoid ossicles, the deep-water bioclastic fraction is characterized by rare globotruncanids (cf. *Rotalipora*; Albian p.p. to Cenomanian), lagenids (*Nodosaria*, *Lenticulina*) and *Textulariina*; the neritic fraction comprises bioclasts of bryozoans, brachiopods and corals. Notably, also calpionellids and a few clasts of shallow-water limestones (e.g., bioclastic grainstones) were identified in the matrix. The co-presence of cf. *Rotalipora* with calpionellids (up to Valanginian) indicates substantial reworking – as supported also by the clasts of shallow-water limestones – and a sediment record up to at least the middle to upper Albian (maximum: Cenomanian, because of total range of *Rotalipora*) (MOSNA, 2010).

Stop 11. Lofer beds at base of Gerhardstein klippe, and Lerchkogel limestone at Litzlkogel

Coordinates: E 12.77970, N 47.55053.

Altitude: 650 m.

We continue on the dirt broad to a small saddle at 1460 m, and follow the footpath toward Litzlkogel (165 m elevation difference). At 1500 m, we pass a preliminary section (Fig. 15C) through the upper part of the exposed succession displays a vertical packaging between: (a) backweathering, more-or-less marly, bedded wacke- to packstones (Fig. 19A) that grade up-section into (b) outweathering, thick-bedded to unbedded intervals with boundstones. The wacke-packstones are rich in smaller benthic foraminifera, peloids, fragments of dasycladalean algae and of corals, echinoderm ossicles (e.g., echinoid spines), brachiopods, *Tubiphytes* and, in a few intervals, coalified plant debris. The boundstones, in turn, contain dendroid corals and *Milleporidium* (Figs. 19B, C) that may show complex encrustation successions. The matrix of these boundstones contains fragments of diverse dasycladaleans, benthic foraminifera and serpulids; locally, boundstones of 'Porostromates' of type *Cayeuxia*, and discrete masses of microbialites are present (Figs. 19D, E, F).

The significance of the rhythmic packaging between wacke-packstones and boundstones is not fully clear as yet. If the wacke-packstones represent a bathymetrically deeper facies than the boundstones, at least the upper three packages may represent upward-shoaling/cleaning cycles. In the lower part of the section, however, input of siliciclastic sediment took place also during boundstone accumulation. More detailed sampling were required to better resolve bathymetric trends and patterns of siliciclastic input associated with sediment packaging.

The summit of Litzlkogel offers a wide view of the surrounding mountains. In the east, an open, NW plunging anticline is seen in the cliffs below the Kammerlinghorn summit (Hundstod anticline; TOLLMANN, 1969). In map view, the trace of the axial plane of this anticline is parallel to the trace of the syncline of the Weißbach syncline. The Gerhardstein and Hochkranz klippen are in the western limb of this syncline. The summits in the north are in the Middle Triassic Ramsau dolomite of the Upper Juvavic nappe. In the valley east of the Hirschbichl saddle the Tirolic nappe complex disappears below the Upper Juvavic unit, and all units dip to NW. This northwesterly dip is also seen in the section 2 of Figure 20 below the Hochkranz klippe, that we see south of Litzlkogel, and is a regional feature. The Weißbach syncline and the adjacent NW-plunging Hundstod anticline seem to be a local feature that

is oblique to most of the structures of the Northern Calcareous Alps. The Weißbach syncline is parallel to the Hundstod thrust ("Hundstod-Aufschuppung"; BARTH, 1968; HAHN, 1913a; TOLLMANN, 1969, 1976b), and may be interpreted on terms of drag along the fault, thus not related to regional folding event.

The Hintertal syncline has a very open monoclinal geometry (section 2 of Fig. 20), while the Weißbach syncline has a tighter hinge zone in directly adjacent to the Hundstod thrust. The overprint of two generations of folds with perpendicular fold axis leads to a Type 1 fold interference pattern (Fig. 21). Because of the monoclinal shape of the Hintertal syncline the elongate basin is open to the NW and SW, and is comparable to a quarter bathtub.

Stop 12. Base of a slide block in Early Jurassic sediments (Weißbach Formation)

Coordinates: E 12.77402, N 47.50857.

Altitude: 1100 m.

We return from Litzlkogel to Pürzlbach, and follow the dirt road from Pürzlbach toward Kopfstein. After crossing the Brechlbach creek, the road follows a layer of incompetent rock between Dachstein limestone (Fig. 17).

These rocks are red bedded limestones that are a local equivalent of the Adnet Formation of the Red limestones, and have been defined as Weißbach Formation (KRAINER et al., 1994; MOSTLER & KRAINER, 1993). These limestones were deposited on a slope, and contain breccia beds. On top of the Weißbach Formation, the base of a Dachstein slide block is exposed. The sediment is seen to be ploughed by the block during roughly N- to NW-directed movement (KRAINER et al., 1994 and own data). The slide block is overlain by alternating breccias and megabreccias of the Adnet Formation and two Dachstein slide blocks (Fig. 17). The capping sequence of the megabreccias ends with manganese rich laminated marls of Toarcian age of the younger Allgäu Formation (KRAINER et al., 1994). Laterally, this breccia succession is replaced by the Allgäu Formation (Figs. 3, 17).

Stop 13. Basinal sedimentary succession from Early to Late Jurassic, soft-sediment deformation in Upper Jurassic

Coordinates: E 12.77992, N 47.51542 and E 12.79117, N 47.51333.(two substops, see text)

Altitude: 1200 m.

We return to Pürzlbach and follow the dirt road toward the Kallbrunnalm. Between 1160 and 1250 m the sedimentary succession from the Allgäu Formation into the Ruhpolding radiolarite and Oberalm Formation is exposed. The Allgäu Formation includes bioturbated cherty limestones and marls („Fleckenkalke und Fleckenmergel“), shales rich in manganese and cm-bedded siliceous limestones to cherts (KRAINER et al., 1994). The dirt road exposes the uppermost part of the succession, starting with the thin-bedded siliceous limestones and cherts, that can be compared to the Chiemgau beds of Middle Jurassic age (TOLLMANN, 1976a). Cm- to dm-bedded cherts of the Ruhpolding radiolarite follow on top, and then micritic limestones of the Oberalm Formation A set of NE-dipping normal to oblique normal faults crosscuts the Oberalm Formation, and some of the faults are sealed within the Oberalm Formation (Fig. 22).

Where the dirt road crosses the Brechlbach, a NE-striking fault separates the Oberalm Formation on the NW side from the Allgäu Formation on the SE side. There, the succession on top of the olistolithes starts with a few meters of grey to red limestones, followed by manganese ore and then manganese-rich marls (KRAINER et al., 1994). The geologic map (Fig. 17) shows that the fault delimits the stack of

olistolithes, but does not cut across the lowermost block. This suggests that fault activity was initially related to olistolithe emplacement and persisted into the Late Jurassic. Initially, the Allgäu Formation covered submarine topography, while the stack of olistolithes was still mobile. Glide processes may have evacuated the olistolithes NW of the fault.

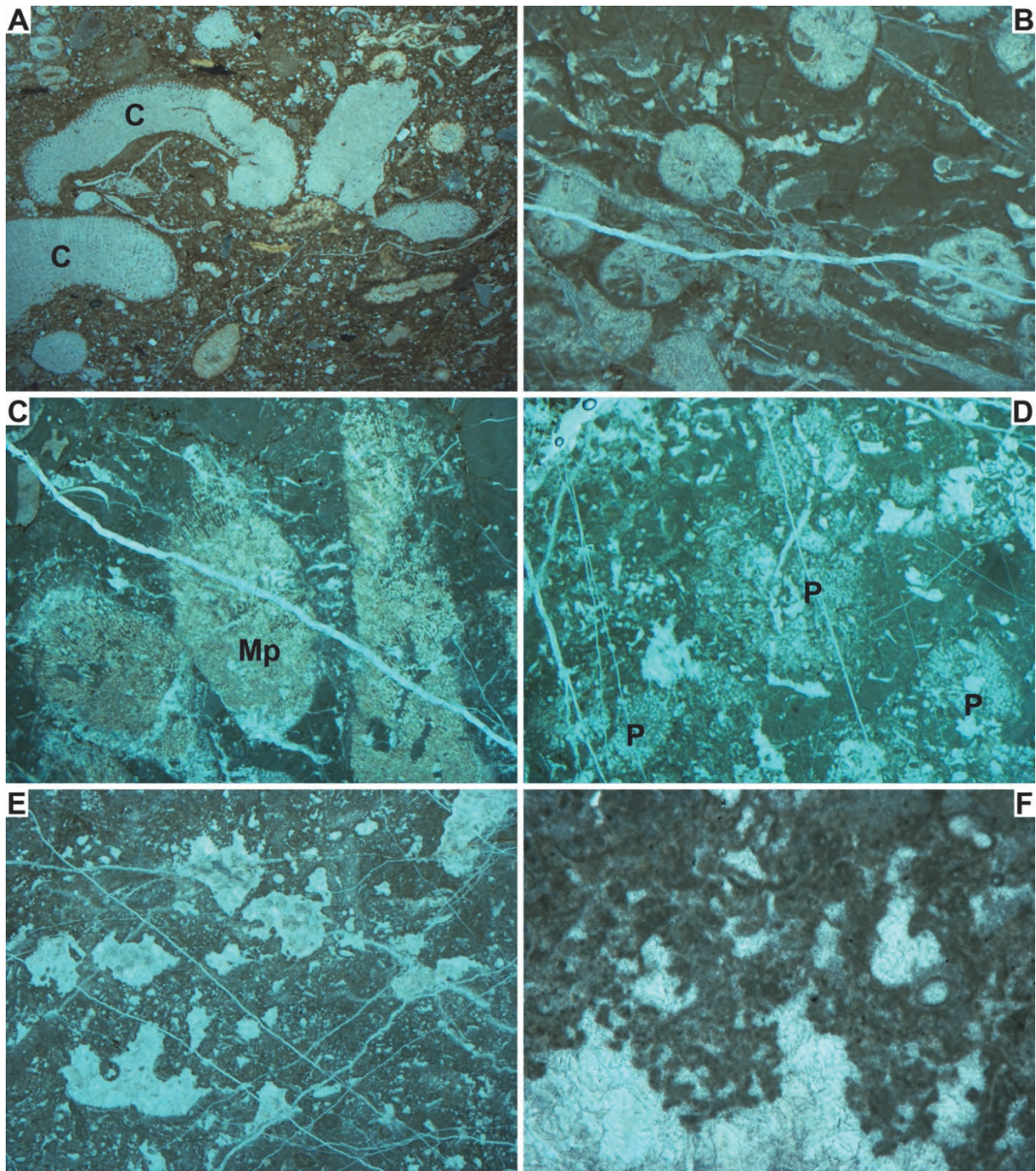


Fig. 19: Litzkogel section. (A) Brown, marly bioclastic packstone with coral fragments (C). Width: 22 mm. (B) Floatstone with dendroid coral. Width: 29 mm. (C) Boundstone with branched *Milleporidium* (Mp). Width: 17.5 mm. (D) Porostromate-microbialite boundstone. Width: 8.5 mm. (E) Fenestral microbialite mainly with thrombolithic fabric. Width: 14 mm. (F) Detail of thrombolithic fabric. Width: 2.2 mm.

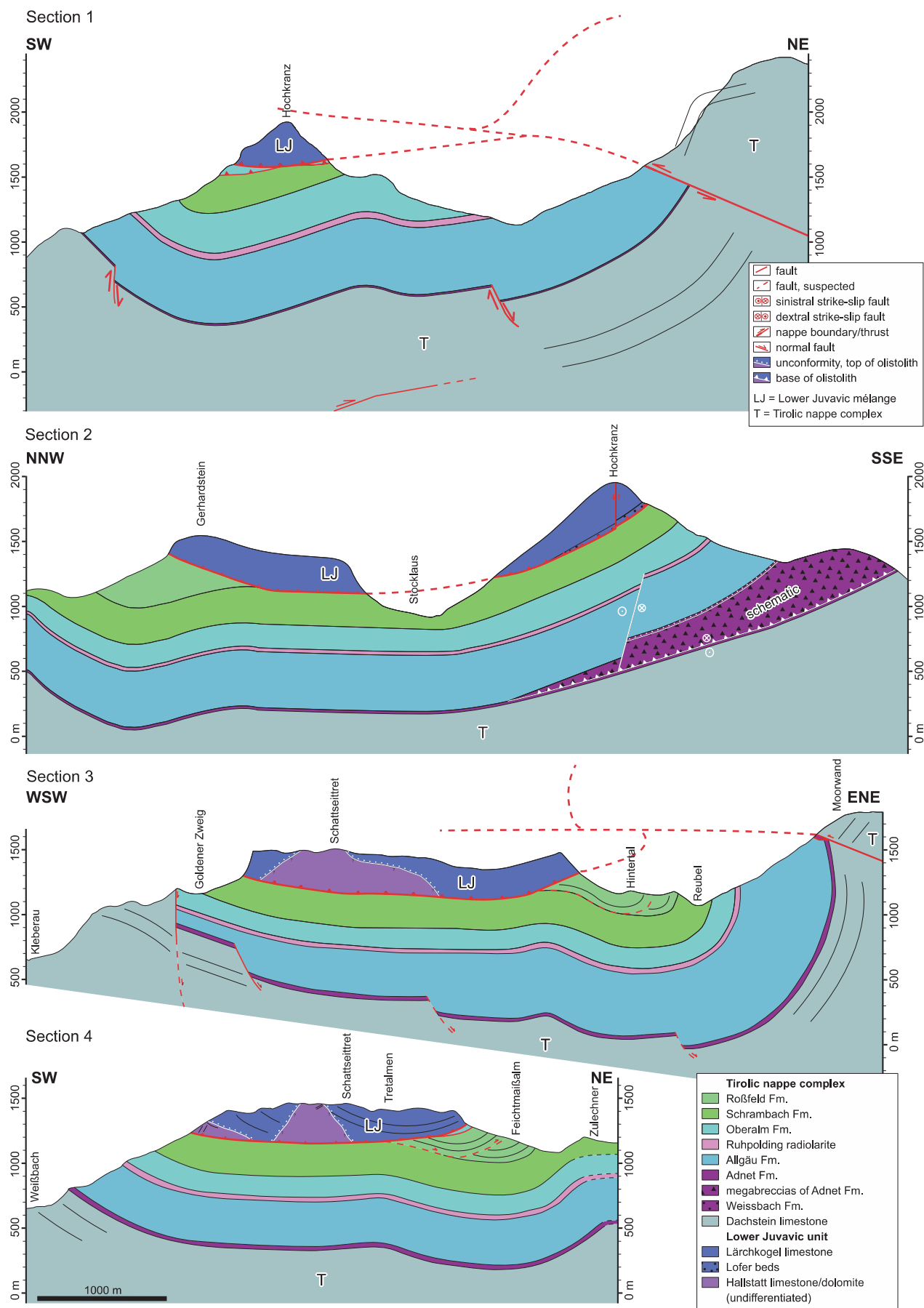


Fig. 20: Cross sections of the Gerhardstein and Hochkranz klippen. See Figure 17 for section traces.

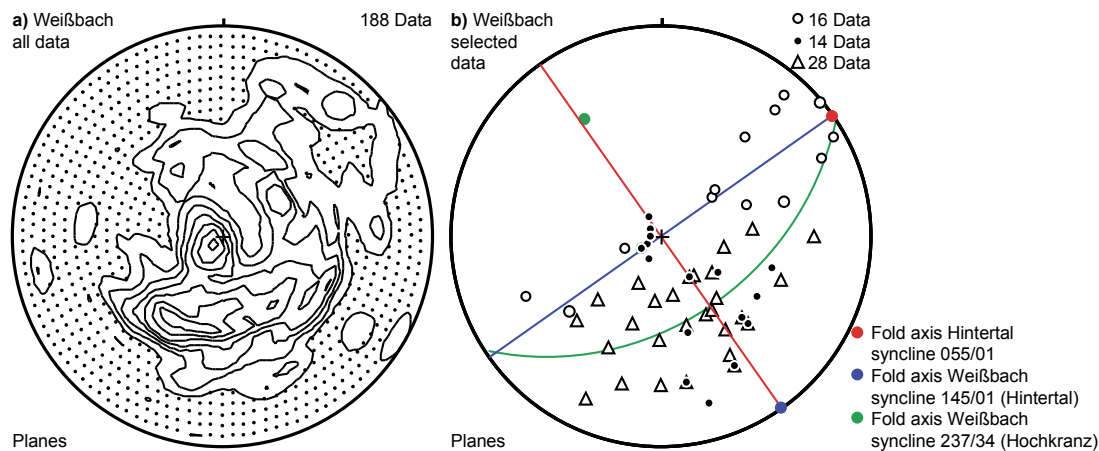


Fig. 21: Analysis of Bedding orientations in the Weißbach area (see Fig. 17). a) Contour plot of all bedding planes of the Weißbach area. There is no straightforward interpretation of the observed distribution of bedding poles. b) Separating data east of Hintertal and Reubel (Fig. 17) allows to calculate a horizontal axis for the Weißbach syncline (poles to bedding shown by open circles and filled blue circle for fold axis). Open triangles indicate bedding poles around Hochkranz, giving a NW-plunging fold axis (filled green circle) for the Weißbach syncline. Bedding orientations selected along the trace of section 2 (black filled circles) allow to calculate an NE-trending axis for the Hintertal syncline.

Where the dirt road crosses the Brechlbach, a NE-striking fault separates the Oberalm Formation on the NW side from the Allgäu Formation on the SE side. There, the succession on top of the olistolithes starts with a few meters of grey to red limestones, followed by manganese ore and then manganese-rich marls (KRAINER et al., 1994). The geologic map (Fig. 17) shows that the fault delimits the stack of olistolithes, but does not cut across the lowermost block. This suggests that fault activity was initially related to olistolite emplacement and persisted into the Late Jurassic. Initially, the Allgäu Formation covered submarine topography, while the stack of olistolithes was still mobile. Glide processes may have evacuated the olistolithes NW of the fault.

The differences in thickness and facies in the Lower Jurassic sediments have been interpreted in terms Early Jurassic transtensive basin formation (CHANNELL et al., 1992; KRAINER et al., 1994), which is supported by the synsedimentary faults in the Oberalm Formation, given that the same fault system remained active into the Late Jurassic.

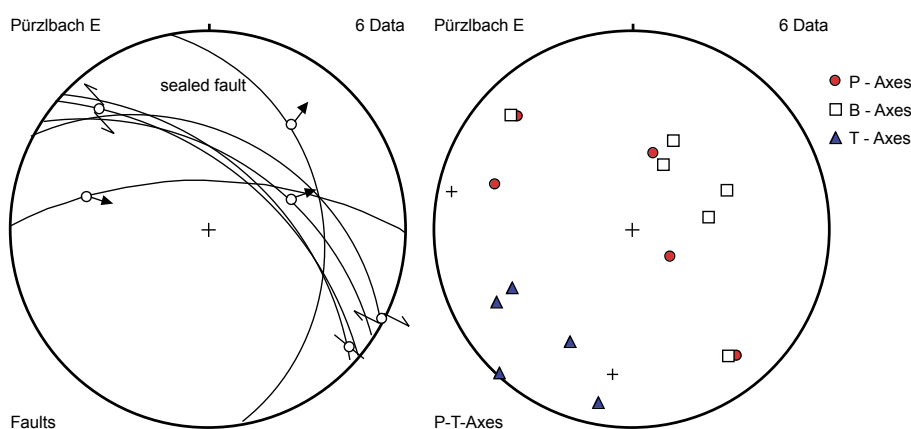


Fig. 22: Faults in the Oberalm Formation at stop 13, that are probably syndepositional. The girdle distribution of P- and B-axes indicates transtension.

Stop 14. View of the Kammerlinghorn from Kallbrunnalm

Coordinates: E 12.81699, N 47.51622.

Altitude: 1450 m.

This stop is a second alternative to stop 11 at the summit of Litzlkogel in case of poor weather conditions.

Concluding remarks

This field trip has shown some key events in the evolution of the NCA:

- 1) Early Jurassic basin formation and associated differentiation of facies and emplacement of huge olistolithes, related to opening of the Central Atlantic.
- 2) Late Jurassic deposition of large breccia bodies and olistolithes. In the Late Jurassic, facies differences are observed between the Tirolic and Lower Juvavic units. Continental to shallow marine deposits are found on top of the Lower Juvavic unit, while allobasic limestones intercalated with pelagic deposits are found on top of the Tirolic unit. However, this event is partly contemporaneous with emplacement of the sedimentary mélange of the Lower Juvavic units into pelagic sediments by glide processes (Fig. 1), and by transpression at the Trattberg rise east of the field trip area (see discussion above, Stop 7). Cross sections in the Salzkammergut area 100 km east of Lofer show very open folds onlapped and sealed by Upper Jurassic sediments (MANDL, 2013), and PICOTTI & COBIANCHI (2017) discussed lithospheric folding to explain thickness differences in Upper Jurassic sedimentary successions of the easternmost Southern Alps. Whatever type of tectonic activity it was, it did cause uplift and erosion in some areas, and subsidence in other areas. The uplifted areas were those affected by erosion and retransgression during the Late Jurassic, and those documented all across the Middle and Eastern NCA (e.g., Loferer beds, Oberalmer Basiskonglomerat, Obersee breccia (e.g., LEIN et al., 2009; PLÖCHINGER, 1953; SANDERS et al., 2007)
- 3) Inversion of the continental margin starting at the end of the Early Cretaceous. During this event, the nappes of the NCA formed (d1 to d4 of Fig. 23). Part of the Lower Juvavic unit, and the Upper Juvavic nappe, were detached and emplaced onto Early Cretaceous synorogenic deposits. Consequently, the Lower Juvavic unit is either „in place“ (i.e., not transported during Lower Cretaceous shortening; in the surrounding of Kuchl in Fig. 1), or it is a nappe (N and SW of Lofer in Fig. 1; see also SCHWEIGL & NEUBAUER, 1997). Transport of the Lower Juvavic nappe was most probably together the Upper Juvavic nappe (G. Mandl in SCHEIDLEDER et al., 2001).
- 4) Cenozoic faulting controls much of the present-day morphology of the NCA. Two dominant processes interact: lateral escape of crustal blocks that affects mainly the internal part of the Eastern Alps, and only the southernmost part of the central NCA (RATSCHBACHER et al., 1991), and postcollisional oblique convergence between the Eastern Alps and the European foreland. The latter causes NE-striking sinistral tear faults rooting at the base of the Subalpine Molasse and/or Helvetic nappes (ORTNER et al., 2015). As lateral escape is increasingly extensional toward the east, these tear faults, i.e. the Saalachtal fault, end in an extensional horse-tail splay toward the south and sinistral offset does not reach the southern margin of the NCA (d5 of Fig. 23).

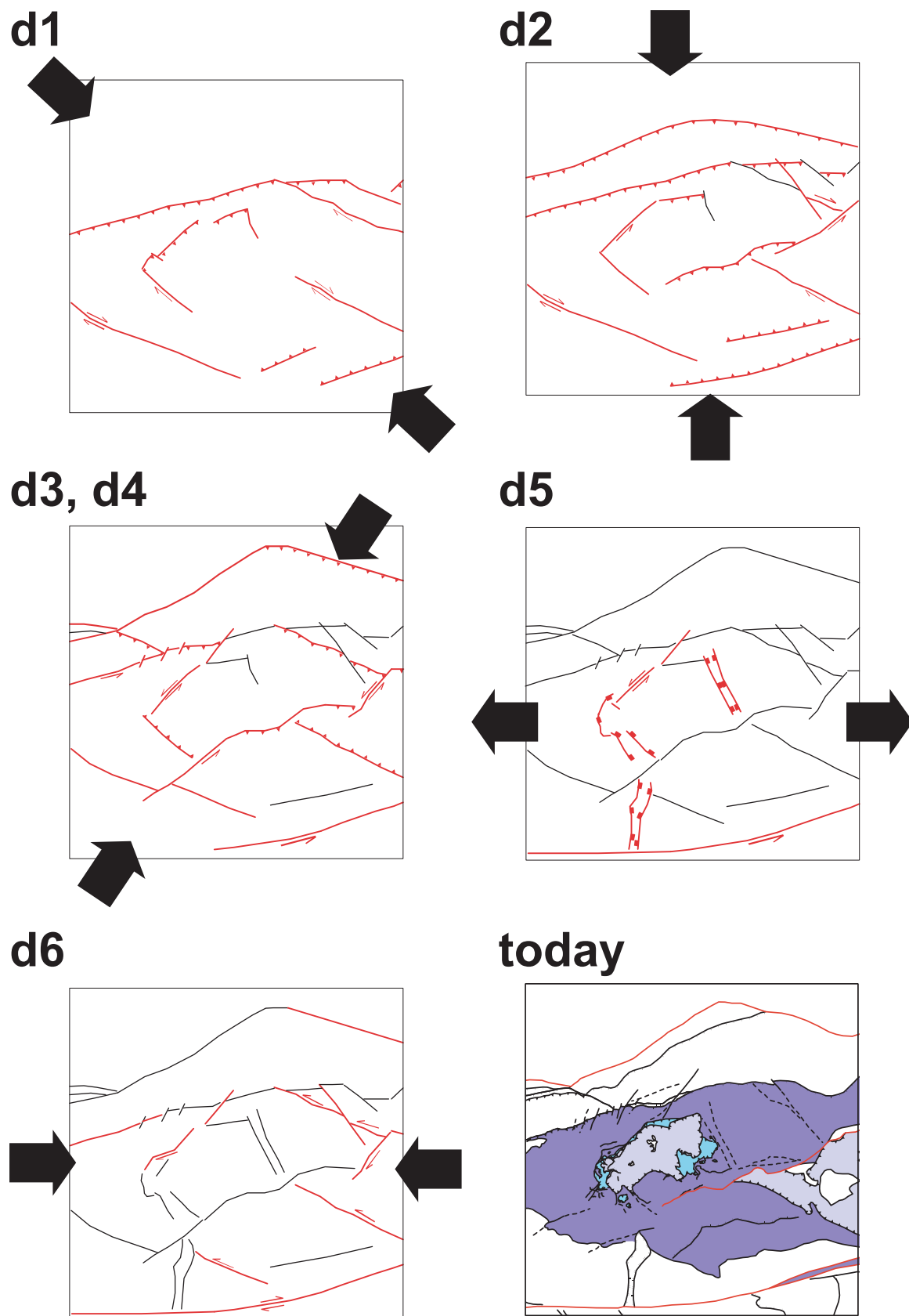


Fig. 23: Attempt to correlate the paleostress tensors of Figures 13 and 14 to the activity of individual faults observed in the field trip area (modified from RITTNER, 2006). Coloring of tectonic units as in Fig. 1.

References

- AMPFERER, O. (1927): Über den Westrand der Berchtesgadener Decke.- Jahrbuch der Geologischen Bundesanstalt, 77, 205 - 232, Wien.
- BARTH, W. (1968): Die Geologie der Hochkalter-Gruppe in den Berchtesgadener Alpen.- Neues Jahrbuch für Geologie und Paläontologie, Abhandlungen, 131, 119-177, Stuttgart.
- BRAUNSTINGL, R. (2005): Geologische Karte von Salzburg 1:200.000.- Geologische Bundesanstalt, Wien.
- CHANNELL, J. E. T., BRANDNER, R., SPIELER, A. & STONER, J. S. (1992): Paleomagnetism and paleogeography of the Northern Calcareous Alps (Austria).- Tectonics, 11, 792 - 810, Washington, D.C.
- DARGA, R. & SCHLAGINTWEIT, F. (1991): Mikrofazies, Paläontologie und Stratigraphie der Lerchkogelkalke (Tithon-Berrias) des Dietrichshorns (Salzburger Land, Nördliche Kalkalpen).- Jahrbuch der Geologischen Bundesanstalt, 134, 205-226,
- DARGA, R. & WEIDICH, K. F. (1986): Die Lackbachschichten, eine klastische Unterkreide-Serie in der Unkener Mulde (Nördliche Kalkalpen, Tirolikum).- Mitteilungen der Bayerischen Staatssammlung für Paläontologie und historische Geologie, 26, 93-112, München.
- DECKER, K., FAUPL, P. & MÜLLER, A. (1987): Synorogenic sedimentation in the Northern Calcareous Alps during the Early Cretaceous.- In: FAUPL, P. & FLÜGEL, H. W. (Eds.), Geodynamics of the Eastern Alps, 126 - 141, Wien (Deuticke).
- DECKER, K., PERESSON, H. & FAUPL, P. (1994): Die miozäne Tektonik der östlichen Kalkalpen: Kinematik, Paläostrukturen und Deformationsaufteilung während der "lateralen Extrusion" der Zentralalpen.- Jahrbuch der Geologischen Bundesanstalt, 137, 5-18, Wien.
- DIERSCHE, V. (1980): Die Radiolarite des Oberjura im Mittelabschnitt der Nördlichen Kalkalpen.- Geotektonische Forschungen, 58, 217 S., Stuttgart.
- FERNECK, F. A. (1962): Stratigraphie und Fazies im Gebiet der mittleren Saalach und des Reiteralm Gebirges: ein Beitrag zur Deckenfrage in den Berchtesgadener Alpen.- 107 S., Diss. LMU München, München
- FISCHER, A. G. (1965): Eine Lateralverschiebung in den Salzburger Kalkalpen.- Verhandlungen der Geologischen Bundesanstalt, 1965, 20-33, Wien.
- FORD, M., WILLIAMS, E. A., ARTONI, A., VERGES, J. & HARDY, S. (1997): Progressive evolution of a fault-related fold pair from growth strata geometries, Sant Llorens de Morunys, SE Pyrenees.- Journal of Structural Geology, 19, 413 - 441, Oxford.
- FRANK, W. & SCHLAGER, W. (2006): Jurassic strike slip versus subduction in the Eastern Alps.- Int. Jour. Earth Sci., 95, 431-450, Stuttgart.
- FROITZHEIM, N. & MANATSCHAL, G. (1996): Kinematics of Jurassic rifting, mantle exhumation, and passive-margin formation in the Austroalpine and Penninic nappes (eastern Switzerland).- Geological Society of America Bulletin, 108, 1120 - 1133, Boulder.
- GARRISON, R. E. & FISCHER, A. G. (1969): Deep water limestones and radiolarites of the Alpine Jurassic.- In: FRIEDMANN, G. M. (Eds.), Depositional environments in carbonate rocks – a symposium, 20-56, Tulsa (SEPM Spec. Publ. 14).
- GAWLICK, H.-J., AUBRECHT, R., SCHLAGINTWEIT, F., MISSONI, S. & PLASIENKA, D. (2015): Ophiolitic detritus in Kimmeridgian resedimented limestones and its provenance from an eroded obducted ophiolitic nappe stack south of the Northern Calcareous Alps (Austria).- Geologica Carpathica, 66, 473-487, Bratislava.
- GAWLICK, H.-J., FRISCH, W., VECSEI, A., STEIGER, T. & BÖHM, F. (1999): The change from rifting to thrusting in the Northern Calcareous Alps as recorded in Jurassic sediments.- Geologische Rundschau, 87, 644 - 657, Stuttgart.
- HAAS, J., KOVÁCS, S., KRYSTYN, L. & LEIN, R. (1995): Significance of Triassic facies zones in terrane reconstructions in the Alpine-North Pannonian domain.- Tectonophysics, 242, 19-40, Amsterdam.

- HAHN, F. F. (1910): Die Geologie der Kammerkehr-Sonntagshorngruppe, I. Teil.- Jahrbuch der k. k. Geologischen Reichsanstalt, 60, 311-419, Wien.
- HAHN, F. F. (1912): Versuch einer Gliederung der austroalpinen Masse westlich der österreichischen Traun.- Verhandlungen der Geologischen Reichsanstalt, 1912, 337-344, Wien.
- HAHN, F. F. (1913a): Geologie des oberen Saalachgebietes zwischen Lofer und Diesbachtal.- Jahrbuch der k. k. Geologischen Reichsanstalt, 63, 1-76, Wien.
- HAHN, F. F. (1913b): Grundzüge des Baues der nördlichen Kalkalpen zwischen Inn und Enns.- Mitteilungen der Österreichischen Geologischen Gesellschaft, 9, 374-500, Wien.
- HANDY, M. R., M. SCHMID, S., BOUSQUET, R., KISLING, E. & BERNOLLI, D. (2010): Reconciling plate-tectonic reconstructions of Alpine Tethys with the geological-geophysical record of spreading and subduction in the Alps.- Earth-Science Reviews, 102, 121-158, Amsterdam.
- HORNSTEINER, G. (1991): Die jurassische Entwicklung auf der Waidringer Steinplatte unter besonderer Berücksichtigung der Scheiblberg Schichten an der Typlokalität.- unpublished Diploma thesis Univ. Innsbruck, 219 S., Innsbruck.
- JACOBSHAGEN, V. & KOCH, K. E. (1959): Verkeilungen als Richtungsanzeiger an Überschiebungen.- Neues Jahrbuch für Geologie und Paläontologie, Monatshefte, 1959, 99-110, Stuttgart.
- KRAINER, K., MOSTLER, H. & HADITSCH, J. G. (1994): Jurassische Beckenbildung in den Nördlichen Kalkalpen bei Lofer (Salzburg) unter besonderer Berücksichtigung der Manganerzen-Genese.- Abhandlungen der Geologischen Bundesanstalt, 50, 257 - 293, Wien.
- LAVIER, L. L. & MANATSCHAL, G. (2006): A mechanism to thin the continental lithosphere at magma-poor margins.- Nature, 440, 324-328, London.
- LEIN, R., SUZUKI, H. & GAWLIK, H.-J. (2009): Die Obersee-Brekzie bei Lunz (Niederösterreich): Revision der Stratigraphie und des Komponentenbestandes.- In: BRYDA, G. (Eds.), Arbeitstagung Blatt 101 Eisenerz: Leoben, 204-210, Wien (Geologische Bundesanstalt).
- LINZER, H.-G., DECKER, K., PERESSON, H., DELL'MOUR, R. & FRISCH, W. (2002): Balancing lateral orogenic float of the Eastern Alps.- Tectonophysics, 354, 211-237, Amsterdam.
- LUKESCH, M. E. (2003): Die Geologie des Nordwest-Randes der Berchtesgadener Masse bei Lofer (Nördliche Kalkalpen) - Genese oberjurassischer Brekzien und das Westende der Saalachtal Störung.- unpublished Diploma thesis Univ. Innsbruck, 127 S., Innsbruck.
- MANDL, G. (2000): The Alpine sector of the Tethyan shelf - examples for Triassic to Jurassic sedimentation and deformation from the Northern Calcareous Alps.- Mitteilungen der Österreichischen Geologischen Gesellschaft, 92, 61-77, Wien.
- MANDL, G. W. (2013): Zur Geologie des Raumes Hüttenneckalm-Sandlingalm-Blaa-Alm (Salzkammergut, Österreich) mit kritischen Anmerkungen zur Sandlingalm-Formation.- Jahrbuch der Geologischen Bundesanstalt, 153, 33-74,
- MISSONI, S. & GAWLICK, H.-J. (2010): Evidence for Jurassic subduction from the Northern Calcareous Alps (Berchtesgaden; Austroalpine, Germany).- International Journal of Earth Sciences, 100, 1605-1631, Stuttgart.
- MOSNA, D. (2010): Die Lärchberg-Schichten im Gebiet des Gerhardsteins nahe Lofer - Dokumentation der Lärchberg-Schichten als Beitrag zur Interpretation der spätjurassischen Paläogeographie.- unpublished Diploma thesis Univ. Innsbruck, 120 S., Innsbruck.
- MOSTLER, H. & KRAINER, K. (1993): Neue Ophiuren aus liassischen Slope-Sedimenten der Nördlichen Kalkalpen in der Umgebung von Lofer (Salzburg).- Geologisch-Paläontologische Mitteilungen Innsbruck, 19, 19-47, Innsbruck.
- ORTNER, H. (2003): Cretaceous thrusting in the western part of the Northern Calcareous Alps (Austria) - evidences from synorogenic sedimentation and structural data.- Mitteilungen der Österreichischen Geologischen Gesellschaft, 94, 63-77, Wien.

- ORTNER, H. (2017a): Geometry of growth strata in wrench-dominated transpression: 3D-model of the Upper Jurassic Trattberg rise, Northern Calcareous Alps, Austria.- *Geophysical Research Abstracts*, 19, EGU2017-9222,
- ORTNER, H. (2017b): Tectonic maps in areas of deposition of exotic olistolithes – application to the Northern Calcareous Alps of Austria.- In: SARIC, K., PRELEVIC, D., SUDAR, M. & CVETKOVIC, V. (Eds.), 13th Workshop of Alpine Geological Studies, Zlatibor, Abstract volume, 79, Belgrade (Sapient Graphics).
- ORTNER, H., AICHHOLZER, S., ZERLAUTH, M., PILSER, R. & FÜGENSCHUH, B. (2015): Geometry, amount and sequence of thrusting in the Subalpine Molasse of Western Austria and Southern Germany, European Alps.- *Tectonics*, 34, 1-30, Hoboken.
- ORTNER, H., KOSITZ, A., WILLINGSHOFER, E. & SOKOUTIS, D. (2016): Geometry of growth strata in a transpressive fold belt in field and analogue model: Gosau Group at Muttekopf, Northern Calcareous Alps, Austria.- *Basin Research*, 28, 731–751, doi: 10.1111/bre.12129
- ORTNER, H., USTASZEWSKI, M. & RITTNER, M. (2008): Late Jurassic tectonics and sedimentation: breccias in the Unken syncline, central Northern Calcareous Alps.- *Swiss Journal of Geosciences*, 101, Supplement 1, S55-S71, Basel.
- PAVLIK, W. (2006): Provisorische Geologische Karte von Österreich, Blatt 92 - Lofer, GeoFAST 1:50.000.- Geologische Bundesanstalt, Wien.
- PERESSON, H. & DECKER, K. (1997): The Tertiary dynamics of the northern Eastern Alps (Austria): changing palaeostresses in a collisional plate boundary.- *Tectonophysics*, 272, 125 - 157, Amsterdam.
- PICOTTI, V. & COBIANCHI, M. (2017): Jurassic stratigraphy of the Belluno Basin and Friuli Platform: a perspective on far-field compression in the Adria passive margin.- *Swiss Journal of Geosciences*, 110, 833-850, Basel.
- PILLER, W. E., EGGER, H., ERHART, C. W., GROSS, M., HARZHAUSER, M., HUBMANN, B., VAN HUSEN, D., KRENMAYR, H.-G., KRYSYNSKI, L., LEIN, R., LUKENEDER, A., MANDL, G. W., RÖGL, F., ROETZEL, G., RUPP, C., SCHNABEL, W., SCHÖNLAUB, H.-P. S., H., WAGREICH, M. & WESSELY, G. (2004): Die stratigraphische Tabelle von Österreich 2004 (sedimentäre Schichtfolgen).- (Kommission für die paläontologische und stratigraphische Erforschung Österreichs der Österreichische Akademie der Wissenschaften und Österreichische Stratigraphische Kommission).
- PLÖCHINGER, B. (1953): Der Bau der südlichen Osterhorngruppe und die Thiton-Neokomtransgression.- *Jahrbuch der Geologischen Bundesanstalt*, 96, 257-273, Wien.
- RASSER, M. W., VASICEK, Z., SKUPIEN, P., LOBITZER, H. & BOOROVA, D. (2003): Die Schrambach-Formation an ihrer Typuslokalität (Unter-Kreide, Nördliche Kalkalpen, Salzburg): Lithostratigraphische Formalisierung und "historische" Irrtümer.- In: PILLER, W. E. (Eds.), *Stratigraphia Austriaca*, Schriftenreihe der Erdwissenschaftlichen Kommission, 16, 193-216, Wien (Österreichische Akademie der Wissenschaften).
- RATSCHBACHER, L., FRISCH, W., LINZER, G. & MERLE, O. (1991): Lateral extrusion in the Eastern Alps, Part 2: Structural analysis.- *Tectonics*, 10, 257 - 271, doi: 10.1029/90TC02623
- RECHES, Z. & DIETERICH, J. H. (1983): Faulting of rocks in three-dimensional strain fields. I. Failure of rocks in polyaxial, servo-controlled experiments.- *Tectonophysics*, 95, 111-132, Amsterdam.
- RITTNER, K. M. (2006): Geologie der östlichen Unkener Mulde am Kontakt zur Berchtesgadener Masse - Strukturgeologie und elektronische Verarbeitung geologischer Daten.- unpublished Diploma thesis Univ. Innsbruck, 104 S., Innsbruck.
- ROSENBERG, C. L., BRUN, J.-P., CAGNARD, F. & GAPAIS, D. (2007): Oblique indentation in the Eastern Alps: Insights from laboratory experiments.- *Tectonics*, 26, TC2003, Washington, D.C.
- SANDERS, D., LUKESCH, M., RASSER, M. & SKELTON, P. (2007): Shell beds of Diceratid rudists ahead of a low-energy gravelly beach (Thitonian, Northern Calcareous Alps, Austria): paleoecology and taphonomy.- *Austrian Journal of Earth Sciences*, 100, 186-199, Wien.
- SCHEIDLEDER, A., BOROVICZENY, F., GRAF, W., HOFMANN, T., MANDL, G. W., SCHUBERT, G., STICHLER, W., TRIMBORN, P. & KRALIK, M. (2001): Pilotprojekt "Karstwasser Dachstein": Band 2: Karsthydrologie und Kontaminationsrisiko von Quellen.- *Archiv für Lagerstättenforschung*, 21, 1-155,

- SCHLAGER, W. & SCHLAGER, M. (1973): Clastic sediments associated with radiolarites (Tauglbodenschichten, Upper Jurassic, Eastern Alps).- *Sedimentology*, 20, 65-89, Amsterdam.
- SCHMID, S. M., BERNOULLI, D., FÜGENSCHUH, B., MATENCO, L., SCHEFER, S., SCHUSTER, R., TISCHLER, M. & USTASZEWSKI, K. (2008): The Alpine-Carpathian-Dinaride-orogenic system: correlation and evolution of tectonic units.- *Swiss Journal of Geosciences*, 101, 139-183, Basel.
- SCHMID, S. M., FÜGENSCHUH, B., KISSLING, E. & SCHUSTER, R. (2004): Tectonic map and overall architecture of the Alpine orogen.- *Eclogae Geologicae Helvetiae*, 97, 93-117, Basel.
- SCHWEIGL, J. & NEUBAUER, F. (1997): Structural evolution of the central Northern Calcareous Alps: Significance for the Jurassic to Tertiary geodynamics of the Alps.- *Eclogae Geologicae Helvetiae*, 90, 1 - 19, Basel.
- SIEWERT, W. (1973): Zur Tektonik der nördlichen Ausläufer des Steinernen Meeres (Gebiet um den Hochkranz).- *Verhandlungen der Geologischen Bundesanstalt*, 1973, 255-265, Wien.
- STAMPFLI, G. M. & BOREL, G. D. (2002): A plate tectonic model for the Paleozoic and Mesozoic constrained by dynamic plate boundaries and restored synthetic oceanic isochrons.- *Earth and Planetary Science Letters*, 196, 17-33, Amsterdam.
- STEIGER, T. (1981): Kalkturbidite im Oberjura der Nördlichen Kalkalpen (Barmsteinkalke, Salzburg, Österreich).- *Facies*, 4, 215-348, Erlangen.
- TOLLMANN, A. (1969): Tektonische Karte der Nördlichen Kalkalpen, 2. Teil: Der Mittelabschnitt.- *Mitteilungen der Österreichischen Geologischen Gesellschaft*, 61 (1968), 214-181, Wien.
- TOLLMANN, A. (1976a): Analyse des klassischen nordalpinen Mesozoikums.- 580 S., Monographie der Nördlichen Kalkalpen, Teil II, Wien (Deuticke).
- TOLLMANN, A. (1976b): Der Bau der Nördlichen Kalkalpen.- 449 S., Monographie der Nördlichen Kalkalpen, Teil III, Wien (Deuticke).
- TOLLMANN, A. (1985): Geologie von Österreich, Band 2.- 710 S., Wien (Deuticke).
- TRÜMPY, R. (1988): A possible Jurassic-Cretaceous transform system in the Alps and the Carpathians.- *Geological Society of America Special Paper*, 218, 93-109, Boulder.
- VECSEI, A., FRISCH, W., PIRZER, M. & WETZEL, A. (1989): Origin and tectonic significance of radiolarian chert in the Austroalpine rifted continental margin.- In: HEIN, J. R. & OBRADOVIC, J. (Eds.), *Siliceous Deposits of the Tethys and Pacific Regions*, 65-80, New York (Springer).
- VORTISCH, W. (1931): Tektonik und Breccienbildung in der Kammerkehr-Sonntagshornguppe.- *Jahrbuch der Geologischen Bundesanstalt*, 80, 81-96, Wien.
- WÄCHTER, J. (1987): Jurassische Massflow- und Internbrekzien und ihr sedimentär-tektonisches Umfeld im mittleren Abschnitt der nördlichen Kalkalpen.- *Bochumer geol. und geotechn. Arbeiten*, 27, 239 S., Bochum.
- WEISSERT, H. J. & BERNOULLI, D. (1985): A transform margin in Mesozoic Tethys: evidence from the Swiss Alps.- *Geologische Rundschau*, 74, 665-679, Stuttgart.
- WOLFGRUBER, S. (2010): Die Lärchberg-Schichten im Gebiet des Gerhardsteins nahe Lofer - Untersuchung der Schwermineralspektren der Loferer Schichten als Grundlage für einen möglichen Beitrag zur spätjurassischen Paläogeographie.- unpublished Diploma thesis Univ. Innsbruck, 107 S., Innsbruck.



Field Trip Pre-EX-6

Paleogene Events in the sedimentary record of outcrops in Salzburg and eastern Bavaria

HANS EGGER¹, ALFRED UCHMAN²

¹ Geological Survey of Austria, Neulinggasse 38, 1030 Vienna, Austria. johann.egger@geologie.ac.at

² Institute of Geological Sciences, Jagiellonian University, Kraków, Poland. alfred.uchman@uj.edu.pl

Editorial note

With the exception of Stop 4 and additional information on Stop 1, this guidebook is a short version of the field trip guidebook for the “Climate and Biota of the Early Paleogene” Conference, held in Salzburg in June 2011. Bibliographic reference to this publication: Egger, H. (ed): Climate and Biota of the Early Paleogene, Field-Trip Guidebook, 5–8 June, Salzburg, Austria. Berichte der Geologischen Bundesanstalt. 86, 132pp. This publication can be downloaded from the webpage of the Geological Survey of Austria. The help of Markus Kogler in preparing the figures is gratefully acknowledged.

Introduction

Hans Egger

The Eastern Alps, a 500 km long segment of the Alpine fold-and-thrust belt, originate from the northwestern Tethyan realm. The modern structure of the Eastern Alps is the result of the convergence between the European and the Adriatic Plates (Fig. 1). Separation of these plates started by oblique rifting and spreading in the Permian and Triassic and continued during the Jurassic by the formation of oceanic lithosphere in the Penninic basin. The structural evolution of this basin was linked to the opening of the North Atlantic (e.g. Frisch, 1979; Stampfli et al., 2002). Due to the presence of lower Eocene deep-marine sedimentary rocks in the Penninic units, it is clear that the final closure of the Penninic Ocean did not occur before the Eocene (see Neubauer et al., 2000 for a review).

As a result of the oblique collision of the European and Adriatic plates the elimination of the Penninic Ocean started in the West and prograded continuously to the East. Thrusting in the Eastern Alps started at latest in the Middle Eocene whereas in the adjacent Western Carpathians the onset of thrust formation was around the Eocene-Oligocene boundary (see Decker & Peresson, 1996 for a review). In the Eastern Alps continuing convergence during the Miocene caused lateral tectonic escape of crustal wedges along strike slip faults, which strongly affected the nappe complex of the Eastern Alps. A recent review on the complicated structural development of the Eastern Alps is given by Brückl et al. (2010).

The northern rim of the Eastern Alps consists of detached Jurassic to Paleogene deposits, which tectonically overlie Oligocene to lower Miocene Molasse sediments. From north to south these thrust units originate from (1) the southern shelf of the European Plate (Helvetic nappe complex), (2) the adjacent passive continental margin (Ultrahelvetic nappe complex), (3) the abyssal Penninic Basin (Rhenodanubian nappe complex) and (4) the bathyal slope of the Adriatic Plate (nappe complex of the

Northern Calcareous Alps). Thrusting and wrenching from the Upper Eocene on destroyed the original configuration of these depositional areas and, therefore, the original palinspastic distance between the sedimentary environments of the studied sections is not known. During our field trip, Paleogene sections along a north-south transect within these four nappe complexes will be visited.

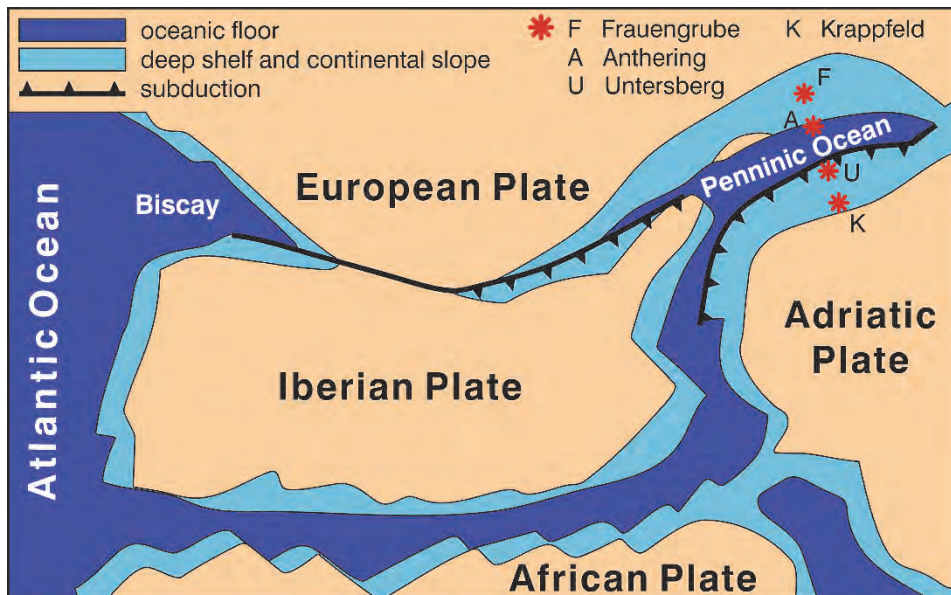


Fig. 1: Schematic paleogeographic map of the NW Tethys and neighbouring areas showing the location of the Alpine environmental areas in the early Paleogene /simplified and modified after Stampfli et al., 1998).

The shallow water sedimentary record of the **Helvetic shelf** is punctuated by a number of stratigraphic gaps, which become more pronounced in direction to the coast of the European continent in the north. So, in the North-Helvetic realm, Paleocene deposits are absent because there the basal Lutetian (calcareous nannoplankton Sub-Zone NP15a) of the Adelholzen beds (STOP 4) with an erosional unconformity overlies the Maastrichtian of the Gerhartsreith Formation (Fig. 3). The Adelholzen Beds (Schafhärtl, 1846) are an equivalent of the Bürgen Formation in Switzerland where an equivalent hiatus between the Cretaceous and the Eocene occurs (Menkeld-Gföllner, 1997). Basinward, this main hiatus is less extended and comprises only the uppermost Paleocene (upper part of Zone NP9) and the lowermost Eocene (Zones NP10 and NP 11 - Egger et al., 2009) in the southern part of the Helvetic shelf (Frauengrube section – STOP 3). A tectonically disturbed but continuous record exists across the K/Pg-boundary of the South-Helvetic domain (Kuhn & Weidich, 1987).

Towards south, the Helvetic shelf gradually passed into the **Ultrahelvetic continental slope**. Depending on the paleodepth at this slope, the pelitic rocks of the Ultrahelvetic unit display varying contents of carbonate. Since Prey (1952), these pelitic deposits were assembled to the informal lithostratigraphic unit Buntmergelserie, which was thought to comprise the Albian to upper Eocene. However, only very few small outcrops of Paleocene to middle Eocene have been recognized and most of them have unclear tectonic positions due to a strong tectonic overprint.

Recently, Egger & Mohamed (2010) recognized a stratigraphic contact between upper Maastrichtian (calcareous nannoplankton Zone CC25) Buntmergelserie and the uppermost Maastrichtian (CC26) to lowermost Eocene (NP11, NP12?) turbidite succession of the Achthal Formation at the Goppling section (STOP 5). This 350 m thick formation is interpreted as the infill of a slope basin, which formed

as a result of block faulting of the continental margin. Deposition took place partly below the planktonic foraminiferal lysocline and partly below the CCD.

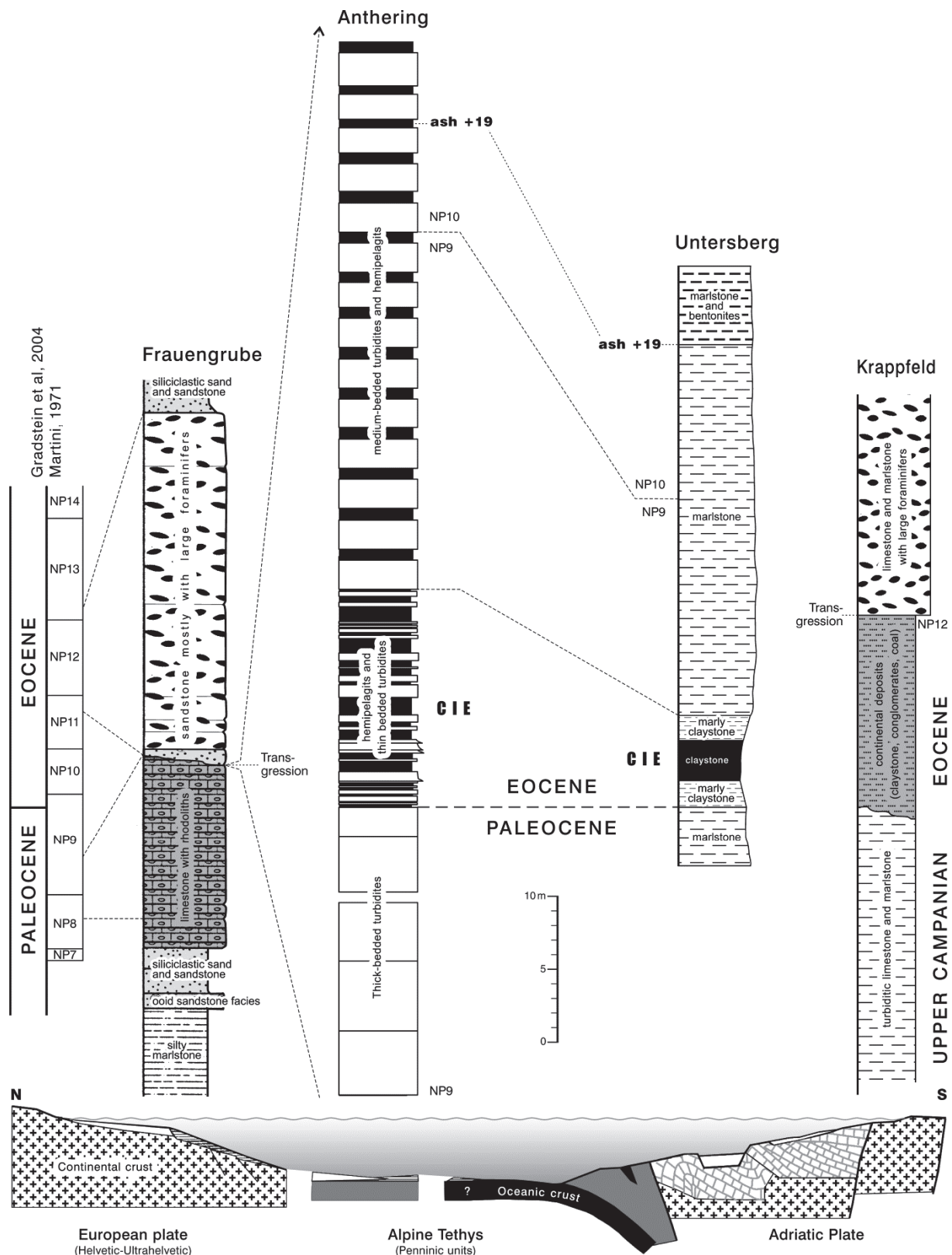


Fig. 2: Correlation and paleogeographic position of Paleogene sections across the Penninic Basin.



Fig. 3: Transgressional contact between the Gerhardtsreit Formation (Maastrichtian) and glauconitic sandstone of the Adelholzen Formation (Lutetian) at the Wimmern section (Bavaria).

Sedimentary successions rich in turbidites other than the Achthal Formation, are known from a number of Ultrahelvetic sites. In Vorarlberg (westernmost Austria), grey turbidites and hemipelagic marlstone (Kehlegg beds) were assigned to the Ultrahelvetic unit by Oberhauser (1991). The base of the Kehlegg beds is situated around the K/Pg-boundary. The unit comprises the entire Paleocene (Egger, unpublished) and its top is tectonically truncated by an overthrust. In a more southerly paleogeographic position on the slope, the deep-water system of the Feuerstätt thrust unit was deposited, exposed in Vorarlberg and southwestern Germany (see Schwerd and Risch, 1983 for a review). There, turbidites and intervening red claystone ("Rote Gschief-Schichten") of Paleocene and early Eocene age may represent the in-fills of adjacent slope basins at different paleodepths on the continental slope (Weidich and Schwerd, 1987; Schwerd, 1996). Farther to the east, in Lower Austria, Paleocene to Eocene turbidite successions associated with Buntmergelserie are reported by Prey (1957).

In summary, the style of early Paleogene turbidite sedimentation on the European continental margin seen at the Goppling section was not a unique phenomenon. Rather, it occurred at several sites along the strike of the Ultrahelvetic thrust unit in the Eastern Alps. Nevertheless, it is unlikely that these deposits originated from the same basin. Instead, a number of small sub-basins can be assumed, which due to the different subsidence histories and their different bathymetric positions, probably cannot be directly correlated.

The largely synchronous formation of different sub-basins along the strike of the Ultrahelvetic slope points to large-scale tectonic deformation of the continental margin, starting in the late Maastrichtian. The subsidence of intra-slope basins can be related to an extensional tectonic regime. However, for the same period, Nachtmann and Wagner (1987), Wessely (1987), and Ziegler et al. (2002) all document strong intra-plate compressional deformation of the foreland of the Eastern Alps. Together with the data from the Goppl section and other occurrences of the Ultrahelvetic unit, this implies that the southern European plate was simultaneously affected by extension and compression. Here, this style of deformation is typical for anastomosing strike-slip fault zones in convergent settings (e.g. Crowell, 1974).

The well-established contractional deformation event, which affected the European plate in Late Cretaceous times, was explained by two different models. In the first one, strike-slip faulting was driven by the oblique convergence of the European and African plates resulting in a dextral transpressional tectonic regime subsequently to the onset of the collision (Ziegler, 1987). In the second model, this deformation is seen as the result of an important change in relative motion between the European and African plates causing pinching of Europe's lithosphere between Africa and Baltica (Kley and Voigt, 2008). This model explains better than the collision model the uniform N to NE intraplate shortening of the European plate during the Late Cretaceous event and is also consistent with the NE-SW trending strike-slip faults, which affected the European margin and led to the formation of slope-basins.

Syndepositional faulting and the associated alteration in margin topography, changed sediment dispersal and accumulation not only on the slope but also in the adjacent "Rhenodanubian Flysch" of the **Penninic basin**. There, a dearth of turbidite sedimentation (=Strubach-Tonstein) has been recognized in the Paleocene of the Rhenodanubian Group (Egger, 1995). This was interpreted to be the result tectonic activity that caused a cut-off of the basin from its source areas (Egger et al., 2002). More precisely, the data presented suggest that the above mentioned structurally controlled slope-basins acted as sediment traps and prevented turbidity current by-pass to the main basin.

The Rhenodanubian Flyschzone constitutes an imbricated nappe complex trending parallel to the northern margin of the Eastern Alps. The deep-water sediments of Barremian to Ypresian age were formalized as Rhenodanubian Group (RG) by Egger and Schwerd (2008). The RG consists primarily of siliciclastic and calcareous turbidites but thin, hemipelagic claystone layers occur in all formations of the RG and indicate a deposition below the local calcite compensation depth, probably at palaeodepths >3000 m (Butt, 1981; Hesse, 1975). Paleocurrents and the pattern of sedimentation suggest that the deposition occurred on a flat, elongate, weakly inclined abyssal basin plain (Hesse, 1975, 1982). Compared to other turbidite basins, the depositional area of the Rhenodanubian Group is characterized by low sedimentation rates. An average sedimentation rate for the Cretaceous basin fill, incorporating both turbidites and hemipelagites, of only 25 mm kyr⁻¹ has been calculated (Egger & Schwerd, 2008).

Lithostratigraphic classification of the Paleogene deposits of the Rhenodanubian Flysch has been proposed by Egger (1995) who distinguished three distinct lithological units in the area of Salzburg. In the upper Maastrichtian and Danian the Acharting Member of the Altlengbach Formation is characterized by thin- to medium-bedded turbidites, which display base-truncated as well as complete Bouma sequences. Usually the upper part of the Bouma sequences consist of medium-grey clayey marl which represents c. 35 % of this member whereas the percentage of intervening green coloured hemipelagic shale layers is less than 15 %. A distinct feature of this turbidite facies is the intercalation

of thick-bedded and coarse grained sandstones with high amounts of mica and quartz. These are marker beds for mapping the Altengbach Formation. Calcareous nannoplankton zone NP3 was found in a sequence of very thin-bedded and fine-grained turbidites. Further up-section, hemipelagic claystone (Strubach Tonstein) becomes the dominant rock-type suggesting starvation of turbidite sedimentation. This claystone-rich interval is regarded as part of the Acharting Member.

The lower boundary of the 50 m thick Strubach Tonstein is within Zone NP3. New increased input of turbiditic material started within nannozone NP8 and continued until the upper part of zone NP10. In Zone NP8 and in the lower part of Zone NP9 the facies is very similar to that of the Danian part. In the upper part of zone NP9 graded silty marls of the Anthering Formation become the predominant rock type at the expense of sandstones and siltstones. The base of the Anthering Formation is at the P/E-boundary, which is characterized by the common occurrence of hemipelagic claystone.

The rate of hemipelagic sedimentation in the Paleocene can be calculated using the Strubach Tonstein, which was deposited during a period of about 6 my between calcareous nannoplankton Zones NP3 and NP8. Excluding the turbidites the rate of hemipelagic sedimentation has been calculated as ca. 8 mmky⁻¹. Similar values (7 mmky⁻¹ resp. 9 mmky⁻¹) were assessed for the middle and upper part of Zone NP10, whereas a hemipelagic sedimentation rate of 49 mmky⁻¹ has been calculated for the Carbon Isotope Event (CIE)-interval at the Paleocene/Eocene-boundary (Egger et al., 2003). From this it can be summarized that in the Penninic basin the CIE was associated with an increase in the sedimentation rate of siliciclastic hemipelagic material by a factor of six.

In general, the input of terrestrially derived material into the basins increases during episodes of low sea-level as a result of enhanced topographical relief. In the Anthering section, the thickest turbidites of the Thanetian and Ypresian occur in the uppermost 13 m of the Thanetian (Egger et al., 2009). This suggests an episode of massive hinterland erosion, indicating a sea-level drop just prior to the onset of the CIE. This is consistent with data from the Atlantic region (Heilmann-Clausen, 1995; Knox, 1998; Steurbaut et al., 2003; Pujalte and Schmitz, 2006; Schmitz and Pujalte, 2007). The synchronicity of this sea-level drop in the Atlantic and Tethys regions indicates a eustatic fluctuation. Starting with the onset of the CIE, mainly fine-grained suspended material came into the basin and caused a strong increase in hemipelagic sedimentation rates. Such an increase associated with decreasing grain-sizes has been reported from P/E-boundary sections elsewhere and interpreted as an effect of a climate change at the level of the CIE, affecting the hydrological cycle and erosion (Schmitz et al., 2001).

In the lowermost Eocene of the eastern Alps (sub-Zone NP10a) twenty-three layers of altered volcanic ash (bentonites) originating from the North Atlantic Igneous Province have been recorded in lower Eocene deposits (calcareous nannoplankton Sub-Zone NP10a – STOP 2) at Anthering, about 1,900 km away from the source area (Egger et al., 2000). The Austrian bentonites are distal equivalents of the “main ash-phase” in Denmark and the North Sea basin (Fig. 4). The total eruption volume of this series has been calculated as 21,000 km³, which occurred during 600,000 years (Egger and Brückl, 2006). The most powerful single eruption of this series took place 54.0 million years ago (Ma) and ejected ca. 1,200 km³ of ash material which makes it one of the largest pyroclastic eruptions in geological history. The clustering of eruptions must have significantly affected the incoming solar radiation in the early Eocene by the continuous production of stratospheric dust and aerosol clouds. This hypothesis is corroborated by oxygen isotope values which indicate a global decrease of sea surface temperatures between 1–2°C during this major phase of explosive volcanism.

Equivalents of these bentonites were found also in the sedimentary record of the northern Adriatic Plate within the succession of the Northern Calcareous Alps at Untersberg (STOP 1, Egger et al., 1995) and Gams (Egger et al., 2004). The Cretaceous to Paleogene deposits of the Adriatic Plate lithostratigraphically are formalized as Gosau Group. This group comprises mainly siliciclastic and mixed siliciclastic-carbonate strata deposited after Early Cretaceous thrusting. The Gosau Group of the Northern Calcareous Alps can be divided into two parts – a lower part consisting of terrestrial and shallow-water sediments, including bauxites, coal seams, rudist biostromes, and several key stratigraphic horizons rich in ammonites and inoceramids (Lower Gosau Subgroup, Turonian to lower Campanian), and an upper part, comprising deep-water marlstone, mudstone and turbidites (Upper Gosau Subgroup, upper Campanian to Pribonian). Deposition of the Gosau Group was the result of transtension, followed by rapid subsidence into deep-water environments due to subduction and tectonic erosion at the front of the Adriatic Plate (Wagreich, 1993).

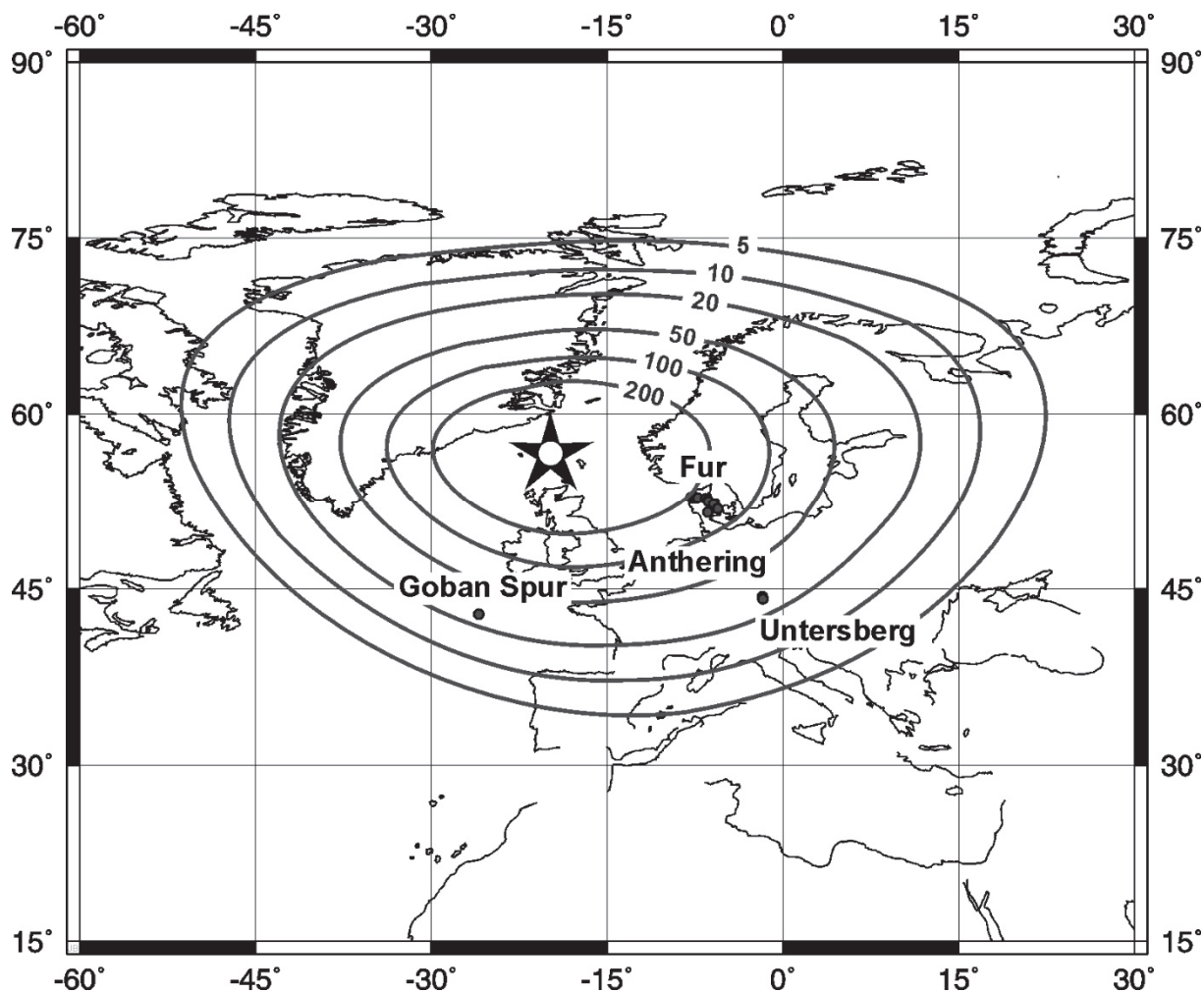


Fig. 4: Map showing the plate tectonic situation at 54 Ma (rotated present day shore lines), the rotated locations where layer +19 was found (solid spheres and locality names), and elliptical isopachs of layer +19 (grey contours, tephra thicknesses in mm) with assumed NAIP-source (star) at one focus.

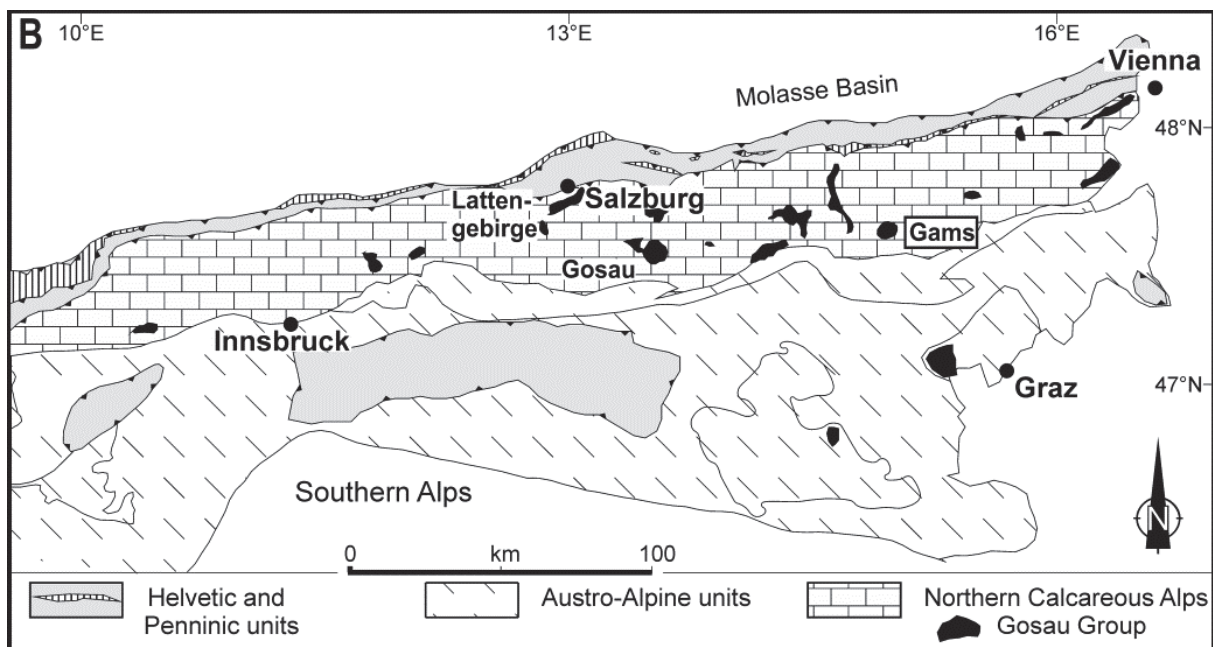


Fig. 5: Location of Gosau deposits in the Eastern Alps.

The Cretaceous/Paleogene-boundary has been studied in five sections of the Nierental Formation of the Upper Gosau Subgroup of the Northern Calcareous Alps (Fig. 5). The first K/Pg boundary in the region was discovered in the *Wasserfallgraben section* of the Lattengebirge in Bavaria (Herm et al. 1981). Perch-Nielsen et al. (1982) reported on biostratigraphical and geochemical results, and Graup and Spettel (1989) measured bulk Ir contents of 4-5 ppb in the boundary clay from this section. The second K/Pg boundary site was identified in the *Elendgraben section* near the village of Gosau in Salzburg (Preisinger et al. 1986; Stradner et al. 1987). The boundary is marked by a 2-4 mm thick yellowish clay layer, which contains up to 14.5 ppb iridium. The third K/Pg boundary site was recognized in the *Knappengraben section* at Gams (Stradner et al. 1987). Again, the boundary clay is of light yellow color and contains up to 7 ppb iridium. Lahodinsky (1988) studied the lithology of the Knappengraben and Elendgraben sections and interpreted their sedimentological and geochemical features as the result of extensive volcanic eruptions. Recently, Grachev et al. (2005, 2007, 2008) followed this interpretation. The fourth K/Pg boundary site has been described at the *Rotwandgraben section* also near the village of Gosau, about 2.5 km to the southeast of the Elendgraben section (Peryt et al. 1993, 1997). The maximum Ir content in the boundary clay has been determined to be 7 ppb.

In the Northern Calcareous Alps, Paleocene/Eocene (P/E)-boundary sections were studied at Untersberg near Salzburg (Egger et al., 2005) and Gams in Styria (Egger et al., 2009; Wagreich et al., 2011). At the Untersberg section the P/E-boundary is characterized by grey and red claystone intercalated into the dominating marlstone of the succession. At its top, the claystone displays a gradual increase in calcium carbonate contents. This transition zone from the red claystone to the overlying grey marlstone indicates a deposition within the lysocline. The gradual change of carbonate content within the transition zones suggests a slow shift of the level of the lysocline and CCD at the end of the CIE and has been described also from other sections (e.g. Zachos et al., 2005).

Like on the Helvetic shelf in the north of the Penninic basin (see above), a major stratigraphic gap exists in the sedimentary record of the **shelf of the Adriatic plate** at the southern rim of the basin. Lower Eocene deposits rest with an erosional unconformity on Upper Campanian marlstone of the *Tranolithus phacelosus* Zone (Sub-Zone CC23a). In the Pemberger quarry (unfortunately, this outcrop

was destroyed in 2011), from the base of the marine deposits *Assilina placentula*, *Nummulites burdigalensis kuepperi*, *Nummulites increscens*, and *Nummulites bearnensis* were described (Schaub, 1981; Hillebrandt, 1993). This fauna is indicative of the lower part of shallow benthic zone SBZ10, which has been correlated with calcareous nannoplankton zone NP12 (Serra-Kiel et al., 1998).

Due to their similar stratigraphic positions, Egger et al. (2009) assumed that the Ypresian transgressions at the shelves of the European and Adriatic Plates originated from the same eustatic event, which was the highstand of the TA2 supercycle in the global sea-level curve (Haq et al., 1987). At the Adriatic Plate, at the base of the marine transgression, black shales occur containing a rich and well preserved tropical palynoflora, indicating *Nypa*-dominated mangrove type forests, which reflect the early Eocene climate optimum (Hofmann et al., 2011). The onset of this episode of tropical climate was near the top of magnetic Chron 24, which coincides with the NP11/NP12 zonal boundary (Collinson, 2000; Gradstein et al., 2004).

The youngest deposits of the Gosau Group at Krappfeld are of Lutetian age. Hillebrandt (1993) reported both *Nummulites hilarionis* and *Nummulites boussaci*, which indicate shallow benthic zone SBZ14, and *Nummulites millecaput*, which is indicative for shallow benthic zone SBZ15. These foraminiferal zones can be correlated with the upper part of calcareous nannoplankton Zone NP15 and the lower part of Zone NP16 (Serra-Kiel et al., 1998).

Stop 1 Untersberg Section near Fürstenbrunn

Hans Egger, Alfred Uchman

Topic: Paleocene/Eocene-boundary and lower Eocene bentonites section in bathyal marlstone and claystone

Tectonic unit: Northern Calcareous Alps (Adriatic Plate)

Lithostratigraphic unit: Gosau Group, Nierental Formation

Chronostratigraphic units: Upper Paleocene to Lower Eocene

Biostratigraphy: Calcareous Nannoplankton Zones NP9 and NP10a; Planktonic Foraminifera Zones P5 to E3

Location: Tributary of the Kühlbach near Fürstenbrunn (Fig. 6B)

Coordinates: 47° 44' 19" N, 012° 59' 04" E

References: Egger et al. (2005), Egger & Brückl (2006), Hillebrandt (1962), Hagn (1981)

Stop 1a: Paleocene/Eocene-boundary

From the bus stop it is a 10 minute downhill walk through the forest (no trail!) to reach the outcrops, which are located along the course of a creek. Estimated duration of the stop is 1.5 hours.

The Paleogene deposits of the Untersberg region were examined by von Hillebrandt (1962 and in Hagn, 1982. The more than 1000 m thick Paleogene succession of the Untersberg area consists predominantly of marlstone displaying carbonate contents between 40wt% and 50wt%. Abundant planktonic foraminifera and calcareous nannoplankton are the main source of the carbonate. Von Hillebrandt (1962) already recognized the importance of the benthic foraminiferal extinction at the end of the Paleocene and Egger et al. (2005) re-examined this outcrop. However, at that time the exposure was worse and only part of the CIE-interval was outcropping. In 2010, a flood event due to torrential rain significantly improved the outcrop situation and revealed also minor faults along the dipping planes.

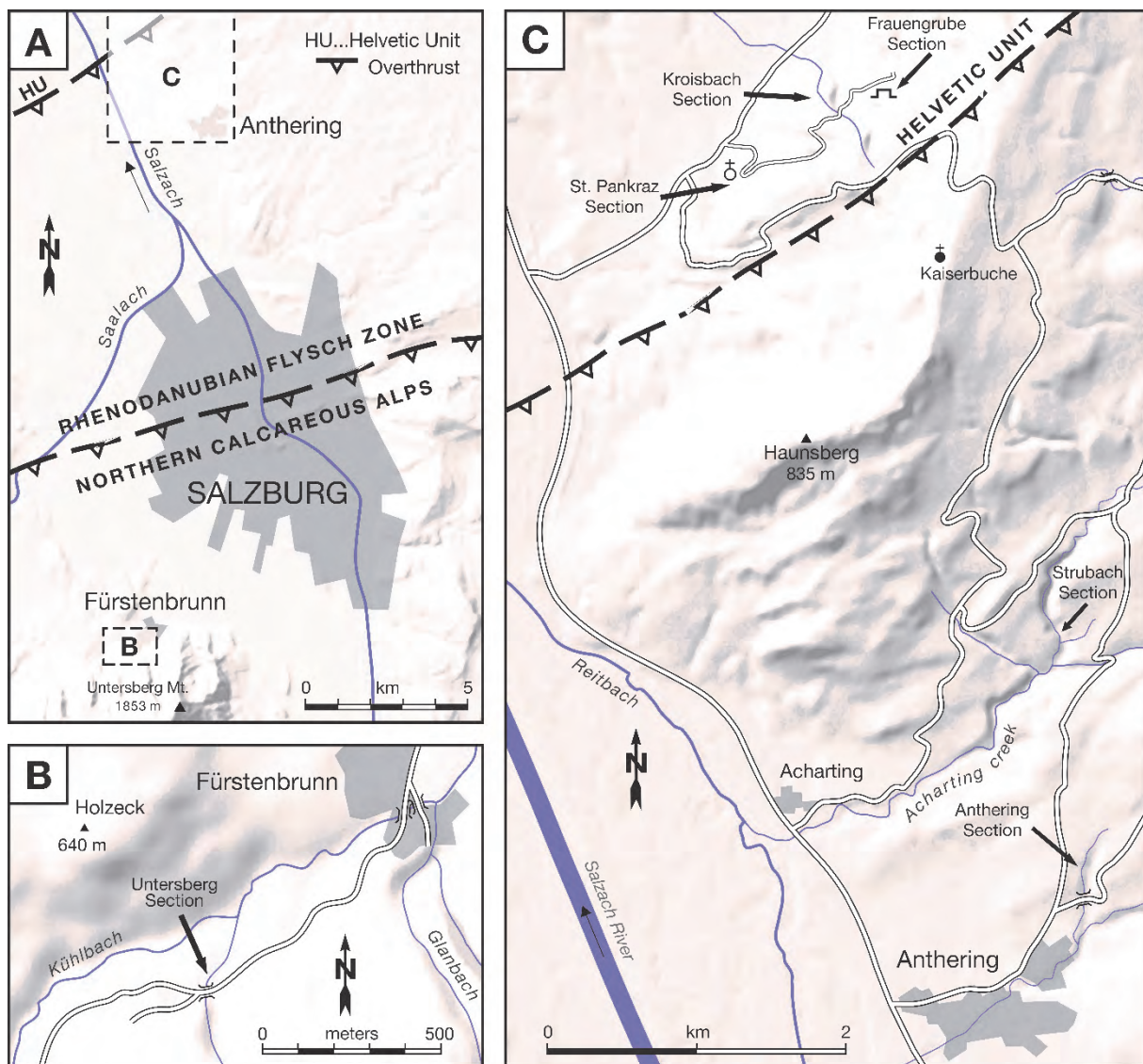


Fig. 6: Route map for outcrops 1 – 3 of the field trip.



Fig. 7: Photograph of the outcrop 1a at Untersberg showing the CIE-interval.

At the base of the new outcrop (Fig. 7) grey marlstone shows a sharp contact to grey claystone, which is overlain by red claystone. The claystone at the P/E-boundary indicates a deposition below the CCD. Excluding the carbonate content, the mean percentages of the siliciclastic components are almost identical below and above the CIE-interval: 16.3% quartz and feldspar and 83.7% clay minerals from the interval above the CIE and 16.6% quartz and feldspar and 83.4% clayminerals below the CIE. However, within the CIE-interval the mean percentage of quartz and feldspar is 24.8%, which is equivalent to an increase of 49% in relation to the other parts of the section.

The clay mineral assemblage at Untersberg is strongly dominated by smectite (72wt%), followed by illite (18wt%), kaolinite (6wt%) and chlorite (4wt%) (Fig. 8). The abundance of smectite throughout the studied section, together with the absence of mixed-layers, indicates that the rocks of the Untersberg section were not affected by deep-burial diagenesis. Consequently, diagenetic effects on the composition of clay mineral assemblages can be ruled out.

At its top, this claystone displays a gradual increase in calcium carbonate contents (Fig. 9) already documented by Egger et al. (2005). This transition zone to the overlying grey marlstone indicates a deposition within the lysocline, which is the water depth where carbonate dissolution rates are greatly accelerated (Berger, 1970). The gradual change of carbonate content within the transition zones suggests a slow shift of the level of the lysocline and CCD at the end of the CIE and has been described also from sections elsewhere (Zachos et al., 2005).

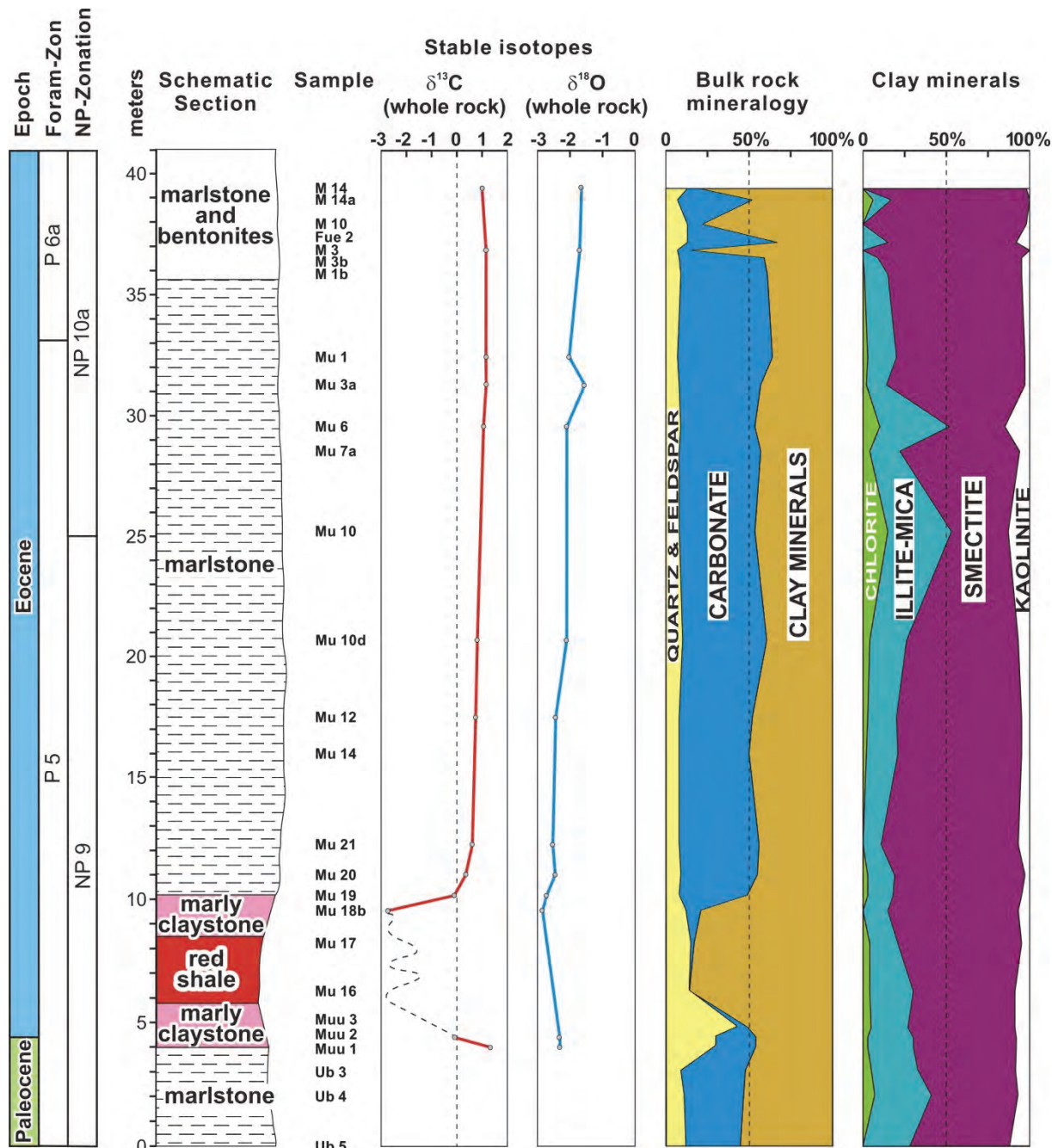


Fig. 8: Carbon isotope values, bulk rock mineralogy, and composition of clay mineral assemblages across the Paleocene–Eocene boundary.

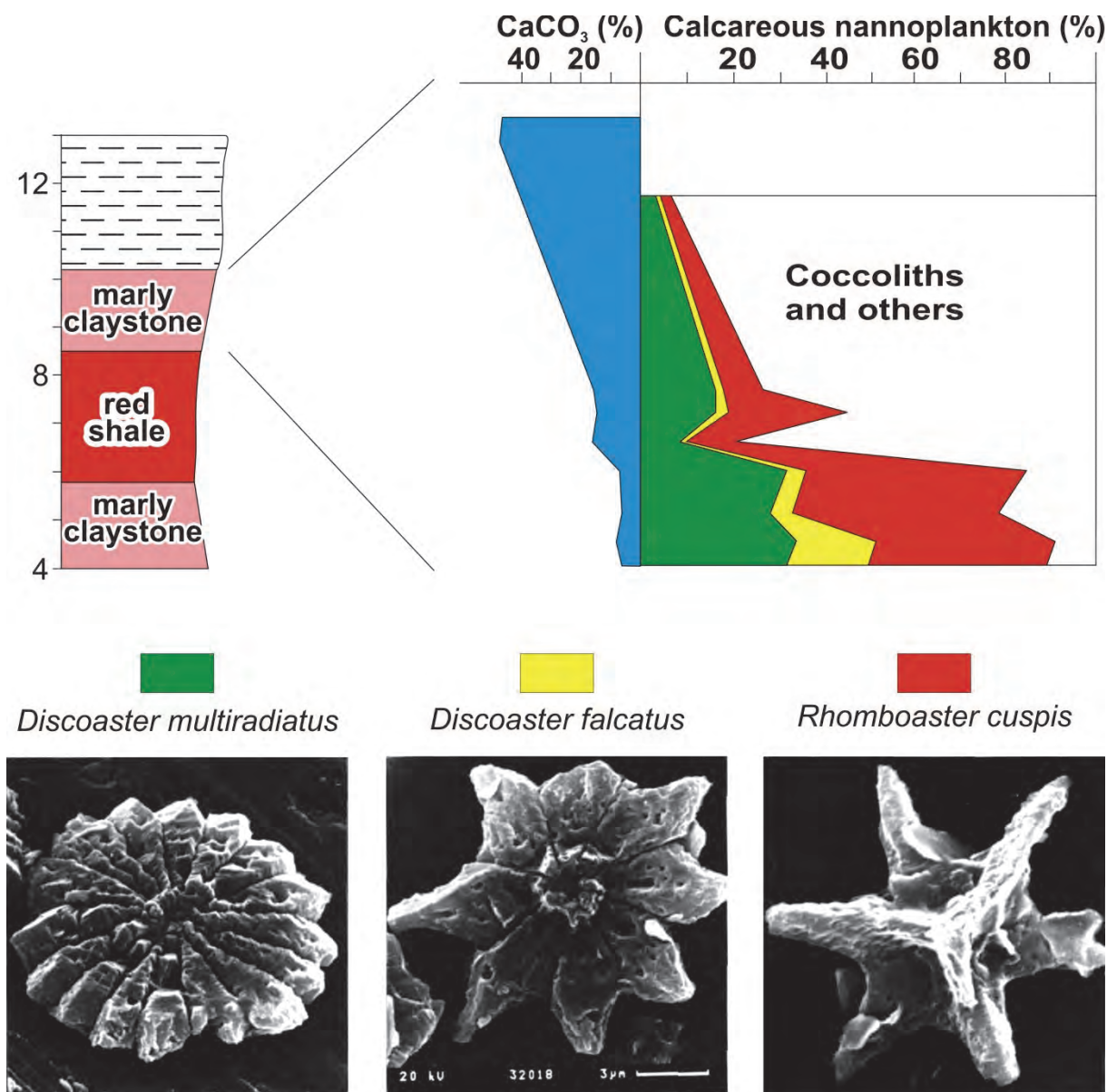


Fig. 9: Percentages of *Discoaster multiradiatus*, *Discoaster falcatus*, and *Rhomboaster cuspis* in the calcareous nannoplankton assemblages and calcium carbonate percentages at the top of the CIE-interval (scale bar represents 3 μm for all photographs).

Calcareous nannoplankton

Calcareous nannofossils were found in the marlstone and in the transition zones (marly claystone) between the marlstone and the shale. They are abundant (> 30 specimens per field of view) in the samples from the marlstone, whereas their abundance is low (< 10 specimens per field of view) in the samples from the transition zones. The preservation of nannofossils is moderate in the marlstone and poor in the transition zone according to the classification of Steinmetz (1979). In the moderately preserved samples the majority of the specimens are slightly etched but all taxa can be easily identified and diversity is about 16 species per sample on average. In the poorly preserved samples, the majority of specimens are deeply etched, identification of taxa is difficult and the diversity is only about 6 species per sample.

Reworked specimens are present in the marlstone samples, with rare Cretaceous species appearing (less than 1% of the nannofossil assemblage). Reworking has affected mainly Upper Cretaceous deposits, indicated by the occurrences of *Micula decussata*, *Prediscosphaera cretacea*, *Lucianorhabdus cayeuxii*, *Broinsonia parca*, *Ceratolithoides aculeus*, *Uniplanarius trifidus* and *Arkhangelskiella cymbiformis*. In one sample (M3b) typical Lower Cretaceous species (*Micrantonolithus hoschulzii* and *Nannoconus steinmannii*) were also found. However, the relatively common *Watznaueria barnesae* specimens in most samples may in part also originate from Lower Cretaceous deposits, as this species is abundant throughout the entire Cretaceous.

The Paleogene nannoflora is dominated by *Coccolithus pelagicus*, which usually accounts for about 90% of the nannoplankton assemblages, with the exception of the poorly preserved assemblages of the CIE-interval. *Discoaster multiradiatus*, the index species of Zone NP9, is another common species and occurs in all samples. Species of the stratigraphically important genus *Fasciculithus* are rare in the Untersberg section, except in the samples from below the CIE. *Scapholithus apertus* is the only species which becomes extinct at the Palaeocene-Eocene boundary of the Untersberg section.

The first specimens of the genus *Rhomboaster* occur just below the base of the CIE. There, short-armed specimens of *Rhomboaster cuspis* are exceedingly rare. In contrast, in the samples from the top of the CIE-interval *Rhomboaster cuspis* is the dominant species (up to 49% of the assemblages) followed by *Discoaster multiradiatus* and *Discoaster falcatus* and *Discoaster araneus*. In other Tethyan sections *Discoaster anartios* (Bybell and Self-Trail, 1994) co-occurs with *Discoaster araneus*; however, this species has not been found at Untersberg. Coccoliths are absent or extremely rare in this CIE-assemblage.

The unusual composition of the nannoplankton assemblage of the marly claystone at the top of the CIE-interval is an effect of carbonate dissolution because, synchronously with increasing carbonate content, the calcareous nannoplankton shows better preservation and a higher diversity (Fig. 9). The species diversity in nannoplankton assemblages is, to large extent, controlled by selective dissolution of skeletal elements. Bukry (1971) recognized that *Discoaster* is the most dissolution-resistant genus among the Cenozoic genera, followed by the genus *Coccolithus*. At Untersberg, the high percentages of *Rhomboaster* in the transition zone assemblages are most probably an effect of selective dissolution, indicating that *Rhomboaster* has a similar resistance to dissolution as *Discoaster*.

Foraminifera

Planktonic and benthic foraminifera are very abundant in most of the studied samples, although, as a result of carbonate dissolution, their preservation is poor across the CIE-interval. There, the assemblages are strongly dominated by agglutinating taxa. A specific determination was often difficult to make as many planktonic foraminifera specimens are corroded or deformed. For this reason no quantitative analysis of the foraminifera fauna was conducted, despite recording 191 different taxa in 19 samples, excluding species reworked from the Upper Cretaceous and Lower Paleocene (mainly Danian). The planktonic foraminiferal biozonation follows the criteria of Berggren and Pearson (2005).

Zone P5 (*Morozovella velascoensis* Partial-range Zone), the uppermost zone in the Paleocene, is defined by the highest occurrence (HO) of *Globanomalina pseudomenardii* and the lowest occurrence (LO) of *Acarinina sibaiyaensis*. At Untersberg, only reworked specimens of *G. pseudomenardii* occur, whereas *A. sibaiyaensis* is absent and has not been found in Eastern Alpine sections till now. The assignment of the lowermost part of the studied section to Zone P5 is due to the occurrence of

Morozovella subbotinae, which has a stratigraphic range from Zone P5 to Zone E5. In this part of the section also *M. aequa* and *M. gracilis* occur.

Due to the scarcity of planktonic foraminifera in the claystone of the CIE-interval no zonal attribution was possible. In the overlying marlstone (sample MU 19/97) *Pseudohastigerina wilcoxensis* was found, indicating Zone E2 (*Pseudohastigerina wilcoxensis/Morozovella velascoensis* Concurrent-range Zone). This zone is defined as the interval between the lower occurrence (LO) of *P. wilcoxensis* and the highest occurrence (HO) of *M. velascoensis*.

M. velascoensis has its HO in sample MU 10d/97. Further up-section, rare specimens of this species (sample MU 6/97) are considered to be reworked. The LO of *Morozovella edgari* is used to assign the highest part of the section to Zone E3 (*Morozovella marginodentata* Partial-range Zone). This zone is defined by the HO of *M. velascoensis* and the LO of *M. formosa*, however, the latter species does not occur in our samples.

The distribution of calcareous benthic foraminifera is similar to those of other deep-water sections (see Thomas, 1998, for a review). *Gavelinella cf. beccariiformis* has its HO at the onset of the CIE. The post-extinction calcareous benthic foraminifera assemblages are dominated by *Nuttalides truempyi* (very small specimens), *Abyssamina poagi*, *Anomalinoides nobilis*, *A. praeacutus*, *Oridorsalis spp.* and a number of pleurostomellids (e.g. *Ellipsoglandulina*, *Ellipsoidella*, *Ellipsopolymorpha*, *Nodosarella*, *Pleurostomella*). This assemblage is typical of lower bathyal to abyssal environments (van Morkhoven et al., 1986). For example, *Abyssamina poagi* occurs between 1700 m and 4000 m depth, and *Oridorsalis lotus* indicates a depth of between 800 m and 1900 m. This suggests a palaeodepth of about 2000 m (lower bathyal) for the deposition of Untersberg section.

The agglutinating foraminiferal fauna consists of 68 species, 25 of which (37% of the entire fauna) occur exclusively at the base of the succession and end within the CIE-interval. These species are *Ammodiscus cretaceus*, *Aschemocella carpathica*, *A. grandis*, *Bathysiphon? annulatus*, *Caudammina arenacea*, *C. excelsa*, *C. ovulum*, *Dorothia beloides*, *Glomospira diffundens*, *G. glomerata*, *G. serpens*, *Haplophragmoides walteri*, *Hormosinella distans*, *Hyperammina lineariformis*, *Karrerulina horrida*, *Psammotodendron? gvidoensis*, *Psammosiphonella sp.*, *Remesella varians*, *Rzehakina fissistomata*, *Saccamina grzybowskii*, *Silicobathysiphon sp.*, *Subrheophax pseudoscalaris*, *S. splendidus*, *Trochamminoides folius*, and *T. subcoronatus*. In the upper part of the succession the typical assemblage with *Paratrocchaminoides* and *Trochamminoides* has disappeared, but *Recurvooides gerrochi* and *R. pseudoregularis* are still common. Within the CIE-interval the agglutinated assemblage is dominated by *Glomospira* spp. Such assemblages, similar to the „Biofacies B“ assemblage or to the „*Glomospira* event“ occur in the Cretaceous and in the Early Eocene of the North Atlantic and Tethys (comp. Kuhnt et al., 1989; Kaminski et al., 1996).

Radiolarians

Occurrences of radiolarians are restricted to the lower part of the section, where they are abundant from samples Mu18a to Mu14 and common in samples Muu2, Mu10, and Mu10d. In the finest grained sieve-residue of sample Mu19, radiolarians are the dominant component. The radiolarians are all spheroidal spumellarians, but are taxonomically indeterminable, since their siliceous skeletons are poorly preserved, due to their replacement by smectite. The abundance of siliceous plankton indicates high nutrient levels in oceanic surface waters in the basal Eocene. A coeval increase in both sedimentation rates and the amounts of terrestrially derived quartz and feldspar suggests that this

high primary productivity was the result of enhanced continental run-off. No radiolarians were found further up-section in outcrop 1b.

Trace fossils

The trace fossil assemblage is low diverse and consists only of four ichnotaxa: *Chondrites* isp., *Planolites* isp., *Thalassinoides* isp., and *Zoophycos* isp. They are mostly visible in cross section what precludes determinations at the ichnospecies level.

The trace fossil distribution pattern of the studied section shows a clear three-fold subdivision. The highest abundance and diversity of trace fossils was recognized in the lower part of the section (0 - 2.40 m), where *Chondrites* isp., *Planolites* isp., *Thalassinoides* isp., *Zoophycos* isp., and large unidentified burrows occur. All ichnotaxa show a more or less continuous record, with the exception of *Zoophycos* and the undeterminable large burrows, which are restricted to a few horizons. Disrupted primary lamination is locally recognized but the major part consists of grey and greenish grey mudstone with occasional red coloured spots and layers.

The middle part of the section (2.40–4 m) is characterized by the presence of primary lamination in a more or less continuous 1.5 m-thick interval, with only very scarce trace fossils. This interval mainly consists of non-calcareous red mudstones, locally with green spots and laminae. Around 3.1 m from the base, primary lamination is undisturbed, while in the remaining part of the interval the primary lamination is disrupted.

The upper part of the section shows less abundant and less diverse trace fossil assemblage than the lower part. *Chondrites* shows a more or less continuous record, and *Thalassinoides* is common, while *Planolites* occurs only sporadically, and *Zoophycos* is absent. One thin layer displays primary lamination.

The trace fossil assemblage is typical of the *Zoophycos* ichnofacies, which is depauperated in some section segments. The *Zoophycos* ichnofacies in Palaeogene is typical for lower bathyal-abyssal depths and low-energy fine-grained facies.

The study of bioturbational structures suggests a temporarily complete extinction of the macrobenthic community during the Paleocene-Eocene transition. Similar observations were made by Nicolo et al. (2010) in the South Pacific and Rodriguez-Tovar et al. (2011) at the Zumaia section at the Bay of Biscay. Both publications explain the severe crisis of benthic communities as a result of oxygen depleted bottom waters. However, the P/E-boundary at the Untersberg and Zumaia sections manifests as a red claystone horizon deposited in an oxic environment. Several factors can be invoked to explain this situation. Extreme oligotrophy on the sea floor can be considered when temperature of deep waters increased by at least few degrees during Paleocene-Eocene transition (e.g. Bowen et al., 2006). The waters can be dense and saline (Braas et al., 1982). Moreover, methane which was released from methane clathrates after the increase in temperature (see Dickens, 2000) might saturate the pore waters and prevent burrowing by macroorganisms. It is an open question, if one of these factors or their combination stopped bioturbation.

Stop 1b: Volcanic ash-layers in the Lower Eocene

Hans Egger

Within grey marlstone (calcareous nannoplankton sub-Zone NP10a; planktonic foraminifera Zone E3) thirteen light yellowish layers consisting essentially of smectite were found. These 0.2 cm to 3 cm thick bentonite layers are interpreted as volcanic ashes. No bentonites were found in either the lower part of zone NP9 or in the overlying sub-zone NP10b, which are exposed in other outcrops of the area. The occurrence of bentonites is therefore exclusively restricted to sub-zone NP10a.

Due to their complete conversion to smectitic clay the original chemical composition of the bentonites must have strongly changed. Consequently, only the immobile elements have been used to assess the composition of the original magma (Winchester and Floyd, 1977). The immobile element contents of most of these altered ash layers show very little variation: Nb 28.3 ± 4.7 ppm, Zr 259 ± 104 ppm, Y 25.0 ± 9.5 ppm, and TiO₂ 4.82 ± 0.7 wt.% (see Fig. 10).

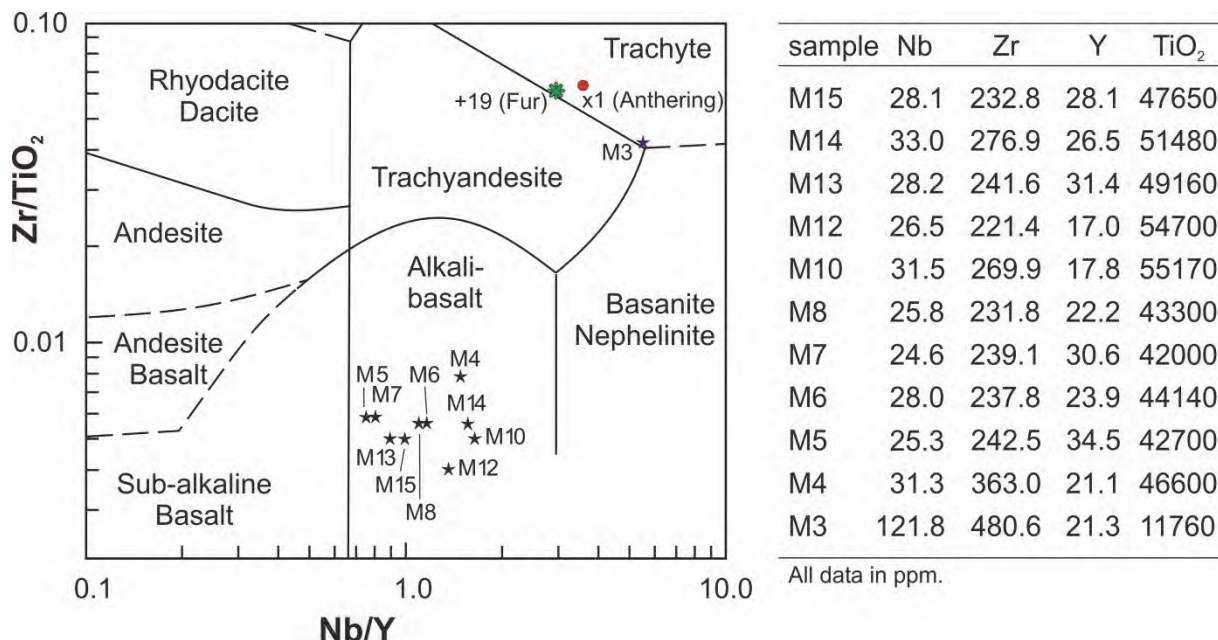


Fig. 10: Magma composition of different ash-layers by means of immobile element distribution (after Winchester and Floyd, 1977). For comparison, sample +19 from the Danish Fur Formation and sample X1, from the Austrian Anthering Formation, are plotted (from Egger et al., 2000).

These samples plot in the discrimination diagram of different magma sequences in the field of alkali-basalts. Basaltic ashes are rare in the geological record as the generation of basaltic pyroclastics requires an interaction between basaltic lavas and meteoritic water (see Heister et al., 2001, for a review). Layer M3 (Figure 10) has a totally different composition with highly enriched Nb and Zr, equal Y, and depleted TiO₂ compared to the other bentonites. It is the oldest and thickest layer of the ash-series and plots at the border of trachyte and trachy-andesite.

The biostratigraphical and geochemical correspondence of these tephrae with ashes from the North Sea Basin suggests that these pyroclastic deposits are related to the continental breakup of Europe and Greenland (Egger et al., 2000; Huber et al., 2003; Egger & Brückl, 2006). There, the North Atlantic Igneous Province (NAIP), which is one of the largest basaltic lava accumulations on Earth, formed in the early Paleogene (62–53 Ma), prior to and during the continental break-up between Europe and Greenland (Eldholm & Grue, 1994; Ritchie & Hitchen, 1996; Ross et al., 2005). Beside voluminous flood

basalts and associated igneous intrusions, it produced widespread pyroclastic deposits. From the early Eocene Fur Formation in Denmark more than 200 ash-layers of predominantly basaltic composition have been recorded from this explosive volcanic activity (Knox & Morton 1988; Heister et al. 2001). A numbering system for most of these layers was introduced by Bøggild (1918) and is still in use: The upper, closely spaced layers constitute the “positive series”, with layers numbered +1 to +140 in ascending order. The lower, more widely spaced and generally thinner layers make up the “negative series”, and are numbered -1 to -39 in descending order.

The paroxysm of this volcanic activity, the positive ash-series, consists of tholeiitic ferrobasaltic layers with the exception of layer +19. In the immobile element diagram of Floyd and Winchester (1976) this layer plots at the border between trachyte and trachyandesite, whereas more detailed geochemical investigations indicate a rhyolitic composition of the original magma (Huber et al., 2003; Larsen et al. 2003). Some of the ashes of the positive series have also been found at many other sites in Denmark, the North Sea, England, the Goban Spur southwest of Ireland, and the Bay of Biscay (Knox, 1984). Based on detailed multi-stratigraphic and geochemical investigations, the most distal equivalents of layer +19 and 22 other layers have been identified in the Antherring and Untersberg outcrops of the Austrian Alps near Salzburg (Egger et al. 2000 and 2005; Huber et al. 2003).

It can be assumed that the ash-layers of the NAIP form important correlation horizons for lower Eocene deposits in large areas of Europe. In addition to the Austrian outcrops, reports of lower Eocene basaltic ash layers exist from Switzerland and Poland (Winkler et al. 1985; Waśkowska-Oliwa & Leśniak 2002), although stratigraphic and geochemical information from these deposits is insufficient for a detailed correlation.

Stop 2 Antherring Section

Hans Egger

Topics: Paleocene/Eocene-boundary section in a succession of deep-water turbidites and hemipelagites

Tectonic unit: Rhenodanubian Flysch Zone (Penninic Basin)

Lithostratigraphic unit: Rhenodanubian Group, Antherring Formation

Chronostratigraphic units: Upper Paleocene to Lower Eocene

Biostratigraphy: Upper part of calcareous nannoplankton Zone NP9 to upper part of Zone NP10

Location: Outcrops of the Kohlbachgraben near Antherring (Figs. 6C, 11)

Coordinates: 47° 53' 19" N, 013° 01' 17" E

References: Heilmann-Clausen & Egger (1997), Egger, Heilmann-Clausen & Schmitz (2000), Crouch et al. (2001), Egger et al. (2003), Egger & Brückl (2006), Iakovleva & Heilmann-Clausen (2007), Egger et al. (2009).

From the carpark at the Reintthal inn it is an approx. 10 minutes walk on a small road to the first outcrop of the section, which is located along the course of the Kohlbach creek (no trail!). We examine the section (Fig. 11) walking up-stream from the lower Eocene (NP10) to the uppermost Paleocene (NP9).

The Antherring section is located about 18 km to the north of the Untersberg section as the Antherring and Untersberg sections are separated by the thrust between the Northern Calcareous Alps and the Rhenodanubian Flysch zone, the original palinspastic distance between them must have been much greater than at present. However, reliable data on this distance are lacking.

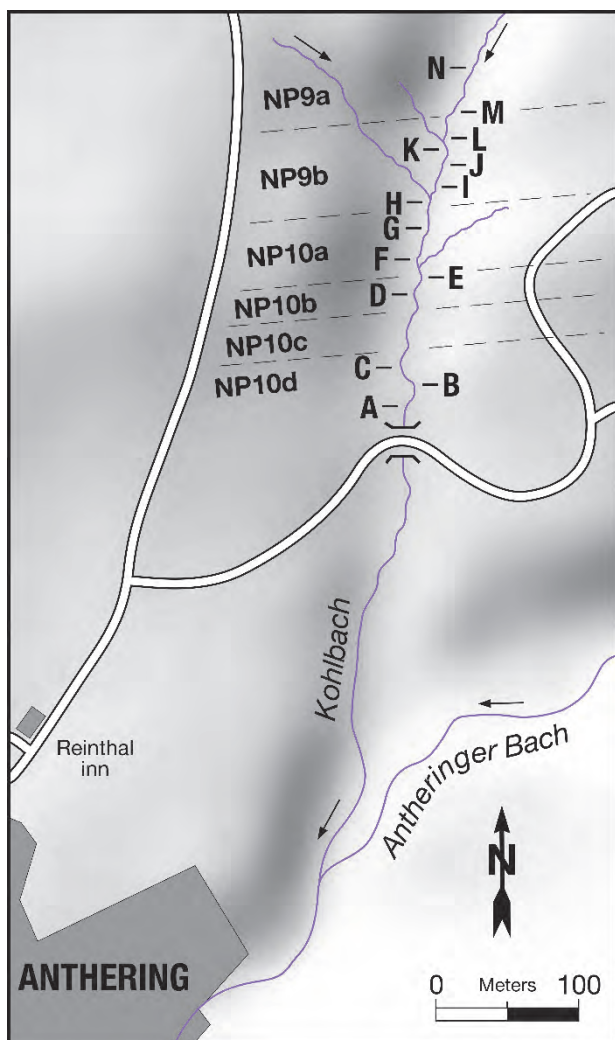


Fig. 11: Location of outcrops and biostratigraphy of the Anthering section.

The 250 m thick upper Paleocene to lower Eocene deposits of the Anthering section, spanning calcareous nannoplankton Zones NP9 and NP10. These sediments comprise the youngest part of the Rhenodanubian Group. This group was deposited on the continental rise to the south of the European plate, which was the main source for the siliciclastic detritus entering the basin. The section is composed of calcareous mud-turbidites with intervening hemipelagic claystone indicating a deposition below the calcite compensation depth. The general sedimentary record of the Anthering-section is typical for an abyssal plain facies. Paleo-water depth estimations by Butt (1981), using foraminifera assemblages, range between 3000 to 5000 m.

In the Eocene part (Anthering Formation) of the section, the turbidite succession is characterized by the predominance of graded silty marlstone, which form about 85% of the succession (Anthering Formation). Occasionally, these turbiditic marlstone layers overlie silty to sandy beds deposited from the same turbidity current. The turbidites usually display base-truncated Bouma-sequences. Turbidites displaying complete Bouma-sequences are very rare. Single turbidite layers can reach thicknesses up to 2 m. The finegrained sand-fraction represents, on average, 5% of the sedimentary rocks and exceptionally up to 10%. The fine-grained (silty-clayey) sediment displays carbonate contents of 29% to 53%. The clay fraction is dominated by smectite.



Fig. 12: Photograph showing outcrop B.

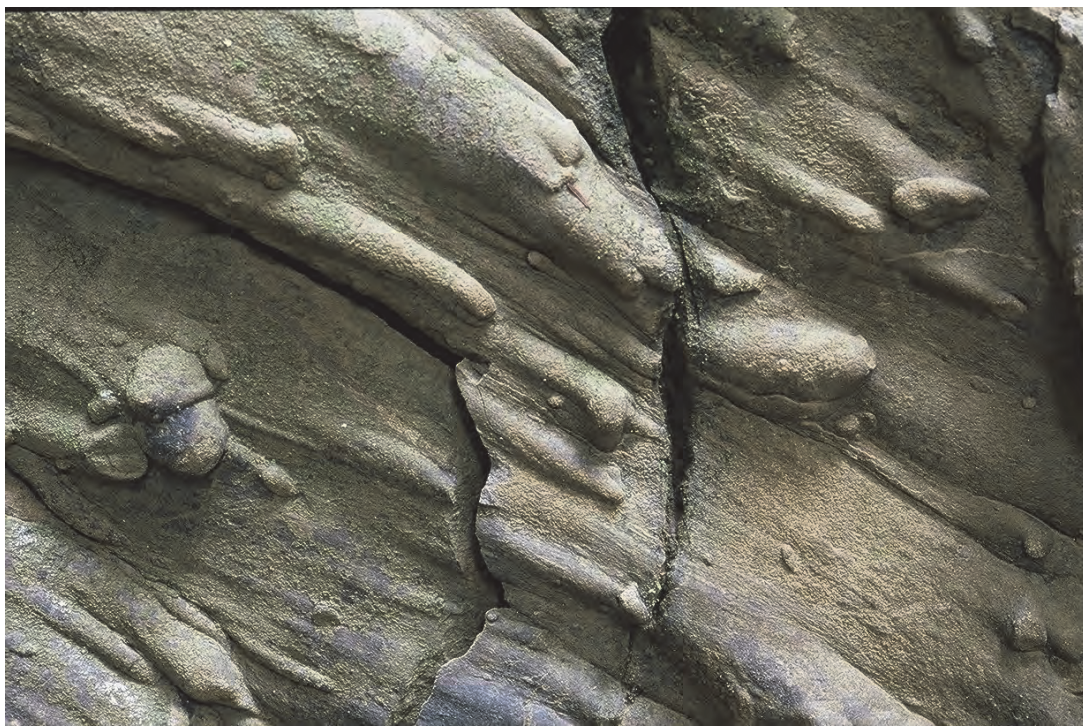


Fig. 13: Flute casts at outcrop B.

Common intercalations of hemipelagic claystone occur between the individual mud-turbidite beds (Fig. 12, 14). The hemipelagic claystones prove a position of the basin-floor below the local calcite compensation depth. They are devoid of carbonate and display sharp contacts to the turbiditic marls. Usually the claystones show a greenish to greyish colour (0.15wt% organic carbon on average) with a large number of dark spots as indications of intensive bioturbation. Only in the middle part of the section (outcrop E and one layer in outcrop D) darkgrey homogeneous claystones with abundant pyrite framboids and relatively high contents of organic carbon (0.94wt% on average) occur (Fig. 15). These black shales indicate an oxygen deficient environment at the basin floor. As they occur together with bentonite layers, volcanism might have led to eutrophic conditions and high plankton productivity responsible for the anoxic conditions.

In the lowermost Eocene (Subzone NP10a) at the Anthering section, 23 layers of altered volcanic ash (bentonites) originating from the North Atlantic Igneous Province have been recorded, about 1,900 km away from the source area (Egger et al., 2000). The Austrian bentonites are between 1mm and 30 mm thick and are considered to be distal equivalents of the “main ash-phase” in Denmark and the North Sea basin. Egger & Brückl (2006) have calculated the total eruption volume of this series as 21,000 km³, which occurred in 600,000 years. The most powerful single eruption of this series took place 54.0 million years ago (Ma) and ejected ca. 1,200 km³ of ash material which makes it one of the largest pyroclastic eruptions in geological history. The clustering of eruptions must have significantly affected the incoming solar radiation in the early Eocene by the continuous production of stratospheric dust and aerosol clouds. This hypothesis is corroborated by oxygen isotope values which indicate a global decrease of sea surface temperatures between 1–2°C during this major phase of explosive volcanism.

The Anthering section displays the global negative carbon isotope excursion (CIE) and the acme of the dinoflagellate species *Apectodinium augustum* (Fig. 17) in the upper part of zone NP9 (Heilmann-Clausen and Egger, 1997; Egger et.al., 2000; Crouch et al., 2001). The onset of the CIE is characterized by the presence of the thickest hemipelagic layers of the entire Anthering Section. About 45 % of the rock is claystone, whereas the average percentage of claystone in the overlying NP10 is only 14 %, and even less in the lower part of NP9. The CIE-interval attains a thickness of 15 m, comprising turbidites and hemipelagites. The thickness of the turbidites varies between 0.08 m and 2.25 m, although only the thickest layer exceeds 1 m thickness. The average thickness of the turbidite beds is 0.39 m and sand-grade material, which makes up 2 % of this facies, occurs only in the thickest layers. Excluding the turbidites the remaining thickness of hemipelagic claystone is 8.4m. Using Fe– and Ca–intensity curves which probably represent precessional cycles, Röhl et al. (2000) calculated that the CIE interval lasted for 170 ky. From this, a hemipelagic sedimentation rate of 49 mmky⁻¹ has been calculated for the compacted sediment across the CIE.

This value is ca. six times higher than the hemipelagic sedimentation rate in the Paleocene (Egger et al., 2009). The increased rate of hemipelagic sedimentation at the CIE suggests a high input of siliciclastic suspension into the basin. At the level of the CIE clay mineral assemblages of hemipelagic claystone display a distinct increase of smectite and kaolinite at the expense of illite and chlorite (Egger et al., 2002). This indicates a decrease of bedrock erosion in the adjoining land areas. Well-developed smectitic soils with a mixture of kaolinite are mostly restricted to subtropical climates with a well-marked dry season (see Thiry, 2000 for a review). During the rainy season continental erosion of such areas is very pronounced (see van der Zwan, 2002, for a review) and will result in a strong increase in hemipelagic sedimentation rates (Schmitz et al., 2001).

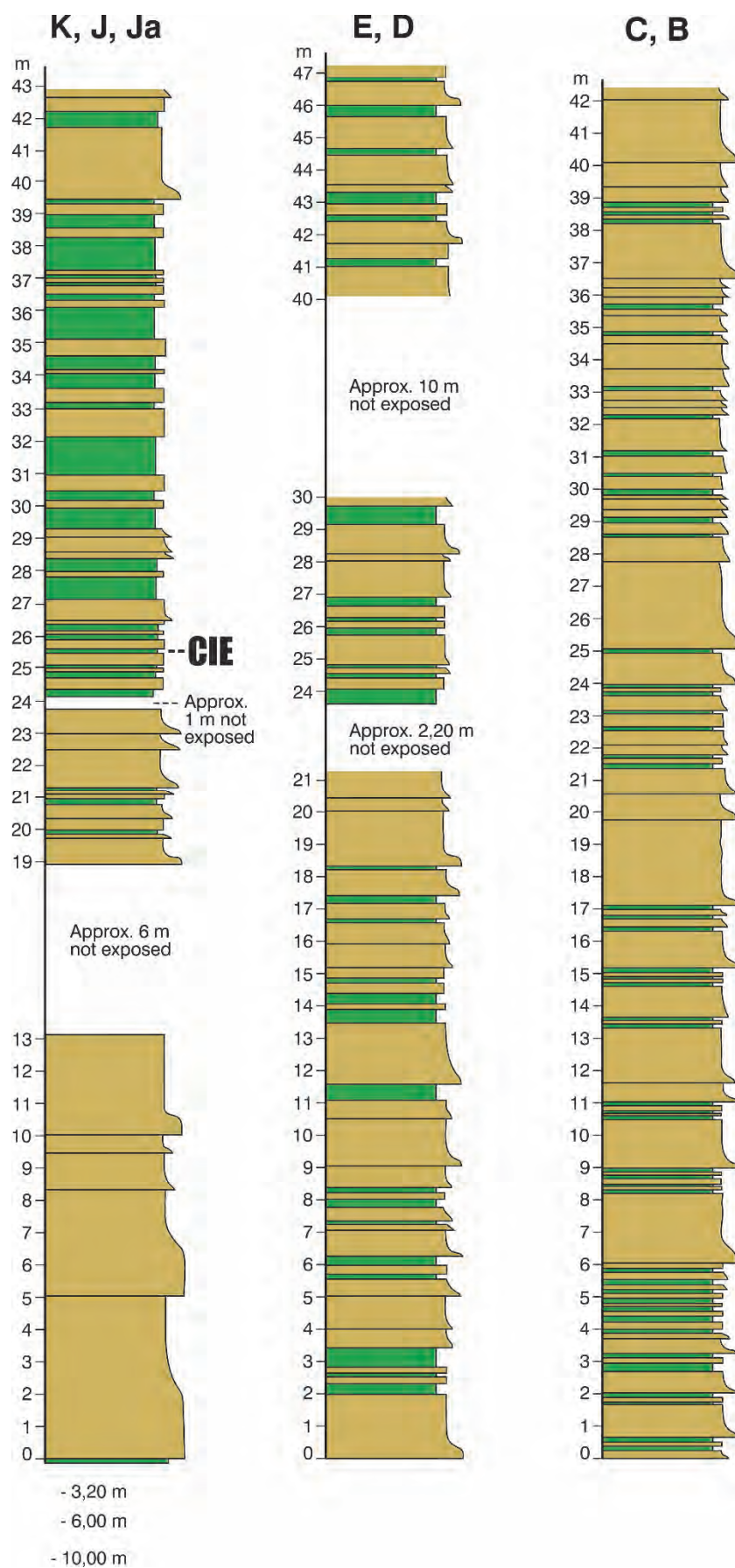


Fig. 14: Lithologic logs of outcrops at Anthering.

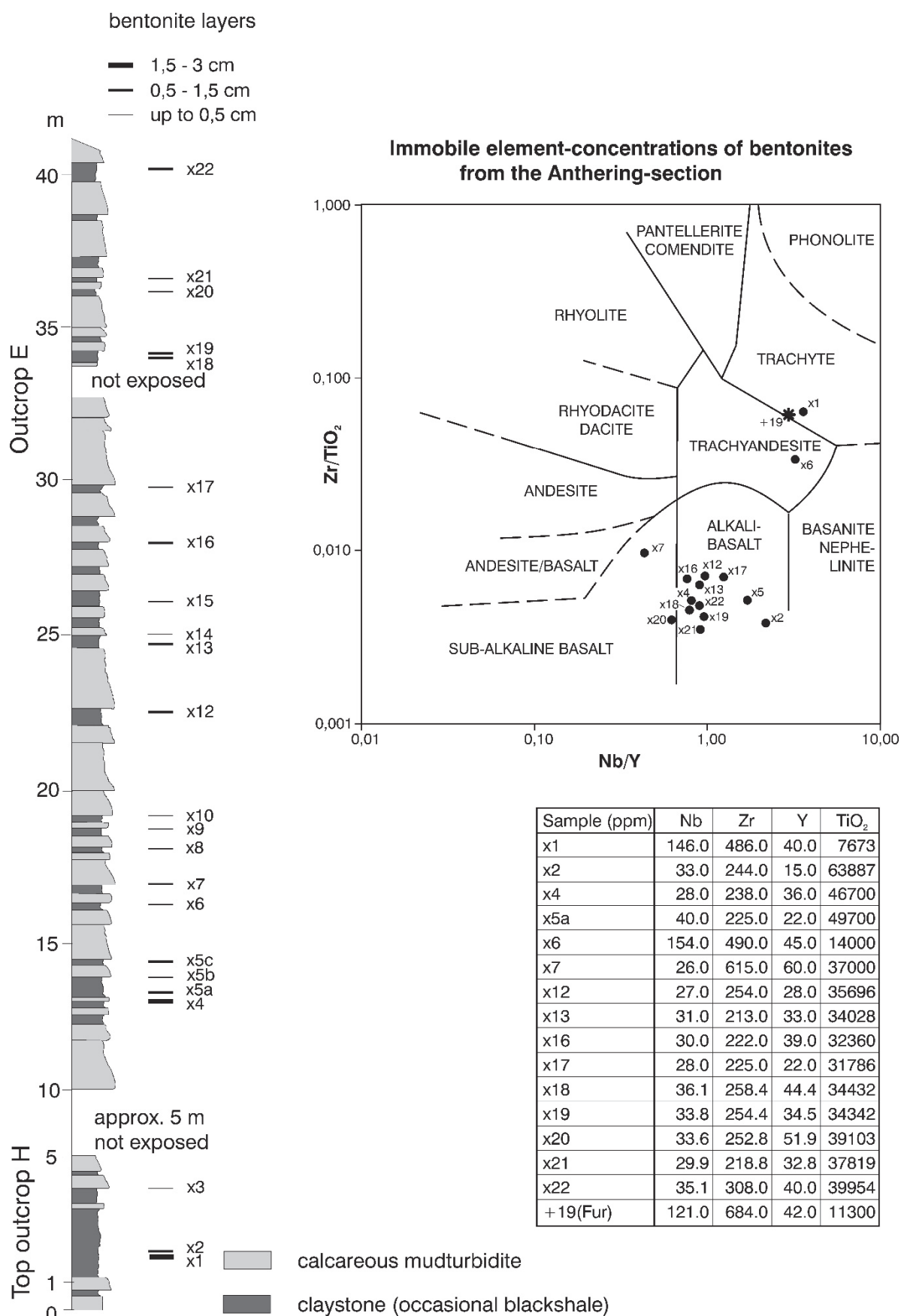


Fig. 15: Log of outcrop E showing positions of bentonites and immobile element concentrations of bentonites.

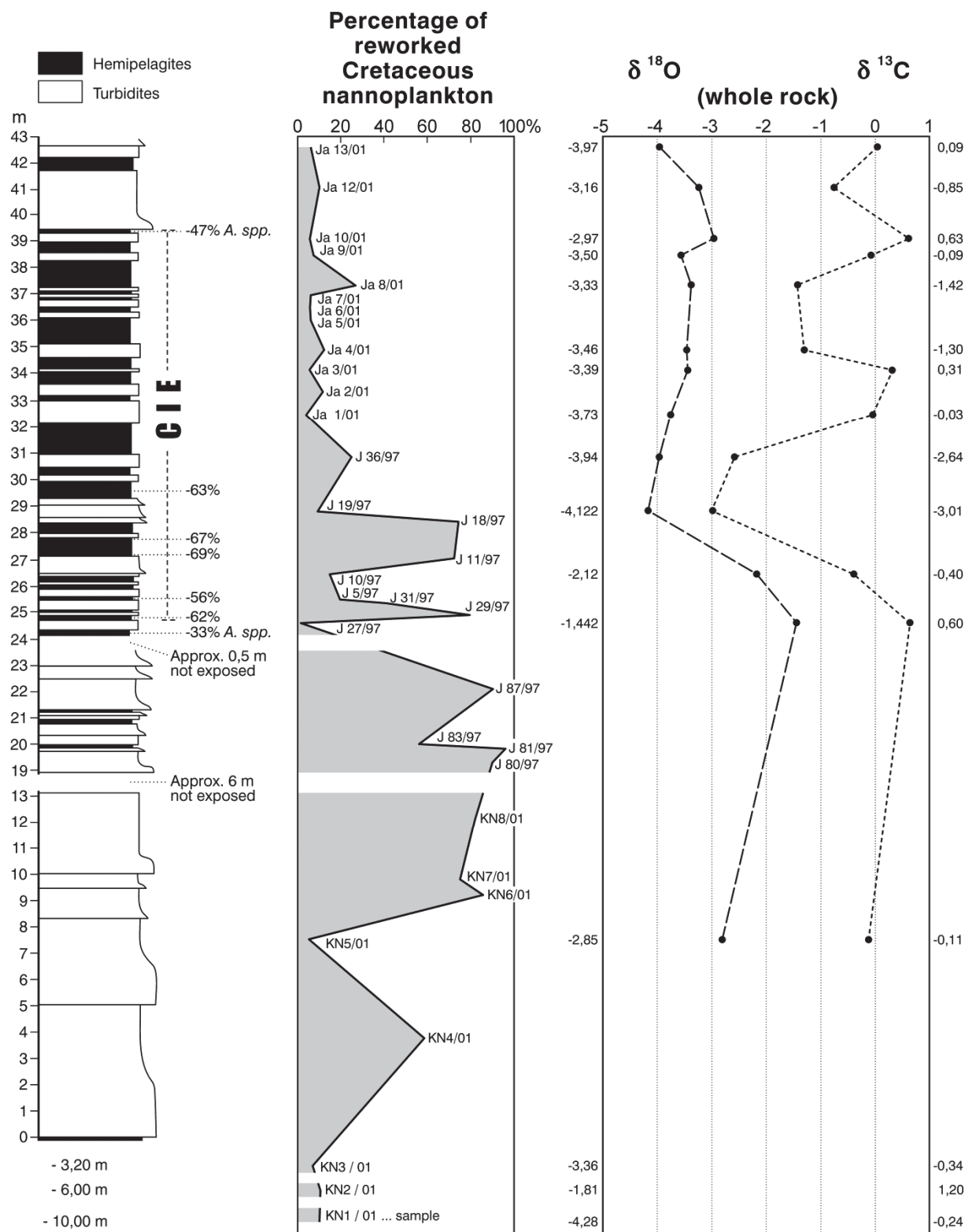


Fig. 16: Lithostratigraphy, percentages of redeposited Cretaceous nannoplankton, and stable isotope record of oxygen and carbon across the CIE-interval at Anthering. A. spp. percentages of the genus *Apectodinium* in the dinoflagellate assemblage (Egger et al., 2009).

Enhanced erosion of land areas around the CIE-interval can also be inferred from the composition of calcareous nannoplankton assemblages. Whereas, in general, reworked Cretaceous species form only 2–3 % of the calcareous nannoplankton assemblages of the Anthering section, substantial Cretaceous admixtures are present in many samples from across the CIE. The oldest nannoplankton assemblage showing a high percentage (>50 %) of reworked specimens originates from a turbidite bed 22 m below the onset of the CIE. Three metres above the onset of this geochemical marker, the youngest assemblage with a similar percentage of reworked Cretaceous specimens has been found (Fig. 16).

Most of the reworked specimens consist of species with a long stratigraphic ranges (*Wattnaueria barnesae*, *Micula staurophora*, *Retecapsa crenulata*, *Cribrosphaerella ehrenbergii*, *Eiffellithus turriseiffelii*). Biostratigraphically important species that were found in all of the counted samples include *Brownsonia parca*, *Arkhangelskiella cymbiformis* (small specimens), *Calculites obscurus*, *Lucianorhabdus cayeuxii* and *Eiffellithus eximius* whilst *Marthasterites furcatus*, *Erolithus floralis* and *Lithastrinus grillii* were found only occasionally. This assemblage suggests that predominantly lower to middle Campanian deposits were reworked at the end of the Paleocene. Probably, the erosional area was the North-Helvetic shelf at the southern European Plate where the Middle Eocene is resting with an erosional unconformity on the Upper Cretaceous.

Substantial reworking of the Cretaceous started already in the latest Paleocene. At Anthering, the uppermost 20 m of the Paleocene succession are formed by the thickest turbidites (up to 5 m) of the entire section. The siliciclastic sand-fraction in the turbidites forms around 30 % of the rocks in this part of the section (Altlengbach Formation). This suggests that a sea-level drop took place shortly before the onset of the CIE. This is consistent with data from the Atlantic region (Heilmann-Clausen, 1995; Knox, 1998; Steurbaut et al., 2003; Pujalte and Schmitz, 2006; Schmitz and Pujalte, 2007). The synchronicity of this sea-level drop in the Atlantic and Tethys regions indicates a eustatic fluctuation. Starting with the onset of the CIE, mainly fine-grained suspended material came into the basin and caused an increase in hemipelagic sedimentation rates by a factor of 5 or 6. Such an increase associated with decreasing grain-sizes has already been reported from P/E-boundary sections elsewhere and interpreted as an effect of a climate change at the level of the CIE, affecting the hydrological cycle and erosion (Schmitz et al., 2001).

Dinoflagellates

Information on the distribution of organic-walled dinoflagellate cysts in the Anthering section has previously been briefly published by Egger et al. (1997 and 2000), Heilmann-Clausen and Egger (2000) and Crouch et al. (2001). With results obtained during the present study the data can be summarized as follows. Common genera and species occurring throughout the section are *Apectodinium* spp., *Areoligera* spp., *Glyptolytocysta* spp., *Spiniferites* spp., *Polysphaeridium zoharyi*, *Homotryblium tenuispinosum*, *Operculodinium centrocarpum*, and *Phthanoperidinium crenulatum*. *Lingulodinium machaeorophorum* occurs sporadically and is usually rare.

The overall composition of the dinoflagellate assemblages allows a simple subdivision of the section into three parts: The lower and upper intervals are characterized by generally low dominance and relatively high species richness. These two intervals are separated by a middle interval coinciding with the CIE (outcrops J and JA). There the genus *Apectodinium* which usually accounts for 5 % - 20 % of the dinoflagellate assemblages is dominant and reaches abundances up to 69 % in hemipelagic samples. The genus *Apectodinium* includes several intergrading species, which form a closely related group

(Harland, 1979). In spite of the strong dominance, the species richness remains relatively high within the CIE interval.

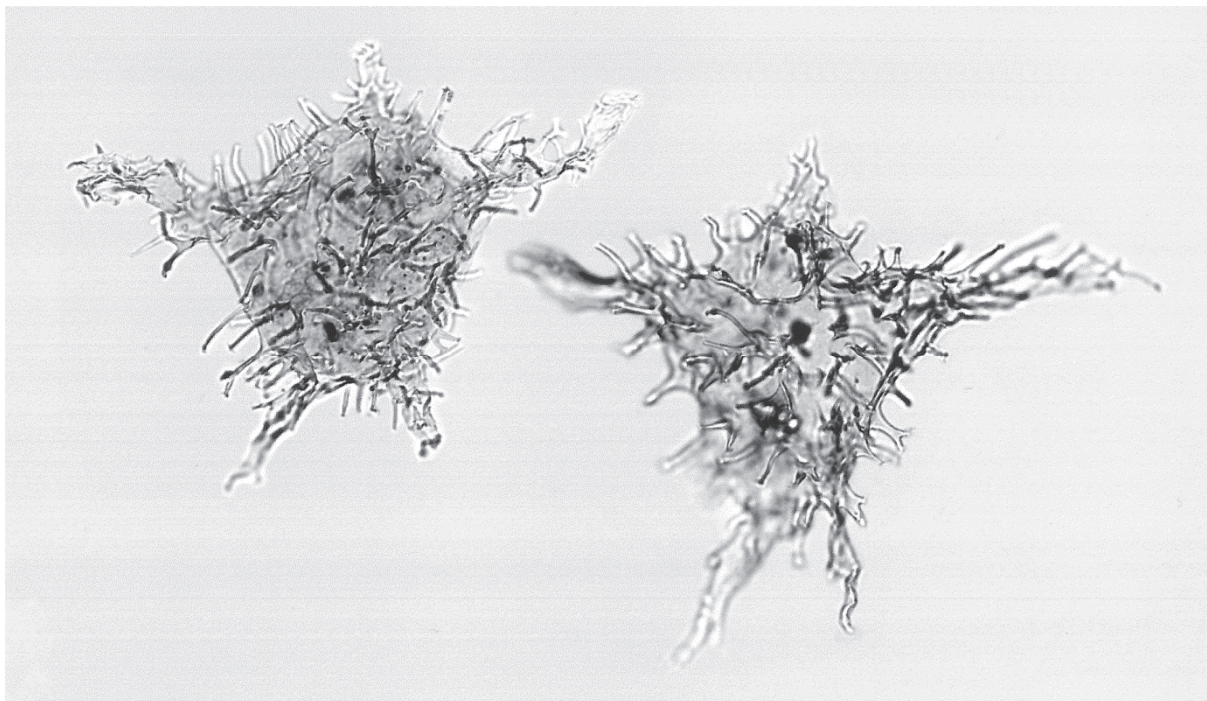


Fig. 17: *Apectodinium augustum*. Left specimen from Anthering, outcrop j. Right specimen from the CIE-interval in Denmark (Viborg Borehole).

Quantitative dinoflagellate cyst data from hemipelagic layers at outcrop J reveal there is a ten-fold to forty-fold increase in the total number of cysts within the CIE interval (where *Apectodinium* dominates). Above the CIE, counts reveal fluctuations in cyst numbers with a general trend towards reduction, which parallel the declining percentages of *Apectodinium*. The total number of cysts is low in sample J4 from the CIE-interval, with dominant *Apectodinium*, but this sample is from a layer with a minimum in the TOC which suggests increased oxygenation at this level. The *Apectodinium* percentages are increased in sample J26 (33 %) and J28 (62 %), but no data of absolute dinoflagellate abundances are available for these two samples.

Relying on information from modern cyst production (e.g. Dale, 1996), the Anthering Section must have been deposited below neritic waters, or waters which originated in the neritic zone. The genus *Impagidinium*, which is today purely oceanic, is present in several samples (especially in outcrop N), but usually rarer than 1-2 %. Such low occurrences indicate the neritic/oceanic boundary interval (Dale 1996). It should be noted that the boundary between neritic and oceanic waters today does not strictly follow bathymetry and presence of neritic waters need not conflict with the interpretation of the depositional environment at Anthering being an abyssal basin floor (Egger et al., 2000). It is also well known that neritic cysts are today transported over long distances with currents, and are deposited in various basinal parts of the Atlantic Ocean (e.g. Dale, 1996).

The continuous presence of *Polysphaeridium zoharyi* and *Homotryblium tenuispinosum* is evidence of a rather constant, and significant, mixing of the water masses at Anthering. *Polysphaeridium zoharyi* today mainly characterizes equatorial lagoons (Dale, 1996), and the extinct *Homotryblium* is a dominant form in several well-documented inner neritic, probably lagoonal settings of various ages

(e.g. Köthe, 1990; Brinkhuis, 1994; Dybkjær and Rasmussen, 2000; and personal observation of Heilmann-Clausen in the basal Oligocene Heide Sand, Belgium).

Siliceous plankton

Throughout the Anthering section the fossil remains of siliceous plankton (radiolaria, diatoms as well as rare ebridians and silicoflagellates) have been replaced by pyrite. Silica dissolution prior to this replacement, and damage caused by the pressure of pyrite crystals growing inside the shells, can make identification difficult. In particular, radiolarians are very poorly preserved and are all taxonomically indeterminate spheroidal or lenticular spumellarians (Christopher Hollis, oral communication). If pyrite fillings only are preserved, the outline and shape of diatom frustules can be recognized, but a specific and often generic determination is impossible. However, in the more robust frustules, even relatively fine pores and cribra covering the areolae are preserved, and thus allow species determination.

Most samples have diatom floras dominated by the taxa *Paralia sulcata* var. *biseriata*, *Paralia sulcata* var. *crenulata*, *Coscinodiscus antiquus*, and by species of the genera *Auloplacata* and *Stephanopyxis*. The recent relatives of the latter two genera occur in coastal-neritic as well as in oceanic environments. This may also be the case for the less common species of the genera *Hemiaulus* (e.g. *H. peripterus*), *Actinoptychus* and *Sceptroneis*. Species of the genus *Trochosira*, which are also rather rare, are considered to have been fully planktonic, whereas specimens of *Craspedodiscus*, *Trinacia*, *Sheshukovia* and *Aulacodiscus* probably indicate a coastal-neritic environment. Other genera can be considered to have been fully benthic, e.g. species of the genera *Auliscus* and *Arachnodiscus*. In neritic assemblages, resting spores should be abundant, but in the studied samples only single specimens of resting spores were found. These belong to the form groups *Xanthiopyxis*, *Pterotheca* and *Bicornis*. As resting spores are most resistant to dissolution, their scarcity indicates that the encountered diatoms represent an oceanic assemblage (Fenner, 1994). The minor admixture of coastal and neritic specimens may have been caused by storm events that whirled up freshly deposited sediment in shallow regions which thereafter settled out from suspension beyond the shelf edge.

The occurrence of *Craspedodiscus* spp. and *Trinacia* spp. in deep-water deposits at Anthering is highly remarkably as these genera are usually restricted to neritic environments. We can rule out redeposition of these specimens because in that case, resting spores and benthic species would have been redeposited in considerable amounts. This suggests that water-depth was not the limiting factor for the occurrence of *Craspedodiscus* spp. and *Trinacia* spp.. Probably, the preference of these genera for neritic settings was due to the higher level of dissolved nutrients in these areas.

Agglutinating foraminifera

Individual samples contain up to 65 species and more than 700 specimens agglutinated foraminifera. More than 90 species were identified and grouped into four morphogroup assemblages (tubular genera, infaunal passive deposit feeders, active deposit feeders, epifaunal active herbivores and omnivores). Distributional patterns of morphogroups of agglutinating foraminifera are related, more or less directly, to food supply and food utilisation processes (Jones and Charnock, 1985).

At Anthering, tubular forms comprise the genera *Nothia*, *Rhabdammina*, *Rhizammina*, *Psammosiphonella* and *Bathysiphon*. These typical „flysch-type“ elements have been interpreted as sessile suspension feeders (morphogroup A of Jones and Charnock). However, the ecological interpretation of some of these deep-sea genera is still under discussion (Gooday et al., 1997), e.g. the life habitat of *Nothia* has been re-interpreted as epibenthic detritivore (Geroch and Kaminski, 1992).

Epi- and infaunal passive deposit feeders (morphogroup B1) comprise *Saccammina*, *Psammospaera*, *Hormosina*, *Hormosinella*, *Trochamminoides*, *Paratrocchamminoides*, *Lituotuba*, *Hyperammina* and *Kalamopsis*. Another epifaunal and shallow infaunal group of active deposit feeders (morphogroup B2) corresponds to the *Ammodiscus* - *Glomospira* assemblage of „Biofacies B“ (Kuhnt et al., 1989). It consists of the genera *Ammodiscus*, *Glomospira* and *Rzehakina*. The B3 assemblage of epifaunal active herbivores and omnivores (*Haplophragmoides*, *Trochammina* s.l.) may be restricted to omnivores in this deep-sea environment. The C-morphogroup of infaunal forms (*Gerochammina*, *Karrerulina*, *Reophax*, *Subreophax*, *Spirolectammina*) are negligible in the abyssal setting of the Anthering section. The genera *Recurvoides* and *Thalmannammina* were summarized as *Recurvoides*-assemblage. The microhabitat preferences of this assemblage are questionable. In the Cretaceous „Hatteras Fauna“ of the Fardes Formation in southern Spain it co-occurs with *Glomospira* and *Ammodiscus*, and might, therefore, be indicative of oxygen deficient conditions (Kaminski et al., 1999). In our samples we did not find this correlation because the highest percentages of the *Recurvoides*-assemblage occur in high diversity faunas without any indication of oxygen depletion. It is noteworthy, that the *Recurvoides*-assemblage usually forms more than 10% of the agglutinated faunas within nannoplankton zone NP9 whereas in zone NP10 this percentage is much lower.

The highest diversity and the highest abundance of agglutinated specimens occur in the lower part of the section (samples NF2 to LF1). These assemblages display balanced proportions of infaunal, epifaunal and suspension feeding species. The high diversity of these agglutinated faunas is seen as typical for oligotrophic, food-limited environments where the various microhabitats are fully occupied. Several taxa have their last occurrences in this part of the section: *Ammodiscus cretaceus*, *Aschemocella* cf. *carpathica*, *A. grandis*, *Haplophragmoides horridus*, *H. suborbicularis*, *Hormosina trinitatensis*, *Karrerulina* cf. *coniformis*, *Paratrocchamminoides heteromorphus*, *P. multilobus*, *Recurvoides walteri*, *Remesella varians*, *Rzehakina complanata*, *R. epigona*, *R. fissistomata*, *Spirolectammina* cf. *dentata*, *Spirolectammina spectabilis*, *Thalmannammina* n. sp., *Thurammina papillata*.

Further up-section (samples J85 to JaF1) impoverished faunas with a predominance of the genus *Glomospira* appear. This “*Glomospira* event” has been observed at numerous localities in the Tethys and northern North Atlantic (see Kaminski et al., 1996 for a review). Kaminski et al. (1989) speculated that the predominance of *Glomospira* indicates areas of high surface productivity that caused low-oxygen levels at the sea-floor. However, this assemblage occurs also in well oxidized sediments and, therefore, it may be opportunistic rather than a reliable indicator for high productivity (Galeotti et al., 2000; Kaminski et al., 1996). With the onset of the CIE, even this opportunistic assemblage disappeared and over a period of at least 180 000 years the benthic communities suffered severely from unfavorable habitat conditions.

Between samples HF2 to EF1 the majority of the hemipelagic layers have an organic carbon content between 0.14% and 0.17% (0.15% on average), but several black shale layers (up to 1.22% TOC) occur. This suggests periodic eutrophication of the sea water probably by volcanic ashfall as closely spaced bentonites were found in that part of the section (Egger et al., 2000). The black shales are usually devoid of benthic foraminifera and contain common framboidal pyrite indicating anoxic conditions (Egger et al., 1997). The agglutinating faunas of these layers are not as rich and diverse as those from further down the section. *Glomospira glomerata* has its first appearance in this part of the section. The faunal assemblage changed to a predominance of passive deposit feeders (B1-assemblage) and tubular

genera (A-assemblage). These assemblages are dominant along the continental rises where bottom currents or distal turbidity currents occur (Kaminski et al., 1996).

In the uppermost part of the Anthering section (samples DA64a to BF1) a strong increase in the number of species and specimens of the DWAF, with relatively balanced assemblages, occurs indicating the return of ecological conditions similar as those at the base of the section.

Stop 3 Frauengrube Section near St. Pankraz

Hans Egger

Topic: Erosional unconformity between the Thanetian and Ypresian

Tectonic unit: South Helvetic nappe complex (European Plate)

Lithostratigraphic unit: Kressenberg Formation, Fackelgraben Member, Frauengrube Member

Chronostratigraphic units: Thanetian, Ypresian

Biostratigraphy: Calcareous Nannoplankton Zones NP9 and NP12

Location: Frauengrube Quarry (Fig. 6C)

Coordinates: 47° 56' 11" N, 013° 00' 06" E

References: Egger et al., 2009, Rasser & Piller, 1999 and 2001

In the Haunsberg area, the Frauengrube section and the immediately adjoining Kroisbach section are both part of the South-Helvetic nappe complex. The base of the succession is a grey mica-bearing marlstone of the Maastrichtian Gerhartsreit Formation, which is overlain by silty claystones and clayey siltstones of the Paleocene Olching Formation. Detailed nannoplankton studies at the Cretaceous/Paleogene-boundary indicate continuous sedimentation across the boundary, since the uppermost Maastrichtian (*Micula prinsii* Zone) and the lowermost Paleocene (*Markalius inversus* Zone) have been discovered (Stradner, pers. comm. 2005). Around the boundary, the amount of terrestrially-derived sediment input strongly increases at the expense of carbonate. This shift in the lithological composition defines the lithostratigraphic boundary between the Gerhartsreit and Olching formations.

The Olching Formation is overlain by the Kroisbach Member of the Kressenberg Formation. This member is characterized by glauconite-bearing quartz-sandstones with abundant brachiopods (*Crania austriaca* Traub) in the lower part and oysters (*Pycnodonte* spp.) in the upper part. The glauconitic matrix of the oyster-beds contains calcareous nannoplankton of the Upper Thanetian *Heliolithus riedelii* Zone (NP8) and very well preserved pollen and spores (Stradner, in Gohrbandt, 1963; Kedves, 1980; Draxler, 2007).

The Kroisbach Member is overlain by the rhodolithic limestone of the Fackelgraben Member (Figs. 18 and 19). Samples from thin intervening marlstone layers in the upper part of this member contained poorly preserved calcareous nannoplankton of the *Discoaster multiradiatus* Zone (NP9), of latest Paleocene age: *Chiasmolithus* sp., *Coccolithus pelagicus*, *Discoaster falcatus*, *Discoaster multiradiatus*, *Discoaster mohleri*, *Fasciculithus tympaniformis*, *Neochiastozygus perfectus*, *Thoracosphaera* sp., *Toweius callosus*, *Toweius pertusus*. Reworking of Cretaceous species has not been observed.

The Fackelgraben Member and the overlying Frauengrube Member are separated by an irregular erosional surface (Fig. 20), that has been described previously from other outcrops in the Salzburg area (Vogeltanz, 1977). Clasts of the Fackelgraben Member are reworked in the basal part of the Frauengrube Member (Rasser and Piller, 2001), which comprises 0.5 m of brownish sandstone with a

marly matrix, that contains poorly preserved calcareous nannoplankton. Reworked species from the Campanian and Maastrichtian make up about 5% of the nannoplankton assemblage (*Arkhangelskiella cymbiformis*, *Broinsonia parca*, *Cribrosphaerella ehrenbergii*, *Cyclagelosphaera reinhardtii*, *Eiffellithus eximus*, *Markalius inversus*, *Micula staurophora*, *Prediscosphaera cretacea*, *Watznaueria barnesae*). The rest of the species observed have their first occurrence during the Paleocene (*Campylosphaera eodela*, *Chiasmolithus bidens*, *Chiasmolithus consuetus*, *Chiasmolithus danicus*, *Coccolithus pelagicus*, *Discoaster barbadiensis*, *Discoaster multiradiatus*, *Thoracosphaera* sp., *Toweius* spp.) or in the lower Eocene (*Neochiastozygus junctus*, *Pontosphaera versa*, *Pontosphaera duocava*, *Rhabdosphaera solus*, *Transversopontis pulcher*, *Zygrhablithus bijugatus*). Unfortunately, no marker species of the lowermost Eocene, in particular of the *Rhomboaster-Tibrachiatus* lineage, have been encountered in our samples. However, *Tibrachiatus orthostylus* (Type B = without bifurcated rays) has been described from the base of the Frauengrube Member from another outcrop in the Haunsberg area (Stradner in Gohrbandt, 1963). This finding indicates that the onset of the transgression did not take place before the *Discoaster binodosus* Zone (NP11).

Beside calcareous nannoplankton, the samples from the base of the Frauengrube Member contain marine and terrestrial palynomorphs. The terrestrial flora indicates a subtropical to tropical climate containing Sapotaceae and Matixiaceae pollen among other floral elements (*Dictyophyllidites* sp., *Pityosporites* sp., *Nudopollis* sp., *Subtriporopollenites* sp., *Cupuliferoidaepollenites liblarensis*). Palmpollen have not been found (Draxler, pers. comm. 2006).

The marine flora contains very similar, relatively well preserved dinoflagellate assemblages dominated by *Homotryblium tenuispinosum* ("tasmaniense-type"), *Polysphaeridium zoharyi* and *Apectodinium* spp. (excluding *A. augustum*). The three taxa are equally common, and together are estimated to constitute 60-90% of the dinoflagellate assemblages. Of relevance for age-determination is the occurrence of the *Areoligera undulata* – *A. sentosa* group (present in each sample), *Glaphyrocysta* cf. *semitecta* (samples 1 and 3), *Deflandrea oebisfeldensis* (2 specimens in sample 1) and *Phthanoperidinium* cf. *echinatum* (1 or 2 specimens in sample 1). In addition to these taxa, the samples also include low abundances of several long ranging taxa without stratigraphic value. *Spiniferites* spp. and *peridinioids*, apart from *Apectodinium*, are rare.

The *Areoligera undulata* – *A. sentosa* group, *Glaphyrocysta* cf. *semitecta* and *Phthanoperidinium* cf. *echinatum* were not recorded in the Anthering Formation at Anthering, from where dinoflagellates were previously studied (Egger et al., 2000; 2003). This suggests a younger age for the Frauengrube Member. The *Areoligera undulata* – *A. sentosa* group is probably of inner neritic-lagoonal origin and has previously been recorded in the Lutetian in southern England (Eaton, 1976; Bujak et al., 1980). Little is known about its stratigraphical distribution elsewhere. The several specimens of *Glaphyrocysta* (cf.) *semitecta* are very close to, but perhaps not identical with *Glaphyrocysta semitecta*, a taxon previously recorded from NP15 to near the Eocene/Oligocene boundary in NW Europe (e.g. Bujak et al., 1980; Heilmann-Clausen and Van Simaeys, 2005). Nothing else in the samples suggests such a young age. The abundance of *Apectodinium* points to an age no younger than the Ypresian-Lutetian transition, most likely early Ypresian or older. The two specimens of *Deflandrea oebisfeldensis* also point to an early Ypresian or older age, as this form becomes extinct in the lower Ypresian in NW Europe (probably in or near top of NP11, e.g. Heilmann-Clausen and Costa, 1989; Luterbacher et al., 2004).

In summary, the calcareous nannoplankton and dinoflagellate assemblages of the Frauengrube section indicate an erosional gap across the P/E-boundary, spanning the upper part of zone NP9, the entire zone NP10, and at least a large part of zone NP11.

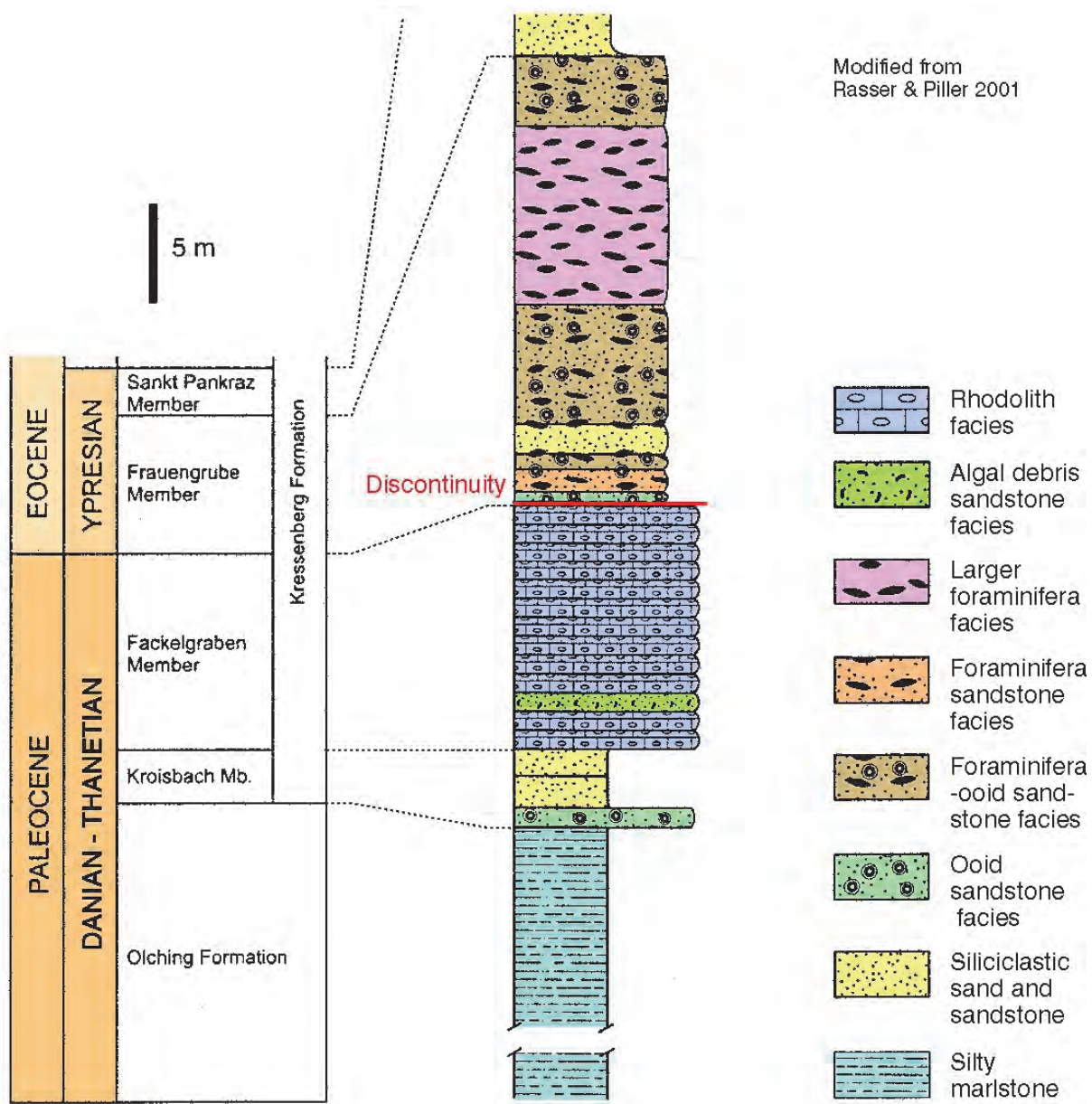


Fig. 18: Lithologic log of the Paleogene of the South Helvetic sucession in Salzburg.

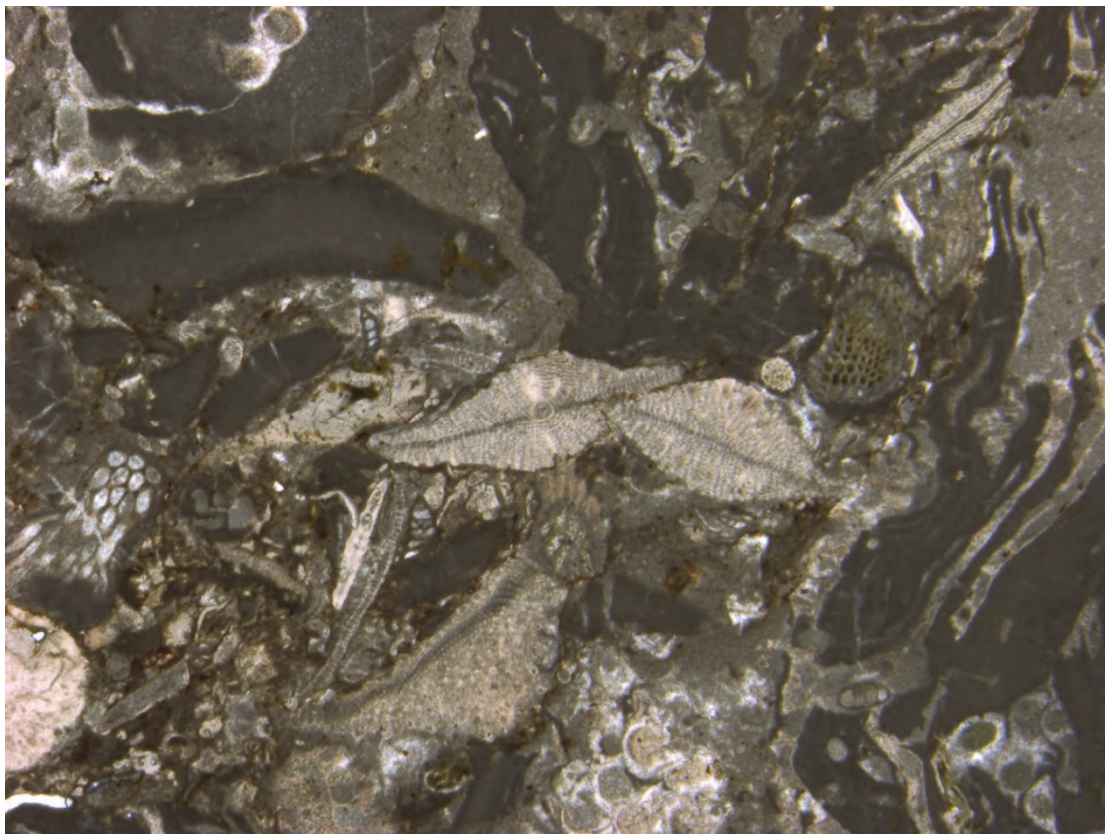


Fig. 19: Image of a thin section of rhodolithic limestone with *Discocyclina* sp. (Fackelgraben Member).



Fig. 20: Photograph of the type locality of the Frauengrube Member (Note the erosional unconformity between the Fackelgraben Member (left) and the Frauengrube Member (right)).

Stop 4 Wimmern Section

Hans Egger

Topics: Transgression of the Adelholz Formation on the Gerhardtsreit Formation

Tectonic unit: North Helvetic Nappe Complex (European Plate)

Lithostratigraphic units: Adelholz Formation, Gerhardtsreit Formation

Chronostratigraphic units: Maastrichtian, Lutetian

Biostratigraphy: Calcareous nannoplankton Sub-Zones NP15a and NP15b

Location: Outcrops near Wimmern (Fig. 21)

Coordinates: 47° 52' 09" N, 012° 49' 57" E

References: Egger, H. et al. (2011)

At Wimmern (Fig. 21), the Maastrichtian is overlain by 4 m thick glauconite rich sand of the lower Adelholzen beds (Fig. 22). Poorly preserved calcareous nannoplankton assemblages from the basal 50 cm of the sand contain *Chiasmolithus grandis*, *Chiasmolithus solitus*, *Cyclicargolithus floridanus*, *Nannotetraena cristata*, and *Sphenolithus spiniger*, indicating calcareous nannoplankton Sub-Zone NP15a at the base of the Adelholzen beds. *Chiasmolithus gigas*, the index species for Sub-Zone NP15b has its first occurrence 4 m above the transgressional surface and is still present at the top of the section (7.5 m above the transgressional surface). Sub-Zone NP15b is presented by marlstone containing high numbers of larger foraminifera and foraminiferal limestone.

The poor preserved planktonic foraminifera assemblage from the glauconitic sand at the base of the section yields *Acarinina coalingensis*, *A. esnehensis*, *A. interposita*, *Igorina broedermannii*, and *Pseudohastigerina wilcoxensis*. Fifty centimetres above the transgression *Acarinina bullbrookii*, *A. cuneicamerata*, and *Pseudohastigerina micra* have their first occurrences. The assemblage suggests an assignment to planktonic foraminiferal Zone E7 in the zonation scheme of Wade et al. (2011).

The age of the transgression of the Adelholzen beds (which is called Bürgen Formation in Switzerland) is equivalent to the age of the transgression of the Lutetian at the Lutetian stratotype (St. Leu d'Esserent in the Paris Basin) where Aubry (1991) attributed the base of the type Lutetian to calcareous nannoplankton Subzone NP14b. Contrary to previous opinions (e.g. Hagn et al., 1982), this suggests that the North-Helvetic domain was affected by an eustatic sea-level rise in the Lutetian and not by tectonic subsidence.

Stop 5 Goppling section

Hans Egger

Topics: Cretaceous-Paleogene transition in an active tectonic deep-water setting. Slope basin formation on the bathyal to abyssal southern slope of the European Plate.

Tectonic unit: Ultrahelvetic Nappe Complex (European Plate)

Lithostratigraphic units: Buntmergelserie, Achthal Formation (type locality)

Chronostratigraphic units: Upper Maastrichtian to Ypresian

Biostratigraphy: Calcareous nannoplankton Zones CC26 to NP11

Location: Stecherwald southwest of Teisendorf (Fig. 23)

Coordinates: 47° 50' 51" N, 012° 47' 42" E (base of the section)

References: Egger, H. & Mohamed, O. (2010)

The type area of the Achthal Formation is the forest ("Stecherwald") southwest of Teisendorf. The base of the composite type section of the Achthal Formation (Goppling section) is located in creek 3 ("Gopplingbach"), ca. 15 m south of the hiking trail bridge. Further up-stream the Danian, Selandian and lower Thanetian all show excellent exposures, which end at the hamlet of Goppling. The upper Thanetian is seen only in small and poor exposures, in the two gullies east of creek 3 (Fig. 23). The Eocene part of the section is well exposed along creek 4, with the first outcrop ca. 20 m downstream from the hiking trail (coord. E 012° 48' 02", N 47° 50' 48").

The lithostratigraphic term "Achthaler Sandstein" dates back to Gümbel (1862, p.616). Although Schlosser (1925, p.167) mentioned a Thanetian macrofauna from this unit ("Achthaler Grünsand"), it can be assumed that these fossils originated from the tectonically neighbouring shallow-water deposits of the South-Helvetic thrust unit. Ganss and Knipscheer (1956) report on Paleocene foraminifera faunas and interpreted the outcrops as a special facies (Teisendorf facies) of the Helvetic sedimentation area. Hagn (1960 and 1967) recognized the deep-water character of the deposits and assigned them to the southern part of the Ultrahelvetic sedimentation area, which interpretation is adopted by Egger & Mohamed (2010), who introduced the term "Achthal Formation" for the deep-water turbidite succession. The base of the Achthal Formation (coord. E 012° 47' 42", N 47° 50' 51"), which conformably overlies the Buntmergelserie, is defined by the onset of turbiditic sedimentation in the uppermost Maastrichtian. The stratigraphic top is unknown because of the tectonic truncation of the Goppling section. However, deposition of the Achthal Formation probably ended in the Ypresian because grey calcareous marlstone of early Lutetian age occurs in the Ultrahelvetic thrust unit at Mattsee in Austria (Rögl and Egger, 2010), only ca. 25 km northeast of Teisendorf.



Fig. 21: Location of the Wimmern outcrop.

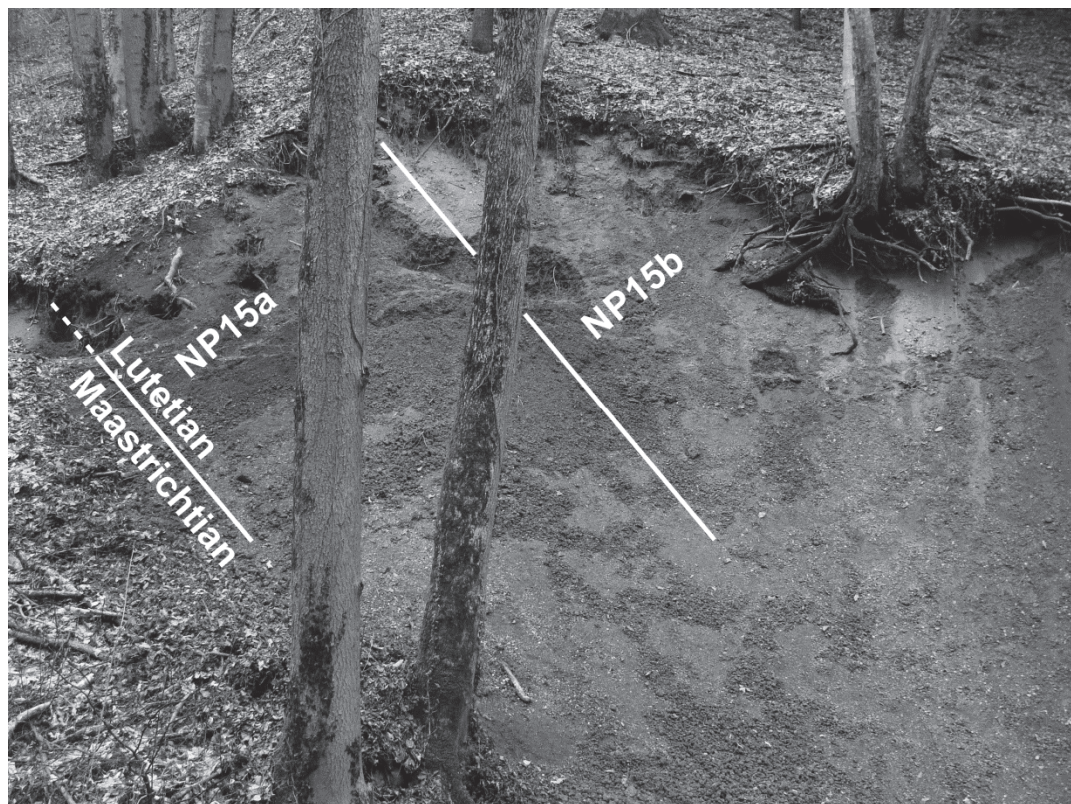


Fig. 22: Photograph of the Wimmern outcrop.

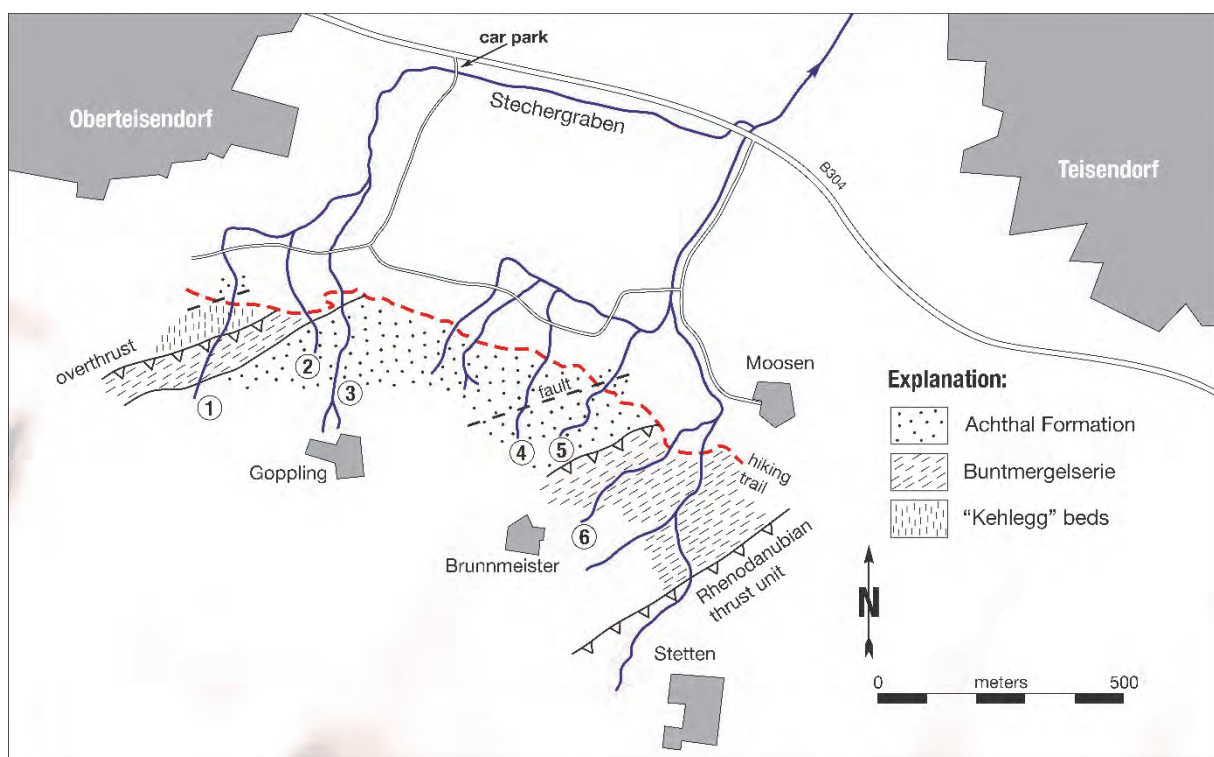


Fig. 23: Sketch map of the area investigated. Numbers indicate the most important creek sections mentioned in the text.

The deep-water system of the Achthal Formation is interpreted to have initially filled a slope depression lying above a subsiding basement fault block. Initial subsidence occurred in the latest Maastrichtian and continued into the early Paleogene. Synsedimentary tectonic activity was the primary control on the depositional evolution of the slope-basin.

In the forest south of Teisendorf and Oberteisendorf, a number of small creeks have created excellent exposures of the Achthal Formation. Almost all such outcrops lie to the south of the hiking trail running between the two villages. For better orientation, the more important creeks have been numbered (Fig. 23). The Ultrahelvetic nappe complex in the area is composed of three tectonic slices exposing beds continuously dipping to the southeast. During the field trip we will see part of the ca. 320 m thick sedimentary succession of the Goppling slice, which comprises Maastrichtian to lower Eocene deposits (Fig. 24).

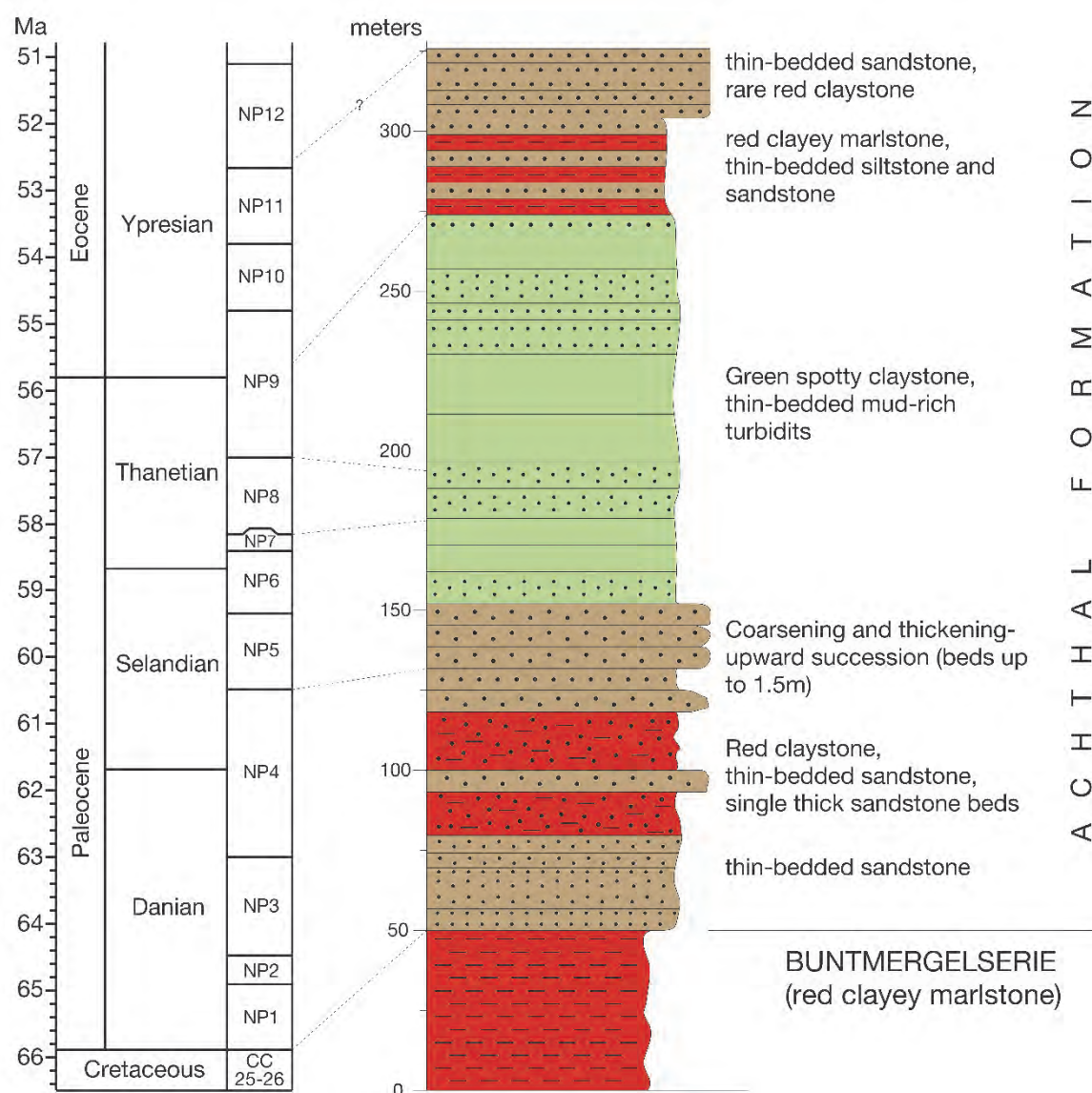


Fig. 24: Composite log of the Achthal Formation in the type area.

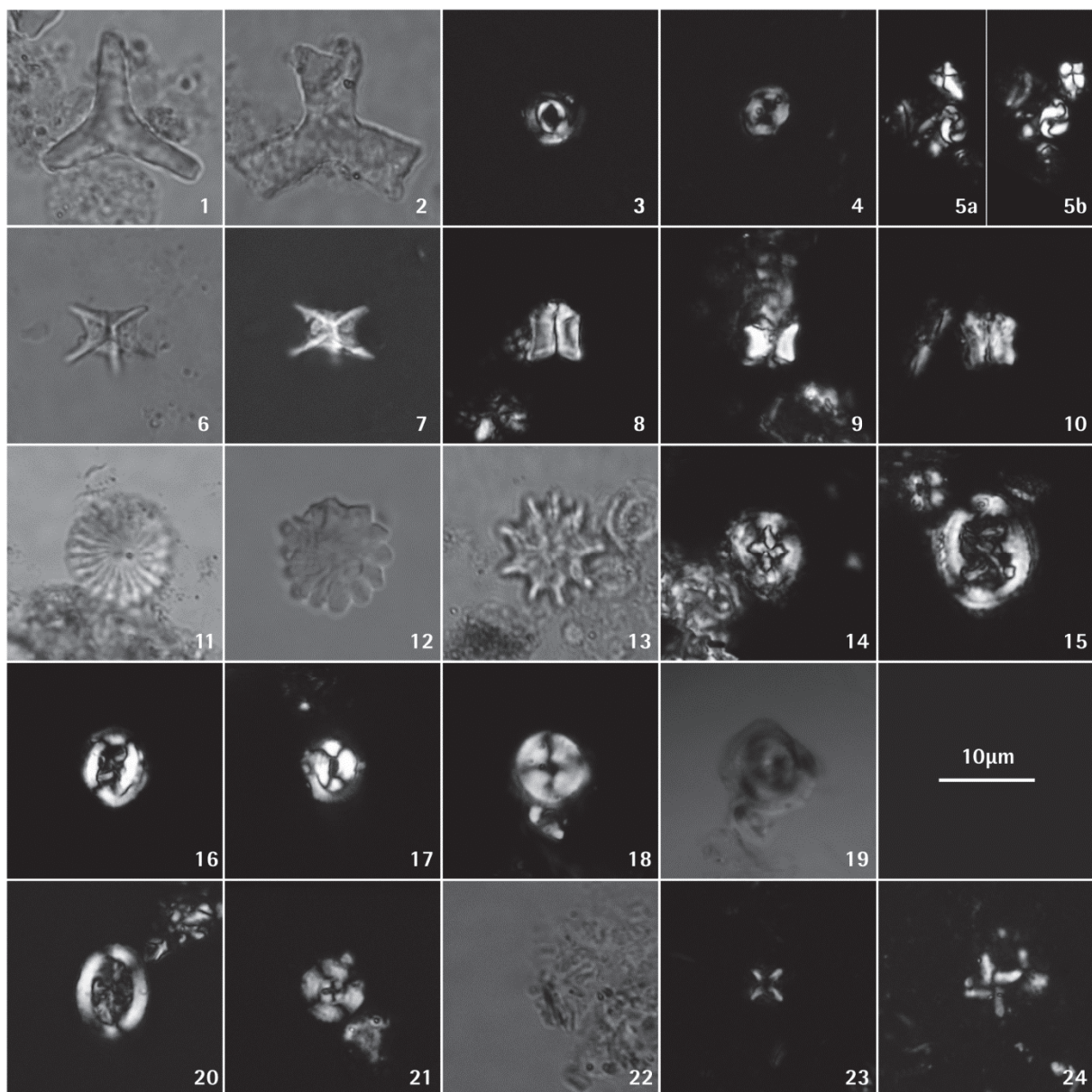


Fig. 25: Calcareous nannoplankton from the Goppling section.

Paleogene species: 1) *Tribrachiatus orthostylus* - Gstetten18/09; 2) *Tribrachiatus digitalis* - Gstetten10/09; 3) *Toweius callosus* - Gstetten22/09; 4) *Toweius occultatus* - Gstetten22/09; 5 a and b) *Sphenolithus anarrhopus* - Achthal 12/09; 6 and 7) *Rhomboaster cuspis* - Gstetten22/09; 8) *Fasciculithus tympaniformis* - Achthal12/09; 9) *Fasciculithus billii* - Achthal28/09; 10) *Fasciculithus ulii* - Achthal28/09; 11) *Discoaster multiradiatus* - Gstetten13/09; 12) *Discoaster mohleri* - Achthal12/09; 13) *Discoaster falcatus* - Gstetten13/09; 14) *Cruciplacolithus tenuis* - Achthal12/09; 15) *Chiasmolithus bidens* - Achthal12/09; 16) *Chiasmolithus danicus* - Achthal12/09; 17) *Coccolithus pelagicus* - Achthal12/09; 18 and 19) *Bomolithus elegans* - Achthal28/09.

Maastrichtian: 20) *Arkhangelskiella cymbiformis* - Achthal18/09; 21) *Ceratolithoides cf kampfneri* - Achthal18/09; 22) *Cyclagelosphaera reinhardtii* - Achthal18/09; 23) *Micula staurophora* - TS10/09; 24) *Micula prinsii* - TS10/09.

Stratigraphic Framework of the Goppling Section

Maastrichtian

The basal part of the Goppling section is formed by ca. 50 m of bioturbated red clayey marlstone, which is assigned to the Buntmergelserie. The top of this red-bed succession is exposed in creek 3 ("Goppling creek"), immediately south of the hiking trail bridge. There, the marlstone contains 19 wt% carbonate. The nannoplankton assemblages are dominated by *Micula staurophora*, whereas all other species are rare and most specimens are preserved only as fragments. Apart from *Lithraphidites quadratus*, the zonal marker for the upper Maastrichtian Zone CC25, *Arkhangelkiella cymbiformis* (Fig. 25/20), *Cyclagelosphaera reinhardtii* (Fig. 25/22), *Eiffellithus turriseiffeli*, *Micula staurophora*, *Prediscosphaera cretacea*, *Retecapsa crenulata*, and *Watznaueria barnesae* occur. At the top of the red marlstone outcrop, small specimens of *Ceratolithoides* cf *kamptneri* were observed (Fig. 25/21), indicating already Zone CC26.

Two samples for foraminifera studies were taken from the red marlstone at the outcrop in creek 3 outcrop. The assemblages consist essentially of a rich agglutinated fauna and a small number of calcareous benthic species. Very small planktic species were found only in one sample and display excellent grain-size sorting suggesting reworking by current activity.

Predominant dissolution-resistant species in the calcareous nannoplankton assemblages and the composition of foraminifera assemblages indicate sedimentation of the Maastrichtian red clayey marlstone in a deep-water environment. The absence of an authochthonous planktic fauna indicates deposition below the foraminiferal lysocline, where all planktic foraminifera are dissolved (Berger, 1970). Below the lysocline and above the calcite compensation depth (CCD) calcareous nannoplankton form coccolith ooze, because in spite of their small size, some coccoliths are more dissolution-resistant than foraminifera (see Hay, 2004, for a review).

In the latest Maastrichtian (*Micula prinsii*-Zone), rapid subsidence brought the Ultrahelvetic sea-floor to below the CCD. The red marlstone transitionally passes into ca. 5 m of grey marlstone with intercalated thin carbonate-cemented parallel-laminated turbiditic siltstone and sandstone beds. The best outcrop of these rocks was found in creek 2 about 10 m south of the hiking trail. In the lower part of this outcrop, carbonate values of three samples (TS2/09, TS7/09 and TS9/09) range between 20.8 wt% and 21.5 wt%. In the upper part carbonate values decrease to 9.4 wt% (TS10/09) and finally to less than 2 wt% (TS12/09, TS13/09 and TS14/09). Dinoflagellate cyst assemblages indicate a Maastrichtian age of the claystone as in the uppermost sample *Dinogymnum acuminatum* occurs (Fig. 26/1), which does not cross the K/Pg-boundary (e.g. Stover et al. 1996).

Associated with this regional subsidence along the southern continental margin of the European Plate, was the onset of turbidite sedimentation. Turbidity currents running parallel with the strike of the slope indicate an opposing topographic high, which caused deflection of the down slope sediment transport (Kneller and McCaffrey, 1999). Subsidence of the sea-floor associated with the deposition of sediment-gravity flows and the coeval generation of a sea-ward bounding topographic high suggest the formation of an intra-slope basin on subsiding crustal fault blocks.

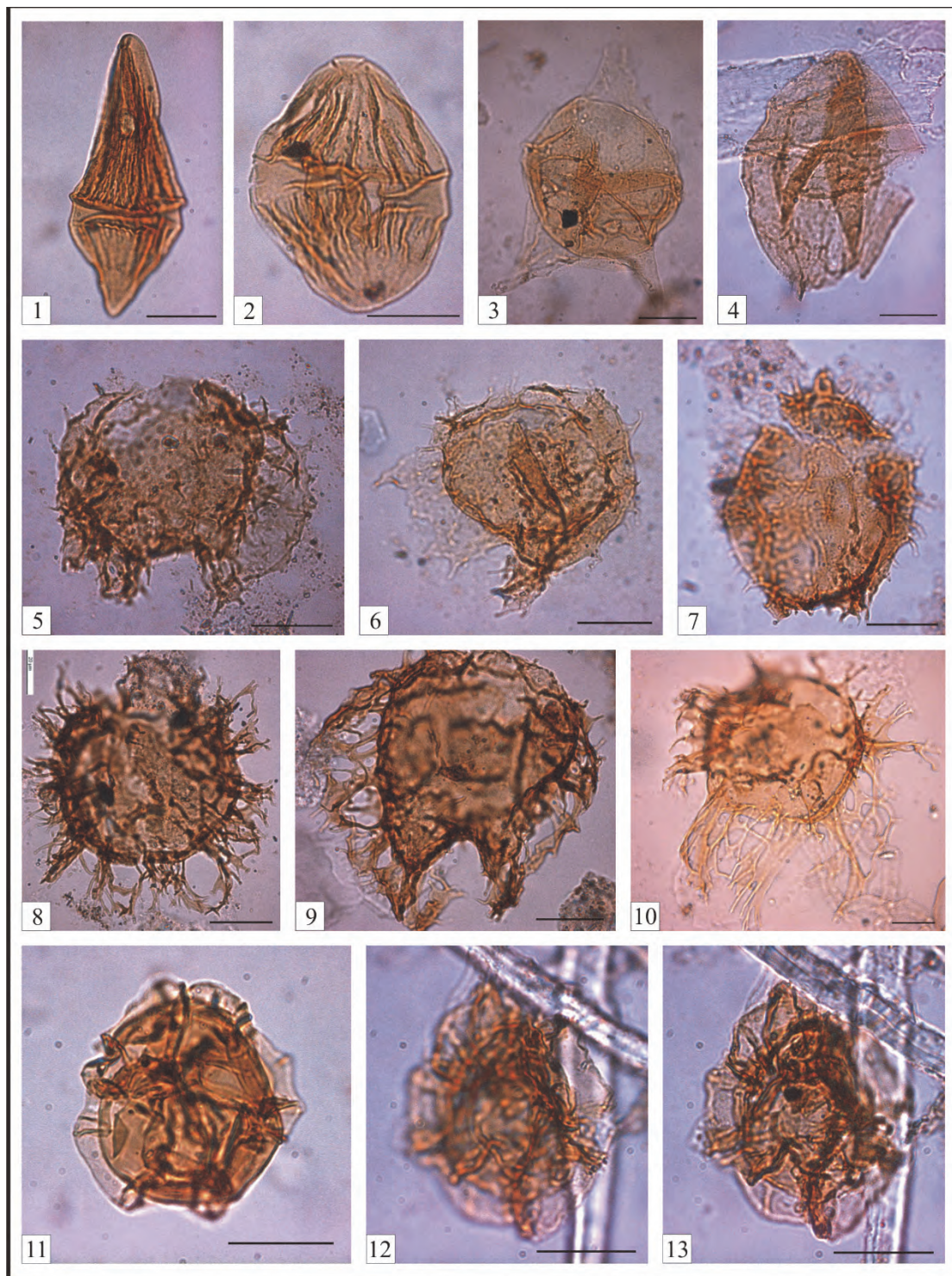


Fig. 26: Dinoflagellate taxa from the Goppling section. The species name is followed by sample location and England Finder coordinates (for localization of the specimen on the slide). Scale is 20 µm.
1) *Dinogymnium acuminatum* - TS11/09/a, O24; 2) *Dinogymnium* sp., TS11/09/a, F7/3; 3) *Cerodinium* sp., TS11/09/a, X16/3; 4) *Trityrodinium suspectum* - TS8/09/a, B24/2; 5) *Palynodinium grallator* - TS13/09/a, C40; 6) *Palynodinium grallator* - TS11/09/a, W36; 7) *Palynodinium minus* - TS13/09/b, Y27; 8) *Areoligera volata* - Ach.2/09/a, G12; 9) *Areoligera coronata* - Ach.1/09/a, A3; 10) *Areoligera gippingensis* - TS11/09/a, X34; 11) *Pterodinium cingulatum* subsp. *cingulatum* - TS12/09/a, W33/4; 12 and 13) *Pterodinium aliferum* - TS8/09/a, D6/1.

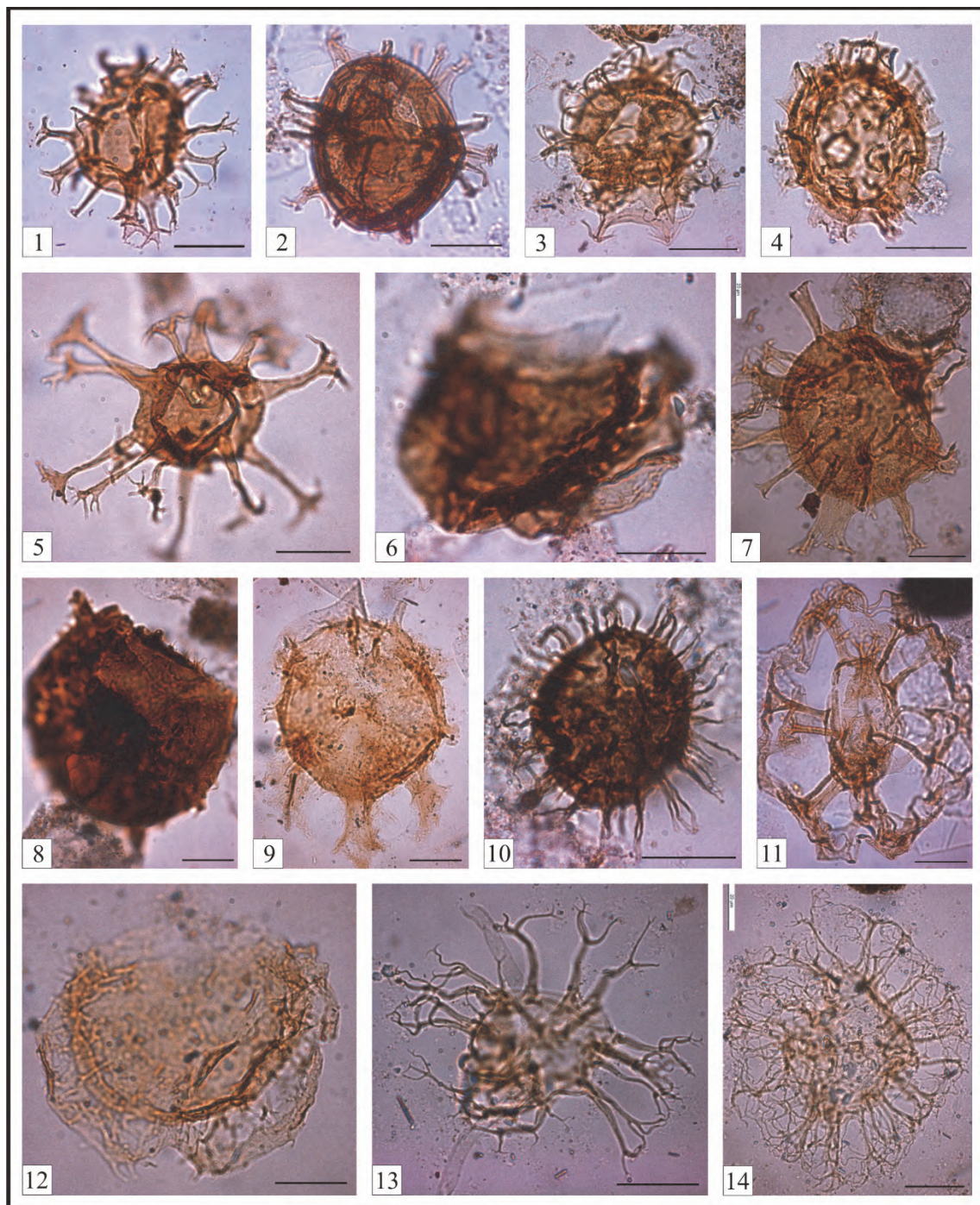


Fig. 27: Dinoflagellate taxa from the Goppling section (continuation). The species name is followed by sample location and England Finder coordinates (for localization of the specimen on the slide). Scale is 20 µm. 1) *Achromosphaera* cf. *alcicornu* - TS13/09/b, N5; 2) *Spiniferites pseudofurcatus* - TS4/09/b, X51/1; 3) *Hystrichostrogylon membraniphorum* - TS12/09/a, N24/2; 4) *Achilleodinium biformoides* - TS11/09/a, X8; 5) *Oligosphaeridium complex* - Ach. 2/09/a, G12; 6) *Senoniasphaera inornata* - Ach. 2/09/b, F40; 7) *Cordosphaeridium fibrospinosum* - TS12/09/a, B36/3; 8) *Carpatella cornuta* - Ach.1/09/b, K16; 9) *Damassadinium californicum* - TS11/09/a, P10; 10) *Operculodinium centrocarpum* - Ach.2/09/b, B25/4; 11) *Rigaudella aemula* - TS4/09/b, D18/1; 12) *Glaphyrocysta perforata* - TS11/09/a, S14/1; 13) *Surculosphaeridium longifurcatum* - TS11/09/a, M46/2; 14) *Trabeculidium quinquetrum* - TS12/09/a, D34/2.

Danian

Danian and Selandian deposits are almost continuously exposed in the Goppling creek gully. Due to the carbonate depletion, no calcareous plankton could be found in the siliciclastic succession, although dinoflagellate assemblages of samples Ach1/09 and Ach2/09 (see Fig. 27/6, 8 and 9) contain *Carpatella cornuta*, *Damassadinium californicum* and *Senoniasphaera inornata*, which have their first appearance date in the early Danian. *Palynodinium grallator* (Figs. 26/5 and 6) has its highest occurrence in the lowermost Danian planktonic foraminiferal Zone P1a (Habib et al., 1996; Dam et al., 1998; Brinkhuis et al., 1998). The samples were taken at the base (Ach1/09) and top (Ach2/09) of the same outcrop. Consequently, this outcrop can be assigned to Zone P1a in the zonation of Berggren et al. (1995).

The Danian shows a two-fold lithological subdivision. The 30 m thick lower part is dominated by thin-bedded (< 40 cm) parallel-laminated sandstone turbidites, that rarely show thin capping mudstone. In contrast to the Maastrichtian turbidites, the Danian ones are not calcite cemented and do not contain carbonate at all. They are fine-grained (grain diameters up to 0.2 mm), show clast supported fabrics, and have a quartzarenitic composition. Beside quartz (ca. 90 % of the grains), feldspar, chert and glauconite occur as components. Freimoser (1972) noted that the heavy mineral assemblages of these Paleocene sandstones are essentially composed of zircon, tourmaline and rutile (together about 90 % of the assemblage). Hemipelagic claystone between the turbidite beds is rare and when present only a few millimeters thick indicating that (1) turbidity currents entered the basin with a high frequency and (2) deposition took place below the local CCD.

In the 40 m thick upper part of the Danian, hemipelagic layers are common and often display red colors. Packages of red hemipelagic claystone contain thin base truncated turbiditic siltstone to sandstone beds. These packages are separated by single thick (>0.5 m) medium to coarse-grained sandstone beds showing grain diameters up to 1.0 mm. As in the lower Danian, only K-feldspar components can be observed and plagioclase is entirely absent. The beds are either massive or show stratification defined by 2-5 cm thick laminae. Graded (Ta) and parallel laminated (Tb) Bouma divisions form the major parts of these beds. Small-sized terrestrial plant remnants are commonly concentrated in horizontal Td-layers near the top of the beds and indicate a derivation of the turbidite material from land areas. Submarine erosion is evidenced by flute casts, which indicate sediment transport predominantly from the west, parallel to the approximately east-west trending slope.

One sample (Ach3/09) of the red claystone was studied for dinoflagellates but contained only *Areoligera senonensis*, which has a range from the Cretaceous to the Paleogene. Together with the last red hemipelagites, grey turbiditic clayey marlstones occur, containing strongly corroded nannoplankton assemblages. Beside substantial admixtures of Cretaceous species, *Chiasmolithus danicus*, *Cruciplacolithus tenuis*, *Coccolithus pelagicus* and *Toweius* spp. are indicative for the Danian (*Chiasmolithus danicus* Zone, NP3). However, the absence of *Ellipsolithus macellus*, the zonal marker for Zone NP4, might only be a consequence of the poor preservation in this sample.

Selandian

About 10 m up-section from the above mentioned Danian sample, nannoplankton assemblages contain *Fasciculithus tympaniformis*, the zonal marker for the calcareous nannoplankton Zone NP5 of earliest Selandian age. With the disappearance of red hemipelagites the discrimination between turbiditic and non-turbiditic rocks becomes difficult. Single turbidites show a distinct pelitic component (Bouma Td) in this part of the Goppling section, with approximately the same thickness as the sandy

part of the turbidite. This turbiditic mudstone only occasionally contains carbonate. In most cases it is devoid of carbonate and displays the same grey color as the supposed hemipelagic mudstone.

The Selandian, which forms the morphologically steepest part in the course of creek 3, is composed of a ca. 25 m thick thickening and coarsening upward succession. In the lower part of this succession decimeter-scale turbidites occur. Continuing up the exposure, the bed thicknesses gradually increase up to 1.5 m at the top of the succession. These sandstone beds are the thickest beds in the entire Achthal Formation and do not display turbiditic mudstone. In part, they contain intraformational mudstone clasts with diameters up to 0.2 m. Flute casts indicate paleotransport from west to east and thus an orientation parallel to the trend of the paleoslope.

Thanetian

In spite of excellent exposures along creek 3, the boundary between the Selandian and Thanetian is difficult to fix precisely due to carbonate depletion and the lack of calcareous plankton. Ca. 20 m downstream from the confluence in the uppermost part of creek 3 (Fig. 23), *Fasciculithus billii* is indicative for the upper part of Zone NP5. From here on upstream, a ca. 40 m thick part of the section is characterized by abundant olive-green strongly bioturbated „spotty“ claystone. Probably, the majority of the oval spots in these hemipelagic deposits represent cross sections of the trace fossils *Planolites* and *Thalassinoides* (Uchman, 1999). *Thalassinoides* spp. and a strongly fragmented specimen of *?Scolica strozzii* were found also as semi-reliefs at the base of turbidite beds (Fig. 28/4, 28/5 and 28/6).

The turbidites intervening with the claystone are mostly thin bedded and occasionally display substantial amounts of glauconite, resulting in green rock colors. Glauconite was deformed during burial and flowed around adjacent quartz grains. This is indicated by the patchy distribution of glauconite-filled areas, which are much larger than normal pores.

Some beds show a lenticular shape. The orientation of paleoflow indicators (flute casts and erosional channels) suggest paleotransport from north to south, following the gradient of the south-facing paleoslope. *Discoaster mohleri* (Fig. 25/12) indicative of Thanetian zone NP7, was found in the eastern branch of creek 3, about 50 m up-stream from the confluence with the western branch (Fig. 23). *Discoaster multiradiatus* (Fig. 25/11), the zonal marker of Zone NP9, was found in the uppermost part of the western branch.

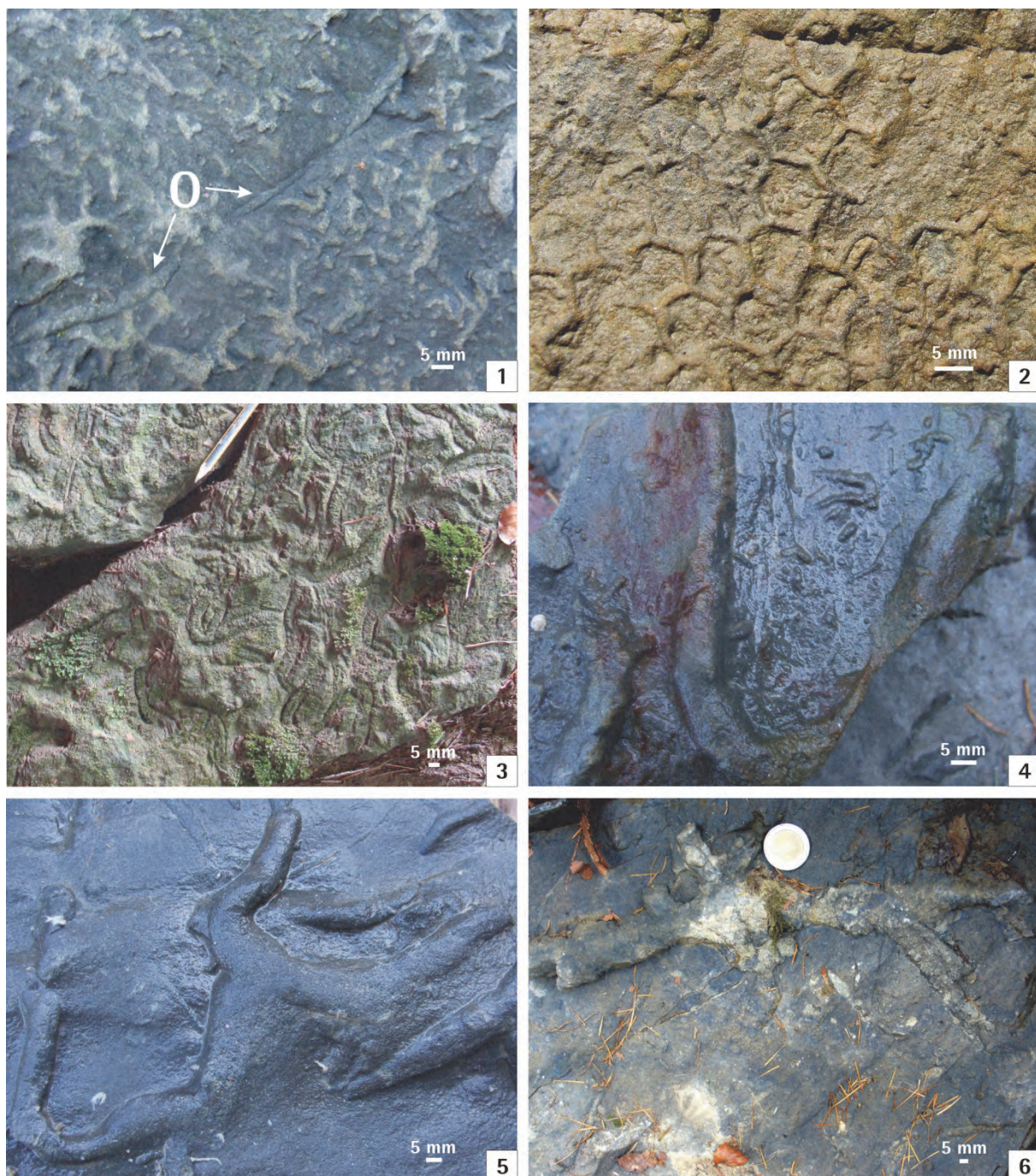


Fig. 28: Ichnofossils from the Thanetian (creek 3) and Ypresian (creek 4) of the Goppling section
1) *Ophiomorpha annulata* (O) and ?*Protopaleodictyon* isp. – creek 3; 2) *Paleodictyon majus.* – creek 4;
3) *Scolicia prisca* – creek 4; 4) ?*Scolicia strozzii* – creek 3; 5) *Thalassinoides* isp. – creek 3;
6) *Thalassinoides* isp. – creek 3.

Ypresian

The Ypresian of the Goppling section shows a two-fold lithological subdivision. The lower part consists of a ca. 50 m thick succession of decimeter-scale turbiditic sandstone and siltstone beds alternating with red colored marly claystone. The latter rock is often bioturbated and probably represents hemipelagic non-turbiditic material. As its carbonate values range between 4 wt% and 8 wt%, sedimentation slightly above the CCD can be assumed.

Samples containing *Rhomboaster cuspis* (Fig. 25/6 and 7) were found in the lower part of creek 5, about 20 m to the north of the hiking trail. *R. cuspis* has its first appearance date at the Paleocene/Eocene-boundary, which is situated in the upper third of Zone NP9. About 25 m to the south of the hiking trail, *Tribrachiatus digitalis* (Fig. 25/2) occurs, the marker fossil of sub-Zone NP10b in the refined zonation scheme of Aubry (1992). About 15 m further up-section, another outcrop of the red bed facies occurs and provided *Tribrachiatus orthostylus* (Fig. 25/1), whereas *T. contortus*, which has its highest occurrence at the NP10/NP11-boundary is absent. Therefore these samples can be assigned to the lower part of NP11 (*Discoaster binodosus*-Zone). Thus, in summary, the red bed facies encompasses the upper part of NP9 to the lower part of NP11.

Along strike to west, red beds containing *R. cuspis* were found in the upper part of creek 4. These deposits are separated by a fault from the underlying part of the succession in creek 4. In this gully, the topographically lowest outcrops lie just down-stream the hiking trail. *T. orthostylus* with pointed rays (Fig. 25/1) co-occurs with *Chiasmolithus bidens*, *Coccolithus pelagicus*, *Discoaster barbadiensis*, *D. multiradiatus*, *Ellipsolithus macellus* and *Sphenolithus primus*. Whereas the robust and dissolution resistant *Tribrachiatus* specimens may be common in the samples, the other species, in particular the discoasterids, are exceedingly rare due to dissolution. Carbonate values of two samples from this outcrop were 4.2 wt% and 4.8 wt%.

A few meters up-stream from the hiking trail the red bed facies in creek 4 shows a sharp sedimentary contact to an overlying ca. 60 m thick sand-rich and thin-bedded turbidite succession that displays only rare and very thin carbonate depleted hemipelagic layers. This suggests that the upper part of the Ypresian succession was deposited below the CCD and hence another subsidence pulse can be assumed. This interpretation is supported by the orientation of flute casts, which indicate paleoflow directions from west to east.

This part of the Goppling section commonly contains trace fossils (e.g. *Paleodictyon majus* and *Scolicia prisca*, see Fig. 28/2 and 3). According to Uchman (1999) the ichnogenus *Paleodictyon* probably reflects a moderate shortage of food. These generally oligotrophic conditions were interrupted by periodic accumulation of organic detritus (e.g. plant detritus) by turbidity currents. These more eutrophic episodes favored the ichnogenera *Ophiomorpha* and *Scolicia*. In the Rhenodanubian Group (Egger and Schwerd, 2008) of the adjacent abyssal Penninic basin, the ichnogenera *Ophiomorpha*, *Paleodictyon* and *Scolicia* are known exclusively from the Greifenstein Formation of Eocene age (Uchman, 1999).

Depositional evolution

Due to the lack of information about the three-dimensional geometry of the basin-fill, the scale and shape of this basin is unknown. It can be assumed that it was a narrow elongate, structurally controlled depression where tectonic activity was the primary control on sedimentation. Presumably, this confined basin was too small for the development of a large-scale deep-sea fan. Instead a channelized deep-water system could be expected, with the bounding slopes of the basin acting as channel walls

(Fig. 29). Gravity-induced flows entering a sub-basin drop their sediment load and prograde across the depression forming a thickening and coarsening upward succession (Anderson et al., 2006; Shultz and Hubbard, 2005).

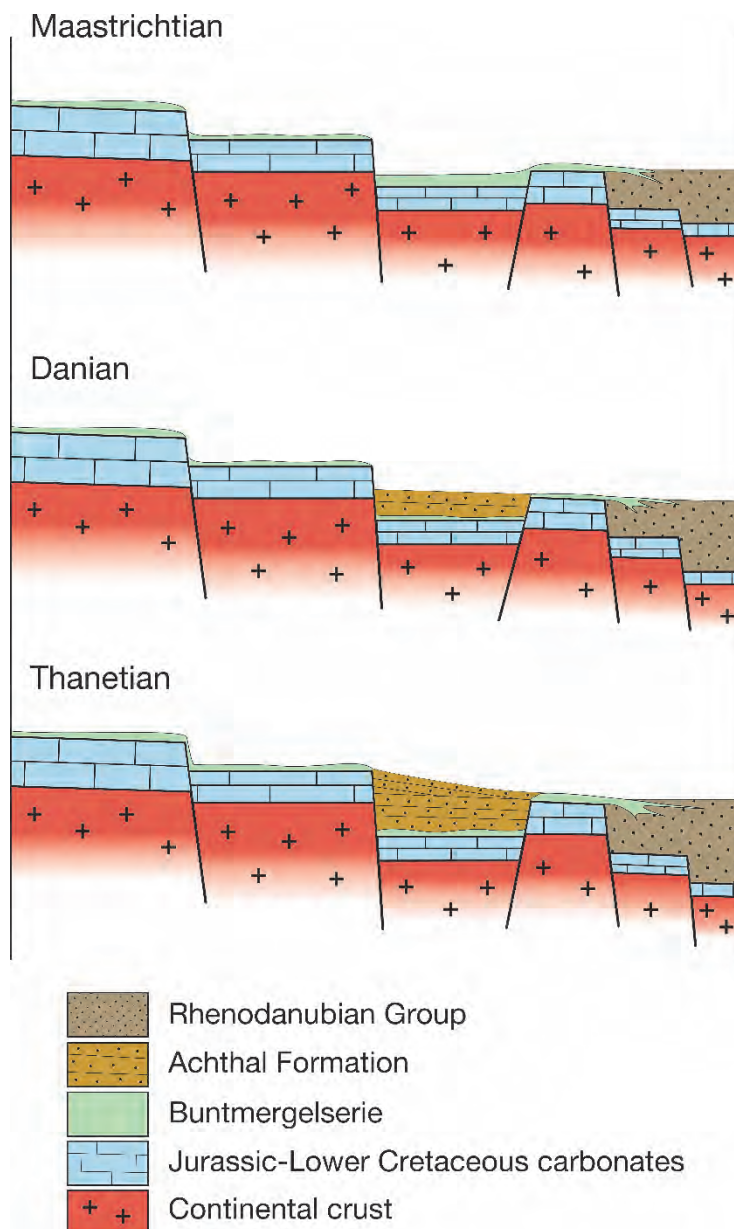


Fig. 29: Slope basin model for the deposition of the Achthal Formation.

At the front of this prograding lobe-like body the thin-bedded sand-rich turbidite succession of early Danian age was deposited (e.g. Crabaugh and Steel, 2004). The lack of muddy tops can be interpreted as an effect of flow-stripping of the fine-grained component of the turbidity currents (e.g. Piper and Normark, 1983; Sinclair and Tomasso, 2002). This indicates that during this early stage of basin evolution, the confining sill was still low. Hence it could be surmounted by the lower-density fraction of the turbidity currents, while the coarse-grained higher density portions of the flows were deflected and preserved upstream of the barrier. The rare and thin hemipelagites indicate the existence of high-

frequency trigger mechanisms (e.g. earthquakes) for turbidity currents during the onset of basin formation.

In a conventional fan model, the upper Danian packages of thin-bedded turbidites and red hemipelagic mudstone, which are separated by single thick sandstone beds, can be interpreted as interchannel deposits. In such a model, the thin-bedded turbidites are thought to result from low-density currents overflowing adjacent active channels, while the thicker beds are explained as the result of crevasses in the channel levee, which let high density turbidity currents (Lowe, 1982) escape to the basin floor (e.g. Mutti, 1977). This model implies the existence of subordinate fairways within the slope-basin.

Alternatively, the upper Danian facies can be seen as the result of an episode of comparatively tectonic quiescence. Siliciclastic material accumulated at the shelf edge over time and larger turbidity currents triggered by earthquakes or gravity load entered the slope-basin with low periodicity. This is indicated by the common occurrence of intervening hemipelagic red claystone as their deposition indicates very low sedimentation rates. The lack of muddy tops of the thick-bedded turbidites can again be explained as a result of flow-stripping as flow thickness was determined as the primary control of the run-up distance of a turbidity current onto the opposing slope (Muck and Underwood, 1990). It is assumed, that high-density currents (Lowe, 1982) lost their fine-grained component by down-spill, so that only their coarse-grained material is preserved in the sub-basin. Low-density currents had not the potential to surmount the bounding slope and remained completely in the sub-basin.

Increased subsidence at the end of the Danian caused ponding of the turbidity currents, which display a distinct pelitic component. However, sedimentation rates quickly outpaced subsidence rates and deposition reduced the relief sufficiently to allow spill down-slope. The filling up of the basin to the spill-point is indicated by downslope paleotransport directions in the upper Selandian and Thanetian. Due to the gradient reduction in the area of the former basinal structure turbidites were deposited on this flat surface and the ca. 95 m thick basin-fill succession of Danian and Selandian age became buried by slope deposits developing into a healed slope (e.g. Smith, 2004).

References

- ANDERSON, K.S., GRAHAM, S.A. AND HUBBARD, S.M., 2006. Facies, architecture, and origin of a reservoir-scale sand-rich succession within submarine canyon fill: insights from Wagon Caves Rock (Paleocene), Santa Lucia Range, California, U.S.A. *Journal of Sedimentary Research* 76, 819–838.
- AUBRY, M.-P., 1991. Sequence stratigraphy: Eustasy or tectonic imprint? *Journal of Geophysical Research* 96, 6641–6679.
- AUBRY, M.-P., 1992. Towards an upper Paleocene - lower Eocene high resolution stratigraphy based on calcareous nannofossil stratigraphy. *Israel Journal of Earth Sciences* 44, 239–253.
- BERGER, W.H., 1970. Planktonic foraminifera: selective solution and paleoclimatic interpretation. *Marine Geology* 8, 111–138.
- BERGGREN, W.A., KENT, D.V., SWISHER, C.C. AND AUBRY, M.-P., 1995. A revised cenozoic geochronology and chronostratigraphy. *Society for Sedimentary Geology Special Publication* 54, 129–212.
- BERGGREN, W.A. AND PEARSON, P.N., 2005. A revised tropical to subtropical Paleogene planktonic foraminiferal zonation. - *Journal of Foraminiferal Research*, 35, 279–298.
- BØGGILD O.B., 1918. Den vulkanske Aske i Moleret samt en Oversigt over Danmarks ældre Tertiærkjærgarter. *Danmarks Geologiske Undersøgelse (Series 2)* 33, 1–159.
- BOWEN, G.J., BRALOWER, T.J., DELANEY, M.L., DICKENS, G.R., KELLY, D.C., KOCH, P.L., KUMP, L.R., MENG, J., SLOAN, L.C., THOMAS, E., WING, S.L. AND ZACHOS, J.C., 2006. Eocene hyperthermal event offers insight into greenhouse warming. *EOS* 87, 165–169.
- BRASS, G. W., SOUTHAM, J. R. AND PETERSON, W. H., 1982. Warm saline bottom water in the ancient ocean. *Nature*, 296, 620–623.
- BRINKHUIS, H., 1994. Late Eocene to Early Oligocene dinoflagellate cysts from the Priabonian type-area (Northeast Italy): biostratigraphy and paleoenvironmental interpretation. – *Palaeogeography, Palaeoclimatology, Palaeoecology*, 107, 121–163.
- BRINKHUIS, H., BUJAK, J.P., VERSTEEGH, G.J.M. AND VISSCHER, H., 1998. Dinoflagellate-based sea surface temperature reconstructions across the Cretaceous-Tertiary boundary. *Palaeogeography, Palaeoclimatology, Palaeoecology* 141, 67–83.
- BRÜCKL, E., BEHM, M., DECKER, K., GRAD, M., GUTERCH, A., KELLER, G.R. AND THYBO, H., 2010. Crustal structure and active tectonics in the Eastern Alps. *Tectonics* 29, doi:10.1029/2009TC002491.
- BUKRY, D., 1971. Cenozoic calcareous nannofossils from the Pacific ocean. *Transactions San Diego Society of Natural History*, 16, 303–328.
- BUJAK, J.P., DOWNIE, C., EATON, G.L. AND WILLIAMS, G.L., 1980. Dinoflagellate cysts and acritarchs from the Eocene of Southern England. *Special Papers in Palaeontology*, 24, 3–100.
- BUTT, A., 1981, Depositional environments of the Upper Cretaceous rocks in the northern part of the Eastern Alps: Cushman Foundation Foraminiferal Research, Special Publication, 20, 121 p.
- BYBELL, L.M. AND SELF-TRAIL, J.M., 1994. Evolutionary, biostratigraphic, and taxonomic study of calcareous nannofossils from a continuous Paleocene–Eocene boundary section in New Jersey. U.S. Geological Survey Professional Papers, 1554, 1–107.
- COLLINSON, M.E., 2000. Fruit and seed floras from the Palaeocene/Eocene transition and subsequent Eocene in southern England: Comparison and palaeoenvironmental implications. In: SCHMITZ, B., SUNDQUIST, B. AND ANDREASSON, F.P. (eds.). *Early Paleogene Warm Climates and Biosphere Dynamics*, GFF (Journal of the Geological Society of Sweden), 122, 36–37.

- CRAABAUGH, J.P. AND STEEL, R.J., 2004. Basin-floor fans of the Central Tertiary Basin, Spitsbergen: relationship of basin-floor sand-bodies to prograding clinoforms in a structural active basin. In: LOMAS, S.A. AND JOSEPH, P. (eds.): Confined turbidite systems. Geological Society, London, Special Publication 222, 187–208.
- CROUCH, E. M., HEILMANN-CLAUSEN, C., BRINKHUIS, H., MORGANS, H.E.G., ROGERS, K.M., EGGER, H. AND SCHMITZ, B., 2001. Global dinoflagellate event associated with the Late Paleocene Thermal Maximum: *Geology*, 29, 315–318.
- CROWELL, J.C., 1974. Origin of late Cenozoic basins in southern California. In: Dickinson, W.R. (ed.): Tectonics and Sedimentation. Society of Economic Paleontologists and Mineralogists Special Publication 22, 190–204.
- DALE, B., 1996. Dinoflagellate cyst ecology: modelling and geological applications: In: JANSONIUS, J. AND McGREGOR, D.C. (eds.), Palynology: principles and applications; American Association of Stratigraphic Palynologists Foundation, 3, 1249–1275.
- DAM, G., NØHR-HANSEAN, H. AND KENNEDY, W. J., 1998. The northernmost marine Cretaceous-Tertiary boundary section: Nuussuaq, West Greenland. *Geology of Greenland Survey Bulletin* 180, 138–144.
- DECKER, K. AND PERESSON, H., 1996. Tertiary kinematics in the Alpine-Carpathian-Pannonian system: links between thrusting, transform faulting and crustal extension. In: Wessely, G. and Liebl, W.: Oil and gas in Alpidic thrustbelts and basins of central and eastern Europe. – EAGE Special Publication, 5, 69–77.
- DICKENS, G.R., 2000. "Methane oxidation during the late Palaeocene thermal maximum". *Bulletin Société Géologique de France*, 171, 37–49.
- DRAXLER, I., 2007. Significant Palynomorphs from the Thanetian Kroisbach-Member in Salzburg (Eastern Alps, Austria). *Jahrbuch der Geologischen Bundesanstalt*, 357–377.
- DYBKJÆR, K. AND RASMUSSEN, E.S., 2000. Palynological dating of the Oligocene – Miocene successions in the Lillebælt area, Denmark: *Bulletin of the Geological Society of Denmark*, 47, 87–103.
- EATON, G.L., 1976. Dinoflagellate cysts from the Bracklesham Beds (Eocene) of the Isle of Wight, Southern England. *Bulletin of the British Museum of Natural History and Geology*, 26, 227–332.
- EGGER, H., 1995. Die Lithostratigraphie der Altengbach-Formation und der Anthering-Formation im Rhenodanubischen Flysch (Ostalpen, Penninikum). *Neues Jahrbuch für Geologie und Paläontologie Abhandlungen* 196, 69–91.
- EGGER, H., BICHLER, M., HOMAYOUN, M., KIRCHNER, C. AND SURENIAN, R., 1995. Spätpaläozäne Bentonite aus der Gosau-Gruppe des Untersberg-Vorlandes (Nördliche Kalkalpen, Salzburg). *Jahrbuch der Geologischen Bundesanstalt*, 139, 13–20.
- EGGER H., LOBITZER, H., POLESNY, H. AND WAGNER, L.R., 1997. Trip#1 – Cross section through the oil and gas-bearing Molasse basin into the alpine units in the area of Salzburg, Austria-Bavaria). Guidebook AAPG International Conference and Exhibition, 104p.
- EGGER, H., HEILMANN-CLAUSEN, C. AND SCHMITZ, B., 2000. The Paleocene/Eocene-boundary interval of a Tethyan deep-sea section and its correlation with the North Sea Basin. *Société Géologique de France Bulletin*, 171, 207–216.
- EGGER, H., HOMAYOUN, M. AND SCHNABEL, W., 2002. Tectonic and climatic control of Paleogene sedimentation in the Rhenodanubian Flysch Basin (Eastern Alps, Austria). *Sedimentary Geology* 152, 247–262.
- EGGER, H., FENNER, J., HEILMANN-CLAUSEN, C., RÖGL, F., SACHSENHOFER, R.F. AND SCHMITZ, B., 2003. Paleoproductivity of the northwestern Tethyan margin (Anthering Section, Austria) across the Paleocene-Eocene transition. In: WING, S.L., GINGERICH, P., SCHMITZ, B., THOMAS, E. (eds.), Causes and Consequences of Globally Warm Climates in the Early Paleogene, Geological Society of America Special Paper, 369, 133–146.
- EGGER, H., RÖGL, F. AND WAGREICH, M., 2004. Biostratigraphy and facies of Paleogene deep-water deposits at Gams (Gosau Group, Austria). *Annalen Naturhistorisches Museum Wien*, 106A, 281–307.
- EGGER, H., HOMAYOUN, M., HUBER, H., RÖGL, F. AND SCHMITZ, B., 2005. Early Eocene climatic, volcanic, and biotic events in the northwestern Tethyan Untersberg section, Austria. *Palaeogeography, Palaeoclimatology, Palaeoecology* 217, 243–264.

- EGGER, H. AND BRÜCKL, E., 2006. Gigantic volcanic eruptions and climatic change in the early Eocene. *International Journal Earth Sciences*, 95, 1065–1070.
- EGGER, H. AND SCHWERD, K., 2008. Stratigraphy and sedimentation rates of Upper Cretaceous deep-water systems of the Rhenodanubian Group (Eastern Alps, Germany). *Cretaceous Research* 29, 405–416.
- EGGER, H., HEILMANN-CLAUSEN, C. AND SCHMITZ, B., 2009. From shelf to abyss: Record of the Paleocene/Eocene-boundary in the Eastern Alps (Austria). *Geologica Acta*, 7, 215–227.
- EGGER, H. AND MOHAMED, O., 2010. A slope-basin model for early Paleogene deep-water sedimentation (Achthal Formation nov. nom.) at the Tethyan continental margin (Ultrahelvetic realm) of the European Plate (Eastern Alps, Germany). *Austrian Journal of Earth Sciences* 103, 121–137.
- EGGER, H., RÖGL, F., BIJL, P., BRINKHUIS, H. AND DARGA, R., 2011. The Middle Eocene transgression on the southern European shelf (Adelholzen beds, Eastern Alps, Bavaria. In: EGGER, H. (ed): Climate and Biota of the Early Paleogene, Conference Program and Abstracts, 5–8 June 2011, Salzburg, Austria. Berichte der Geologischen Bundesanstalt, 85, p.70.
- ELDHOLM, O. AND GRUE, K., 1994. North-Atlantic Volcanic Margins: Dimensions and Production-Rates. *Journal Geophysical Research*, 99, 2955–2968.
- FENNER, J., 1994. Diatoms of the Fur Formation, their taxonomy and biostratigraphic interpretation.– Results from the Harre borehole, Denmark: Aarhus Geoscience 1, 99–163.
- FREIMOSER, M., 1972. Zur Stratigraphie, Sedimentpetrographie und Faziesentwicklung der Südostbayerischen Flyschzone und des Ultrahelvetikums zwischen Bergen / Obb. und Salzburg. *Geologica Bavaria* 66, 7–91.
- FRISCH, W., 1979. Tectonic progradation and plate tectonic evolution of the Alps. *Tectonophysics* 60, 121–139.
- GEROCH, S. AND KAMINSKI, M. A., 1992. The morphology, palecology and systematics of *Nothia excelsa* (Grzybowski), a deep-water agglutinated foraminifer. *Annales Societas Geologorum Poloniae*, 62, 255–265.
- GOODAY, A. J., SHIRES, R. AND JONES, A.R., 1997. Large, deep-sea agglutinated foraminifera: two different kinds of organization and their possible ecological significance. *Journal of Foraminiferal Research*, 27, 278–291.
- GALEOTTI, S., ANGORI, E., COCCIONI, R., FERRARI, G., GALBRUN, B., MONECHI, S., PREMOLI-SILVA, I., SPEIJER, R. AND TURI, B., 2000. Integrated stratigraphy across the Paleocene/Eocene boundary in the Contessa Road section, Gubbio (central Italy). *Société Géologique de France Bulletin*, 171, 355–366.
- GANSS, O. AND KNIPSCHEER, H.C.G., 1956. Die Maastricht-Eozän-Folge des Helvetikums im Sprunggraben bei Oberteisendorf (Obb.) und ihre Gliederung mit Hilfe pelagischer Foraminiferen. *Geologisches Jahrbuch* 71, 617–630.
- GOHRBANDT, K., 1963. Zur Gliederung des Paläogen im Helvetikum nördlich Salzburg nach planktonischen Foraminiferen. *Mitteilungen der Geologischen Gesellschaft in Wien*, 56, 1–116.
- GRAUP, G. AND SPETTEL, B., 1989. Mineralogy and phasechemistry of an Ir-enriched pre-K/T layer from the Lattengebirge, Bavarian Alps, and significance for the KTB problem. *Earth and Planetary Science Letters* 95, 271–290.
- GRACHEV, A.F., KORCHAGIN, O.A., KOLLMANN, H.A., PECHERSKY, D.M. AND TSELMOVICH, A., 2005. A new look at the nature of the transitional layer at the K/T boundary near Gams, Eastern Alps, Austria, and the problem of the mass extinction of the biota. *Russian Journal of Earth Sciences*, 7, 1–45.
- GRACHEV, A.F., KORCHAGIN, O.A., TSELMOVICH, V.A. AND KOLLMANN, H.A., 2008. Cosmic dust and micrometeorites in the transitional clay layer at the Cretaceous-Paleogene boundary in the Gams Section. *Physics of the Solid Earth*, 44, 555–569.
- GRACHEV, A.F., KAMENSKY, I.L., KORCHAGIN, O.A. AND KOLLMANN, H.A., 2007. The first data on helium isotopy in a transitional clay layer at the Cretaceous-Paleogene boundary (Gams, Eastern Alps). *Physics of the Solid Earth*, 43:766–772.
- GRADSTEIN, F., OGG, J. AND SMITH, A., 2004. *A Geologic Time Scale*, 589 p. (Cambridge University Press).

- GÜMBEL, C.W., 1862. Geognostische Beschreibung des bayerischen Alpengebirges und seines Vorlandes. 950 pp., Gotha (Justus Perthes).
- HABIB, D., OLSSON, R.K., LIU, C. AND MOSHKOVITZ, S., 1996. High-resolution biostratigraphy of sea-level low, biotic extinction, and chaotic sedimentation of the Cretaceous-Tertiary boundary in Alabama, north of the Chicxulub crater. In: RYDER, G., FASTOVSKY, D. AND GARTNER, S. (Eds.), *The Cretaceous/Tertiary Event and Other Catastrophes in Earth history*. Geological Society of America, Special Paper 307, 243–252.
- HAGN, H., 1960. Die stratigraphischen, paläogeographischen und tektonischen Beziehungen zwischen Molasse und Helvetikum im östlichen Oberbayern. *Geologica Bavaria* 44, 5–208.
- HAGN, H., 1967. Das Alttertiär der Bayerischen Alpen und ihres Vorlandes. *Mitteilungen Bayerische Staatssammlung Paläontologie und historische Geologie* 7, 245–320.
- HAGN, H., 1981. Die Bayerischen Alpen und ihr Vorland in mikropaläontologischer Sicht (Exkursionsführer 17. Europäisches Mikropaläontologisches Kolloquium). *Geologica Bavaria* 82, 1–408.
- HAGN, H., COSTA, L.I., HERM, D., HILLEBRANDT, A. V., HÖFLING, R., LINDBERG, H.G., MALZ, H., MARTINI, E., MOUSSAVIAN, E., PERCH-NIELSEN, K., PFEIL, F.H., RISCH, H., SCHaub, H., SCHMIDT, K., SCHROEDER, R., ULRICH, M., VOIGT, E., WEHNER, H., WEISS, W. AND WITT, W., 1981. Die Bayerischen Alpen und ihr Vorland in mikropaläontologischer Sicht (Exkursionsführer 17. europäisches Mikropaläontologisches Kolloquium). *Geologica Bavaria* 82, 1–408.
- HAQ, B.U., HARDENBOL, J. AND VAIL, P.R., 1987. Mesozoic and Cenozoic Chronostratigraphy and eustatic cycles. *Society of Economic Paleontologists and Mineralogists Special Publication* 42, 71–108.
- HARLAND, R., 1979. The Wetzelia (Apectodinium) homomorpha plexus from the Paleogene/earliest Eocene of North-West Europe. IV International Palynological Conference, Lucknow (1976–1977), 2, 59–70.
- HAY, W.W., 2004. Carbonate fluxes and calcareous nannoplankton. In: THIERSTEIN, H.R. AND YOUNG, J.R. (eds.): *Coccolithophores*, 509–528 (Springer).
- HEILMANN-CLAUSEN, C., 1985. Dinoflagellate stratigraphy of the uppermost Danian to Ypresian in the Viborg 1 borehole, central Jylland, Denmark: Danmarks Geologiske Undersøgelse, ser. A, 7, 1–69.
- HEILMANN-CLAUSEN, C. AND COSTA, L.I., 1989. Dinoflagellate Zonation of the Uppermost Paleocene? to Lower Miocene in the Wursterheide Research Well, NW Germany. *Geologisches Jahrbuch, Ser. A*, 111, 431–521.
- HEILMANN-CLAUSEN, C., 1995. Palæogene aflejringer over Danskekalken. In: NIELSEN, O.B. (ed.). *Danmarks geologi fra Kridt til i dag*. Aarhus Geokompender No. 1, 70–114.
- HEILMANN-CLAUSEN, C. AND EGGER, H., 1997. An ash-bearing Paleocene/Eocene sequence at Anthering, Austria: biostratigraphical correlation with the North Sea Basin. *Danmarks og Grønlands undersøgelse rapport*, 1997/87, 13.
- HEILMANN-CLAUSEN, C. AND EGGER, H., 2000. The Anthering outcrop (Austria), a key section for correlation between Tethys and northwestern Europe near the Paleocene/Eocene boundary: *GFF (Journal of the Geological Society of Sweden)*, 122, 69.
- HEILMANN-CLAUSEN, C. AND SCHMITZ, B., 2000. The late Paleocene thermal maximum $\delta^{13}\text{C}$ excursion in Denmark? – *GFF (Journal of the Geological Society of Sweden)*, 122, p. 70.
- HEILMANN-CLAUSEN, C. AND VAN SIMAEYS, S., 2005. Dinoflagellate cysts from the Middle Eocene to ?lowermost Oligocene succession in the Kysing research borehole, central Danish Basin. *Palynology*, 29, 141–204.
- HEISTER, L.E., O'DAY, P.A., BROOKS, C.K., NEUHOFF, P.S. AND BIRD, D.K., 2001. Pyroclastic deposits within the East Greenland Tertiary flood basalts. *Journal Geological Society London*, 158, 269–284.
- HERM, D., HILLEBRANDT, A. AND PERCH-NIELSEN, K., 1981. Die Kreide/Tertiärgrenze im Lattengebirge (Nördliche Kalkalpen) in mikropaläontologischer Sicht. *Geologica Bavaria*, 82, 319–344.
- HESSE, R., 1975. Turbiditic and non-turbiditic mudstone of Cretaceous flysch sections of the East Alps and other basins. *Sedimentology*, 22, 387–416.

- HESSE, R., 1982. Cretaceous-Paleogene Flysch Zone of the east Alps and Carpathians: identification and plate-tectonic significance of „dormant“ and „active“ deep-sea trenches in the Alpine-Carpathian Arc. In: LEGGETT, J.K. (Ed.). Trench-forearc geology. Geological Society of London Special Publication 10, 471–494.
- HILLEBRANDT, A. v., 1962. Das Paleozän und seine Foraminiferenfaunen im Becken von Reichenhall und Salzburg. Bayerische Akademie der Wissenschaften mathematisch-naturwissenschaftliche Klasse Abhandlungen, 108, 1–113.
- HILLEBRANDT, A. v., 1993. Nummuliten und Assilinen aus dem Eozän des Krappfeldes in Kärnten (Österreich). Zitteliana, 20, 277–293.
- HOFMANN, CH.-CH., PANCAST, R., OTTNER, F., EGGER, H., TAYLOR, K., MOHAMED, O. AND ZETTER, R., 2011. Palynology, biomarker assemblages and clay mineralogy of the Early Eocene Climate Optimum (EECO) in the transgressive Krappfeld succession (Eastern Alps, Austria). Austrian Journal of Earth Sciences, 105/1, 224–239.
- HUBER, H., KOEBERL, C. AND EGGER, H., 2003. Geochemical study of Lower Eocene volcanic ash layers from the Alpine Anthering Formation, Austria. Geochemical Journal, 37, 123–134.
- IAKOVLEVA, A.I. AND HEILMANN-CLAUSEN, C., 2007. *Wilsonidium pechoricum* new species – a new dinoflagellate species with unusual asymmetry from the Paleocene/Eocene transition. J. Paleont. 8, 1020–1030.
- JONES, R.W. AND CHARNOCK, M.A., 1985. „Morphogroups“ of agglutinating foraminifera. Their life positions and feeding habits and potential applicability in (paleo)ecological studies. Revue Paleobiologique, 4, 311–320.
- KAMINSKI, M.A., GRADSTEIN, F.M. AND BERGGREN, W.A., 1989. Palaeogene benthic foraminifer biostratigraphy and Palaeoecology at Site 647, southern Labrador Sea. In: SRIVASTAVA, S.P., ARTHUR, M.A. AND CLEMENT, B. et al., Proceedings of the Ocean Drilling Program, Scientific Results, 105, 705–730.
- KAMINSKI, M.A., KUHNT, W. AND RADLEY, J.D., 1996. Palaeocene–Eocene deep water agglutinated foraminifera from the Numidian Flysch (Rif, Northern Morocco): their significance for the palaeoceanography of the Gibraltar gateway. Journal of Micropalaeontology, 15, 1–19.
- KAMINSKI, M.A., KUHNT, W. AND MOULLADE, M., 1999. The evolution and paleobiogeography of abyssal foraminifera since the Early Cretaceous: a tale of four faunas: Neues Jahrbuch Geologie Paläontologie Abhandlungen, 212, 401–439
- KEDVES, M., 1980. Palynological investigations on Austrian Upper Cretaceous and Lower Tertiary sediments. Acta Biologica Szeged, 26, 63–77.
- KLEY, J. AND VOIGT, T., 2008. Late Cretaceous intraplate thrusting in central Europe: Effect of Africa-Iberia-Europe convergence, not Alpine collision. Geology 36, 839–842.
- KNELLER, B. AND McCAFFREY, W., 1999. Depositional effects of flow nonuniformity and stratification within turbidity currents approaching a bounding slope: deflection, reflection and facies variation. Journal of Sedimentary Research 69, 980–991.
- KÖTHE, A., 1990. Paleogene Dinoflagellates from Northwest Germany. Geologisches Jahrbuch, Serie A, 118, 3–111.
- KNOX, R.W.O'B., 1984. Nannoplankton zonation and the Paleocene/Eocene boundary beds of northwestern Europe: An indirect correlation by means of volcanic ash layers. Journal Geological Society London 141:993–999.
- KNOX, R.W.O'B. AND MORTON, A. C., 1988. The record of early Tertiary North Atlantic volcanism in sediments from the North Sea Basin. Early Tertiary Volcanism and the Opening of the NE Atlantic (MORTON, A. C. AND PARSON, L. M., eds.), Geological Society London Special Publication, 39, 407–419.
- KNOX, R.W.O'B., 1998. The Tectonic and Volcanic History of the North Atlantic Region During the Paleocene-Eocene Transition: Implications for the NW European and Global Biotic Events. In: AUBRY, M.-P., LUCAS, S. AND BERGGREN, W.A. (Eds.), Late Paleocene-Early Eocene Climatic and Biotic Events in the Marine and Terrestrial Records, Columbia University Press, New York, 91–102.

- KUHN, W. AND WEIDICH, K.F., 1987. Neue mikropaläontologische Ergebnisse aus dem Paleozän des Haunsberg-Helvetikums (Salzburg, Österreich). *Paläont. Zeitschrift* 61, 181–201.
- KUHNT, W., KAMINSKI, M.A. AND MOULLADE, M., 1989. Late Cretaceous deep-water agglutinated foraminiferal assemblages from the North Atlantic and its marginal seas. *Geologische Rundschau*, 78, 1121–1140.
- LAHODYNSKY, R., 1988. Lithostratigraphy and sedimentology across the Cretaceous/Tertiary Boundary in the Flyschglosau (Eastern, Alps, Austria). – *Revista Espanola Paleontologia Special Volume*, 1988, 73–82.
- LARSEN, L.M., FITTON, J.G. AND PEDERSEN, A.K., 2003. Paleogene volcanic ash layers in the Danish Basin: compositions and source areas in the North Atlantic Igneous Province. *Lithos*, 71, 47–80.
- LOWE, D.R., 1982. Sediment gravity flows: II. Depositional models with special reference to the deposits of high-density turbidity currents. *Journal of Sedimentary Petrology* 52, 279–297.
- LUTERBACHER, H. P., ALI, J. R., BRINKHUIS, H., GRADSTEIN, F.M., HOOKER, J.J., MONECHI, S., OGG, J.G., POWELL, J., RÖHL, U., SANFILIPPO, A. AND SCHMITZ, B., 2004. The Paleogene Period. In: GRADSTEIN, F.M., OGG, J.G. AND SMITH, A.G., (eds.). *A Geologic Time Scale 2004*. Cambridge University Press, 384–408.
- MENKVOLD-GFELLNER, U., 1997. Die Bürgen-Fm. Und die Klinsenhorn-Fm.: Formelle Definition zweier lithostratigraphischer Einheiten des Eozäns der helvetischen Decken. *Eclogae geol. Helv.* 90, 245–261.
- MUCK, M.T. AND UNDERWOOD, M.B., 1990. Upslope flow of turbidity currents: A comparison among field observations, theory, and laboratory models. *Geology* 18, 54–57.
- MUTTI, E., 1977. Distinctive thin-bedded turbidite facies and related depositional environments in the Eocene Hecho Group (South-central Pyrenees, Spain). *Sedimentology* 24, 107–131.
- NACHTMANN, W. AND WAGNER, L., 1987. Mesozoic and early Tertiary evolution of the Alpine foreland in Upper Austria and Salzburg, Austria. *Tectonophysics* 137, 61–76.
- NEUBAUER, F., GENSER, J. AND HANDLER, R., 2000. The Eastern Alps: Result of a two-stage collision process. *Mitteilungen österreichische geologische Gesellschaft*, 92, 117–134.
- NICOLO, M.J., 2008. Multiple early Eocene hyperthermal events: Their lithologic expressions and environmental consequences. Unpublished PhD Thesis, Rice University (<http://scholarship.rice.edu/handle/1911/26797>).
- OBERHAUSER, R., 1991. Erläuterungen zur geologischen Karte der Republik Österreich 1: 25.000 Blatt 110 St. Gallen Süd und 111 Dornbirn Süd. 72 pp., Vienna (Geologische Bundesanstalt).
- PERCH-NIELSEN, K., MCKENZIE, J. AND HE, Q., 1982. Biostratigraphy and isotope stratigraphy and the „catastrophic“ extinction of calcareous nannoplankton at the Cretaceous/Tertiary boundary.- In: SILVER, L.T. AND SCHULTZ, P.H. (eds.): *Geological Implications of Impacts of Large Asteroids and Comets on the Earth*. Geological Society of America Special Paper, 190, 353–371.
- PERYT, D., LAHODYNSKY, R., ROCCHIA, R. AND BOCLET, D., 1993. The Cretaceous/Paleogene boundary and planktonic foraminifera in the Flyschglosau (Eastern Alps, Austria). *Palaeogeography, Palaeoclimatology, Palaeoecology*, 104, 239–252.
- PERYT, D., LAHODYNSKY, R. AND DURAKIEWICZ, T., 1997. Deep-water agglutinated foraminiferal changes and stable isotope profiles across the Cretaceous-Paleogene boundary in the Rotwand section, Eastern Alps (Austria). *Palaeogeography, Palaeoclimatology, Palaeoecology*, 132, 287–307.
- PIPER, D.J.W. AND NORMARK, W.R., 1983. Turbidite-deposits, patterns and flow characteristics, Navy Submarine Fan, California borderland. *Sedimentology* 30, 681–694.
- PREISINGER, A., ZOBETZ, E., GRATZ, A., LAHODYNSKY, R., BECKE, M., MAURITSCH, H.J., EDER, G., GRASS, F., RÖGL, F., STRADNER, H. AND SURENIAN, R., 1986. The Cretaceous/Tertiary boundary in the Gosau Basin, Austria. *Nature*, 322, 797–799.
- PREY, S., 1952. Aufnahmen in der Flyschzone auf den Blättern Gmunden-Schafberg (4851) und Kirchdorf/Krems (4852) (Gschliefgraben), sowie den Blättern Ybbs (4754) und Gaming-Mariazell (4854) (Rogatsboden). – *Verhandlungen der Geologischen Bundesanstalt* 1952, 41–45.

- PREY, S., 1957. Ergebnisse der bisherigen Forschungen über das Molassefenster von Rogatsboden (NÖ.). Jahrbuch der Geologischen Bundesanstalt 100, 299–358.
- PUJALTE, V. AND SCHMITZ, B., 2006. Abrupt climatic and sea level changes across the Paleocene-Eocene boundary, as recorded in an ancient coastal plain setting (Pyrenees, Spain). Climate and biota of the Early Paleogene Abstracts, p. 103 (Bilbao).
- RASSER, M.W. AND PILLER, W.E., 1999. Kroisbachgraben und Frauengrube: Lithostratigraphische Typuslokalitäten für das paläogene Helvetikum in Salzburg. Abhandlungen Geologische Bundesanstalt, 56, 713–722.
- RASSER, M.W. AND PILLER, W.E., 2001. Facies patterns, subsidence and sea-level changes in ferruginous and glauconitic environments: The Paleogene Helvetic shelf in Austria and Bavaria. Österreichische Akademie der Wissenschaften Schriftenreihe der Erdwissenschaftlichen Kommissionen, 14, 77–110.
- RITCHIE, J. D. AND HITCHEN, K., 1996. Early Paleogene offshore igneous activity to the northwest of the UK and its relationship to the North Atlantic igneous province. Correlation of the Early Paleogene in Northwest Europe (KNOX, R. W. O'B., CORFIELD, R. M. AND DUNAY, R. E., eds.), Geological Society London Special Publication, 101, 63–78.
- RODRÍGUEZ-TOVAR, F.J., UCHMAN, A., ALEGRET, L. AND MOLINA, E., 2011. Impact of the Paleocene-Eocene Thermal Maximum on the macrobenthic community: ichnological record from the Zumaia section, northern Spain. Marine Geology, 282, 178–187.
- RÖGL, F. AND EGGER, H., 2010. The missing link in the evolutionary origin of the foraminiferal genus Hantkenina and the problem of the lower-middle Eocene boundary. Geology 38, 23–26.
- RÖHL, U., BRALOWER, T.J., NORRIS, R.D. AND WEFER, G., 2000. New chronology for the late Palaeocene thermal maximum and its environmental implications. Geology, 28, 927–930.
- ROSS, P.S., UKSTINS, A., PEATE, I., MCCLINTOCK, M.K., XU, Y.G., SKILLING, I.P., WHITE, J.D.L. AND HOUGHTON, B.F., 2005. Mafic volcaniclastic deposits in flood basalt provinces: A review. Journal Volcanology Geothermal Research, 145, 281–314.
- SCHAFFHÄUTL, K., 1846. Beiträge zur näheren Kenntnis der Bayerischen Voralpen. Neues Jahrbuch für Mineralogie, Geognosie, Geologie und Petrefaktenkunde 1846, 641–695 (Stuttgart).
- SCHAUB, H., 1981. Nummulites et Assilines de la tethys paleogene, taxonomie, phylogénese et biostratigraphie. Mémoires Suisses de Paleontologie 104, 1–236.
- SCHLOSSER, M., 1925. Die Eocänaufnahmen der bayerischen Alpen. 1. Teil: Die Faunen des Unter- und Mitteleocaen. Abhandlungen Bayerische Akademie der Wissenschaften, Mathematisch-naturwissenschaftliche Abteilung, 30, 1–207.
- SCHMITZ, B., PUJALTE, V. AND NUNEZ-BETELU, K., 2001. Climate and sea-level perturbations during the Initial Eocene Thermal Maximum: evidence from siliciclastic units in the Basque Basin (Ermua, Zumaia and Trabakua Pass), northern Spain. Palaeogeography, Palaeoclimatology, Palaeoecology, 165, 299–320.
- SCHMITZ, B. AND PUJALTE, V., 2007. Abrupt increase in extreme seasonal precipitation at the Paleocene-Eocene boundary. Geology, 35, 215–218.
- SCHWERD, K., 1996. Ultrahelvetikum. In: Freudenberg, W. and Schwerd, K.: Erläuterungen zur Geologischen Karte von Bayern 1:500 000, 205–210.
- SCHWERD, K. AND RISCH, H., 1983. Zur Stratigraphie und Herkunft der Feuerstätter Decke im Oberallgäu. Jahresberichte Mitteilungen der oberrheinischen geologischen Vereinigung Neue Folge 65, 279–290.
- SERRA-KIEL, J., HOTTINGER, L., CAUS, E., DROBNE, K., FERRANDEZ, C., JAURHI, A.K., LESS, G., PAVLOVEC, R., PIGNATTI, J., SAMSO, J.M., SCHAUB, H., SIREL, E., STROUGO, A., TAMBARÉAU, Y., TOSQUELLA, J. AND ZAKREVSKAYA, E., 1998. Larger foraminiferal biostratigraphy of the Tethyan Paleocene and Eocene. Société Géologique de France Bulletin, 169, 281–299.

- SHULTZ, M.R. AND HUBBARD, S.M., 2005. Sedimentology, stratigraphic architecture, and ichnology of gravity-flow deposits partially ponded in a growth-fault-controlled slope minibasin, Tres Pasos Formation (Cretaceous). *Journal of Sedimentary Research* 75, 440–453.
- SINCLAIR, H.D. AND TOMASSO, M., 2002. Depositional evolution of confined turbidite basins. *Journal of Sedimentary Research* 72, 451–456.
- SMITH, R., 2004. Silled sub-basins to connected tortuous corridors: sediment distribution systems on topographically complex sub-aqueous slopes. In: LOMAS, S.A. AND JOSEPH, P. (Eds.): *Confined Turbidite Systems*. Geological Society London Special Publication 222, 23–43.
- STAMPFLI, G.M., MOSAR, J., MARQUER, D., MARCHANT, R., BAUDIN, T. AND BOREL, G., 1998. Subduction and obduction processes in the Swiss Alps. *Tectonophysics*, 296, 159–204.
- STAMPFLI, G.M., BOREL, G., MARCHANT, R. AND MOSAR, J., 2002. Western Alps geological constraintson western Tethyan reconstructions. *Journal virtual explorer* 8, 77–106.
- STEINMETZ, J.C., 1979. Calcareous nannofossils from the North Atlantic ocean, Leg 49, Deep Sea Drilling Project. *Initial Reports of the Deep Sea Drilling Project*, 49, 519–531.
- STEURBAUT, E., MAGIONCALDA, R., DUPUIS, C., VAN SIMAEYS, S., ROCHE, E. AND ROCHE, M., 2003. Palynology, paleoenvironments, and organic carbon isotope evolution in lagoonal Paleocene–Eocene boundary settings in North Belgium. In: WING, S.L., GINGERICH, P., SCHMITZ, B., THOMAS, E. (eds.), *Causes and Consequences of Globally Warm Climates in the Early Paleogene*, Geological Society of America Special Paper, 369, 291–317.
- STOVER, L.E., BRINKHUIS, H., DAMASSA, S.P., DE VERTEUIL, L., HELBY, R.J., MONTEIL, E., ARTRIDGE, A.D., POWELL, A.J., RIDING, J.B., SMELROR, M. AND WILLIAMS, G.L., 1996. Mesozoic-Tertiary dinoflagellates, acritarchs and prasinophytes. In: JANSONIUS, J. AND MCGREGOR, D.C. (Eds.), *Palynology: principles and applications*. American Association of Stratigraphic Palynologists Foundation, Dallas 2, 641–750.
- STRADNER, H., EDER, G., GRASS, F., LAHODYNSKY, R., MAURITSCH, H.J., PREISINGER, A., RÖGL, F., SURENIAN, R., ZESSL, W. AND ZOBETZ, E., 1987. New K/T boundary sites in the Gosau Formation of Austria. *Terra cognita*, 7, 212 (Paris).
- THIRY, M., 2000. Palaeoclimatic interpretation of clay minerals in marine deposits: an outlook from the continental origin. *Earth Science Reviews* 49, 201–221.
- UCHMAN, A., 1999. Ichnology of the Rhenodanubian Flysch (Lower Cretaceous-Eocene) in Austria and Germany. *Beringeria* 25, 67–173.
- VAN MORKHOVEN, F.P.C.M., BERGGREN, W.A. AND EDWARDS, A.S., 1986. Cenozoic cosmopolitan deep-water benthic foraminifera. *Bulletin Centres Recherches Exploration-Production Elf-Aquitaine Memoir* 11, 1–421.
- VOGELTANZ, R., 1977. Geologie des Wartstein-Straßentunnels, Umfahrung Mattsee (Land Salzburg). *Verhandlungen der Geologischen Bundesanstalt*, Jahrgang 1977, 279–291.
- WADE, B.S., PEARSON, P.N., BERGGREN, W.A. AND PÄLKE, H., 2011. Review and revision of Cenozoic tropical planktonic foraminiferal biostratigraphy and calibration to the geomagnetic polarity and astronomical time scale. *Earth-Science Reviews* 104, 111–142.
- WAGREICH, M., 1993. Subcrustal tectonic erosion in orogenic belts – A model for the Late Cretaceous subsidence of the Northern Calcareous Alps (Austria). *Geology*, 21, 941–944.
- WAGREICH, M., EGGER, H., GEBHARDT, H., MOHAMED, O., SPÖTL, C., KOUKAL, V. AND HOBIGER, G., 2011. A new expanded record of the Paleocene-Eocene transition in the Gosau Group of Gams (Eastern Alps, Austria). *Annalen Naturhistorisches Museum Wien*, A113, 35–65.
- WAŚKOWSKA-OLIWA, A. AND LEŚNIAK, T., 2002. Lower Eocene tuffites in the Żegocina Zone (Polish Flysch Carpathians). *Geologica Carpathica*, 53, 45–47.
- WEIDICH, K.F. AND SCHWERD, K., 1987. Über den Feuerstätter Flysch im Allgäu. *Neues Jahrbuch für Geologie und Paläontologie Abhandlungen* 174, 193–212.

- WESSELY, G., 1987. Mesozoic and Tertiary evolution of the Alpine-Carpathian foreland in eastern Austria. *Tectonophysics* 137, 45–59.
- WINCHESTER, J.A. AND FLOYD, P.A., 1977. Geochemical discrimination of different magma series and their differentiation products using immobile elements. *Chemical Geology*, 20, 325–343.
- WINKLER W., GALETTI G. AND MAGGETTI, M., 1985. Bentonite im Gurnigel-, Schlieren- und Wägital-Flysch: Mineralogie, Chemismus, Herkunft. *Eclogae Geologica Helveticae*, 78, 545–564.
- ZACHOS, J.C., RÖHL, U., SCHELLENBERG, S.A., SLUIJS, A., HODELL, D.A., KELLY, D.C., THOMAS, E., NICOLO, M., RAFFI, I., LOURENS, L.J., McCARREN, H. AND KROON, D., 2005. Rapid acidification of the ocean during the Paleocene-Eocene thermal maximum. *Science* 308, 1611–1615.
- ZIEGLER, P.A., 1987. Late Cretaceous and Cenozoic intra-plate compressional deformations in the Alpine foreland – a geodynamic model. *Tectonophysics* 137, 389–420.
- ZIEGLER, P.A., BERTOTTI, G. AND CLOETHING, S., 2002. Dynamic processes controlling foreland development – the role of mechanical (de)coupling of orogenic wedges and forelands. In: Bertotti, G. et al. (eds.): Continental collision and the tectono-sedimentary evolution of forelands. EGU Stephan Müller Special Publication Series 1, 17–56.



Field Trip Post-EX-1

Transect across the Eastern Alps

FRANZ NEUBAUER & JOHANN GENSER

(with contributions by BIANCA HEBERER, ANDREAS ETZEL & OLIVER STAUBER)

Department Geography and Geology, University of Salzburg, Hellbrunnerstr. 34, 5020 Salzburg, Austria.
franz.neubauer@sbg.ac.at; johann.genser@sbg.ac.at

1 Tectonic evolution of the Eastern Alps: From Permian rifting to Cretaceous and Cenozoic collisions

FRANZ NEUBAUER & JOHANN GENSER

1.1 Introduction

Facts and models on geology of the Eastern Alps made rapid progress during the last two decades mainly due deep seismic profiling, palaeogeographical, structural, petrological and geochronological investigations (Handy et al., 2010, 2015 and references therein; Schmid et al., 2004). These, together with results of the TRANSALP seismic line (TRANSALP Working Group, 2002, Lüschen et al., 2006; Lippitsch et al., 2003), studies on the crustal structure (Brückl et al., 2010; Bianchi and Bokelmann, 2014) and lithospheric-scale geophysical investigations including the recent Alp-Array (Lippitsch et al., 2003; Hetényi et al., 2018), allow new insights into the present-day structure of the Eastern Alps and surrounding areas (Belinić et al., 2018). These triggered new models, which fundamentally changed ideas on the geological evolution of the Eastern Alps.

Despite although old controversies remain and new controversies arised (for reviews, see e.g. Frank, 1987; Mandl, 2000; Neubauer et al., 2000; Schmid et al., 2004; Handy et al., 2010, 2015). Furthermore, the geological evolution of the Eastern Alps can be only understood when data from the north-eastern extension of the Eastern Alpine units in the Western Carpathians are considered in models, too (e. g., Dallmeyer et al., 1996; Froitzheim et al., 2008; Pomella et al., 2015; Plašienka, 2018). There, passive continental margin successions similar to the Austroalpine units sensu lato of the Eastern Alps are exposed, which are overlain by the blueschist-bearing, partly oceanic Meliata unit.

This review synthesizes the principal structural data of the Eastern Alps in respect to the distribution of the Alpine metamorphic overprint, its timing and the general tectonic framework of its evolution. A further goal is to discuss some specific processes and concepts found in the Eastern Alps for the first time, which were later applied in many other orogens (see, e.g., Neubauer, 2014).

Eastern and Western Alps display a fundamentally different geological structure (see below), geological development and in part a distinct geomorphology (Schmid et al., 2004). The boundary between Western (respectively Swiss Central) Alps and Eastern Alps is a thrust at the base of the Austroalpine unit exposed ca. along the Rhine valley S of Lake Constance (Fig. 1). The most prominent

mountain peaks are along the central axis in the Eastern Alps and the Swiss Central and French/Italian Western Alps. East of the Tauern window area, the topography gradually changes from high elevations in the Hohe Tauern area into the Neogene Pannonian basin with its plains and a very low elevation above sea level.

The present structure and the Late Paleozoic to Recent geological evolution of the Eastern Alps are reviewed mainly in respect to the distribution of Alpidic, Cretaceous and Cenozoic aged metamorphic overprint and the corresponding ductile structure (for details of various views, see Faupl and Wagreich, 2000; Mandl, 2000; Neubauer et al., 2000; Schmid et al., 2004; Froitzheim et al., 2008). Following these data, the Alps as a whole, and the Eastern Alps in particular, are the result of two independent Alpine collisional orogenies: The Cretaceous orogeny formed the present Austroalpine units *sensu lato* (including from footwall to hangingwall the Austroalpine *s. str.* unit, the Meliata unit, and the Upper Juvavic unit). The Eocene-Oligocene orogeny resulted from oblique continent-continent collision and overriding of the stable European continental lithosphere by the combined Austroalpine/Adriatic continental microplate (TRANSALP Working Group, 2002; Schmid et al., 2004; Handy et al., 2015). Consequently, a fundamental difference in the present-day structure of the Eastern and Central/Western Alps resulted (Fig. 1). The Western Alps expose deep structural levels, particularly the Penninic units, which are found in Eastern Alps only in the Lower Engadin, Tauern and Rechnitz windows.

1.2 Tectonic units of the Eastern Alps

In the following, we briefly discuss the tectonic units of the Eastern Alps (Fig. 1) and their metamorphic overprint (Fig. 2). These ages are compiled in Frank et al. (1987a), Dallmeyer et al. (1998), Neubauer et al. (1999), Thöni (1999, 2002) and Schuster et al. (2003) and are also graphically summarized in Frey et al. (1999) and Oberhänsli et al. (2004). For tectonic subdivision of Austroalpine units we do not use the new subdivision proposed of Schmid et al. (2004) because of some significant objections, but follow the older terminology introduced by Tollmann (1977 and references therein) as used, e.g., in Neubauer et al. (2000). A simplified comparison of the Austroalpine units between the two terminologies will be given during the excursion. The TRANSALP section extending from NE München to N of Venezia displays the overall crustal-scale structure (Fig. 2) with the Tauern window in the centre of the section.

The Eastern Alps comprise several principal tectonic units. These are discussed from north to south. The Helvetic unit represents a thin-skinned tectonic wedge along the northern margin of the Alpine orogen and is the detached Jurassic to Eocene sedimentary sequence of the passive continental margin of stable Europe.

The Penninic units are mainly exposed in the Tauern window (Kurz et al., 1998; Schmid et al., 2004, 2013). Here, we use a simplified terminology, and the units include from base to top: (1) In the center of the Tauern window, a parautochthonous basement consisting of a pre-Upper Carboniferous basement complex is intruded by Variscan granitoids, the so-called Zentralgneis (Central Gneiss). On top is a primary Permo-Mesozoic cover sequence, the Silbereck Group in this area and the Hochsteggen zone in the western Tauern window. (2) These units are overlain by basement-cover nappes with a Mesozoic cover parts derived from continental margin successions. The Eclogite zone occurs only in the central-southern Tauern window and represents part of one of these nappes. The seemingly parautochthonous unit the basement-cover nappes form the sub-Penninic nappes. (3) The Glockner nappe comprises of ophiolites mainly volcano-sedimentary sequences of the South Penninic oceanic basin (e.g., Höck and Koller, 1989). The overlying Matrei and the Nordrahmen units are considered to

represent a tectonic/sedimentary mélange deposited during the active margin stage (Frisch et al., 1987).

The Lower Cretaceous to Eocene Rhenodanubian Flysch zone along northern margin of the Eastern Alps is of a Penninic palaeogeographic origin and represents largely the sedimentary cover on rarely preserved oceanic crust (Fig. 1). Furthermore, the sub-Penninic nappes exposed in the Tauern window represent a thick-skinned wedge detached from stable Europe, too.

The Austroalpine and Southalpine units are of continental affinity and comprise a pre-Variscan and Variscan basement (usually coined as “Altkristallin”), mostly in a polyphase amphibolite-facies metamorphic grade, and an Upper Carboniferous to Cretaceous, respectively, Palaeogene sedimentary cover (Fig. 1). The Austroalpine nappe complex is exposed to the north of the dextral Periadriatic fault, the Southalpine unit to the south of it (Figs. 1, 2, 3). Both comprise a Variscan basement, which is metamorphosed within anchizonal to granulite-/eclogite-grade conditions during Carboniferous and locally during Permian times (Frey et al., 1999; Oberhänsli et al., 2004), and Upper Carboniferous/Permian to Palaeogene cover successions. The Southalpine unit remained largely unaffected by Alpine metamorphism except some small portions with very-low- and low-grade metamorphism along the Periadriatic fault (e.g., Läufer et al., 1977; Rantitsch, 1997; Hoinkes et al. 1999). The Austroalpine domain is variably affected by Cretaceous (Eo-Alpine) metamorphism ranging from very low-grade to ultra-high pressure conditions (Fig. 3). The Austroalpine domain is considered to represent a Permian to Middle Triassic rift succession, and Middle Triassic passive continental margin in the NW of the Meliata ocean. During the Jurassic, the Austroalpine domain separated from stable Europe by opening of the Penninic ocean in between.

The Meliata unit exposed in the Eastern Alps comprises distal continental margin deposits and recently detected oceanic sedimentary rocks of Middle Triassic to Doggerian age (Mandl and Ondrejíkova, 1991; Kozur, 1991; Mandl, 2000 and references). These include Middle and Late Triassic pelagic carbonates, Late Triassic radiolarites and the Doggerian Florianikogel Formation with shales, volcanogenic greywackes and ashfall tuffs (Kozur and Mostler, 1992). Late Jurassic and Cretaceous tectonic events of the central Northern Calcareous Alps have been related to the closure of the Meliata ocean (e.g., Faupl and Wagreich, 2000, Gawlick et al., 1999, Missoni and Gawlick, 2011 and references therein). The enigmatic very low- to low-grade metamorphic overprint of the structural base of the Northern Calcareous Alps at ca. 149–135 Ma argues for a major tectonic event at that time (Spötl et al., 1998; Vozárova et al., 1999; Schorn et al., 2013). This event likely represents the onset of collision but needs further confirmation (see also Frank and Schlager, 2006).

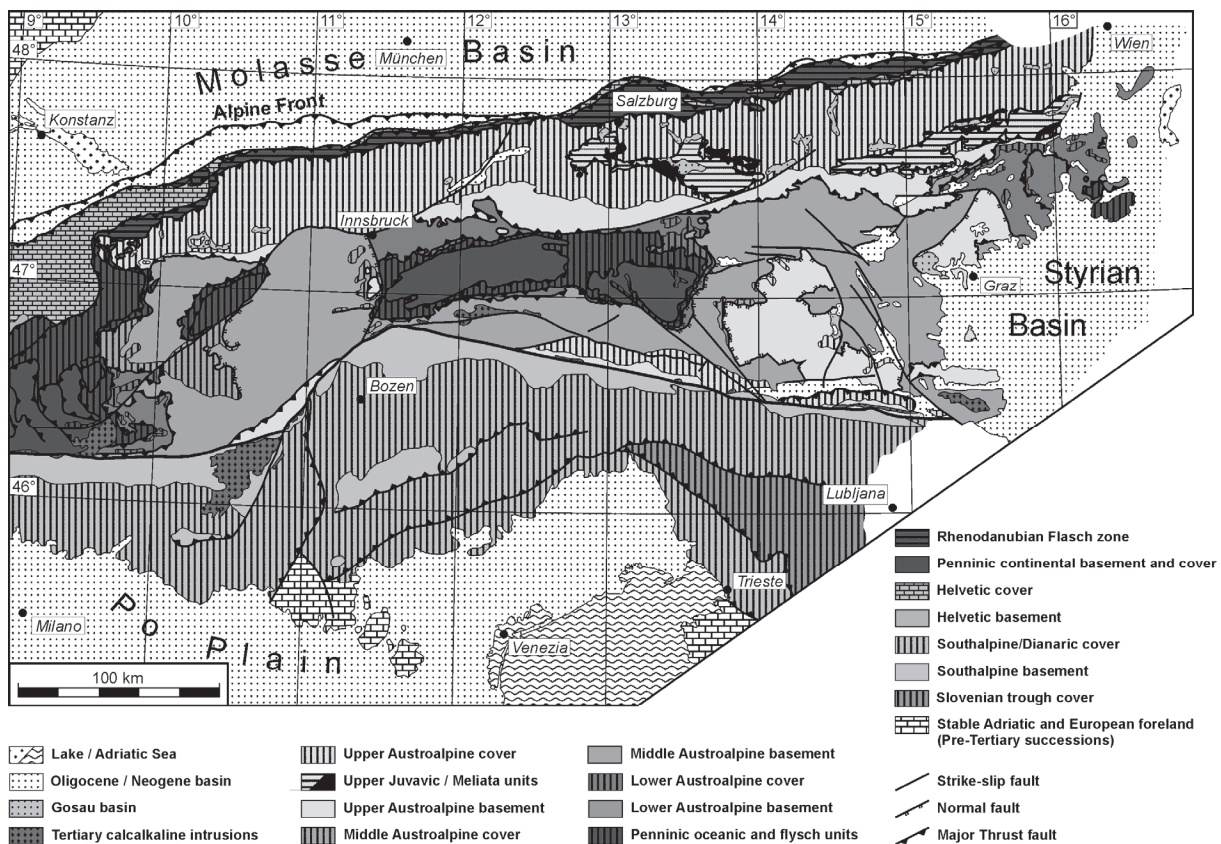


Fig. 1: Simplified geological map of Eastern Alps.

The Austroalpine nappe complex represents a Middle-Late Cretaceous nappe complex, which formed by ductile top-W to WNW shear contemporaneous with amphibolite- to eclogite-grade metamorphism in basement rocks (e.g., Ratschbacher, 1986; Dallmeyer et al., 1998; Hoinkes et al., 1999; Thöni, 1999). The age of peak conditions of metamorphism of Austroalpine units is at 95–90 Ma (Thöni, 2002), and $^{40}\text{Ar}/^{39}\text{Ar}$ mineral ages prove cooling through the Ar retention temperature of white mica between ca. 120 Ma in uppermost tectonic levels to ca. 80 Ma lowermost units (Dallmeyer et al., 1998; Wiesinger et al., 2006) locally overprinted by rare Eocene ages (ca. 50 Ma; Liu et al., 1999). The general Cretaceous nappe transport direction was towards the WNW (D_1) and N (D_2), respectively (e.g., Ratschbacher, 1986; Krohe, 1987; Neubauer et al., 2000; Kurz and Fritz, 2003 and references therein). The related thrust structures are overprinted by ESE-directed ductile low-angle normal faults (D_3), which were operative during exhumation of previously buried Middle Austroalpine units between ca. 87 and 80 Ma (Neubauer et al., 1995; Koroknai et al., 1999 and references therein). These are associated with orogenic collapse of the over-thickened orogenic wedge and formation of Turonian to Palaeogene collapse basins, the so-called Gosau basins. These unconformably overstep earlier structures of the uppermost nappes (Ratschbacher et al., 1989; Wagreich, 1995; Neubauer et al., 1995; Willingshofer et al., 1999b; Wagreich and Decker, 2001).

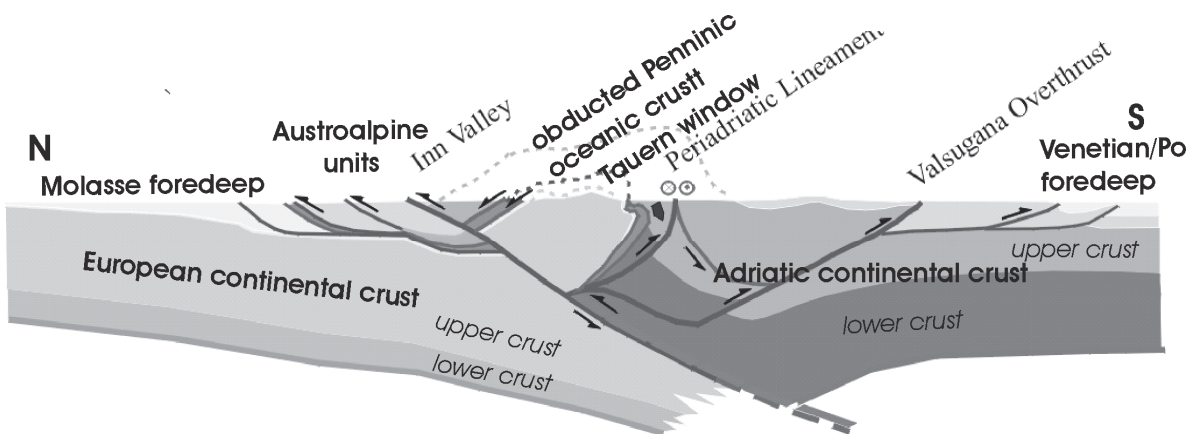


Fig. 2: TRANSALP section showing the overall structure of Eastern Alps (modified from TRANSALP Working Group, 2002).

In contrast, the Southalpine unit is not affected at all by Cretaceous-aged deformation and metamorphism, and is largely unmetamorphosed except some small units with low-grade metamorphism at ca. 50 Ma (own unpublished data). For the tectonic evolution of the eastern Southalpine unit, see Castellarin et al. (2006). Furthermore, there is no Cretaceous unconformity in the sedimentary succession, although the Lombardian and Slovenian Flysch successions (Fig. 3) are considered to monitor Late Cretaceous tectonic processes in the Austroalpine units (Castellarin et al., 2006). The dextral Cenozoic offset of the Periadriatic fault is ca. 150 to 400 km (Schmid et al., 1989; Haas et al., 1995). Structural relationships suggest that the Austroalpine nappe complex represents the orogenic wedge, and the Southalpine unit a retro-wedge.

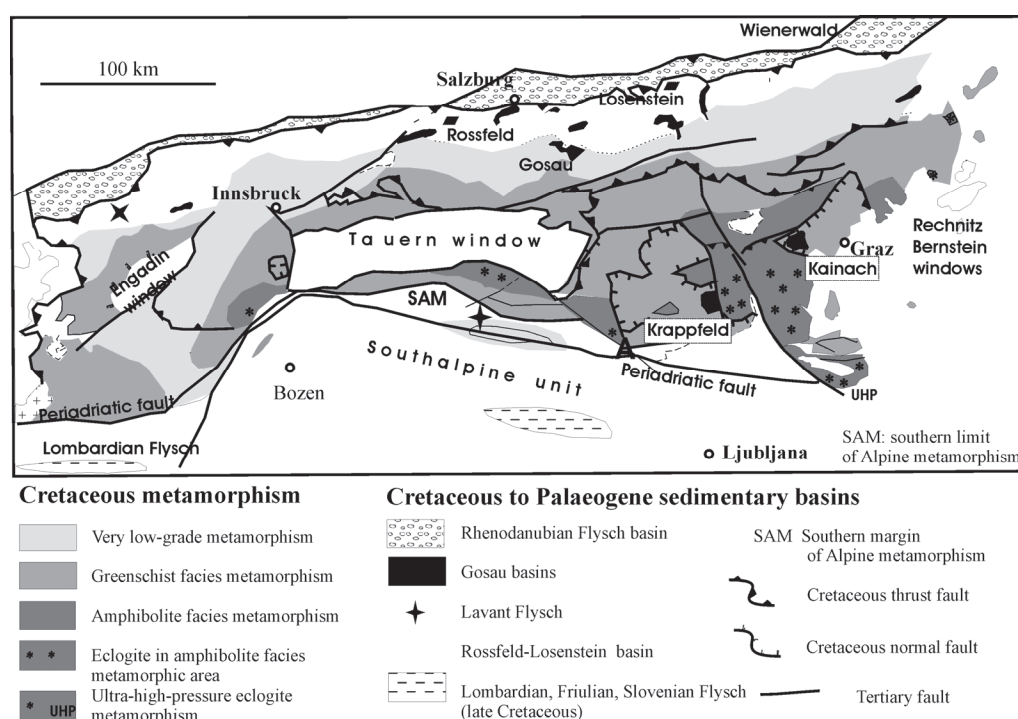


Fig. 3: Distribution of Cretaceous orogenic metamorphism in the Eastern Alps and their relationship to some Cretaceous sedimentary basins. PF – Periadriatic fault, SAM – southern limit of Alpine metamorphism, UHP – ultra-high pressure.

The overriding of the Penninic oceanic and Subpenninic continental units by Austroalpine units occurred during Palaeogene (Liu et al., 2001), and plate collision started with flexure of the European foreland in Late Eocene times. Penninic and Subpenninic units are exposed in the Tauern and other windows. Metamorphism within Penninic and sub-Penninic units peaked at ca. 30 Ma and K-Ar and $^{40}\text{Ar}/^{39}\text{Ar}$ white mica ages are between 38 and 18 Ma (Frank et al., 1987a; Liu et al., 2001).

Nearly all tectonic units of the Austroalpine nappe complex and the Southalpine unit include a Variscan basement. In the Austroalpine units, the basement is exposed mainly along central sectors of the Eastern Alps (Grauwackenzone and klippens like the Gurktal and Graz nappe complexes) (Fig. 1). The composition and evolution of the Austroalpine basement units is not considered in detail here. However, it must be noted that each Alpine nappe (see Fig. 4) comprises a basement that differs from under- and overlying basement units in composition, age and degree of pre-Alpine tectono-thermal events (e.g., Neubauer et al., 1999, and Schuster et al., 2004, and references). For example, the Upper Austroalpine units comprise fossil-bearing Ordovician to Lower Carboniferous successions only affected by a late Variscan (ca. 300 – 320 Ma) and/or Cretaceous very low- to low-grade metamorphic overprint and white mica ages range between 123 and 95 Ma (Dallmeyer et al., 1998; Schuster and Frank, 1999; Frank and Schlager, 2006; Wiesinger et al., 2006). In contrast, various units of the Middle Austroalpine nappe complex comprise a mostly medium-grade polymetamorphic basement (Schuster et al., 2001; Gaidies et al., 2006; Miller et al., 2005) and age groups of white mica are (ca. 340 – 300 Ma, 270 – 240 Ma, and 88 – 80 Ma (Dallmeyer et al., 1998; Schuster and Frank, 1999; Schuster et al., 2001; Wiesinger et al., 2006). The Lower Austroalpine nappe complex is variably affected within low-grade to rare medium-grade metamorphic conditions at ca. 82 and 72 Ma as $^{40}\text{Ar}/^{39}\text{Ar}$ white mica ages indicate (Frank et al., 1996; Dallmeyer et al., 1998; Müller et al., 1999; Heidorn et al., 2003). Pre-Alpine $^{40}\text{Ar}/^{39}\text{Ar}$ white mica ages are often well preserved.

1.3 Lithospheric-scale structure

The common interpretation for the late-stage evolution of Eastern Alps was that the European plate was bent underneath the Eastern Alps. This is expressed as by flexure of the European crust and formation of the ca. 4 km deep North-Alpine Molasse basin. Mantle tomography revealed a polarity change in the central part of Eastern Alps implying subduction of the Adriatic lithosphere (Lippitsch et al., 2003) as well as slab-break-off of the Adriatic lithosphere in the southeast adjacent Dinarides (Wortel and Spakman, 2000). Recent work is both in support (Héteniy et al., 2018; Fig. 4) and in contradiction (Belinić et al., 2018). Ustaszewski et al. (2008) prepared a first palaeogeographic restoration for the case of polarity change and late-stage subduction of the Adriatic plate underneath the Eastern Alps. A geological argument in contraction of Adriatic plate subduction is the missing flexure of the foreland base along the Southalpine front when the available high-quality seismic lines are considered (Fantoni and Franciosi, 2010) are taken into consideration. Two parts of the Adriatic plate, Istria and Monte Euganei, are directly attached to the Southalpine and Dinaric thrust front (Fig. 1).

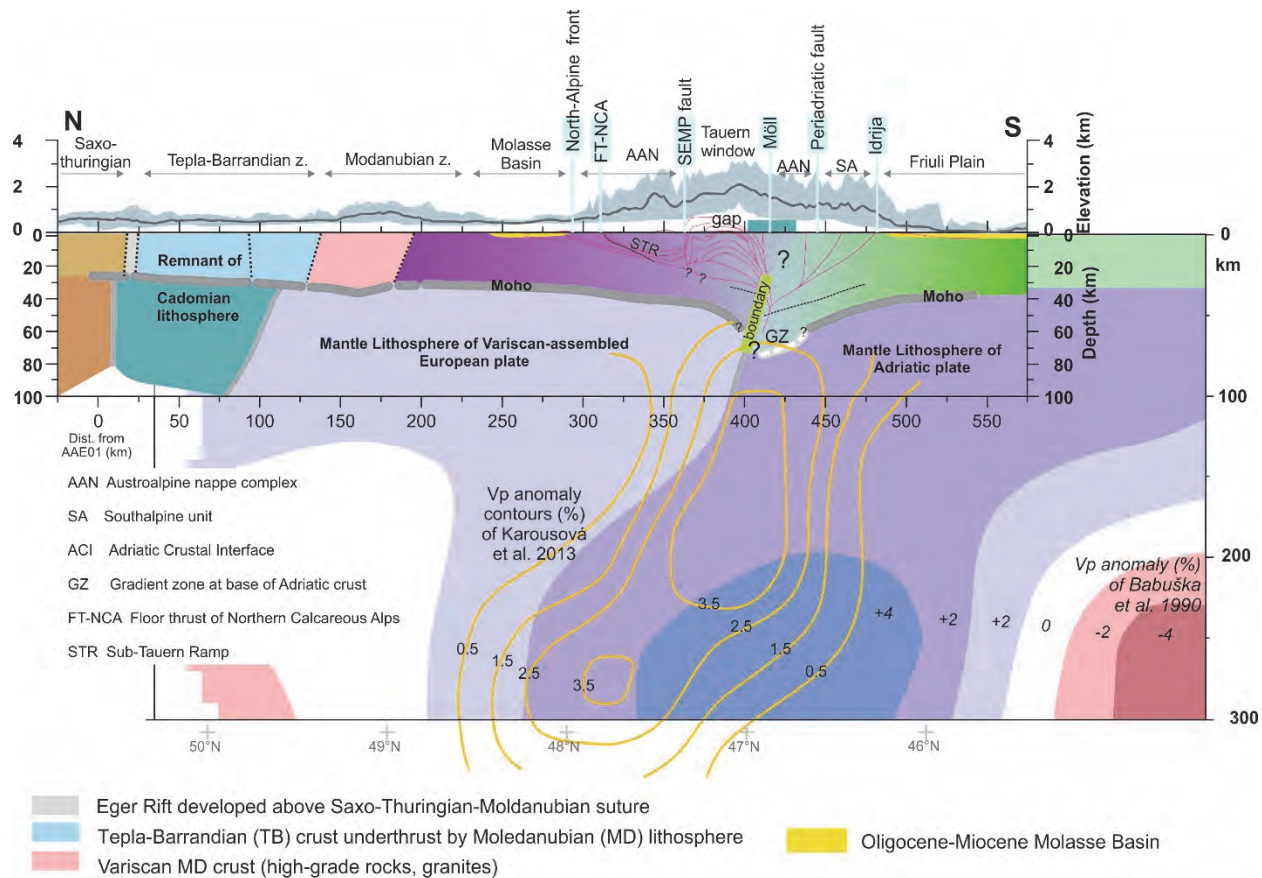


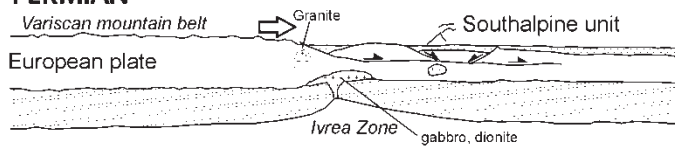
Fig. 4: Lithospheric-scale structure of the Eastern Alps (modified after Héteniy et al., 2018).

1.4 Tectonic evolution

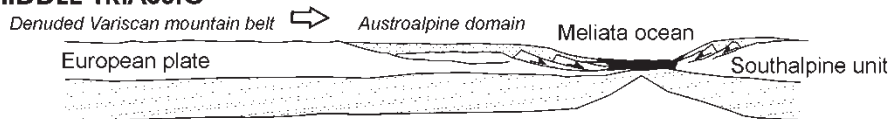
In terms of orogenic high-pressure and regional metamorphism and associated deformation, the Alps are divided into three units: (1) The Austroalpine units s.l., Meliata-Hallstatt units, and Upper Juvavic units which were overprinted by Cretaceous deformation, W- to NW-directed, ductile thrusting (Ratschbacher, 1986; Ratschbacher et al., 1989); (2) the Penninic continental and oceanic units, and the Helvetic units which were partly overprinted by Cenozoic metamorphism and associated N- to W-directed ductile deformation (Kurz et al., 2001 and references); and (3) the Southalpine units, which are largely unaffected by metamorphism except northernmost sectors adjacent to the Periadriatic fault and which were mainly deformed during Cenozoic, c. S-directed thrusting and shortening (e.g. Läufer et al., 1997).

In the following, we discuss principal stages of Permian to Recent tectonic evolution of the Eastern Alps (Fig. 5). Large-scale tectonic restoration can be found in, e.g., Stampfli and Mosar (1999), Schmid et al. (2004) and Handy et al. (2010, 2015).

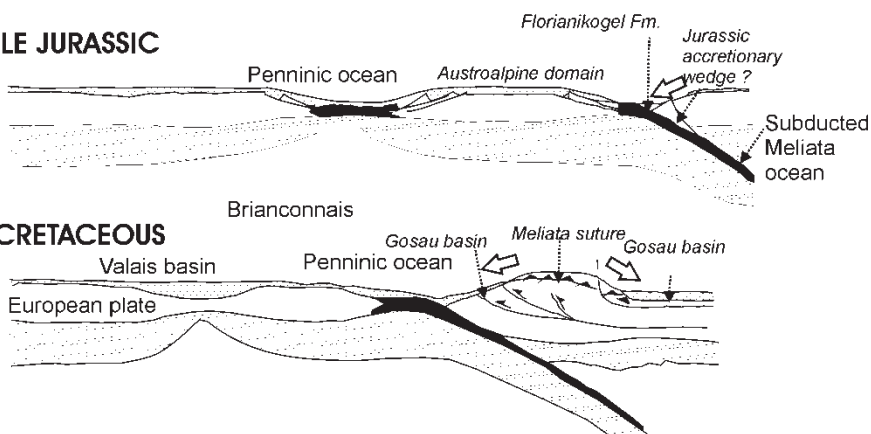
EARLY PERMIAN



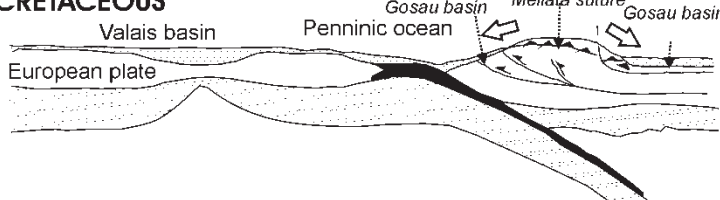
MIDDLE TRIASSIC



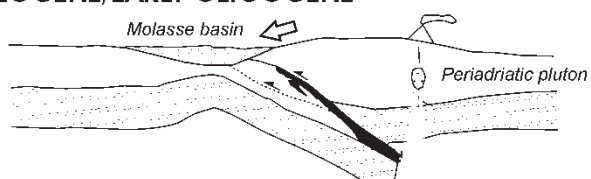
MIDDLE JURASSIC



LATE CRETACEOUS



LATE EOCENE/EARLY OLIGOCENE



NEOGENE

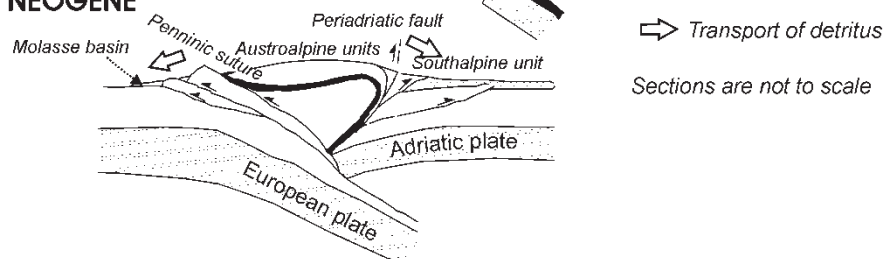


*Fig. 5: Schematic tectonic model of the tectonic evolution of the Eastern Alps for time slices represented in this study. From top to base: **Early Permian** lithospheric-scale extension, heating and subsequent cooling of crustal rocks due to exhumation, surface subsidence and onset of sedimentation. **Middle Triassic** opening of the Meliata ocean. (**Middle**) **Jurassic** opening of the Piemont (Penninic) ocean separating Austroalpine and Penninic continental units with shear zone formation at the continental margin. **Early Late Cretaceous** nappe stacking with deformation of higher nappes of the Lower Austroalpine unit and subsequent formation of the Gosau collapse basins. **Late Eocene** collision between the Austroalpine and Penninic continental units, break-off of the subducted lithosphere and deformation of the lowermost Lower Austroalpine nappe. **Late Oligocene to early Neogene** exhumation of the overthickened Penninic nappe complex by activity along the ductile low-angle normal fault zone separating the Penninic and Austroalpine tectonic units.*

Permian to early Mid-Triassic rifting: The Alpine tectonic evolution started with Permian rifting immediately following the Variscan orogeny and after deposition of Late Carboniferous molasse in all future continental domains. Rifting may have resulted by continuous dextral transtensional shear between Gondwana and Laurussia (e.g., Muttoni et al., 1996). Evidence for strong early to late Permian tectonic subsidence and extension is in the eastern Southalpine units where a carbonate platform was established during the Permian, and the Palaeotethys Sea transgressed from SE towards NW, respectively W. Further evidence of divergence and extension of the lithosphere was the emplacement of tholeiitic gabbros, low-pressure metamorphism due to unroofing of metamorphic core complexes, and magmatic underplating during the Permian (Thöni, 1999; Schuster et al., 2001; Schuster and Stüwe, 2008).

Late Mid to Late Triassic drifting of Meliata Ocean: However, the main phase of tectonic subsidence in Austroalpine passive margin was during Middle Triassic times (Lein, 1987) and processes of passive margin formation are getting more obvious. A new shelf carbonate platform established between Southalpine/Austroalpine s. str. and Upper Juvavic domains, facing towards the Meliata oceanic basin forming a passive continental margin. Ladinian and Upper Triassic radiolarites are considered to represent the infilling of the Meliata oceanic basin from which the westernmost remnants were found in the easternmost sectors of Northern Calcareous Alps (Fig. 1).

Latest Triassic to Early Jurassic rifting of the future Penninic Ocean: A further, independent rift stage during late Triassic and early Jurassic led to the opening of the (South) Penninic, Piemontais-Ligurian ocean due to rifting the Austroalpine domain off from stable Europe. Nearly all Penninic ophiolites of the Eastern Alps were metamorphosed during Cenozoic times. They comprise serpentinites, greenschist and prasinite (consisting of albite, chlorite, epidote, and amphibole), and thick clastic-carbonatic schists, the latter typical for narrow oceanic rifts. Recent U-Pb data of a plagiogranite of the Rechnitz window confirm an age of ca. 140 Ma during earliest Cretaceous. Nearly no gabbro or descendants of sheeted dyke rocks were found. The width of the oceanic seaway is estimated as ca. 500 km (Schmid et al., 2004).

Mid Jurassic drifting to early Late Cretaceous convergence and plate collision: On the other hand, the Meliata oceanic basin started to close during the Jurassic, most likely not later than middle Jurassic due to the record of the Lammer unit S of Salzburg (Gawlick et al., 1999; Missoni and Gawlick, 2011) and of the Florianikogel Formation (Neubauer et al., 2000, and references therein). The final closure occurred during the Early Cretaceous with the formation of a deep-sea trench (Roßfeld basin; Faupl and Tollmann, 1978; Schorn et al., 2013). Collision between Austroalpine s. str. units in a footwall position and the Upper Juvavic units in a hangingwall position occurred during early Late Cretaceous with the formation of a nappe pile of basement-cover nappes exposed in the south and cover nappes in northern, external domains (Frank, 1987; Dallmeyer et al., 1996). Nappe stacking likely prograded from SE to NW (e.g., Ratschbacher, 1986; Ring et al., 1989). The eo-Alpine (Cretaceous) metamorphism reached eclogite and UHP eclogite conditions (Jának et al., 2015). Late Cretaceous Gosau basins seal the Meliata suture and nappe stacking structures. The Middle Austroalpine continental eclogite-gneiss units represent the exhuming UHP/HP wedge, which was subducted to depths corresponding to max. ca. 3.0 GPa in southernmost exposures (Jának et al., 2005, 2015) at ca. 95–90 Ma (Thöni and Jagoutz, 1992; Thöni, 1999). In the north, the pressure is ca. 1 GPa. Most pronounced exhumation of the UHP/HP wedge occurred at 90–80 Ma, as cooling ages indicate. Consequently, thrust faults are known in the footwall and a ductile low-angle normal faults in the hangingwall of the eclogite-gneiss unit (Wiesinger et al., 2006).

LATE CRETACEOUS

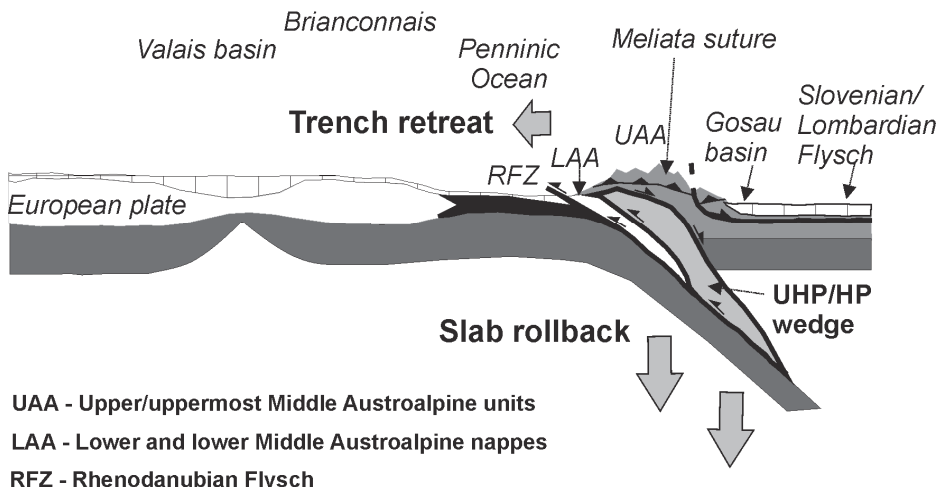


Fig. 6: Generalized (Chemenda-type) model for exhumation of high-/ultra-high-pressure rocks from Middle Austroalpine unit and its relationships to formation of adjacent sedimentary basins.

Late Cretaceous formation of collapse basins: Formation of Gosau basins in the Eastern Alps was associated with sinistral wrenching, normal faulting at shallow crustal levels and exhumation of eclogite-bearing crust within Austroalpine units (Neubauer et al., 1995; Froitzheim et al., 1996; Willingshofer et al., 1999a, b; Kurz and Fritz, 2003). Furthermore, Wagreich (1995) suggested tilting of the Austroalpine nappe stack towards NW associated with final shortening, thrusting and doming, in deep levels of the crust (Neubauer et al., 2000). The Lower Austroalpine nappe complex is variably affected within low-grade to rare medium-grade metamorphic conditions at ca. 82 and 72 Ma as $^{40}\text{Ar}/^{39}\text{Ar}$ white mica ages indicate (Frank et al., 1996; Dallmeyer et al., 1998; Müller et al., 1999; Heidorn et al., 2003). Metamorphism was associated with ductile thrusting at that time. Pre-Alpine $^{40}\text{Ar}/^{39}\text{Ar}$ white mica ages are often well preserved in Lower Austroalpine units.

The Austroalpine nappe complex is continental basement-cover nappe complex with southward increasing, Cretaceous-age metamorphic overprint, which received its final internal structure largely by middle-late Cretaceous tectonic processes. During this time, subduction of the Penninic (Piemontais-Ligurian) Ocean beneath the Austroalpine units started. In detail, the Lower Austroalpine and the lower part of Middle Austroalpine basement-cover nappes represent the footwall of the UHP/HP wedge and were accreted to the exhuming complex at ca. 80 Ma during a pronounced stage of thrusting. In the hangingwall, a series of ductile low-angle normal faults separates the UHP/HP wedge from uppermost Middle Austroalpine and Upper Austroalpine nappes representing the upper plate. Low angle normal faults were most active between 87–80 Ma as published thermochronologic data indicate (summarized in Willingshofer et al., 1999b; Wiesinger et al., 2006). Normal faulting occurred in a sinistral transtensional setting. In consequence of the transtension, collapse basins (Central Alpine Gosau basins) formed on top of the upper plate. We explain this by disturbance of steady-state subduction by oceanward retreat of the subduction zone (Fig. 6). The tectonic unroofing of the UHP/HP wedge continuously increased to and was most pronounced at the rear end of the wedge, so that up to more than 50 km of overburden was cut out. The overall tempo of exhumation can be confronted with the infill history of flexural and collapse basins. These data show rapid exhumation between ca. 87 – 84 Ma and subsequent down-slowning motion. Subsequent footwall

accretion of Lower Austroalpine nappes at ca. 80–78 Ma formed a duplex, which finally led to updoming of the exhuming UHP/HP wedge.

A Chemenda-type model is applied to explain exhumation of high-pressure rocks (Fig. 6). The Chemenda model (Chemenda et al., 1995) predicts exhumation of previously subducted and continental crust metamorphosed at UHP/HP metamorphic conditions mainly driven by both (1) buoyancy of subducted material, and (2) associated surface erosion of the subducted wedge. Thrust surfaces in the footwall and a major normal fault in the hangingwall confine, therefore, the exhuming UHP/HP metamorphic wedge. Clastic material mainly derived from the surface of the uplifting subductional wedge infill a synorogenic flexural sedimentary basin located on top of the lower plate in front of the UHP/HP wedge. Material mainly derives from the surface of the uplifting previously subducted wedge, which commonly form a mountain range at this stage. A cross-section through an orogen exposes, therefore, the following units: (1) the non-subducted lower plate rocks with a collapse basin at the top, (2) the exhumed, previously subducted wedge with a nappe stack, which is dominated by cover rocks at the leading edge front and exhumed metamorphic, mostly polymetamorphic basement rocks, all metamorphosed at HP/UHP conditions at the rear front and all these units were accreted from the footwall plate, and (3) the upper plate with collapse-type basins at top only in the case when extension-induced subsidence exceeds uplift. This is not the case in setting of steady-state subduction. The subhorizontal attitude of nappes originates from subsequent processes.

Eocene/Oligocene continent-continent collision: The Piemontais ocean of the Eastern Alps was closed not earlier than early Eocene because of (1) the presence of pelagic Eocene sediments both in Eastern and Western Alps, and (2) Eocene ages of thrusting in the Penninic/Austroalpine boundary in the northeast and northwest of the Tauern window (Dingeldey et al., 1997; Liu et al., 2001; Heidorn et al., 2003). Obviously, the subduction not only included oceanic crust but also distal Penninic continental crust in Eastern and Western Alps (Kurz et al., 2001, and references therein). Break-off of the subducted lithosphere and associated magmatism are considered to represent important mechanisms of continent-continent collision (von Blanckenburg and Davies, 1995). Upper sectors of the crust were later detached from the downgoing continental lithosphere due to lowering of strength because of temperature increase. Exhumation of these crustal pieces was associated with final thrusting, tectonic unroofing and surface denudation within the uprising mountain chain (e.g., Ratschbacher et al., 1989; Frisch et al., 2000a, 2000b; Fügenschuh et al., 2000).

Final collision was driven by oblique indentation of the Adriatic microplate into the Alpine nappe edifice (e.g., Ratschbacher et al., 1989; Rosenberg et al., 2007, 2018; Wölfle et al., 2011; van Gelder et al., 2017). This resulted in Late Oligocene/Early Miocene sinistral wrenching, and subsequent eastward extrusion of blocks in the Eastern Alps, and westward motion and W-directed indentation of the Adriatic microplate forming the West-Alpine arc (e.g., Ratschbacher et al., 1989, 1991a). Due to effects of ca. S-directed back-thrusting along the Periadriatic fault and within the Southalpine units, upper crustal levels of the down-going Penninic and European continental lithosphere were delaminated and accumulated within a double-vergent orogenic wedge. Exhumation of metamorphic crust, as exposed e.g. within the Tauern window, is achieved, therefore, by the combined effects of shortening (Lammerer and Weger, 1998), and gravity-driven tectonic unroofing in upper levels of the crust and raft tectonics away from the Tauern window towards the Pannonian basin (Keil and Neubauer, 2015).

Extrusion tectonics: Neogene tectonics of Eastern Alps is governed by indentation of the stiff Adria microplate (e.g., Willingshofer and Cloetingh, 2003) into the Alpine orogenic wedge, and associated eastward lateral extrusion of eastern part of Eastern Alps along sinistral (Inn Valley, Salzach-Enns and Mur-Mürz fault systems) and dextral strike-slip faults (Periadriatic fault; Fig. 7; Ratschbacher et al., 1989, 1991a). Extrusion tectonics is also responsible for high heat flow in Austroalpine units during Early Miocene (Sachsenhofer, 2001). Within an overstep between the Salzach-Enns and DAV faults, the Tauern window uprisen in a sort of pull-apart dome (Gensler and Neubauer, 1989; Neubauer et al., 1999; Scharf et al., 2013). This model is highly debated, however explains contemporaneous activation of N-S trending Brenner and Katschberg normal faults (Fig. 7). In principle, extrusion tectonics is still in operation as earthquakes along the sinistral Inn Valley, Salzach-Enns, and Mur-Mürz faults and dextral Save fault and GPS data indicate (Grenerczy & Kenyeres, 2006; Caporali et al., 2013). This is explained by the ongoing indentation of the Venetian Platform at the northern tip of the Adriatic microplate. Further geodetic measurements display pronounced surface uplift of the Hohe Tauern area (Cheloni et al., 2014 and references).

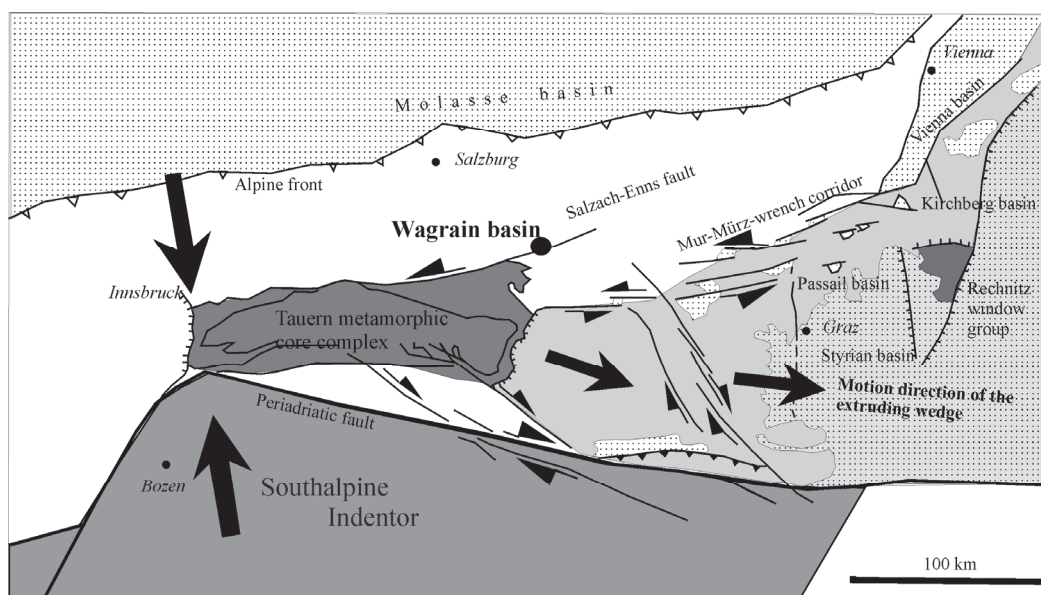


Fig. 7: Extrusion tectonics.

Pliocene to Quaternary deformation: The subsidence of westernmost sectors within the Pannonian basin is related to extrusion (e.g., Sachsenhofer et al., 1997). Furthermore, surface uplift east of the Tauern window is moderate (Hejl, 1997; Frisch et al., 2000b). The process of extrusion is still ongoing as the distribution of earthquakes indicate (Reinecker and Lenhardt, 1999).

Based on deformational characteristics and paleomagnetism of Alps, the Adriatic microplate is interpreted to have moved first to the NW (ca. Oligocene) and later to the N (mostly Miocene). In the eastern sectors, the stiff South-Alpine block in front of the Adriatic microplate indented into the weak Alpine orogen and contributed to crustal thickening, exhumation of previously subducted Penninic units, and to lateral extrusion of central sectors of the Eastern Alps. This scenario indicates a dextral Late Miocene-Pliocene transpressional setting in the Dinarides and back-thrusting along the front of Southern Alps. As GPS data and seismicity suggest, the northward motion is still ongoing, although slowed down, and is diminishing towards north (to ca. 2.4 mm/a) and is east-directed (ca. 1 mm/a) in the Eastern Alps. In this scenario, several features remain unexplained: (1) the age and mode of formation of the Friuli Orocline, a feature showing the change from ENE-strike to SE-trend of Dinarides

in front of the Venetian Platform; (2) the apparent ca. 20–25 degree Late Miocene-Pliocene counterclockwise block rotation of combined Eastern Alps, Adria, and northeastern Dinarides with a pole of rotation located to the SW of present Italian peninsula (Márton et al., 2003; Ortner et al., 2006; Robl and Stüwe, 2005); and (3) the strong Pleistocene sediment accumulation (1 mm/a) of northern Adria (around Venice) in front of the Friuli Orocline (Stefani, 2002). The strong subsidence of Northern Adria is opposite to surface uplift to the N of Alps and Pannonian basin and could be explained by flexural loading or by slab pull in front of a slab tear as slab break-off at the transition southeastern Alps to Dinarides has been suggested by Lippitsch et al. (2003) or as a distal effect flexuring of Appennines.

Quaternary and Recent deformation structures of Central Eastern Alps are studied in Pleistocene conglomerates in various, in partly still ongoing projects. These data indicate maximum NNW-SSE horizontal stresses and shortening and ca. E-W extension in accordance with above mentioned northward indentation.

The tectonic signal of surface uplift is superposed by the signal of post-glacial unloading and is estimated at ca. 1.5 mm/a, which is obviously related to the distribution of the last, Würm ice shield. For Holocene, series of elevated river terraces indicate stepwise surface uplift with increasing surface elevation from external Alps towards the Hohe Tauern with a minimum of 60 meters of terrace elevation in the centre. The present-day rivers incise into bedrocks, sometimes blanketed by moraines, so that the apparent Holocene uplift is ca. 6 mm/yr close to the Hohe Tauern, more than in external sectors of Eastern Alps where the Holocene river terraces are at much lower elevation. Cyclic Pleistocene surface uplift is potentially monitored by a number of other geomorphologic effects including: (1) river terraces (“Niederterrassen”) external to the area covered by the Alpine ice shield, (2) bedrock terraces along valleys in the centre of the Eastern Alps, (3) gorges along rivers, which could have been formed during rapid surface uplift due to rapid post-glacial river incision, and (4) elevated Pleistocene karst caves relative close to the present-day river levels.

1.5 Morphology formation

Significant work on formation of the morphology of Eastern Alps was done initially by the Tübingen working group (e.g., Frisch et al., 2000a, b). The group recognized the morphological difference between Hohe Tauern/Niedere Tauern with a young morphology and the Austroalpine domain with an old morphology, which formed since Oligocene and includes now uplifted peneplanation surfaces (Frisch et al., 2001). Much work has been done by using low-temperature geochronology explaining the differences of exhumation and surface uplift between different areas (Luth and Willingshofer, 2008 and references therein; Wölfler et al., 2011; Heberer et al., 2017). This type is representative for the eastern part of the Eastern Alps. Robl et al. (2008a, b) and Bartosch et al. (2017) modelled the morphology development by interaction of shortening and erosion and could explain the formation of longitudinal fault-controlled valleys by lateral extrusion. The incision of rivers into older Miocene landscapes is young and surface uplift is dated at ca. 6 – 3 Ma before present (Wagner et al., 2011; Legrain et al., 2014).

2 Northern Calcareous Alps and Radstadt Mountains

Aim: The aim of this part of the excursion is:

- (1) introduce into some important aspects of the rift and two-stage passive margin successions exposed in the Northern Calcareous Alps,
- (2) to examine some aspects of the cover successions of the Lower Austroalpine nappe complex and of its LateCretaceous deformation,
- (3) to demonstrate the footwall propagation of thrusting during formation of the Austroalpine nappe complex between ca. 110 and 50 Ma, as a result closure of the Meliata Ocean and subsequent Penninic Ocean, and
- (4) to check the significance of the Salzach-Enns-Mariazell-Puchberg (SEMP) fault and the related Miocene Wagrain basin on the northern edge of Miocene lateral extrusion wedge.

2.1 Introduction

The Northern Calcareous Alps are part of the Upper Austroalpine nappe complex and represent a ca. 600 km long and ca. 40 km wide cover nappe succession dominated by Middle to Upper Triassic dolomites and limestones (Fig. 1). The succession starts with thick uppermost Carboniferous and Permian terrestrial siliciclastic deposits, which are locally overlain by evaporites (Haselgebirge Fm.) with salt and sulfates, which particularly important and widespread in the surroundings of Salzburg (salt = Salz in German, e.g., Salzburg, Salzkammergut). The Permian siliciclastic strata are interpreted to represent a rift, with halfgraben formation with up to 1.5 km thick sediments (Fig. 8). Recently, an inverted Permian normal fault was identified (see below). In earliest Triassic, a gradual transition from siliciclastic rocks to marine carbonates occurred, which form the thick carbonates on a passive continental margin opening towards the evolving Meliata Ocean (Lein, 1987; Kozur, 1991; Mandl, 2000). A classical lithostratigraphic section is shown for the Tennengebirge massif (Fig. 9). Here, we detected an also a Middle-Upper Triassic northward tilted block (Figs. 10, 11). This is now explained as raft tectonics and a corresponding model is shown in Figure 11. Thick Upper Triassic reef and lagoonal deposits are overlying these units.

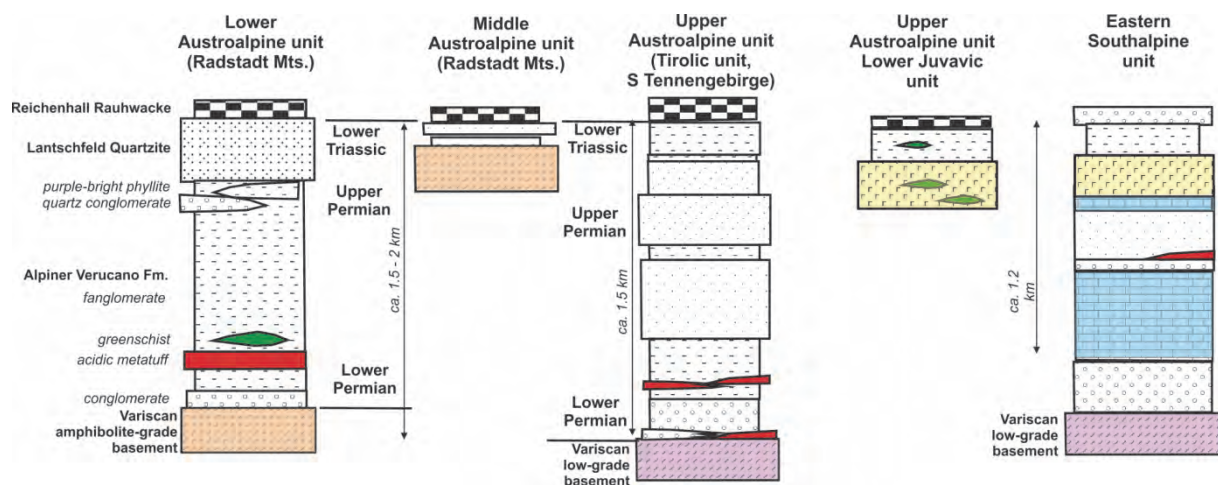


Fig. 8: Basal formations of the Upper Paleozoic cover successions of the Austroalpine and Southalpine units.

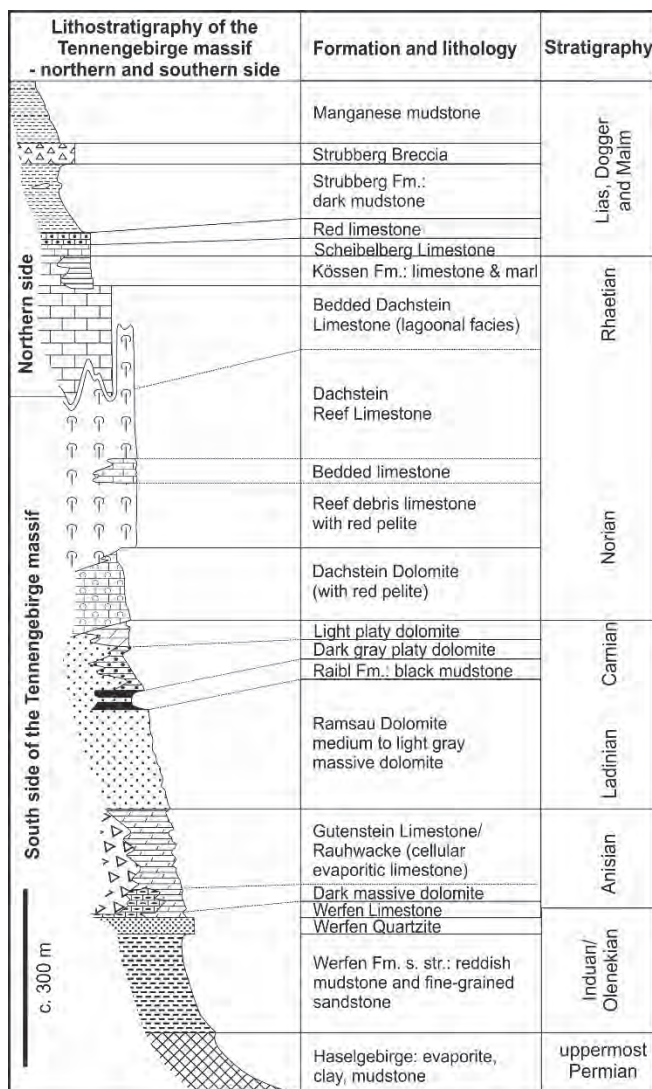


Fig. 9: Lithostratigraphic section of the Tennengebirge block of Northern Calcareous Alps (modified after an unpublished sketch of Gottfried Tichy).

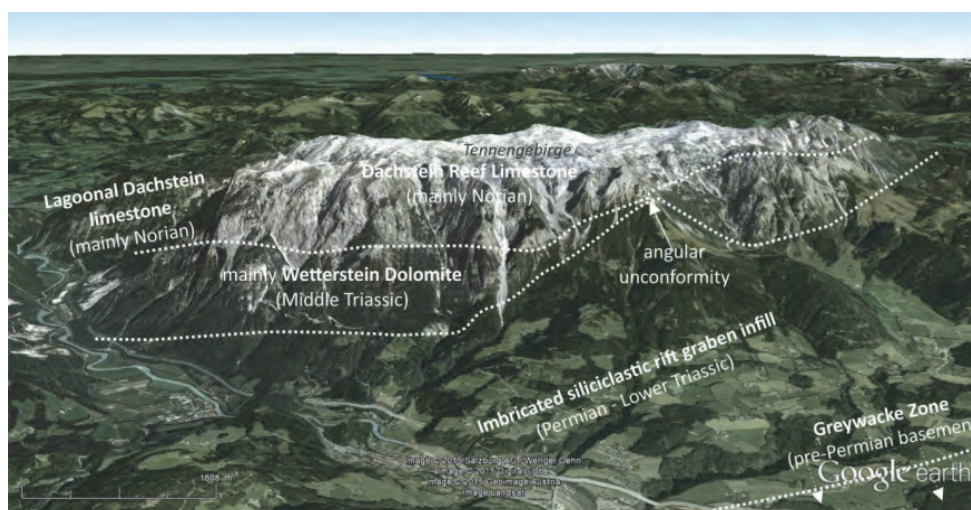


Fig. 10: Google Earth view of the Tennengebirge massif interpreted as Middle-Upper Triassic tilted block (base: www.googleearth.com).

During latest Triassic to Early Jurassic, the shallow water deposits suddenly disappeared and were replaced by reddish pelagic limestones (e.g., by the Adnet Limestone, an ammonitico rosso-type limestone). These features have been interpreted to result from ongoing subsidence related to the extension during rifting of the future Penninic Ocean. Later, radiolarites were deposited as well as the well bedded Oberalm Limestone exposed to the southeast of Salzburg. The subsidence of the Upper Jurassic successions is interpreted to relate to the ongoing closure of the oceanic Meliata rift (Missoni and Gawlick, 2011). Following a marly interval (Schrambach Fm.), these are then overlain by the Lower to lowermost Upper Cretaceous Rossfeld Group, a trench fill mixed of siliciclastic and carbonates due to the closure of the Meliata Ocean (e.g., Faupl and Tollmann, 1978; Krische et al., 2014; Krische and Gawlick, 2015). These latter units are part of the Tirolic nappes, which are overridden by the Juvavic units (Juvavum: Roman word for Salzburg). The tectonics are discussed to result from Late Jurassic gravity gliding (Missoni and Gawlick, 2011) or Early to earliest Late Cretaceous nappe tectonics (Schorn et al., 2013 and references therein). The palaeogeographic development is shown in Faupl and Wagreich, 2000). The Cretaceous and Eocene nappe structures and brittle deformation are discussed in Linzer et al. (1995, 1997).

The St. Martin-Werfen Imbricate zone is exposed south of the Tennengebirge and represents a zone of structural imbricates composed of Permian to Lower Triassic siliciclastic formations and Middle Triassic carbonates. Only a few structural studies did deal with that zone (e.g., Rossner, 1977) and top-s vs. top-N imbrication was discussed.

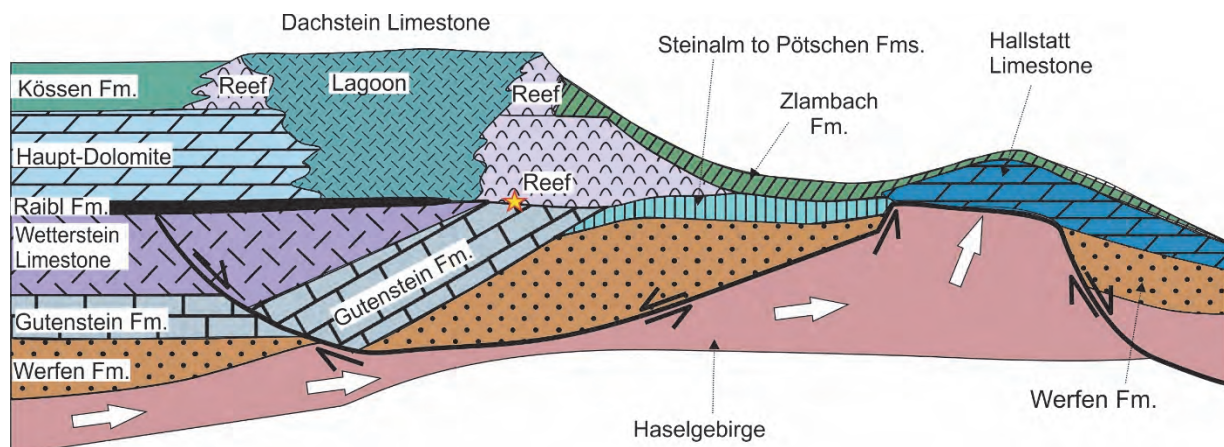


Fig. 11: Tectonic model of the passive margin formation involving raft tectonics on uppermost Permian Haselgebirge evaporites (from Neubauer et al., 2017; palaeogeographic section is based on Mandl, 2000 and references therein).

Upper Cretaceous to Eocene Gosau basins are collapse basin on top of the Cretaceous-aged Upper Austroalpine nappe edifice. The succession of these Gosau basins are divided into basal terrestrial and shallow water deposits gradually changing into marly and turbiditic deep-water deposits.

The Lower Austroalpine nappe complex of the northern Radstadt Mountains is characterized by largely inverted nappes (with mainly Permian to Jurassic successions) including the prominent Quartzphyllite nappe (see also Rossner, 1976). The sections include very thick Permian to Lower Triassic siliciclastic strata, which are overlain by a thick Middle to Upper Triassic dolomites (Rossner, 1979) and Jurassic marls, breccias and radiolarites (Häusler, 1988).

A structural map is shown in Figure 12 and the tectonostratigraphy in Figure 13. These Lower Austroalpine nappes are thrusted over Penninic tectonic units of the NE edge of Tauern window during Eocene as dating of ductile fabrics of the Hochfeind nappe suggests (c. 50–54 Ma; Liu et al., 2001; Fig. 13). Successions of the Quartzphyllite nappe show a dominant foliation and a ca. WNW-trending stretching lineation formed during deformation stage D₁ during nappe transport towards WNW during Late Cretaceous (⁴⁰Ar/³⁹Ar white mica: c. 78–80 Ma). Ductile shear zones in overlying basement units and isoclinal km-scaled folds with subhorizontal axial surfaces and local internal thrust splays in the Quartzphyllite nappe are associated with D₁ deformation. D₁ fabrics are overprinted by D₂ ductile fabrics at the structural base of the Quartzphyllite nappe to the underlying Penninic units. In the interior of the Quartzphyllite nappe, the foliation S₁ is overprinted by kilometer-meter-scaled open N-vergent, ENE to E plunging D₃ folds with amplitudes of ca. 1 – 2 km. These folds also affect the D₂ thrust boundary of Penninic to Lower Austroalpine nappe complex (Fig. 14) and postdate, therefore, plate collision. In outcrops, a non-penetrative axial plane foliation S₃ formed by pressure solution or cataclastic deformation, and no recrystallization of these fabrics occurred. The D₃ folding postdates, therefore, D₂ thrusting dated at ca. 50–54 Ma and indicates a previously unrecognized stage of shortening of Lower Austroalpine units. This folding stage with a minimum shortening estimate of c. 30 percent is interpreted to be associated with internal dome formation within the Tauern window. Regional considerations allow date D₃ N-S shortening to latest Eocene to earliest Miocene. D₃ shortening is overprinted by D₄ activation of the SEMP strike-slip fault and finally by Early Miocene ESE-directed D₄ ductile normal faulting (Katschberg fault) and contemporaneous activation of the Mur-Mürz fault.

The new data are similar to D₃ N-S shortening structures occurring over the whole N-S section in the Eastern and Southern Alps. These structures include internal thrusts within Northern Calcareous Alps (NCA), the footwall accretion and deformation of Penninic units along the northern floor thrust of Eastern Alps.

Taking all the evidence from this section together, the Eastern Alps expose the plate boundary between the combined Europe-derived lower plate continental units and obducted Mesozoic Penninic ocean basin fill and the overlying continental Austroalpine nappe complex in the dome-shaped Tauern window. A structural study in Radstadt Mountains associated with reinterpretation of Ar-Ar geochronology of ductile low-grade metamorphic fabrics and the interpretation of a N-S cross-section of Eastern Alps allow recognize the following major processes: (1) A regular footwall progradation of thrusting from ca. 110 Ma to ca. 50 Ma is partly contemporaneous with orogen-parallel extension (Late Cretaceous and Miocene) in uppermost units (Fig. 14). (2) Latest Eocene and earliest Miocene post-collisional plate boundary folding and shortening formed in the rheologically weak center of the orogen. (3) The interplay of Miocene outward thrust propagation and strike-slip faults is potentially controlled by inherited rift structures in the subducted plate.

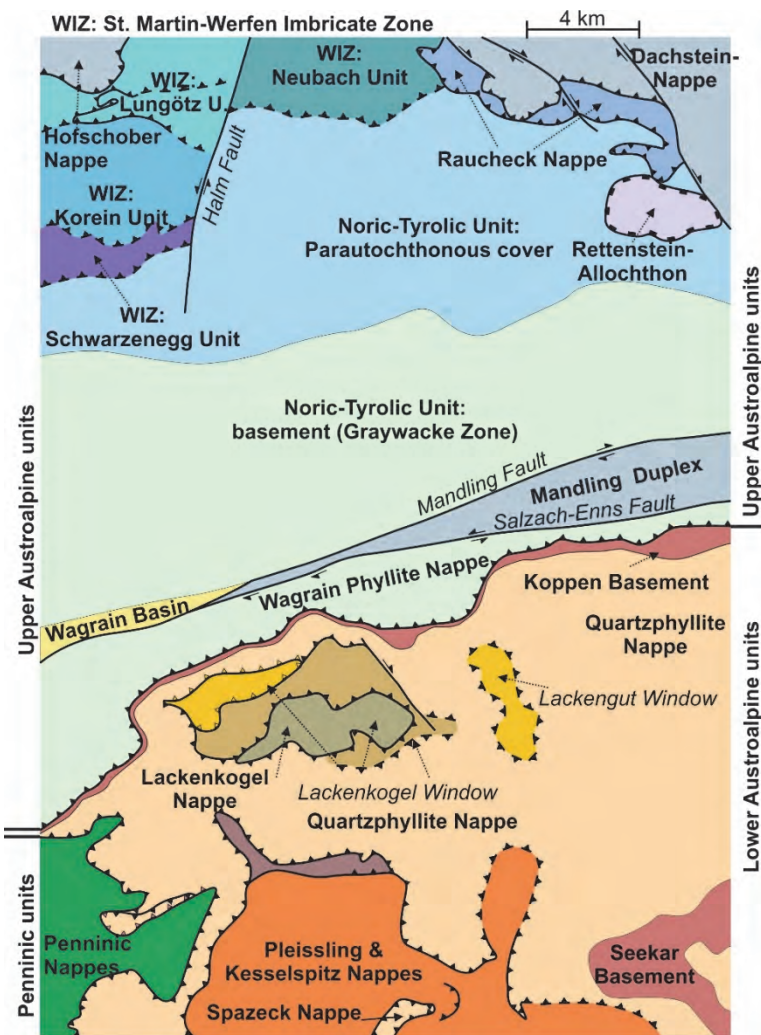


Fig. 12: Tectonic map of the area between St. Martin-Werfen Imbricate zone and uppermost Penninic units.

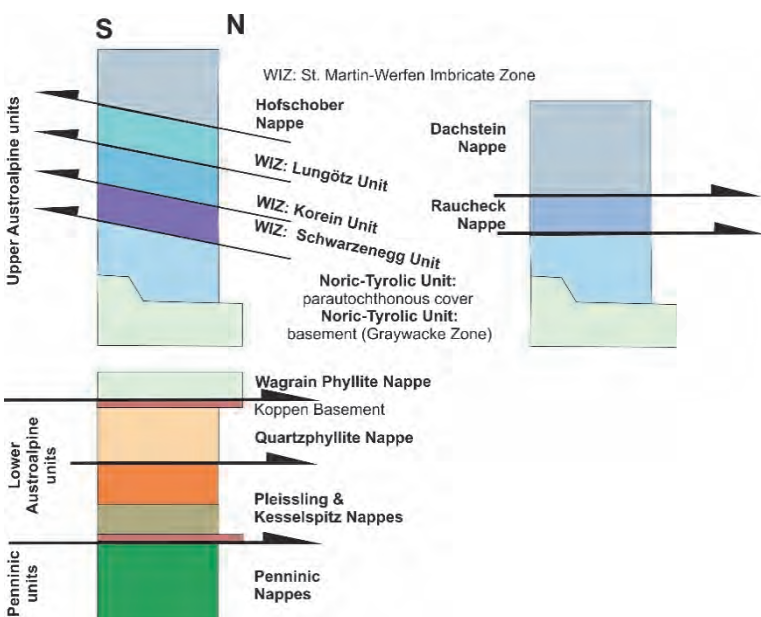


Fig. 13: Tectonostratigraphy of the area between the St. Martin-Werfen Imbricate zone and uppermost Penninic units.

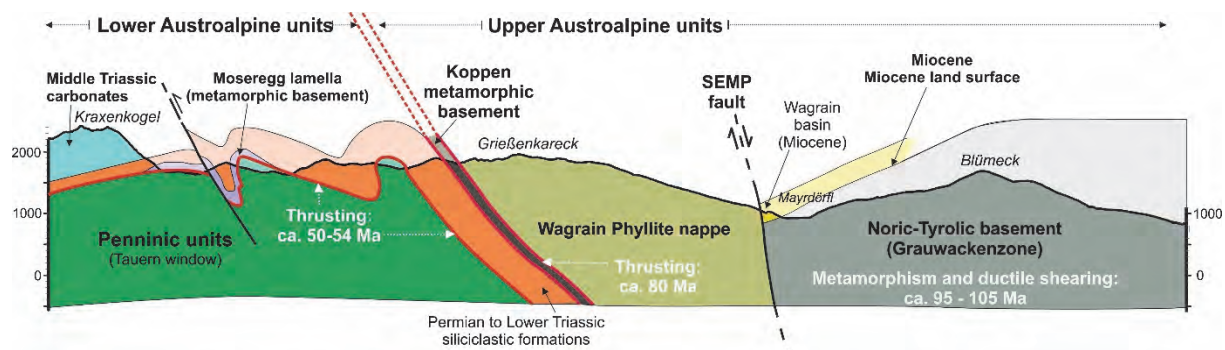


Fig. 14: Simplified cross-section showing the structure of Lower Austroalpine units.

2.2 Stops

Stop 1-1: Adnet quarries Lienbacher quarry: Liassic Adnet Limestone

Location: N47° 41' 47.7" E13° 08' 17.6"; ÖK 50, sheet 94 Hallein; the quarries are located to the NE of the village Adnet. ÖK 50: older version of the Austrian topographic map, scale 1 : 50,000.

In the surroundings of Adnet-Langmoos the Adnet-limestone is cut in numerous quarries, some are active and others are abandoned and overgrown. Detailed descriptions can be found in Böhm (1992) and Dorner et al. (2009). The Adnet Limestone is a red lutitic nodular limestone. The ferro-manganese crusts and the halmyrolysis (submarine weathering) indicate the strongly condensed sequence (Fig. 15). There are only 30 meters compared with about 300 meters of the Glasenbach gorge section in the north. Within the condensed horizons, ammonites are frequent, but it is very hard to get them out. The fossils are not well preserved. Within the threshold facies, *Psiloceras planorbis* (Sowerby) is missing, but not so in Glasenbach gorge. The sequence starts here with *Schlotheimia angulata* (Schlotheim). Neptunian dykes filled with bioclastic detritus occasionally occur. The Adnet Limestone is also strongly deformed with stylolites and abundant signs of pressure solution.

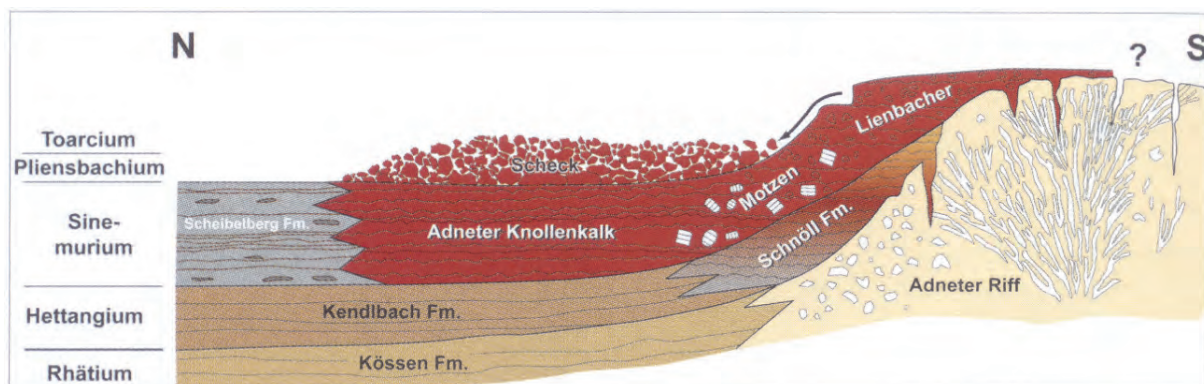


Fig. 15: Various lithotypes of the Adnet Limestone and its relationships to underlying formations (from Dorner et al., 2009).

Stop 1-2: Pass Lueg, Upper Trias: Dachstein Limestone

Location: N47° 34' 30.1" E13° 11' 46.5"; ÖK 50, sheet 94 Hallein; road cut to the South of Pass Lueg along the Federal Road.

The road cut exposes bedded Dachstein Limestone with the famous loferite cycle. The exposure, an ice-polished surface, is rich in megalodonts (*Conchodus infraliasicus* STOPPANI) and shows complete Norian loferite cycles (Plöchinger, 1983).

Stop 1-3: Middle and Upper Triassic carbonate platforms; viewpoint

Location: N47° 31' 58.9" E13° 10' 07.6"; ÖK 50, sheet 94 Hallein; parking place on the western side on the federal road between Pass Lueg and Sulzau

A N-S cross-section through western Tennengebirge is shown in Fig. 16. The panoramic view to the steep western slope of the Tennengebirge massif (shows the thick succession of Lower to Upper Triassic carbonate platform with Ladinian Wetterstein Limestone and Upper Triassic bedded Dachstein Limestone formed by the loferite cycles in an lagoonal depositional environment. No strata of the Carnian Raibl Fm. occur. The whole section with always shallow water deposits is well preserved and displays a thickness of ca. 2 km of Middle-Upper Triassic units (Figs 16, 17) implying rapid subsidence interpreted to represent the tectonic subsidence during opening of the Meliata Ocean.

Stop 1-4: Obermoos W Filzmoos: Overview on structural/stratigraphic base of Northern Calcareous Alps

Location: N47° 26' 04.5" E13° 29' 46.6"; ÖK 50, sheet 126 Radstadt; forest ca. 400 m NW the village Obermoos W Filzmoos.

The roadcut along a forest road exposes a succession of low-grade metamorphic greyish sandstones and quartz-conglomerates of the Filzmoos conglomerate. This unit is interpreted to represent an intramontane molasse basin deposited on top the Ordovician to Devonian Grauwackenzone basement (Figs 18, 19). No unconformity was found in that region. The metaclastic succession is foliated, and traces of axial surface foliation can be found recording the Cretaceous deformation during nappe stacking associated with coeval metamorphism. $^{40}\text{Ar}/^{39}\text{Ar}$ white mica ages from nearby outcrops are at ca. 100 Ma although some older ages up to 120 Ma were recorded, too Frank and Schlager, 2006) potentially due to inherited detrital grains.

During Late Eocene, the NCA were transported towards N and loaded onto the European lithosphere. Based on the top-S imbricates south of the Tennengebirge (Fig. 12), the St. Martin-Werfen imbricate zone, the Northern Calcareous Alps represent a large-scale pop-up (Fig. 20).

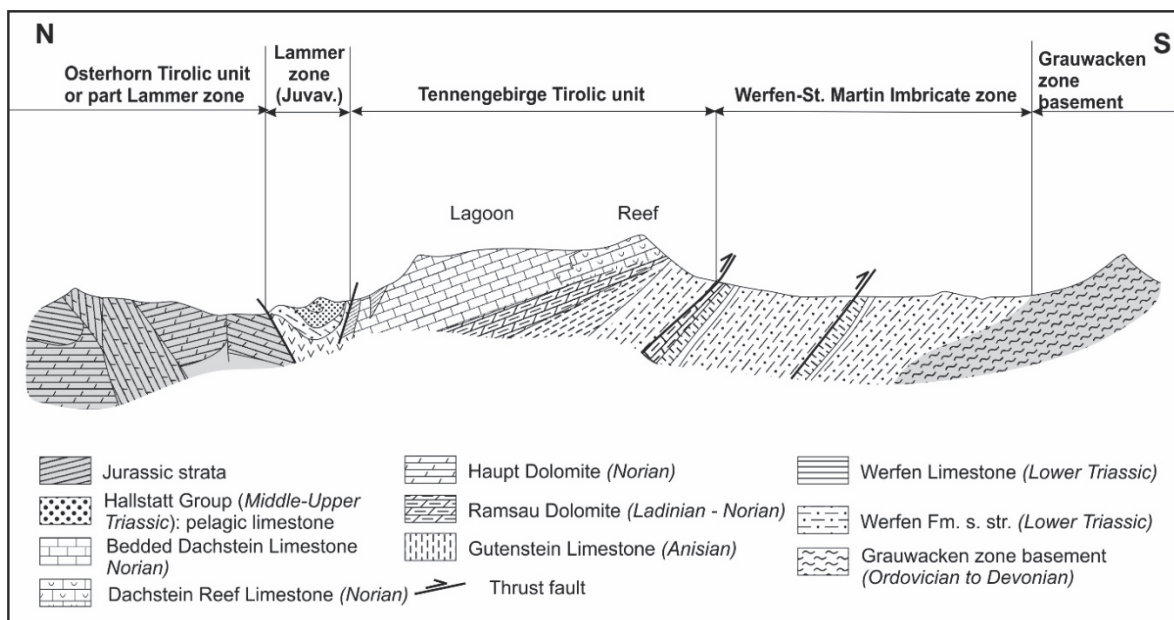


Fig. 16: Cross-section across the Tennengebirge block (modified from Schramm and Tichy, unpublished sketch).



Fig. 17: Google Earth image of the Tennengebirge massif with the Wetterstein Dolomite at the base and Bedded Dachstein Limestone at top and northern margin (from Google Earth Pro). The whole Middle to Upper Triassic shallow water succession is more than 2 km thick indicating rapid subsidence during passive margin formation. Note also the transition from Dachstein reefs in the south to lagoonal well bedded Dachstein Limestone in the north, as well as the Early Miocene Dachstein peneplanation surface on top.

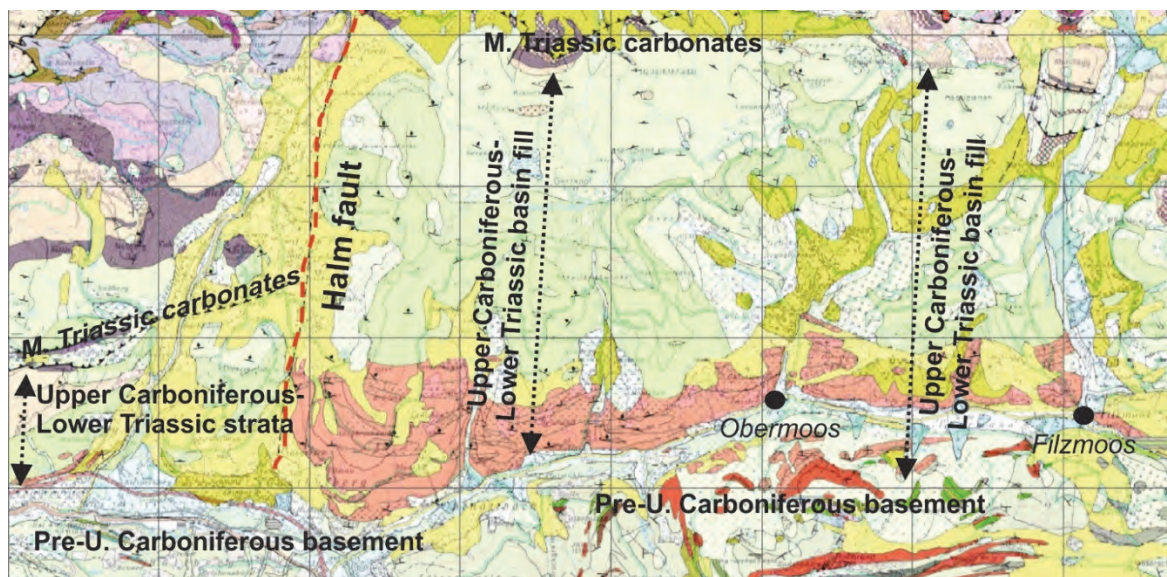


Fig. 18: Geological map of the Filzmoos region exposing a thick succession of Upper Carboniferous to Lower Triassic siliciclastic strata in contrast to area to the west of the Halm fault. The Halm fault is now a strike-slip tear fault separating the thick infill of a halfgraben from a thin succession west of it.

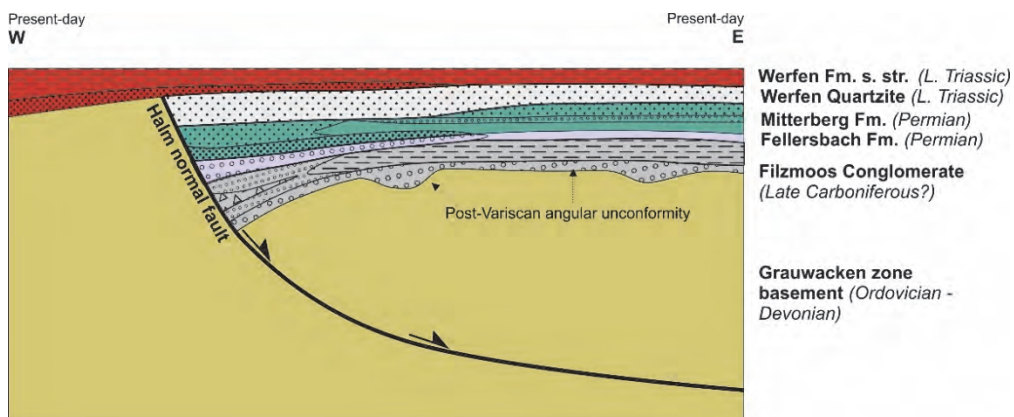


Fig. 19: Tectonic model of the Upper Carboniferous (?) to Permian successions interpreted as a Permian halfgraben.

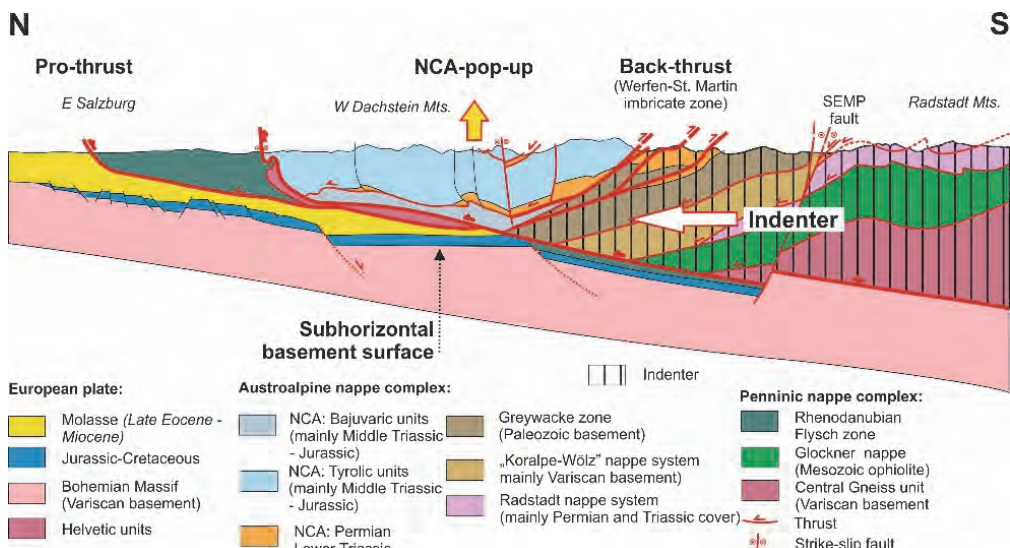


Fig. 20: Cross-section across the northern part of Eastern Alps.

Stop 1-5: E of Wagrain: uppermost part of the Miocene Wagrain basin fill and SEMP fault

Location: N47° 20' 50.8" E13° 20' 05.1" ; ÖK 50, sheet 125 Bischofshofen; artificial water reservoir at middle cable car station SE Weberland hill east of Wagrain

The outcrop exposes the uppermost part of the Wagrain basin fill of the coaly sandstone lithofacies (Neubauer, 2016). The preserved Wagrain basin (Fig. 21) is ca. 200 m thick, with an angular unconformity over phyllites of the Grauwackenzone basement at its base. The SEMP fault stretches in the south and can be traced only by morphology due to intense weathering of the cataastically deformed rocks.

In this exposure, grey-brown sandstones grade into 6–8 m thick dark greyish to locally black, coaly sandstones (Fig. 22). These sandstone beds are internally massive and ca. 10–60 cm thick. Single-grain $^{40}\text{Ar}/^{39}\text{Ar}$ dating of detrital white mica yields an age peak between 85.9 ± 3.6 and 109.2 ± 4.9 with a majority around 100 Ma (Fig. 23). One grain is younger (77.5 ± 3.3 Ma) and a few grains are slightly older (119.0 ± 5.9 Ma; 148.2 ± 11.1 Ma) and one grain is dated at 382.2 ± 7.5 Ma. The dominating Cretaceous-age population indicates a nearly exclusive origin of the dated detrital white mica from higher greenschist facies to medium-grade metamorphic rocks largely overprinted by eo-Alpine metamorphism. Based on this age populations and apatite fission track ages, Neubauer (2016) proposed that the Bösenstein area is the likely source because it already cooled during the Eocene through ca. 100 °C-isotherm, as apatite fission track ages indicate (Hejl, 1997). The high white mica and garnet contents could have their origin in the spatially widespread Wölz Micaschist complex with its abundant garnet micaschists. This implies a sinistral displacement of ca. 40 km along the SEMP fault after deposition of these strata of the Wagrain basin (Fig. 24).

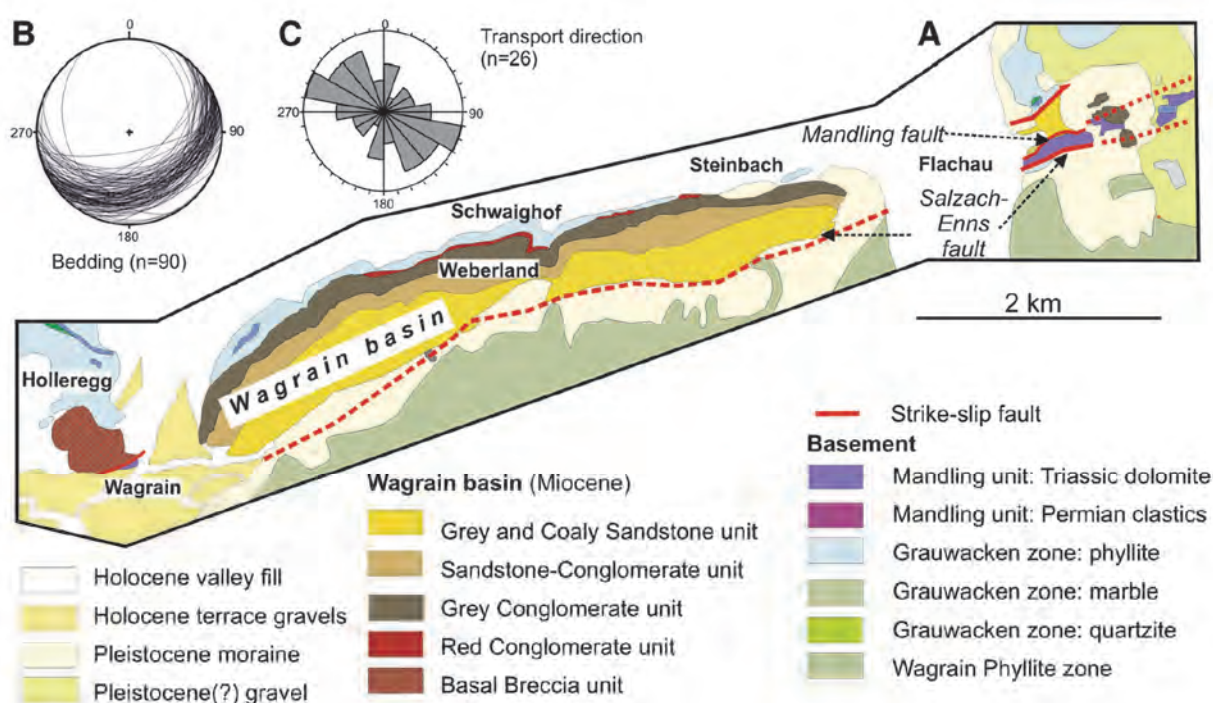
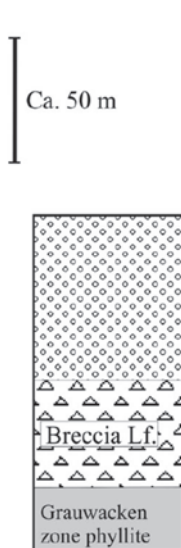


Fig. 21: Geological map of the Wagrain basin (from Neubauer, 2016).

WSW

Wagrain



ENE

Weberland

S Steinbach

NE Flachau

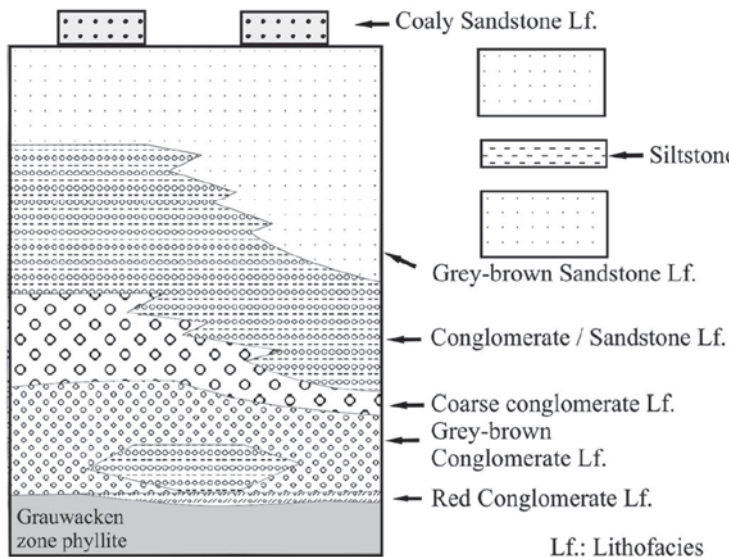


Fig. 22: Lithostratigraphic sections showing the distribution of various lithofacies types (from Neubauer, 2016).

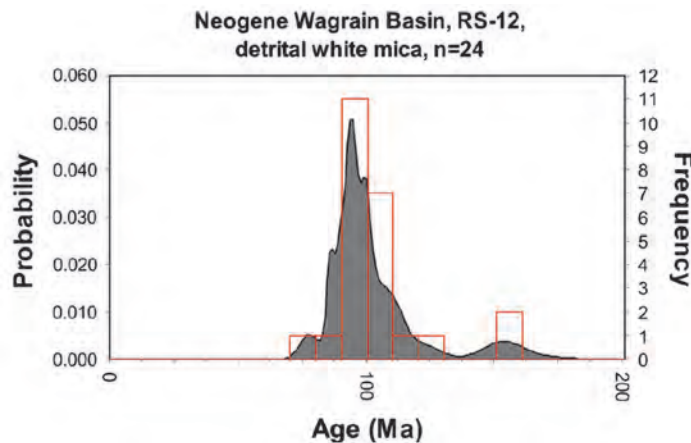


Fig. 23: Ar-Ar ages of detrital single grains of the coaly sandstone lithofacies (from Neubauer, 2016).

Stop 1-6: Radstadt: Upper Ordovician porphyroid of Grauwackenzone

Location: N47° 23' 01.2" E13° 27' 40.9"; ÖK 50, sheet 126, Radstadt; base of tower in the southwestern corner of the medieval city wall

The small outcrop exposes the Middle-Upper Ordovician Blasseneck Porphyroid, a distinct widespread element of the Grauwackenzone basement. The rock well exposes the porphyric texture of the precursor volcanic rock. This is overprinted by Cretaceous greenschist facies-grade metamorphism and top WNW-directed ductile deformation similar as in Upper Carboniferous to Triassic cover successions.

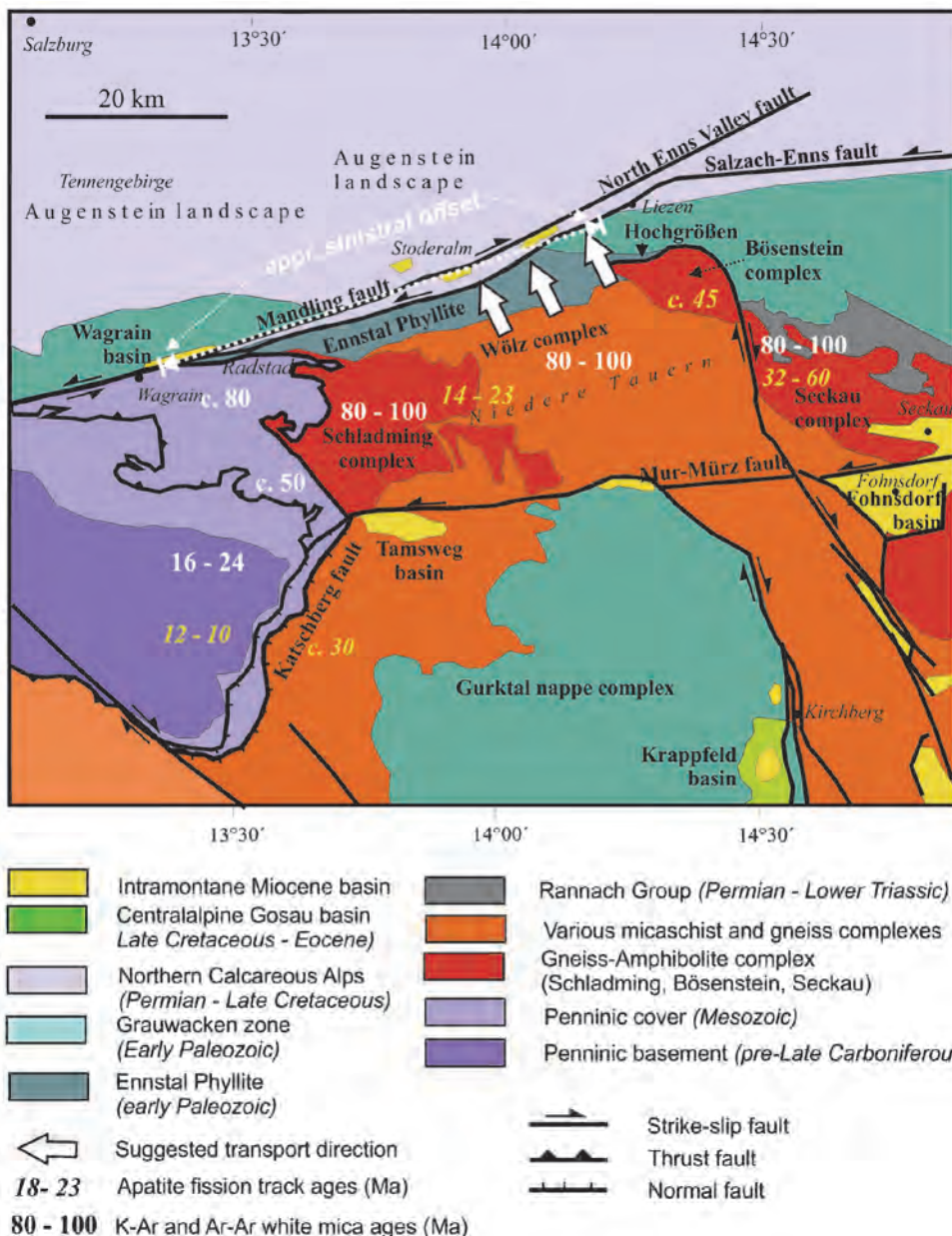


Fig. 24: Model of potential provenance in the eastern Niedere Tauern and Bösenstein areas for the Wagrain basin fill (from Neubauer, 2016).

Stop 1-7: Gnadenalm: “Black” middle Triassic facies of the Pleising nappe

Location: N47° 16' 13.2" E13° 30' 00.2"; ÖK 50, sheet 126, Radstadt; south of Gnadenalm meadow

These exposures along the road 'to Obertauern and the access road to the Gnadenalm expose unusual, dark-colored and bedded dolomite. These dolomites are interpreted as lagoonal deposits (Rossner, 1979). The dark-greyish to black color is unusual for the Middle Triassic successions. Although representing lagoonal deposits, a partly anoxic facies ("black "Anisian/Ladinian" according to older papers of Tollmann, 1977) can be assumed. The area is also rich intraformational monomictic breccia so that fault-controlled escarpment breccia formation is assumed along margins of deepening, increasingly anoxic basins.

Stop 1-8: Obertauern road, W Obertauern: Overview on partly inverted nappes of central Radstadt Mts.

Location: N47° 15' 07.9" E13° 31' 38.2"; ÖK 50, sheet 126, Radstad; parking place at access to Johannisfall.

The viewpoint with a view to the west allows explain a peculiar feature of this part of Radstadt Mountains. The upper nappe, the Quartzphyllite nappe, is inverted and comprises the Permian Alpine Verrucano Fm. at top and underlying Lantschfeld Quartzite (Fig. 25). North of this viewpoint, the amphibolite-grade metamorphic Seekar crystalline basement with Variscan relics is the likely basement of the Quartzphyllite nappe. The Quartzphyllite nappe is underlain by the Pleising nappe with thick Middle Triassic to Carnian carbonate deposits which also include dark phyllites and fine-grained metasandstones of Raibl Formation. The ductilely deformed limestones are within greenschist facies metamorphism and $^{40}\text{Ar}/^{39}\text{Ar}$ white mica ages indicate ages of ca. 78 – 80 Ma (Late Cretaceous). Consequently, the nappe structure is considered to be of Late Cretaceous age (ca. 78 – 80 Ma).



Fig. 25: View towards the Spatzeck and Spirzinger showing the inverted Quartzphyllite nappe.

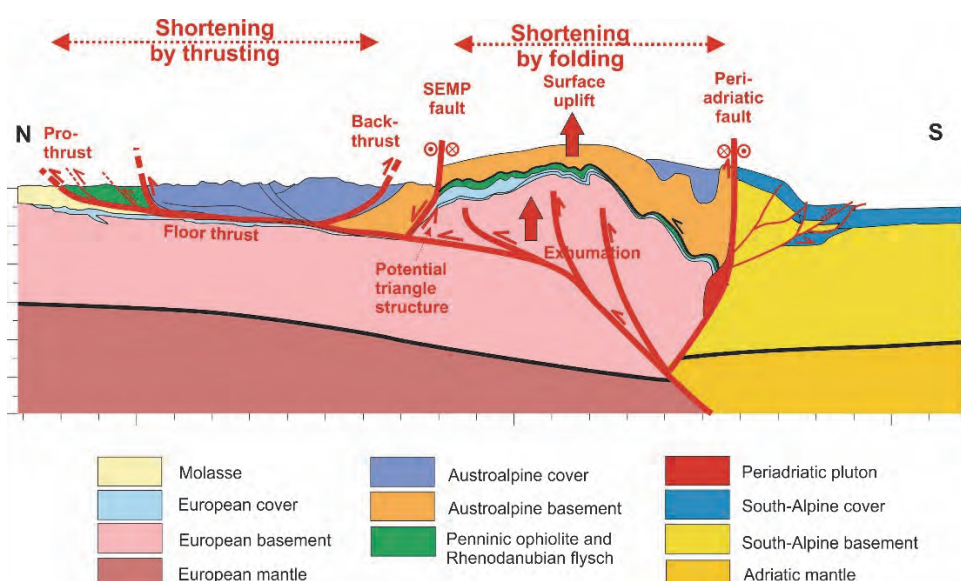


Fig. 26: Tectonic model for the Late Paleogene to Miocene tectonic processes of Eastern Alps in the section across the Eastern Tauern window.

This feature allows discussion of the overall late-stage structure in a N-S cross-section across the Eastern Alps (Fig. 26). We interpret the shortening features by folding as contemporaneous with thrust shortening and fore- and back-thrust of the NCA pop-up (Fig. 26).

Stop 1-9: Obertauern: Paleogene metamorphism in Jurassic successions

Location: N47° 14' 35.5" E13° 34' 00.6"; ÖK 50, sheet 156, Muhr; SE of Obertauern village

This exposure reveals phyllites, marbles, metasandstones, calcareous phyllites of Jurassic age. Single grain $^{40}\text{Ar}/^{39}\text{Ar}$ ages of detrital white mica reveal an early Eocene age (ca. 50 Ma). This indicate that this part was already affected by heating by the underlying Penninic units and represents the age of thrusting of Lower Austroalpine units over Penninic units as initially postulated, in the area further south, by Liu et al. (2001). This implies a footwall propagation of thrusting within Austroalpine units.

3 The eastern Tauern window: deformation phases and age data of the Austro-Alpine – Penninic plate boundary

JOHANN GENSER

3.1 Introduction

One of the main questions regarding the tectonic evolution of the Eastern Alps is the relation between nappe stacking and metamorphism in the Austro-Alpine unit to the subduction of the Penninic units beneath, as new data challenge important assumptions of present (plate)tectonic models (Hawkesworth et al., 1975; Frisch, 1979; Tollmann, 1987; Frank, 1987; Behrmann, 1990; Scharf et al., 2013; Schmid et al., 2013; Rosenberg et al., 2018). These models relate the early to middle Cretaceous nappe stacking and Barrovian type metamorphism in the Austro-Alpine unit to the subduction of the South Penninic ocean beneath or to the final collision with the Middle Penninic basement complex, exposed in the Tauern Window. Recognition of a Cretaceous high-P metamorphism (Thöni and Jagoutz, 1992) in the Austro-Alpine unit in the last years points to a Cretaceous subduction of the AA and hence a lower plate position for this unit during that time span, rather. The two mega-units also show very different timings of the metamorphic evolution, but very similar metamorphic paths (eclogite facies followed by amphibolite facies). In the Austro-Alpine, the temperature peak occurred in the early Late Cretaceous, cooling below c. 300 °C was completed in the late Cretaceous already. In the Penninic units, the thermal peak falls into the late Palaeogene, cooling into the Miocene (Frank et al., 1987a, b) (Fig. 27).

The following is a presentation and discussion of mainly structural and thermochronological data from the Eastern Tauern window, where in the area of the Malta and Lieser valleys, a continuous profile from the deepest tectonic units of the eastern Tauern window up to the Middle Austro-Alpine units is exposed (Fig. 28). It is situated ideally, therefore, to study the relationships between the two mega-units. The area of the eastern TW includes three tectonic mega-units, the Austro-Alpine upper plate, the Glockner Nappe and the basement units of the Venediger Nappe (Fig. 28). The Austro-Alpine unit consists of three individual nappes in the area that were stacked during the Cretaceous and subsequently thrusted onto the Penninic unit. The Penninic unit comprises the remnants of the South Penninic oceanic crust, the Glockner Nappe, and Middle Penninic units comprising a basement complex and an overlying Permo-Mesozoic cover unit. Between the Glockner Nappe and the

parautochthonous basement are several nappes that were derived from the Middle Penninic continental complex (Kurz et al., 1998; Schmid et al., 2013).

Alpine metamorphism Tauern Window

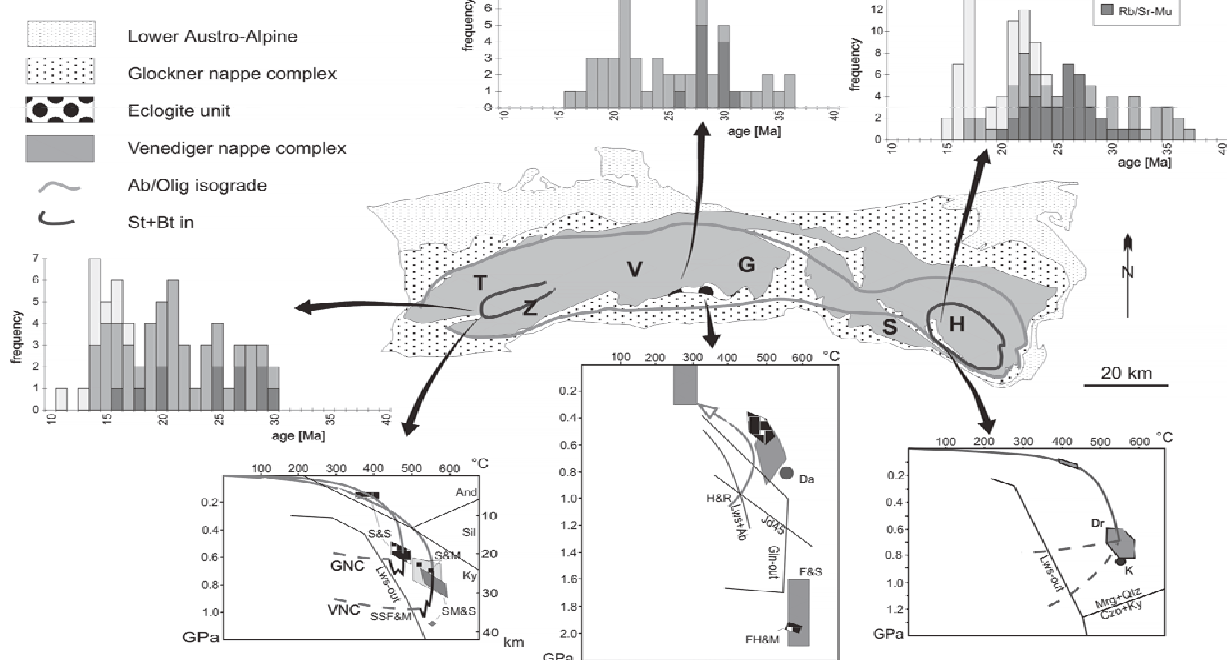


Fig. 27: Alpine metamorphism in the Tauern window with p-T paths and radiometric age data (from Genser et al., 1996; see references therein).

3.2. Tectonic setting and structural evolution of Penninic units

From bottom to top we can distinguish the following tectonic units (Fig. 28), which can be correlated over the entire Tauern window (Kurz et al., 1998; Schmid et al., 2004, 2013). Here, the previous terminology is used:

1. Parautochthonous basement consisting of a pre-Permian basement complex intruded by Variscan granitoids, the Zentralgneis (Central gneisses). On top is a primary Permo-Mesozoic cover sequence, the Silbereck Group in this area.
2. The Eclogite zone, that occurs only in the middle part of the Tauern window.
3. Nappes that consist of basement and cover parts that were derived from continental margin sequences of the Middle Penninic terrane.
4. The Glockner nappe, comprising ophiolites and mainly volcano-sedimentary sequences of the South Penninic oceanic basin.
5. The Matrei and the Nordrahmen units, melange units deposited during the active margin stage.

This study describes the area around Malta and Lieser valley. Beside early work (e.g. Cliff et al., 1971) and mapping (Exner, 1980b, 1983b), further recent data concerning the eastern Tauern window can be found: petrological studies in Kruhl (1993), Scharf et al. (2013), structural and geochronological data and geodynamic interpretations in Bertrand et al. (2015, 2017), Favaro et al. (2015), Neubauer and

Genser (1990), Ratschbacher et al. (1989), Scharf et al. (2016), Schmid et al. (2013) and Rosenberg et al. (2007, 2015, 2018).

In detail, the basement essentially consists of migmatitic paragneisses and minor micaschists and amphibolites (e.g., Frisch et al., 1993). The Variscan granitoids represent intrusions ranging from tonalites to granites, with the main members (Holub and Marschallinger, 1989; Marschallinger and Holub, 1991; Finger et al., 1993): a high-K, calc-alkaline I-type series with syenite, Malta tonalite, Hochalm porphyrygranite, Kölnbrein leucogranite, and two-mica granite and the Na-rich Göß granodiorites to granites. These Variscan granites occur in several cores, divided by metasedimentary basement units. In the eastern Tauern Window (TW), these are the Göß, Hochalm, Hölltor, Sieglitz and Sonnblick cores.

These basement units are overlain by the post-Variscan, Permo-Mesozoic sedimentary sequence of the Silbereck Group. It comprises basal quartzites, overlain by marbles, cagneuls, dolomites and finally calcschists, phyllites to micaschists and minor greenschists. Thrusted onto this parautochthonous unit are the Mureck and the Storz Nappe that comprises mainly Variscan metamorphic paragneisses, amphibolites and micaschists (Vavra, 1989; Vavra and Frisch, 1989; Frisch et al., 1993) and minor granites that intruded during the Variscan (Vavra and Hansen, 1991). The overlying Murtörl unit consists of black albite-phyllites, chloritoid-bearing chlorite-micaschists and graphitic quartzites that are probably of post-Variscan age (because of missing intrusions) and the primary cover of the Storz Group (Kurz et al., 1998).

The Schrovin Nappe comprises orthogneisses and mainly Permo-Mesozoic sediments, quartzites, calcite and dolomite marbles and calcschists. It must be derived from a continental shelf sequence, too (Exner, 1990).

The Glockner Nappe is delineated by some ophiolitic remnants (serpentinites, MOR-basalts) at its base (Höck and Miller, 1987). It mainly consists of the so called Bündner schists, calcschists, grading into marbles and phyllites, and greenschists, deposits of a deep oceanic basin. In this area, the relationship of the basement rocks of the Storz Nappe to the overlying sequence of black phyllites, a Permotriassic shelf sequence and the deep-sea sediments of the Glockner facies is obscured by the strong tectonic overprint, expressed in the parallelism of all the lithological boundaries and also in the strong thinning of the units. All the post-Variscan series are therefore often subsumed in the Peripheral Schieferhülle.

Detailed descriptions of the rock successions and lithologies can be found in the papers by Exner (1971, 1980b, 1982, 1983, 1984, 1989, 1990).

The oldest brittle to semiductile deformation structures in the Penninic units are overprinted by the main, ductile deformation. Indications of earlier deformations under cooler conditions are imbrications of different rock units and parallel trails of graphitic material, preserved in porphyroblasts (mainly albite), pointing to pressure solution as an early deformation mechanism.

The earliest kinematically interpretable deformation structures are a mylonitic foliation parallel to the lithological boundaries with only few intrafolial isoclinal folds (transposition) and a related N-S trending stretching lineation (Fig. 29). Kinematic indicators, as asymmetric porphyroclasts in granitoids and asymmetric quartz textures, the latter preserved in Triassic quartzites of the Peripheral Schieferhülle, indicate tectonic transport top to the N.

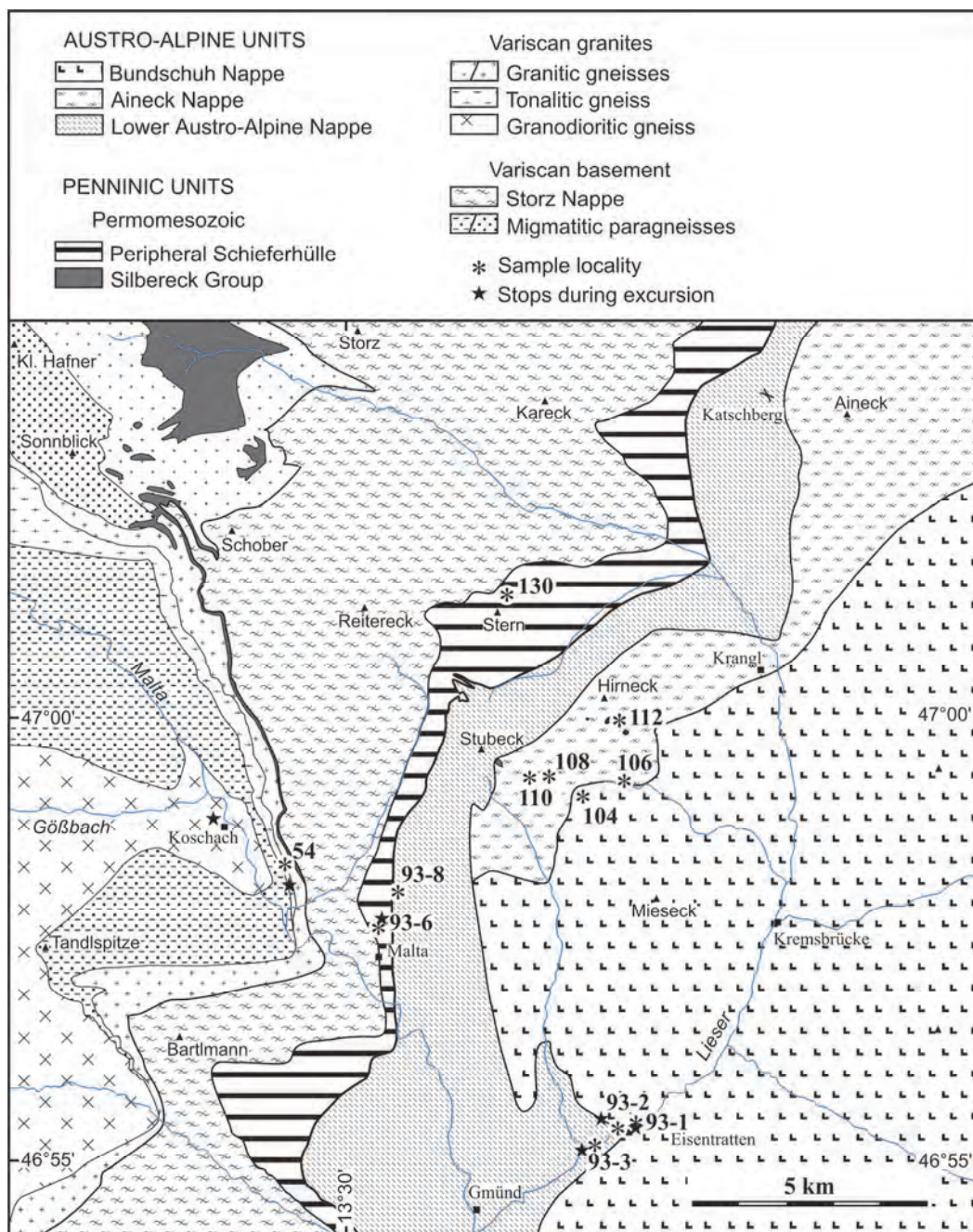


Fig. 28: Geological map of the area of the eastern Tauern window, Lieser and Malta valleys. The numbers relate to samples with new petrological, microstructural and geochronological data.

This N-S trending stretching lineation can be traced from the Peripheral Schieferhülle down to the base of the Silbereck-Fm., affecting the uppermost part of the basement locally (Fig. 29). A mylonitic foliation with N-S trending stretching lineations can be found throughout the Storz nappe, especially well developed in granitic rocks and amphibolites. In paragneisses and micaschists an older (pre-Alpine?) foliation is folded isoclinally and transposed by this foliation. The structures related to this deformation are best preserved in Triassic rocks of the Peripheral Schieferhülle in northern parts of the investigated area (around Stern). Quartzites, dolomites and intercalated calcite marbles display a strong mylonitic foliation with a pronounced N-S trending stretching lineation. Earlier planar structures, as graphitic trails, are folded isoclinally, but also the mylonitic foliation can show a progressive isoclinal refolding with fold axes parallel to the stretching lineation. During this

deformation quartz, calcite, and dolomite recrystallised dynamically. In the Peripheral Schieferhülle this deformation occurred until peak metamorphic conditions were reached, as dolomite was deformed by crystal-plastic mechanisms. Dolomite marbles and quartzites kept their synkinematic deformation features, only calcite shows evidence for a subsequent static recrystallization (Genser, 1992).

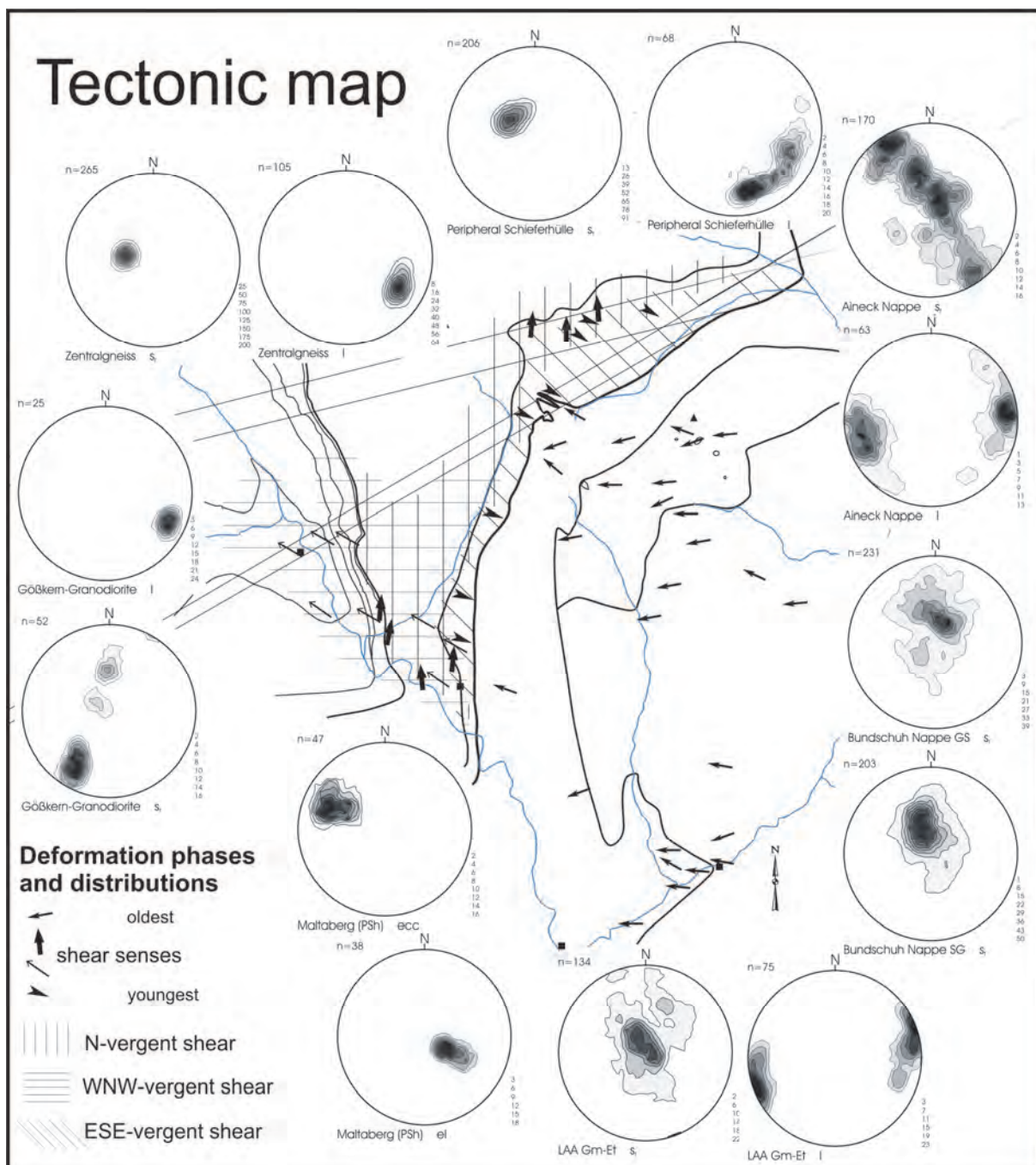


Fig. 29: Tectonic map showing the spread of deformation structures, shear senses, and plots (equal area, lower hemisphere) of foliations and lineations. s_f and l are the penetrative foliations and stretching lineations, ecc and el extensional crenulation cleavage and related extensional lineation, respectively.

In deeper Penninic units, this deformation preceded the temperature peak, but occurred at higher pressure conditions than those of the metamorphic peak. This deformation started within the stability field of albite, even at tectonic levels that later on reached the oligoclase field during metamorphic peak conditions. Granitic gneisses affected by this deformation display the growth of white mica, with celadonite-rich cores and celadonite-poor rims, pointing to a pressure decrease during this deformation.

The next deformation phase affects almost all of the Penninic units in the investigated area and represents the main deformation phase in the mass of the Variscan granitoids. Only parts of the deeper Peripheral Schieferhüllle and also parts of the deeper basement complex remain spared. It develops a mylonitic foliation with a very consistent WNW-ESE trending stretching lineation (Fig. 29). Numerous sense-of-shear criteria, as asymmetric porphyroclasts (δ - and σ -clasts), shear bands, C/S structures and quartz textures unequivocally prove shear of top-to-the WNW.

In the higher Penninic parts, especially in the Storz-Nappe, this deformation is expressed in discrete, W-dipping shear bands with WNW-ESE trending striations, without obliterating the penetrative N-S trending stretching lineation. But quartz textures, mainly oblique cross to single girdle c-axes distributions, indicating WNW-directed shearing, prove a penetrative deformation during this phase in these parts, too. In deeper parts, this deformation phase is the first penetrative event, except in country rocks of the Variscan granitoids that display pre-Alpine deformation structures (sometimes even several phases of superposed folding sealed by Variscan intrusions). Along the northern side of the Malta valley the foliation dips to the E to SE, the stretching lineations to the ESE, in the deepest exposed levels the stretching lineation keeps this very consistent plunge to the ESE, but the foliations display a great circle distribution around this lineation (Fig. 29). Across the Malta valley the foliations in the granodiorites of the Göß core dip gently to the ESE on the northern side of the valley, steeply to the NNE in the middle (Koschach) and moderately to the S on the southern side. In the central part no foliation can be defined, the rocks display apparently uniaxial extension. In the area of steep foliations pronounced stretching lineations also point to deformation in the constrictional field, but some shear criteria, as asymmetric porphyroclasts, asymmetric quartz textures, and asymmetric distributions of extensional and compressional quadrants of aplitic veins point to general non-coaxial deformation with a right-lateral sense of shear. In the granitoids of the Göß core, discordant aplitic and pegmatitic veins show a strong deformation too, although not very obvious macroscopically. It is expressed in a strong recrystallization of feldspars and quartz, mostly occurring in elongated aggregates, and strong lattice preferred orientations of quartz.

During this deformation all major rock forming minerals recrystallised dynamically. It continued until peak metamorphic conditions were reached in deeper tectonic levels. Feldspars recrystallised dynamically, with inversely zoned recrystallised grains of oligoclase, pointing to deformation at at least uppermost greenschist facies conditions.

The last main deformation event led to the exhumation of the Penninic unit. The main shearing was concentrated within a low-angle fault zone in the top of the Glockner Nappe, displacing the AA nappe stack to the ESE (Gensler and Neubauer, 1989; Elsner, 1991). Structures range from mylonitic shear zones with penetrative deformation, especially in calcschists, to the development of a discrete extensional crenulation cleavage, often as multiple sets. Other structures are extension veins and boudinage of competent rock layers. Numerous shear criteria prove shearing top-to-the-ESE. This deformation started at elevated temperatures (crystal-plastic deformation of quartz), but continued

until cool, brittle conditions under the same kinematic frame (Kurz et al., 1994, 1996). In deeper parts, flat-lying, conjugate shear zones are related to this event. Prominent examples are fine grained, cm-thick shear zones in granitoids of the Göß core, that cross-cut the main foliation. In these shear zones, feldspars, quartz, and biotite recrystallised dynamically, quartz-c-axes textures show a maximum parallel to the Y-axis. Deformation here also started near peak metamorphic conditions, but can then be followed to cool, brittle conditions within the same kinematic frame.

3.3. Tectonic setting and structural evolution of Austro-Alpine units

In the area of investigation (Fig. 28), the Austro-Alpine (AA) unit can be divided into three nappes: from the top to the bottom, the (1) Bundschuh Nappe, the (2) Aineck or Radenthein Nappe, and (3) the LAA Nappe (Theiner, 1987). These nappes are distinguished by distinct pre-Alpine and Alpine metamorphic conditions.

The Bundschuh Nappe comprises mainly paragneisses, micaschists and granitic gneisses and shows a two-stage metamorphic evolution. The Bundschuh Nappe shows widespread Variscan amphibolite facies metamorphism, with garnet and staurolite (Exner, 1980a). The Alpine metamorphism reached lower amphibolite facies conditions, leading to the growth of a second, Alpine garnet generation, often as rims around pre-Alpine garnet cores (Schimana, 1986; Theiner, 1987) (Fig. 30). Thermobarometry on the Alpine paragenesis yielded c. 600°C and 10 kbar for the Alpine metamorphic peak.

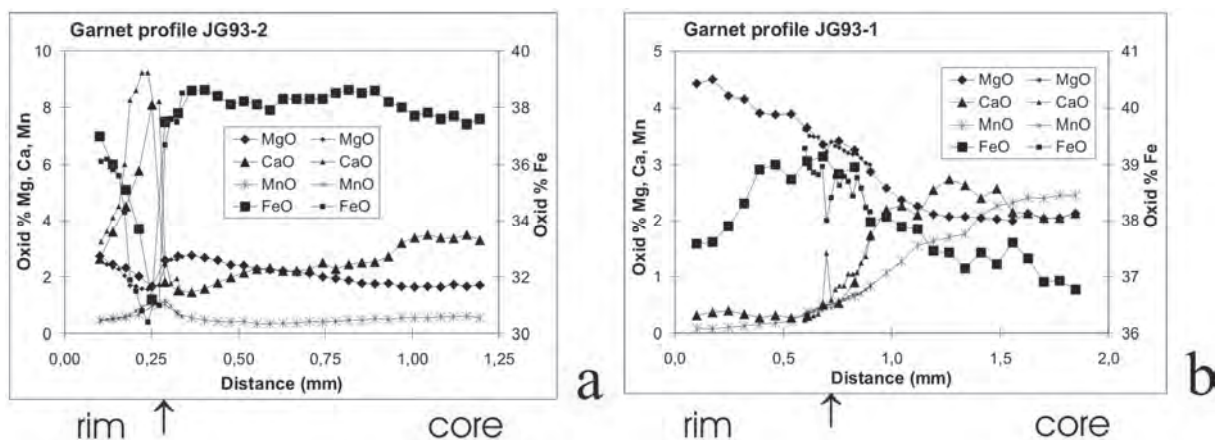


Fig. 30: a, b) Two-phase garnets from micaschists of the Bundschuh nappe. Alpine rims are separated from Variscan cores by a strong increase in Ca and a decrease in Fe. Mg and Mn show only minor variations (boundary is indicated by arrow). Sample JG93-1 contains no plagioclase, so the break is less pronounced. Locations are shown in Fig. 28.

The underlying Aineck Nappe includes garnet-micaschists, paragneisses, and amphibolites and shows only one peak metamorphic assemblage of upper greenschist facies conditions. Garnets typically show continuous zonations and the same suite of inclusion minerals from the core to the rim (Theiner, 1987) (Fig. 30). Thermobarometry gave conditions for the metamorphic peak of approximately 540°C and 9 kbar. The Radenthein unit that underlies the Bundschuh Nappe in the south, displays also only a single stage metamorphism, but shows somewhat higher temperatures (amphibolite facies conditions) (Schimana, 1986).

The LAA Nappe along the eastern margin of the Tauern window is only a remnant of the prominent development at the north-eastern corner in the Radstädter Tauern. There, the Lower Austro-Alpine unit consists of several nappes, build up of pre-Alpine basement slices (para- and orthogneisses, often retrogressed) and thick Permo-Mesozoic cover units of a terrestrial to shallow marine evolution (e.g., Tollmann, 1977; Becker, 1993). In this area, the only remaining nappe displays an inverted tectonic and metamorphic position with pre-Alpine relics of upper greenschist facies minerals, as e.g. garnet, in tectonic higher parts, and only lower greenschist facies conditions in deeper parts. This setting is also evidenced by a remnant Permo-Mesozoic cover sequence at the base of the unit, which is inverted too (Exner, 1971; 1982).

The main deformation event in the Bundschuh Nappe, related to thrusting, occurred prior to the metamorphic peak. This deformation is characterised by an E–W-trending stretching lineation and the transposition of a pre-Alpine planar fabric (Fig. 29). Pre-Alpine garnets are broken and pulled apart, the individual pieces overgrown by a rim of Alpine garnet. Micas show only weak alignments in the Alpine foliation, quartz has recrystallised statically as well (random lattice preferred orientations). The main deformation must have taken place in the ductile domain, however, i.e. at least within greenschist facies conditions. The thermal peak must have outlasted the thrust-related deformation, however, and annealed earlier deformation fabrics.

In the Aineck Nappe, the main deformation, again with an E–W-trending stretching lineation (Fig. 29), is pre- to syn-metamorphic. Micas are aligned in the foliation, garnets show helicitic inclusion trails and quartz various degrees of lattice preferred orientations. The main foliation is folded into upright folds around NE–SW-trending axes, with white mica of the first generation folded around fold hinges. This fabric is overprinted by a static recrystallization under lower greenschist facies conditions, with the growth of white mica, chlorite, albite, and rare stilpnomelane randomly across the older fabric. The main deformation must thus have occurred under upper greenschist facies conditions, followed by a phase of cooling and folding of the main foliation. The static overprint happened under lower greenschist facies conditions, most likely driven by fluid infiltration.

The nappe contact between the Bundschuh Nappe and the Aineck Nappe is cut by the basal thrust that carried the two units on top of the LAA Nappe (Fig. 28). Thrusting must thus post-date the internal imbrication within the MAA units.

The LAA Nappe shows the same E–W-trending stretching lineation as the Bundschuh Nappe and the Aineck Nappe (Fig. 29), but the main deformation occurred under lower greenschist facies conditions. Quartz was deformed by low-temperature plasticity and shows lattice preferred orientations typical for cool deformation conditions. Pre-Alpine garnets are mostly chloritised and deformed into elongated ellipsoids. White micas are frequently rotated into the main Alpine foliation, but also occur in microlithons, tracing an older foliation.

3.4 Ar/Ar mineral data

Single grain $^{40}\text{Ar}/^{39}\text{Ar}$ laser probe (step-wise heating) dating was carried out on white mica, biotite, and amphibole across the Penninic–Austro-Alpine suture at the eastern margin of the Tauern Window in order to constrain the timing of the main Alpine deformation events that led to the juxtaposition of the regarded units. Selected age data for white mica are presented in Fig. 31.

The Bundschuh Nappe, mainly deformed prior to the metamorphic peak of lower amphibolite facies conditions, yielded an integrated age of 107.5 ± 1.3 Ma for muscovite, giving a minimum age for the

main deformation. The next deeper unit (Aineck Nappe), deformed close to the metamorphic peak of slightly lower temperatures, gave an integrated age of 83.5 ± 2.3 Ma for white mica of the peak metamorphic assemblage. White mica of a second generation, grown due to a static, fluid-driven metamorphic overprint, gave ages of 80.8 ± 6.1 Ma. The static metamorphic overprint of lower greenschist facies conditions in the Aineck Nappe should be constrained in time by the age of the second generation of muscovite, as the temperature of this event is below or at about the closure temperature of muscovite. The cooling age of Mu I (110) of c. 85 Ma gives a lower age limit for the penetrative deformation in the Aineck Nappe, related to the W-directed nappe stacking process. From these data a short time interval between cooling from the metamorphic peak (Mu I, sample 110) and the static metamorphic overprint (Mu II, sample 106) can be deduced, as the ages are the same within the 2σ -error limits. A common cause for cooling from the peak metamorphic conditions, for shortening, expressed in the folding of the penetrative foliation at already cooler conditions, and for the subsequent static metamorphic overprint by fluid infiltration can be the thrusting of the Aineck Nappe onto a cool, fluid-rich unit. This could be the LAA unit, derived from the continental margin, on the one hand and the oceanic South Penninic unit on the other hand. The LAA contains mainly low-grade metamorphic pre-Alpine basement rocks and a Mesozoic, carbonate shelf cover sequence that should be rather depleted in fluids in comparison with the shaly-marly deep sea sequence of the South Penninic unit. Also the retrogressive overprint of the LAA with chloritization of garnet needs external fluid sources. These fluids, infiltrating the base of the MAA, are therefore most likely derived from the South Penninic unit, and give a possible age constraint on the subduction of the South Penninic ocean beneath the AA continental margin.

The deepest, Lower AA Nappe, yielded Variscan white mica ages (242.9 ± 2.2 and 239.6 ± 1.1 Ma) from tectonically high levels and strongly disturbed ages of c. 100 Ma from the base. Alpine metamorphic conditions were obviously too low to reset the Ar-system of white mica completely, consistent with the observed deformation conditions and metamorphic assemblages. From the presented data no direct time constraint on the deformation of this unit can be given, but if no marked inverted thermal gradient existed during deformation, the Alpine deformation must be younger than the 85 Ma of Mu I of the overlying Aineck Nappe (sample 110). Thermal models indicate that in shallow to medium crustal levels, that are appropriate for the burial of the LAA in this area, no inverted thermal gradients occur at reasonable thrusting rates (Genser et al., 1996). Additionally, the age sequence with cooling of the higher nappe well before cooling of deeper levels indicates that no inverted geothermal gradient existed during nappe stacking within the exposed crustal levels. The observed inverted metamorphic gradient in the AA edifice must therefore be attributed to the late to post-metamorphic transport of those nappes over deeper ones.

For the LAA Nappe in this area, no pressure data are available that could constrain its burial depths. Its position at the base of the AA nappe complex, however, points to burial depths that are in the same order as for the overlying units. This would imply reduced geothermal gradients during underthrusting of the LAA, a scenario that could be met in an oceanic subduction zone environment. Beginning subduction of the SP oceanic lithosphere, together with the leading edge of the AA continental margin that is deformed into the LAA nappe complex, and fluid infiltration of the base of the MAA, fit into this scenario (Kurz et al., 1996). Tectonic inversion of the continental margin, as presently exposed, at the beginning of oceanic subduction conforms, too. We thus correlate the underthrusting of the LAA with the beginning of subduction of the SP ocean rather than with the end, as proposed by Slapansky and

Frank (1987), who connected it with the collision of the AA and the MP units. It is constrained in time by the second generation of muscovite in the Aineck Nappe at about 80-85 Ma.

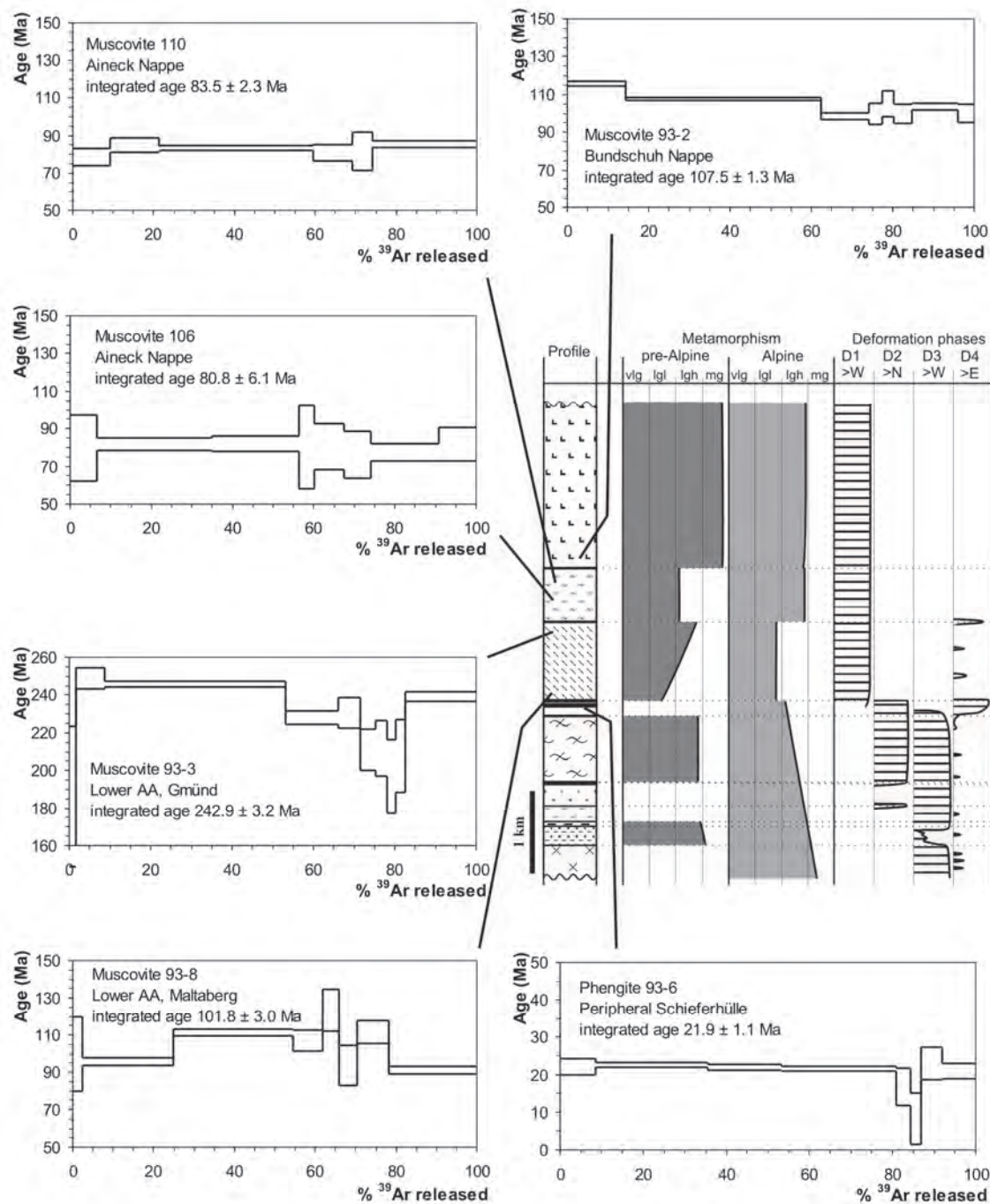


Fig. 31: $^{40}\text{Ar}/^{39}\text{Ar}$ age diagrams of single grains of white mica and profile of the tectonic units at the eastern margin of the Tauern window. Distributions of pre-Alpine and Alpine metamorphic conditions (vlg: very low grade, lgl, lgh: low grade, mg: medium grade) and parts affected by the main deformation phases are given. For location of samples see also Fig. 28.

A white mica from tectonically high parts of the Penninic unit, showing a normal metamorphic gradient of greenschist facies conditions, yielded an age of 21.9 ± 1.1 Ma. The flat age spectra record the cooling of the Peripheral Schieferhülle through c. 400° C. The second penetrative deformation event in the Penninic units, the WNW-directed shearing that occurred on the heating path and at thermal peak conditions, that were higher than the closure temperature of phengite, must thus precede these ages. This deformation event should thus be Late Oligocene (Cohen et al., 2013) in age. The cooling age of 22 Ma gives the onset or an upper age constraint for the ESE-directed shearing, as structural features (e.g. low-temperature plasticity of quartz, calcite twinning) indicate that this deformation started at lower greenschist facies conditions at these tectonic levels, hence at or below the closure temperature of this system. The resulting differential uplift of the Penninic unit should continue to c. 16.5 Ma, the cooling ages of biotite (Rb/Sr) across the centre of the Hochalm Dome (Cliff et al., 1985).

3.5. Discussion

Structural, metamorphic and age data demonstrate distinct Alpine evolutions for the Austro-Alpine and Penninic units. Thrusting in the Austro-Alpine units is generally towards the W, following by folding around E-W to NE-SW trending axes. This thrusting occurred over an extended time-span. The Alpine thrusting in the highest unit (pre-metamorphic) and the subsequent cooling from the highest greenschist to lower amphibolite facies to about 400° C predates 100 Ma. In the next lower unit, thrusting could have persisted until ca. 85 Ma. Nappe stacking must have propagated from the hangingwall to the footwall, therefore, incorporating successively more external and deeper units.

The attainment of higher peak temperatures in higher nappes of the Austro-Alpine unit and the subsequent thrusting onto progressively cooler units of the same mega-unit points to a continuous accretion of parts of the footwall to the hangingwall in the stacking process. Thus thrusting could be explained by an intra-Austro-Alpine subduction. This progressive accretion can also explain the observed inverted metamorphic gradient, without need to invoke inverted temperature gradients.

The beginning of subduction of the oceanic Penninic lithosphere could be dated by the second generation of white mica at the base of the Austro-Alpine unit, that grew due to fluid infiltration. The ages of 80 – 85 Ma indicate a possible interference between intra-Austro-Alpine thrusting and commencing subduction of the Penninic ocean beneath.

In the Penninic units, three distinct deformation stages can be distinguished, that can be found in a very consistent manner over the entire Tauern window (Kurz et al., 1996). The oldest deformation is a shearing top-to-the N to NE, and is found especially the South Penninic Glockner nappe and the underlying gneiss nappes. This event is followed by a shearing top-to-the WNW that affected most of the units, particularly the deeper parautochthonous Zentralgneis unit. The main deformation in the higher Penninic parts, related to their subduction and intra-Penninic stacking is pre- to synmetamorphic. Hence the oldest ages from that unit of about 30 – 32 Ma, already cooling ages, give a minimum age for N-directed shearing, the oldest, ductile deformation. The ages of about 22 Ma place a lower age limit on the WNW-directed shearing, occurring at about peak metamorphic conditions, and an upper age constraint on the subsequent ESE-directed, extensional shearing. K/Ar ages from 22 to 17 Ma for white mica are common along the central dome of the eastern Tauern window, biotite Rb/Sr ages are very uniform at about 15.5 - 17 Ma (Cliff et al., 1985). These ages point to rapid exhumation of the Penninic units from depths of 25 to 20 km to near to the surface in this time span (Cliff et al., 1985). This rapid exhumation was enabled by the tectonic unroofing of the Tauern window along the low-angle normal faults along the Penninic–Austro-Alpine interface. Laterally, the window is

bound by sinistral strike-slip faults, indicating that extension subparallel to the orogen took place in a wrench regime (Genser and Neubauer, 1989; Kurz and Neubauer, 1996).

Thermal modelling of the metamorphism in and around the Tauern window by Genser et al. (1996) also substantiates an independent Alpine evolution of the Penninic and Austro-Alpine units, respectively. A model, where subduction of the South Penninic ocean commenced after the main nappe stacking in the Austro-Alpine unit (Fig. 32), give P-T-t paths, that are in accordance with petrological and thermochronological data (Fig. 27). Models that relate compression and metamorphism in the Austro-Alpine to subduction of the South Penninic ocean and its subsequent collision with the Middle Penninic continental block are grossly inconsistent with these constraining data. A sketch of our preferred model of the relative and absolute timing of the major events is given in Figure 32.

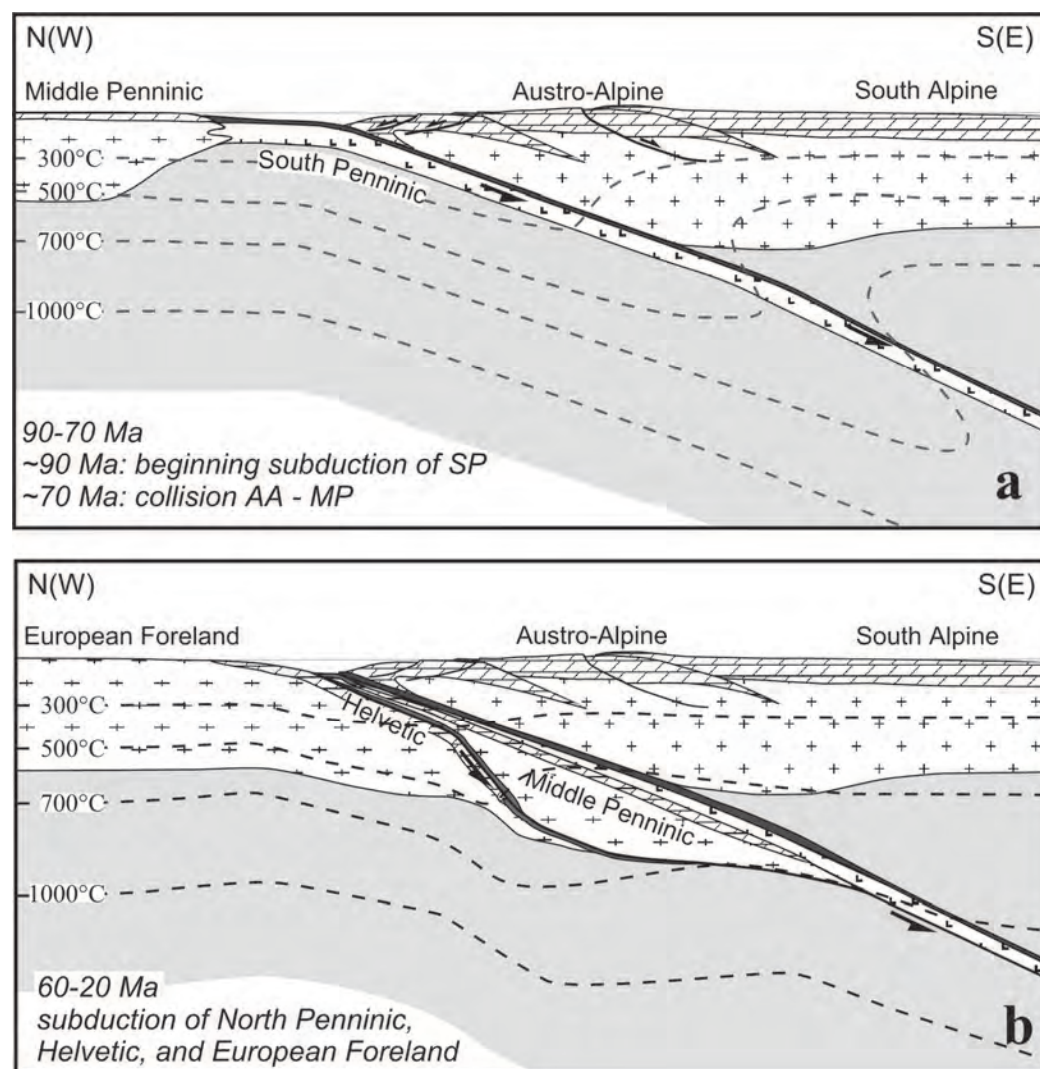


Fig. 32: Thermo-tectonic model for the subduction of the Penninic and Helvetic units beneath the Austro-Alpine hangingwall plate (from Genser et al., 1996).

3.6 Stops

Stop 2-1: Greenschists and calcschists of the Glockner nappe.

Location: N47° 08' 17.2" E13° 32' 06.6"; ÖK 50, sheet 156 Muhr; national road at highway bridge at Kraglau, c. 1.2 km SE of Zederhaus village.

Greenschists and calcschists of the Glockner nappe, which represent metamorphic volcanics (mainly basic tuffs) and sediments (mainly marls), respectively, which were deposited on an oceanic basement.

Stop 2-2: Graphitic phyllites with dolomite clasts of the Nordrahmenzone

Location: N47° 10' 27.7" E13° 26' 56.6"; ÖK 50, sheet 156 Muhr; national road at highway bridge c. 1 km SE of highway tunnel.

Biotite phyllites with cm thick layers of graphitic quartzites and massive clasts of unfoliated dolomite, several metres to deca-metres thick. This unit belongs to the Matrei zone (Nordrahmenzone) and is interpreted to represent the trench fill during subduction of the Penninic ocean (Frisch et al., 1987).

Stop 2-3: Ductile to brittle low-angle normal faulting to the ESE in the Peripheral Schieferhüllle.

Location: N46°57'34.4"N, E13°30'18.7" to N46°57'33.5"N, E13°30'32.0"; ÖK 50, sheet 182 Spittal an der Drau; road cut from second turn at elevation 1010 m upwards on the road Malta – Maltaberg. From Malta village by car (difficult access by big bus) or on foot (ca. 25 minutes to walk).

This roadcut exposes a succession from the uppermost Storz Group (Vavra & Frisch, 1989), a pre-Variscan basement unit, here mainly amphibolites and plagioclase gneisses, overlain by the post-Variscan sequence of the Peripheral Schieferhüllle. The latter sequence starts, approximately 70 m after the crossing path, with black albite porphyroblast schists. Then follow whiteschists, strongly retrogressed orthogneisses, and quartzites of probably Permo-Triassic age, and finally calcschists with intercalated greenschists and metapelites, the so called Bündner Schiefer, Jurassic-Cretaceous deep-sea metasediments and -volcanics. A detailed description of this section can be found in Exner (1980b), of structures in Genser and Neubauer (1989). Alpine metamorphic parageneses comprise:

Quartz-albite-phengite-phlogopite-calcite-ilmenite (quartzites)

Albite-quartz-phengite-biotite-chlorite-calcite-ilmenite (semipelites)

Calcite-quartz-albite-muscovite-rutile-chlorite (calcschists)

Amphiboles-chlorite-albite-epidote-quartz-titanite-biotite-calcite (greenschists)

Two structural events can be distinguished in these outcrops:

1) A penetrative foliation with an only weakly developed stretching lineation. The foliation dips moderately to the ESE, the lineation trends NNE-SSW. These structures can best be seen in the rocks of the Storz Group, in higher units they are strongly overprinted by the second deformation. In deeper parts of the Storz unit and in more northerly parts of the Peripheral Schieferhüllle, where these structures are often well preserved, a tectonic transport of top-to-the N can be derived. This deformation occurred close to metamorphic peak conditions.

2) The second deformation led to a further flattening of the older foliation and an extension in an ESE-WNW-direction. The deformation is noncoaxial, expressed in ESE-dipping shear bands, which often occur in multiple sets with different dip angles. A conjugated, WNW-dipping set of shear bands is only weakly developed and restricted to strongly deformed domains. Lineations on the shear bands plunge

to the ESE and WNW, respectively. In calcschists zones with a new mylonitic foliation, angular to the older foliation, develop. This structures, as well as asymmetric calcite-c-axes textures, prove a dominant normal shear of the hanging-wall to the ESE. Other structures related to this extension are extension veins and boudins, mainly in competent quartzites. Small-scale, asymmetric folds that are overturned to the ESE are related to this shearing, too.

This deformation commenced after metamorphic peak conditions, as evidenced by greenschist facies minerals (chlorite, epidote) in shear zones in amphibolites and continued to cool conditions up to the formation of brittle normal faults. The main part of this deformation is ductile, however.

This deformational event, a low-angle normal faulting, led to the unroofing of the metamorphic dome of the Tauern Window by displacement of the Austro-Alpine upper crust to the ESE. $^{40}\text{Ar}/^{39}\text{Ar}$ dating of a single phengite grain from the quartzites yielded a plateau age of 21.9 ± 1.1 Ma. This age should give the age of cooling below ca. 375 °C and hence an upper limit for the low-angle normal faulting. This event must be placed in the lower Miocene, hence. This is also corroborated by data from Cliff et al. (1985), which indicate nearly isothermal decompression and a following rapid cooling of the Penninic units in the time span between 20 and 16 Ma.

Stop 2-4: Granodiorite of the Göß core

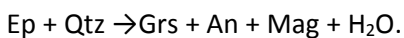
Location: N46°58'45.3", E13°27'44.5"; ÖK 50, sheet 182 Spittal an der Drau; quarry Koschach.

Gmünd-Malta-Koschach (bridge across the Malta river)

In the Göß valley the structurally lowest units of the eastern Tauern Window (and also the Eastern Alps) are exposed (Göß core). It consists mainly of different orthogneisses, ranging from granites to tonalites that represent deformed Variscan granites (intrusion ages of ca. 320 Ma according to Cliff and Cohen, 1980). These orthogneisses are separated from the orthogneisses of the Hochalm core by a paragenetic series. In the Koschach quarry, a strongly lineated, light grey granodioritic augengneiss that is crosscut by several generations of pegmatites to aplites, is exposed.

The magmatic paragenesis of the granodiorite comprises plagioclase, K-feldspar (Karlsbad twinning), quartz, biotite, titanite, allanite, epidote, zircon, and apatite. Geochemically, the rocks resemble Na-rich, high K calc-alkaline I-type granitoids, in part featuring almost trondhjemite affinity (Marschallinger and Holub, 1991). Trace elements show VAG characteristics with selective enrichment of LIL elements and low Rb/Zr.

The Alpine metamorphic paragenesis includes oligoclase, K-feldspar, quartz, biotite, clinozoisite(epidote), garnet, magnetite and sphene. Oligoclase displays inverse zoning (c. An₁₅ in center to An₂₅ at rim), K-feldspar is marginally replaced by myrmekite. Garnet formed due to the general reaction



In this outcrop, one can distinguish 3 main deformational events:

1) The main deformation is responsible for the formation of the penetrative foliation and the pronounced lineation of the orthogneisses. Pegmatite veins are sometimes folded due to this deformation, older aplitic veins mostly not, pointing to low viscosity contrasts during deformation. The strain distribution is generally very homogenous. The dominant stretching lineation indicates constrictional deformation geometry, corroborated by quartz-c-axes distributions (type I crossed girdles). In the Koschach quarry, the foliation dips steeply to the NNE (30/70), on the southern side of

the Malta valley to the S (180/40), on the northern side to the ESE. The poles to the foliation hence display a great circle distribution around the stretching lineation (120/20), which is very consistent over the whole area. This distribution we interpret also to have formed in the constrictional deformation field, and not due to later folding. Shear criteria that are mostly only weakly expressed and quartz-c-axes distributions indicate a non-coaxial deformation path with a dextral shear component. This deformation occurred at elevated temperatures up to the Alpine metamorphic peak, with dynamic recrystallization of plagioclase, K-feldspar and quartz.

This deformation event must be placed in Oligocene times, based on radiometric dating of the metamorphic peak at about 20 Ma in deep tectonic levels of the eastern Tauern Window by Cliff et al. (1985).

2) Conjugate, ductile shear zones that are a few mm to cm wide, cut discordantly across the penetrative foliation. These shear zones dip to the ESE and WNW, and show a normal sense of shear to the ESE and WNW, respectively. This deformation led to a subvertical shortening and ESE-WNW-directed extension, therefore. In the shear zones, plagioclase, quartz, and biotite recrystallised, green amphiboles and calcite, respectively, formed. This indicates an activity of these structures at still elevated temperatures (upper greenschist to lower amphibolite facies conditions). This ESE-WNW extension is related to the uplift of the Penninic units.

3) Steeply dipping, ESE-WNW-trending faults (parallel to the main foliation) that show a normal sense of shear of the northern hangingwall indicate an extension in NNE-SSW direction, too. They were active from near peak metamorphic conditions (asymmetric folding of biotite schists and aplites, with static recrystallization of biotite after this deformation) to cool conditions (slickensides, cacirites, fault gouges).

4 The Nock area: tectonic evolution of the Gurktal Extensional Allochthon, Eastern Alps

FRANZ NEUBAUER, JOHANN GENSER & OLIVER STAUBER

Aim: The main aims of examining the north-western boundary of the Gurktal nappe complex overlying there the Mesozoic cover units (and the underlying Bundschuh basement are:

- (1) to look for the arguments for the Cretaceous nappe structure and, therefore, for the controversy on tectonic reconstruction of Middle vs. Upper Austroalpine units,
- (2) and to examine the subsequent Late Cretaceous extensional tectonics, which is ignored in many recent reconstructions.

4.1 Introduction

The nature and extent of Alpine thrusting of the Gurktal nappe complex, which is part of the Upper Austroalpine nappe complex, represents one of the most controversial topics of geology of Eastern Alps (Clar, 1965 and Frank, 1987 vs. Tollmann, 1975, 1987).

4.2 Austroalpine units east of the Tauern window

East of the Penninic Tauern window, all major Austroalpine units are exposed in the classical Bundschuh area where Holdhaus (1921) argued for an intra-Austroalpine nappe structure based on the discovery of Late Triassic fossils (Fig. 33). Here, the Austroalpine units comprise, from footwall to hangingwall (Tollmann, 1977; von Gosen, 1989a; Koroknai et al., 1999; Schuster and Frank, 1999):

(1) the Radenthein micaschist complex (RMC), a basement complex constituting the Radenthein nappe; (2) the Bundschuh nappe including the Bundschuh complex (BC), a gneissic, pre-Permian basement unit, and a Permian to Mesozoic cover sequence (Pistotnik, 1973/74; here coined as Stangalm Group); the Radenthein and Bundschuh nappes are classically interpreted to represent part of the Middle Austroalpine units in the sense originally defined by Tollmann (1977 and references therein); (3) the Murau nappe with a phyllitic Paleozoic basement; and (4) the Stolzalpe nappe also with a phyllitic Paleozoic basement (e.g., Neubauer and Pistotnik, 1984), and Late Carboniferous to Triassic cover sequences (Kristan-Tollmann & Tollmann, 1964; Pistotnik, 1973/74; Krainer, 1987, 1989).

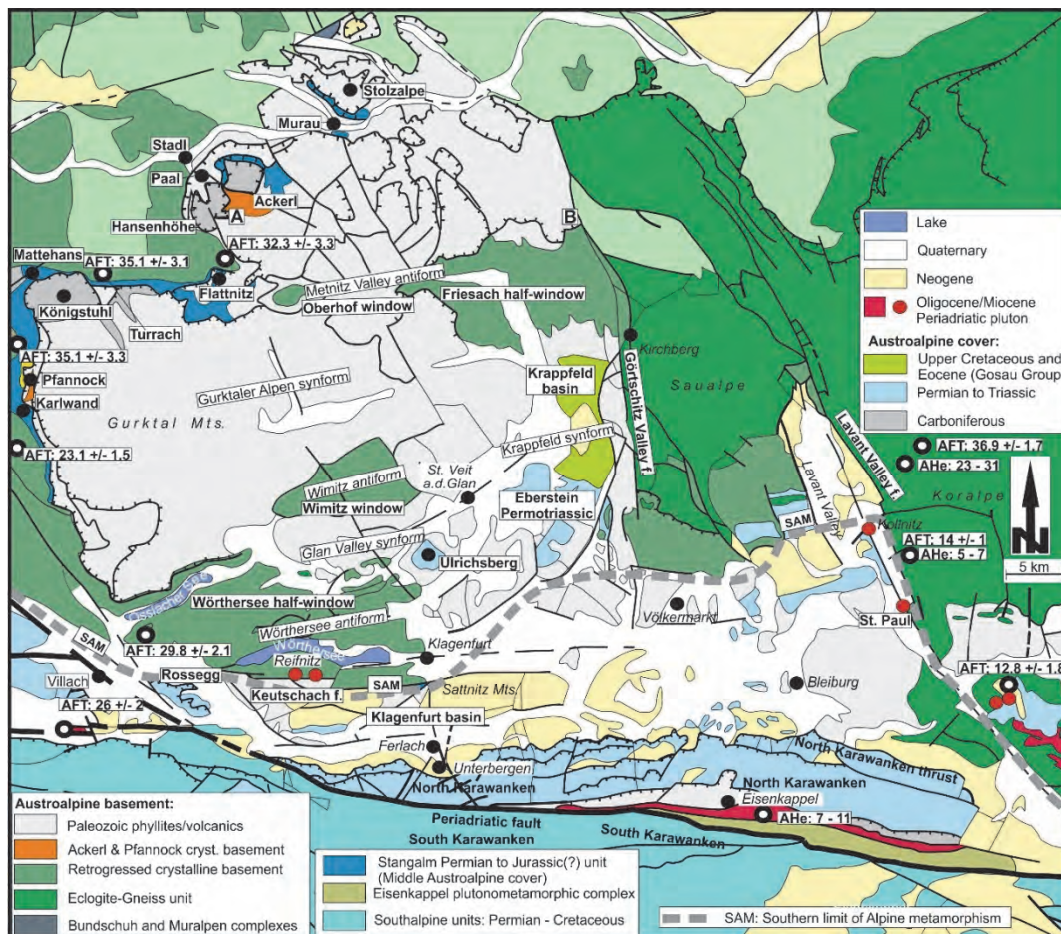


Fig. 33: Simplified geological overview map the Gurktal nappe complex and neighbour units. Late-stage structures and thermochronologic ages are shown, too. AFT – apatite fission track ages, AHe – (U-Th)/He ages. Note also gently late-stage folding of the whole region. Modified after Neubauer et al. (2018), where also data sources can be found.

Furthermore, a post-Variscan angular unconformity below the Lower Triassic Stangalm Quartzites (Pistotnik, 1976) proves the preservation of style and orientation of Variscan structures in the Bundschuh basement unit (see below). Lithostratigraphic peculiarities of the Stangalm Group in comparison to Upper Austroalpine strata include (Figs. 34, 35): only a thin siliciclastic Permian, if any, and thin Lower Triassic quartzites (Pistotnik, 1976; Krainer, 1984), black phyllites, black calc-schists and related synsedimentary ore mineralizations of Anisian age, relatively thin Middle and Upper Triassic dolomites separated by Carnian siliciclastic beds - the latter show extreme thickness variations interpreted to result from synsedimentary normal faulting - and Jurassic cherty limestones and thin Upper Jurassic cherts (Pistotnik, 1973/74; Fig. 34). In contrast, the cover units intercalated between

the Murau and Stolzalpe nappes range from Permian Alpine Verrucano Fm., Buntsandstein-type quartzites, Anisian rauhwacke to Anisian black marble/black calcareous schists.

The Murau and Stolzalpe nappes are part of the Gurktal nappe complex (Upper Austroalpine nappe complex or Central Upper Austroalpine according to Frank, 1987 and Schmid et al., 2004) and are separated from each other by intercalated Triassic successions along northern margins of the Gurktal nappe complex. Both Murau and Stolzalpe nappes comprise a Ordovician to Devonian volcanic-sedimentary successions (Neubauer and Pistotnik, 1984; Giese, 1988). Along the western margin of the Gurktal nappe complex, the Pfannock unit represents a separate tectonic unit (Pistotnik, 1996). It comprises the Pfannock orthogneiss as the basement, and an Upper Carboniferous to Upper Triassic cover succession, which is virtually non-metamorphic (von Gosen et al., 1987; Rantitsch and Russegger, 2000). Among the cover formations, the Anisian Pfannock Fm. represents the transition between clastic Upper Carboniferous and overlying thin Permian and Lower Triassic siliciclastics and Middle-Upper Triassic carbonates (Pistotnik, 1996), which paleogeographically correlated with the Drauzug by Frank (1987). Th section is completrd by Hauptdolomite and Kössen Fm. (with the fossil locality of Holdhaus, 1921). The succession is similar to such in the Northern Calcareous Alps.

Cover of Middle Austroalpine unit: Stangalm Group

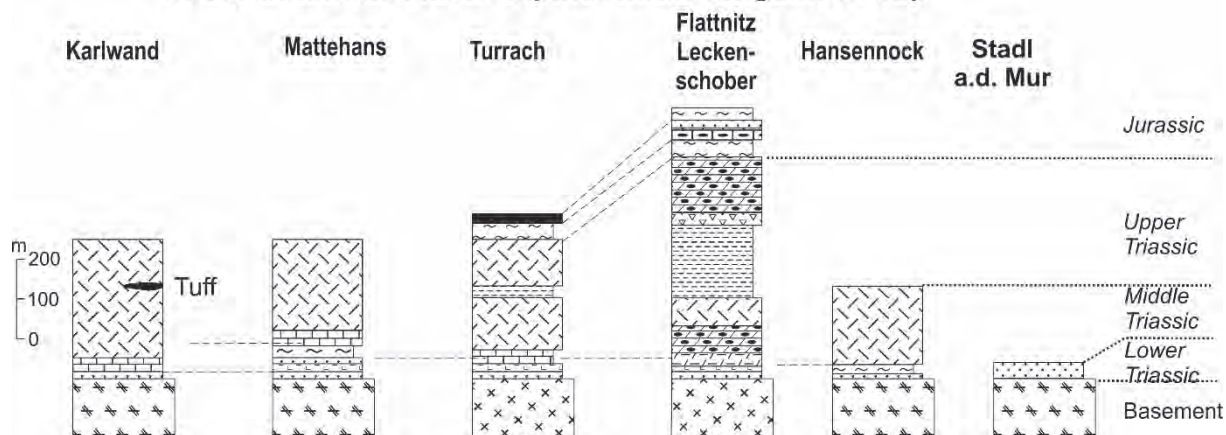


Fig. 34. The Mesozoic cover, the Stangalm Group on the Middle Austroalpine basement.

The unmetamorphic to very low-grade metamorphic cover on the overlying Stolzalpe nappe starts with the post-Variscan intramontane molasse-type uppermost Carboniferous Stangnock and thin Permian Werchzirm Formations (Fritz et al., 1990; Krainer, 1987), which is separated from other portions of the Stolzalpe nappe.

The present superposition of the Gurktal nappe complex over Middle Austroalpine units is interpreted to result from Cretaceous nappe stacking within ductile deformational conditions (Tollmann, 1977; Neubauer, 1987; Ratschbacher and Neubauer, 1989; von Gosen, 1989a; Kurz and Fritz, 2003) although there is still a wide disagreement on the nature and extent of displacement (e.g., Clar, 1965; Tollmann, 1975; Frank, 1987; Frimmel, 1986; 1988). Based on scarce shear sense criteria, a top to the W (WNW) displacement of hangingwall units was proposed (Neubauer, 1987; Ratschbacher and Neubauer, 1989; Ratschbacher et al., 1989; von Gosen, 1989a). Furthermore, many structural data favour an overprint by a second ductile phase with a general top to the ESE displacement (Neubauer, 1987), which was interpreted to represent subsequent Late Cretaceous east-directed motion due to extension

(Ratschbacher and Neubauer, 1989; Ratschbacher et al., 1989; Koroknai et al., 1999). The second event was also interpreted to be responsible for a break in Cretaceous peak metamorphic conditions between the Middle Austroalpine units and the Gurktal nappe complex (Ratschbacher et al., 1991a; Koroknai et al., 1999) and our new geochronological data clearly underline this interpretation.

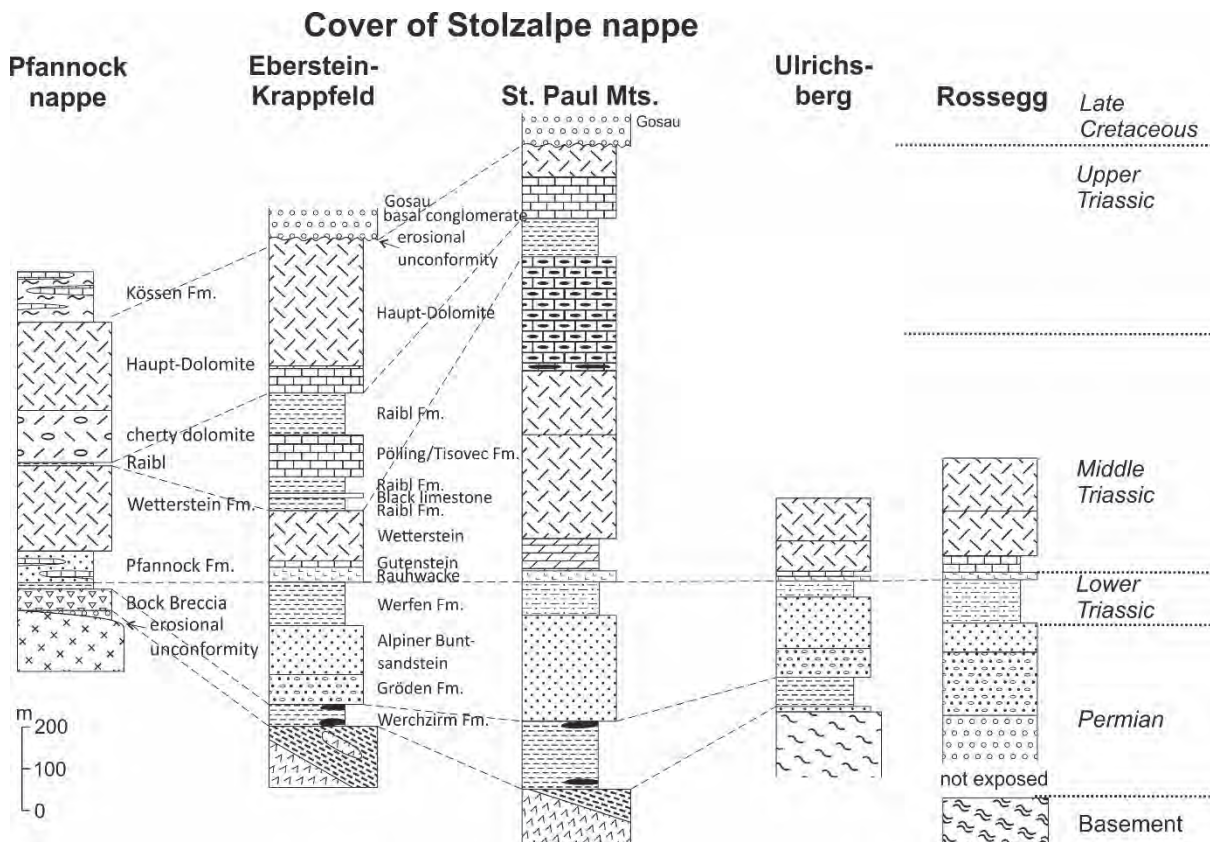


Fig. 35: The autochthonous Permian to Mesozoic cover on Pfannock nappe and Stolzalpe nappe. In comparison to the Stangalm Group, thick Permian strata predate the carbonatic Mesozoic units. Tectonically separated Upper Carboniferous to Permian successions of northwestern Stolzalpe nappe are not shown (for sources, see text).

Based on older microfabric observations (Exner, 1980a) and garnet-biotite geothermometry, Theiner (1987) found a polymetamorphic evolution with a Variscan metamorphic overprint on the Bundschuh complex at ca. 600 – 640°C and, in nearby localities, Alpine temperatures ranging from 500 to 520°C. The age of the Bundschuh orthogneiss is Ordovician according to U-Pb zircon ages (462.5 ± 6.5 Ma; Genser Liu, unpubl. data). Previous Rb-Sr whole rock investigations resulted in sets of subparallel isochrons with model ages between 371 and 397 Ma and high initial $^{87}\text{Sr}/^{86}\text{Sr}$ ratios between 0.721 and 0.739 (Frimmel, 1988). Geochemistry and petrography indicate a syn-collisional origin of the granites (Frimmel, 1988).

Previous geochronological data constraining the age of the metamorphic event(s) of the investigated tectonic units were published by Frimmel (1986), Schimana (1986), Hawkesworth (1976) and Schuster and Frank (1999). The minimum age of metamorphism in the Radenthein nappe is about 88–84 Ma according to Rb/Sr small-scale whole rock and mineral isochrones. K/Ar data record an Alpine age in the Radenthein and Bundschuh (Priedröf) nappes mostly in the range of 70–110 Ma. From the Wölz

micaschist underlying the Bundschuh orthogneiss, Schuster and Frank (1999) report several Sm-Nd garnet ages ranging from 84 ± 6 Ma to 100.6 ± 6.3 Ma. Furthermore, they report white mica and biotite K-Ar ages ranging from 82 ± 2 to 88 ± 3 Ma and Rb-Sr biotite ages of 73.9 ± 0.7 to 77.9 ± 0.8 Ma, representing cooling through appropriate closure temperatures. Rb-Sr white mica ages of the Bundschuh orthogneiss from the Innerekrems area range between 305 ± 12 and 119 ± 1 Ma (Theiner, 1987). The muscovite K/Ar age from the Stangalm Mesozoic cover rocks is about 70 Ma (Schimana, 1986). Rb/Sr muscovite ages from the Bundschuh orthogneiss indicate an early Variscan metamorphic event (350–354 Ma) within these rocks. The Bundschuh orthogneiss was deformed intensely during Cretaceous metamorphism and Rb/Sr mineral ages (muscovite, feldspar) were variably reset to 119 to 91 Ma (Frimmel, 1986). This was confirmed by Sm-Nd garnet data with ages at ca. 80 Ma (Schuster and Frank, 1999). Altogether, according to these data, the Radenthein and Bundschuh tectonic units were strongly affected by Cretaceous metamorphism, while pre-Alpine metamorphism is restricted to the Bundschuh basement unit.

We interpret the very thin siliciclastic successions at the base of the Stangalm Group to represent deposition on a rift shoulder - this feature contrasts with many other Austroalpine Permian to Mesozoic cover successions. We interpret the Triassic strata of the Stangalm Group to reflect extension of the rifting stage, which also enhanced synsedimentary Early Anisian iron mineralizations potentially related to normal faults as well as a second stage of extension during Early Carnian.

The Upper Carboniferous to Triassic cover successions of the GNC are dissimilar to those of the Drauzug unit, which exposed to the SW of the GNC, and resemble those of the westernmost Northern Calcareous Alps. The new data makes it necessary to reconsider currently popular paleogeographic and tectonic models of the Austroalpine domain. The term Drauzug-Gurktal nappe system should be dismissed because: (1) the Drauzug unit does not represent a nappe in contrast to the GNC, (2) the palaeogeographic dissimilarities of Permian and Triassic successions, and (3) eastern palaeogeographic extension of the Drauzug unit in the North Karawanken thrust sheet overlying there the southern margin of the GNC.

4.3 Stops

Stop 2-5: Middle Austro-Alpine basement with Priedröf micaschist/paragneiss and Bundschuh orthogneiss; Alpine metamorphic overprint.

Location: N46° 57' 46.8" E13° 43' 41.4"; ÖK 50, sheet 50, sheet 183, Radenthein; road exposure along the Nockalm road in the Heiligenbach valley, ca. 400 metres South of the custom-house at Innerekrems.

Both the Priedröf micaschist/quartzitic paragneisses (footwall) and the Bundschuh orthogneisses (hangingwall) are exposed along the Nockalm road and along the opposite wall of the valley. The Priedröf micaschist/paragneiss essentially contain quartz, feldspar, biotite, muscovite, garnet and rare pseudomorphs after staurolite. The Bundschuh orthogneiss is composed of K-feldspar porphyroclasts, quartz, plagioclase and light-greenish white mica.

Theiner (1987) found a polymetamorphic evolution with a Variscan metamorphic overprint in nearby localities with ca. 600 – 640 °C and Alpine temperatures ranging from 500 to 520 °C based on garnet-biotite geothermometry. The age of the Bundschuh orthogneiss is uncertain. Rb-Sr whole rock investigations resulted in sets of subparallel isochrons with model ages between 371 and 397 Ma and high Sr₀ ratios between 0.721 and 0.739 (Frimmel, 1988). White mica of the Bundschuh orthogneiss from the Innerekrems area range between 305 ± 12 and 119 ± 1 Ma (Theiner, 1987). Geochemical and

petrography indicate a syn-collisional granites (Frimmel, 1988). The first age is interpreted to be close to the time of Variscan metamorphism, the second age as result of Cretaceous resetting of the Rb-Sr isotopic system.

Both lithologies contain an ESE plunging stretching lineation. Shear criteria suggest both a first top WNW shear and a later, semiductile ESE displacement.

Stop 2-6: Bridge Postmeister Alm. Primary base of the Stangalm Mesozoic sequence.

Location: N46° 56' 48.6" E13° 43' 58.9"; ÖK 50, sheet 183, Radenthein; road exposure along the Nockalm road in the Heiligenbach valley, E of bridge E PostmeisterAlm.

The outcrop exposes the primary contact between the basement (micaschist) and the transgressively overlying Quartzite (Lower Triassic, previous "Skythian" stage; Fig. 36). The basement micaschist displays open folds, which are discordantly overlain by quartzites of suggested Lower Triassic age. The quartzite represents the basal formation of the Stangalm Mesozoic sequence. Hangingwall sectors of the quartzite are well foliated and display an E-dipping foliation. New sericite is grown on the foliation plane. A new ^{40}Ar - ^{39}Ar age of a concentrate of a few grains yielded a plateau age of ca. 89.0 ± 0.6 Ma.

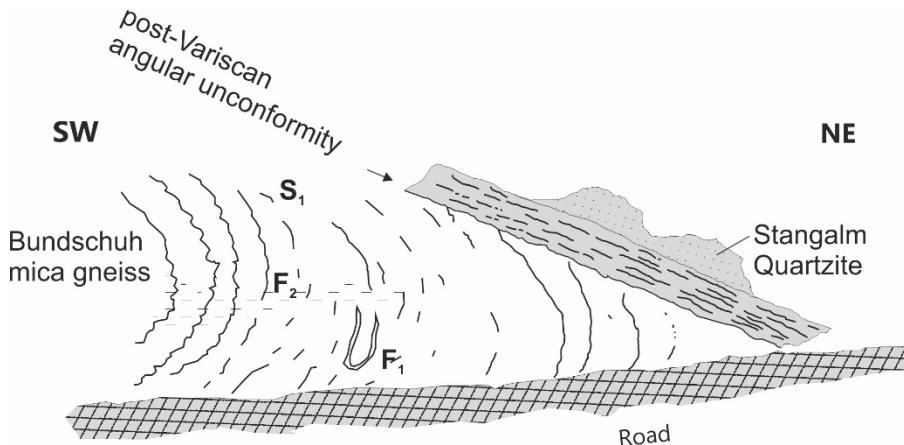


Fig. 36: Sketch showing the structural relationships between folded micaschists the Buntschuh basement and thin quartzites at the base of the Stangalm Group.

Stop 2-7: Ductile low angle normal fault at the tectonic boundary between the Stangalm and Pfannock Permo-Mesozoic sequences and the Gurktal thrust system.

Location: N46° 56' 33.2" E13° 45' 40.3" and N46° 56' 07.3" E13° 45' 32.8"; ÖK 50, sheet 183, Radenthein; Nockalm road. Park your car at the Eisentalhöhe parking place.

Follow the path to the Eisentalhöhe (exposure of Hauptdolomite and Kössen Formation of the Pfannock slice of the Gurktal Nappe Complex). Follow ridge from the Eisentalhöhe to the west, which exposes the phyllonite zone and the underlying dolomite marble of the Stangalm unit. A plateau age of 89.0 ± 0.6 Ma was found for newly grown white mica in the basal Lower Triassic Stangalm Quartzite exposed at the base of the Mesozoic cover succession on the Buntschuh basement.

The dolomite marbles of the Stangalm Mesozoic sequence are in part strongly foliated and lineated. The lineation plunges E and ESE. Dolomite microfabrics of the metamorphic Stangalm Mesozoic comprise symmetric as well as asymmetric fabrics indicating a mixture of coaxial and non-coaxial deformation regimes implying partitioning of shear strain. Calcite-dolomite thermometry gives a

bimodal distribution of temperatures with maxima at approx. 360°C and approx. 450°C, while a white mica concentrate gives an Ar-Ar plateau age of 96.2 ± 0.4 Ma.

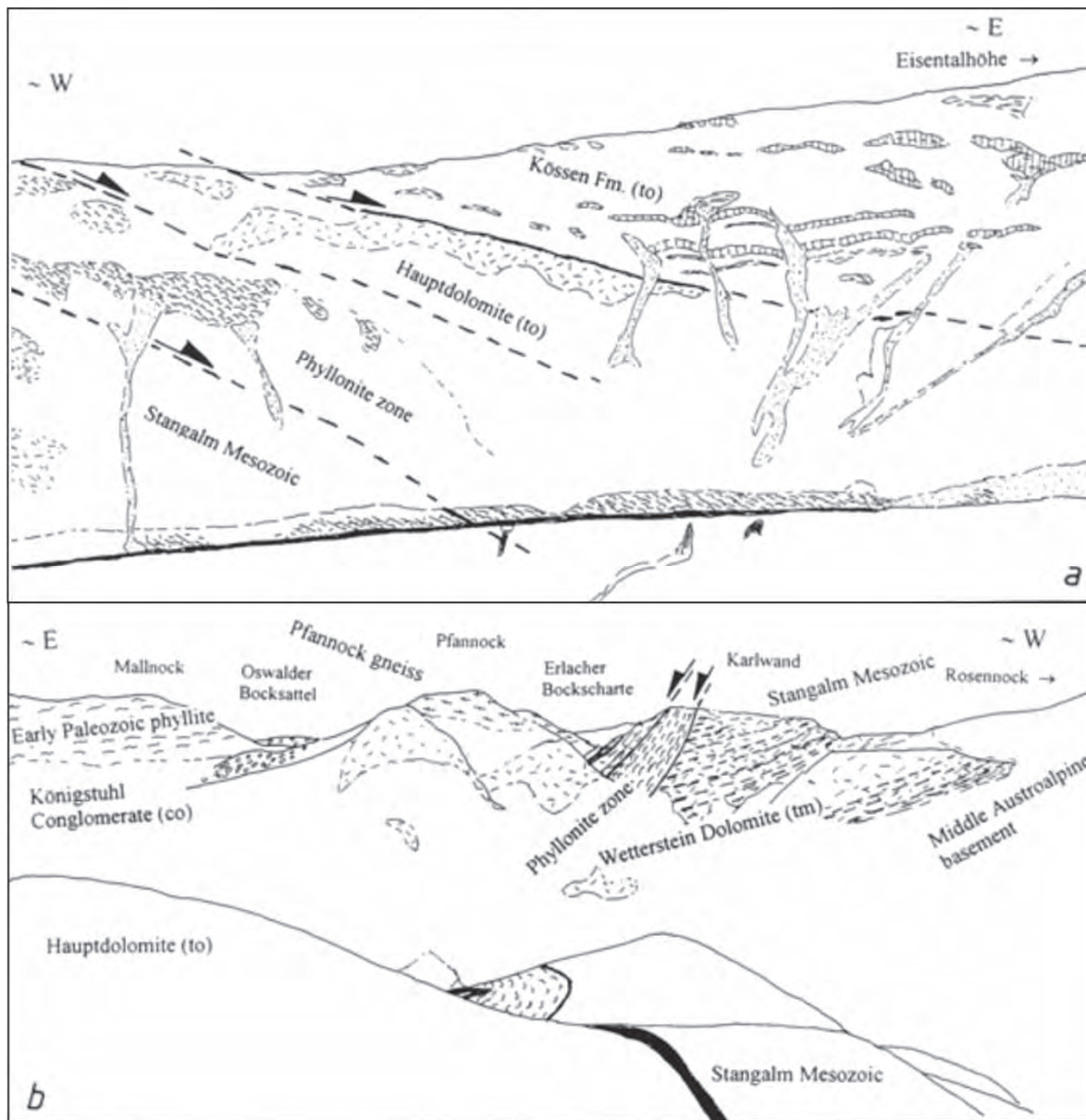


Fig. 37: View from the parking place "Eisentalhöhe" towards N displaying the low-angle normal fault contact between Middle and Upper Austroalpine structural units. a - View from the parking place "Eisentalhöhe" towards . b –View to the south displaying a high-angle normal fault contact between Middle and Upper Austroalpine structural units.

The marbles are overlain by a several tens of metres thick phyllonite, which exhibits a clearly visible extensional crenulation cleavage fabric. Sense of displacement is top to the E/ESE. The phyllonite was interpreted as Carnian Raibl Formation. But the inclusion of chlorite schists exclude this stratigraphic interpretation. This level is now interpreted as part of the Murau Nappe of the Gurktal Nappe Complex because lithological composition and continuous exposure to true Murau Nappe along the structural base of the Gurktal nappe complex.

For the first time, a plateau age of 85.78 ± 0.33 Ma demonstrates the pervasive Late Cretaceous metamorphic overprint on the Murau nappe in the footwall of the regional, ESE-directed ductile detachment fault. This age is interpreted to date cooling after the throughout recrystallization of rocks composing the Murau nappe. A further white mica concentrate gives an Ar-Ar plateau age of 87.1 ± 0.5 Ma (age of ductile shearing), whereas another sample gives a mixed Ar-Ar age of 204.3 ± 0.5 Ma suggesting the polymetamorphic nature of the Phyllonite zone. White micas of the first sample shows a more phengitic composition than that one with the older age.

Views from the parking place to the N (Fig. 37a) and to the S show the structural contacts between various structural units (Fig. 37b).

In the hangingwall, dark Upper Triassic limestones of the Kössen Fm., which belong to the cover of the Pfannock Nappe of the Gurktal Nappe Complex, are exposed. According to Holdhaus (1921 and Kristan-Tollmann and Tollmann (1964), these limestones include in part rich faunas (e.g., *Thamnasteria rectilamellosa*, *Isoclinus bavaricus*, *Cardita austriaca*).

5 The “Carboniferous of Nötsch” and the pre-Alpine Gailtal basement: Significance for Alpine-Carpathian tectonics and palaeogeography

Aim: The aim for looking to the pre-Alpine Gailtal basement and the Carboniferous of Nötsch in the southernmost Austroalpine region is to discuss the significance of the peculiar tectonostratigraphy of tectonic units in the wider Nötsch area, which is similar to the Grauwackenzone succession of the northern Austroalpine units south of Northern Calcareous Alps. From there, these units extend also to the eastern part of Western Carpathians. These relationships to the Nötsch area show that these units were potentially rooted in that area close to the Periadriatic fault and were then thrusted towards NW or N.

5.1 Regional geology

Among all distinct Austroalpine tectonic basement units of Eastern Alps and Western Carpathians, the Nötsch-Veitsch-Ochtina (NVO) unit is particularly interesting because of two reasons: (1) It comprises elsewhere unknown Lower Carboniferous clastic shallow water formations overlain by Upper Carboniferous terrestrial conglomerates and sandstones, which are interpreted to represent deep to shallow marine molasse deposits following initial stages of the early Late Carboniferous Variscan orogeny (Schönlau, 1985; Krainer, 1992); and (2) the Veitsch (Eastern Alps) (Ratschbacher, 1984) and Ochtina/North Gemicic unit (Western Carpathians) (Vozárová et al., 2013) nappes containing similar strata are overlain by a pre-Variscan amphibolite-grade metamorphic basement unit and a Lower Paleozoic phyllitic basement (Kaintaleck basement; Neubauer et al., 1994, 2002), all representing tectonic units in the footwall of the Late Jurassic/Early Cretaceous oceanic Meliata suture similar as in West Carpathians.

The Nötsch area is located between the Periadriatic and the Bleiberg fault (Fig. 38), the latter being part of a major regional strike-slip fault (Drau Range South Margin fault) in the southernmost part of the Austroalpine domain (Bartel et al., 2014) subparallel to the Periadriatic fault. To the north of the the Bleiberg fault, the Drauzug s. str. (Drau Range) containing there Pb-Zn mineralizations is exposed. The Nötsch area comprises, from base to top, similar three tectonic units as the Grauwackenzone (incl. the NVO unit) in the northern part of the Austroalpine nappe complex (Figs. 38, 39): (1) the unmetamorphic Carboniferous Nötsch Group (Schönlau, 1985), (2) the retrogressed amphibolite

facies-grade metamorphic Nötsch crystalline basement ("Granite of Nötsch" of Exner, 1985), and (3) the rarely fossil-bearing (Silurian-Devonian) greenschist facies-grade metamorphic Gailtal crystalline basement (Schönlau, 1979).

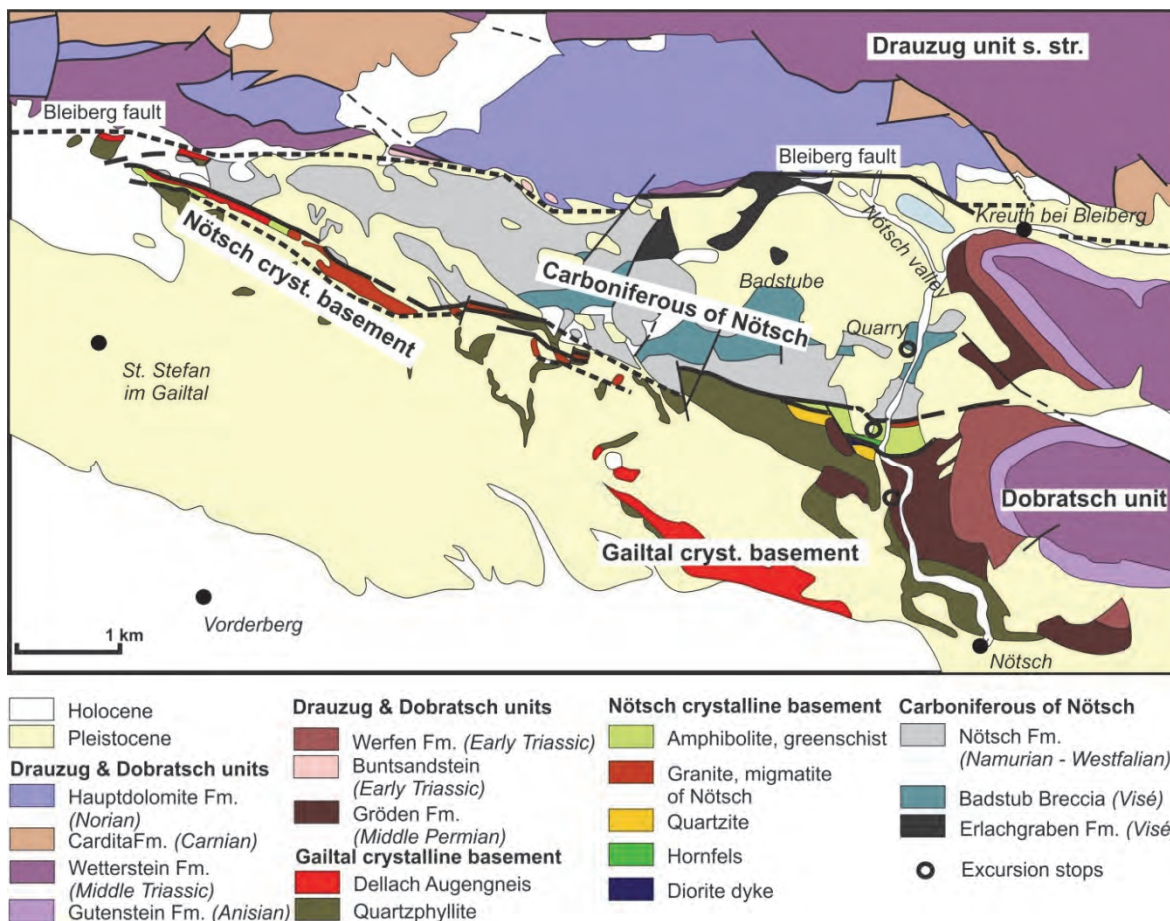


Fig. 38: Geological map of the Nötsch area (after Anderle, 1977 and Schönlau, 1989).

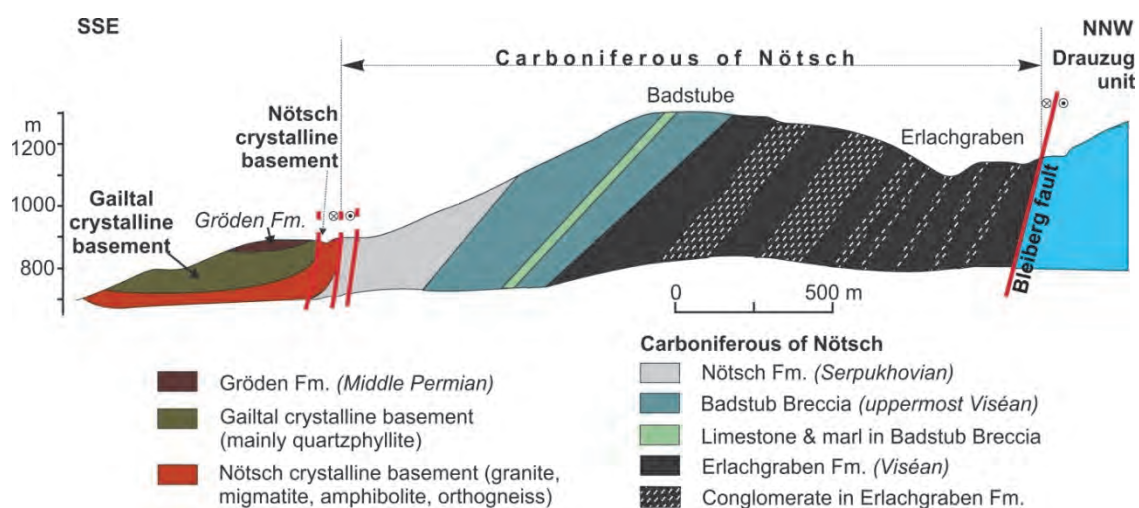


Fig. 39: Section along the western ridge of the Nötsch valley (modified after Schönlau, 1985).

The eastern Gailtal crystalline basement consists mostly of quartz-phyllite, within which Silurian conodonts were found in a marble horizon (Schönlau, 1979). According to own unpublished data, the Dellach augengneiss with the U-Pb zircon age of 441.6 ± 6.7 Ma is a tectonic lens within the Gailtal basement and represents a Silurian magmatic rock overprinted by Carboniferous metamorphism (Ar-Ar sericite ages of 321 ± 1 Ma to 345 ± 1 Ma) and a second thermal stage with a maximum age of 265 ± 3 Ma. Ductile shearing can be recognized (Fig. 40b) and we tentatively relate the Permian age to this event.

By an angular unconformity (Fig. 40f), the Gailtal crystalline basement is covered by the Gröden Fm. at the base of the Upper Permian to Upper Triassic cover of the Dobratsch. Consequently, the Gailtal crystalline basement is part of the Dobratsch unit. The cover has some distinct features, e.g. Middle Triassic volcanics and some pelagic Upper Triassic limestones making it distinct from the Drauzug s. str. north of the Bleiberg fault.

The eastern Gailtal crystalline basement consists mostly of quartz-phyllite, within which Silurian conodonts were found in a marble horizon (Schönlau, 1979). According to own unpublished data, the Dellach augengneiss with the U-Pb zircon age of 441.6 ± 6.7 Ma is a tectonic lens within the Gailtal basement and represents a Silurian magmatic rock overprinted by Carboniferous metamorphism (Ar-Ar sericite ages of 321 ± 1 Ma to 345 ± 1 Ma) and a second thermal stage with a maximum age of 265 ± 3 Ma. Ductile shearing can be recognized (Fig. 40b) and we tentatively relate the Permian age to this event.

By an angular unconformity (Fig. 40f), the Gailtal crystalline basement is covered by the Gröden Fm. at the base of the Upper Permian to Upper Triassic cover of the Dobratsch. Consequently, the Gailtal crystalline basement is part of the Dobratsch unit. The cover has some distinct features, e.g. Middle Triassic volcanics and some pelagic Upper Triassic limestones making it distinct from the Drauzug s. str. north of the Bleiberg fault.

In the underlying amphibolite-grade Nötsch crystalline basement (Figs. 38, 39, 40a), U-Pb zircon ages of 480.3 ± 9.4 Ma and 442.5 ± 1.7 Ma from mylonitic orthogneisses indicate a similar age of intrusion of granitoids as the Dellach augen-gneiss. However, Ar-Ar white mica ages range from 408 ± 2 Ma to maximum 430 ± 2 Ma constraining cooling after a pre-Variscan stage of amphibolite-grade metamorphism. Biotite and K-feldspar plateau ages are at 344 ± 2 Ma to 337 ± 2 Ma are overprinted by a younger event between 213 ± 1 Ma and 198 ± 1 Ma interpreted to result from an advanced stage of Alpine rifting. The lower boundary of the Nötsch crystalline basement is a cataclastic shear zone (Fig. 40c).

The Carboniferous of Nötsch is a famous fossil-rich very-low grade to unmetamorphic Lower Carboniferous succession with the Erlachgraben Fm. at the base, the Badstube Breccia (Fig. 40d) in middle part of the section and the Nötschgraben Fm. at the top. The nature of the contact to the overlying Permian Gröden Fm., sedimentary or tectonic, is unknown. Rich flora (van Amerom and Schönlau, 1992) and faunas (e.g., Schraut, 1999) proof an age from latest Viséan to early Bashkirian (Schönlau in Hubmann et al., 2014) of the Carboniferous of Nötsch. Recently, Vachard et al. (2018) described limestone clasts within the Badstube Breccia, reworked from a carbonate shelf, indicating that they are older than the Badstube Fm. Microfacies and fossil assemblages with abundant algae indicate that a shallow marine carbonate shelf was developed at the northern margin of the deep-sea basin of Nötsch.

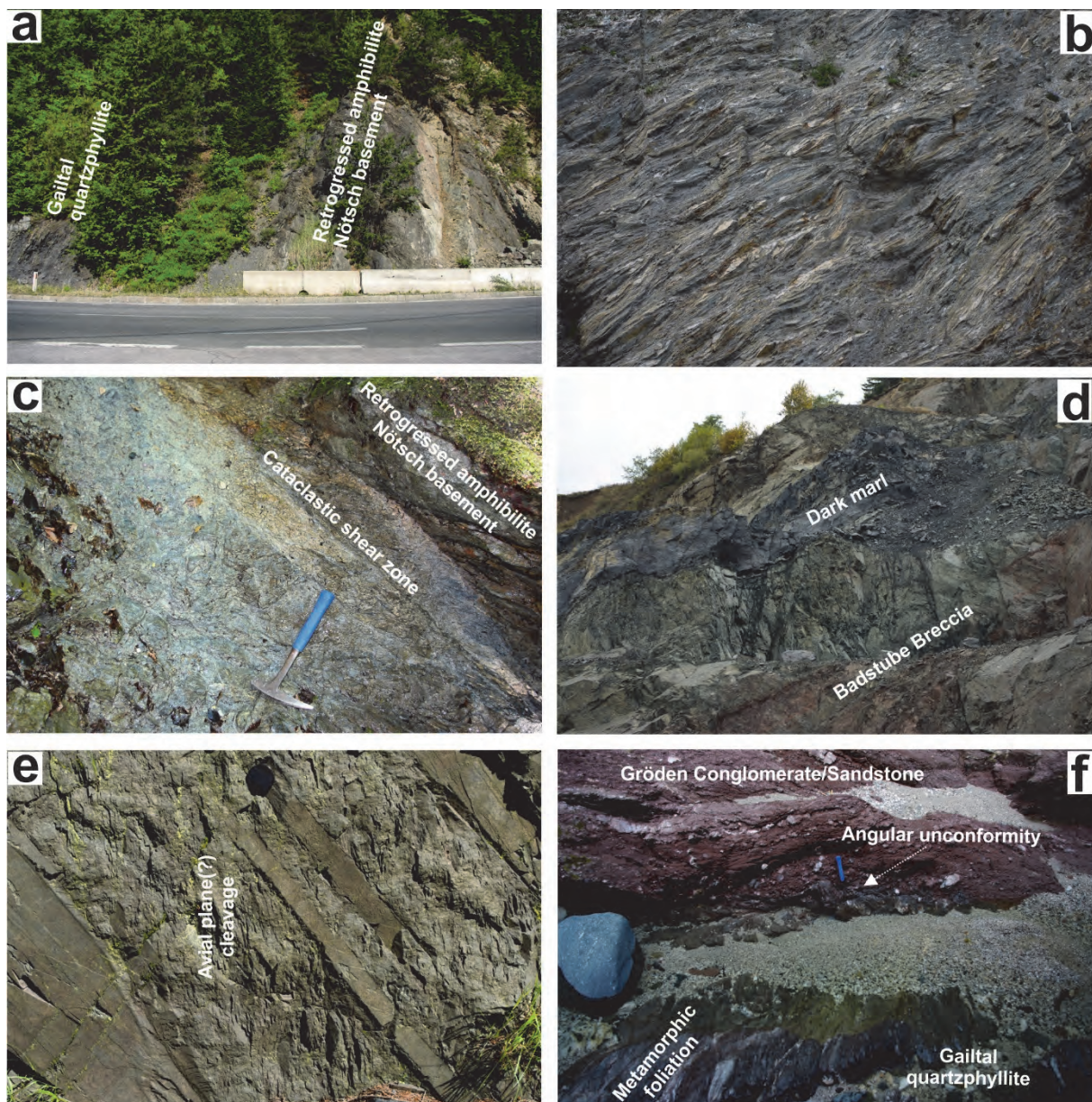


Fig. 40: Field photographs of various rocks of the retrogressed Nötsch basement, the Gailtal crystalline basement and of the Carboniferous of Nötsch.

Own data, white mica Ar-Ar ages from orthogneiss boulders (Exner, 1983a) of the Pölland area at the western margin of the Nötschgraben Fm. (Fig. 38), show plateau ages ranging from 343 ± 4 Ma to 380 ± 2 Ma and are affected by a post-depositional very low-grade metamorphic overprint, which is also reflected in rare axial plane cleavage (Fig. 40e).

The new data has significance for the Variscan history. We assume that an early Variscan amphibolite-grade metamorphic unit was exhumed along a thrust fault and shed clasts into the molasse-type basin in the footwall (Fig. 42 for a model). This metamorphic unit was not the Nötsch crystalline basement, which has a different age pattern.

The new data demonstrate, beside its significance for the Variscan history, that the tectonic succession of the Nötsch area at the southernmost part of the Austroalpine unit has a strong similarity to the nappe stack (including the NVO unit) of the northern Austroalpine sectors (Grauwacken zone and Ochtina/North Gemic unit in western Carpathians; see Fig. 43 for details of correlation). We consider,

therefore, these three units of the Nötsch area as a remnant of the root zone of the basement and cover nappes in the footwall of the Meliata suture. The structural relationships demonstrate >150–200 km large-scale nappe transport of the Meliata suture remnants in the Eastern Alps and the involvement of large, hitherto undetected Cenozoic strike-slip faults within the Austroalpine nappe structure.

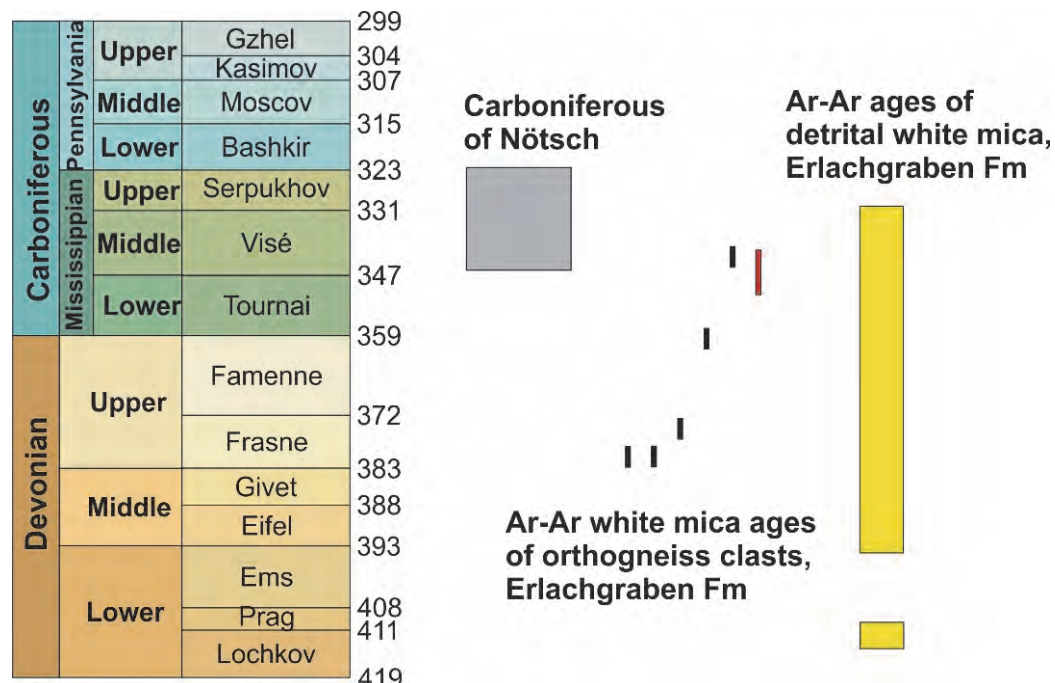


Fig. 41: Detrital white mica ages in comparison to the depositional age of the Carboniferous of Nötsch.

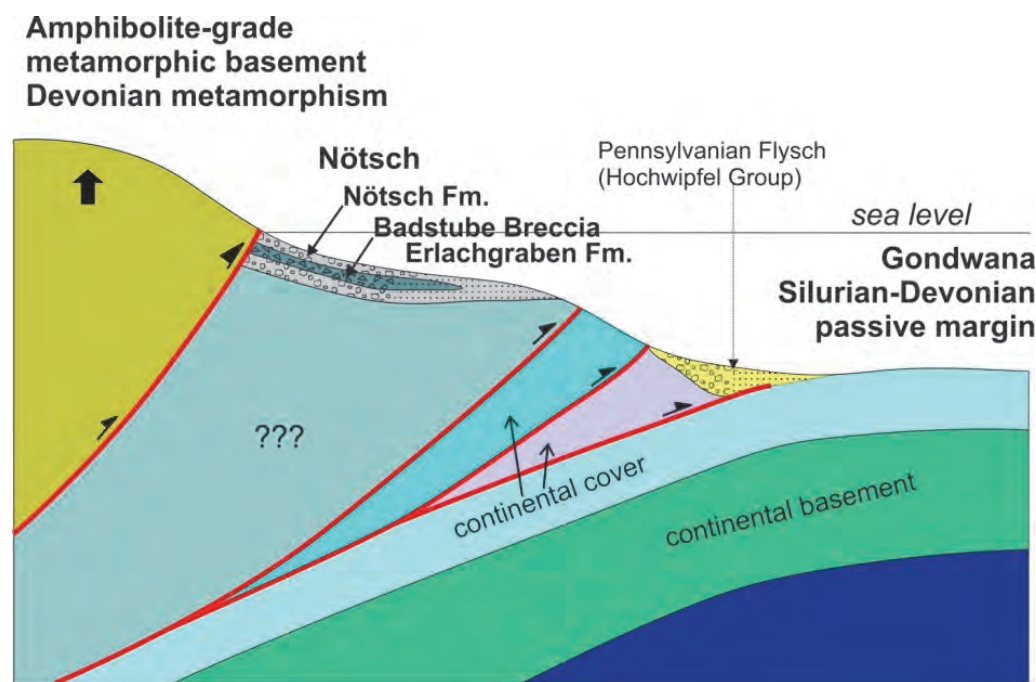


Fig. 42: Tectonic model of the Carboniferous of Nötsch.

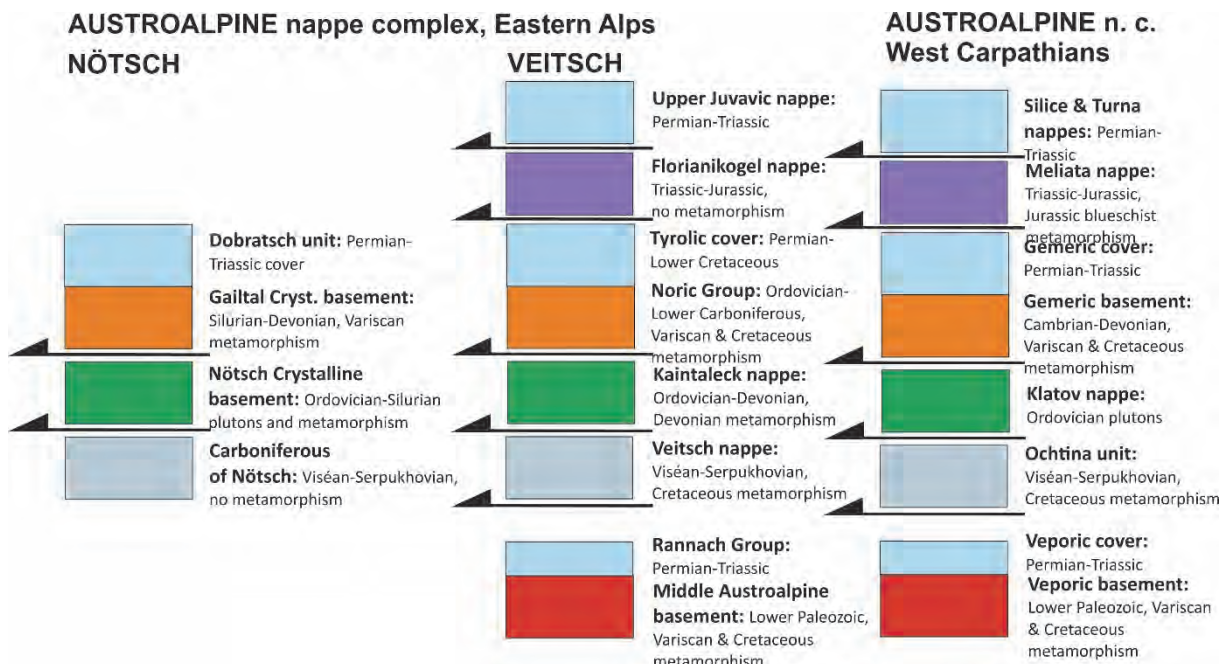


Fig. 43: Comparison of the tectonostratigraphy of the Nötsch area with that of the northeastern Austroalpine nappe complex and with Western Carpathians. Note that the age of thrusting in the Nötsch area is uncertain, whereas in the other areas the age of thrusting was during Cretaceous.

5.2 Stops

Stop 3-1: Nötschgraben quarry with Badstub Breccia

Location: N46° 37' 01.9" E13° 36' 52.0"; ÖK 50, sheet 200 Arnoldstein; Jakomini quarry.

The quarry exposes mainly the Badstub Breccia overlying the Erlachgraben Fm. and underlying the Nötsch Fm. According to Krainer and Mogessie (1991), the Upper Visean Badstub Fm. consists of amphibolite breccias and conglomerates with intercalated sandstones, siltstones and shales. In the upper part of the sequence, these sedimentary rocks contain some fossils, e.g., brachiopod shells. Based on structural, textural and compositional features, these authors suggested that these sediments represent submarine resedimented deposits formed by sediment gravity flows on a proximal fan or slope (fan delta, slope apron) along an active strike-slip fault zone parallel to a continental margin. We interpret this fault as a thrust. Major and minor element chemistry of the amphibolite clasts argue for metamorphosed tholeiitic ocean floor basalts of the amphibolite clasts.

Stop 3-2: Nötsch Valley: Road cut with Nötsch crystalline basement, boundary to Gaital Phyllite

Location: N46° 36' 35.7" E13° 36' 35.1"; ÖK 50, sheet 200 Arnoldstein.

This road cut exposes the boundary of retrogressed amphibolites of the pre-Variscan Nötsch crystalline basement to the overlying Variscan Gaital Quartzphyllite (Fig. 40a). The boundary shows ductile fabrics overprinted by late stage cataclastic fabrics. The Gaital Quartzphyllite is ductilely deformed and exhibits boudinage (Fig. 40b). Depending on the state of vegetation, the boundary of the retrogressed Nötsch crystalline basement to the Nötsch Formation of the Carboniferous of Nötsch can be seen, too.

Stop 3-3: Nötschgraben – Angular unconformity at base of Dobratsch unit

Location: N46° 36' 29.3" E13° 36' 35.5"; ÖK 50, sheet 200 Arnoldstein.

The outcrop in the Nötsch Valley exposes the angular unconformity between the Variscan Gailtal Quartzphyllite with a Variscan age of greenschist facies metamorphism and red overlying conglomerate and sandstone of the Permian Gröden Fm. of the Dobratsch unit. This proves that the Gailtal crystalline basement is part of the Dobratsch unit.

6 Periadriatic fault and the Eastern Carnic Alps and Karawanken

FRANZ NEUBAUER, JOHANN GENSER, ANDREAS ETZEL & BIANCA HEBERER

Aim: The aims of this part of the excursion are:

- (1) to examine the Southalpine unit, particularly regarding the differences of the Permian to Middle Triassic successions in comparison to the Austroalpine domain,
- (2) to investigate the complexities of the Periadriatic fault and the Late Miocene and Pliocene formation of the Klagenfurt basin and its overriding by the North Karawanken, and
- (3) to assess the significance of exhumed tectonic basements units exposed along the Periadriatic fault in the Eisenkappel area.

6.1 Periadriatic fault system

The Periadriatic fault is the longest and most important strike-slip fault system of the Alpine mountain belt and separates the Southalpine units in the south from the Penninic units in its western part and Austroalpine units in its eastern part. The eastern PAF is considered as southern confining fault of the Late Oligocene to Early Miocene extruding wedge (Neubauer, 1988; Neubauer and Genser, 1990; Ratschbacher et al., 1989, 1991a, 1991b; Schmidt et al., 1991). Several distinct connotations are generally associated with the Periadriatic fault: (1) A major dextral strike fault with an offset between 150 to 400 km, (2) a separation of vergency: to the north north of the fault, to the south in the Southalpine unit, (3) a metamorphic boundary, (4) Eocene to Oligocene slab break-off magmatism along its trace. Although distinct reviews exist for major portions of the Periadriatic fault (Schmid et al., 1989; Rosenberg, 2004), not much attention has been paid to its eastern part.

This contribution is aimed to fill this gap and discusses important issues on the eastern part of the Periadriatic fault from the Lesach Valley to the eastern Karawanken Mountains. The Periadriatic fault is the most important strike-slip fault in the Alps and separates the Southalpine unit in the south, with top to-the-south motion from the Austroalpine and Penninic units with a top-north or northwest transport in the north (e.g., Schmid et al., 1989, 2004; Fodor et al., 1998). The Periadriatic fault can be traced from the Po Plain west of Torino to the Pannonian basin. It extends for approximately 700 km from NW Italy to NE Slovenia, where it disappears beneath Neogene sediments of the Pannonian basin (Fodor et al., 1998). The Periadriatic fault (PAF) (Figs 1, 3, 7,) strikes largely E–W parallel to the Alps, except for its central segment, the NW–SE striking Giudicarie fault (Pomella et al., 2012 and references therein).

The eastern segments of the PAF are called Gailtal and Pustertal faults and the eastern extension in the Karawanken Mts. has no special name. It represents a fault system composed of several distinct faults, which are from west to east: the eastern segment between Mules and Pannonian basin, which

is also often called Gail Valley fault, which is cross-cut by two NW-trending faults, the Möll Valley and the Lavant Valley faults. The eastern PAF exposes a flower structure (Polinski and Eisbacher, 1992). These allow a further distinction of three segments of the eastern PAF because of their peculiar structure: (1) The segment between Mules and Hochstuhl fault is straight and separates mainly basement (Brixen Quartzphyllite unit; Lower Palaeozoic to Lower Carboniferous Variscan basement of the Southalpine unit in the south and mostly basement rocks, the Gailtal basement in the eastern segment and the Defereggel quartzphyllite unit in the north. (2) The segment between Hochstuhl and Lavant Valley faults is characterized by the juxtaposition of Permomesozoic strata of the Southalpine unit to the North Karawanken unit, which overrode the Neogene Klagenfurt basin. Furthermore, in contrast to the western segment of the Southalpine unit, the Lower Palaeozoic to Lower Carboniferous basement only occurs in inliers within anticlines. (3) The eastern segment is poorly exposed and separates the Pohorje basement from Neogene sediments in the south.

In the Eastern Alps, the PAF separates the Southalpine units from the Austroalpine units. The units on either side of the PAF show differences in tectonic style, paleogeography, facies and degree and age of metamorphism (e.g. Schmid et al., 1989; Tollmann, 1977). During Alpine collision, the Austroalpine units underwent a complex tectonic and metamorphic evolution, whereas the Southalpine unit largely escaped Alpine metamorphism (e.g., Bistacchi et al., 2010). The eastern PAF also represents a boundary of metamorphic overprint separating the largely unmetamorphic Southalpine unit (with the exception of the small Eder unit – a strike-slip duplex with greenschist facies metamorphic overprint: Läufer et al., 1997), from Austroalpine units with Cretaceous-age low-grade metamorphic conditions (e.g., Müller et al., 2001, 2002). The PAF consists of bundles of kinematically linked large-scale faults. Fault rocks along the PAF comprise a several kilometer wide mylonitic belt for deeper crustal levels and a few tens of meters wide cataclasitic zone at shallower levels (Rosenberg, 2004). The TRANSALP transect near Bruneck proved the subvertical trend of the PAF near the surface and a continuous bend to the S up to ~60° dip near the upper/lower crustal boundary (Bleibinhaus and Groschup, 2008; Bleibinhaus et al., 2009).

The transpressional PAF shows, with exception of the Giudicarie fault segment, a dextral displacement, whereas estimations of the lateral offset range from 150 km to 450 km (e.g. Haas et al., 1995). Rare evidence for local sinistral displacements and reactivation is reported, too (Mancktelow et al., 2001; Nemes, 1997; Rathore and Becke, 1980), which verifies polyphase activation of the fault. Along the PAF, a vertical offset of several kilometers occurs locally (Läufer et al., 1997; Nemes, 1997; Schmid et al., 1989; von Blanckenburg et al., 1998; Heberer et al., 2017).

Along the eastern part of the Periadriatic fault, a number of small lamellae of basement and cover rock successions as well as generally Oligocene tonalites are exposed. These include:

- (1) The Lesach lamella with Permian Gröden Sandstone in the Lesach Valley (western extension of the Gail Valley) (Sassi et al., 1974; Zanferrari, 1976; Nemes, 1997). Note that further west, additional lamellae are known, including the Winnebach-Bruneck and Mauls-Pens lamellae, which are not discussed here;
- (2) the Eisenkappel crystalline basement in the surrounding;
- (3) the Eisenkappel Paleozoic unit, and
- (4) Oligocene tonalites.

6.2 Lesach lamella

The Lesach lamella with its Permian Gröden Sandstone is located c. 3 km south of similar lithologies within the Drau Range and is separated from this unit by the Gailtal crystalline basement. The Dobrautsch is the only location within the DR, where Permian redbeds (Gröden Fm.) are located nearby the PAF (Anderle, 1977). We suggest as the most appropriate origin of the Lesach lamella the southern Dobrautsch and its eastern extension. This implies a dextral strike-slip duplication of Permian strata compared to the base of the DR strata in the north and a minimum dextral offset of 50 – 60 km of the Lesach lamella along the PAF.

6.3 Eisenkappel crystalline basement

The Eisenkappel area in the eastern Karawanken Mountains in Austria and Slovenia exposes north to the Periadriatic fault, metamorphic and plutonic units, which include a deformed tonalite lamella, the Eisenkappel crystalline basement with the Eisenkappel pluton and the Eisenkappel Paleozoic units. The Eisenkappel pluton intruded into amphibolite-facies rocks ("Altkristallin") to the south (Exner, 1972; Faninger and Štruc, 1978; for a map, see Bauer et al., 1981). It is composed of mainly granites and diorites and minor gabbro, monzonite, and granodiorite (Visonà and Zanferrari, 2000; Bole et al., 2001). According to Miller et al. (2011), contact metamorphism of the Eisenkappel granite to the Eisenkappel Paleozoic unit implies an emplacement pressure of ≤ 350 MPa (Exner, 1972, 1976). Based on mineral age date done in the mid-70s, an early Triassic intrusion age was postulated (e.g., Cliff et al., 1975; Scharbert, 1975). In order to improve on these data, Genser and Liu (2010) dated zircons from seven samples and titanite from one sample by U/Pb LA-ICP-MS at Xi'an and amphiboles and biotites from four samples, and K-feldspars from five samples by the Ar-Ar method at Salzburg University. According to their data, one diorite sample (with very small zircon grains) from Slovenia gave U/Pb ages between 450 and 500 Ma. Zircons from the main rocks of the Karawanken pluton (biotite-granite, granodiorite, amphibole-granite) often show a spread of data points along the concordia with a maximum between 280 and 300 Ma and a smaller cluster at about 240-250 Ma. The titanite gave ages of about 245 Ma. Ar-Ar dating yielded ages between 245 and 260 Ma for amphiboles from granitic rocks and an age of 235 Ma for a K-rich amphibole from a gabbro. Biotites gave ages of 245 Ma, 242 Ma, and 232 Ma for granitic rocks, and 228 Ma for biotite from the gabbro. K-feldspars show patterns with increasing ages with high-temperature gas release steps. The ages reach (pseudo)plateaus of about 170-180 Ma, reliable low-temperature release steps are at about 70-80 Ma. Genser and Liu (2010) draw the following main conclusions from their ages:

- (1) There is an Ordovician magmatic event preserved in the Karawanken belt.
- (2) The time of intrusion of the main Eisenkappel granitoids is between 280 and 300 Ma, i.e. of early Permian age.
- (3) The spread of U/Pb zircon ages along the concordia down to about 245 Ma points to elevated temperatures up to the end of the Permian. This is also supported by the U/Pb titanite age and Ar-Ar amphibole ages; the latter confirming cooling below ca. 550 °C between 260 and 245 Ma.
- (4) Cooling below 300 °C (biotite ages) occurred in the Middle Triassic.
- (5) K-feldspar Ar-Ar ages indicate cooling below ca. 250 °C in mid-Jurassic time and probably some reheating in the Cretaceous.

Miller et al. (2011) reported mineral-whole rock Sm–Nd analyses of two cumulate gabbros of 249 ± 8.4 Ma and 250 ± 26 Ma (ϵ_{Nd} : +3.6) from an alkaline gabbro body with within-plate geochemical characteristics. Garnet-whole rock Sm–Nd analyses of two associated silicic samples yielded well-constrained ages of 238.4 ± 1.9 Ma and 242.1 ± 2.1 Ma (ϵ_{Nd} : -2.6) indicating Triassic magmatism.

6.4 Eisenkappel Paleozoic unit

The very low-grade metamorphic Eisenkappel Paleozoic unit consists of slates, greywackes and includes a prominent pillow diabase horizon, which shows mildly alkaline geochemical characteristics (Loeschke, 1970). The age of the Eisenkappel Paleozoic unit is still uncertain and is interpreted either as Ordovician or Early Carboniferous (Loeschke and Schnepf, 1987). The Eisenkappel Paleozoic unit is welded with contact metamorphism with Eisenkappel crystalline basement (Exner, 1972, 1976).

6.5 Oligocene tonalites

The eastern Periadriatic fault includes Oligocene tonalites, which intruded during initial fault motion at uncertain depths (>15 km) and which were later exhumed to the surface (Pomella et al., 2011; Neubauer et al., 2018). The pressure estimates for the depth of intrusion are as follows: 6.2 to 7.5 kbar for the Mauls tonalite, 3.5 to 4 kbar (Finkenstein; Diener, 2002), 4.1 to 5.5 kbar for the Karawanken (=Eisenkappel) tonalite (Elias, 1998; Table 1). This results in intrusion depth of 23 to 29 km for Mauls, 9 – 13 km for Finkenstein and 15 – 20 km for the Eisenkappel tonalite (Elias, 1998; Diener, 2002).

The main displacement initiated during the intrusion of tonalites, which ranges in age from 32.9 ± 0.2 to 29.00 ± 0.97 Ma, although in this segment, reliable ages are still scarce (Rosenberg, 2004 for data compilation). The tonalite intrusion is considered to result from slab-break-off (von Blanckenburg and Davies, 1995), which resulted in rheological weakening and mechanical decoupling of the Southalpine unit from the Austroalpine/Penninic units (von Gosen, 1989b; Handy et al., 2005; Rosenberg, 2004). A wide range of fault rocks is reported ranging from ductile mylonites to fault gouge as some well-exposed sections testify (von Gosen, 1989b; Nemes, 1997; Handy et al., 2005). Mylonites from the Eisenkappel area gave a preliminary Ar-Ar biotite age of 19.0 ± 0.3 Ma (own unpublished age). Activity along the fault started in the mid-Oligocene, coeval with the intrusion of tonalitic and subordinate granodioritic bodies adjacent to the fault (e.g., Rosenberg, 2004; von Blanckenburg and Davies, 1995; von Blanckenburg et al., 1998). Most of the linearly aligned plutons are located north of the fault and magmas ascended along the fault system (Rosenberg, 2004; Schmid et al., 2004). Different models of the transport of the magma up to the plutons are discussed: The initiation is considered by slab breakoff (von Blanckenburg and Davies, 1995; von Blanckenburg et al., 1998), the linearly aligned plutons weakened the crust and triggered the fault, whereas plutons developed from the geometry of the mylonitic foliation (Rosenberg, 2004; von Gosen, 1989b).

Both basaltic and granitic magmatism took place during continental collision between 42 and 25 Ma (von Blanckenburg and Davies, 1995), but most plutons are almost isochronic with ages ranging from 28 to 34 Ma (e.g. Rosenberg, 2004) as e.g. the ~32 Ma old tonalite gneisses along the Gailtal and Pustertal faults (Nemes, 1997; Rosenberg, 2004; Sassi et al., 1974). The chemistry of the basalts proves partially molten metasomatic parts of the lithospheric mantle as the source of the magma feeding (von Blanckenburg et al., 1998).

Location	Rock type	Depth of intrusion (kbar)	Method	Age ± error (Ma)	Reference
Mauls	Tonalite	6.2–7.5	U-Pb Zr	29.00 ± 0.97	Elias, 1998
Mauls	Fault gouge		K-Ar	15.89 ± 0.33	Zwingmann and Mancktelow, 2004
Nampolach	Tonalite gneiss		AFT	25.2 ± 1.9	Hejl, 1997
Finkenstein	Tonalite	3.5–4.0	U-Pb Zr	32.9 ± 0.2	Diener, 2002
Finkenstein	Tonalite		AFT	26 ± 2	Hejl, 1997
Eisenkappel	Tonalite	4.1–5.5	U-Pb Zr	31.4 ± 0.7	Elias, 1998
Eisenkappel	Tonalite		K-Ar Bt	29± 6, 28± 4	Scharbert, 1975
Eisenkappel	Tonalite		AFT	16–20	Nemes, 1997
Eisenkappel	Tonalite		AHe	6.4 – 11.4	Heberer et al., 2017
Pohorje	Granodiorite		U-Pb Zr	18.64 ± 0.11	Fodor et al., 2008

Table 1: Geochronological ages from the eastern segment of the Periadriatic fault. AFT – apatite fission track, Bt – biotite, Zr – zircon.

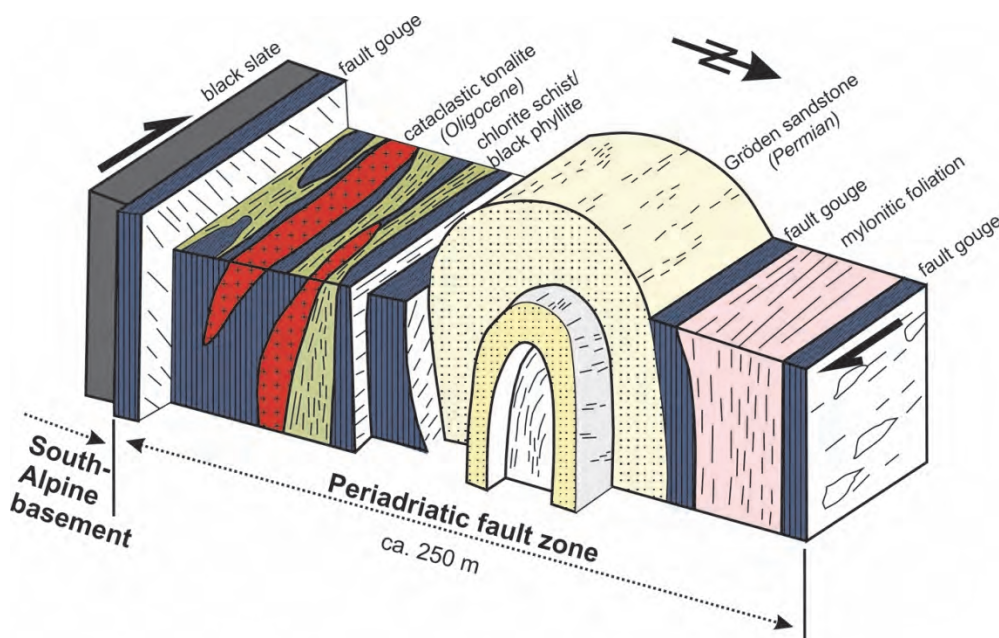


Fig. 44: Cross-section across the Periadriatic fault in the central part of the Periadriatic fault (modified from Nemes, 1997 and Cao and Neubauer, 2016).

6.6 Fault rocks along the Periadriatic fault

The tonalites and accompanying shear lenses include a wide variety of fault rocks ranging from mylonite and low-grade phyllonites, pseudotachylites over a wide variety of cataclastic rocks to fault gouge (von Gosen, 1989b; Nemes, 1997). The fault contains many narrow and long tonalite lenses,

which are preserved in many different structural states as undeformed bodies, tonalite gneisses, phyllonites/chlorite schist and cataclastic tonalite (Fig. 44). The tonalites and accompanying shear lenses include a wide variety of fault rocks ranging from mylonite and low-grade phyllonites, pseudotachylytes over a wide variety of cataclastic rocks to fault gouge (von Gosen, 1989b; Nemes, 1997). The fault rocks are considered to have formed by mainly dextral strike-slip and subordinate late-stage top-S reverse faulting (Nemes, 1997).

6.7 Stops

The Nassfeld region is a classical area well described by Schönlaub and Forke (2007), which also includes the detailed geological map (Fig. 45).

Stop 3-4: Tröpolach: Marble of Eder unit with Alpine ductile fabrics along the Periadriatic fault

Location: N46° 36' 02.3" E13° 17' 12.0"; ÖK 50, sheet 198 Weißbriach; roadcut on Naßfeld road, ca. 700 metres SSW to Oselitzen near Tröpolach (north bridge at 734 NN).

The outcrop exposes steeply dipping, E-trending mylonitic Eder marble, actually a greenschist-facies-grade mylonite, with a prominent foliation and a subhorizontal stretching lineation. The mylonite is interpreted to represent an expression of Oligocene deformation along the Periadriatic fault. Läufer et al. (1997) and Nemes (1997) describe a polyphase calcite fabric. According to some preliminary Ar-Ar white ages at ca. 30 Ma, this unit was affected by Oligocene ductile shearing during an early stage of motion along the Periadriatic fault.

Stop 3-5: Lower Carboniferous Hochwipfel Group

Location: N46° 35' 58.1" E13° 17' 09.4"; ÖK 50, sheet 198 Weißbriach; east Oselitzen river bed, below curve/bridge of Naßfeld road, ca. 700 metres S to Oselitzen near Tröpolach.

The outcrop exposes greyish to dark siltstones and graywackes of the Hochwipfel Group (Early Carboniferous). The Hochwipfel Group is interpreted to represent the infilling of a synorogenic flysch basin on top of the Devonian carbonate platform. Mader et al. (2007) describe an Early Variscan, early Carboniferous metamorphic source for the Hochwipfel flysch.

Stop 3-6: Upper Carboniferous to Middle Triassic of the Southalpine unit. Nassfeld: Walking tour from mountain hut Watschiger Alm to Kammleiten summit

Location: N46° 33' 54.8", E13° 17' 12.0" to N46° 34' 33.1" E13° 17' 45.9"; ÖK 50, sheet 198 Weißbriach.

A walking tour down from the top station of the cable-car down to Naßfeld saddle allows to study cyclic marine/terrestrial Upper Carboniferous formations of the Auernig Group, various Permian formations including Permian shallow water carbonates and overlying mostly marine Lower and Middle Triassic strata. The details are well described in Schönlaub and Forke (2007). The Middle to Upper Carboniferous Auernig Group monitors marine transgression in a post-Variscan intramontane molasse basin on top of the Variscan nappe structure of Carnic Alps. The marine Upper Carboniferous and Permian sedimentation is distinct from that of the Austroalpine units north of the Periadriatic fault, which is purely terrestrial. The Middle Triassic Muschelkalk Conglomerate is likely a result of extensional tectonics indicating Middle Triassic reorganization of the depositional realm.

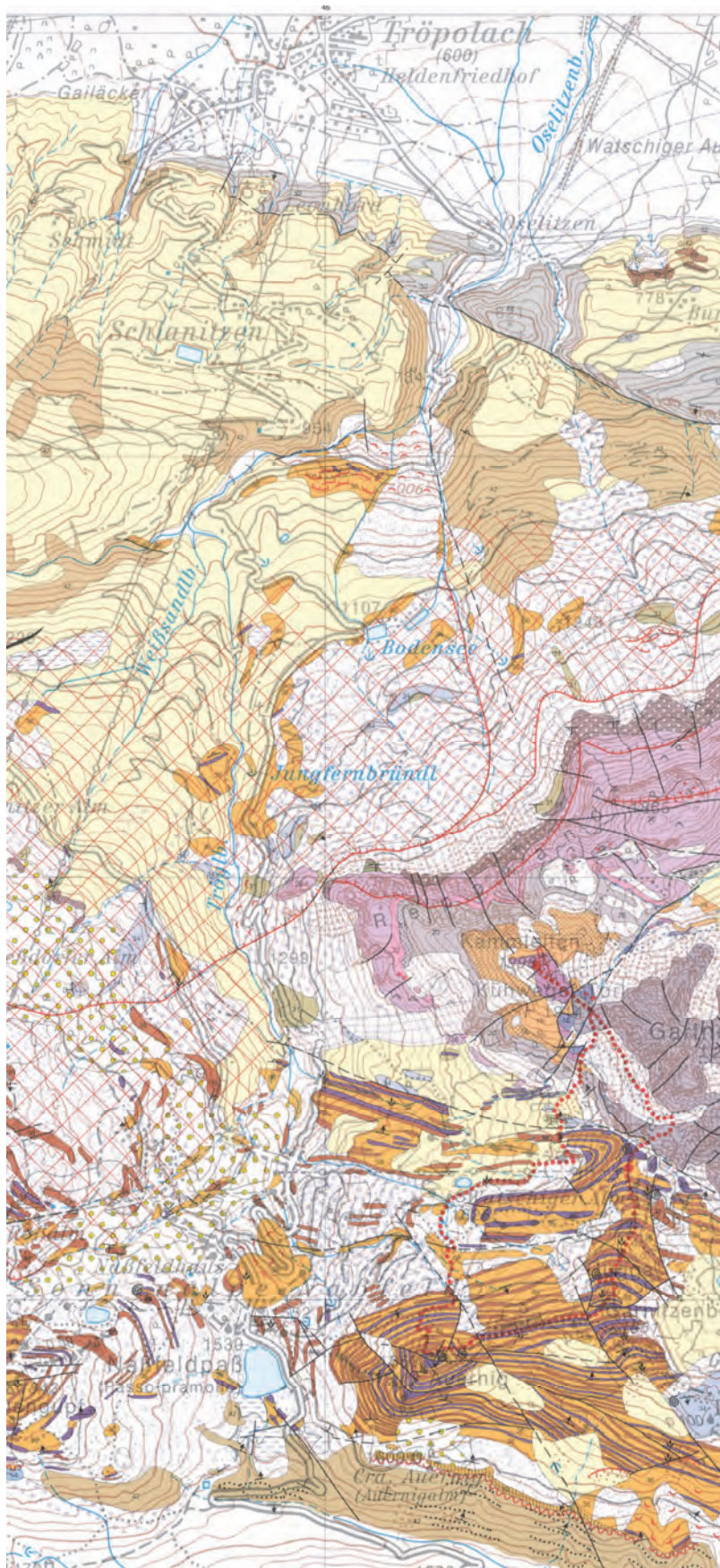


Fig. 45: Detailed geological map of the Nassfeld region (from Schönlaub and Forke, 2007).

 1	Jüngste Flussablagerung, Wildbachschutt Deposito fluviale più recente, deposito torrentizio	 24	Treßdorf-Kalk (Unteres Perm) Calcare di Tressdorf (Permiano Inferiore)
 2	Murenschutt Detrito di debris flow	 25	Trogkofel-Konglomerat, Trogkofelbrekzie (Unteres Perm) Conglomerato di Trogkofel, breccia di Trogkofel (Permiano Inferiore)
 3	Schwemmkegel Cono alluvionale	 26	Trogkofel-Kalk (Unteres Perm), S Spaltenfüllungen Calcare di Trogkofel (Permiano Inferiore), S fissuri
 4	Hangschutt, Schutthalde Detrito di versante, falda di detrito	 27	Zweikofel-Formation (Unteres Perm) Formazione di Zweikofel (Permiano Inferiore)
 5	Blockwerk, Bergsturzmaterial Detrito a grossi blocchi, deposito di frana di crollo	 28	Konglomeratlage darin Livello di conglomerato della Formazione di Zweikofel
 6	Vernässung, Moor Zona palustre, torbiera	 29	hellgrauer, massiger Kalk darin Formazione di Zweikofel (presenza di calcare massiccio grigio chiaro)
 7	Abrisslinie Orlo di distacco di frana	 30	Schieferlage darin Livello di scisti della Formazione di Zweikofel
 8	Zerrspalte Fessura, crepa	 31	Grenzland-Formation (Schiefer, grauer und grüner Sandstein; Unteres Perm) Formazione di Grenzland (scisti, arenarie grigie e verdi; Permiano Inferiore)
 9	Stark bewegter, aufgelockerter Bereich Zona mobile ed instabile	 32	Kalklage darin Livello di calcare della Formazione di Grenzland
 10	Große Wanderblöcke N Tressdorfer Höhe Massi erratici N Tressdorfer Höhe	 33	Konglomeratlage darin Livello di conglomerato della Formazione di Grenzland
 11	Moränenstreu Morenico sparso	 34	Schulterkofel-Formation (Ober-Karbon) Formazione di Schulterkofel (Carbonifero Superiore)
 12	Localmoräne mit groben Blockwerk, Wall Morena locale con grandi massi, con diga naturale	 35	Schiefer-, Konglomeratlage darin Formazione di Schulterkofel (presenza di strati scistosi)
 13	(Grund-)Moräne Morena basale	 36	Auernig-Formation (graubrauner Siltschiefer und Sandstein; Ober-Karbon) Formazione di Auernig (scisti argillosi grigi-bruni e arenarie; Carbonifero Superiore)
 14	Schlern-Dolomit (Ladinium) Dolomia dello Sciliar (Ladinico)	 37	Kalklage darin Livello di calcare della Formazione di Auernig
 15	Kalk darin Dolomia dello Sciliar (relitti di calcare)	 38	Quarzitischer Sandstein, Quarzkonglomeratlage darin Livello di arenarie quarzoso, conglomerato della Formazione di Auernig
 16	Muschelkalk (Anisium) Muschelkalk (Anisico)	 39	Trögl-Kalk (Echinodermenschutt- und Fusilinenkalk; Ober-Karbon) Calcare di Creta di Rio Secco (Calcare massiccio a echinoderme e fusilinidi; Carbonifero Superiore)
 17	Tuff- und Agglomerat darin Tufi ed agglomerati del Muschelkalk	 40	Auernigalm-Kalkbrekzie (Ober-Karbon) Brecchia calcarea di Casera Auernig (Carbonifero Superiore)
 18	Muschelkalk-Konglomerat (Anisium) Conglomerato di Muschelkalk (Anisico)	 41	Postvariszische Transgressionsbildungen (Lyditbrekzie, Konglomerat bis Geröllschiefer, Schiefer, Malinfiere-Fm.; Ober-Karbon-Kasimov-Stufe) Sedimenti trasgressivi post ercinica (brecchia lìdica, conglomerati e scisti di detrito, scisti, calcari; Carbonifero Superiore - Kasimoviano Inferiore)
 19	Werfen-Formation (Kalke und Schiefer, tieferer Teil dolomitisiert; "Skyth") Formazione di Werfen (calcari e scisti; parte inferiore dolomitizzata, Scitico)	 42	Hochwipfel-Formation (Schiefer, Sandstein, Grauwacke; Unter- bis Mittel-Karbon) Formazione di Hochwipfel (scisti, arenarie, grovacche; Carbonifero Inferiore-Medio)
 20	Bellerophon-Formation (Oberes Perm) Formazione a Bellerophon (Permiano Superiore)	 43	Lyditbrekzien-Lage darin Strato di brecchia lìdica della Formazione di Hochwipfel
 21	Bellerophon-Formation, dunkelgrauer Mergel und Schiefer an der Basis (Oberes Perm) Marne grigie scure e scisti alla base della Formazione a Bellerophon (Permiano Superiore)	 44	Debritlegge (mit Kalkgeröll) darin Strato di con ciottoli calcarei della Formazione di Hochwipfel
 22	Gröden-Formation (Mittleres Perm); S Spaltenfüllung in Trogkofel-Kalk (Trogkofel, Zweikofel Ost, Obere Garnitenklamm) Formazione di Val Gardena (Permiano Medio); S = riempimento di fessura nel calcare del Trogkofel/Creta di Aip, Zweikofel orientale, alta gola di Garnitz)		
 23	Gröden-Formation mit Tarvis-Brekzie an Basis (Dolomit- und Kalkbrekzie mit violetter und brauner Matrix; Unteres Perm) Formazione di Val Gardena con breccia di Tarvisio alla base (breccia di calcare e dolomia con matrice viola e marrone-rossiccia; Permiano Inferiore)		

Fig. 45 continued. Legend to the detailed geological map of the Nassfeld region (from Schönlaub and Forke, 2007).

Stop 3-7: Bärental Valley Bärental Conglomerate (Pliocene) and North Karawanken thrust

Location: N46° 29' 44.0" E14° 09' 44.0"; ÖK 50, sheet 211 Windisch Bleiberg; Bärental/Feistritzbach.

The group of outcrops along the road exposes the North Karawanken thrust over the Miocene to Pliocene Bärental Conglomerate, which is part of the Klagenfurt basin (Nemes et al., 1997). Close to the thrust surface, the conglomerate is well affected by brittle deformation with slickensides and striae showing a two-stage kinematics, oblique shortening and dextral strike-slip (Etzel, 2013). This group of outcrops is situated close to the western termination of the North Karawanken thrust, but east of Hochstuhl fault, which transects the Periadriatic fault. The Hochstuhl fault was active during Late Miocene to Pliocene times and is potentially active as some earthquake hypocenters indicate (Reinecker and Lenhardt, 1999).

The formation of the flexural Klagenfurt basin and the interaction with the North Karawanken thrust and Hochstuhl fault is shown in Figure 46 according to a recent MSc thesis (Etzel, 2013 resp. manuscript in preparation).

Stop 3-8: Viewpoint Schaidasattel: Trace of the Periadriatic fault east of Zellpfarre and of the northern parallel fault of pre-Alpine basement

Location: N46° 28' 44.2" E14° 28' 02.7"; ÖK 50, sheet 212 Vellach; Schaidasattel, parking place.

The viewpoint from the Schaidasattel (drainage divide between rivers following the Periadriatic fault system) is along the northern boundary fault between North Karawanken cover rocks and the Eisenkappel Paleozoic unit. To the SW, the Koschuta Mts. with its subvertical northern slope can be seen. With its impressive steep northern wall formed by Dachstein reef limestone belonging to the Southalpine unit, and the trace of the PAF follows the E-W valleys north of it. The North Karawanken unit belongs, in terms of Triassic facies, to the Drau Range unit, and is different in facies. The Northern Karawanken including the crystalline rocks north of the Periadriatic fault are exhumed during Late Miocene tectonic processes as (U-Th)/He data testify (Heberer et al., 2017; Fig. 47).

Stop 3-9: Eisenkappel granite

Location: N46° 27' 01.3" E14° 28' 27.6"; ÖK 50, sheet 212 Vellach.

Along this roadcut, a prophyric variety of the Eisenkappel granite, dated as Permian, is exposed. The granite has an intrusional contact to paragneisses of Eisenkappel crystalline basement (Exner, 1972, 1976).

Stop 3-10: Eisenkappel, Ebriach gorge: Diabase pillow basalt

Location: N46° 28' 39.3" E14° 33' 24.4"; ÖK 50, sheet 212 Vellach; abandoned quarry W Eisenkappel

The gorge well exposes subvertical pillow basalts with a fine-grained plagioclase center and greenish, chlorite-rich rims. Younging is towards south. Best examples of pillows are in the river bed as well as in an abandoned quarry. The age of the pillow basalts is uncertain, interpreted either as Ordovician in comparison with the Magdalensberg Group of the Stolzalpe nappe within the Gurktal nappe complex, or Early Carboniferous (Loeschke and Schnepf, 1987).

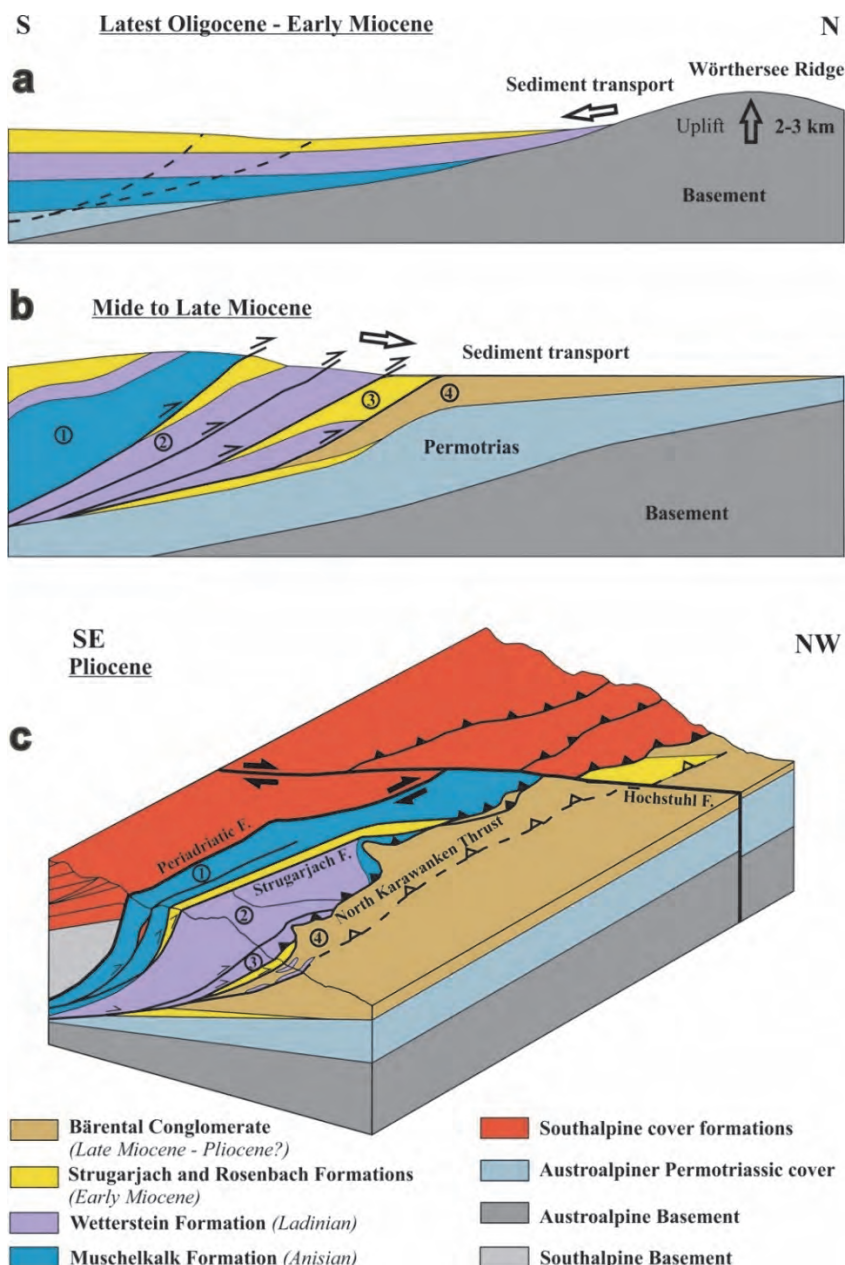


Fig. 46: Tectonic model of the evolution of the flexural Klagenfurt basin and the interaction with the North Karawanken thrust and Hochstuhl fault in three steps (modified from Etzel, 2013; resp. manuscript in preparation).

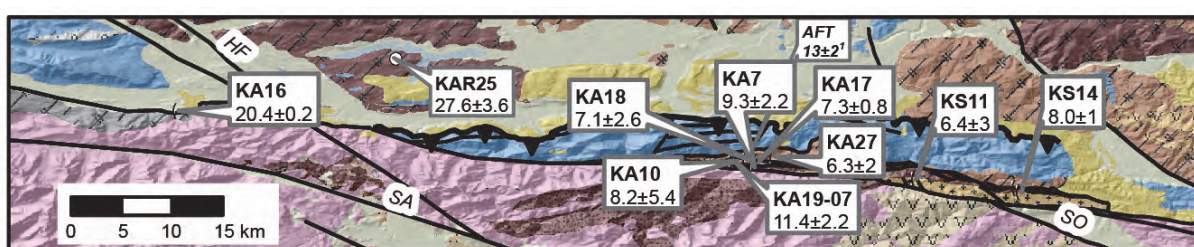


Fig. 47: Map showing apatite (U-Th)/He ages from plutonic rocks in the Karawanken exposed north of the Periadriatic fault. The young ages ranging from 6 to 11 Ma imply significant exhumation during Late Miocene to Pliocene times associated with thrusting of the North Karawanken unit onto the Klagenfurt basin. From Heberer et al. (2017).

Stop 4-1 (first stop of excursion day 4): S of Hagenegg castle SW Eisenkappel: Permian/Triassic gabbro and diorite

Location: N46° 28' 31.76", E14° 35' 22.5", ÖK 50, sheet 213 Eisenkappel; dell immediately SW Eisenkappel, near tennis court.

This exposure shows the mutual relationship mainly between cumulate gabbro, gabbro and diorite. The cumulates are composed of olivine, plagioclase, clinopyroxene, brown amphibole and phlogopite. Olivine is the most abundant mafic phase, and is included in poikilitic plagioclase or clinopyroxene (Miller et al., 2011). Miller et al. (2011) found that the Eisenkappel gabbro formed at 1000 ± 20 °C and 0.38–0.47 GPa. Mineral-whole rock Sm–Nd analyses of two cumulate gabbros yielded ages of 249 ± 8.4 Ma and 250 ± 26 Ma implying intrusion at ca. the Permian-Triassic boundary.

Stop 4-2: Kupitz gorge: Eisenkappel tonalite

Location: N46° 28' 01.2" E14° 36' 55.1"; ÖK 50, sheet 213 Eisenkappel; Kupitz gorge south of Remscheniggraben.

The Kupitz gorge is a confluent to the Remschenig valley and exposes ductilely deformed Oligocene tonalite juxtaposed to Middle Triassic successions of the Southalpine unit with a phyllonitic contact to the Eisenkappel crystalline basement. Elias (1998) reported a U-Pb zircon age of the Eisenkappel tonalite of 31.4 ± 0.7 and a pressure, based on Al-in-hornblende barometry of 4.1–5.5 kbar. Heberer et al. (2017) found (U-Th)/He ages of 6.3 ± 2 to 11.4 ± 2.2 Ma for tonalite and metamorphic basement implying a Late Miocene to Pliocene age of rock exhumation interpreted to relate to emplacement of the North Karawanken thrust wedge.

Stop 4-3: Eisenkappel basement, Rapakiwi granodiorite

Location: N46° 28' 28.9" E14° 35' 37.7"; ÖK 50, sheet 213 Eisenkappel; path east river Vellach south of Remschenigbach confluence.

Within the Karawanken pluton, Exner (1972, 1976) described a granodiorite with Rapakiwi-type K-feldspar mantled by oligoclase. It forms a ca. 10 m thick dyke, which can be followed over 100s of meters.

7 Cretaceous and Miocene extension processes at the eastern edge of the Gurktal nappe complex

FRANZ NEUBAUER, BIANCA HEBERER & JOHANN GENSER

Aim: The aims of visiting the Saualpe-Krappfeld area, which is part of the Austroalpine nappe complex, are two-fold:

- (1) The close relationship of exhumation of Cretaceous-aged eclogites with the rapidly subsiding Krappfeld basin, which represents a Late Cretaceous collapse basin, shows the Late Cretaceous age of ca. ESE-WSW extension following subduction and collision of the Eclogite-Gneiss unit. The area with the rapidly subsiding basin represents the counterpart of the Nock detachment (visited during the excursion) at the western margin Gurktal extensional allochthon.
- (2) The area exposes a succession of superimposed sedimentary units in the wider Krappfeld basin, which reactivated the brittle Görtschitz Valley fault during Miocene times. The Görtschitz Valley fault is a dextral transtensional fault with an apparent vertical throw of ca. 3 to 5 km, representing

one of the largest Miocene faults of Eastern Alps, but hitherto forgotten in most compilations. Transtension reflects the eastward lateral rafting on the Miocene Katschberg normal shear zone towards the Pannonian basin.

7.1 Introduction

In terms of tectonostratigraphic units (Figs. 48, 49, 50), the Saualpe block comprises at the base, the Koriden Gneiss-Eclogite complex, a continental unit that suffered Cretaceous-aged eclogite metamorphism during A-type subduction (e.g., Miller et al., 2005; Wiesinger et al., 2006 and references therein). An ESE-directed ductile low-angle normal fault separates the Koriden Eclogite-Gneiss complex from the overlying Micaschist complexes (Wiesinger et al., 2006), which underwent Cretaceous-aged amphibolite to upper greenschist facies-grade metamorphism. The Micaschist complexes are exposed along the southern Saualpe block due to the Saualpe South Margin Flexure and within the Friesach half window (Fig. 33). Another ductile low-angle normal fault separates the Micaschist complexes from the overlying Phyllite unit, which is conventionally considered as a part of the lower (Murau) nappe of the large Gurktal nappe complex. The upper nappe (Stolzalpe nappe) of the Gurktal nappe complex comprises very low-grade Ordovician to Lower Carboniferous fossil-rich volcanosedimentary successions of the Magdalensberg Group exposed along the margins of the Krappfeld basin area (e.g., Thiedig et al., 1999). Above the post-Variscan unconformity and metamorphic hiatus, Permian to Triassic cover units with clastics and dolomites (Eberstein Permotriassic) are exposed in the southern Krappfeld area. The Eberstein Permotriias is tilted towards north (Figs. 48, 49) and is also affected by internal thrusts and normal faults (Appold and Pesch, 1984; Ratschbacher and Neubauer, 1989) predating the deposition of the Krappfeld Gosau Group above an erosional contact and angular unconformity (Hermann and Wascher, 1972).

In the central axis of the Austroalpine units in the Eastern Alps, the Upper Cretaceous Gosau Group is exposed in collapse basins on top of the Lower Cretaceous Austroalpine nappe stack formed during Early Cretaceous plate collision. The Krappfeld Group comprises, from base to top, the St. Florian Fm. with basal dolomite conglomerate and shallow water limestones, the turbiditic Wietersdorf Fm. with thick olistostromes and breccia layers (Fig. 50), and the Pemberg Fm. with orbitoid-bearing turbidites and marls (Thiedig, 1975; Leggewie and Thiedig, 1977; Zetter and Dimter, 1992; Thiedig et al., 1999), together ranging from Santonian to earliest Late Maastrichtian (Fig. 50) (van Hinte, 1963; Thiedig and Wiedmann, 1975; Neumann, 1989). Beside, intraformational olistostromes of reef detritus (Thiedig, 1975), the Wietersdorf Fm. includes numerous angular siliciclastic clasts from the Magdalensberg Group mainly demonstrating the erosion of this shallow basement level. The large olistostromes were sourced from the east, likely from reefs at the top of the future Saualpe block (Thiedig, 1975; Neumann, 1989; Sanders et al., 2004), which is taken as evidence for a Late Cretaceous precursor fault of the Miocene Görtschitz Valley fault system.

Above a Paleocene hiatus, a latest Paleocene to Eocene succession is exposed in three separate areas unconformably postdating the Krappfeld Gosau (Figs. 48, 49, 50). It includes: the Holzer Fm. at the base, with red clay, coal, sandstone, dark marls (Zetter and Hofmann, 2001; Drobne et al., 2011) and the Dobranberg Fm. with marine nummulite-rich shallow water limestones and marls (Fig. 51c) (Wilkins, 1989a, 1989b; Kázmér et al., 2003 and references therein; Drobne et al., 2011). The reddish bauxite-like red clay of the Guttaring area is now considered as latest Paleocene in age and as part of the Holzer Formation (Kuhlemann et al., 2008). A few remnants of large blocks of Eocene limestone overly the Phyllite Group exposed to the north of the Guttaring fault, which indicates a widening of

the Eocene land surface west of the Görtschitz Valley fault (Fig. 49). Vitrinite reflectance studies of the coal from the Holzer Fm. exhibit low values ($R < 0.4$) implying only a thin overburden (Sachsenhofer, 1992). There are also some unconsolidated mudstones with coaly layers of uncertain Paleogene to early Miocene age south of Guttaring here considered as Dachberg Fm. (Figs. 49, 50; Appold et al., 1986).

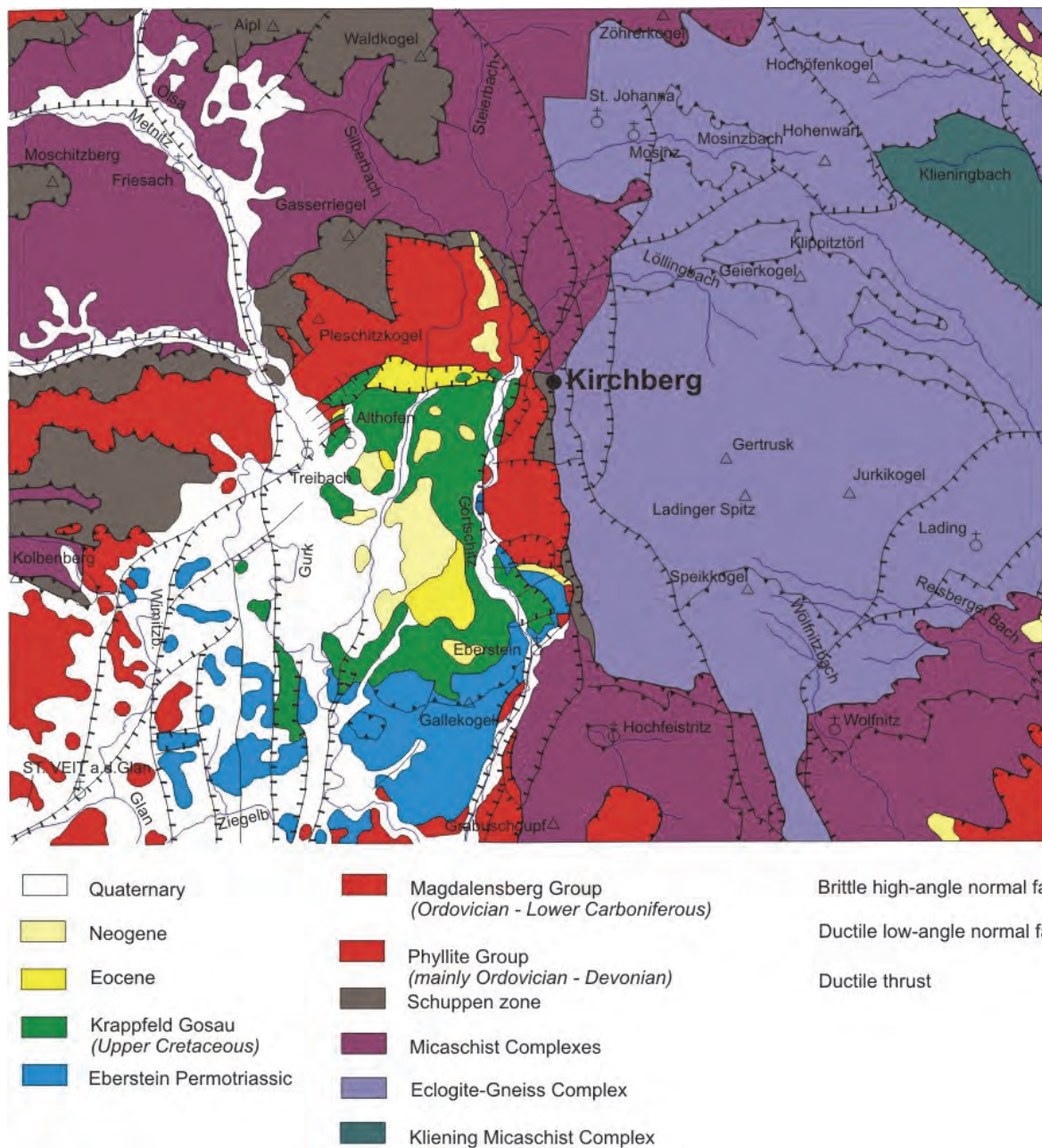


Fig. 48: Simplified geological map of the Krappfeld basin and the Saualpe area (modified after Thiedig et al., 1999 and Weissenbach and Pistotnik, 2000).

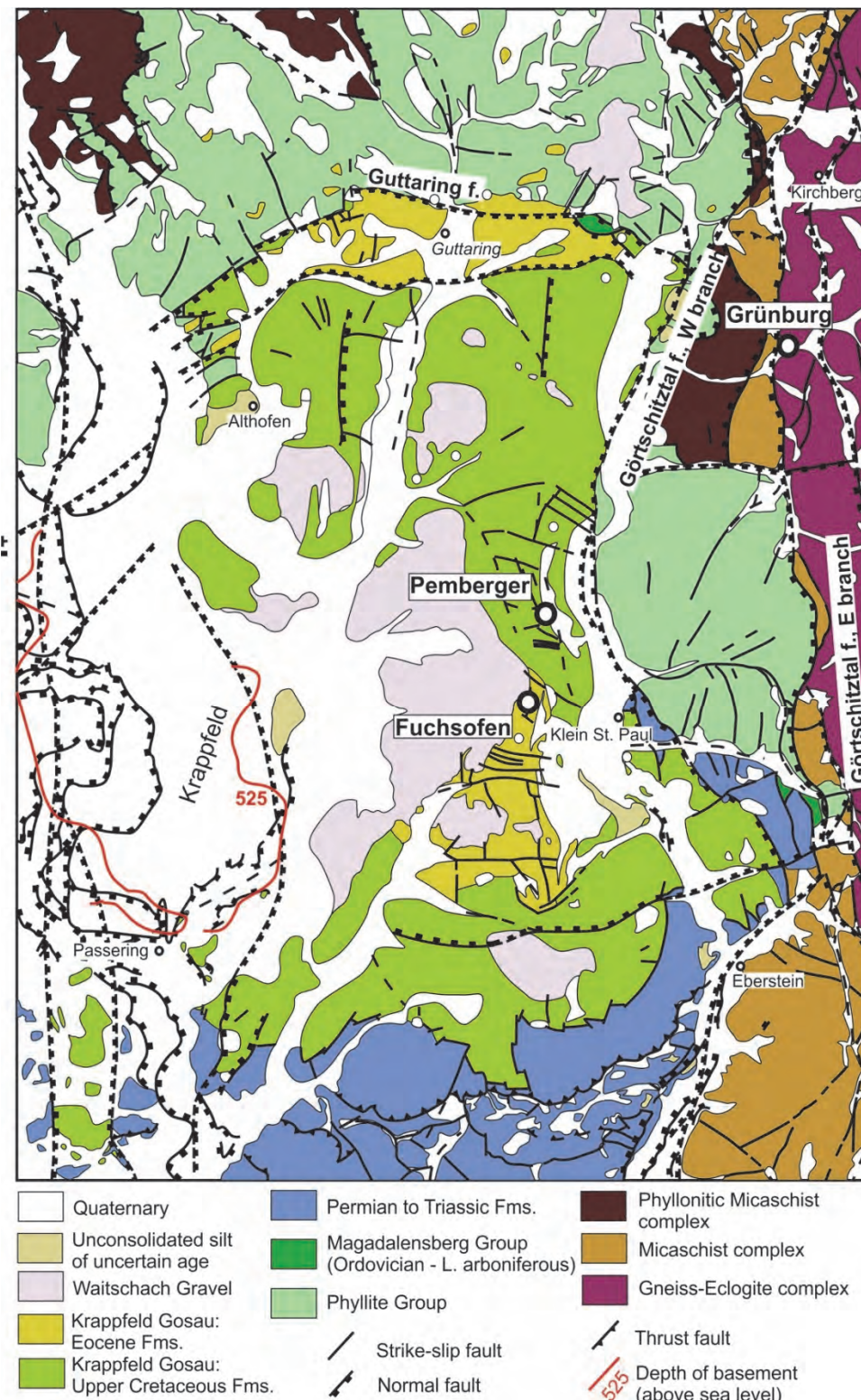


Fig. 49: Detailed geological map of the Krappfeld basin and Saualpe area (modified after Thiedig et al., 1999).

The Miocene Waitschach Gravels are overlying both the Phyllite Group north of the E-W trending Guttaring fault and the former Krappfeld basin west of the Görtschitz valley. Small remnants of Waitschach Gravel on Phyllite Group are exposed west of the Krappfeld basin (Fig. 49) (van Husen, 1976, 1989; Thiedig et al., 1999). The Waitschach Gravels in the eastern part of the Krappfeld basin

comprise abundant large, meter-sized boulders of pegmatite gneiss, paragneiss, quartzite, vein quartz as well as rare eclogite typical for the Koriden Gneiss-Eclogite unit exposed to the east of the Görtschitz Valley (Fritsch, 1962; van Husen, 1989). Consequently, previous researchers argued since Fritsch (1962) that the present-day N-S Görtschitz Valley was not in existence during deposition of the Waitschach Gravels.

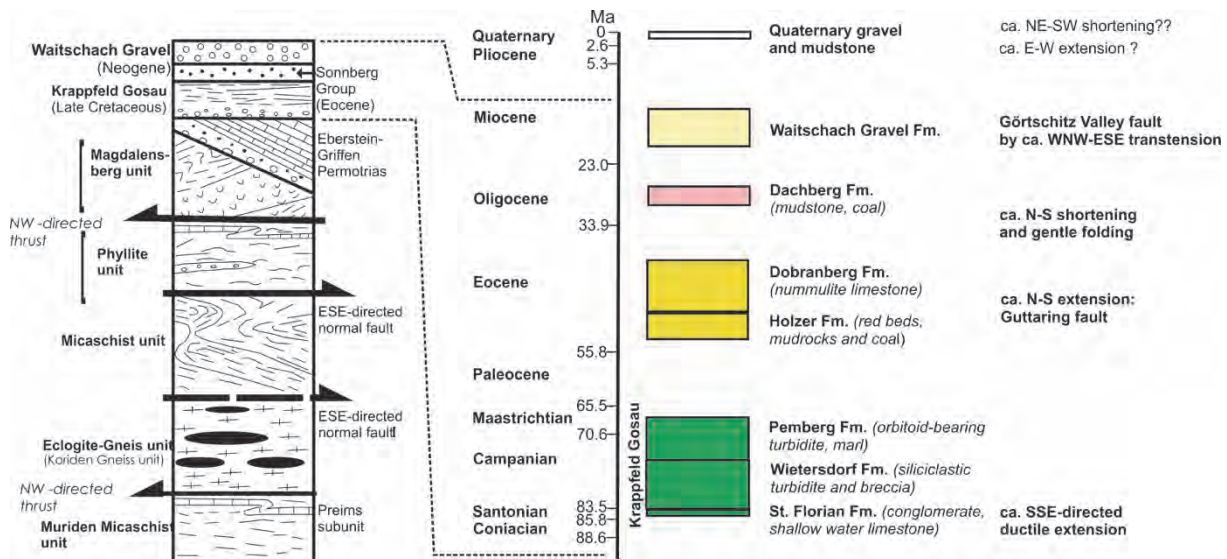


Fig. 50: Left side: Simplified tectonostratigraphy of the Saualpe and Krappfeld region (modified from Wiesinger et al., 2006). Right side shows sedimentary strata of the Krappfeld basin fill and supposed tectonic events affecting that area since Late Cretaceous.

The present-day Krappfeld itself is a small Quaternary basin with a flat morphology (Fig. 49). It was not glaciated, at least not during the last (Würmian) glaciation (Hiller, 1973; van Husen, 1989). Fluvial gravels and lacustrine silts form the basin fill. According to geophysical investigations, the basin is ca. 150 – 180 meter deep (van Husen, 1989; Walach, 1989). A c. 100 m deep outlet was found at the southern edge by geophysical methods.

The Görtschitz valley fault with ca. 15 – 20 km apparent dextral and ca. 3 to 5 km apparent vertical displacement is the most prominent fault within the central Eastern Alps. The Görtschitz valley follows the western branch of the ca. NNW-trending Görtschitz valley fault, which separates, between Mösel and Eberstein (Fig. 49), the Upper Cretaceous Krappfeld basin fill from Phyllite unit, the Magdalensberg Group and fault-bounded slices of the Eberstein Permotrias. The Görtschitz Valley was not glaciated during the Würmian glaciation (Schillig, 1966; van Husen, 1989). The valley itself includes a few gravel terraces believed to be of Holocene age. Two river terraces are prominent: the upper one at ca. at 670 to 680 m elevation, ca. 110 meters above the present-day valley (e.g. at 565 m elevation at Mösel), and the lower one at ca. 580–590 m elevation, ca. 25–35 m above the present-day valley floor.

7.2 Tectonics and geomorphology

The morphology and the post-collisional evolution of the Eastern Alps were heavily affected by eastward-directed lateral extrusion during Late Oligocene to Early Miocene times and intra-orogenic raft tectonics (Neubauer and Genser, 1990; Ratschbacher et al., 1991a; Keil and Neubauer, 2015; . We explain this stage as driven by eastward floating raft tectonics of upper crustal blocks along the basal Katschberg ductile low-angle normal fault away from the Tauern window. The extrusional and rafting

stage was overprinted by south-directed flexure forming the Late Miocene-Pliocene Klagenfurt basin in front of the North Karawanken thrust (Nemes et al., 1997). This refined tectonic model of the interior of the East Alpine extrusional wedge is based on new structural field data and a reassessment of the existing, but hitherto overlooked geological record from the ca. NNW-trending dextral transtensional Götschitz Valley fault system. As discussed before, this fault system with ca. 3 to 5 km apparent vertical displacement is one of the most prominent faults within the central Eastern Alps (Thiedig and Weißenbach, 1975) and juxtaposes the Krappfeld basin with superimposed Upper Cretaceous, uppermost Paleocene–Middle Eocene, Lower Miocene and Quaternary successions to the uplifted Saualpe basement block with its Cretaceous-aged eclogite to greenschist facies grade rocks in the east (Fig. 48). The geometry of and kinematics affecting the Krappfeld basin fill allow defining the superimposed Late Cretaceous to Recent succession of basin-forming tectonic events of the eastern part of central Eastern Alps (Fig. 52): (1) Following Cretaceous continental subduction, exhumation of previously subducted Cretaceous eclogites occurred along an array of ductile low-angle normal faults during Late Cretaceous times and the upper block subsided below sea level forming the collapse-type Krappfeld basin due to extreme ESE–WNW extension (Willingshofer et al., 1999a). (2) After a period of Paleocene non-deposition and deep subtropical weathering (Thiedig, 1970; Kuhlemann et al., 2008), an Eocene marine transgression occurred due to N–S extension forming the Krappfeld basin. (3) Subsequent N–S shortening resulted in gentle Oligocene folding of the Upper Cretaceous-Eocene basin fill. (4) This stage is followed by NE–SW extension consistent with activation of the transtensional Götschitz Valley fault system and at least ca. 2.5 to 3 km apparent vertical offset as part of a raft system of the eastward extruding ALCAPA block (Keil and Neubauer, 2015), in which the Götschitz Valley fault system represents an antithetic transtensional fault to the ductile Katschberg low-angle normal fault at the eastern margin of the Tauern window. The fluvial Waitschach Gravel of likely Karpatian age (Early Miocene) was deposited along the western branch of the Götschitz valley fault system and received detritus from the uppermost units of the Saualpe block in the east (e.g., Fritsch, 1962). Incision of the Götschitz Valley along the western branch of the Götschitz Valley fault started in post-Karpatian times most likely during the Late Miocene-Pliocene flexure of the Klagenfurt basin in the south (Nemes et al., 1997) and resulted in a modified regional drainage system, which reoriented the drainage pattern from east-directed respectively W-directed to a south-directed one.

7.3. Stops

Stop 4-4: Wietersdorf, Gosau quarry “Pemberger Riegel”

Location: N46° 50' 44.1" E14° 31' 40.6"; ÖK 50, sheet 186 St. Veit an der Glan; quarry Pemberger Riegel W Wietersdorf.

The quarry exposes grey calcareous turbidites intercalated with grey marls, which generally dip steeply to the west. The graded turbidite beds include abundant very low-grade angular volcano-sedimentary clasts of the Magdalensberg Group as well as intraformational marly limestone clasts with grain sizes of 6 – 8 cm. The transport direction is supposed to have been from a nearby source located in the east receiving shallow water carbonates. The basin indicates significant subsidence and topography during Late Cretaceous extension. The marly rich succession is partly folded and an even axial surface foliation has been documented (von Gosen and Thiedig, 1980).

Stop 4-5: Wietersdorf, Gosau quarry “Fuchsofen”, Eocene limestone quarry

Location: N46° 50' 17.2" E14° 31' 33.6"; ÖK 50, sheet 186 St. Veit an der Glan; quarry Fuchsofen W Wietersdorf.

The quarry exposes Eocene limestones of the Dobranberg Fm. with light-colored yellowish marine nummulite-rich shallow water limestones and rare marls (Fig. 51c). These are overlain, above an erosional unconformity, by Miocene unconsolidated gravels of the Waitschach Fm. on top of the Fuchsofen hill. The facies and fossils are described in Kázmér et al. (2003 and references therein) and Drobne et al. (2011). Biostratigraphy indicate a lower to middle Cuisian to Lutetian age (Drobne et al., 2011 and references therein). The limestones dip gently to SW and are transected by ca. N-S trending dextral strike-slip faults (Fig. 51c).

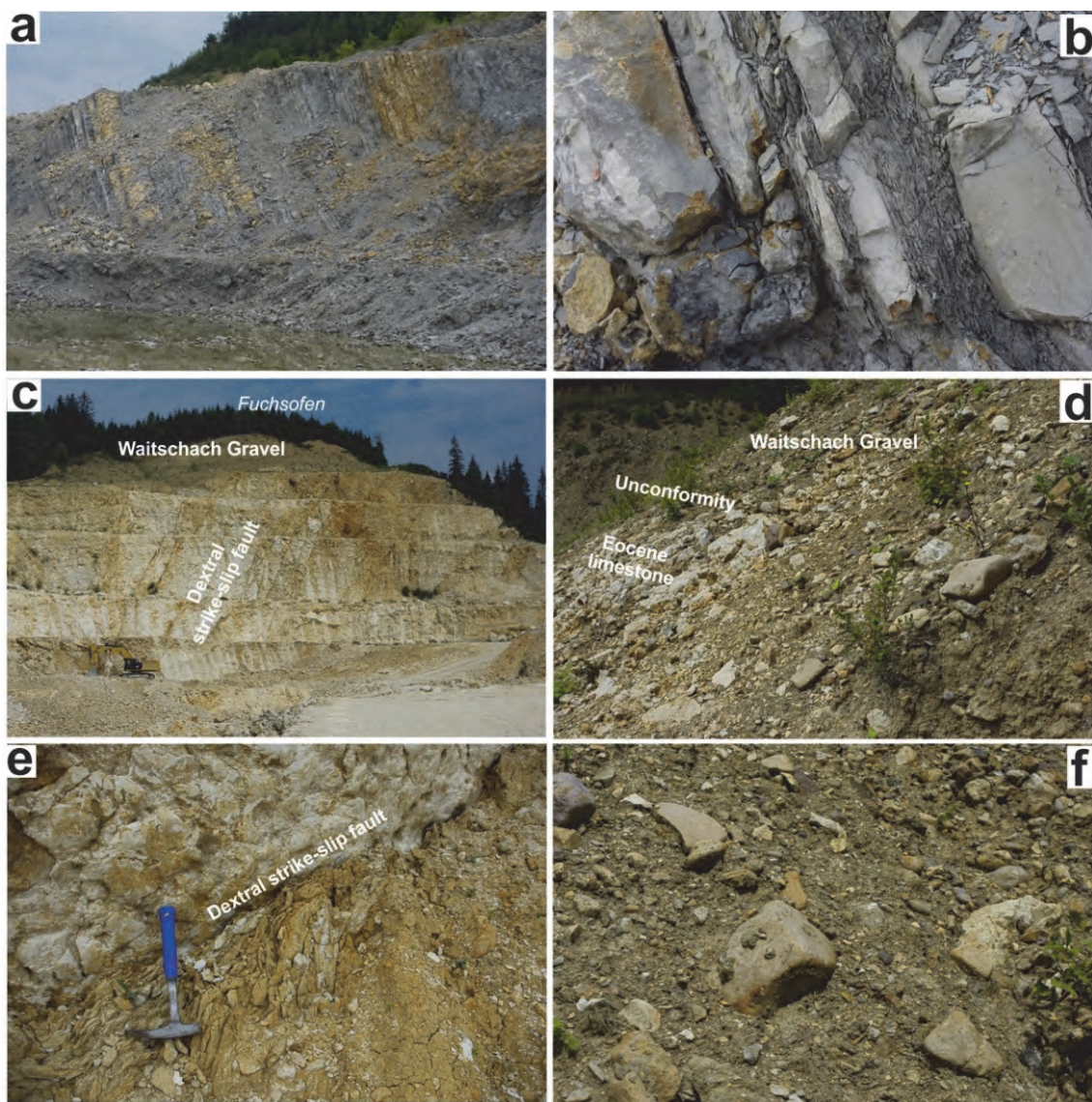


Fig. 51: (a) Late Cretaceous (Santonian) marly turbidites. (b) Detail of turbidites with graded bedding. The left bed shows angular marly limestone clasts. Thickness of the bed: ca. 25 cm. (a) and (b) are from the Pemberger Riegel quarry. (c) Northern slope of the Fuchsofen quarry with massive Eocene limestone overlain by the Miocene Waitschach Gravel at top. (d) Unconformity between Eocene limestone and Miocene Waitschach Gravel. (e) Dextral strike-slip fault transecting the Eocene limestone. (f) Variety of clasts in the Waitschach Gravel at Fuchsofen top.

The Waitschach Gravel at top of Fuchsofen exhibits clasts mostly reworked from the immediate Eocene underground, from the Eberstein Permotrias (e.g. red sandstone of the Gröden Fm.), volcanosedimentary material from the Magdalensberg Group and rare vein quartz and some eclogite from the Saualpe. The occurrence at the top of the Fuchsofen shows the post-depositional post-Miocene uplift of the Krappfeld basin and incision of the Görtschitz Valley.

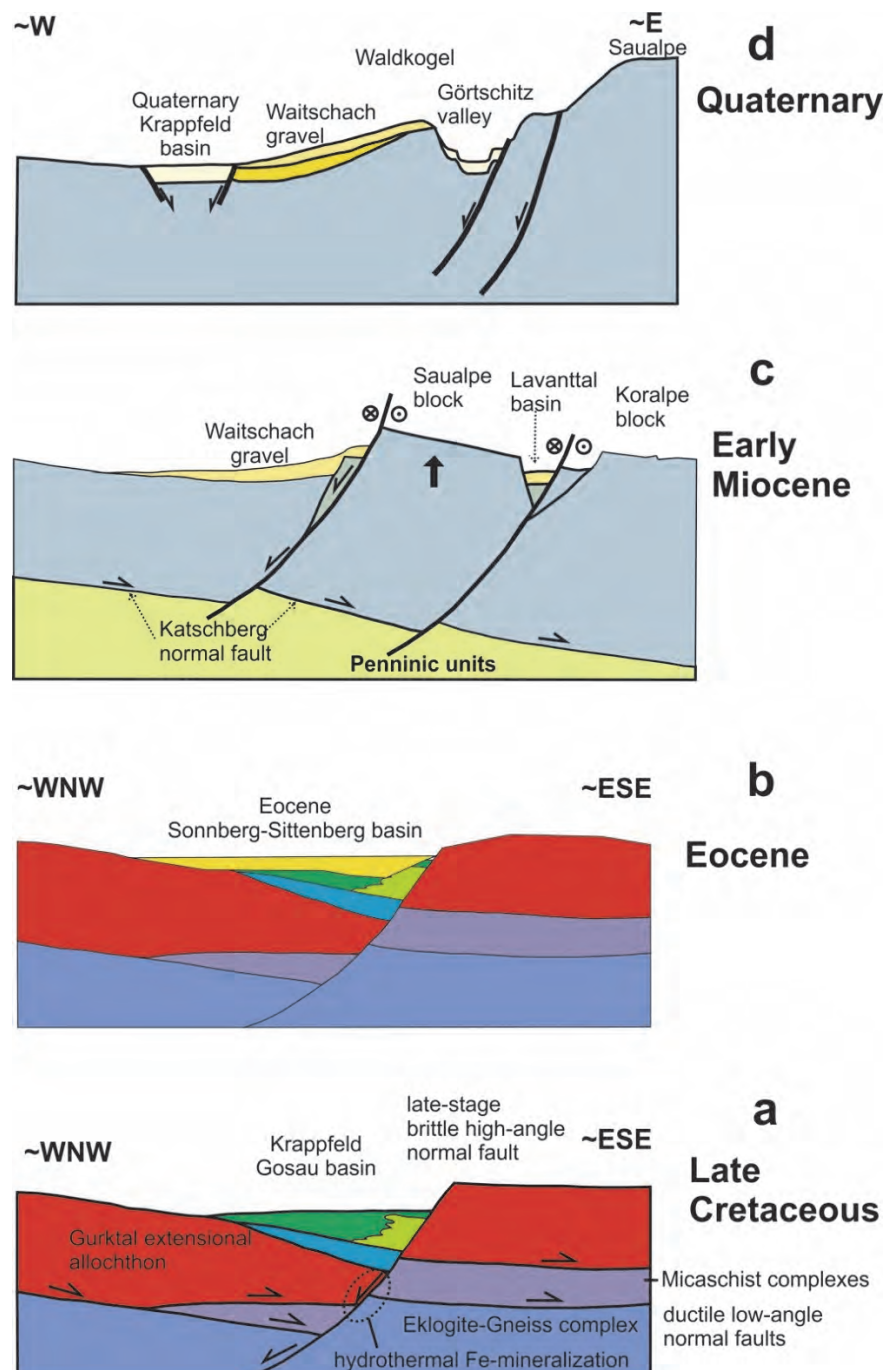


Fig. 52: Tectonic evolution of the Krappfeld basin area in comparison with the basement units exposed to the east. (a) Late Cretaceous extension and formation of the Krappfeld Gosau basin. (b) Eocene shallow water limestone deposition during a tectonically rather quiet period. (c) Early Miocene eastward rafting along the ductile Katschberg normal fault and transtensional reactivation of the Görtschitz Valley fault. (d) Quaternary surface uplift and erosion and incision of the Görtschitz Valley during waning stages along the transtensional Görtschitz Valley fault.

Stop 4-6: Grünburg, Cretaceous eclogite

Location: N46° 51' 23.3" E14° 34' 25.3"; ÖK 50, sheet 186 Sankt Veit an der Glan; Grünburger Bach, slope west/southwest R. Grünburg.

The description of the petrology of this outcrop follows Miller et al. (2005). This outcrop is part of an eclogite lens with a length of about 1500 m and about 150 m wide, intercalated with country rock mica-schists and gneisses. Near the base of the outcrop a pegmatoid dyke containing muscovite, plagioclase and quartz intruded this eclogite parallel to the foliation. The fine- to medium-grained eclogites are of the Fe- and quartz-rich "metabasaltic" variety and consist of garnet + omphacite + quartz + rutile + apatite ± amphibole ± phengite ± clinozoisite ± zircon ± pyrite. Garnet is slightly zoned with rim compositions of $\text{Prp}_{35-37}\text{Alm}_{39-40}\text{Grs}_{22-24}\text{Sps}_{0.5-0.6}$ and contains inclusions of rutile, quartz, clinozoisite, apatite and zircon. Omphacite is unzoned with 0.34–0.35 mol% jadeite and, together with clinozoisite, defines the foliation and mineral lineation. Subcalcic magnesiohornblende is present as texturally late poikiloblastic grains overgrowing garnet, clinozoisite, quartz and rutile.

The geochemistry of the quartz-rich eclogite from the Grünburger Graben, Saualpe is close to N-MOR basalt, particularly based on a flat chondrite-normalized rare earth element pattern. Heede (1997) attempted to date zircon (multigrain) separates from this eclogite, but without success due to their extremely low U contents (3.6-4.6 ppm) and Pb contamination problems. Sm-Nd studies are in progress (Miller et al., 2005) but were not published yet. The Rb-Sr age of the muscovite from the pegmatoid is 81.1 ± 1.5 Ma, with an initial Sr isotope ratio of 0.71127 ± 8 (Heede, 1997).

Acknowledgements: The authors gratefully acknowledge discussions with many persons including Wolfgang Frisch, Robert Handler, Walter Kurz and the TRANSALP Working Group. Work has been supported by grants (nos. P8652, P9918, P14028, P22110, P22728) of the Austrian Science Fund (FWF).

References

- ANDERLE, N., 1977. Geologische Karte der Republik Österreich 1 : 50 000, 200 Arnoldstein. Geologische Bundesanstalt, Wien.
- APPOLD, T. & PESCH, P., 1984. Die Tektonik der postvariskischen Transgressionsserie im Krappfeld (Kärnten/Österreich). Carinthia II, 174/94, 319–337.
- APPOLD, T., THIEDIG, F., VOLLMER, T. & WILKENS, E., 1986. Ein neues Alttertiärvorkommen am Dachberg südlich Guttaring/Kärnten (Österreich). Carinthia II, 176/96, 303–310.
- BARTEL, E.M., NEUBAUER, F., HEBERER, B. & GENSER, J., 2014. States of paleostress north and south of the Periadriatic fault: Comparison of the Drau Range and the Friuli Southalpine wedge. Tectonophysics, 637, 305–327.
- BARTOSCH, T., STÜWE, K. & ROBL, J., 2017. Topographic evolution of the Eastern Alps: The influence of strike-slip faulting activity. 9, 384–398.
- BAUER, F.K., BUCKENBERGER, U., SCHULZE, R., EXNER, C., KUPSCHE, F., LÖSCHKE, J., ROLSER, J., SUETTE, G., TESSENHOHN, F., VAN HUSEN, D. & WALTZ, W., 1981. Geologische Karte der Karawanken 1:25.000, Ostteil (2 sheets), Wien (Geologische Bundesanstalt).
- BECKER, B., 1993. The Structural Evolution of the Radstadt Thrust System, Eastern Alps, Austria - Kinematics, Thrust Geometries, Strain Analysis, Diss., Univ. Tübingen, 76 p., 1993.
- BEHRMANN, J.H., 1990. Zur Kinematik der Kontinentkollision in den Ostalpen, Geotekt.Forsch., 76, 1-180, 1990.

- BELINIĆ, T., STIPČEVIĆ, J., ŽIVČIĆ, M. & ALP-ARRAYWORKING GROUP, 2018. Lithospheric thickness under the Dinarides. *Earth Planet. Sci. Lett.*, 484, 229–240.
- BERTRAND, A., ROSENBERG, C. L. & GARCIA, S., 2015. Fault slip analysis and late exhumation of the Tauern Window, Eastern Alps. *Tectonophysics*, 649, 1–17.
- BERTRAND, A., ROSENBERG, C., RABAUTE, A., HERMAN, F. & FÜGENSCHUH, B., 2017. Exhumation mechanisms of the Tauern Window (Eastern Alps) inferred from apatite and zircon fission track thermochronology, *Tectonics*, 36, <https://doi.org/10.1002/2016TC004133>.
- BIANCHI, I. & BOKELMANN, G., 2014. Seismic signature of the Alpine indentation, evidence from the Eastern Alps. *J. Geodyn.*, 82, 69–77.
- BISTACCHI, A., MASSIRONI, M. & MENEGON, L., 2010. Three-dimensional characterization of a crustal-scale fault zone: The Pusteria and Sprechenstein fault system (Eastern Alps). *J. Struct. Geol.*, 32, 2022–2041.
- BLEIBINHAUS, F. & GROSCHUP, R., 2008. Structure of the Periadriatic Fault in the Eastern Alps from reflection seismic imaging, AGU, San Francisco.
- BLEIBINHAUS, F., LINCK, R., GROSCHUP, R. & GEBRANDE, H., 2009. Seismic structure of the Eastern Alps – TRANSALP revisited, EGU, Wien.
- BÖHM, F., 1992. Mikrofazies und Ablagerungsmilieu des Lias und Dogger der Nordöstlichen Kalkalpen. *Erlanger Geologische Abhandlungen*, 121, 55–217.
- BOLE, M., DOLENEC, T., ZUPANIČ, N. & ČINČ-JUHANT, B., 2001. The Karavanke Granitic Belt (Slovenia)—a bimodal Triassic alkaline plutonic complex. *Schweiz. Mineral. Petrograph. Mitt.*, 81, 23–38.
- BRÜCKL, E., BEHM, M., DECKER, K., GRAD, M., GUTERCH, A., KELLER, G. R. & THYBO, H., 2010. Crustal structure and active tectonics in the Eastern Alps. *Tectonics*, 29, TC2011, <https://doi.org/10.1029/2009TC002491>.
- CAO, S. & NEUBAUER, F., 2016. Deep crustal expressions of exhumed strike-slip fault systems: Shear zone initiation on rheological boundaries. *Earth Sciences Reviews*, 162, 155–176.
- CAPORALI, A., NEUBAUER, F., STANGL, G. ZULIANI, D., 2013. Modeling surface GPS velocities in the Southern and Eastern Alps by finite dislocations at crustal depths. *Tectonophysics*, 590, 136–150.
- CASTELLARIN, A., VAI, G.B. & CANTELLI, L., 2006. The Alpine evolution of the Southern Alps around the Giudicarie faults: A Late Cretaceous to early Eocene transfer zone: *Tectonophysics*, 414, 203–223.
- CHELONI, D., D'AGOSTINO, N. & SELVAGGI, G., 2014. Interseismic coupling, seismic potential, and earthquake recurrence on the southern front of the Eastern Alps (NE Italy). *J. Geophys. Res.: Solid Earth*, 119, 4448–4468.
- CHEMENDA, A.I., MATTAUER, M. & BOKUN, A.N., 1995. Continental subduction and a mechanism for exhumation of high pressure metamorphic rocks: new modelling and field data from Oman. *Earth Planet. Sci. Lett.*, 143, 173–182.
- CLAR, E., 1965. Zum Bewegungsbild des Gebirgsbaues der Ostalpen. *Zeitschr.ift der Deutschen Geologischen Gesellschaft*, 116, 267–291.
- CLIFF, R., HOLZER, H. & REX, D., 1975. The age of the Eisenkappel granite, Carinthia and the history of the Periadriatic lineament. *Verh. Geol. Bundesanst*, 1975, 347–350.
- CLIFF, R.A & COHEN, A., 1980. Uranium-lead isotope systematics in a regionally metamorphosed tonalite from the Eastern Alps. *Earth Planet. Sci. Lett.*, 50, 211–218.
- CLIFF, R.A., DROOP, G.T.R. & REX, D.C., 1985. Alpine metamorphism in the south-east Tauern Window, Austria 2: Rates of heating, cooling and uplift. *J. Metam. Geol.*, 3, 403–415.
- CLIFF, R.A., NORRIS, R.J., OXBURGH, E.R. & WRIGHT, R.C., 1971. Structural, Metamorphic and Geochronological Studies in the Reißeck and the Southern Ankogel Groups, the Eastern Alps. *Jahrb. Geol. Bundesanst.*, 114, 121–272.
- COHEN, K.M., FINNEY, S.C., GIBBARD, P.L. & FAN, J.-X., 2013. The ICS International Chronostratigraphic Chart. *Episodes*, 36, 199–204.

- DALLMEYER R.D., NEUBAUER F., HANDLER R., FRITZ H., MÜLLER W., PANA D. & PUTIS M., 1996. Tectonothermal evolution of the internal Alps and Carpathians: Evidence from $^{40}\text{Ar}/^{39}\text{Ar}$ mineral and whole rock data. *Eclogae Geologie Helvetica*, 89, 203–227.
- DALLMEYER, R.D., HANDLER, R., NEUBAUER, F. & FRITZ, H., 1998. Sequence of thrusting within a thick-skinned tectonic wedge: Evidence from $^{40}\text{Ar}/^{39}\text{Ar}$ ages from the Austroalpine nappe complex of the Eastern Alps. *J. Geology*, 106, 71–86.
- DIENER, R., 2002. Die siliziklastischen Sedimente der synorogenen Hochwipfel-Formation im Karbon der Westkarawanken (Österreich/Slowenien/Italien): Sedimentologie, Geochemie und Provenienz. PhD Dissertation, Univ. Stuttgart, p. 366.
- DINGELDEY, CH., DALLMEYER, R.D., KOLLER, F. & MASSONNE, H.-J., 1997. P-T-t history of the Lower Austroalpine Nappe Complex in the "Tarntaler Berge" NW of the Tauern Window: implications for the geotectonic evolution of the central Eastern Alps: Contributions to Mineralogy and Petrology, 129, 1–19.
- DORNER, R., HÖFLING, R. & LOBITZER, H., with contributions of FEITZINGER, G., SVOBODOVÁ, M. & ŠVABENICKÁ, L., 2009. Nördliche Kalkalpen in der Umgebung Salzburgs (Exkursion H am 17. April 2009). Jahresberichte und Mitteilungen des Oberrheinischen Geologischen Vereines, Neue Folge, 91, 317–366.
- DROBNE, K., EGGER, H., HOFMANN, C., MOHAMED, O., OTTNER, F., RÖGL, F., 2011. Stop A3/6 - Pemberger and Fuchsofen quarries to the west of Klein St. Paul. Berichte der Geologischen Bundesanstalt, 85, 111–117.
- ELIAS, J., 1998. The Thermal History of the Ötztal-Stubai Complex (Tyrol, Austria/Italy) in the Light of the Lateral Extrusion Model. *Tübinger Geowiss. Arb. Reihe A* 42, 1–169
- ELSNER, R., 1991. Geologie des Tauern-Südostrandes und geotektonische Konsequenzen, Jahrb. Geol. BUNDESANST., 134, 561–645.
- ETZEL, A., 2013. The Hochstuhl Fault and its relation to the Periadriatic Fault and the North Karawanken Thrust. Master thesis Faculty of Sciences, University of Salzburg, pp. V + 83.
- EXNER, C., 1985. Petrographie und Tektonik des Granitzuges von Nötsch (Kärnten). *Jahrb. Geol. Bundesanst.*, 127, 557–570.
- EXNER, C., 1971. Geologie der peripheren Hafnergruppe (Hohe Tauern). *Jb. Geol. Bundesanst.*, 114, 1–119.
- EXNER, C., 1972. Geologie der Karawankenplutone östlich Eisenkappel, Kärnten. *Mitteilungen der Geologischen Gesellschaft Wien* 64, 1–108.
- EXNER, C., 1976. Die geologische Position der Magmatite des periadriatischen Lineamentes. *Verhandlungen der Geologischen Bundesanstalt* 1976 (2), 3–64.
- EXNER, C., 1980a. Das Kristallin östlich der Katschbergzone, Mitt. Österr. Geol. Ges., 71/72, 167–189.
- EXNER, C., 1980b. Geologie der Hohen Tauern bei Gmünd in Kärnten. *Jahrb. Geol. Bundesanst.*, 123, 343–410.
- EXNER, C., 1982. Geologie der zentralen Hafnergruppe (Hohe Tauern). *Jahrb. Geol. Bundesanst.*, 125, 51–154.
- EXNER, C., 1983a. Zur Petrographie von Gneisgerölle im Karbon von Nötsch (Kärnten). *Jahrb. Geol. Bundesanst.*, 126, 215–217.
- EXNER, C., 1983b. Geologische Karte der Hafnergruppe 1 : 25.000, mit Erläuterungen, Mitt. Ges. Geol. Bergbaustud. Österr., 29, 41–74.
- EXNER, C., 1984. Der Südrand des Tauernfensters bei Spittal an der Drau, *Jb. Geol. Bundesanst.*, 127, 349–367.
- EXNER, C., 1989. Geologie des mittleren Lungaus, *Jahrb. Geol. Bundesanst.*, 132, 7–103.
- EXNER, C., 1990. Erläuterungen zur Geologischen Karte des mittleren Lungaus, Mitt. Ges. Geol. Bergbaustud. Österr., 36, 1–38.
- FANINGER, E. & ŠTRUCL, I., 1978. Plutonic emplacement in the eastern Karavanke Alps. *Gelogija*, 21, 81–87.
- FANTONI, R. & FRANCIOSI, R., 2010. Tectono-sedimentary setting of the Po Plain and Adriatic foreland. *Rend. Fis. Acc. Lincei*, 21 (Suppl 1), S197–S209.

- FAUPL, P. & TOLLMANN, A., 1978. Die Roßfeldschichten: Ein Beispiel für Sedimentation im Bereich einer tektonisch aktiven Tiefseerinne aus der kalkalpinen Unterkreide. *Geologische Rundschau*, 68, 93–120.
- FAUPL, P. & WAGREICH, M., 2000. Late Jurassic to Eocene Paleogeography and Geodynamic Evolution of the Eastern Alps. *Mitteilungen der Österreichischen Geologischen Gesellschaft* 92, 79–94.
- FAVARO, S., SCHUSTER, R., HANDY, M. R., SCHARF, A. & PESTAL, G., 2015. Transition from orogen-perpendicular to orogen-parallel exhumation and cooling during crustal indentation – key constraints from $^{147}\text{Sm}/^{144}\text{Nd}$ and $^{87}\text{Rb}/^{87}\text{Sr}$ geochronology (Tauern Window, Alps). *Tectonophysics*, 665, 1–16.
- FINGER, F., G. FRASL, B. HAUNSCHMID, H. LETTNER, A. VON QUADT, A. SCHERMAIER, A. O. SCHINDLMAYR, & STEYRER, H.-P., 1993. The Zentralgneise of the Tauern Window (Eastern Alps): Insight into an intra-Alpine Variscan batholith. In: RAUMER, J.F. VON & NEUBAUER, F., eds., *Pre-Mesozoic geology in the Alps*. pp. 375–391, Springer-Verlag, Berlin Heidelberg New York.
- FODOR, L., GERDES, A., DUNKL, I., KOROKNAI, B., PÉCSKAY, Z., TRAJANOVA, M., HORVÁTH, P., VRABEC, M., BALOGH, K., JELEN, B. & FRISCH, W. 2008. Miocene emplacement and rapid cooling of the Pohorje pluton at the Alpine-Pannonian-Dinaric junction: a Geochronological and structural study. *Swiss J. Geosci.*, 101 Supplement 1, S255–S271.
- FODOR, L., JELEN, B., MÁRTON, E., SKABERNE, D., CAR, J. & VRABEC, M., 1998. Miocene-Pliocene tectonic evolution of the Slovenian Periadriatic fault: Implications for Alpine-Carpathian extrusion models. *Tectonics* 17, 690–709.
- FRANK, W. & SCHLAGER, W., 2006. Jurassic strike slip versus subduction in the Eastern Alps. *International Journal of Earth Sciences* 95, 431–450.
- FRANK, W., 1987. Evolution of the Austroalpine elements in the Cretaceous. In: FLÜGEL, H.W. & FAUPL, P., eds., *Geodynamics of the Eastern Alps*. Deuticke, Wien, pp. 379–406.
- FRANK, W., KRALIK, M., SCHARBERT, S. & THÖNI, M., 1987a. Geochronological data from the Eastern Alps. In: Flügel, H. W. & P. Faupl, P., eds., *Geodynamics of the Eastern Alps*. pp. 272–281, Deuticke, Vienna, 1987.
- FRANK, W., HÖCK, V. & MILLER, C., 1987b. Metamorphic and tectonic history of the central Tauern Window. In: FLÜGEL, H.W. & FAUPL, P., eds., *Geodynamics of the Eastern Alps*. pp. 34–54, Deuticke, Vienna.
- FRANK, W., LELKES-FELVÁRI G. & DUNKL I., 1996. Thermal history of Austroalpine basement rocks of the borehole Fertörákos-1004, Western Hungary.: Advances in Austrian-Hungarian Joint Geological Research, Budapest, 1996, 177–195.
- FREY, M., DESMONS, J. & NEUBAUER, F., 1999. The new metamorphic maps of the Alps: Introduction: *Schweizerische Mineralogische und Petrographische Mitteilungen*, 79, 1–4.
- FRIMMEL, H., 1986. Isotopengeologische Hinweise für die paläogeographische Nachbarschaft von Gurktaler Decke (Oberostalpin) und dem Altkristallin östlich der Hohen Tauern (Österreich). *Schweizerische Mineralogische und Petrographische Mitteilungen*, 66, 193–208.
- FRIMMEL, H., 1988. Metagranitoide am Westrand der Gurktaler Decke (Oberostalpin) – Genese und paläotektonische Interpretation. *Jahrbuch der Geologischen Bundesanstalt*, 131, 575–592.
- FRISCH, W., 1979. Tectonic progradation and plate tectonic evolution of the Alps. *Tectonophysics*, 60, 121–139.
- FRISCH, W., DUNKL, I. & KUHLEMANN, J., 2000a. Post-collisional orogen-parallel large-scale extension in the Eastern Alps. *Tectonophysics*, 327, 239–265.
- FRISCH, W., G. VAVRA & M. WINKLER, 1993. Evolution of the Penninic basement of the Eastern Alps, in *Pre-Mesozoic geology in the Alps*, edited by J. F. von Raumer, and F. Neubauer, pp. 349–360, Springer-Verlag, Berlin Heidelberg New York.
- FRISCH, W., GOMMERINGER, K., KELM, U. & POPP, F., 1987. The Upper Bündner Schiefer of the Tauern Window—a key to understanding Eoalpine Orogenic processes in the Eastern Alps. In: FLÜGEL, H.W. & FAUPL, P., eds., *Geodynamics of the Eastern Alps*. pp. 55–69, Deuticke, Vienna.

- FRISCH, W., KUHLEMANN, J., DUNKL, I., & SZÉKELY, B., 2001. The Dachstein paleosurface and the Augenstein Formation in the Northern Calcareous Alps—a mosaic stone in the geomorphological evolution of the Eastern Alps. *Internal Journal of Earth Sciences*, 90, 500–518.
- FRISCH, W., SZÉKELY, B., KUHLEMANN, J. & DUNKL, I., 2000b. Geomorphological evolution of the Eastern Alps in response to Miocene tectonics. *Z. Geomorph. N. F.*, 44, (1), 103–138.
- FRITSCH, W., 1962. Geröllfunde vom Fuchsofen bei Klein St. Paul im Görtschitztal. *Carinthia II*, 72, 75–78.
- FRITZ, A., BOERSMA, M. & KRAINER, K., 1990. Steinkohlenzeitliche Pflanzenfossilien aus Kärnten. *Carinthia II*, Sonderheft, 49, 1–189.
- FROITZHEIM, N., SCHMID, S. M. & FREY, M., 1996. Mesozoic paleogeography and the timing of eclogite-facies metamorphism in the Alps: A working hypothesis. *Eclogae geol. Helv.*, 89, 81–110.
- FROITZHEIM, N., PLASIENKA, D. & SCHUSTER, R., 2008. Alpine Tectonics of the Alps and Western Carpathians. Mesozoic and Cenozoic. In: McCann, T., ed., *The Geology of Central Europe, Volume 2*. Geological Society, London, pp. 1141–1232.
- FÜGENSCHUH, B., MANCKTELOW, N. & SEWARD, D., 2000. Cretaceous to Neogene cooling and exhumation history of the Oetztal-Stubai basement complex, eastern Alps: A structural and fission track study. *Tectonics*, 19, 905–918.
- GAIIDES, F., ABART, R., DE CAPITANI, C., SCHUSTER, R., CONNOLLY, J.A.D. & REUSSER, E., 2006. Characterization of polymetamorphism in the Austroalpine basement east of the Tauern Window using garnet isopleth thermobarometry. *Journal of metamorphic Geology*, 24, 451–475.
- GAWLICK, H.-J., FRISCH, W., VECSEI, A., STEIGER, T. & BÖHM, F., 1999. The change from rifting to thrusting in the Northern Calcareous Alps as recorded in Jurassic sediments. *Geologische Rundschau*, 87, 644–657.
- GENSER, J. & LIU, X., 2010. On the age of the Eisenkappel granites. *Journal of Alpine Geology*, 52, 121–122 (PanGeo Austria 2010, Abstract volume).
- GENSER, J. & NEUBAUER, F., 1989. Low angle normal faults at the eastern margin of the Tauern window (Eastern Alps). *Mitt. Österr. Geol. Ges.*, 81(1988), 233–248.
- GENSER, J., 1992. Struktur- Gefüge- und Metamorphoseentwicklung einer kollisionalen Plattengrenze: Das Beispiel des Tauernstrandes (Kärnten/Österreich). Unpubl. Diss. Univ. Graz, 379 pp.
- GENSER, J., CLOETINGH, S. & NEUBAUER, F., 2007. Late orogenic rebound and oblique Alpine convergence: New constraints from subsidence analysis of the Austrian Molasse basin. *Global Planet. Change* 58, 214–223.
- GENSER, J., J.D. VAN WEES, S. CLOETINGH, S. & NEUBAUER, F., 1996. Eastern Alpine tectono-metamorphic evolution: constraints from two-dimensional P-T-t modelling. *Tectonics*, 13, 584–604.
- GIESE, U., 1988. Lower Paleozoic volcanic evolution at the northwestern border of the Gurktal nappe Upper Austroalpine, eastern Alps. *Schweizerische Mineralogische und Petrographische Mitteilungen*, 68, 381–396.
- GRENERCZY, G. & KENYERES, A., 2006. Crustal deformation between Adria and the European platform from space geodesy. In: PINTER, N. ET AL., EDs., *The Adria Microplate: GPS Geodesy, Tectonics and Hazards*, NATO Sci. Ser. IV, vol. 61, , pp. 321–334, Springer, Dordrecht, Netherlands, https://doi.org/10.1007/1-4020-4235-3_22.
- HAAS, J., KOVACS, S., KRYSTYN, L. & LEIN, R., 1995. Significance of Late Permian Triassic facies zones in terrane reconstructions in the Alpine North Pannonian domain. *Tectonophysics* 242, 19–40.
- HANDY, M.R., BABIST, J., WAGNER, R., ROSENBERG, C. & KONRAD, M., 2005. Decoupling and its relation to strain partitioning in continental lithosphere: insight from the Periadriatic fault system (European Alps). *Geol. Soc. Lond. Spec. Publ.*, 243, 249–276.
- HANDY, M.R., USTASZEWSKI, K., KISSLING, E., 2015. Reconstructing the Alps–Carpathians–Dinarides as a key to understanding switches in subduction polarity, slab gaps and surface motion. *Int. J. Earth Sci.*, 104, 1–26.

- HANDY, R., SCHMID, S.M., BOUSQUET, R., KISSLING, E. & BERNOULLI, D., 2010. Reconciling plate-tectonic reconstructions of Alpine Tethys with the geological-geophysical record of spreading and subduction in the Alps. *Earth Sci. Rev.*, 102, 121–158.
- HÄUSLER, H., 1988. Unterostalpine Jurabreccien in Österreich. Versuch einer sedimentologischen und paläogeographischen Analyse nachtriadischer Breccienserien im Unterostalpinen Rahmen des Tauernfensters (Salzburg – Tirol). *Jahrb. Geol. Bundesanst.*, 131, 21–125.
- HAWKESWORTH, C.J., 1976. Rb/Sr Geochronology in the Eastern Alps. *Contrib. Mineral. Petrol.*, 54, 225–244.
- HAWKESWORTH, C.J., WATERS, D.J. & BICKLE, M.J., 1975. Plate tectonics in the Eastern Alps. *Earth Planet. Sci. Lett.*, 24, 405–413.
- HEBERER, B., REVERMAN, R. L., FELLIN, M. G., NEUBAUER, F., DUNKL, I., ZATTIN, M., SEWARD, D., GENSER, J. & BRACK, P. 2017. Postcollisional cooling history of the Eastern and Southern Alps and its linkage to Adria indentation. *Int. J. Earth Sci.*, 106, 1557–1580.
- HEEDE, H. U., 1997. Isotopengeologische Untersuchungen an Gesteinen des ostalpinen Saualpenkristallins, Kärnten-Österreich. - Münstersche Forschungen zur Geologie und Paläontologie 81, 168 pp.
- HEIDORN, R., NEUBAUER, F., GENSER, J. & HANDLER, R., 2003. $^{40}\text{Ar}/^{39}\text{Ar}$ mica age constraints for the tectonic evolution of the Lower Austroalpine to Penninic nappe boundary, Austria: TRANSALP Conference, Extended abstract of oral and poster presentations, Trieste, 10 – 12 February 2003, *Mem. Sci. Geol. (Padova)*, 54, 217–220.
- HEJL, E., 1997. ‘Cold spots’ during the Cenozoic evolution of the Eastern Alps: thermochronological interpretation of apatite fission-track data: *Tectonophysics*, 272, 159–172.
- HERMANN, P. & WASCHER, W., 1972. Basiskonglomerate der Krappfeldgau bei Rottenstein/Kärnten. *Verhandlungen der Geologischen Bundesanstalt (Wien)*, 1972, 299–308.
- HETÉNYI, G., PLOMEROVÁ, J., BIANCHI, J., KAMPFOVÁ EXNEROVÁ, H., BOKELMANN, G., MARK R. HANDY, M., BABUŠKA, V., ALPARRAY-EASI WORKING GROUP, 2018. From mountain summits to roots: Crustal structure of the Eastern Alps and Bohemian Massif along longitude 13.3°E. *Tectonophysics* 744, 239–255.
- HILLER, O. K., 1973. Zur Morphogenese des Krappfeldbeckens in Kärnten. *Mitt. Österr. Geogr. Ges.* 115, 86–105.
- HÖCK, V., & MILLER, C., 1987. Mesozoic ophiolitic sequences and non-ophiolitic metabasites in the Hohe Tauern. In: FLÜGEL, H.W. & FAUPL, P., eds., *in Geodynamics of the Eastern Alps*. pp. 16–33, Deuticke, Vienna, 1987.
- HÖCK, V., KOLLER, F., 1989. Magmatic evolution of the Mesozoic ophiolites in Austria. *Chem. Geol.*, 77, 209–227.
- HOINKES, G., KOLLER, F., RANTITSCH, G., DACHS, E., HÖCK, V., NEUBAUER F. & SCHUSTER, R., 1999. Alpine metamorphism of the Eastern Alps: *Schweizerische Mineralogische und Petrographische Mitteilungen*, 79, 155–181.
- HOLDHAUS, K., 1921. Über die Auffindung von Trias im Königstuhlgebietes in Kärnten. *Anzeiger der Akademie für Wissenschaften Wien mathematisch-naturwissenschaftliche Klasse*, 58, 19–21.
- HOLUB, B. & MARSCHALLINGER, R., 1989. Die Zentralgneise im Hochalm-Ankogel-Massiv (östliches Tauernfenster). Teil I: Petrographische Gliederung und Intrusionsabfolge, *Mitt. Österr. Geol. Ges.*, 81, 5–31, 1989.
- HUBMANN, B., EBNER, F., FERRETTI, A., KIDO, E., KRAINER, K., NEUBAUER, F., SCHÖNLAUB, H.P. & SUTTNER, T. J., 2014. The Paleozoic Era(the) Abhandlungen der Geologischen Bundesanstalt, 66 (Sec. Ed.), 9–135.
- JANÁK, M., FROITZHEIM, N., K. YOSHIDA, K., SASINKOVÁ, V., NOSKO, M., KOBAYASHI, HIRAJIMA, T., VRABEC, M., 2015. Diamond in metasedimentary crustal rocks from Pohorje, Eastern Alps: a window to deep continental subduction. *Journal of Metamorphic Geology*, 33,
- JÁNAK, M., FROITZHEIM, N., LUPTÁK, B., VRBEC, M. & KROGH RAVNA, E.J., 2005. First evidence for ultrahigh-pressure metamorphism of eclogites in Pohorje, Slovenia: tracing deep continental subduction in the Eastern Alps. *Tectonics*, 23, TC5014, <https://doi.org/10.1029/2004TC001641>.
- KÁZMÉR, M., DUNKL, I., FRISCH, W., KUHLEMANN, J. & OZSVÁRT, P., 2003. The Palaeogene forearc basin of the Eastern Alps and Western Carpathians: subduction erosion and basin evolution. *J. Geol. Soc.*, 160, 413–428.

- KEIL, M. & NEUBAUER, F., 2015. Orogen-parallel extension and topographic gradients east of the Tauern window: a possible indication of intra-orogenic raft tectonics? *Austrian Journal of Earth Sciences*, 108, 1, 6–17.
- KOROKNAI, B., NEUBAUER, F., GENSER, J. & TOPA, D., 1999. Metamorphic and tectonic evolution of the Austroalpine units at the western margin of the Gurktal nappe complex, Eastern Alps. *Schweizerische Mineralogische und Petrographische Mitteilungen*, 79, 277–295.
- KOZUR, H. & MOSTLER, H. 1992. Erster paläontologischer Nachweis von Meliaticum und Süd-Rudabanyaicum in den Nördlichen Kalkalpen (Österreich) und ihre Beziehung zu den Abfolgen der Westkarpaten. *Geologisch-Paläontologische Mitteilungen der Universität Innsbruck*, 18, 87–129.
- KOZUR, H., 1991. The Evolution of the Meliata-Hallstatt ocean and its significance for the early evolution of the Eastern Alps and Western Carpathians. *Palaeogeography, Palaeoclimatology, Palaeoecology* 87, 109–135.
- KRAINER, K. & MOGESSIE, A., 1991. Composition and Significance of Resedimented Amphibolite Breccias and Conglomerates (Badstub Formation) in the Carboniferous of Nötsch (Eastern Alps, Carinthia, Austria). *Jahrbuch der Geologischen Bundesanstalt*, 134, 65–81.
- KRAINER, K., 1984. Sedimentologische Untersuchungen an permischen und untertriadischen Sedimenten des Stangalm-Mesozoikums (Kämten/Österreich). *Jahrbuch der Geologischen Bundesanstalt*, 127,
- KRAINER, K., 1987. Das Perm der Gurktaler Decke: eine sedimentologische Analyse Carinthia II, 177/97, 49–92.
- KRAINER, K., 1989. Molassesedimentation im Oberkarbon der Ostalpen am Beispiel der Stangnock Formation am NW-Rand der Gurktaler Decke (Österreich). *Zentralblatt für Geologie und Paläontologie Teil 1*, 1988, H. 7/8, 807–820.
- KRAINER, K., 1992. Fazies Sedimentationsprozesse und Paläogeographie im Karbon der Ost- und Südalpen. *Jahrbuch der Geologischen Bundesanstalt*, 135, 99–193.
- KRISCHE, O. & GAWLICK, H.-J., 2015. Age and significance of Lower Cretaceous mass flows: Ischler Breccia revisited (Rossfeld Formation, Northern Calcareous Alps, Austria). *Austrian Journal of Earth Sciences*, 108, 128–150.
- KRISCHE, O., GORIČAN, S. & GAWLICK, H.-J., 2014. Erosion of a Jurassic ophiolitic nappe-stack as indicated by exotic components in the Lower Cretaceous Rossfeld Formation of the Northern Calcareous Alps (Austria). *Geologica Carpathica*, 65, 3–24.
- KRISTAN-TOLLMANN, E. & TOLLMANN, A., 1964. Das mittelostalpine Standardprofil aus dem Stangalm-Mesozoikum (Kärnten). *Mitteilungen der Geologischen Gesellschaft Wien*, 56(1963), 539–589.
- KROHE, A., 1987. Kinematics of Cretaceous nappe tectonics in the Austroalpine basement of the Koralpe region (eastern Austria): *Tectonophysics*, 136, 171–196.
- KRUHL, J.H., 1993. The P-T-d development at the basement-cover boundary in the north-east Tauern Window (Eastern Alps): Alpine continental collision, *J. metamorphic Geol.*, 11, 31–47.
- KUHLEMANN, J., TAUBOLD, H., VENNEMANN, T., DUNKL, I. & FRISCH, W., 2008. Clay mineral and geochemical composition of Cenozoic paleosol in the Eastern Alps (Austria). *Austrian J. Earth Sci.*, 108, 60–69.
- KURZ W & FRITZ H., 2003. Tectonometamorphic Evolution of the Austroalpine nappe complex in the Central Eastern Alps—Consequences for the Eo-Alpine Evolution of the Eastern Alps. *Int. Geol. Rev.*, 45, 1100–1127.
- KURZ, W. & NEUBAUER, F., 1996. Deformation partitioning and shear localization during the updoming of the Sonnblick area in the Tauern Window (Eastern Alps, Austria), *J. Struct. Geol.*, 18, 1327–1343, 1996.
- KURZ, W., F. NEUBAUER, H. GENSER. H. & HORNER, H., 1994. Sequence of Tertiary brittle deformations in the eastern Tauern Window (Eastern Alps). *Mitt. Österr. Geol. Ges.*, 86 (1993), 153–164.
- KURZ, W., NEUBAUER, F. & GENSER, J., 1996. Kinematics of Penninic nappes (Glockner Nappe and basement-cover nappes) in the Tauern Window (Eastern Alps, Austria) during subduction and Penninic-Austroalpine collision, *Ecl. geol. Helv.*, 89, 573–605.
- KURZ, W., NEUBAUER, F., GENSER, J. & DACHS, E., 1998. Alpine geodynamic evolution of passive and active continental margin sequences in the Tauern Window (Eastern Alps, Austria, Italy): a review. *Geol. Rundsch.* 87, 225–242.

- KURZ, W., NEUBAUER, F., GENSER, J., UNZOG, W. & DACHS, E., 2001. Tectonic Evolution of Penninic Units in the Tauern Window during the Paleogene: Constraints from Structural and Metamorphic Geology. In: PILLER W.E. & RASSER M.W. (eds.), Paleogene of the Eastern Alps, Österr. Akademie der Wissenschaften, Schriftenreihe der Erdwissenschaftlichen Kommissionen, 14, 347–375.
- LAMMERER, B. & WEGER, M., 1998. Footwall uplift in an orogenic wedge: the Tauern Window in the Eastern Alps of Europe. *Tectonophysics*, 285, 213–230.
- LÄUFER, A.L., FRISCH, W., STEINITZ, G. & LOESCHKE, J., 1997. Exhumed fault-bounded Alpine blocks along the Periadriatic lineament: the Eder unit (Carnic Alps, Austria). *Geologische Rundschau*, 86, 612–626.
- LEGGEWIE, R. & THIEDIG, F., 1977. Oberkreidesedimente am Ostrand des Krappfeldes (Kärnten, Österreich). *Mitteilungen des Geologisch-Paläontologischen Institutes der Universität Hamburg* 47, 229–246.
- LEGRAIN, N., STÜWE, K. & WÖLFER, A., 2014. Incised relict landscapes in the eastern Alps: Geomorphology, 221, 124–138.
- LEIN, R., 1987. Evolution of the Northern Calcareous Alps during Triassic times. In: FLÜGEL, H.W. & FAUPL, P., eds., *Geodynamics of the Eastern Alps*. Deuticke, Vienna, pp. 85–102.
- LINZER, H.G., MOSER, F., NEMES, F., RATSBACHER, L. & SPERNER, B., 1997. Build-up and dismembering of the eastern Northern Calcareous Alps. *Tectonophysics*, 272, 97–124.
- LINZER, H.-G., RATSBACHER, L. & FRISCH, W., 1995. Transpressional collision structures in the upper crust: the fold-thrust belt of the Northern Calcareous Alps. *Tectonophysics*, 242, 41–61.
- LIPPITSCH, R., KISSLING, E. & ANSORGE, J., 2003. Upper mantle structure beneath the Alpine orogen from high-resolution teleseismic tomography. *J. Geophys. Res.*, 108, 2376. <https://doi.org/10.1029/2002JB002016>.
- LIU, Y., GENSER, J., HANDLER, R., FRIEDL, G. & NEUBAUER, F., 2001. $^{40}\text{Ar}/^{39}\text{Ar}$ muscovite ages from the Penninic/Austroalpine plate boundary, Eastern Alps. *Tectonics*, 20, 528–547.
- LOESCHKE, J. & SCHNEPF, H., 1987. Zur Geologie des Diabaszuges östlich Eisenkappel (Kärnten/Österreich). *N. Jb. Geol.-Paläont. Abh.*, 174, 303–329.
- LOESCHKE, J., 1970. Zur Geologie und Pétrographie des Diabaszuges westlich Eisenkappel (Ebriachtal/Karawanken/Österreich). *Oberrhein. geol. Abh.*, 19, 73–100.
- LÜSCHEN, A., BORRINI, D., GEBRANDE, H., LAMMERER, B., MILLAHN, K., NEUBAUER, F., NICOLICH, R., TRANSALP WORKING GROUP, 2005. TRANSALP – deep crustal Vibroseis and explosive seismic profiling in the Eastern Alps. *Tectonophysics*, 414, 9–38.
- LUTH, S.W. & WILLINGSHOFER E., 2008. Mapping of the post-collisional cooling history of the Eastern Alps. *Swiss J. Geosci.*, 101:207–223.
- MADER, D., NEUBAUER, F. & HANDLER, R., 2007: $^{40}\text{Ar}/^{39}\text{Ar}$ dating of detrital white mica of Late Palaeozoic sandstones in the Carnic Alps (Austria): implications to provenance and tectonic setting of sedimentary basins. *Geologica Carpathica*, 58 (2), 133–144.
- MANCKTELOW, N.S., STÖCKLI, D. F., GROLLIMUND, B., MÜLLER, W., FÜGENSCHUH, B. & VIOLA, G., 2001. The DAV and the Periadriatic fault system in the Eastern Alps south of the Tauern window. *Int. J. Earth Sci.*, 90, 593–622.
- MANDL, G. W., 2000. The Alpine sector of the Tethyan shelf – Examples pf Triassic to Jurassic sedimentation and deformation from the Northern Calcareous Alps: *Mitt. Österr. Geol. Ges.*, 92(1999), 61–77.
- ANDL, G. W. & ONDREJKOVA, A., 1991. Über eine triadische Tiefwasserfazies (Radiolarite, Tonschiefer) in den Nördlichen Kalkalpen – ein Vorbericht: *Jahrbuch der Geologischen Bundesanstalt (Wien)*, 134, 309–318.
- MARSCHALLINGER, R. & HOLUB, B., 1991. Die Zentralgneise im Hochalm-Ankogel-Massiv (östliches Tauernfenster) Teil II: Geochemische und zirkontypologische Charakteristik. *Mitt. Österr. Geol. Ges.*, 82, 19–48.
- MÁRTON, E., DROBNE, K., COSOVIC, & MORO, A., 2003. Paleomagnetic evidence for Tertiary counterclockwise rotation of Adria. *Tectonophysics*, 377, 143–166.

- MILLER, C., THÖNI, M., GOESSLER, W. & TESSADRI, R., 2011. Origin and age of the Eisenkappel gabbro to granite suite (Carinthia, SE Austrian Alps). *Lithos* 125, 434–448.
- MILLER, C., THÖNI, M., KONZETT, J., KURZ, W. & SCHUSTER, R., 2005. Eclogites from the Koralpe and Saualpe type-localities, Eastern Alps, Austria: Mitteilungen der Österr. Mineralogischen Gesellschaft, 150, 227–263.
- MISSONI, S. & GAWLICK, H.-J., 2011. Evidence for Jurassic subduction from the Northern Calcareous Alps (Berchtesgaden; Austroalpine, Germany). *International Journal of Earth Sciences (Geologische Rundschau)* 100, 1605–1631.
- MÜLLER, W., DALLMEYER, R.D., NEUBAUER, F. & THÖNI, M. 1999. Deformation-induced resetting of Rb/Sr and $^{40}\text{Ar}/^{39}\text{Ar}$ mineral systems in a low-grade, polymetamorphic terrane (eastern Alps, Austria). *Journal of the Geological Society (London)*, 156, 261–278.
- MÜLLER, W., KELLEY, S. P. & VILLA, I. M., 2002. Dating fault-generated pseudotachylites: comparison of Ar-40/Ar-39 stepwise-heating, laser-ablation and Rb-Sr microsampling analyses. *Contrib. Mineral. Petrol.* 144, 57–77.
- MÜLLER, W., PROSSER, G., MANCKTELOW, N., VILLA, I., KELLEY, S., VIOLA, G. & OBERLI, F., 2001. Geochronological constraints on the evolution of the Periadriatic Fault System (Alps). *Int. J. Earth Sci.*, 90, 623–653.
- MUTTONI, G., KENT, D.V. & CHANNELL, J.E.T., 1996. Evolution of Pangea: Paleomagnetic constraints from the southern Alps, Italy: *Earth and Planetary Science Letters*, 140, 97–112.
- NEMES, F., 1997. Kinematics of the Periadriatic Fault in the Eastern Alps - Evidence from structural analysis, fission track dating and basin modelling. Doctoral Thesis Faculty of Sciences, University of Salzburg, pp. 225.
- NEMES, F., NEUBAUER., F., CLOETINGH, S. & GENSER, J., 1997. The Klagenfurt Basin in the Eastern Alps: a decoupled intra-orogenic flexural basin? *Tectonophysics*, 282, 189–204.
- NEUBAUER, F., 1987. The Gurktal Thrust System within the Austroalpine region – some structural and geometrical aspects. In: FLÜGEL, H.W. & FAUPL, P., eds., *Geodynamics of the Eastern Alps*. Deuticke, Wien, pp. 226–236.
- NEUBAUER, F., 1988. Bau und Entwicklungsgeschichte des Rennfeld-Mugel- und des Gleinalmkristallins (Ostalpen). *Abh. Geol. Bundesanst.*, 42: 1–137.
- NEUBAUER, F., 2014. The structure of the Eastern Alps: from Eduard Suess to present-day knowledge. *Austrian Journal of Earth Sciences*, 107/1, 83–93.
- NEUBAUER, F., 2016. Formation of an intra-orogenic transtensional basin: the Neogene Wagrain basin in the Eastern Alps. *Swiss Journal of Geosciences*, 109, 37–56.
- NEUBAUER, F. & GENSER, J., 1990. Architektur und Kinematik der östlichen Zentralalpen – eine Übersicht. *Mitteilungen des Naturwissenschaftlichen Vereines für Steiermark*, 120, 203–219.
- NEUBAUER, F. & PISTOTNIK., J., 1984. Das Altpaläozoikum und Unterkarbon des Gurktaler Deckensystems (Ostalpen) und ihre paläogeographischen Beziehungen. *Geologische Rundschau*, 73, 149–174.
- NEUBAUER, F., DALLMEYER, R.D., DUNKL I. & SCHIRNIK, D., 1995. Late Cretaceous exhumation of the metamorphic Gleinalm dome, Eastern Alps: kinematics, cooling history and sedimentary response in a sinistral wrench corridor: *Tectonophysics*, 242, 79–89.
- NEUBAUER, F., FRISCH, W. & HANSEN, B.T., 2002. Early Palaeozoic tectonothermal events in basement complexes of the eastern Graywacke Zone (Eastern Alps. evidence from U-Pb zircon data. *International Journal of Earth Sciences*, 91, 775–786.
- NEUBAUER, F., GENSER, J. & HANDLER, R., 2000. The Eastern Alps: result of a two-stage collision process. *Mitteilungen der Österr. Geologischen Gesellschaft*, 92, 117–134.
- NEUBAUER, F., HANDLER, R., HERMANN, S. & PAULUS, G., 1994. Tectonostratigraphy and structure of the eastern Graywacke Zone, Eastern Alps. *Mitt. Österr. Geol. Ges. (ALCAPA issue)*, 87: 61–74.
- NEUBAUER, F., HOINKES, G., SASSI, F.P., HANDLER, R., HöCK, V., KOLLER, F. & FRANK, W., 1999. Pre-Alpine metamorphism of the Eastern Alps. *Schweizerische Mineralogische und Petrographische Mitteilungen*, 79. p. 41–62.

- NEUBAUER, F., BERNROIDER, M., LEITNER, C., SCHORN, A., ZIEGLER, T. & GENSER, J., 2017. Die Evaporite des Haselgebirges als metamorphe Gesteine: Bildung, Umwandlung, Gefüge, Alter und Konsequenzen für die Struktur der Nördlichen Kalkalpen. Arbeitstagung „Angewandte Geowissenschaften an der GBA“, Bad Ischl, Hallstatt, Gmunden, p. 29–37, Geologische Bundesanstalt, Wien.
- NEUBAUER, F., HEBERER, B., DUNKL, I., LIU, S., BERNROIDER, M., DONG, Y., 2018. The Oligocene Reifnitz tonalite (Austria) and its host rocks: implications for Cretaceous and Oligocene-Neogene tectonics of southeastern Eastern Alps. *Geologica Carpathica*, 69, 237–253.
- NEUMANN, H.-H., 1989. Die Oberkreide des Krappfeldes. Arbeitstagung Geologische Bundesanstalt, 1989, 70–79.
- OBERHÄNSLI, R., BOUSQUET, R., ENGI, M., GOFFÉ, B., GOSSO, G., HANDY, M., HÖCK, V., KOLLER, F., LARDEAUX, J. M., POLINO, R., ROSSI, P.L., SCHUSTER, R., SCHWARTZ, S., SPALLA, I., 2004. Metamorphic structure of the Alps 1: 100000000. Paris, Commission for the Geological Map of the World.
- ORTNER, H., REITER, F. & BRANDNER, R., 2006. Kinematics of the Inntal shear zone–sub-Tauern ramp fault system and the interpretation of the TRANSALP seismic section, Eastern Alps, Austria. *Tectonophysics*, 414, 241–258.
- PISTOTNIK, J., 1973/74. Zur Geologie des NW-Randes der Gurktaler Masse (Stangalm-Mesozoikum, Österreich). *Mitteilungen der Österreichischen Geologischen Gesellschaft*, 66/67, 127–142.
- PISTOTNIK, J., 1976. Ein Transgressionskontakt des Stangalm-Mesozoikums (Gurktaler Alpen, Kärnten/Österreich). *Carinthia II*, 166/86, 127–131.
- PISTOTNIK, J., 1996. Geologische Karte der Republik Österreich 1 : 50.000, Blatt 183 Radenthein. Geologische Bundesanstalt, Wien.
- PLAŠIENKA, D., 2018. Continuity and episodicity in the early Alpine tectonic evolution of the Western Carpathians: How large-scale processes are expressed by the orogenic architecture and rock record data. *Tectonics*, 37, 2029–2079. <https://doi.org/10.1029/20792017TC004779>.
- PLÖCHINGER, B., 1983. Salzburger Kalkalpen. Sammlung geol. Führer 73, 144 p., Borntraeger, Berlin., Stuttgart.
- POLINSKI, R.K. & EISBACHER, G.H., 1992. Deformation partitioning during polyphase oblique convergence in the Karawanken Mountains, southeastern Alps. *Journal of Structural Geology* 14, 1203–1213.
- POMELLA, H., FLÖSS, D., SPECKBACHER, R., TROPPER, P., FÜGENSCHUH, B., 2015. The western end of the Eoalpine High-Pressure Belt (Texel unit, South Tyrol / Italy). *Terra Nova*, 28, 60–69.
- POMELLA, H., KLÖTZLI, U., SCHOLGER, R., STIPP, M. & FÜGENSCHUH, B., 2011. The Northern Giudicarie and the Meran-Mauls fault (Alps, Northern Italy) in the light of new paleomagnetic and geochronological data from boudinaged Eo-/Oligocene tonalites. *International Journal of Earth Sciences*, 100, 1827–1850.
- POMELLA, H., STIPP, M. & FÜGENSCHUH, B., 2012. Thermochronological record of thrusting and strike-slip faulting along the Giudicarie fault system (Alps, Northern Italy). *Tectonophysics*, 579, 118–130.
- RANTITSCH, G., 1997. Thermal history of the Carnic Alps (Southern Alps, Austria) and its palaeogeographic implications: *Tectonophysics*, 272, 213–232.
- RANTITSCH, G. & RUSSEGGER, B., 2000. Thrust-related very low grade metamorphism within the Gurktal nappe complex (Eastern Alps). *Jahrbuch der Geologischen Bundesanstalt*, 142, 219–225.
- RATHORE, J.S. & BECKE, M., 1980. Magnetic fabric analyses in the Gail Galley (Carinthia, Austria) for the determination of the sense of movements along this region of the Periadriatic Line. *Tectonophysics* 69, 349–368.
- RATSCHBACHER, L., 1984. Beitrag zur Neugliederung der Veitscher Decke (Grauwackenzone) in ihrem Westabschnitt (Obersteiermark Österreich). *Jahrbuch der Geologischen Bundesanstalt* 127, 423–453.
- RATSCHBACHER, L., 1986. Kinematics of Austro-Alpine cover nappes: changing translation path due to transpression: *Tectonophysics*, 125, 335–356

- RATSCHBACHER, L. & NEUBAUER, F., 1989. West-directed decollement of Austro-Alpine cover nappes in the eastern Alps: geometrical and rheological considerations. In: COWARD, M.P., DIETRICH, D. & PARK, R.G., Eds., Alpine Tectonics. Geological Society [London] Special Publication, 45, 243–262.
- RATSCHBACHER, L., FRISCH, W., NEUBAUER, F., SCHMID, S.M. & NEUGEBAUER, J., 1989. Extension in compressional orogenic belts: The eastern Alps. *Geology*, 17, 404–407.
- RATSCHBACHER, L., FRISCH, W., LINZER, H.G. & MERLE, O., 1991a. Lateral extrusion in the Eastern Alps, part 2: Structural analysis: *Tectonics*, 10, 257–271
- RATSCHBACHER, L., MERLE, O., DAVY, P. & COBBOLD, P., 1991b. Lateral extrusion in the Eastern Alps, part 1. boundary-conditions and experiments scaled for gravity. *Tectonics*, 10, 245–256, <https://doi.org/10.1029/90tc02622>.
- REINECKER, J. & LENHARDT, W.A., 1999. Present-day stress field and deformation in eastern Austria. *International Journal of Earth Sciences*, 88, 532–550.
- RING, U., RATSCHBACHER, L., FRISCH, W., BIEHLER, D. & KRALIK, M., 1989. Kinematics of the Alpine plate-margin – structural styles, strain and motion along the Penninic-Australpine boundary in the Swiss-Austrian Alps: *Journal of the Geological Society (London)*, 146, 835–849.
- ROBL, J. & STÜWE, K., 2005. Continental collision with finite indenter strength: 2. European Eastern Alps. *Tectonics* 24, TC4014. <https://dx.doi.org/10.1029/2004TC001741>.
- ROBL, J., HERGARTEN, S. & STÜWE, K., 2008a. Morphological analysis of the drainage system in the Eastern Alps. *Tectonophysics*, 460, 263–277
- ROBL, J., STÜWE, K., HERGARTEN, S., EVANS, L., 2008b. Extension during continental convergence in the Eastern Alps: The influence of orogen-scale strike-slip faults. *Geology* 36, 963–966.
- ROSENBERG, C. L., 2004. Shear zones and magma ascent: A model based on a review of the Tertiary magmatism in the Alps, *Tectonics*, 23, TC3002, <https://dx.doi.org/10.1029/2003TC001526>.
- ROSENBERG, C.L., BERGER, A., BELLAHSEN, N. & BOUSQUET, R., 2015. Relating orogen-width to shortening, erosion, and exhumation during Alpine collision. *Tectonics* 34, 1306–1328. <https://dx.doi.org/10.1002/2014TC003736>.
- ROSENBERG, C.L., BRUN, J.-P., CAGNARD, F. & GAPAIS, D., 2007. Oblique indentation in the Eastern Alps: insights from laboratory experiments. *Tectonics* 26 (TC2003). <https://doi.org/10.1029/2006TC001960>.
- ROSENBERG, C. L., SCHNEIDER, S., SCHARF, S., BERTRAND, A., HAMMERSCHMIDT, K., RABAUTE, A. & BRUN, J.-P., 2018. Relating collisional kinematics to exhumation processes in the Eastern Alps. *Earth-Sci. Rev.*, 176, 311–344.
- ROSSNER, R., 1976. Struktur und Position der Quarzphyllitdecke im Rahmen des Unterostalpins der Radstädter Tauern. *N. Jb. Geol. Paläont. Abh.*, 151, 281–303.
- ROSSNER, R., 1977. N-Vergenz oder S-Vergenz im Schuppenbau der Werfen St. Martiner Zone (Nordkalkalpen, Österreich)? *N. Jb. Geol. Paläont. Mh.*, 419–432.
- ROSSNER, R., 1979. Gebirgsbau und alpidische Tektonik am Nordostrand des Tauernfensterrahmens (Nördliche Radstädter Tauern, Österreich). *Jb. Geol. Bundesanst. Wien*, 122, 251–387.
- SACHSENHOFER, R. F., 1992. Coalification and thermal histories of Tertiary basins in relation to late Alpidic evolution of the Eastern Alps. *Geologische Rundschau*, 81, 291–308.
- SACHSENHOFER, R. F., 2001. Syn- and post-collisional heat flow in the Cenozoic Eastern Alps. *Int. J. Earth Sci.* 90, 579–592.
- SACHSENHOFER, R.F., LANKREIJER, A., CLOETINGH, S. & EBNER, F., 1997. Subsidence analysis and quantitative basin modelling in the Styrian Basin (Pannonian Basin System, Austria). *Tectonophysics*, 272, 175–196.
- SANDERS, D., PONS, J. M., CAUS, E., 2004. Shallow-water limestone clasts in a Campanian deep-water debrite (Krappfeld, Central Alps, Austria): implications for carbonate platform history. *Ann. Naturhist. Mus. Wien*, 106 A, 139–165

- SASSI, F.P., ZANFERRARI, A., ZIRPOLI, G., BORSI, S. & DEL MOO, A., 1974. The Austrides to the south of the Tauern Window and the periadriatic lineament between Mules and Mauthen. *Neues Jahrbuch für Geologie und Paläontologie - Monatshefte*, 421-434.
- SCHARBERT, S., 1975. Radiometrische Altersdaten von Intrusivgesteinen im Raum Eisenkappel (Karawanken, Kärnten). *Verh. Geol. Bundesanst.*, 1975, 301-304.
- SCHARF, A., HANDY, M. R., SCHMID, S. M., FAVARO, S., SUDO, M., SCHUSTER, R., & HAMMERSCHMIDT, K., 2016. Grain-size effects on the closure temperature of white mica in a crustal-scale extensional shear zone—Implications of in-situ $^{40}\text{Ar}/^{39}\text{Ar}$ laser-ablation of white mica for dating shearing and cooling (Tauern Window, Eastern Alps), *Tectonophysics*, 674, 210–226.
- SCHARF, A., HANDY, M. R., ZIEMANN, M. A. & SCHMID, S. M., 2013. Peak-temperature patterns of polyphase metamorphism resulting from accretion, subduction and collision (eastern Tauern Window, European Alps)—A study with Raman microspectroscopy on carbonaceous material (RSCM). *J. Metamorph. Geol.*, 31, 863–880.
- SCHARF, A., HANDY, M.R., FAVARO, S., SCHMID, S.M. & BERTRAND, A., 2013. Modes of orogen-parallel stretching and extensional exhumation in response to microplate indentation and roll-back subduction (Tauern Window, Eastern Alps). *Int. J. Earth Sci.*, 102, 1627–1654.
- SCHILLIG, D., 1966. Geomorphologische Untersuchungen in der Saualpe (Kärnten). *Tübinger Geogr. Stud.*, 21, 1–81.
- SCHIMANA, R., 1986. Neue Ergebnisse zur Entwicklungsgeschichte des Kristallins um Radenthein (Kärnten, Österreich), *Mitt. Ges. Geol. Bergbaustud. Österr.*, 33, 221–232.
- SCHMID, S.M., AEBLI, H.R., HELLER, F. & ZINGG, A., 1989. The role of the Periadriatic Line in the tectonic evolution of the Alps. In: COWARD, M.P., DIETRICH, D. & PARK, R.G., eds., *Alpine Tectonics*. Geol. Soc. London Spec. Publ., 45, pp. 153–171.
- SCHMID, S.M., FÜGENSCHUH, B., KISSLING, E. & SCHUSTER, R., 2004. Tectonic map and overall architecture of the Alpine orogen. *Eclogae Geologicae Helvetiae*, 97, 93–117.
- SCHMID, S.M., SCHARF, A., HANDY, M.R. & ROSENBERG, C.L., 2013. The Tauern Window (Eastern Alps, Austria): a new tectonic map, with cross-sections and a tectonometamorphic synthesis. *Swiss J. Geosci.*, 106, 1–32.
- SCHMIDT, T., BLAU, J. & KAZMER, M., 1991. Large-scale strike-slip displacement of the Drauzug and the Transdanubian mountains in Early Alpine history - evidence from Permo-Mesozoic facies belts. *Tectonophysics*, 200, 213–232.
- SCHÖNLAUB, H. P., 1979. Das Paläozoikum in Österreich. *Abhandl. Geol. Bundesanst.*, 33, 1–124.
- SCHÖNLAUB, H.P., 1985. Das Karbon von Nötsch und sein Rahmen. *Jahrb. Geol. Bundesanst.*, 127, 673–692.
- SCHÖNLAUB, H.P., 1989. Geologische Karte der Republik Österreich 1 : 50 000, 199 Hermagor. *Geologische Bundesanstalt*, Wien.
- SCHÖNLAUB, H. P. & FORKE, H. C., 2007. Die post-variszische Schichtfolge der Karnischen Alpen – Erläuterungen zur Geologischen Karte des Jungpaläozoikums der Karnischen Alpen 1:12500. *Abhandlungen der Geologischen Bundesanstalt*, 61, 3–157.
- SCHORN, A., NEUBAUER, F., GENSER, J. & BERNROIDER, M., 2013. The Haselgebirge evaporitic mélange in central Northern Calcareous Alps (Austria): part of the Permian to Lower Triassic rift of the Meliata ocean? *Tectonophysics*, 583, 28–48.
- SCHRAUT, G., 1999. Paläofaunistische Untersuchungen aus dem Unterkarbon von Nötsch (Kärnten, Österreich), Teil 2: Cephalopoda (Nautiloidea, Ammonoidea), Crustacea (Phyllocarida) Echinoidea. *Jahrbuch der Geologischen Bundesanstalt*, 141, 503–517.
- SCHUSTER, R. & FRANK, W., 1999. Metamorphic evolution of the Austroalpine units east of the Tauern Window: Indications for Jurassic strike-slip tectonics. *Mitteilungen der Gesellschaft der Geologie- und Bergbaustudenten Österreichs*, 42(1999), 37–58.

- SCHUSTER, R. & STÜWE, K., 2008. Permian metamorphic event in the Alps. *Geology*, 36, 603–606.
- SCHUSTER, R., KOLLER, F., HOECK, V., HOINKES, G. & BOUSQUET, R., 2004. Explanatory notes to the map: Metamorphic structure of the Alps – Metamorphic evolution of the Eastern Alps. *Mitteilungen der Österreichischen Mineralogischen Gesellschaft* 149, 175–199.
- SCHUSTER, R., SCHARBERT, S., ABART, R. & FRANK W., 2001. Permo-Triassic extension and related HAT/LP metamorphism in the Austroalpine–Southalpine realm: *Mitt. Ges. Geol. Bergbaustrud. Österr.* v. 45, 111–141.
- SPÖTL, C., LONGSTAFFE, F.J., RAMSEYER, K., KUNK, R. & WIESHEU, R., 1998. Fluid-rock reactions in an evaporitic mélange, Permian Haselgebirge, Austrian Alps: *Sedimentology*, 45, 1019–1945.
- STAMPFLI, G. M. & MOSAR J., 1999. The making and becoming of Apulia. *Mem. Sci. Geol.*, 51, 141–154.
- STEFANI, C., 2002. Variation in terrigenous supplies in the Upper Pliocene to Recent deposits of the Venice area. *Sedimentary Geology*, 153, 43–55.
- THEINER, U., 1987. Das Kristallin der NW-Nockberge - Eine kristallingeologische Neuuntersuchung, Unveröff. Diss. formal-naturw. Fak. Univ. Wien, pp. 154.
- THIEDIG, F. 1970. Verbreitung, Ausbildung und stratigraphische Einstufung neogener Rotlehme und Grobschotter in Ostkärnten (Österreich). *Mitt. Geol.-Paläont. Inst. Univ. Hamburg*, 38, 97–116.
- THIEDIG, F., 1975. Submarine Brekzien als Folge von Felsstürzen in der Turbidit-Fazies der Oberkreide des Jrappfeldes in Kärnten (Österreich). *Mitt. Geol.-Paläont. Inst. Universität Hamburg* 44, 495–516.
- THIEDIG, F., VAN HUSEN, D. & PISTOTNIK, J., 1999. Geologische Karte der Republik Österreich 1 : 50.000, 186 Sankt Veit an der Glan. *Geologische Bundesanstalt*, Wien.
- THIEDIG, F., WEISSENBACH, N., 1975. Die Junge Bruchtektonik der Saualpe. *Clausthaler Geologische Abhandlungen*, Sonderband, 1, 155–174.
- THIEDIG, F., WIEDMANN, J., 1976. Ammoniten und das Alter der höheren Kreide (Gosau) des Krappfeldes in Kärnten (Österreich). *Mitt. Geol.-Paläont. Inst. Univ. Hamburg*, 45, 9–27.
- THÖNI, M., 1999. A review of geochronological data from the Eastern Alps. *Schweiz. Mineral. Petrogr. Mitt.*, 79, 209–230
- THÖNI, M., 2002. Sm-Nd isotope systematics in garnet from different lithologies (Eastern Alps) – age results, and an evaluation of potential problems for garnet Sm-Nd Chronometry. *Chemical Geology*, 194, 353–379.
- THÖNI, M. & JAGOUTZ, E., 1992. Some new aspects of dating eclogites in orogenic belts: Sm-Nd, Rb-Sr, and Pb-Pb isotope results from the Austroalpine Saulape and Koralpe type-locality (Carinthia/Styria, southeastern Austria): *Geochimica et Cosmochimica Acta*, 56, 347–368.
- TOLLMANN, A., 1975. Die Bedeutung des Stangalm-Mesozoikums in Kärnten für die Neugliederung des Oberostalpins in den Ostalpen. *Neues Jahrbuch für Geologie und Paläontologie Monatshefte*, 150, 19–43.
- TOLLMANN, A., 1977. Die Geologie von Österreich (Band I): Die Zentralalpen. Deuticke, Wien.
- TOLLMANN, A., 1987. The Alpidic Evolution of the Eastern Alps. In: FLÜGEL, H.W. & FAUPL, P., eds., *Geodynamics of the Eastern Alps*. Deuticke, Wien, pp. 361–378.
- TRANSALP Working Group: Gebrände H., Lüschen E., Bopp M., Bleibinhaus F., Lammerer B., Oncken, O., Stiller, M., Kummerow, J., Kind, R., Millahn K., Grassl H., Neubauer, F., Bertelli L., Borrini D., Fantoni R., Pessina C., Sella M., Castellarin A., Nicolich R., Mazzotti A. & Bernabini M., 2002. First deep seismic reflection images of the Eastern Alps reveal giant crustal wedges and transcrustal ramps: *Geophysical Research Letters*, 29/10, 92-1–92-4.
- USTASZEWSKI, K., SCHMID, S.M., FÜGENSCHUH, B., TISCHLER, M., KISSLING, E. & SPAKMAN, W., 2008. A map-view restoration of the Alpine–Carpathian–Dinaridic system for the early Miocene. *Swiss J. Geosci.*, 101, 273–294.
- VACHARD, D., KRAINER, K. & SCHÖNLAUB, H. P., 2018. Lower Serpukhovian (Steshevian) foraminifers and algae from exotic limestone clasts of Nötsch (Eastern Alps, Austria). *Geobios*, 51, 75–100.

- VAN AMEROM, H. W. J. & SCHÖNLAUB, H. P., 1992. Pflanzenfossilien aus dem Karbon von Nötsch und der Hochwipfel-Formation der Karnischen Alpen (Österreich). *Jahrb. Geol. Bundesanst.*, 135, 195–216.
- VAN GELDER, I., WILLINGSHOFER, E., SOKOUTIS, D., CLOETINGH, S.A.P.L., 2017. The interplay between subduction and lateral extrusion: a case study for the European Eastern Alps based on analogue models. *Earth Planet. Sci. Lett.*, 472, 82–94.
- VAN HINTE, J. E., 1963. Zur Stratigraphie und Mikropaläontologie der Oberkreide und des Eozäns des Krappfeldes (Kärnten). *Jb. geol. Bundesanstalt, Sdb.* 8, 1–147.
- VAN HUSEN, D., 1976. Zur quartären Entwicklung des Krappfeldes und des Berglandes um St. Veit an der Glan. *Mitt. Ges. Geol. Bergbaustud. Österreichs*, 23, 55–68.
- VAN HUSEN, D., 1989. Die Entwicklung des Krappfeldes und seiner weiteren Umgebung im Pliozän und Pleistozän. *Arbeitstagung Geologische Bundesanstalt 1989*, 107–119.
- VAVRA, G. & FRISCH, W., 1989. Pre-Variscan back-arc and island arc magmatism in the Tauern Window (Eastern Alps). *Tectonophysics*, 169, 271–280.
- VAVRA, G. & HANSEN, B.T., 1991. Cathodoluminescence studies and U/Pb dating of zircons in pre-Mesozoic gneisses of the Tauern Window: implications for the Penninic basement evolution. *Geol. Rundschau*, 80, 703–715, 1991.
- VAVRA, G., 1989. Die Entwicklung des penninischen Grundgebirges im östlichen und zentralen Tauernfenster der Ostalpen - Geochemie, Zirkontypologie, U/Pb-Radiometrie. *Tüb. Geowiss. Abh. Reihe A*, 6, 1–150.
- VISONÀ, D. & ZANFERRARI, A., 2000. Some constraints on geochemical features in the Triassic mantle of the easternmost Austroalpine–Southalpine domain: evidence from the Karawanken pluton (Carinthia, Austria). *International Journal of Earth Sciences*, 89, 40–51.
- VON BLANCKENBURG, F. & DAVIES, J. H., 1995. Slab breakoff: A model for syncollisional magmatism and tectonics in the Alps. *Tectonics*, 14, 120–131.
- BLANCKENBURG, F., KAGAMI, H., DEUTSCH, A., OBERLI, F., MEIER, M., WIEDENBECK, M., BARTH, S. & FISCHER, H., 1998. The origin of Alpine plutons along the Periadriatic Lineament. *Schweizerische Mineralogische und Petrographische Mitteilungen* 78, 55–66.
- VON GOSEN, W., 1989a. Gefügeentwicklungen, Metamorphosen und Bewegungen der ostalpinen Baueinheiten zwischen Nockgebiet und Karawanken (Österreich). *Geotektonische Forschungen*, 72, 1–247
- VON GOSEN, W., 1989b. Fabric developments and the evolution of the Periadriatic Lineament in southeast Austria. *Geological Magazine*, 126, 55–71.
- VON GOSEN, W., THIEDIG, F., 1980. Erster Nachweis alpidischer Schieferung in postvariszischer Transgressionsserie und Oberkreide des Krappfeldes und der Griffener-St. Pauler Berge (Kärnten/Österreich). *Verhandlungen der Geologischen Bundesanstalt Wien* 1979, 313–335.
- VON GOSEN, W., PISTOTNIK, J. & SCHRAMM, J. M., 1987. Schwache Metamorphose in Gesteinsserien des Nockgebietes und im Postvariszikum des Karawankenvorlandes (Ostalpen, Kärnten). *Jahrbuch der Geologischen Bundesanstalt*, 130, 31–36.
- VOZÁROVÁ, A., LAURINC, D., ŠARINOVÁ, K., LARIONOV, A., PRESNYAKOV, S., RODIONOV, N. & PADERIN, I., 2013. Pb ages of detrital zircons in relation to geodynamic evolution: Paleozoic of the Northern Gmericum (Western Carpathians. Slovakia). *Journal of Sedimentary Research*, 83, 915–927.
- VOZÁROVA, A., VOZÁR, J. & MAYR, M., 1999. High-pressure metamorphism of basalts in the evaporitic sequence of the Haselgebirge: An evidence from Bad Ischl (Austria): *Abhandl. Geol. Bundesanst. (Wien)*, 56, 325–330.
- WAGNER, T., FRITZ, H., STÜWE, K., NESTROY, O., RODNIGHT, H., HELLSTROM, J. & BENISCHKE, R., 2011. Correlations of cave levels, stream terraces and planation surfaces along the River Mur—Timing of landscape evolution along the eastern margin of the Alps. *Geomorphology*, 134, 62–78.
- Wagreich, M. & Decker, K., 2001. Sedimentary tectonics and subsidence modelling of the type Upper Cretaceous Gosau basin (Northern Calcareous Alps, Austria). *Int. J. Earth Sciences*, 90, 714–726.

- WAGREICH, M., 1995. Subduction tectonic erosion and Late Cretaceous subsidence along the northern Austroalpine margin (Eastern Alps, Austria). *Tectonophysics*, 242, 63–78.
- WALACH, G., 1989. Geophysikalische Prospektionsprojekte auf ÖK-Blatt 186 St. Veit/Glan. Arbeitstagung Geologische Bundesanstalt, 1989, 122–125.
- WEISSENBACH, N. & PISTOTNIK, J., 2000. Geologische Karte der Republik Österreich 1 : 50000, 186 Sankt Leonhard im Lavanttal. Geologische Bundesanstalt, Wien.
- WIESINGER, M., NEUBAUER, F. & HANDLER, R., 2006. Exhumation of the Saualpe eclogite unit, Eastern Alps: constraints from $^{40}\text{Ar}/^{39}\text{Ar}$ ages: Mineralogy and Petrology, 88, 149–180.
- WILKENS, E., 1989a. Paläogene Sedimente des Krappfeldes und seiner Umgebung. Arbeitstagung Geologische Bundesanstalt 1989, 85–99.
- WILKENS, E., 1989b. Entstehung von Großforaminiferen-Akkumulationen, Biofabric-Entwicklung und Bioklastaggregationen im Alttertiär des Sonnberges. Arbeitstagung Geol. Bundesanst., 1989, 100–106.
- WILLINGSHOFER, E. & CLOETINGH, S., 2003. Present-day lithospheric strength of the Eastern Alps and its relationship to neotectonics. *Tectonics* 22, 1075, <https://doi.org/10.1029/2002tc001463>.
- WILLINGSHOFER, E., NEUBAUER, F. & CLOETINGH, S. 1999a. Significance of Gosau basins for the upper Cretaceous geodynamic history of the Alpine—Carpathian belt: Physics and Chemistry of the Earth Part A: Solid Earth and Geodesy, 24, 687–695.
- WILLINGSHOFER, E., WEES, J.D. VAN, CLOETINGH, S. A. P. L. & NEUBAUER, F. 1999b. Thermomechanical evolution of an accretionary wedge: the Austroalpine of the Eastern Alps – indications and implications from 2D-numerical modelling. *Tectonics*, 18, 809–826.
- WÖLFLER, A., KURZ, W., FRITZ, H. & STÜWE, K., 2011. Lateral extrusion in the Eastern Alps revisited: Refining the model by thermochronological, sedimentary, and seismic data. *Tectonics*, 30, TC4006, <https://doi.org/10.1029/2010TC002782>.
- WORTEL, M.J.R. & SPAKMAN, W., 2000. Subduction and slab detachment in the Mediterranean–Carpathian region. *Science*, 290, 1910–1917.
- ZANFERRARI, A., 1976. On the occurrence of a Permo-Scythian syncline outcropping in the middle Lesachtal along the Gailtal line (Carinthia, Austria). *Neues Jahrb. Geologie und Paläontologie - Monatshefte* 2, 109–117
- ZETTER, R., DIMTER, A., 1992. Palynostratigraphische Untersuchungen oberkretazischer Sedimente des Krappfeldes (Kärnten). *Mitt. Gesellschaft der Geologie- und Bergbaustudenten in Österreich*, 38, 175–183.
- ZETTER, R., HOFMANN, C.-C., 2001. New aspects of the palynoflora of the lowermost Eocene (Krappfeld Area, Carinthia). In: Piller, W.E., Rasser, M.W. (eds.), *Paleogene of the Eastern Alps*, Österr. Akad. Wiss. Schriftenr. Erdwiss. Komm. 14, 473–507.
- ZWINGMANN, H. & MANCKTELOW, N., 2004. Timing of Alpine fault gouges. *Earth. Planet. Sci. Lett.* 223, 415–425.



Field Trip Post-Ex-2

Latest Jurassic to Early Cretaceous evolution in the central Northern Calcareous Alps

OLIVER KRISCHE¹, JACEK GRABOWSKI², LÁSZLÓ BUITOR³ & HANS-JÜRGEN GAWLICK⁴

¹ Technisches Büro für Geologie DI Dr. mont. Thomas Unterweissacher, Regio Tech 1, 6395 Hochfilzen, Austria.

² Polish Geological Institute, National Research Institute, Rakowiecka 4, 00-975 Warszawa, Poland.

³ University of Pécs, Department of Geology and Meteorology, 6 Ifjúság útja, 7624 Pécs, Hungary.

⁴ Montanuniversitaet Leoben, Department of Applied Geosciences and Geophysics, Petroleum Geology, Peter-Tunner-Strasse 5, 8700 Leoben, Austria.

Abstract

This field trip will provide new insights in the latest Jurassic to Early Cretaceous depositional history of the central Northern Calcareous Alps based on new data from: biostratigraphy, sedimentology (e.g., facies, component analysis), biogeography, geophysics (e.g., magnetic stratigraphy, magnetic susceptibility, gamma ray spectrometry), and geochemistry from a basinal perspective. Starting in the latest Jurassic we will see deep-water *Calpionella* limestones with intercalated mass transport deposits and turbidites made of shallow-water material from a contemporaneously growing carbonate platform, in parts mixed with older components derived from the Late Permian to earliest Early Triassic Alpine Haselgebirge (Alpine Haselgebirge Mélange). Backstepping of this platform is manifested by a fining upward-trend in the sedimentological record of the age-equivalent basinal sedimentary rocks. The drowning of this platform started in the Middle Berriasian and the final drowning is dated as Late Berriasian. Onset of platform drowning in the Middle Berriasian resulted in the basin in starvation, increasing siliciclastic input, and an isotope excursion. Late Berriasian to Late Valanginian deposition is characterized by marly deposition with intercalated turbidites containing contemporaneous calcareous litho- and bioclasts and siliciclastic material. Still in the Late Valanginian intense redeposition from the hinterland started and mass transport deposits with e.g., components from the obducted Triassic-Jurassic Neotethys-Ocean floor were deposited. Sea-level changes triggered in the timespan Middle/Late Berriasian to Middle Aptian (basin is filled) the depositional history, mass transport deposits occur during lowstand phases. We will present this history on base of a multi-method approach with a lot of additional results regarding e.g., the Jurassic/Cretaceous-boundary, the Early Cretaceous geodynamic history of the Eastern Alps in one of the most prominent areas of the Northern Calcareous Alps: the Salzburg Calcareous Alps.

1 Introduction

During this field trip in one of the geologically most classical areas of the world, the central Northern Calcareous Alps as part of the Eastern Alps (Fig. 1) we will visit locations documenting the whole latest Jurassic (Late Tithonian) to Early Cretaceous (Middle Aptian) depositional history in basinal sequences.

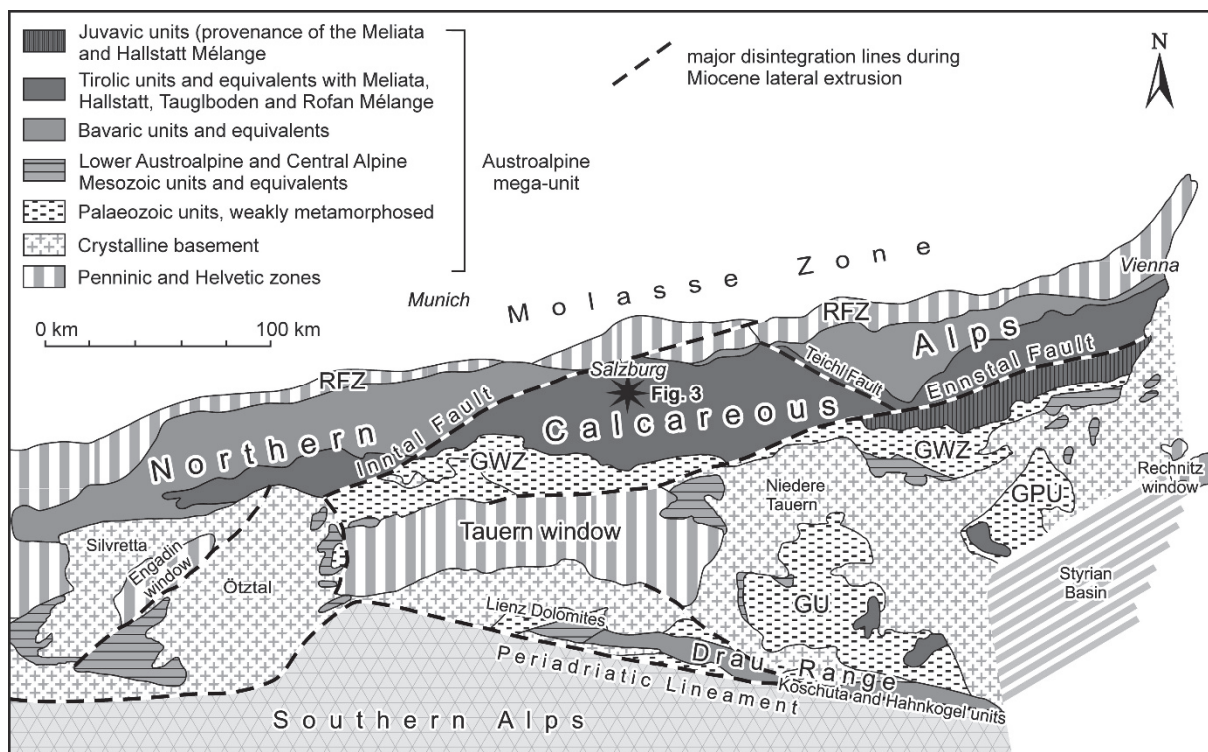


Fig. 1: Tectonic sketch map of the Eastern Alps and field trip area, indicated by an asterisk (compare Fig. 2). After Tollmann (1977) and Frisch & Gawlick (2003). GPU Graz Palaeozoic Unit; GU Gurktal Unit; GWZ Greywacke Zone; RFZ Rhenodanubian Flysch Zone.

Until today there is little consensus on the Late Jurassic to Early Cretaceous geodynamic history of the Northern Calcareous Alps. One crucial problem is the still in cases poorly known stratigraphic and facies evolution of the sedimentary sequences, very often only preserved as pebbles in mass transport deposits. However, in the last few years and still ongoing is progress in e.g.,

1. age dating, lithology, microfacies, geochemical and petrophysical characteristics, and magnetic stratigraphy of the latest Jurassic to Early Cretaceous sedimentary sequences,
2. understanding the history of lost oceanic domains, mainly based on pebble and clast analysis,
3. understanding the geodynamic processes in the Western Tethyan realm and timing of the polyphase thrusting processes in the Northern Calcareous Alps.

It is out of our scope to give in this field trip guide a historical overview about the different views and interpretations during the history of investigations. Therefore only a brief review is given in the description of the formations will be visited and, in addition, several remarks to the discussed topics described in the different chapters. For the wealth of literature about the Northern Calcareous Alps until 1995 see TOLLMANN (1976a, b, 1985) and PLÖCHINGER (1980, 1995). A summary about the different nappe concepts is given in FRISCH & GAWLICK (2003), and MISSONI & GAWLICK (2011a, b). Crucial for the understanding of the Mesozoic geodynamic history of the Northern Calcareous Alps is a restoration of the palaeogeography before the tectonic motions in the frame of the Neogene lateral tectonic extrusion of the Eastern Alps (RATSCHBACHER et al., 1991; LINZER et al., 1995; PUEYO et al., 2007).

2 Latest Jurassic to Early Cretaceous stratigraphy and formations

For definition and detailed description of the Jurassic formations (Fig. 2) see GAWLICK et al. (2009). The formations which will be visited during this field trip were deposited in the Tauglboden Basin (e.g. SCHLAGER & SCHLAGER, 1969, 1973; compare KRISCHE, 2012 who discussed for the Leube quarry a provenance from the southern part of Trattberg Rise) or Tauglboden-Rossfeld Basin, even the Rossfeld Basin has a larger extension to the south. The Tauglboden Basin was formed in Early Oxfordian times as a trench-like basin in front of the Trattberg Rise representing the frontal part of the advancing upper Tirolic nappe (FRISCH & GAWLICK, 2003). Later, in the Late Oxfordian compression moved to the north forming the Brunnwinkl Rise (Fig. 2). From this time onwards the Tauglboden Basin became an isolated basin between two topographic highs on which a shallow-water carbonate platform start to grow from Early Kimmeridgian onwards (Plassen Carbonate Platform; Fig. 2). During the Kimmeridgian to Early Tithonian sediment supply from the platforms into the Tauglboden Basin was rather low. The situation changed with the extensional collapse of the Trattberg Rise from the Early Tithonian onwards which gave way for the Plassen Carbonate Platform in the south to shed carbonate into the Tauglboden Basin to the north. Latest Jurassic (Late Tithonian) to earliest Cretaceous (Middle Berriasian) deposition in the Tauglboden Basin was controlled by this carbonate platform evolution in a highly tectonically active regime. These Tithonian tectonic motions are interpreted by MISSONI & GAWLICK (2011a) as expression of mountain uplift and unroofing. This led in the field trip area, situated to the north, to extension, e.g. expressed in the collapse of the Trattberg Rise and the advancing Haselgebirge Mélange from a more southern palaeogeographic position (Fig. 2). The final drowning of the Plassen Carbonate Platform in the Late Berriasian gave way for an increasing siliciclastic influx from the south from Middle/Late Berriasian times onwards. This siliciclastic influx was mainly controlled by sea-level changes and decreasing tectonic activity during the more or less whole Early Cretaceous. In the Late Berriasian resedimented arenitic beds with calcareous shallow-water clasts within the basinal sequence show the influence of a newly evolving carbonate producing area in the south in a very narrow time span. Successively the Tauglboden Basin (now the Tauglboden-Rossfeld Basin or Rossfeld Basin) became filled, mainly with marls and mixed carbonatic-siliciclastic material, but still a Late Berriasian to Late Valanginian shallow-water area (carbonate-ramp) to the south influenced parts of the basin with resedimented calcareous material. Deposition ended in the Middle Aptian. “Mid-Cretaceous” tectonic motions started slightly later and became sealed by the Late Cretaceous Gosau sedimentary cycle.

In former interpretations the Rossfeld Basin as continuation of the Late Jurassic Tauglboden Basin should be a newly formed Early Cretaceous flysch basin in a migrating foredeep in front of advancing Juvavic nappes (FAUPL & TOLLMANN, 1979; TOLLMANN, 1985; FAUPL & WAGREICH, 2000; NEUBAUER et al., 2000; FRANK & SCHLAGER, 2006). The sedimentation in the basin should have been terminated by the overthrust of these nappes, documented e.g. by the Hallstatt outliers on top of the Rossfeld Formation type-locality. By this interpretation mass-flow deposits, intercalated in calcareous sandstones and cherty limestones of the upper Rossfeld Formation should contain the complete component spectrum of the arriving Juvavic nappes (e.g., PESTAL et al., 2009) as documented in the different Jurassic basins. However, new results on the uninvestigated carbonate components in these mass flows of the type locality and elsewhere (e.g., MISSONI & GAWLICK, 2011b; KRISCHE, 2012, KRISCHE et al., 2014; KRISCHE & GAWLICK, 2015) show only different Late Jurassic to Early Cretaceous shallow-water clasts from the Plassen Carbonate Platform sensu stricto, their drowning sequence, the following Early Cretaceous basinal sediments, and contemporaneous shallow-water clasts derived from an unexplored source in the hinterland beside the already known siliciclastic, volcanic, ophiolitic components (POBER & FAUPL,

1988; FAUPL & POBER, 1991; SCHWEIGL & NEUBAUER, 1997a, b; von EYNATTEN et al., 1996; von EYNATTEN & GAUPP, 1999; FAUPL & WAGREICH 2000), and radiolarite clasts from the Neo-Tethys ocean floor and matrix radiolarites from the ophiolitic mélange (KRISCHE et al., 2014). Triassic-Jurassic components from the Hallstatt Zone (Hallstatt and Pötschen Limestones) or Triassic shallow-water carbonate components of the Upper Tirolic Berchtesgaden (formerly a Juvavic) unit as well as components of the Alpine Haselgebirge are completely absent. Only in few cases not facies indicative clast of the uppermost Werfen to lowermost Gutenstein Formations may occur.

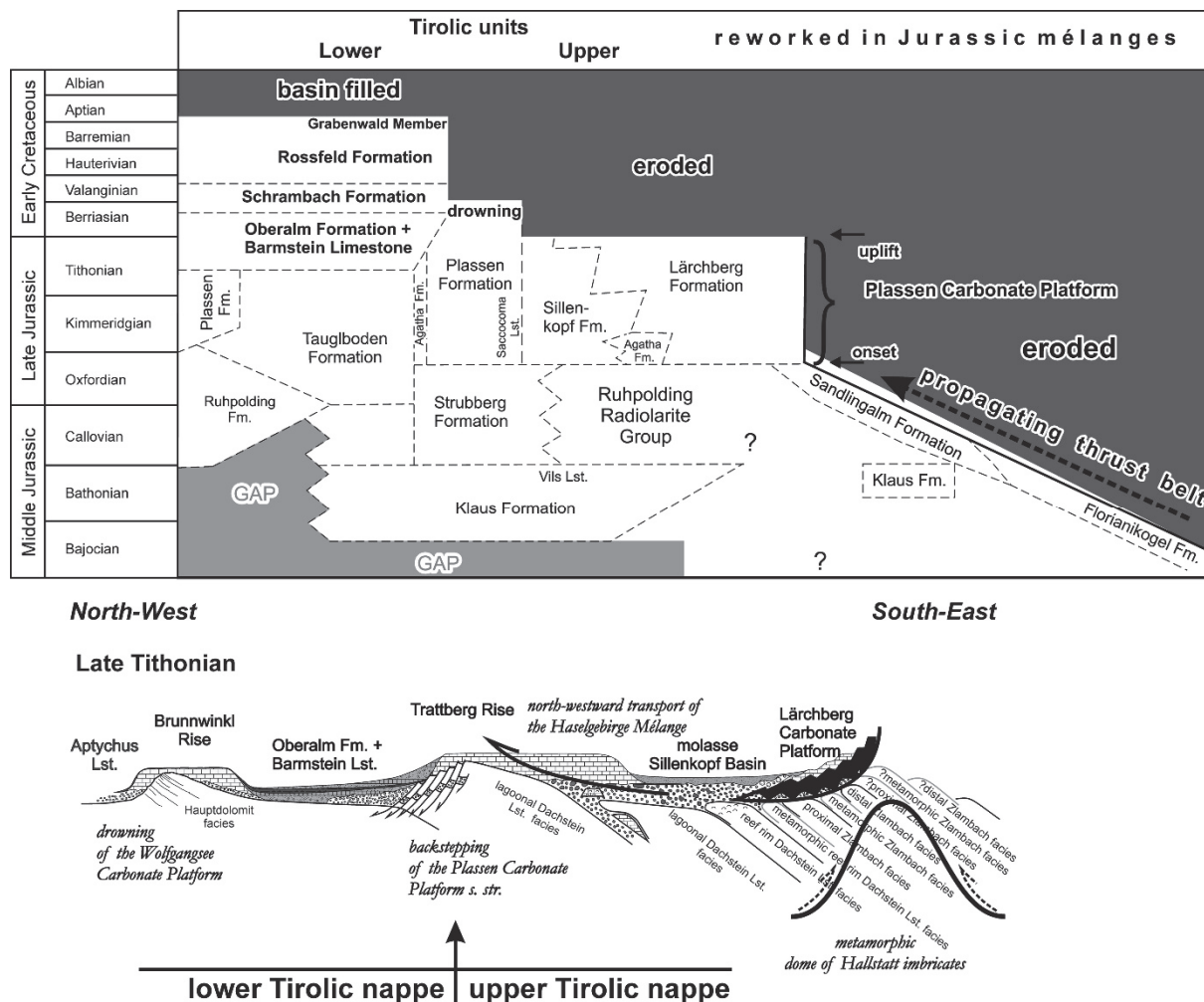


Fig. 2: A) Middle Jurassic to Early Cretaceous stratigraphy of the central Northern Calcareous Alps with an overview of the common formation names, simplified after MISSONI & GAWLICK (2011a). Late Jurassic and Early Cretaceous formation names which will be visited during the field trip are written in bold letters. B) Simplified Late Tithonian basin and rise configuration (after MISSONI & GAWLICK 2011a). The boundary between the lower and the upper Tirolic nappe is the Trattberg Rise, formed in Early Oxfordian times.

Oberalm Formation + Barmstein Limestone: In the Late Jurassic (Middle-Late Tithonian) to Early Cretaceous (Middle Berriasic) Oberalm Formation (LIPOLD, 1854; for complete history and definition see GAWLICK et al., 2009) occur intercalated coarse-grained resediments (mass transport deposits and turbidites) from the Plassen Carbonate Platform, named Barmstein Limestones (GÜMBEL, 1861). The overall depositional trend of the Oberalm Formation is fining upward (MISSONI & GAWLICK, 2011a, b). A special type of Barmstein Limestones was deposited in the latest Tithonian: beside reworked

material from the shallow-water area of the Plassen Carbonate Platform components of the Late Permian Haselgebirge appear (Fig. 2 for explanation). This type of mass transport deposit was named by PLÖCHINGER (1974) as “Tonflatschenbreccia” with its type area in the Leube quarry (see below).

In the upper Oberalm Formation widespread a microfacies and lithological change can be observed between the late Early Berriasian and the Middle Berriasian. Deposition of the more or less variegated, purple to reddish, siliceous to slaty marly limestones of roughly Middle Berriasian age (or late Early Berriasian age; Gutratberg Member of the Oberalm Formation: KRISCHE et al., 2013) is the basinal expression of the stepwise demise of the Plassen Carbonate Platform due to the increasing siliciclastic input. Carbonate production of the Plassen Carbonate Platform decreased since the late Early Berriasian and resulted in its final drowning in the Late Berriasian (GAWLICK & SCHLAGINTWEIT, 2006).

Schrambach Formation: After the final drowning of the Plassen Carbonate Platform in the Late Berriasian (GAWLICK & SCHLAGINTWEIT, 2006) and the rapid decrease of shallow-water carbonate production in basinal areas condensed red marls were deposited (Gutratberg Member as topmost part of the Oberalm Formation: KRISCHE et al., 2013). Above the Gutratberg Member and intercalated in the marls of the typical Schrambach Formation (Late Berriasian to Late Valanginian) first coarse-grained arenitic turbidites were deposited (KRISCHE & GAWLICK, 2010). The Schrambach Formation is mostly developed as a marl and calcareous marl succession, but also resedimented limestone beds consisting of shallow-water material within the marly sequence can be observed.

The age range of the Schrambach Formation (LILL v. LILIENBACH, 1830) is different in different areas of the Northern Calcareous Alps (TOLLMANN, 1976a, 1985 with references therein). A former estimated onset of the Schrambach Formation in the lower Early Berriasian in the type area cannot be confirmed. At the type locality, the Schrambachgraben northwest of the village Kuchl the age range of the Schrambach Formation is Late Berriasian to Early Valanginian (BOOROVÁ et al., 2015 with references therein). In the Leube quarry reference section the Schrambach Formation has an age range of latest Early Berriasian to Late Valanginian (KRISCHE et al., 2013 and herein). The transition between the underlying Oberalm Formation and the Schrambach Formation should be gradual in the type section and no distinct and/or essential lithological changes are observed in the lower horizons of the Schrambach Formation compared with those of the topmost part of the Oberalm Formation except a change in the occurrence and quantity of calcareous dinoflagellates (BOOROVÁ et al., 2015). Therefore also in the youngest study of BOOROVÁ et al. (2015) the change from the Oberalm Formation to the Schrambach Formation is placed at the Middle/Late Berriasian boundary (compare RASSER et al., 2003).

In contrast to the type-locality Schrambachgraben in the Leube quarry to the north or the Weitenau area to the east a significant lithological change between the Oberalm and the Schrambach Formations is observed: A microfacies and lithological change is between Middle and Late Berriasian. In this time interval the carbonate content decreases and the fine-grained siliciclastic content increases permanently with detrital quartz, apatite and garnet becoming more frequent (KRISCHE et al., 2013). Coarse-grained limestone beds above the Gutratberg Member and below the Late Berriasian marly limestone succession (BUJTOR et al., 2013) belong to the basal Schrambach Formation. These turbidite beds in the Leube succession may correspond to the sandy limestones layers in the type section Schrambachgraben slightly above the boundary between the Oberalm and the Schrambach Formation (BOOROVÁ et al., 2015), even such sandy limestones layers with resediments occur in different horizons in the Schrambach Formation (KRISCHE et al., 2013).

However, a characteristic change in the lithology or a direct biostratigraphic proof for the onset of the Schrambach Formation in the Late Berriasian is still missing in the type section. In addition, MISSONI & GAWLICK (2011b) dated the lower part of the Schrambachgraben section by coccolithophorid taxa as Late Berriasian (Middle Berriasian in BOOROVÁ et al., 2015) and attributed also this part of the section to the Schrambach Formation, meaning that the Gutratberg Member and the coarse-grained turbidites are situated below the Schrambachgraben section and covered by dense vegetation or the road. Only magnetostratigraphy of the type section may clarify this open problem.

Rossfeld Formation: In the Early Cretaceous (Valanginian to Aptian: TOLLMANN, 1976a; OBERHAUSER, 1980; PLÖCHINGER, 1990; KRISCHE et al., 2014) Roßfeld Formation (LILL v. LILIENBACH, 1830) and equivalents (Lackbach beds: DARGA & WEIDICH, 1986) several levels of oligo- to polymictic conglomerates, coarse-grained breccias and arenitic turbidites occur. The until recent times commonly accepted interpretation of the Early Cretaceous geodynamic evolution of the Northern Calcareous Alps is a convergent regime mirrored by the coarsening-upward depositional trend in the Late Valanginian to Early Aptian Rossfeld Formation (FAUPL & TOLLMANN, 1979; DECKER et al., 1987; LEISS, 1992). In this scenario the Rossfeld cycle ended with the overthrust of the Tirolic nappe by the Juvavic nappes (e.g., PLÖCHINGER, 1968; TOLLMANN, 1976a, b; SCHWEIGL & NEUBAUER, 1997a, b; SCHORN & NEUBAUER, 2011). The main argument for the overthrust of the Juvavic nappes over the Tirolic nappe are the huge Hallstatt Limestone blocks in the Rossfeld Formation type area, which should rest in the Rossfeld Formation (TOLLMANN, 1976a with reference therein). This view could not be confirmed by reinvestigation of the mass transport deposits and blocks in the type area by MISSONI & GAWLICK (2011b). The Hallstatt Limestone blocks rest tectonically transported (younger than “Mid-Cretaceous”) on top of the Rossfeld Formation. Furthermore, the highest part of the Rossfeld Formation at the type section is Barremian and not Aptian, meaning that parts of the Rossfeld Formation were eroded before the emplacement of the Hallstatt Limestones. In addition, components of Hallstatt Limestones (or other Middle - Late Triassic pebbles) in the various breccia layers of the Rossfeld Formation indicating an arrival of “Juvavic nappes” do not occur.

However, a detailed and systematic description of the very heterogeneous component spectrum in the Rossfeld Formation in a wider scale was until recent times (KRISCHE, 2012) not carried out. Earlier investigations focused on the biostratigraphic age dating of the Rossfeld Formation or the description of some specific components (e.g., KÜHNEL, 1929; WEBER, 1942; DEL-NEGRO, 1949; 1983; PICHLER, 1963; DARGA & WEIDICH, 1986; IMMEL, 1987; SCHWEIGL & NEUBAUER, 1997a). In contrast to the un-investigated radiolarite and carbonate pebbles in the mass-transport deposits, the other components from the ophiolite suite like dolerites, mafic volcanites, intermediate/basic magmatites, ultrabasic rocks and serpentinites were well investigated (e.g. von EYNATTEN & GAUPP, 1999). In addition, the typical heavy minerals like chromium spinel, hornblende, green calcium-rich amphiboles, and brown amphiboles indicating an ophiolitic source area were well described (e.g. WOLETZ, 1963; FAUPL & POBER, 1991; SCHWEIGL & NEUBAUER, 1997a; VON EYNATTEN & GAUPP, 1999). First microfacies studies and biostratigraphic age dating of the radiolarite and carbonate components in the different mass transport deposits in the Rossfeld Formation were carried out by MISSONI & GAWLICK (2011a, b) in the type area of the Rossfeld Formation. A detailed component analysis of the mass transport deposits from all different stratigraphic levels of the Rossfeld Formation in a wider scale was carried out by KRISCHE (2012), KRISCHE et al. (2013, 2014), and KRISCHE & GAWLICK (2015).

The different fining- and coarsening-upward trends in the Rossfeld Basin fill can be best explained by sea-level fluctuations and decreasing tectonic activity in the Jurassic orogen in an underfilled foreland basin.

3 The Field Trip

In Figure 3 the localities which will be visited during this field are shown. In the Leube quarry near the village Gartenau south of Salzburg we will study the latest Jurassic to Late Valanginian sedimentary succession: Oberalm Formation + Barmstein Limestone, Schrambach Formation, and lower part of the Rossfeld Formation. In the Rossfeld area (Germany), type-locality of the Rossfeld Formation, we will study the Late Valanginian to Barremian part of the Rossfeld Formation. In the central Weitenau area we will visit the latest Barremian to Middle Aptian Grabenwald Member of the Rossfeld Formation. The Grabenwald Member is the youngest part of the Rossfeld Basin fill.

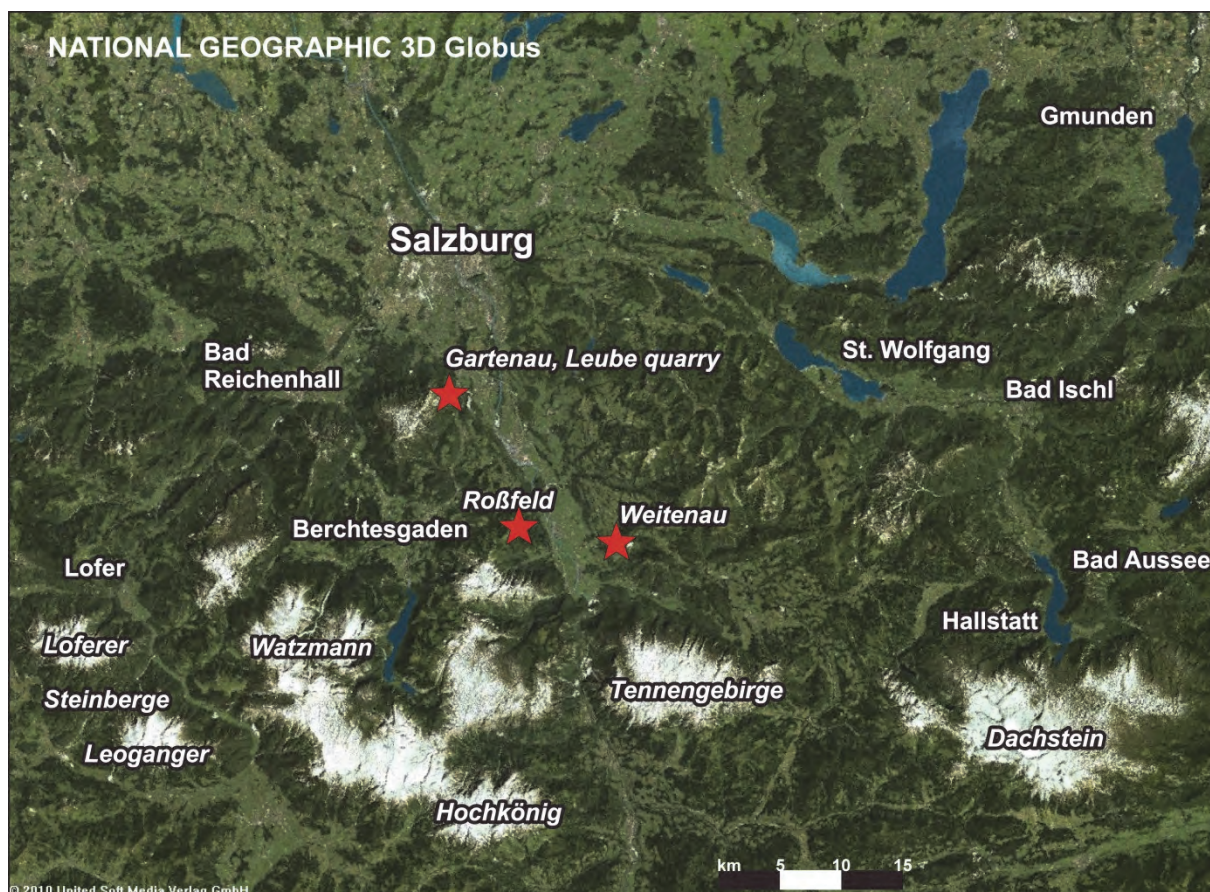


Fig. 3: Satellite image of the central Northern Calcareous Alps, showing the localities which will be visited during this field trip (red stars).

3.1 Gartenau: Leube quarry

The Leube quarry (Fig. 4, 6), where the latest Jurassic to Early Cretaceous sedimentary rocks are exploited for cement production, is located in the central Northern Calcareous Alps south of Salzburg, near to the villages of Gartenau and St. Leonhard. In this quarry, a complete and only slightly disturbed sedimentary succession from the higher Oberalm Formation + Barmstein Limestone to the Roßfeld Formation is well preserved (Fig. 5).

The Leube quarry provides one of the best preserved and exposed uppermost Jurassic to Early Cretaceous sedimentary successions in the central Northern Calcareous Alps. The new calpionellid data, in combination with ammonite, microfacies and lithology analyses, form the basis for a detailed, revised biostratigraphy of this time interval (KRISCHE et al., 2013) and gave rise for further very detailed investigations. Additionally, the investigation of hemipelagic basinal sedimentary sequences is very important for a better understanding of the Late Jurassic to Early Cretaceous evolution of the central Northern Calcareous Alps and also allows new insights into the development of the Late Jurassic to Early Cretaceous shallow-water carbonate platform at the southern rim of the basin (Plassen Carbonate Platform *sensu stricto*). The remarkably rich Late Berriasian ammonite fauna (BUJTOR et al., 2013) reveals strong biogeographic connections toward the Tethyan faunas along the northern margin of the Tethys; many are reported for the first time from Austria (Fig. 11). The presented results contribute to an improvement of the palaeogeographical and geodynamical model of the Northern Calcareous Alps for this time span.

Former and recent investigations at the Leube quarry section

The history of investigations until 2013 is described in detail in KRISCHE et al. (2013). Therefore we see no need to write a new historical overview. We take in general the text from KRISCHE et al. (2013), slightly modified and added: In the last hundred years the classic profile in the northern active Leube quarry was studied several times. The first indication for the presence of ammonites was reported by FUGGER (1907) in "Schrammbach" and Rossfeld beds in the vicinity of the villages of St. Leonhard, Gartenau and Götschen. WEBER (1942) referred the first ammonites (*Pseudothurmannia (Parahoplites) spinigera*) in the Schrambach and the Lower Rossfeld beds nearby the village Gartenau. OEDL (in: PLÖCHINGER, 1955) reported the occurrence of *Fuhriella michaelis* from the marly limestones of the open pit mine. From the underground mine PLÖCHINGER (1961) described the first lithological profile with Oberalm, Schrambach and Rossfeld beds. Mapping of PICHLER (1963) gave information about the lithology, sedimentology and the fossil content of the Schrambach beds. Their age was considered as Berriasian to Early Valanginian, based on ammonite biostratigraphy. PLÖCHINGER (1968) reported *Bochianites neocomiensis* and *Kilianella roubaudiana* from greenish-grey marls, indicating a Valanginian to Early Hauterivian age. PLÖCHINGER (in: MATURA & SUMMESBERGER, 1980) also referred findings of *Olcostephanus*, *Berriasella* and *Neolissoceras* from the quarry. First lithological and microfacies analyses around the Schneiderwald (Fig. 4) and the eastern part of the open pit were carried out by PLÖCHINGER (1974, 1976, 1977) who included calpionellid biostratigraphy in his investigations. IMMEL (1987) described a Late Hauterivian ammonite assemblage with *Oosterella kittli*, *Crioceratites (Crioceratites) nolani* and *Moutoniceras annulare* from sandy limestones (Rossfeld Formation) of the Köppelschneid (Fig. 4).

Starting from the 1990s, WEIDICH (1990), STEIGER (1992), BODROGI et al. (1996), REHÁKOVÁ et al. (1996), BOOROVÁ et al. (1999) and HRADECKÁ (2003) investigated profiles in the open pit mine and delivered litho- and biostratigraphical descriptions of the quarry, based on foraminifers, radiolarians, shallow-water organisms, calpionellids, dinoflagellates and aptychi. BOOROVÁ et al. (1999) and DORNER et al. (2009) mentioned very scarce occurrences of ammonites in their profiles.

Recent investigations were carried out by GAWLICK et al. (2005) in the area of the old, recultivated quarry south of today's open pit and by WAGREICH (2009) in the active Leube quarry. BUJTOR et al. (2013) investigated the ammonite assemblage of the active Leube quarry and described the occurring species palaeontologically and biostratigraphically. KRISCHE et al. (2013) presented a modern analysis of the Late

Tithonian to Valanginian Oberalm Formation + Barmstein Limestones and the Schrambach Formation with exact biostratigraphic ages. KRISCHE et al. (2014) analyzed and dated the exotic components from the mass transport deposits of the lowermost Rossfeld Formation. Ongoing studies deal with isotope stratigraphy (MAIER et al., 2013), magnetostratigraphy, gamma ray spectrometry, AMS studies, and geochemical analysis (GRABOWSKI et al., 2016a, 2017a, b) to enlighten the Early Cretaceous depositional history of the Western Tethyan realm.

During this field trip published results are combined with the recently obtained and still unpublished and here for the first time presented results.

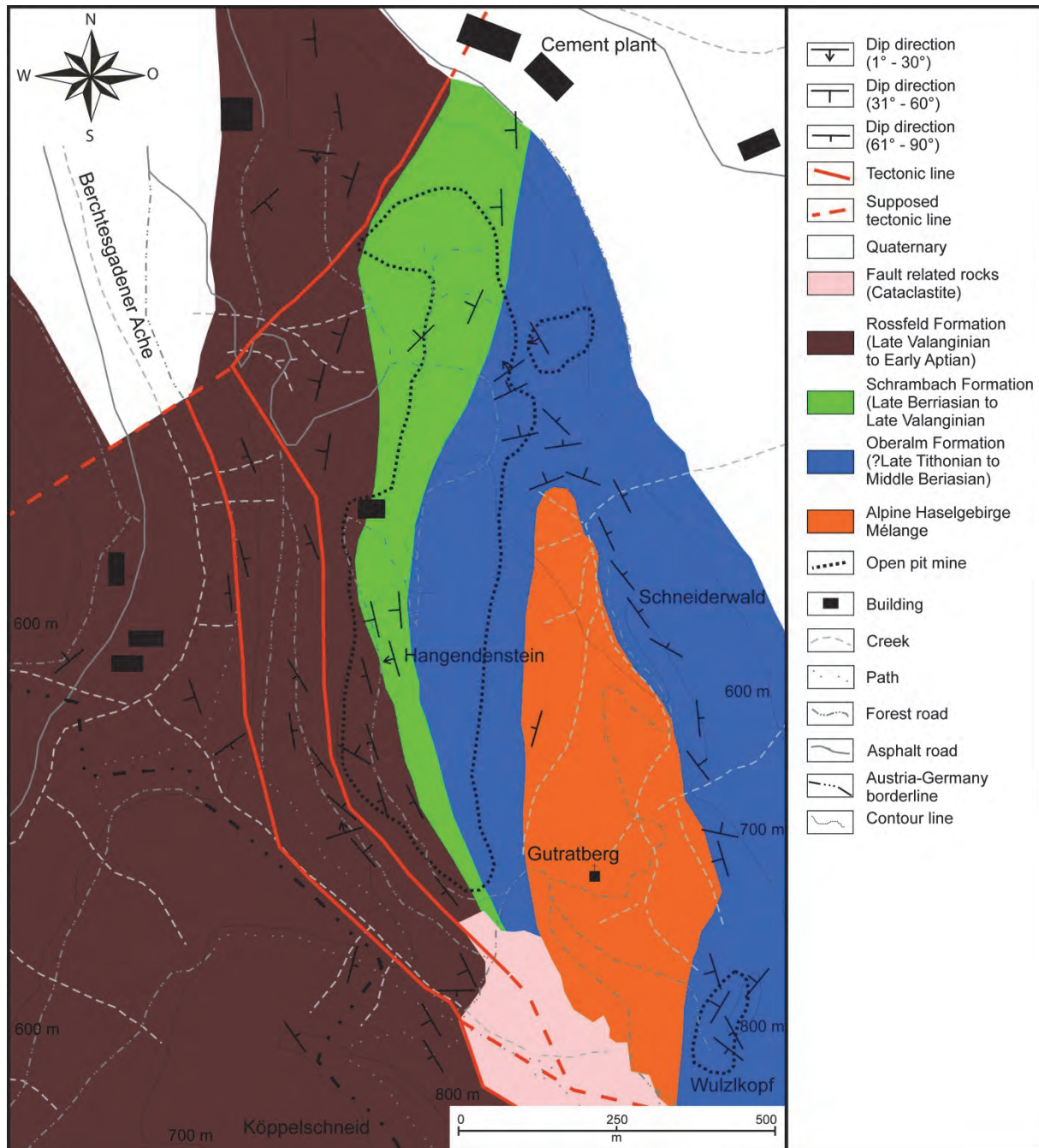


Fig. 4: Geological map of the Leube quarry and the surrounding area, after KRISCHE et al. (2013).

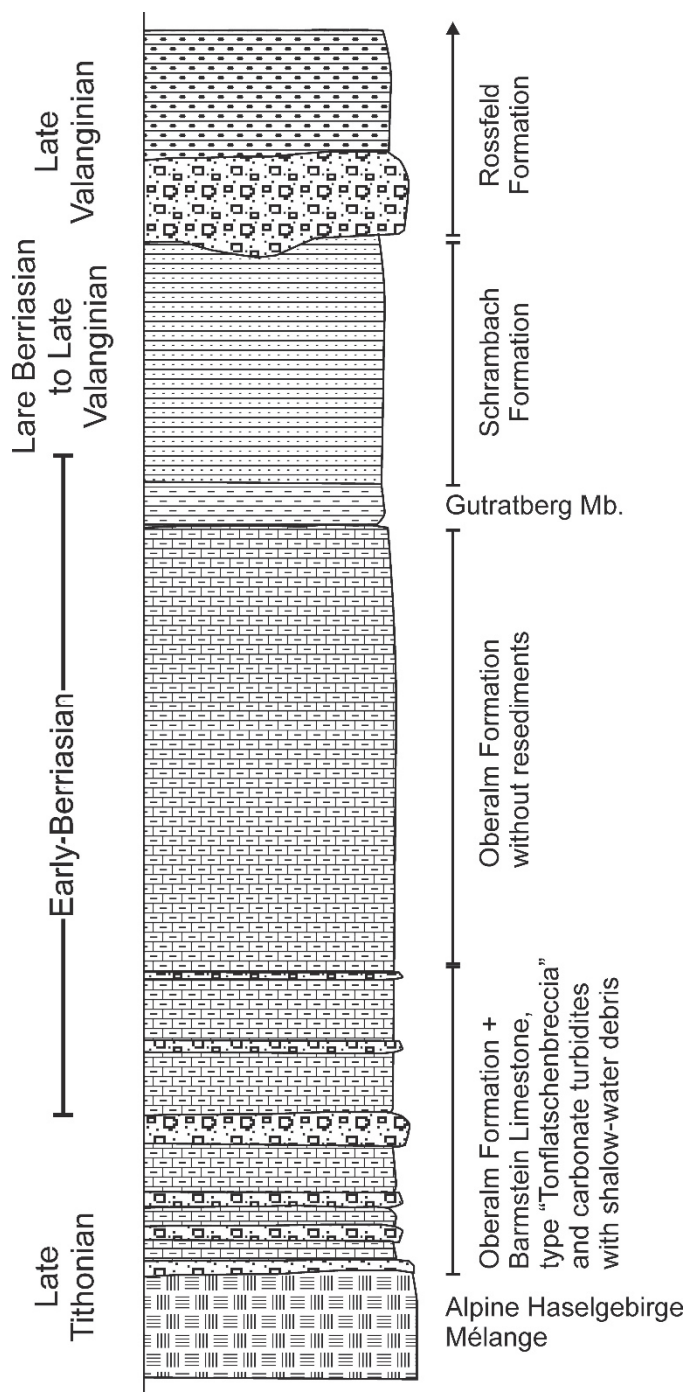


Fig. 5: Overall composite Leube quarry section with the standard lithostratigraphy modified after KRISCHE et al. (2013). Ages adapted according to the new definition of the Jurassic/Cretaceous boundary.

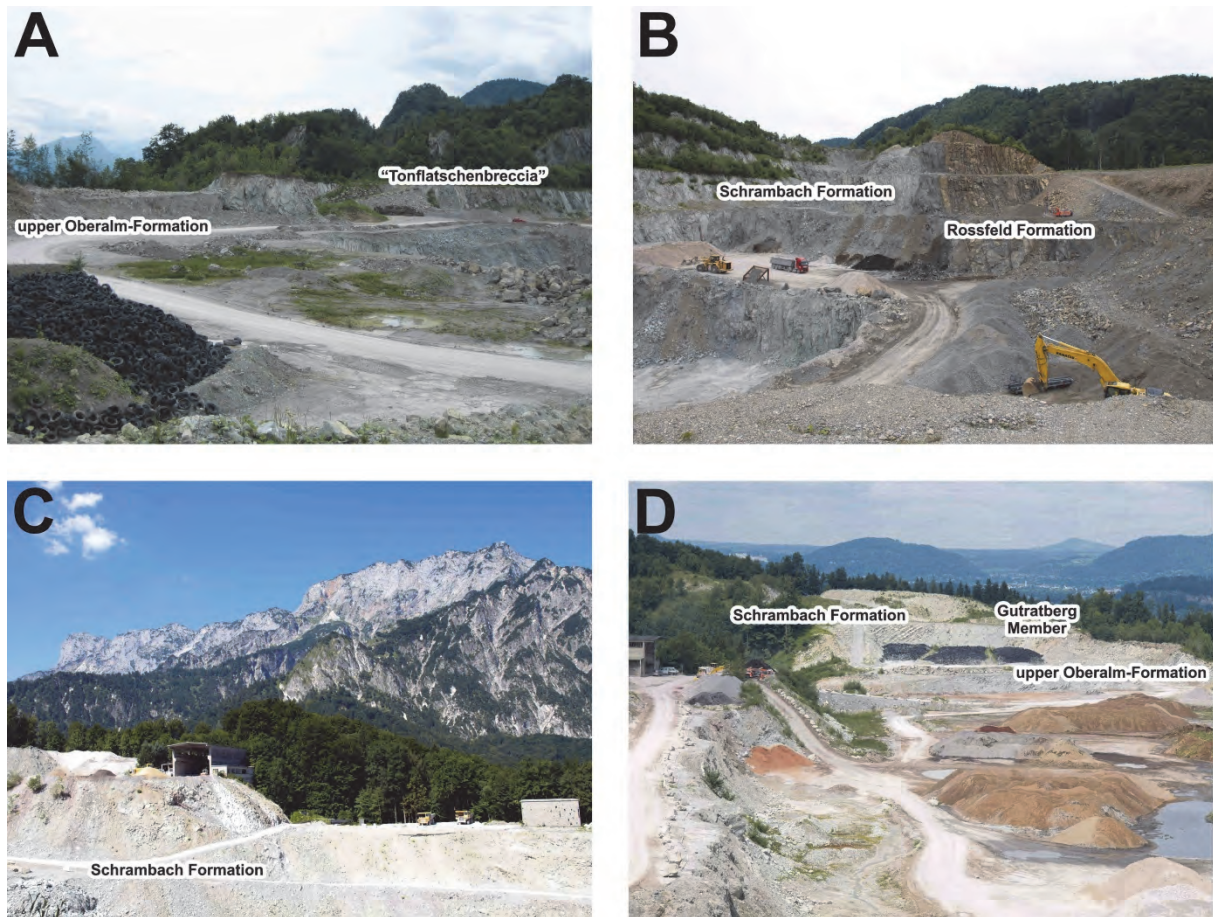


Fig. 6: Different views of the Leube quarry and formations which will be visited. Due to the fact of ongoing exploitation in the quarry the outcrop situation and available parts of the succession may change. A) Northwestern part of the quarry with the Early Berriasian part of the succession. B) Northern part of the quarry with the Early Berriasian (upper Oberalm Formation), the Middle Berriasian (Gutratberg Member of the Oberalm-Formation), and the Late Berriasian (Schrambach Formation). C) Eastern side of the quarry with the in details presented part of the succession for magnetostratigraphy, gamma ray spectrometry, AMS studies, and geochemical analysis. D) Southern part of the quarry with the transition from the Schrambach Formation to the Rossfeld Formation.

Oberalm Formation + Barmstein Limestone

Basal part: Barmstein Limestone: “Tonflatschenbreccia” (PLÖCHINGER, 1974)

A contact between the Alpine Haselgebirge Mélange or a huge Alpine Haselgebirge Mélange block with the overlying Barmstein Limestone with Haselgebirge components and *Calpionella*-limestones of the Oberalm Formation is outcropping in the Ottobau. Here the Oberalm Formation contains *Calpionella alpina* and *Crassicollaria* sp. (KRISCHE et al., 2013) and is Late Tithonian in age.

This is in accordance with the biostratigraphic results of a section to the south, in the so-called Schneiderwald-anticline (PLÖCHINGER, 1974, 1976). Here a roughly 50 m thick succession of the Oberalm Formation + Barmstein Limestone, type “Tonflatschenbreccia” is preserved (Fig. 7). According to GAWLICK et al. (2005) the age of practically the whole part of the succession is early Early Berriasian. A latest Tithonian age for the basal part of the succession cannot be excluded (compare PLÖCHINGER, 1976).

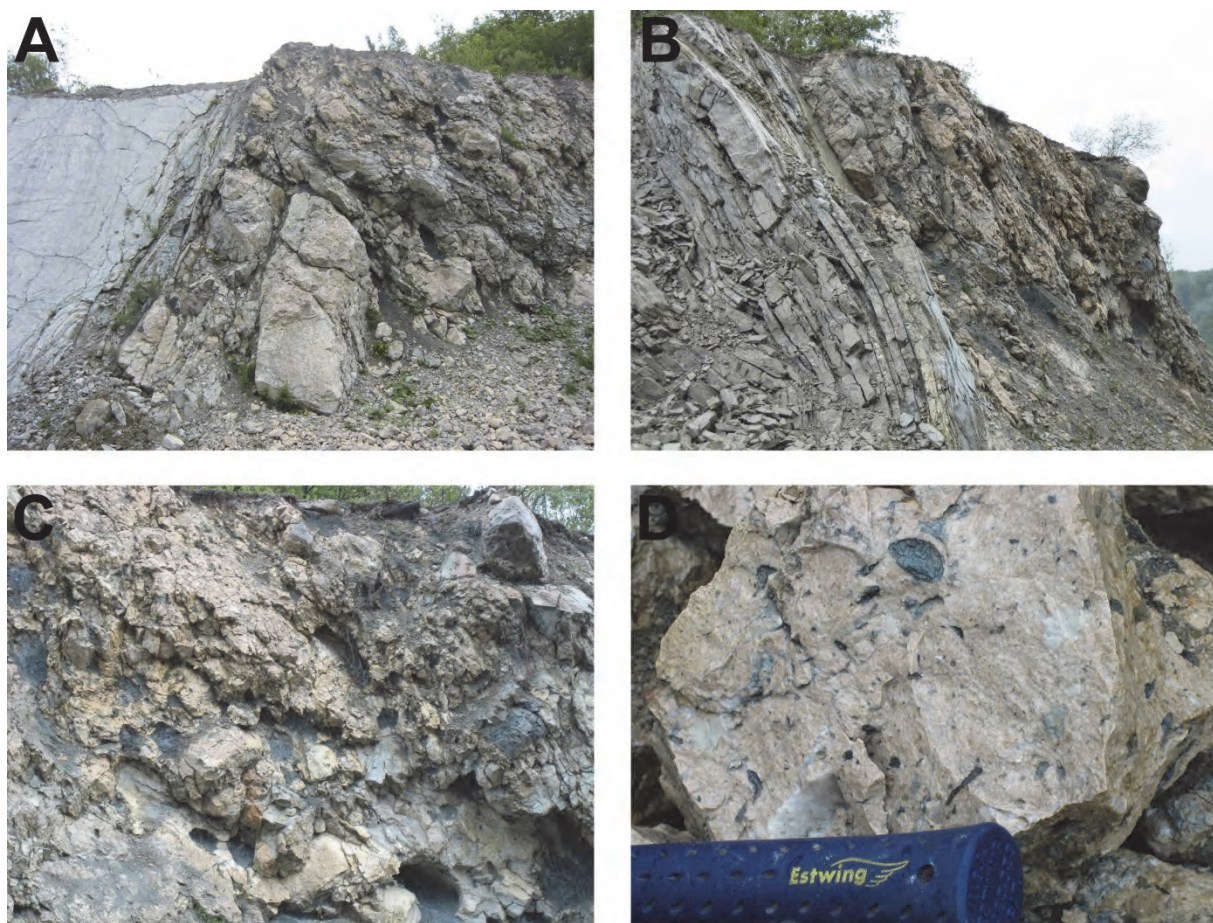


Fig. 7: “Tonflatschenbreccia” in the Leube quarry: mass transport deposit with shallow-water clasts from the Plassen Carbonate Platform s. str. and the Late Permian Alpine Haselgebirge Mélange. **A**) and **B**) Outcrop situation. **C**) and **D**) Details from the “Tonflatschenbreccia”.

In this part of the succession KRISCHE et al. (2013) described several depositional cycles starting with coarse-grained breccia layers at its base overlain by wacke- and packstones with fine-grained biotritus. The top of each cycle is represented by marly wackestones with radiolarians, “filaments” and calpionellids. Aside the different clasts which derive from the Alpine Haselgebirge Mélange several limestone lithoclasts occur: A) Radiolarian-spicula wackestones, B) Calpionellid-radiolarian wackestones, C) slope derived bio- und lithoclastic wacke- to floatstones, D) grainstones with pellets, D) bioclastic lagoonal wackestones. A heterogeneous Triassic clast spectrum as described by GAWLICK et al (2005) from other occurrences of the Barmstein Limestones was not detected in the Leube quarry.

More in the eastern part of the quarry, near the biotope the Jurassic/Cretaceous boundary is preserved in the Oberalm Formation. In the lower part of this section a poorly preserved and re-deposited *Micracanthoceras microcanthum* was referred (FRAU et al., 2016), which was originally described as *?Djurjuriceras* sp. from the “Tonflatschenbreccia” by BUJTOR et al. (2013) referring to the Late Tithonian Microcanthum Zone (Fig. 8). *Micracanthoceras microcanthum* occur together with *Calpionella alpina* and Crasicollarians, indicating the Late Tithonian age of this part of the succession. Ongoing studies will improve the age of this part of the section.



Fig. 8: Re-deposited *Micracanthoceras microcanthum* from the “Tonflatschenbreccia” (BUJTOR et al., 2013).

Upper part: Calpionellid-radiolarian wackestones with intercalated turbidites

Above the graded cycles follow a relative thick series of stratified greenish, marly limestones (radiolarian wackestones with rare calpionellids). They alternate with greenish-grey-brownish marls and contain intercalations of turbiditic radiolarian packstones. The occurrence of *Calpionella alpina* and Remaniellids prove the Early Berriasian age of the rocks.

Both the lithology and the microfacies change in the highest part of the Oberalm Formation (Fig. 9A). Red-green marls, marly limestones (wackestones with radiolarians, calpionellids and spicula) with coarser-grained turbiditic intercalations (packstones with shell fragments, sparite and micrite clasts) and radiolarian packstones occur. A conspicuous, stratified green marly limestone horizon of roughly one metre thickness is referred to as Portland cement bed (PLÖCHINGER, 1976: calpionellid-rich wackestone). In between thicker marl beds green-reddish fine-grained marly limestones (very fine-grained wackestones with some biotritus) occur. The variegated limestone-marl sequence is a characteristic feature within the highest part of the Oberalm Formation, recently defined as Gutratberg Member of the Oberalm Formation (KRISCHE et al. 2013).

Aside the Calpionellid biostratigraphy for the upper part of the Oberalm Formation below the Gutratberg Member (KRISCHE et al., 2013) an Early Berriasian age is also confirmed by following nannofossil assemblage (det. M. Báldi-Beke): *Conusphaera mexicana*, *Cyclagelosphaera margerelii*, *Haqius circumradiatus*, *Polycostella senaria*, *Watznaueria barnesae*, *Watznaueria Britannica*, *Watznaueria fossacincta*, and *Watznaueria manivitiae*. *Polycostella senaria* has the shortest range (Late Tithonian to Early Berriasian). *Haqius circumradiatus* is a typical Cretaceous form (from the Berriasian to Campanian). The range of *Conusphaera mexicana* (Tithonian to Aptian) and the absence of the Nannoconids confirm the age.

Schrambach Formation

The Gutratberg Member is followed by green-brown marls with plant debris and ammonite fragments. These rocks are defined as Schrambach Formation based on the lithological and microfacies change. A coarser alloclastic, cherty limestone bed (KRISCHE & GAWLICK, 2010) terminates the ammonite bearing beds. The marl beds on top are overlain by a well stratified limestone (pellets-sparite packstones with

foraminifera) and marl (marly wackestones with sparite and micrite clasts, calpionellids, filaments, spicula) succession with occasional ammonite fragments. The stratified limestone-marl succession is erosionally truncated by a coarse-grained conglomerate bed of the basal Rossfeld Formation. In general the Schrambach Formation consists of silty or cherty marls and alternating marl-limestone successions (Fig. 9B).

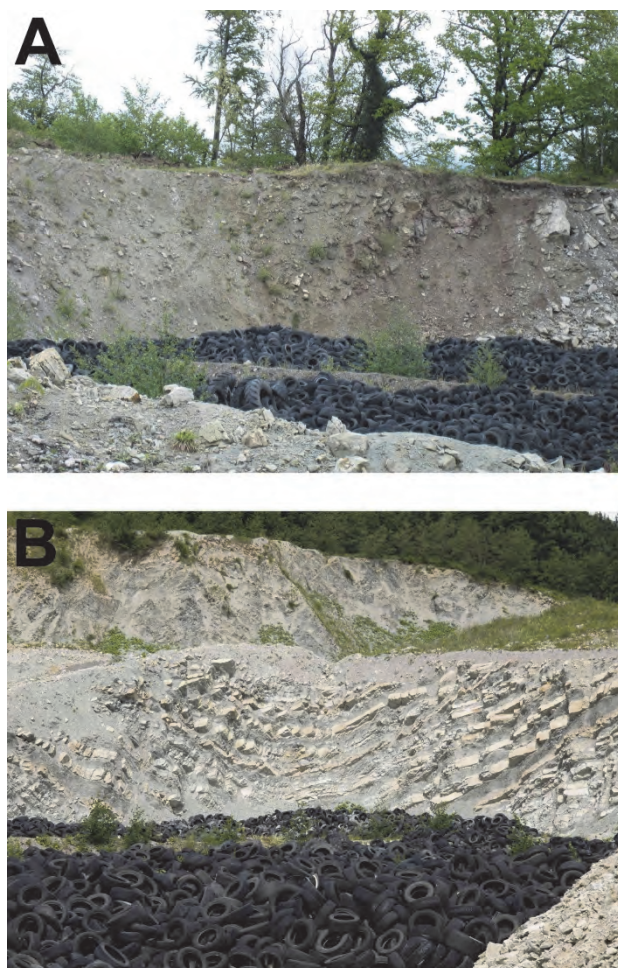


Fig. 9: A) Gutratberg Member of the Oberalm Formation and transition to the Schrambach Formation.
B) Late Berriasian Schrambach Formation.

Of special interest are the various ammonites found in the Late Berriasian part of the Schrambach Formation (BUJTOR et al., 2013), because Berriasian ammonite faunas are rarely reported from Austria (UHLIG, 1882; PLÖCHINGER in MATURA & SUMMESBERGER, 1980). From the marl and alternating marl-limestone part of the Schrambach Formation a Late Berriasian ammonite fauna was collected, which represents the Subthurmannia boissieri Zone. Subzonal division was impossible. The diverse ammonite fauna (Figs. 10, 11) has a Mediterranean character. Besides phylloceratid, lytoceratid and haploceratid ammonoids, a diverse olcostephanid, berriasiellid and neocomitid ammonite assemblage was determined including *Spiticeras cf. bulliforme*, *Spiticeras* div. sp., *Negrelliceras cf. negreli*, *Berriasella (Berriasella) calisto*, *Berriasella (Berriasella)* sp. aff. *picteti*, *Pomeliceras (Mazenoticeras)* sp. aff. *iovkovciense*, *Erdenella cf. isaris*, *Tirnovella cf. alpillensis*, *Fauriella boissieri*, *Fauriella donzei*, *Fauriella shipkokensis*, *Spiticeras* sp., and *Kilianella ex gr. chamalocensis*. Eight species are reported for the first time from Austria. This fauna provides a faunal link between the Mediterranean ammonite faunas from SE Spain, SE France, Bulgaria, and Crimea.

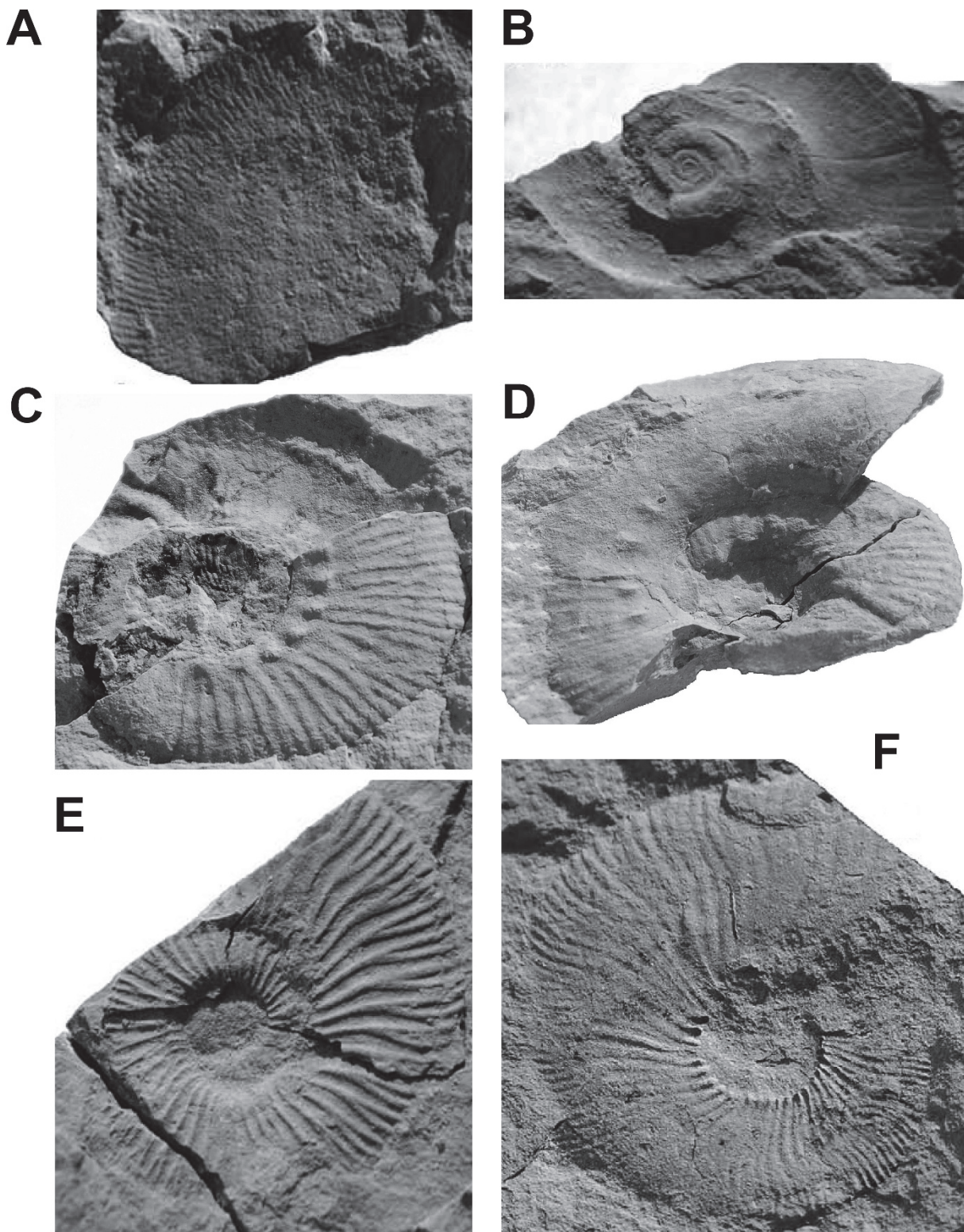


Fig. 10: Ammonites indicating a Tethyan fauna with lyto-, phyllo- and haploceratids, however the abundance of olcostephanid and neocomitid ammonites may refer shallower environments (after BUJTOR et al., 2013). **A)** *Euphylloceras cf. thetys*, **B)** *Lytoceras liebigi*, **C)** *Spiticeras bulliforme*, **D)** *Negrelliceras sp. aff. negreli*, **E)** *Berriasella calisto*, **F)** *Fauriella boissieri*. Not to scale - for dimensions see BUJTOR et al. (2013).

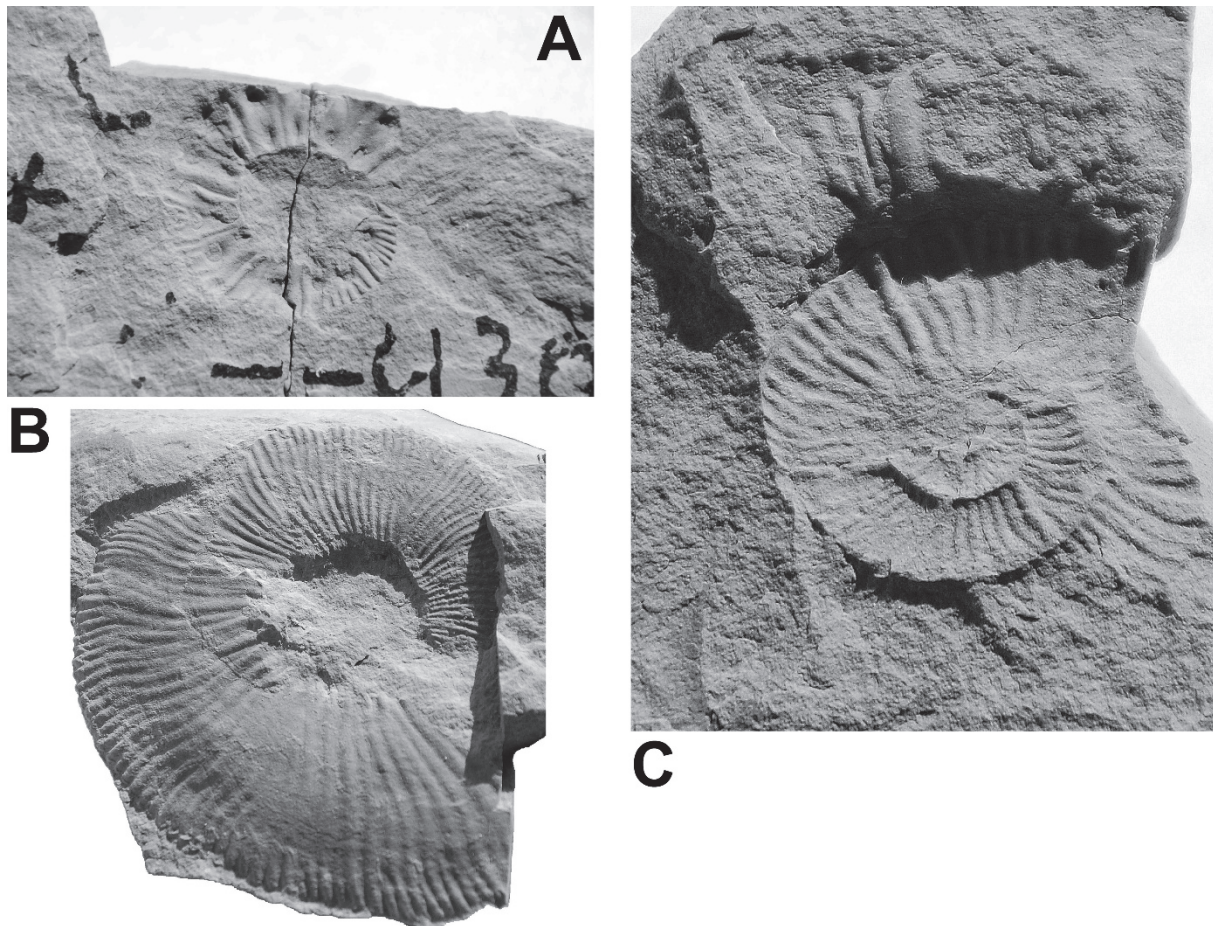


Fig. 11: Ammonites indicating important biogeographically connections toward westward (*Micracanthoceras microcanthum* (Fig. 8) and *Kilianella chamalocensis*) and eastward (*Fauriella shipkovenensis*, and *Pomeliceras (Mazenoticeras) iovkovciense*) along the northern margin of the Tethys. **A)** *Pomeliceras (Mazenoticeras) iovkovciense*, **B)** *Fauriella shipkovenensis*, **C)** *Kilianella chamalocensis*.

In contrast to the well dated lower part of the Schrambach Formation the upper part of the Schrambach Formation and its maximum age range below the Rossfeld Formation is rather poorly known. KRISCHE et al. (2013) dated in several sections the higher part of the Schrambach Formation as Early Valanginian based on Calpionellid associations. In several cases the mass transport deposits of the Rossfeld Formation overlie directly the limestone-marl succession of the Schrambach Formation with an erosional contact. In other cases the topmost part of the Schrambach Formation was not dateable with Calpionellids or ammonites. Under the circumstances that all ages directly obtained from the Schrambach Formation below the basal part of the Rossfeld Formation show Early Valanginian an Late Valanginian age for the topmost part of the Schrambach Formation could be only estimated for the type area. A Late Valanginian age for the mass transport deposits in the lower part of the Rossfeld Formation is proven in the Salzkammergut (Bad Ischl area; KRISCHE & GAWLICK, 2015) and the Rossfeld Formation type locality (see below).

Few samples from the Schrambach Formation directly below the mass transport deposits yielded poorly preserved and rare nannofossil assemblages. All samples were taken from sections in the western part of the quarry, today not anymore existing.

A Valanginian age could be determined by following nannofossil assemblage (det. M. Báldi-Beke): *Calcidcalathina oblongata*, *Cyclagelosphaera argoensis*, *Cyclagelosphaera margerelii*, *Micrantholithus*

obtusus, *Watznaueria barnesae*, *Watznaueria britannica*, *Watznaueria fossacincta*, *Zeugrhabdotus* cf. *cooperi*, and *Zeugrhabdotus embergeri*. *Calcicalathina oblongata* has the shortest range from the very early Valanginian (base of the petransiens ammonite zone) to the early Barremian. Other forms have longer age ranges but are in line: *Nannoconus steinmanni* (since Berriasian) and *Micrantholithus obtusus* (Berriasian to Aptian).

Another sample yielded following Valanginian (to Hauterivian) nannoplankton assemblage (det. M. Báldi-Beke): *Biscutum constans*, *Calcicalathina oblongata*, *Cyclagelosphaera argoensis*, *Cyclagelosphaera margerelii*, *Nannoconus steinmanni*, *Nannoconus kampfneri*, *?Rhagodiscus asper*, *?Sollasites horticus*, and *Watznaueria barnesae*. This nannoplankton assemblage cannot be older than Valanginian, because of the FO of *Calcicalathina oblongata* is in the lowermost Valanginian, at the base of the petransiens Ammonite zone.

An third nannofossil assemblage provided an Late Valanginian (to Early Hauterivian) age (det. M. Báldi-Beke): *Calcicalathina oblongata*, *Cyclagelosphaera argoensis*, *Cyclagelosphaera margerelii*, *Diazomatholithus lehmanii*, *Eiffellithus (Rothia) windii*, *Micrantholithus obtusus*, *Percivalia fenestrata*, *Watznaueria barnesae*, *Watznaueria britannica*, *Watznaueria fossacincta*, and *?Zeugrhabdotus* sp. *Eiffellithus (Rothia) windii* has a very short range in the Late Valanginian to Early Hauterivian and has its FO in the campylotoxus ammonite zone, and the LO is in the radiatus ammonite zone.

Based on this sample the open question of the maximum age range of the Schrambach Formation in the wider area is now solved. The Schrambach Formation has in the type region an age range from Late Berriasian to Late Valanginian.

Magnetostratigraphy, gamma ray spectrometry, AMS studies, and geochemical analysis

A total number of more than 150 oriented drill cores were collected from the roughly 130 m thick Berriasian interval of the Leube quarry section. Sampling covered the upper part of the Oberalm Formation (including Gutratberg Member) and the lower to middle(?) part of the Schrambach Formation (Fig. 12). The samples were demagnetized thermally in the Palaeomagnetic Laboratory of the Polish Geological Institute - National Research Institute. Magnetite was identified as principal magnetic mineral in grey limestones, while magnetization of red beds was related to hematite. Two components of natural remanent magnetization (NRM) were documented. The first component A with low unblocking temperatures (100–300° C) of normal polarity was quite dispersed. The second component B, identified in a temperature range between 350–550° C, is well clustered and revealed both normal and reversed polarities (Fig. 13). The component B is interpreted as primary. The palaeomagnetic vectors revealed NE-SW declination and moderate inclination (ca. 49°), indicating Berriasian palaeolatitude of around 30° N. Several normal and reversed magnetic intervals were correlated with magnetozones M17r (upper part of the Early Berriasian) to M14r (Berriasian/Valanginian-boundary). The lower part of the Schrambach Formation can be correlated with the magnetozones M17r to M16n (Fig. 14) which is consistent with biostratigraphic dating (KRISCHE et al., 2013; BUJTOR et al., 2013).

Our results show that remagnetization of Mesozoic rocks in the Northern Calcareous Alps (PUEYO et al., 2007) did not affect every sedimentary succession of the Tirolic units. Magnetic susceptibility indicates a long term increasing trend (Fig. 14) which is interpreted as manifestation of accelerating siliciclastic input from the hinterland in the south. This result is supported by gamma ray spectrometric measurements which show an increasing trend of K and Th content (Fig. 14). Definite increase of the

siliciclastic input took place in the lower part of M16n. The onset of more marly sedimentation in the lower part of M16n (lower part of *oblonga* calpionellid Subzone) can be well correlated with other sections in the Central Carpathians and the Western Balkan region (GRABOWSKI et al., 2013; 2016b) pointing to a regional event related probably to tectonic uplift or more likely a regression with subsequent sea-level lowstand resulting in increasing erosion of the mountain range at the southern peripheries of the Carpathian-Alpine realm. This would correspond to the sea-level curve of HARDENBOL et al. (1998). Th/U ratio, widely used as redox proxy, show large variations between the beds which might sharp contrasts in oxygenation conditions. A gentle decrease of Th/U ratio towards the top of M16n point to slight deterioration of oxygen availability in the upper part of M16n. High resolution carbon isotope ($\delta^{13}\text{C}$) curve reveals a well-defined second order changes between 0.8 and 1.3 ‰ which is in very good agreement with other magnetostratigraphically calibrated $\delta^{13}\text{C}$ Berriasian trends (see GRABOWSKI et al., 2016b).



Fig. 12: Sampling campaign in the Leube quarry, beds 1-25, lower part of the Late Berriasian. Boundary between magnetozones M16r and M16n is situated between points 11 and 12.

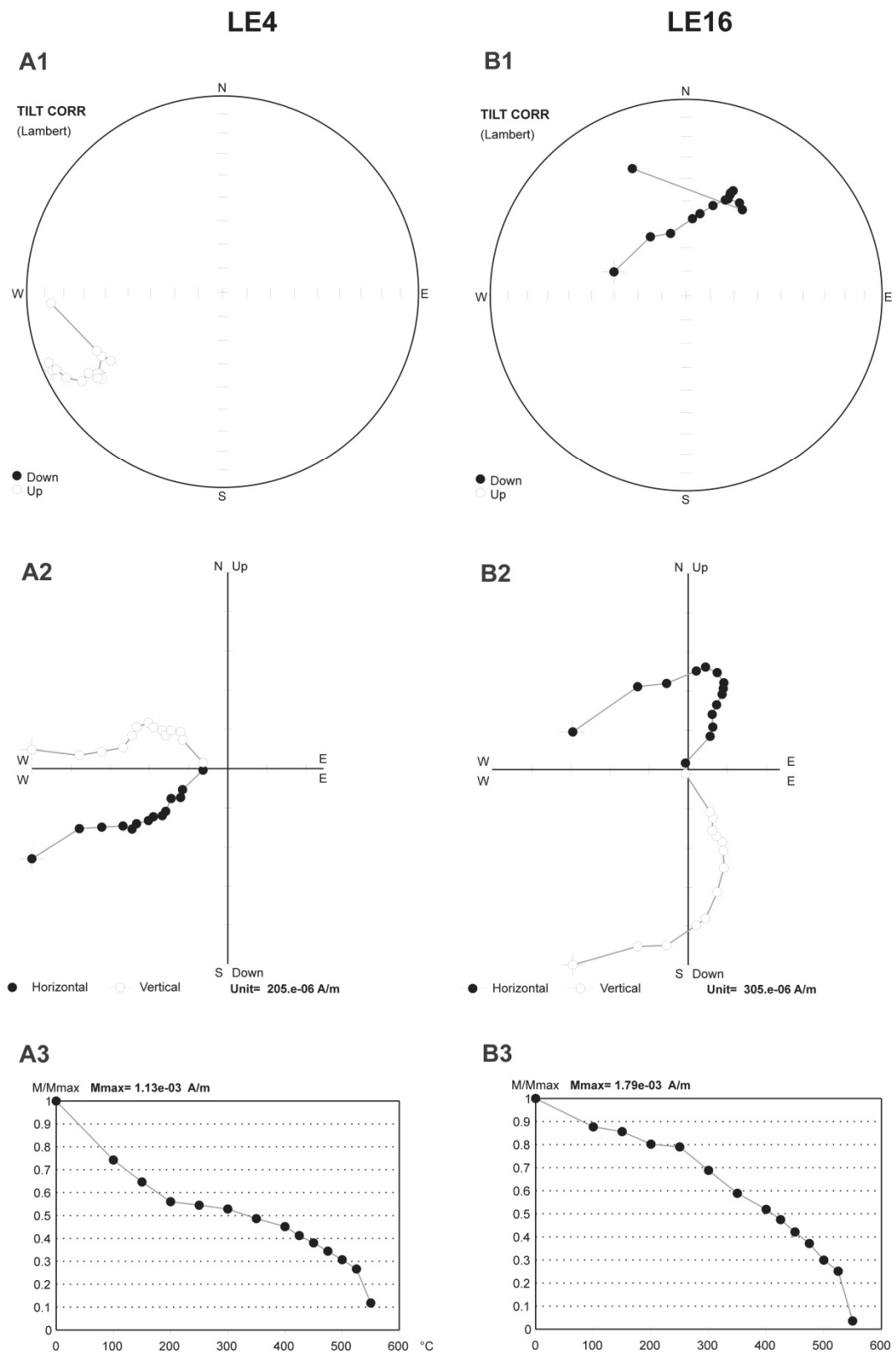


*Fig. 13: Thermal demagnetization of typical specimens with reversed (sample Le 4, left side) and normal polarity (sample Le 16, right side) of the component B. **A1 and B1**) stereographic projection of demagnetization path (after bedding correction). **A2 and B2**) orthogonal projection of demagnetization path (after bedding correction). **A3 and B3**) natural remanent magnetization intensity decay during thermal treatment.*

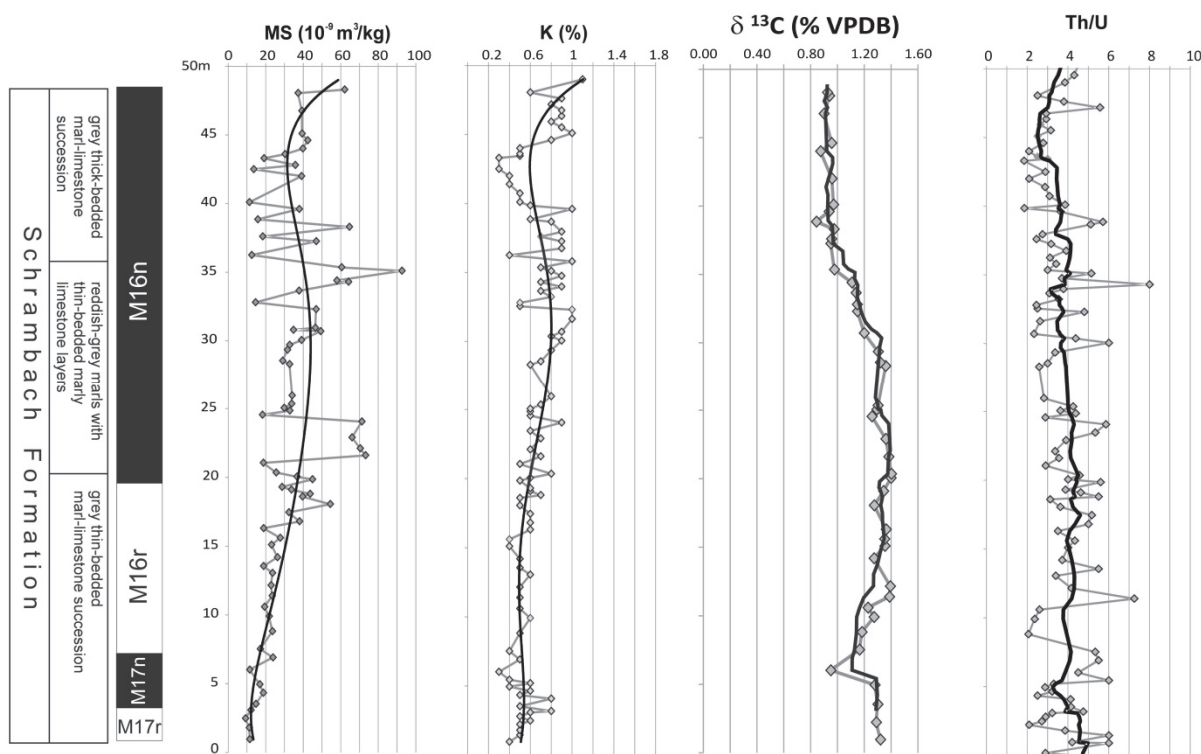


Fig. 14: Magnetic stratigraphy, magnetic susceptibility (MS), gamma ray spectrometry (K and Th/U) and $\delta^{13}\text{C}$ curve from the lower part of Schrambach Formation (Leube quarry). Black - normal polarity; white - reversed polarity.

Rossfeld Formation

The lowermost part of the Rossfeld Formation in the Leube quarry consists of a series of mud and debris flows (Fig. 15). These mass transport deposits overlie the Schrambach Formation with an erosional contact. Therefore the youngest part of the Schrambach Formation is in this part of the succession eroded. Of special interest in these mud flows is the occurrence of well-rounded exotic components, i.e. volcanites and different radiolarite pebbles (Fig. 16).

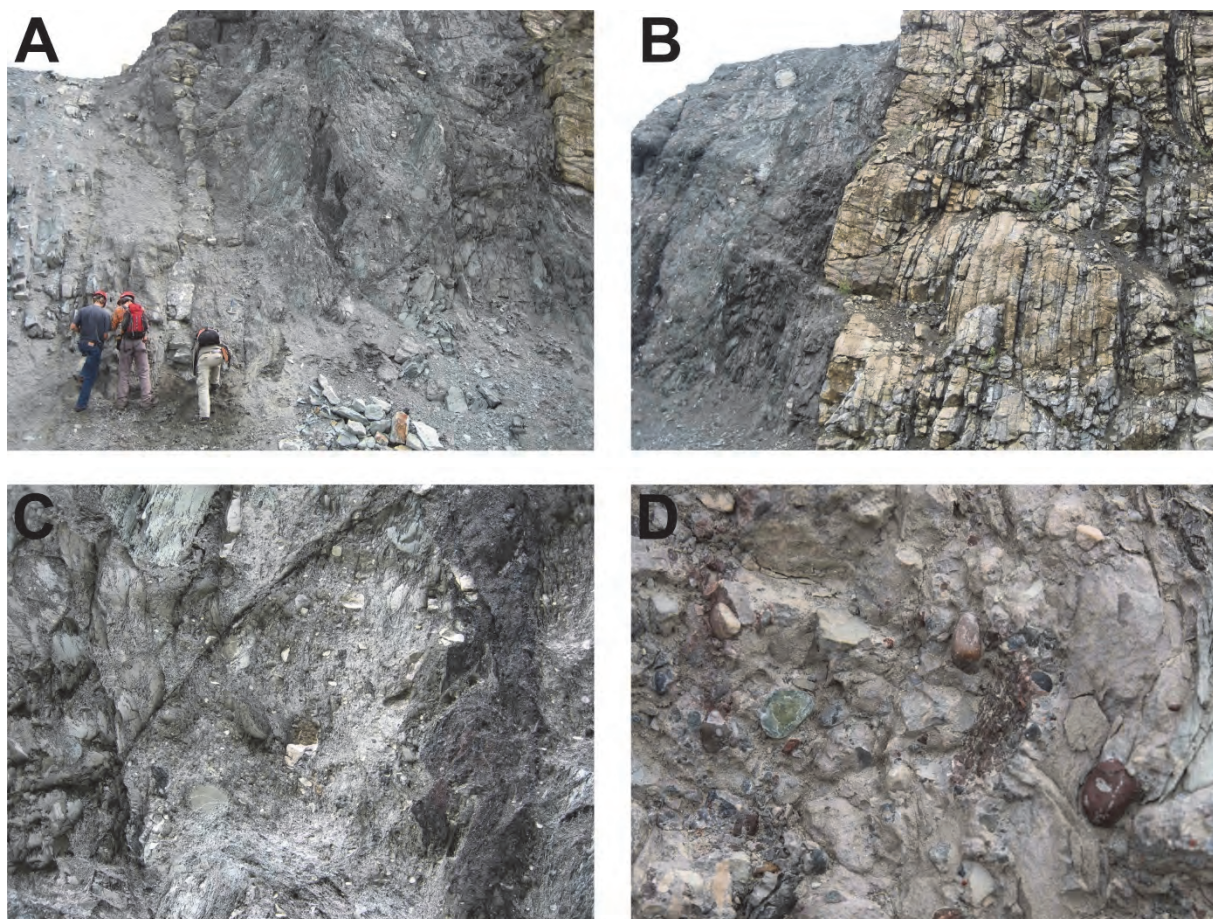


Fig. 15: Field view of the basal part of the Rossfeld Formation. A) Transition from the Schrambach Formation (left side) to the different mass transport deposits of the lower Rossfeld Formation. The contact between the bedded marls succession of the Schrambach Formation and the first mud flow is erosional. This part of the series consists of at least 4 different mud flows and one debris flow (details in Krische et al. 2014). B) The mud flows are overlain by bedded, siliceous arenites. C) and D) Details from the mud-flow deposits with angular carbonate clasts and well-rounded radiolarite and volcanic clasts.

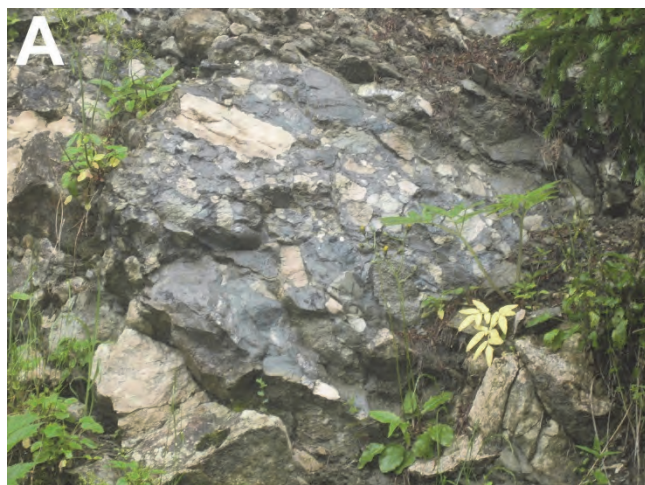


Fig. 16: A) and B) Macroscopic view of the component spectrum of the debris-flow deposit. The predominantly build by different carbonate clast with angular to sub-angular shape debris flows contain rarely exotic clasts of volcanites and different radiolarites with sub-rounded to well-rounded shape.

3.2 Rossfeld

The Rossfeld area (Germany) along the Rossfeld panorama road is the type area of the Early Cretaceous Rossfeld Formation and represents the westward continuation of the Tauglboden Basin north of the Trattberg Rise of Mount Kehlstein. Sedimentation of the Rossfeld Formation in the type area lasted according to TOLLMANN (1985) until the Barremian.

The first stop is located near the toll station of the Rossfeld Panorama road. Along the panorama road and adjacent forest roads the Late Valanginian part of the Rossfeld succession is outcropping: fine-grained siltstones to marls are intercalated with different mass transport deposits (Fig. 17). A Late Valanginian (Peregrinus and Furcillata Zones, HOEDEMAEKER et al. 2003) age is proven by the occurrence of *Himantoceras trinodosum* together with *Haploceras (Neolissoceras) grasiatum* and *Phyllopachyceras* sp. (Fig. 18).



*Fig. 17: Outcrop situation of the Rossfeld Formation near the toll station of the Rossfeld panorama road. **A)** Part of the section with an intercalated coarse-grained mass transport deposit in sandy marls with turbiditic calcareous sandstones. **B)** Most components in the mass transport deposit are angular to subangular carbonate clasts. Exotic components occur only rarely. **C)** Graded calcareous sandstones; the component spectrum in the turbidites is identical to those of the coarse-grained mass transport deposits.*

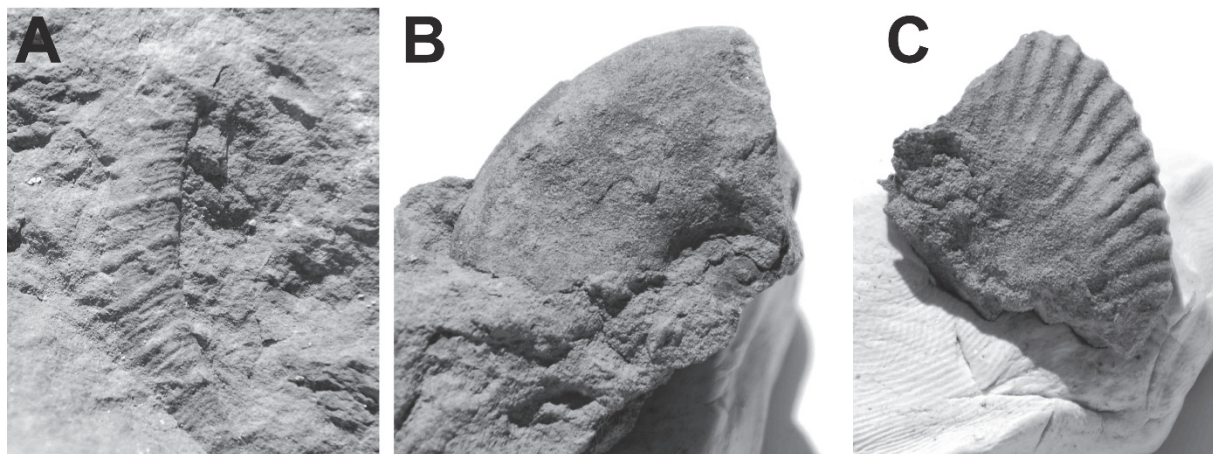


Fig. 18: Late Valanginian ammonites from the Rossfeld Formation near the toll station of the Rossfeld panorama road. **A)** *Himantoceras trinodosum*, **B)** *Haploceras (Neolissoceras) grasiatum*, **C)** *Phyllopachyceras* sp.

The second stop is the Hahnenkamm near the highest point of the Rossfeld panorama road. Here the Barremian part of the Rossfeld succession (TOLLMANN, 1985) is well preserved on an outcrop along the road (Fig. 19). Calcareous sandstones intercalated with several mass transport deposits which contain a similar component spectrum as in the Leube quarry except the Triassic radiolarites. The mass transport deposits show also a lack in components from both the Hallstatt Zone as well the Berchtesgaden unit. The Hallstatt outliers on top of the Rossfeld Formation are explained by MISSONI & GAWLICK (2011b) as southward-thrust elements during the Miocene tectonic extrusion, because they came to their present position after the youngest diagenetic overprint.

All (sub)angular carbonate components derive from a nearby source area and are of Late Jurassic to Early Cretaceous age, similar to the sedimentary succession of Mt. Plassen (Salzkammergut) and the overlying drowning sequence (GAWLICK & SCHLAGINTWEIT, 2006). These components are mixed with significant amounts of siliciclastic and ophiolitic material, indicating both local and distant source areas of continental and oceanic basement (DECKER et al., 1987; FAUPL & WAGREICH, 2000) beside volcanic material (SCHWEIGL & NEUBAUER, 1997b), and rounded Oxfordian radiolarite pebbles (MISSONI & GAWLICK, 2011a). Some radiolarite pebbles look like Triassic radiolarites, but their stratigraphic age is so far not proven.

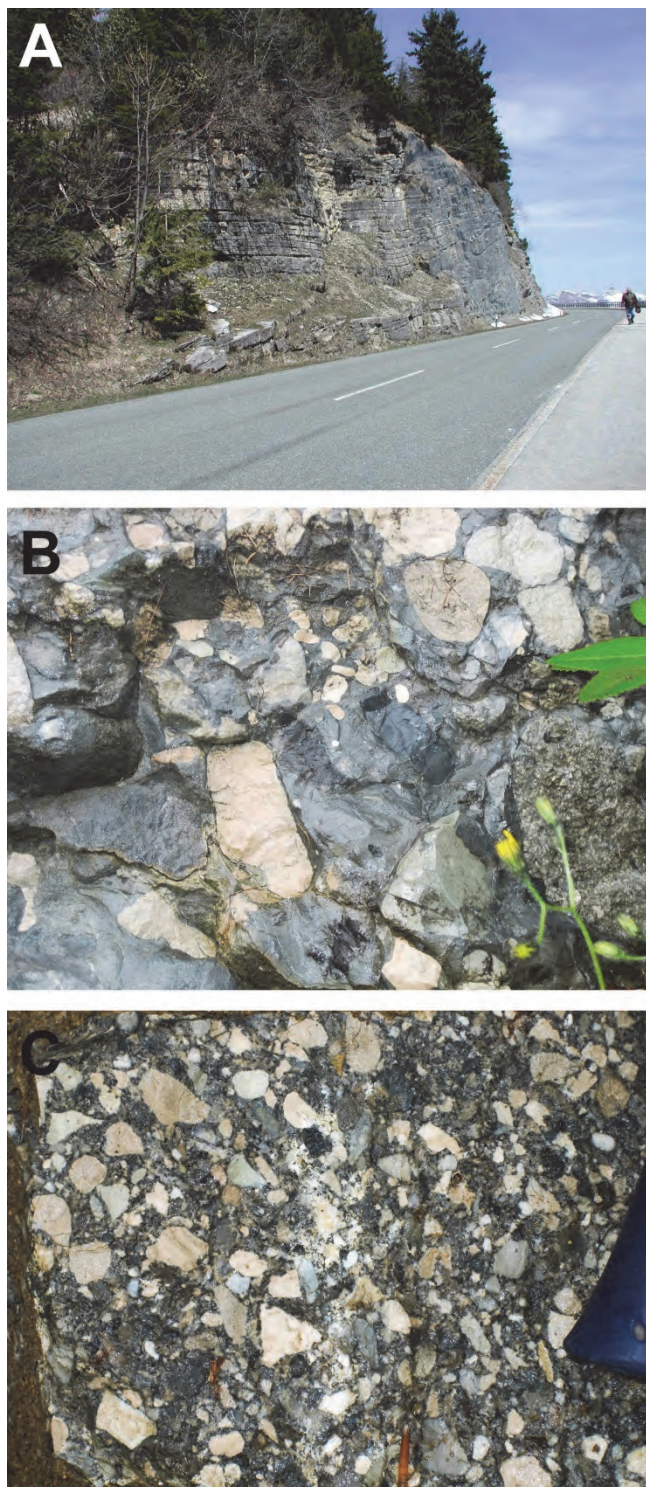


Fig. 19: **A)** Rossfeld Formation at the Hahnenkamm locality on the Rossfeld Panorama road. Calcareous sandstones with intercalated mass transport deposits. **B)** Coarse-grained polymictic breccia. Besides the dominating carbonate clasts (Late Jurassic - Early Cretaceous) few radiolarite components (?Triassic and Jurassic radiolarites) occur. **C)** Finer-grained polymictic breccia. Beside the dominating carbonate clasts radiolarites and ophiolitic grains occur.

Components in the mass transport deposits of the Rossfeld Formation

On base of microfacies analysis and biostratigraphy the components in the different mass transport deposits of the Rossfeld Formation are classified into six groups (KRISCHE, 2012; KRISCHE et al., 2014; KRISCHE & GAWLICK, 2015):

1. Triassic carbonates: uppermost Werfen to lowermost Gutenstein Formations,
2. Late Jurassic to earliest Cretaceous limestones: Oberalm Formation + Barmstein Limestone,
3. Carbonate bioclasts from a proximal Rossfeld basin shallow-water depositional realm,
4. Radiolarites, ophicalcites, siliceous deep-sea claystones, cherts,
5. Volcanic and ophiolite rock fragments
6. Siliciclastics: sand- and siltstones.

Biostratigraphic dating of the different radiolarite pebbles in the mass transport deposits with poor to moderate preserved radiolarians (KRISCHE et al., 2014) show three age clusters:

1. Ladinian to Early Carnian: these radiolarite pebbles are interpreted as derived from the Meliata facies zone (continental slope) or from the Neo-Tethys ocean floor.
2. Late Carnian/Norian: these radiolarite pebbles derive from the original sedimentary cover sequences of the Neo-Tethys ocean floor.
3. Late Bajocian to Callovian. These radiolarite pebbles are interpreted to derive from the matrix of the ophiolitic mélange below the Neo-Tethys obducted ophiolites.
4. Oxfordian: These radiolarite pebbles are interpreted to derive from the matrix of the ophiolitic mélange below the Neo-Tethys obducted ophiolites.

These radiolarite pebbles together with the volcanic and ophiolitic material were eroded in Early Cretaceous times from the ophiolitic nappe stack and transported by a fluvial system to the Rossfeld Basin (Fig. 20). On the way from the ophiolitic nappe stack the fluvial system crossed an area with exposed late Early to early Middle Triassic carbonates, latest Jurassic to earliest Cretaceous basinal sediments of the Plassen Carbonate Platform and the proximal depositional realm of the Rossfeld Basin.

Middle to Late Triassic shallow-water carbonate clasts from the Dachstein and/or Berchtesgaden nappes as commonly interpreted on the basis of the colour of the clasts and without microfacies analyses (KÜHNEL, 1929; WEBER, 1942; MEDWENITSCH, 1949, 1958; DEL-NEGRO, 1949, 1983; PLÖCHINGER, 1955, 1968, 1974, 1990; PICHLER, 1963) are missing, in all mass transport deposits of the Rossfeld Formation. No single grain deriving from the Triassic carbonate platforms or the Hallstatt zone was found in the mass-flows.

The Late Jurassic to earliest Cretaceous shallow-water carbonate clasts derive from the Plassen Carbonate Platform (e.g. Plassen Formation) or represent slope-to-basinal carbonate pebbles (Oberalm Formation and Barmstein Limestone).

Valanginian to Hauterivian carbonate clasts prove the existence of a contemporaneous shallow-water carbonate platform or ramp. Especially the existence of contemporaneous shallow-water carbonate areas, proved by carbonate litho- and bioclasts, was more or less unknown from the Rossfeld Formation.

The siliceous pebbles can be classified by their microfacies into different groups: radiolarites, ophicalcites, siliceous (deep-sea) clays, microcrystalline cherts and brown-black siliceous marlstones. Late Ladinian to Late Triassic ribbon radiolarites are of special interest because they indicate fragments

of the Neotethys oceanic realm. Ophicalcites and colourful siliceous (deep-sea) clays complete the pebble spectrum derived from the Neo-Tethys ocean floor. Intra-oceanic subduction in the Neo-Tethys started around the Early/Middle Jurassic boundary, and ophiolite obduction started in the Bajocian. Ophiolitic mélanges in the Dinarides/Albanides/Hellenides yielded Bajocian to Oxfordian ages from matrix radiolarites (GAWLICK et al., 2016 with references therein). Therefore the proof of Middle and Late Triassic and Middle-Late Jurassic radiolarite pebbles together with ophiolitic and volcanic material is a strong argument for the erosion of an ophiolitic nappe-stack carrying an island arc similar to those of the Dinaridic-Hellenic belt south of the present day Northern Calcareous Alps at that time.

Siliciclastic rocks such as quartz-sandstones, siltstones and singular quartz-grains and specific heavy minerals indicate erosion of a crystalline hinterland and complete the mixed conglomerate and breccia component suite.

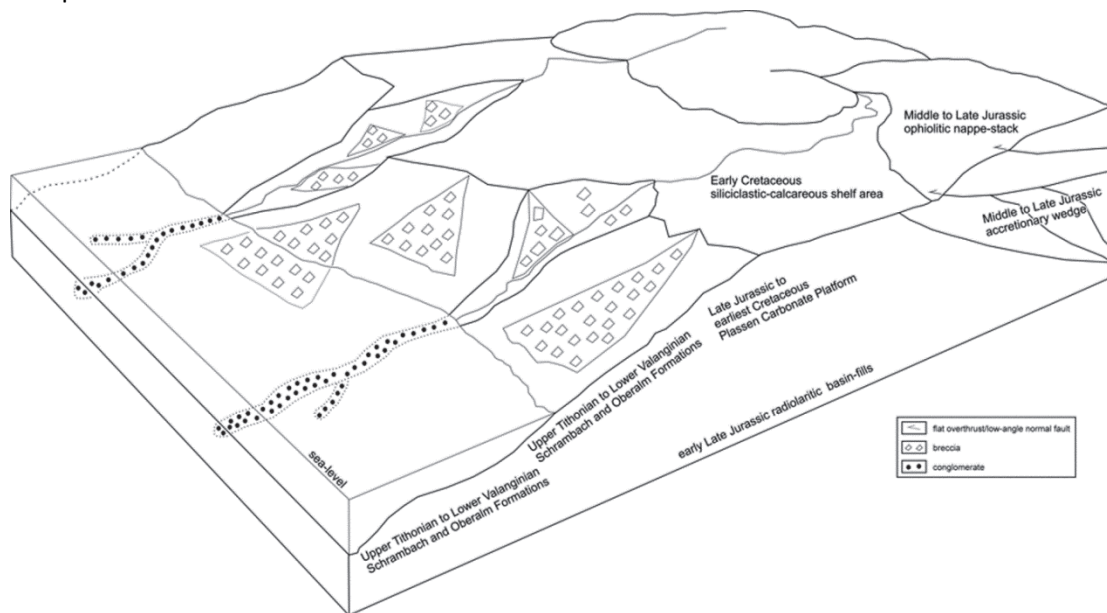


Fig. 20: Simplified sketch of the evolution of the basal conglomerates of the Rossfeld Formation. After the main sea-level lowstand after the late Early Valanginian/early Late Valanginian the rounded components in the mass transport deposits were brought by fluvial systems from the exposed hinterland and shelf area to the deeper parts of the basin. Local material from breccia fans was also incorporated in the mass transport deposits. During the sea-level rise in the Late Valanginian the typical fining-upward sequences of the Rossfeld Formation were deposited, today clearly visible at several outcrops in Bad Ischl, in Gartenua, in the Weitenau area and on the Rossfeld. From KRISCHE et al. (2014).

Panorama view from the Rossfeld road

To the east the Callovian to Oxfordian Lammer Basin fill on the northern side of the Tennengebirge Mt. is visible. The nearly 2000 m thick trench-like basin fill consists of olistostromes and huge slide blocks (Fig. 21) in a radiolaritic matrix. The reworked material derived from the Zlambach facies zone and the Dachstein reef rim. Hallstatt Limestones and material from the continental slope (Meliata facies zone) (Fig. 21) were transported in a piggy-back manner and were reworked in an earlier phase of northward propagating compression. In tectonic sense this basin fill corresponds to the Upper Tirolic nappe (Fig. 2). For a detailed description of the Lammer Basin fill see GAWLICK (1996), MISSONI & GAWLICK (2011b), and GAWLICK et al. (2012).

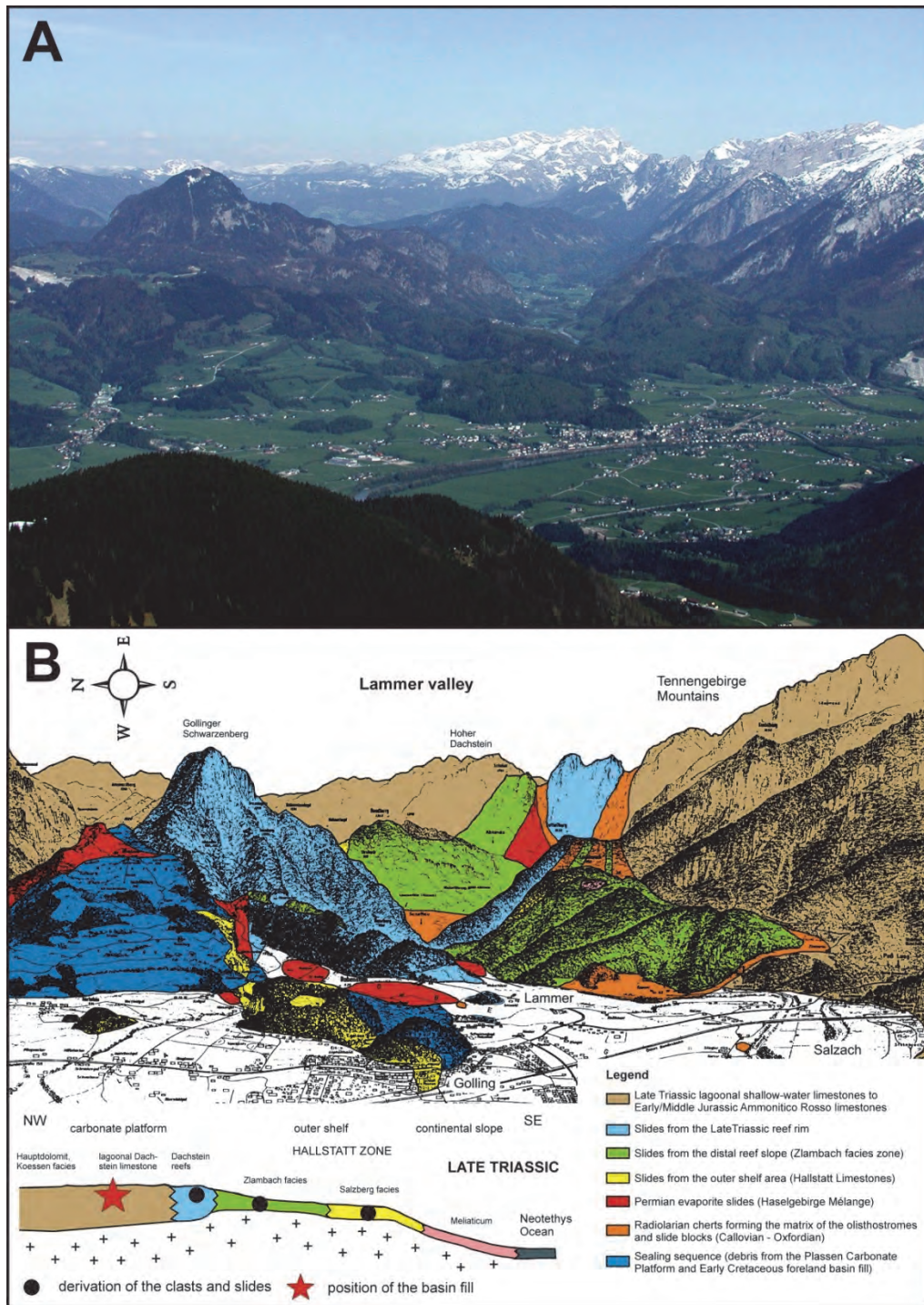


Fig. 21: A) View from the west showing the type area of the Callovian-Oxfordian Lammer Basin fill. B) Geological interpretation of the landscape picture. The basin fill consists of allochthonous material of different age and facies provenance, which generally derives from the outer shelf area transitional to the Neo-Tethys Ocean.

To the south of the Rossfeld Panorama road the Late Triassic sedimentary succession of Mt. Hohes Freieck as eastward continuation Mt. Hoher Göll is visible (Fig. 22). The exposed sedimentary succession represents the southern rim of the Rhaetian Kössen Basin and in tectonic sense the Trattberg Rise, i.e. the since the Early Oxfordian formed nappe front of the Upper Tirolic nappe (Fig. 2). From this nappe front Late Triassic to Middle Jurassic sedimentary rocks were eroded, mobilized as

blocks and slides, and redeposited in the Tauglboden Basin. The Tauglboden Basin and the Rossfeld Basin fill are palaeogeographically situated north of the Trattberg Rise and correspond to the Lower Tirolic nappe (Fig. 2).

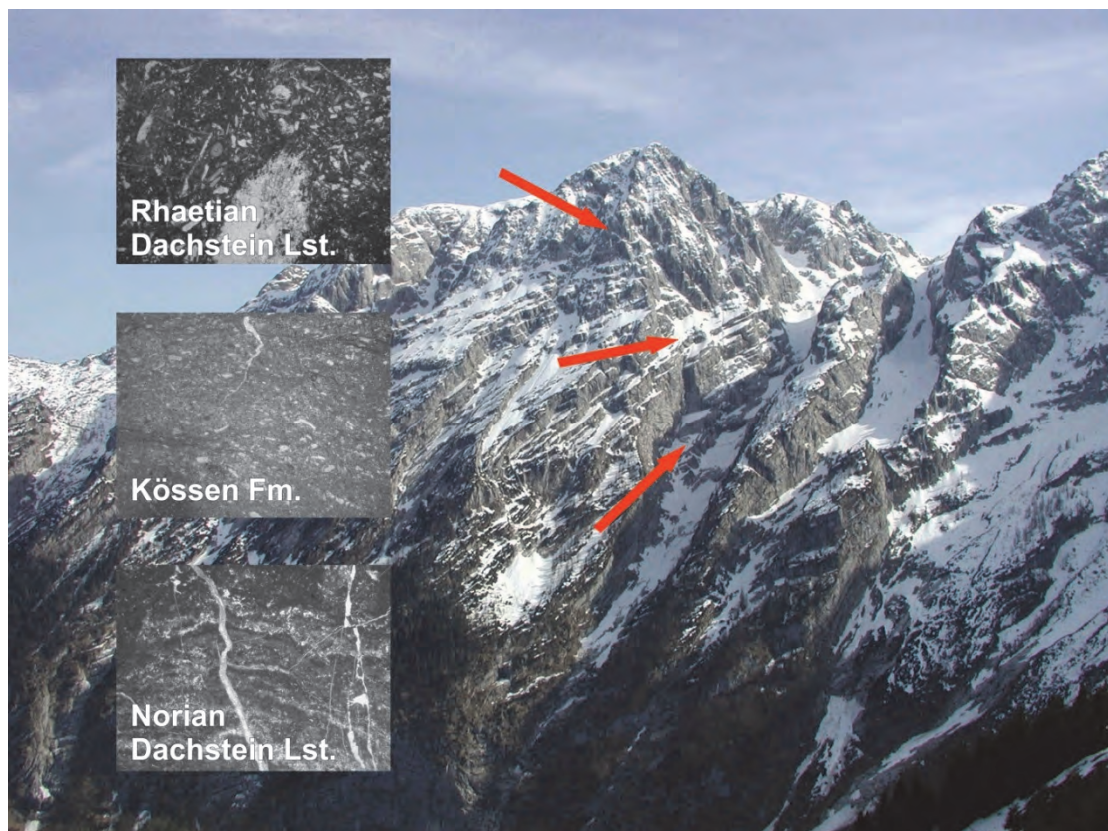


Fig. 22: Late Triassic sedimentary succession of the Trattberg Rise, Mt. Hohes Freieck east of Mt. Hoher Göll. Insets show typical microfacies of the Late Norian to Rhaetian succession. The Rhaetian reefs represent the southern margin of the Kössen Basin to the north. This clearly documents the palaeogeographic position of the area near the southern rim of the Kössen Basin and far away from the Dachstein Limestone reef zone to the south facing the open marine realm (Hallstatt Zone). For details MISSONI & GAWLICK (2011b).

3.3 Weitenau area

The Weitenau area is located between the township Golling to the west and the village Voglau to the east (Fig. 3). Geologically the Weitenau area is built of a different independent blocks of different palaeogeographic origin separated by faults with different character (KRISCHE, 2012; compare PLÖCHINGER 1968, 1990; Fig. 23). Of special interest in the Weitenau area is the preservation of the youngest part of the Rossfeld Formation, the Late Barremian to Middle Aptian shallowing cycle of the basin fill (Grabenwald Member: FUCHS, 1968; Plöchinger, 1968; WEIDICH, 1990; SCHLAGINTWEIT et al., 2012).

The Late Barremian to Middle Aptian Grabenwald Member is characterized by coarse-grained carbonatic sandstones (Fig. 24). Beside remains of corals and red algae also orbitolinids occur (*Montseciella arabica* and *Palorbitolina lenticularis*; SCHLAGINTWEIT et al., 2012) indicating a today eroded shallow-water evolution near the southern rim of the Northern Calcareous Alps. Planktonic foraminifera from the uppermost Grabenwald Member (FUCHS, 1968) were dated as Middle Aptian

(WEIDICH, 1990). However, within the Aptian the filling and shallowing of remaining deeper water areas in the Rossfeld Basin is documented by local remnants of coal and amber (PLÖCHINGER, 1968; WINKLER, 2004).

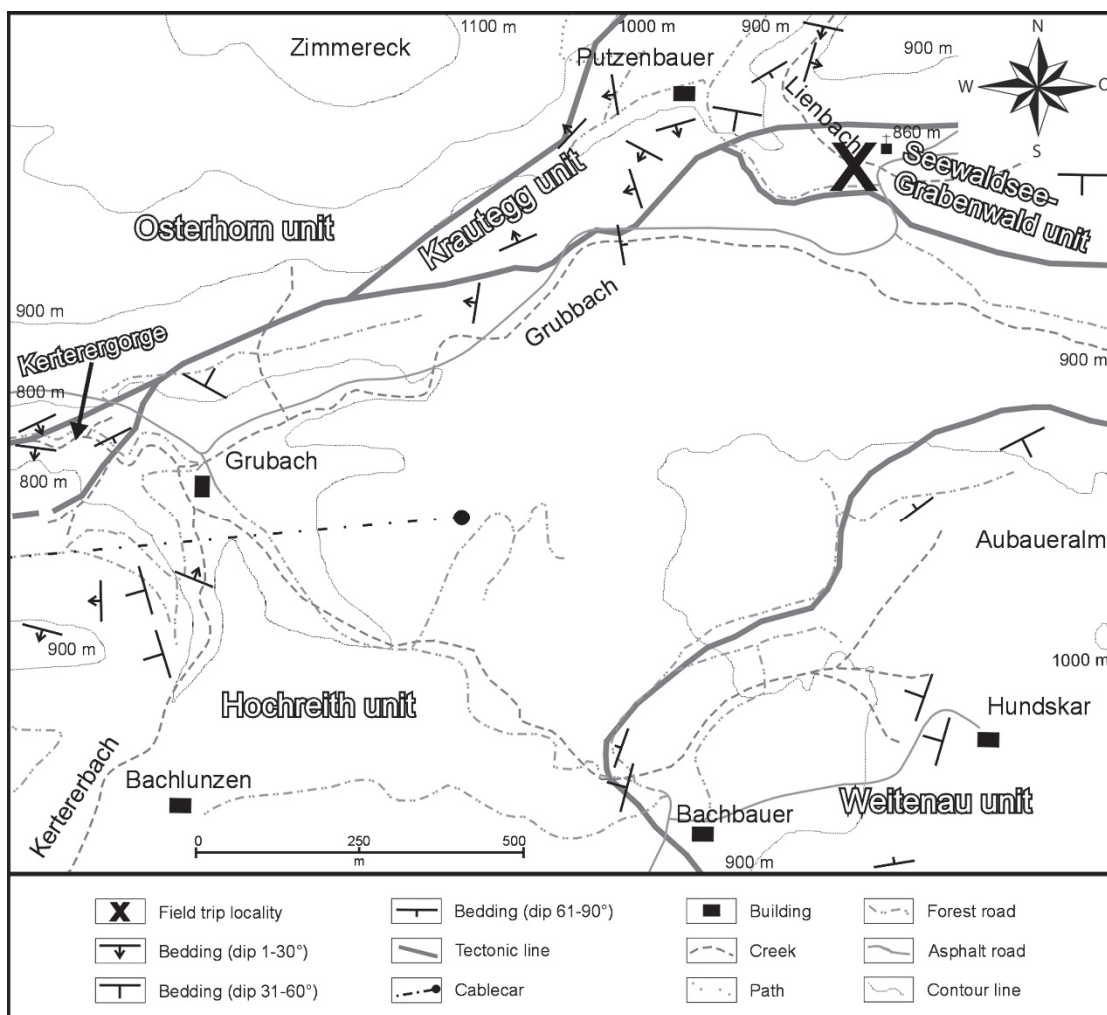


Fig. 23: Locality of the Aptian Orbitolina-bearing sedimentary rocks in the central Weitenau area, located in the Seewaldsee Grabenwald Block (after SCHLAGINTWEIT et al., 2012).

We will visit the Grabenwald outcrop in the central part of the Weitenau area situated in the Seewaldsee Grabenwald Block according to KRISCHE (2012) and SCHLAGINTWEIT et al. (2012). In the Lienbach valley up to 40 cm thick siliciclastic packstone beds are intercalated in turbiditic brownish marls (Fig. 24). Along the forest road to the cottage Putzenbauer the slightly older orbitolinid-bearing sandstones and fine-grained breccias can be studied (Fig. 24). The siliciclastic fraction of these sedimentary rocks consists of subangular quartz grains, quartzites, volcanites, reddish radiolarites, metasedimentary colourless silicified rocks, and yellowish silicified claystones (SCHLAGINTWEIT et al., 2012).



Fig. 24: Outcrop situation of the Aptian sedimentary sequence along the forest road to the cottage Putzenbauer and in the Lienbach valley. **A)** Orbitolina-bearing calcareous coarse-grained turbiditic sandstones. **B)** Marly sequence in the Lienbach valley where up to 40 cm thick siliciclastic packstone beds are intercalated in turbiditic brownish marls of Middle Aptian age.

Acknowledgements

We like to express our special thanks to the Zementwerk LEUBE GmbH for the more than ten years lasting permission to investigate the succession in the open mine, and for the permission to guide this field trip through the quarry. Maria Báldi-Beke (Budapest) determined the nannoplankton from samples of the Leube quarry section. Palaeomagnetic and chemostratigraphic investigations in the Leube quarry were financially supported by the project 2016/21/B/ST10/02941 of the National Science Center (Poland). Special thanks are due to Jolanta Iwańczuk, Ales Vrsic and Artur Teodorski for participation in field and laboratory work.

References

- BODROGI, I., DRAXLER, I., FILACZ, E. & LOBITZER, H., mit Beiträgen von STRADNER, H., EGGER, H., SURENIAN, R., SACHSENHOFER, R. F., KNAUER, J. & KLEIN, P. (1996): Die Mikrofauna und -flora ausgewählter (hemi)pelagischer Oberjura/Unterkreide-Schichtfolgen der Salzburger Kalkalpen sowie ein Vergleich mit der Unterkreide des Gerecse-Gebirges in Ungarn. - Unveröffentlichtes Manuskript, 1-31, Wien.
- BOOROVÁ, D., LOBITZER, H., SKUPIEN, P. & VAŠÍČEK, Z. (1999): Biostratigraphy and Facies of Upper Jurassic-Lower Cretaceous pelagic carbonate sediments (Oberalm-, Schrambach- and Roßfeld-Formation) in the Northern Calcareous Alps, South of Salzburg. - Abhandlungen der Geologischen Bundesanstalt, 56/2: 273-218, Wien
- BOOROVÁ, D., SKUPIEN, P., VAŠÍČEK, Z. & LOBITZER, H. (2015): Biostratigraphy of the Lower Cretaceous Schrambach Formation of the classical locality of Schrambachgraben (Northern Calcareous Alps, Salzburg Area). - Bulletin of Geosciences, 90: 89-131, Prag.
- BUJTOR L., KRISCHE O. & GAWLICK H.-J. (2013): Late Berriasian ammonite assemblage and biostratigraphy of the Leube quarry near Salzburg (Northern Calcareous Alps, Austria). - Neues Jahrbuch für Geologie und Paläontologie - Abhandlungen, 267: 273-295, Stuttgart.
- DARGA, R. & WEIDICH, K.F. (1986): Die Lackbach-Schichten, eine klastische Unterkreide-Serie in der Unkener Mulde (Nördliche Kalkalpen, Tirolikum). - Mitteilungen der Bayerischen Staatssammlung für Paläontologie und historische Geologie, 26: 93-112, München.
- DECKER, K., FAUPL, P. & MÜLLER, A. (1987): Synorogenic Sedimentation on the Northern Calcareous Alps during the Early Cretaceous. - In: FLÜGEL, H.W. & FAUPL, P. (Eds.): Geodynamics of the Eastern Alps, 126-141, (Deuticke) Wien.
- DEL NEGRO, W. (1949): Geologie von Salzburg. - 1-348, (Wagner) Innsbruck.
- DEL NEGRO, W. (1983): Geologie des Landes Salzburg. - Schriftenreihe des Landespressobüros: Serie Sonderpublikationen, 45: 1-152, Salzburg.
- DORNER, R., HÖFLING, R. & LOBITZER, H. (2009): Nördliche Kalkalpen in der Umgebung Salzburgs (Exkursion H am 17. April 2009). - Jahresberichte Mitteilungen Oberrheinischer Geologischer Verein NF, 91: 317-366, Stuttgart.
- FAUPL, P. & POBER, E. (1991): Zur Bedeutung detritischer Chromspinelle in den Ostalpen: Ophiolithischer Detritus aus der Vardarsutur. - Jubiläumsschrift 20 Jahre Geologische Zusammenarbeit Österreich - Ungarn, Teil 1: 133-143, Wien.
- FAUPL, P. & TOLLMANN, A. (1979): Die Roßfeldschichten: Ein Beispiel für Sedimentation im Bereich einer tektonisch aktiven Tiefseerinne aus der kalkalpinen Unterkreide. - Geologische Rundschau, 68: 93-120, Stuttgart.
- FAUPL, P. & WAGREICH, M. (2000): Late Jurassic to Eocene Palaeogeography and Geodynamic Evolution of the Eastern Alps. - Mitteilungen der Österreichischen Geologischen Gesellschaft, 92: 79-94, Wien.
- FRANK, W. & SCHLAGER, W. (2006): Jurassic strike slip versus subduction in the Eastern Alps. - International Journal of Earth Sciences, 95: 431-450, Berlin Heidelberg.
- FRAU, C., BULOT, L.-G., WIMBLEDON, W.A.P. & IFRIM, C. (2016): Upper Tithonian ammonites (Himalayitidae Spath, 1925 and Neocomitidae Salfeld, 1921) From Charens (Drôme, France). - Geologica Carpathica, 67(6): 543-559, Bratislava.
- FRISCH, W. & GAWLICK, H.-J. (2003): The nappe structure of the central Northern Calcareous Alps and its disintegration during Miocene tectonic extrusion - a contribution to understanding the orogenic evolution of the Eastern Alps. - International Journal of Earth Sciences, 92/5: 712-727, Berlin Heidelberg.
- FUCHS, W. (1968): Eine bemerkenswerte, tieferes Apt belegende Foraminiferenfauna aus den konglomeratreichen Oberen Roßfeldschichten von Grabenwald (Salzburg). - Verhandlungen der Geologischen Bundesanstalt, 1968: 87-89, Wien.
- FUGGER, E. (1907): Erläuterungen zur Geologischen Karte der im Reichsrat vertretenen Königreiche und Länder der Österreichisch - Ungarischen Monarchie. SW-Gruppe Nr. 18 Hallein und Berchtesgaden. (Zone 13, Kol.

VIII der Spezialkarte der Österreichisch - Ungarischen Monarchie im Maßstab 1:75:000. - K.K. Geologische Reichsanstalt, 1-34, Wien.

GAWLICK, H.-J. (1996): Die früh-oberjurassischen Brekzien der Stubbergschichten im Lammertal - Analyse und tektonische Bedeutung (Nördliche Kalkalpen, Österreich). - Mitteilungen Gesellschaft Geologie Bergbaustudenten Österreichs, 39/40, 119-186, Wien.

GAWLICK, H.-J. & SCHLAGINTWEIT, F. (2006): Berriasian drowning of the Plassen carbonate platform at the type-locality and its bearing on the early Eoalpine orogenic dynamics in the Northern Calcareous Alps (Austria). - International Journal of Earth Sciences, 95, 451-462, Berlin Heidelberg.

GAWLICK, H.-J., SCHLAGINTWEIT, F. & MISSONI, S. (2005): Die Barmsteinkalke der Typlokalität nordwestlich Hallein (hohes Tithonium bis tieferes Berriasium; Salzburger Kalkalpen) - Sedimentologie, Mikrofazies, Stratigraphie und Mikropaläontologie: neue Aspekte zur Interpretation der Entwicklungsgeschichte der Ober-Jura-Karbonatplattform und der tektonischen Interpretation der Hallstätter Zone von Hallein - Bad Dürrnberg. - Neues Jahrbuch für Geologie und Paläontologie Abhandlungen, 236: 351-421, Stuttgart.

GAWLICK, H.-J., MISSONI, S., SCHLAGINTWEIT, F., SUZUKI, H., FRISCH, W., KRYSTYN, L., BLAU, J. & LEIN, R., (2009): Jurassic Tectonostratigraphy of the Austroalpine Domain. - Journal of Alpine Geology, 50, 1-152, Wien.

GAWLICK, H.-J., MISSONI, S., SCHLAGINTWEIT, F. & SUZUKI, H. (2012): Jurassic active continental margin deep-water basin and carbonate platform formation in the north-western Tethyan realm (Austria, Germany). - Journal of Alpine Geology, 54, 189-292, Wien.

GAWLICK, H.-J., MISSONI, S., SUZUKI, H., SUDAR, M., LEIN, R. & JOVANOVIC, D. (2016): Triassic radiolarite and carbonate components from a Jurassic ophiolitic mélange (Dinaridic Ophiolite Belt). - Swiss Journal Geoscience, 109: 473-494, Basel.

GRABOWSKI, J., SCHNEYDER, J., SOBIEN, K., KOPTIKOVA, L., KRZEMINSKI, A., PSZCZOLKOWSKI, A., HEJNAR, J. & SCHNABL, P. (2013): Magnetic susceptibility and spectral gamma logs in the Tithonian-Berriasian pelagic carbonates in the Tatra Mts (Western Carpathians, Poland): Palaeoenvironmental changes at the Jurassic/Cretaceous boundary. - Cretaceous Research, 43, 1-17.

GRABOWSKI, J., GAWLICK, H.-J., IWANCZUK, J., KRISCHE, O., REHAKOVA, D. & WOJCIK, K. (2016a): Tithonian-Berriasian magnetostratigraphy in the Northern Calcareous Alps (Leube quarry, Northern Calcareous Alps, Austria) - first results. - In: MICHALIK, J. & FEKETE, K. (Eds.): XIIth Jurassica Conference, Field Trip Guide and Abstract Book, 91-92, Earth Science Institute, Slovak Academy of Science, Bratislava.

GRABOWSKI, J., LAKOVA, I., PETROVA, S., STOYKOVA, K., IVANOVA, D., WOJCIK-TABOL, P., SOBIEN, K. & SCHNABL, P. (2016b): Paleomagnetism and integrated stratigraphy of the Upper Berriasian hemipelagic succession in the Barlya section Western Balkan, Bulgaria: Implications for lithogenic input and paleoredox variations. - Palaeogeography, Palaeoclimatology, Palaeoecology, 461, 156-177, Amsterdam.

GRABOWSKI, J., GAWLICK, H.-J., HIRSCHHUBER, H.-J., IWANCZUK, J., KRISCHE, O., REHAKOVA, D., ZIOLKOWSKI, P., TEODORSKI, A. & VRSIC, A. (2017a): Tithonian - Berriasian magnetic stratigraphy, gamma ray spectrometry, AMS studies, and geochemical analyses in the Northern Calcareous Alps (Leube quarry, Salzburg area, Austria) - first results. - Jurassica XIII: Jurassic Geology of Tatra Mts., Abstracts and Field Trip guidebook, 34-35, Koscielisko, Polish Geological Institute.

GRABOWSKI, J., GAWLICK, H.-J., HIRSCHHUBER, H.-J., IWANCZUK, J., KRISCHE, O., REHAKOVA, D., ZIOTKOWSKI, P., TEODORSKI, A. & VRSIC, A. (2017b): Primary magnetization in the Berriasian of the Northern Calcareous Alps (Salzburg area). - In: SARIC, K., PRELEVIC, D., SUDAR, M. & CVETKOVIC, V. (Eds.): Émile Argand Conference - 13th Workshop on Alpine Geological Studies - September 7th-18th 2017, Zlatibor Mts. (Serbia), 37, (University of Belgrade - Faculty of Mining and Geology) Beograd.

GÜMBEL, C.W. von (1861): Geognostische Beschreibung des Bayrischen Alpengebirges und seines Vorlandes. I-XX. - 1-950, (Justus Perthes) Gotha.

HARDENBOL, J., THIERRY, J., HARLEY, M.B., JACQUIN, T., DE GRACIANSKY, P.-C. & VAIL, P.R. (1998): Mesozoic and Cenozoic Sequence Chronostratigraphic Framework of European basins. - SEPM special Publications, 160: 763-786.

- HOEDEMAEKER, PH., REBOULET, S., AGUIRRE-URRETA, M.B., ALSEN, P., AOUTEM, M., ATROPS, F., BARRAGAN, R., COMPANY, M., GONZÁLEZ-ARREOLA, C., KLEIN, J., LUKENEDER, A., PLOCH, I., RAISOSSADAT, N., RAWSON, P.F., ROPOLO, P., VASÍČEK, Z., VERMEULEN, J. & WIPPICH, M.G.E. (2003): Report on the 1st International Workshop of the IUGS Lower Cretaceous Ammonite Working Group, the 'Kilian Group' (Lyon, 11 July 2002). - *Cretaceous Research*, 24: 89-94.
- HRADECKÁ, L. (2003): Srovnání spodnokřídového foraminiferového společenstva z výplní štramberských vápenců lomu Kotouč ve Štramberku na Moravě se společenstvem stejného stáří z lomu Gutrathsberg v Gartenau v Rakousku. - Sbor. věd. prací VŠBTech. univ. Ostrava, Ř. hornicko-geologická, mimoř. čís. ke 4. paleont. semináři, XLIX: 45-47, Ostrava.
- IMMEL, H. (1987): Die Kreideammoniten der Nördlichen Kalkalpen. - *Zitteliana*, 15: 3-163, München.
- KRISCHE, O. (2012): Die Platznahme der Alpinen Haselgebirge Mélange: Die geodynamische Entwicklung der zentralen Nördlichen Kalkalpen im höchsten Ober-Jura und in der Unter-Kreide. - Unpublished PhD Thesis, 1-340, Montanuniversität Leoben, Leoben.
- KRISCHE, O. & GAWLICK, H.-J. (2010): Berriasian turbidites in the central Northern Calcareous Alps (Salzburg, Austria): palaeogeography and hinterland reconstructions. *Schriftenreihe der Deutschen Gesellschaft für Geowissenschaften*, 72: 60, Hannover.
- KRISCHE, O. & GAWLICK, H.-J. (2015): Age and significance of Lower Cretaceous mass flows: Ischler Breccia revisited (Rossfeld Formation, Northern Calcareous Alps, Austria). - *Austrian Journal of Earth Sciences*, 108: 128-150, Wien.
- KRISCHE, O., BUJTOR, L. & GAWLICK, H.-J. (2013): Calpionellid and ammonite biostratigraphy of uppermost Jurassic to Lower Cretaceous sedimentary rocks from the Leube quarry (Northern Calcareous Alps, Salzburg, Austria). - *Austrian Journal of Earth Sciences*, 101: 26-45, Wien.
- KRISCHE, O., GORIČAN, S. & GAWLICK, H.-J. (2014): Erosion of a Jurassic ophiolitic nappe-stack as indicated by exotic components in the Lower Cretaceous Rossfeld Formation of the Northern Calcareous Alps (Austria). - *Geologica Carpathica*, 65: 3-24, Bratislava.
- KÜHNEL, J. (1929): Geologie des Berchtesgadener Salzberges. - *Neues Jahrbuch für Mineralogie, Geologie und Paläontologie Beilagegebände B*, 61: 17-22, Stuttgart.
- LEISS, O. (1992): Orogenically controlled sedimentation in the Lechtaler Kreideschiefer (Lechtal shale; Cretaceous) and geodynamics of the inner western NCA (Northern Calcareous Alps, Lechtal Alps). - *Geologische Rundschau*, 81: 603-634, Stuttgart.
- LILL V. LILIENBACH, A. (1830): Ein Durchschnitt aus den Alpen mit Hindeutung auf die Karpaten. - *Neues Jahrbuch für Mineralogie, Geognosie, Geologie Petrefaktenkunde*, 1: 153-220, Heidelberg.
- LINZER, H.G., RATSBACHER, L. & FRISCH, W. (1995): Transpressional collision structures in the upper crust: the fold-thrust belt of the Northern Calcareous Alps. - *Tectonophysics*, 242: 41-61, Amsterdam.
- LIPOLD, M. v. (1854): Der Salzberg am Dürnberg nächst Hallein. - *Jahrbuch der kaiserlich-königlichen Geologischen Reichsanstalt*, 1854: 590-610, Wien.
- MAIER, G., MLEKUSCH, T., KRISCHE, O. & GAWLICK, H.-J. (2013): Biostratigraphy, isotope stratigraphy ($\delta^{18}\text{O}$, $\delta^{13}\text{C}$) and geochemical characteristics (XRF) of Upper Tithonian to Lower Cretaceous deeper water sedimentary rocks (Northern Calcareous Alps, Salzburg) as a tool to prospect raw material for cement industry. - In: SCHUSTER, R. (Ed.): 11th Workshop on Alpine Geological Studies & 7th European Symposium on Fossil Algae. Abstract & Field Guides. 58, Schladming, Sept. 2013, Wien.
- MATURA, A. & SUMMERSBERGER, H. (1980): Geology of the Eastern Alps (An excursion guide). - *Abhandlungen der Geologischen Bundesanstalt*, 34: 103-170, Wien.
- MEDWENITSCH, W. (1949): Die Geologie der Hallstätterzone von Ischl - Altaussee (mit einer Situationsskizze 1:50000, mit einem N-S- und einem W-E- Tektonogramm 1:25000 als Beilagen). - *Mitteilungen der Gesellschaft der Geologie- und Bergbaustudenten in Wien*, I./Heft 2: 1-27, Wien.

- MEDWENTISCH, W. (1958): Die Geologie der Salzlagerstätten Bad Ischl und Alt-Aussee (Salzkammergut). - Mitteilungen der Geologischen Gesellschaft in Wien, 1957: 133-200, Wien.
- MISSONI, S. & GAWLICK, H.-J. (2011a): Evidence for Jurassic subduction from the Northern Calcareous Alps (Berchtesgaden; Austroalpine, Germany). - International Journal of Earth Sciences, 100/7, 1605-1631, Berlin Heidelberg.
- MISSONI, S. & GAWLICK, H.-J. (2011b): Jurassic mountain building and Mesozoic-Cenozoic geodynamic evolution of the Northern Calcareous Alps as proven in the Berchtesgaden Alps (Germany). - Facies, 57: 137-186, Berlin Heidelberg.
- NEUBAUER, F., GENSER, J. & HANDLER, R. (2000): The Eastern Alps: result of a two-stage collision process. - In: Neubauer, F. & Höck, V. (Eds.): Aspects of geology in Austria. - Mitteilungen Österreichische Geologische Gesellschaft, 92:117-134, Wien.
- OBERHAUSER, R. (1980): Der geologische Aufbau Österreichs. XIX. - 1-701 (Springer) Wien/New York.
- PESTAL, G., HEJL, E., BRAUNSTINGL, R. & SCHUSTER, R. (Eds.) (2009): Erläuterungen Geologische Karte von Salzburg 1:200000. - Geologische Bundesanstalt, 1-162, Wien.
- PICHLER, H. (1963): Geologische Untersuchungen im Gebiet zwischen Roßfeld und Markt Schellenberg im Berchtesgadener Land. - Beihefte zum Geologischen Jahrbuch, 48: 129-204, Hannover.
- PLÖCHINGER, B. (1955): Zur Geologie des Kalkalpenabschnittes vom Torrener Joch zum Ostfuß des Untersberges; die Göllmasse und die Halleiner Hallstätter Zone. - Jahrbuch der Geologischen Bundesanstalt, 98: 93-144, Wien.
- PLÖCHINGER, B. (1961): Bericht 1960 über Aufnahmen auf den Blättern Berchtesgaden (93) und St. Wolfgang (95/N1). - Verhandlungen der Geologischen Bundesanstalt, 1961: A48-A49, Wien.
- PLÖCHINGER, B. (1968): Die Hallstätter Deckscholle östlich von Kuchl/Salzburg und ihre in das Aptium reichende Roßfeldschichten-Unterlage. - Verhandlungen der Geologischen Bundesanstalt, 1968: 80-86, Wien.
- PLÖCHINGER, B. (1974): Gravitativ transportiertes permisches Haselgebirge in den Oberalm Schichten (Tithonium, Salzburg). - Verhandlungen der Geologischen Bundesanstalt, 1974: 71-88, Wien.
- PLÖCHINGER, B. (1976): Die Oberalm Schichten und die Platznahme der Hallstätter Masse in der Zone Hallein-Berchtesgaden. - Neues Jahrbuch Geologie und Paläontologie Abhandlungen, 151: 304-324, Stuttgart.
- PLÖCHINGER, B. (1977): Die Untersuchungsbohrung Gutrathsberg B I südlich St. Leonhard im Salzachtal (Salzburg). - Verhandlungen der Geologischen Bundesanstalt, 1977: 3-11, Wien.
- PLÖCHINGER, B. (1990): Geologische Karte der Republik Österreich 1:50.000, Erläuterungen zu Blatt 94 Hallein. - Geologische Bundesanstalt, 1-76, Wien.
- PLÖCHINGER, B. (1995): Tectonics of the Northern Calcareous Alps: a review. - Mem Sci Geol Padova, 47: 73-86, Padua.
- POBER, E. & FAUPL, P. (1988): The chemistry of detrital chromian spinels and its implications for the geodynamic evolution of the Eastern Alps. - Geologische Rundschau, 77: 641-670, Stuttgart.
- PUEYO, E.L., MAURITSCH, H.J., GAWLICK, H.-J., SCHOLGER, R. & FRISCH, W. (2007): New evidence for block and thrust sheet rotations in the central northern Calcareous Alps deduced from two pervasive remagnetization events. - Tectonics, 26: 1-25.
- RASSER, M.W., VAŠÍČEK, Z., SKUPIEN, P., LOBITZER, H. & BOOROVÁ, D. (2003): Die Schrambach-Formation an ihrer Typlokalität (Unter-Kreide, Nördliche Kalkalpen, Salzburg): Lithostratigraphische Formalisierung und „historische“ Irrtümer. - In: PILLER, W.E. (Ed.): Stratigraphia Austriaca, Schriftenreihe der Erdwissenschaftlichen Kommissionen, 16: 193-216, Wien.
- RATSBACHER, L., FRISCH, W., LINZER, H.G. & MERLE, O. (1991): Lateral extrusion in the Eastern Alps, Part 2: structural analysis. - Tectonics, 10: 257-271.

- REHÁKOVÁ, D., MICHALIK, J. & OŽVOLDOVÁ, L. (1996): New microbiostratigraphical data from several Lower Cretaceous pelagic sequences of the Northern Calcareous Alps, Austria (preliminary results). - *Geologisch-Paläontologische Mitteilungen Innsbruck, Sonderband 4: 57-81*, Innsbruck.
- SCHLAGER, M. & SCHLAGER, W. (1969): Über die Sedimentationsbedingungen der jurassischen Taugl bodenschichten (Osterhorngruppe, Salzburg). - *Anzeiger der Österreichischen Akademie der Wissenschaften. Mathematisch-naturwissenschaftlichen Klasse*, 106: 178-183, (Österreichische Akademie Wissenschaften) Wien.
- SCHLAGER, W. & SCHLAGER, M. (1973): Clastic sediments associated with radiolarites (Taugl bodenschichten, Upper Jurassic, Eastern Alps). - *Sedimentology*, 20: 65-89, (Blackwell) Oxford.
- SCHLAGINTWEIT, F., KRISCHE, O. & GAWLICK, H.-J. (2012): First findings of orbitolinids (larger benthic foraminifera) from the Early Cretaceous Rossfeld Formation (Northern Calcareous Alps, Austria). - *Jahrbuch der Geologischen Bundesanstalt*, 152: 145-158, Wien.
- SCHORN, A. & NEUBAUER, F. (2011): Emplacement of an evaporitic mélange nappe in central Northern Calcareous Alps: evidence from the Moosegg klippe (Austria). - *Austrian Journal of Earth Sciences*, 104: 22-46, Wien.
- SCHWEIGL, J. & NEUBAUER, F. (1997a): New structural, sedimentological and geochemical data on the Cretaceous geodynamics of the central Northern Calcareous Alps (Eastern Alps). – *Zentralblatt Geologie und Paläontologie Teil 1*, 1996: 329-343, Stuttgart.
- SCHWEIGL, J. & NEUBAUER, F. (1997b): Structural evolution of the central Northern Calcareous Alps: Significance for the Jurassic to Tertiary geodynamics in the Alps. - *Eclogae geol. Helvetiae*, 90: 303-323, Basel.
- STEIGER, T. (1992): Systematik, Stratigraphie und Palökologie der Radiolarien des Oberjura-Unterkreide-Grenzbereiches im Osterhorn-Tirolikum (Nördliche Kalkalpen, Salzburg und Bayern). – *Zitteliana*, 19: 1-188, München.
- TOLLMANN A. (1976a): Monographie der Nördlichen Kalkalpen. Teil II. Analyse des klassischen nordalpinen Mesozoikums. Stratigraphie, Fauna und Fazies der Nördlichen Kalkalpen. - 1-580, (Deuticke) Wien.
- TOLLMANN, A. (1976b): Der Bau der Nördlichen Kalkalpen. Orogenic Stellung und regionale Tektonik. - 1-449, (Deuticke) Wien.
- TOLLMANN, A. (1977): Geologie von Österreich, Band 1: Die Zentralalpen. - 1-766, (Deuticke) Wien.
- TOLLMANN, A. (1985): Geologie von Österreich, Band 2: Außerzentralalpiner Anteil. - 1-710, (Deuticke) Wien.
- UHLIG, V. (1882): Zur Kenntnis der Cephalopoden der Rossfeldschichten. *Jahrbuch der Kaiserlich - Königlichen Geologischen Reichsanstalt*, 32/III: 346-396, Wien
- VON EYNATTEN, H. & GAUPP, R. (1999): Provenance of Cretaceous synorogenic sandstones in the Eastern Alps: constraints from framework petrography, heavy mineral analysis and mineral chemistry. - *Sedimentary Geology*, 124: 81-111, Amsterdam.
- VON EYNATTEN, H., GAUPP, R., WIJBRANS, J.R. (1996): $^{40}\text{Ar}/^{39}\text{Ar}$ laser-probe dating of detrital white micas from Cretaceous sedimentary rocks of the Eastern Alps: evidence for Variscan high-pressure metamorphism and implications for Alpine orogeny. - *Geology*, 24: 691-694, Boulder
- WAGREICH, M. (2009): Stratigraphic constraints on climate control of Lower Cretaceous oceanic red beds in the Northern Calcareous Alps (Austria). - *SEPM Special Publication* 91: 91-98, Tulsa.
- WEBER, E. (1942): Ein Beitrag zur Kenntnis der Roßfeldschichten und ihrer Fauna. - *Neues Jahrbuch für Mineralogie, Geologie und Paläontologie Beilage-Bände Abteilung B: Geologie und Paläontologie*, 86: 247-281, Stuttgart
- WEIDICH, K. F. (1990): Die kalkalpine Unterkreide und ihre Foraminiferenfauna. - *Zitteliana*, 17: 1-312, München.
- WINKLER, W. (2004): Eine mineralogische Besonderheit aus dem Lammertal, Salzburg, Österreich - fossile Harze aus der Unterkreide. - *Gmundner Geostudien*, 2: 337-342, Gmunden.
- WOLETZ, G. 1963): Charakteristische Abfolgen der Schwermineralgehalte in Kreide- und Alttertiär-Schichten der nördlichen Ostalpen. - *Jahrbuch der Geologischen Bundesanstalt*, 106: 89-119, Wien.



Field Trip Post-EX-5

Mass transport deposits, geometry, depositional regime and biostratigraphy in a Late Jurassic carbonate-clastic radiolaritic basin fill (Northern Calcareous Alps)

HANS-JÜRGEN GAWLICK¹, HISASHI SUZUKI² & SIGRID MISSONI¹

¹ University of Leoben, Department of Applied Geosciences and Geophysics, Petroleum Geology, Peter-Tunner-Strasse 5, 8700 Leoben, Austria. hans-juergen.gawlick@unileoben.ac.at

² Otani University, Kyoto 603-8143, Japan

Abstract

This field trip will provide insights in the geometry of a Late Jurassic deep-water radiolaritic trench-like basin, which formation started in the Oxfordian. The Oxfordian phase (first cycle) of the marine basin evolution is characterized by a coarsening-upward trend in deposition, reflecting a compressional regime. In the mass transport deposits only redeposited Late Triassic to Middle Jurassic clasts occur. In the Kimmeridgian (second cycle) grey-greenish radiolarite deposition in a starved environment dominated. In the Tithonian (third cycle) restarted sediment recycling. The general sedimentation trend is a fining-upward cycle indicating an extensional regime. At the beginning of this third cycle, the mass-transport deposits contain (predominantly) Late Triassic to rare Jurassic clasts. Higher up in the succession, the deposits are firstly made of a mixture of older clasts and Tithonian reef debris. Upsection the clast spectra consist of shallow-water carbonates originated from a newly formed carbonate platform. In the Late Tithonian until the Jurassic/Cretaceous boundary occur mass transport deposits and turbidites made predominantly of shallow-water material from this carbonate platform, in parts also mixed with older components derived from the Late Permian - earliest Early Triassic Alpine Haselgebirge. In general, the sedimentation in the Tauglboden basin is characterized by fine-grained siliceous organic-rich sedimentary rocks with intercalation of various mass transport deposits (slumps, debris flows, olistostromes and slide blocks). In the proximal basin, the thickness of the Oxfordian part of the basin fill is nearly 700 m, whereas in the central basin the compacted thickness reaches nearly 150 m. In the most distal part of the basin deposited only few tens of meters of radiolarites. In the Tithonian to earliest Berriasian deposited in the more proximal parts roughly 300-400 m, and in the central to distal part of the basin an up to 800 m thick compacted sedimentary sequence. The triggering factors of the gravitational mass transport movements are earthquakes and volcanism, both can be studied in well preserved outcrops. In addition, the Jurassic geodynamic evolution of the Northern Calcareous Alps will be discussed.

1 Introduction

During this field trip in the central Northern Calcareous Alps (Fig. 1), as part of the Eastern Alps and one of the geologically most classical areas of the world, we will visit locations documenting the entire Late Jurassic (Oxfordian-Tithonian) to earliest Cretaceous (Early Berriasian) depositional history in basinal sequences.

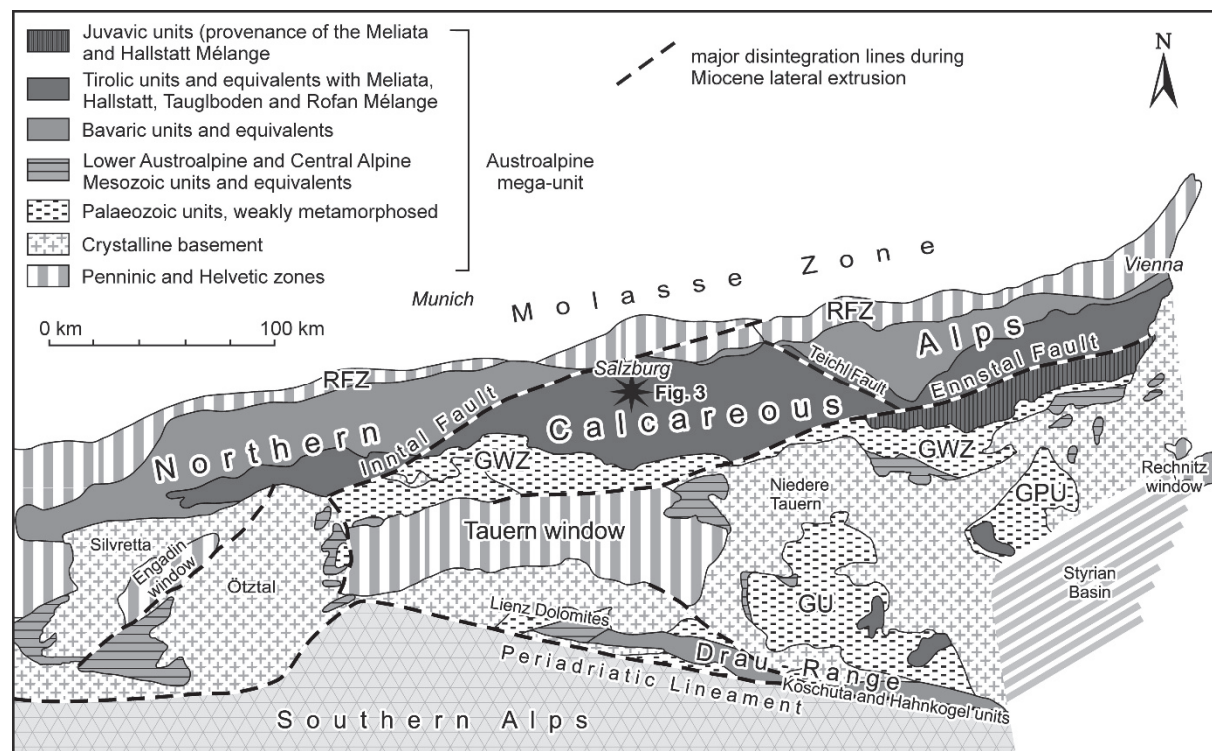


Fig. 1: Tectonic sketch map of the Eastern Alps. The field trip area is indicated by an asterisk (compare Fig. 2). After TOLLMANN (1977) and FRISCH & GAWLICK (2003). GPU Graz Palaeozoic Unit; GU Gurktal Unit; GWZ Greywacke Zone; RFZ Rhenodanubian Flysch Zone.

Until today a lively debate is ongoing on the Middle to Early Cretaceous geodynamic history and the Triassic-Jurassic arrangement of the different facies belts in the Northern Calcareous Alps. It is out of our scope to give a historical overview about the different views and interpretations during the history of investigations. Crucial for the understanding of the Mesozoic geodynamic history of the Northern Calcareous Alps is a restoration of the palaeogeography before the Neogene lateral tectonic extrusion of the Eastern Alps (RATSCHBACHER et al., 1991; LINZER et al., 1995; PUEYO et al., 2007).

Classical nappe concept and historical alternatives

The classic tectonic subdivision of the Northern Calcareous Alps (compare Fig. 1) (in its fundamentals established by HAUG, 1906; later modifications by, e.g., HAHN, 1913; KOBER, 1923; SPENGLER, 1951; PLÖCHINGER, 1980; TOLLMANN, 1976a, b, 1985; compare LINZER et al., 1995) was established in the Berchtesgaden Alps and in the Salzkammergut area and defined three nappe groups. These are, from bottom to top: Bavaric, Tirolic, and Juvavic nappe group. This concept is still widely accepted (see below). Later, a subdivision into three tectonic units (“Stockwerke” *sensu* LEBLING et al., 1935) was proposed: the Tirolic unit (“Tirolische Einheit” *sensu* HAHN, 1913) at the base, overlain by the Lower Juvavic unit (“Tiefjuvavische Einheit”: Hallstatt nappes), and the Upper Juvavic unit (“Hochjuvavische Einheit”: Berchtesgaden and Dachstein nappes). Subsequently, in the salt-mine of Hallein MEDWENITSCH

(1962) subdivided the Lower Juvavic nappe into a Lower (“Untere Hallstätter Decke”: Zlambach nappe - grey Hallstatt facies rocks) and an Upper Hallstatt nappe (“Obere Hallstätter Decke”: Sandling nappe - variously coloured Hallstatt Limestone nappe). In this concept fragmentary blocks of Lower Juvavic Hallstatt Limestones and/or the Alpine Haselgebirge Mélange (TOLLMANN, 1976b) framed the Upper Juvavic nappes (TOLLMANN, 1985 for details and figures).

In an alternative concept, the evaporitic (Alpine) Haselgebirge (Permian salt-mudstone succession; Haselgebirge Mélange according to SPÖTL et al., 1998) acted as a ductile deformation layer. The gravitational tectonic of the Juvavic units should have started in the Oxfordian (e.g., TOLLMANN, 1981, 1987; MANDL, 1982, LEIN, 1985, 1987a) or Late Tithonian (PLÖCHINGER, 1974, 1976, 1984), leading to Late Jurassic to Early Cretaceous sliding of the Alpine Haselgebirge and Hallstatt Limestone successions towards the north.

According to these models (TOLLMANN, 1987; LEIN, 1987b), sliding began in a phase of enhanced radiolarite sedimentation as troughs with deep-marine radiolaritic sedimentation arranged along the median longitudinal axis of the Northern Calcareous Alps (DIERSCHE, 1980). Slump folds are characteristic features in these sediments (e.g., GARRISON & FISCHER, 1969; SCHLAGER & SCHLAGER, 1973; DIERSCHE, 1980; TOLLMANN, 1987). An overall Oxfordian onset of radiolarite sedimentation was estimated, based on ammonite stratigraphy (DIERSCHE, 1980). Hence, the radiolarite basins were filled by deep-water cherty limestones to radiolarites with intercalated breccias and turbidites. The formation of the generally asymmetric radiolarite basins was attributed to extensional tectonics (e.g., SCHLAGER & SCHLAGER, 1973; DIERSCHE, 1980; VECSEI et al., 1989). Another group of authors attributed basin formation and breccia mobilization to strike-slip tectonics (e.g., FISCHER, 1965; WÄCHTER 1987; FRANK & SCHLAGER, 2006; ORTNER et al., 2008).

Current concept

In the current concept we follow:

1. The tectonic subdivision of the Eastern Alps of TOLLMANN (1977) with some modern modifications (FRISCH & GAWLICK, 2003, compare SCHMID et al., 2004) (Fig. 1). A new definition for the nappe groups in the Northern Calcareous Alps, based on new results for the traditional used nappe groups: Bavarian nappes, Tirolian nappes, and Juvavic nappes, is at moment in preparation and discussion (MANDL et al., 2017). In this new concept the Juvavic nappe system is seen as to be formed in Middle-Late Jurassic times with subsequent transport during the Early Cretaceous. The Tirolian nappe system should be formed in the frame of the still enigmatic Mid-Cretaceous (“eoalpine”) tectonic revolution by thrust over the Bavarian unit, and the Bavarian nappe system should be formed post-gosauic by thrust over the Penninic and European units. In general, this proposal follows the concept of FRISCH & GAWLICK (2003): Formation of the Juvavic and Tirolian nappe system with tectonic shortening and nappe thrusting in Middle-Late Jurassic times. From the ancient Juvavic nappe stack mainly erosional products are preserved (Hallstatt Mélange), only in view cases exist remnants of the Juvavic nappes. During the Mid-Cretaceous tectonic period the Jurassic Tirolian nappe system carrying the Hallstatt Mélange and the (at that time still preserved) overlying Juvavic nappe stack with the ophiolite nappes and mélanges on top thrust over on the newly formed Bavarian nappe system. Post-gosauic the entire nappe system of the Calcareous Alps thrust over the Penninic and European derived units.
2. The palaeogeographic reconstruction for the Triassic (valid also for the Early/Middle Jurassic) of KRYSTYN & LEIN in HAAS et al. (1995) with some modifications.

3. The Jurassic geodynamic history of the Austroalpine domain mirrors its palaeogeographic position between two oceanic domains: A) To the west (northwest) the newly formed Penninic Ocean as part of the Alpine Atlantic, where continental extension started in the Hettangian and the first oceanic crust formed in the late Early Jurassic (Toarcian). B) To the east (southeast) the Neo-Tethys Ocean, in which closure started around the Early/Middle Jurassic boundary. Ophiolite obduction started in the Middle Jurassic (Bajocian).

The Juvavic nappe stack of the Northern Calcareous Alps represent the in Jurassic times accreted wedge of the former outer Triassic shelf area (FRISCH & GAWLICK, 2003), i.e. the Hallstatt zone (LEIN, 1987a) and the reef rim. In the central Northern Calcareous Alps remnants of the eroded nappe complex are preserved in the Middle to Late Jurassic radiolaritic trench-like basin fills. These basins were formed in sequence in front of the propagating thrust belt or on top of them and were later overthrust. In these radiolaritic basins occur redeposits of the Meliata facies zone, the Hallstatt facies zone (grey and various coloured Hallstatt zone), and from the reefal belt of the Triassic carbonate platforms. Some blocks or units show transported metamorphism (GAWLICK et al., 1994; GAWLICK & HÖPFER, 1999; MISSONI & GAWLICK, 2011a; compare FRANK & SCHLAGER, 2006).

In the Bajocian/Bathonian the sedimentary evolution in the southern (palaeogeographically southeastern) part of the Tirolic realm as well as in the Hallstatt realm differed from that in the northern (palaeogeographically northwestern) part. Deep-water trench-like basins formed in front of advancing nappes in the course of ophiolite obduction. The first basin group in the southern parts of the Northern Calcareous Alps received mass-flow deposits and large, up to nappe sized slides which derived from the Meliata and Hallstatt Zone (= Meliata and Hallstatt Mélange). The thickness of the Bathonian to Oxfordian basin fills may reach up to 2.000 metres. The nappe stack carrying the Hallstatt Mélange is defined as *Upper Tirolic nappe* (group) (Fig. 2).

The second basin group, the Tauglboden and the Rofan trench-like basins in the north were subjected to high subsidence and sedimentation rates in the Oxfordian to earliest Kimmeridgian. The Trattberg Rise eroded and supplied the Tauglboden Basin to its north with mass transport deposits and slides in Oxfordian times. The nappe carrying the Tauglboden Mélange is defined as *Lower Tirolic nappe* (Fig. 2).

2 Late Jurassic to earliest Cretaceous stratigraphy and formations

For definition and detailed description of the Jurassic formations (Fig. 2) see GAWLICK et al. (2009). The formations, which will be visited during this field trip, were deposited in the Tauglboden Basin (e.g. SCHLAGER & SCHLAGER, 1969, 1973).

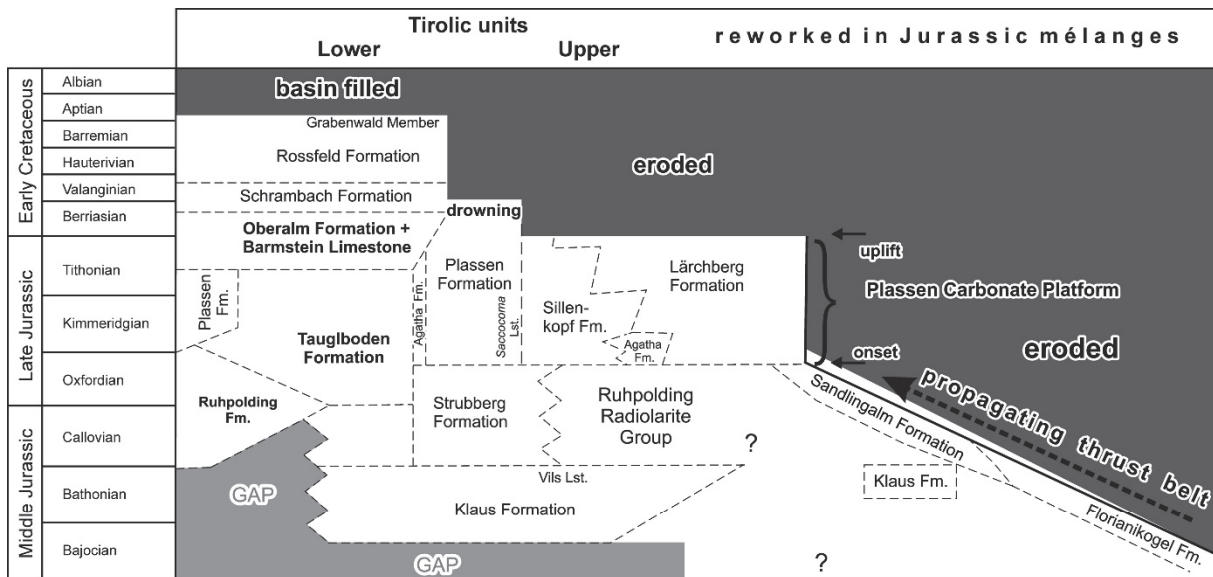
The Tauglboden Basin formed in Early Oxfordian times as a trench-like basin in front of the Trattberg Rise representing the frontal part of the advancing upper Tirolic nappe (Fig. 2). In the Late Oxfordian ongoing compression moved to the north by forming the Brunnwinkl Rise. From this time onwards the Tauglboden Basin became an isolated basin between two topographic highs on which shallow-water carbonate platforms started to be established from the Early Kimmeridgian onwards (Plassen Carbonate Platform). During the Kimmeridgian, the sediment supply from the platforms into the Tauglboden Basin was rather low. The situation changed with the extensional collapse of the Trattberg Rise from the Early Tithonian onwards, which gave way for the Plassen Carbonate Platform in the south to shed resediments into the Tauglboden Basin to the north. Latest Jurassic (Late Tithonian) to earliest Cretaceous (Middle/Late Berriasian) deposition in the Tauglboden Basin was controlled by the

carbonate platform evolution in a tectonically active regime. The tectonic is interpreted by MISSONI & GAWLICK (2011b) as expression of mountain uplift and unroofing (extensional collapse). In the field trip area this extension is expressed in the collapse of the Trattberg Rise, and the formation of steep escarpments and new relief which supplied the Tauglboden Basin again with resediments. Sediment supply from these escarpments increased significantly and cut during the Tithonian more and more into the Kimmeridgian - Early Tithonian Plassen Carbonate Platform. Contemporaneously the evaporitic Haselgebirge Mélange became transported northward, and reached in the Late Tithonian the position of the collapsed Trattberg Rise. In this palaeogeographic position, the evaporitic mélange became reworked and occur as clasts in the coarse-grained breccias, whose components derive mainly from the Plassen Carbonate Platform. During the latest Tithonian to Middle Berriasian Plassen Carbonate Platform underwent backstepping as expressed in the fining-upward trend in the Tauglboden Basin. The final drowning of the Plassen Carbonate Platform in the Late Berriasian gave way for an increasing siliciclastic influx from the south. This siliciclastic influx was mainly controlled by sea-level changes and decreased tectonic activity during the Early Cretaceous. Successively the Tauglboden Basin (now the Tauglboden-Rossfeld Basin or Rossfeld Basin) became filled. Deposition ended in the Middle Aptian (for more details see this volume: KRISCHE et al., 2018).

Ruhpolding Formation: The Middle to Late Jurassic (Late) Bajocian to Early Tithonian Ruhpolding Formation (TRAUTH, 1950; for complete history and definition see GAWLICK et al., 2009), but with a diachronous onset and a diachronous end. This formation included black, green and red radiolarites to cherty limestones and silicified marls/shales in typical microfacies: radiolarian wacke- to packstones. Other organisms beside radiolarians are very rare, e.g. spicula, crinoids (*Saccocoma*), filaments, or in cases *Bositra* shells (DIERSCHE, 1980).

Tauglboden Formation: The Late Jurassic (Early Oxfordian to Early Tithonian) Tauglboden Formation (SCHLAGER, 1956; for complete history and definition see GAWLICK et al., 2009) is defined as radiolarite/cherty marl/cherty limestone succession with intercalated turbidites and mass transport deposits. The Tauglboden Formation can be subdivided into three parts of deposition: A) the lower (Early to ?early Late Oxfordian) part of the sequence is characterized by intense redeposition with a coarsening-upward trend. B) The Late Oxfordian to Kimmeridgian is characterized by a condensed radiolaritic-calcareous sequence. C) The Early Tithonian part of the succession is characterized again by intense redeposition of older material. This part changes gradually into the Oberalm Formation + Barmstein Limestone.

The components in the mass-flow deposits are: Hauptdolomit, lagoonal Dachstein Limestone, Kössen Formation, several limestones of the Adnet Group, Kendlbach and Scheibelberg Formations, Klaus Formation, radiolarites, distal Strubberg Formation and derive from the Trattberg Rise to the south (Fig. 2).



Early/Middle Oxfordian

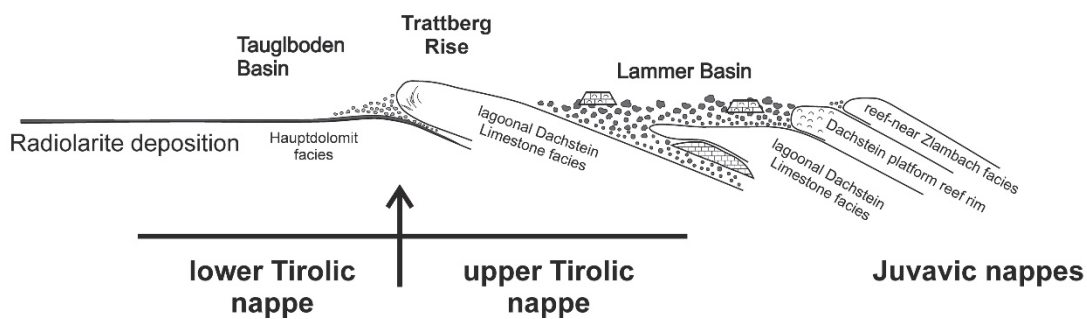


Fig. 2: A) Middle Jurassic to Early Cretaceous stratigraphy of the central Northern Calcareous Alps with an overview of common formation names, simplified after MISSONI & GAWLICK (2011a). Middle Jurassic to earliest Cretaceous formation names, which will be visited during the field trip, are written in bold letters. **B)** After the Middle Jurassic imbrication of the Middle Triassic to Early Jurassic outer shelf region, a new nappe front was formed in the lagoonal Dachstein Limestone facies zone (= Trattberg Rise). North of this nappe front a new deep-water basin was formed (= Taugloden Basin). In contrast to the more northern regions with thin sequences of radiolarites, the sedimentation in the proximal Taugloden Basin was characterized by an up to 700 m thick Early-Middle Oxfordian succession, consisting of radiolarites, slump deposits and different types of mass transport deposits and slides. The Trattberg Rise separated the upper Tirolic nappe from the lower Tirolic nappe.

Oberalm Formation + Barmstein Limestone: In the open-marine Middle/Late Tithonian to Middle Berriasian Oberalm Formation (LIPOLD, 1854; for complete history and definition see GAWLICK et al., 2009; redefined in its uppermost parts by KRISCHE et al., 2013) occur intercalated coarse-grained resediments (mass-transport deposits and turbidites) from the Plassen Carbonate Platform, named Barmstein Limestones (GÜMBEL, 1861). The overall depositional trend of the Oberalm Formation + Barmstein Limestone is fining upward (MISSONI & GAWLICK, 2011a, b). In the latest Tithonian a special type of Barmstein Limestones deposited. In the reworked material from the Plassen Carbonate Platform appear components of the evaporitic Haselgebirge Mélange. This type of mass transport

deposit addressed PLÖCHINGER (1974) as “Tonflatschenbreccia” with its type area in the Leube quarry (for more details see this volume: KRISCHE et al., 2018).

In the upper Oberalm Formation a microfacies and lithological change can be observed between the late Early Berriasian and the Middle Berriasian. Deposition of the variegated, purple to reddish, siliceous to marly limestones with turbidites of roughly Middle Berriasian age (Gutratberg Member of the Oberalm Formation: KRISCHE et al., 2013) is the basinal expression of a stepwise demise of the Plassen Carbonate Platform due to the increasing siliciclastic and organic input. Carbonate production of the Plassen Carbonate Platform decreased significantly since the late Early Berriasian and resulted in its final drowning in the Late Berriasian (GAWLICK & SCHLAGINTWEIT, 2006).

3 The Field Trip

Figure 3 shows the localities that will be visited during this field trip. In the Taugl valley (Tauglboden) we will study the Oxfordian to Early Tithonian Tauglboden Formation (type-locality), which overlies the Early and Middle Jurassic condensed red nodular limestones of the Adnet and Klaus Formations. In the Mörtlbach valley, the Gaissau section offer the Callovian-Oxfordian Ruhpolding Formation (radiolarite) overlain by the Tauglboden Formation. Along the road from Gaissau to Krispl we will see the Late Tithonian part of the Oberalm Formation + Barmstein Limestone. Along the Barmsteine cliffs we will visit the type-locality of the Barmstein Limestone.

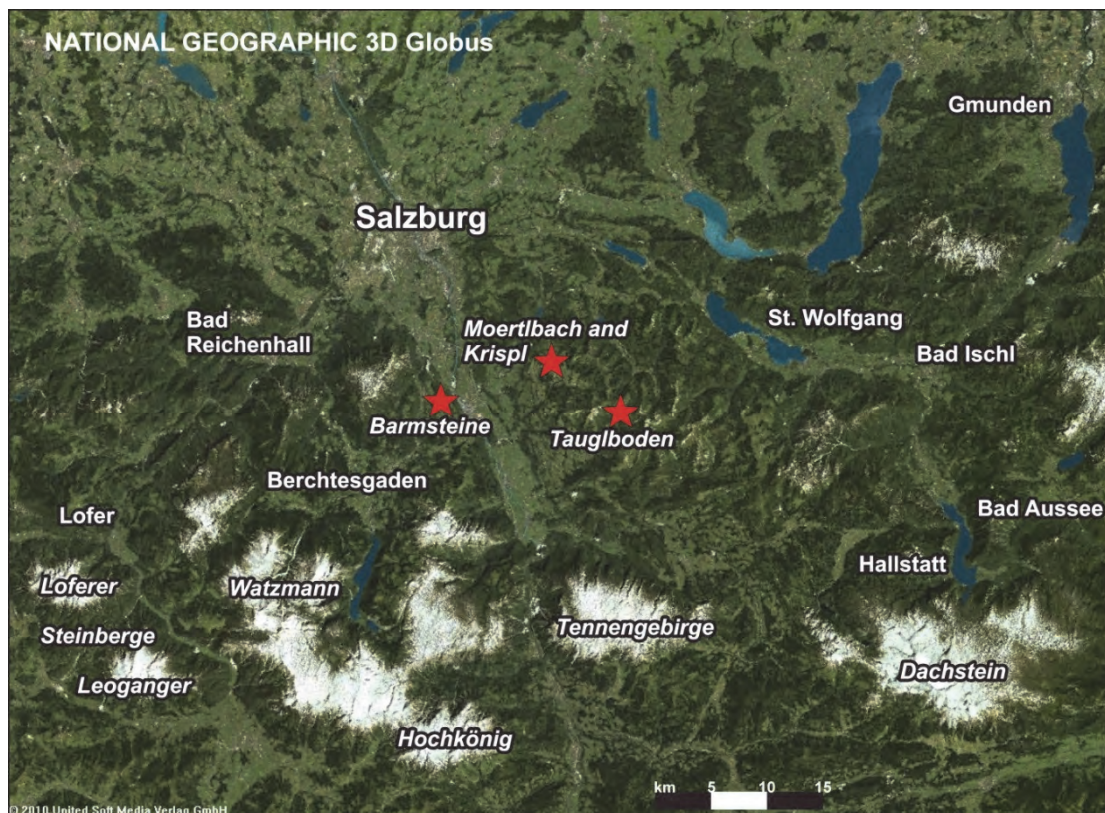


Fig. 3: Satellite image of the central Northern Calcareous Alps, showing the localities of which will be visited during this field trip (red stars).

3.1 Taugl valley (Tauglboden): Tauglboden Formation

In respect to facies, thickness and component content of the mass transport deposits the type area of the Tauglboden Formation in the inner parts of the Osterhorn Block (Fig. 3) represents a central position in the Tauglboden Basin. Proximal parts of the basin are not preserved in the type area, but can be seen in the Knerzenalm area (e.g., MANDL, 1982; WEGERER et al., 2001; GAWLICK et al., 2007) southeast of Bad Ischl, and in the Unken valley (GARRISON & FISCHER, 1969; VECSEI et al., 1989).

In the Taugl valley, geographically situated in the central to southern Osterhorn Mountains (Fig. 3), a complete late Early Jurassic to Late Jurassic sedimentary sequence is preserved. This area was investigated since the second half of the 19th century (SUÈSS & MOJSISCOVICS, 1868) (Fig. 4). As almost everywhere in the Northern Calcareous Alps, the carbonate successions, especially the Jurassic ones, were fairly well dated by means of ammonites (summarized in BÖHM, 1992). In contrast, the age of the radiolaritic sediments remained generally enigmatic until Recent. In the second half of the 20th century the radiolarites were attributed to the Oxfordian or reaching the Kimmeridgian (DIERSCHE, 1980; TOLLMANN, 1985). Recent radiolarian dating constrained the biostratigraphic ages of the radiolarite sequences in numerous areas within the Northern Calcareous Alps (for a review see GAWLICK et al., 2009).

The general sedimentological features and the thickness of the Tauglboden Formation in the type area investigated SCHLAGER & SCHLAGER (1969, 1973) in detail (Fig. 5), and later DIERSCHE (1980) in a more regional context. The age of the succession was attributed to the (Late) Oxfordian to Kimmeridgian on basis of the investigations of SCHLAGER & SCHLAGER (1969) and HUCKRIEDE (1971). HUCKRIEDE (1971) dated the silicified sedimentary rocks below the first red radiolarite bed by means of aptychi as early Oxfordian (Fig. 6). This aptychi-bearing layer yielded also a moderately preserved radiolarian fauna (see below). This radiolarian fauna cannot precisely determine the age of this layer. SCHLAGER & SCHLAGER (1969) mentioned the occurrence of a Kimmeridgian ammonite in the Tauglboden Formation, which limited the age of radiolarite deposition in the Northern Calcareous Alps to the Oxfordian (-Kimmeridgian).

Detailed component analyses and direct biostratigraphic dating of the radiolaritic matrix sediments of various mass transport deposits were carried out since the end of the last century. Modern data resulted in a modified view of the situation of the Tauglboden Basin type-locality.

The radiolarian dating of this paper is based on BAUMGARTNER et al. (1995) and SUZUKI & GAWLICK (2003a), under implementation of the extended age ranges of some species (e.g., SUZUKI et al., 2001; O'DOGHERTY et al., 2006, 2009; SUZUKI & GAWLICK, 2009; AUER et al., 2009; GORIČAN et al., 2012). Nevertheless, we still use here for the presented radiolarian faunas the nomenclature of SUZUKI & GAWLICK (2003b, 2009) (compare O'DOGHERTY et al., 2017).

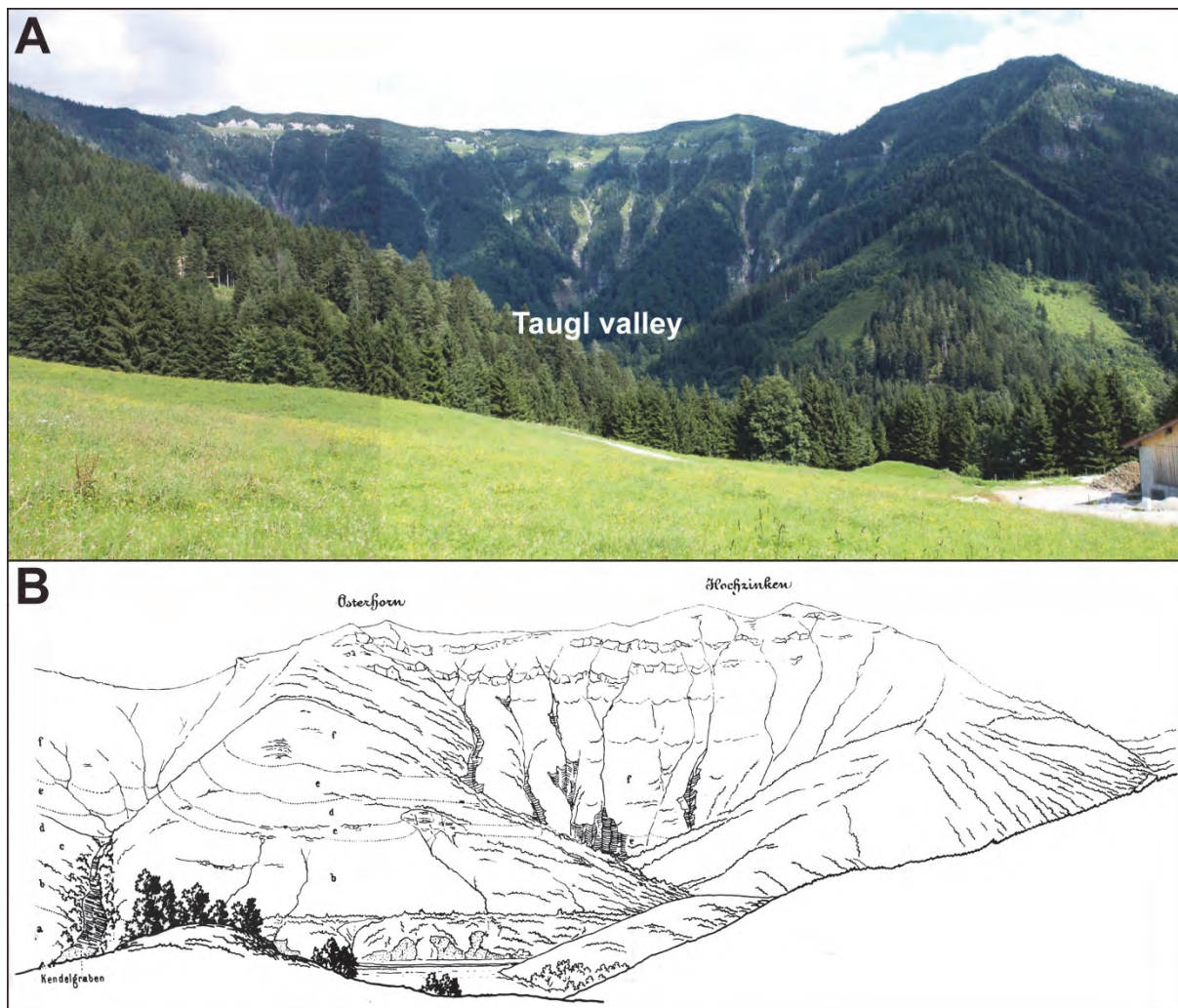


Fig. 4: A) Photo of the central Osterhorn Unit with the Taugl valley. View from the west. B) Original drawing of the central Osterhorn Mountains from SUESS & MOJSISCOVICS (1868). The authors figured out the main characteristics and ages of the Late Triassic to Late Jurassic sedimentary succession. Legend according to SUESS & MOJSISCOVICS (1868) (translated): a - Norian limestones; b - Rhaetian sequence (Kössen Formation and Dachstein Limestone); c - Lower Jurassic and Adnet Limestone (= grey cherty limestones and red nodular limestones); d - bioturbated cherty limestones and marls ("Fleckenmergel"); e - Brown Jurassic (Middle Jurassic); f - White Jurassic (Upper Jurassic). In today's terms, d and e correspond to the Oxfordian to Early Tithonian Tauglboden Formation, f to the late Early Tithonian to Berriasian Oberalm Formation + Barmstein Limestone.

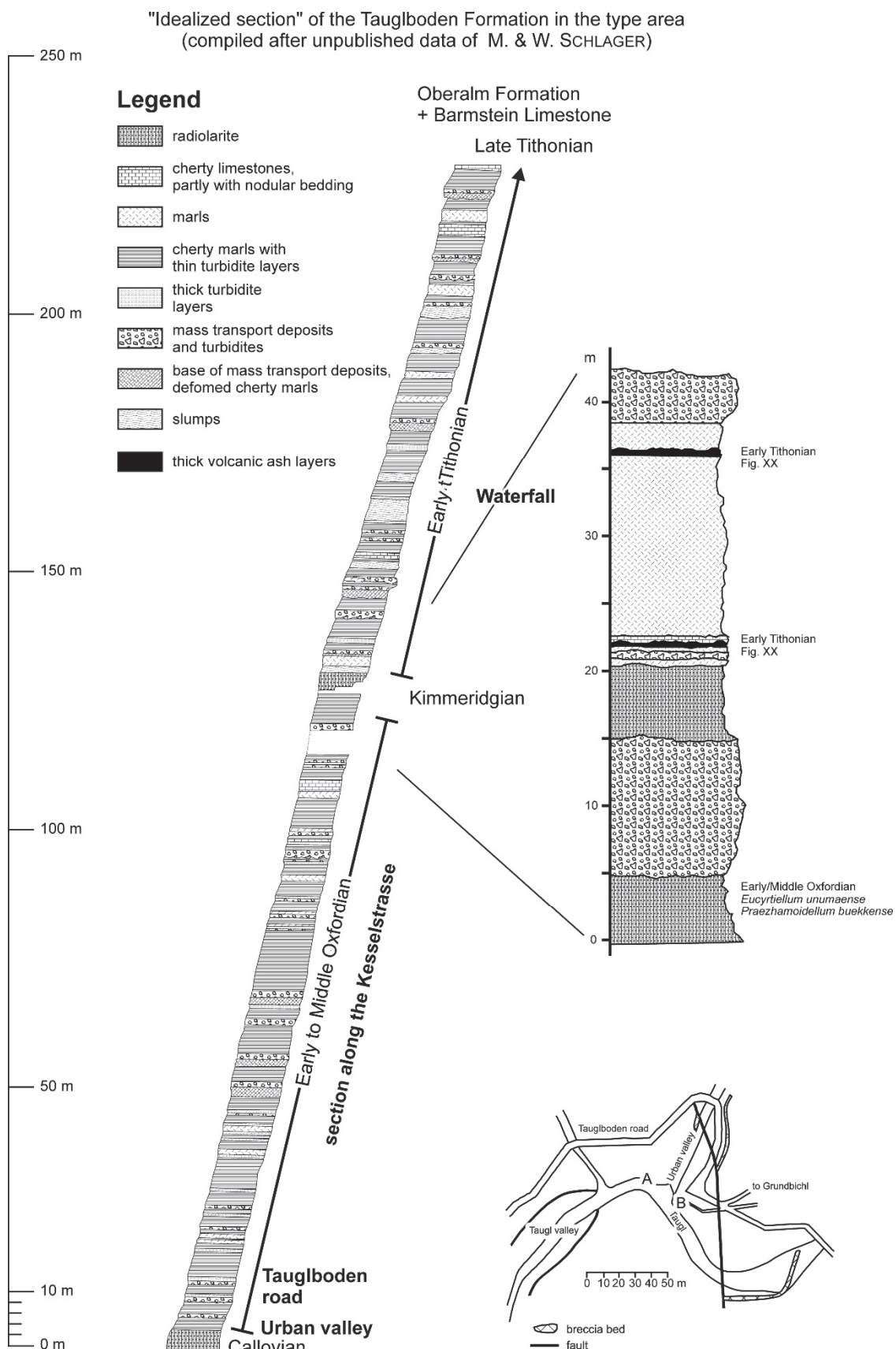


Fig. 5: "Standardized profile" of the Tauglboden Formation (left) in the type area (idealized type section - see SCHLAGER & SCHLAGER, 1973 for details), unpublished profile of M. SCHLAGER & W. SCHLAGER, the central Osterhorn Mountains in the Salzburg Calcareous Alps. Redrawn and printed with permission of

W. SCHLAGER (Amsterdam) in GAWLICK (2000), GAWLICK & FRISCH (2003) and GAWLICK et al. (2012). Ages of different parts of the section according to HUCKRIEDE (1971), GAWLICK et al. (1999), GAWLICK & FRISCH (2003), and new data. Detail section (right) modified from GAWLICK et al. (1999). Map inset: Area of the Urban/Taugl creek exposing excellent sections of the succession around the boundary Klaus Formation/radiolarite (Tauglboden Formation). The drawn detailed section in Figure 6 is from west of the Urban valley (A). An equivalent section is seen east of the Urban creek (B). Redrawn and added after HUCKRIEDE (1971).

Base of the Tauglboden Formation: Urban valley section

The contact between the Early to Middle Jurassic red nodular limestones and the overlying radiolarite sequence is exposed in the junction of the Urban valley with the Taugl valley. The section starts with red nodular limestones, whose age is Late Bathonian to Early Callovian according to HUCKRIEDE (1971) and BÖHM (1992). On top of these red limestones, a condensed layer with feldspar and other volcanic material contains rhyncholiths of (early) Oxfordian age (HUCKRIEDE, 1971). Moderate preserved radiolarians from this layer cannot precise the biostratigraphic age, because of the lack of an Oxfordian marker species. Following species could be determined: *Archaeodictymitra* sp., *Eucyrtidiellum* cf. *unumaense* (Yao), *Gongylothorax favosus* DUMITRICA, *Gongylothorax* aff. *favosus* DUMITRICA, *Lithocampium* sp. A, *Lithocampium* sp., *Loopus* sp., *Stichocapsa naradaniensis* MATSUOKA, *Tricolocapsa conexa* MATSUOKA, *Preazhamoidellum* cf. *parvipora* (TAN), *Tricolocapsa* aff. *fusiformis* Yao, *Tricolocapsa* sp. A sensu OZVOLDOVA, *Tricolocapsa* sp., *Unuma* sp., *Williriedellum crystallinum* DUMITRICA, *Williriedellum marcucciae* CORTESE, *Williriedellum* sp. B, *Zhamoidellum ovum* DUMITRICA, and *Zhamoidellum* sp. (sample TB-Grenzfuge).

The microfacies of the Oxfordian part (HUCKRIEDE, 1971) of the red nodular limestone correspond to that of the overlying red radiolarite: Radiolarian wacke- to packstones predominates. Therefore, this part of the section belongs already to the radiolarite succession.

From the red radiolarite, roughly 50 cm above the boundary layer, following species from a poor preserved radiolarian fauna could be determined: *Emiluvia* sp., *Archaeodictyomitra* sp., *Eucyrtidiellum* cf. *unumaense* (Yao), *Hsuum* cf. *maxwelli* PESSAGNO, *Protunuma* cf. *japonicus* MATSUOKA & Yao, *Triversus* sp., *Williriedellum* sp. B, *Zhamoidellum ovum* DUMITRICA, *Zhamoidellum* sp. (sample TB3).

The radiolarian fauna is similar to those from red radiolarite in the Fludergraben valley. In the Fludergraben valley a roughly two metres thick red radiolarite overlie red nodular limestones of the Klaus Formation (Callovian/Oxfordian boundary according to MANDL, 1982).

In the Tauglboden area the basal radiolarite is well-bedded, of red colour and has at maximum 2 metres thickness. Both, lithology and colour of the radiolarites change gradually upsection. Moreover, the colour of the radiolarites turns from red over grey to finally dark-grey. Only the grey radiolarites are fine laminated, others are massive. The intercalated clay layers between the radiolarite beds increase upsection (Fig. 7). The carbonate content rises as well, whereby the first turbiditic resediments occur after the red to grey colour shift, indicating a change in the basin geometry.

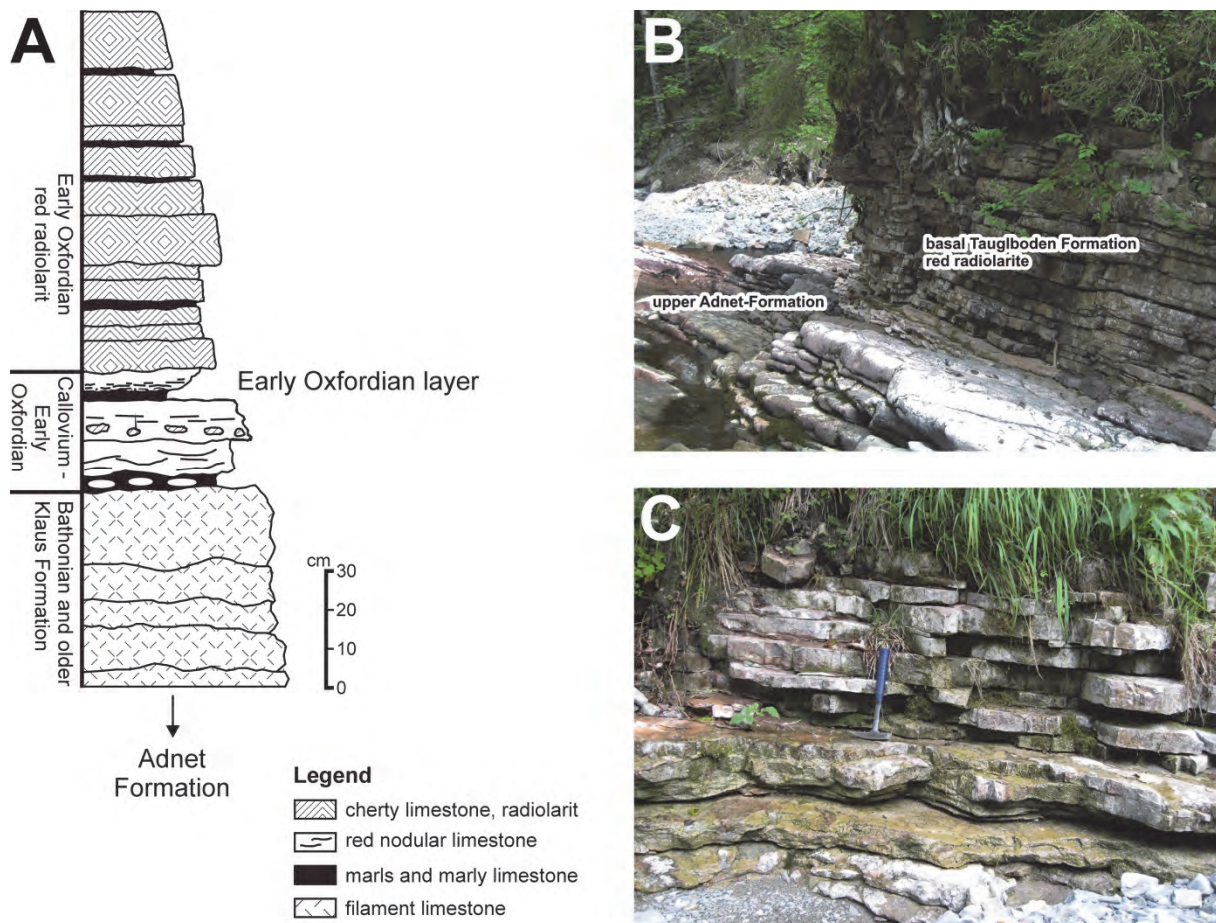


Fig. 6: **A)** Boundary section Klaus Formation to basal Tauglboden Formation (red radiolarite) redrawn and added after HUCKRIEDE (1971). **B)** Exposure east of the Urban creek. **C)** Exposure west of the Urban creek.

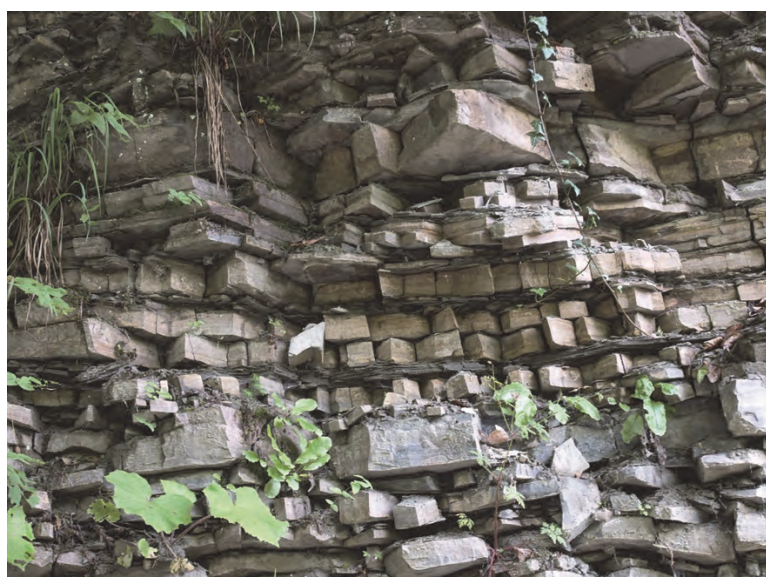


Fig. 7: Reddish-grey massive and laminated Early Oxfordian radiolarite layers with clay intercalations, located in the Taugl valley. Width of the photo: 80 cm.

Radiolarites and mass transport deposits along the Tauglboden road

About five metres above the contact of the red nodular limestone with the radiolarite succession, coarse-grained mass transport deposits are intercalated in the radiolarite sequence. Up to 20 cm thick breccia layers overlie the radiolarite beds practically without basal erosion; obviously the breccia layers seem to be channels deposits (Fig. 8). The structure is fostered by early dewatering of the underlying radiolaritic sediments. Below the breccia layers exist a layers of green-grey volcanic ash, today altered to an illite-bentonite (REITER, 2009). These ashes are locally preserved and acted as slide-plane (Fig. 8).

The components in the slide-flow deposit derive exclusively from the lagoonal Dachstein facies zone. Components of the Early Rhaetian Kössen Formation are rare, whilst components of Rhaetian lagoonal Dachstein Limestone strongly predominate. Early to Middle Jurassic clasts occur in rock-forming quantities, too. Early Jurassic grey cherty limestones (Scheibelberg Formation), chert nodules and red nodular limestones (Adnet Formation) dominate. In contrast, Middle Jurassic *Bositra* Limestone components are rare (details in GAWLICK et al., 2012).

Forest road Kesselstrasse

A highly diverse outcrop situation will be visible on the walk along the forest road Kesselstrasse. In small valleys aside and along the forest road good outcrops with insights into the early evolution of the Tauglboden Basin exist. The age of the succession along the road is still Early to Middle Oxfordian as proven by radiolarians. Dark-grey to black laminated radiolarites with changing clay and carbonate content, slump deposits and mass flows are typical sedimentary features of the succession (Fig. 9). The slump deposits consist partly of cherty sediments without older components, large blocks of older components incorporated in the argillaceous matrix, and debris flows. Generally, the older clasts are the same as in the basal breccia layers (slide flows) along the Tauglboden road. Jurassic clasts are rarer and Triassic clasts older in age appear. The erosion cut deeper into the Norian lagoonal Dachstein Limestone as expressed in the component spectrum. Higher up in the succession the amount of mass transport deposits increased together with the component size. In the curve before the waterfall dark-grey laminated calcareous radiolarites underlie a thick mass transport deposit. According to the poorly preserved radiolarian fauna with *Eucyrtidiellum unumaense* (YAO) and *Praezhamoidellum buekkense* KOZUR (sample TB8) the age of this part of the succession is still Early-Middle Oxfordian. Thus, the entire ca. 150 m thick sequence below this mass flow (Fig. 5) is Early to Middle Oxfordian in age. Above this mass transport deposits follow a roughly 4 metre thick succession of well-bedded grey laminated calcareous radiolarites free of mass transport deposits or turbidites, which are again overlain by mass transport deposits (Fig. 9D). Above these mass transport deposits are up to 15 cm thick layers of volcanic ashes, intercalated between laminated calcareous radiolarites and slide flows (Figs. 9E and F).

Two volcanic ash layers (meta-bentonites) contain both a moderate preserved radiolarian fauna of Early Tithonian age (for details see GAWLICK et al., 1999). In the lower volcanic ash layer following radiolarians were determined: *Sphaerostylus lanceola* (PARONA), *Eucyrtidiellum pyramis* (AITA), *Archaeospongoprnum patricki* JUD, *Archaeodictyomitira apiarium* (RÜST), *Archaeodictyomitira minoensis* (MIZUTANI), *Tricolocapsa funatoensis* (AITA), *Zhamoidellum ovum* DUMITRICA, *Parvingula boesii* (PARONA). In the upper volcanic ash layer following radiolarians were determined: *Archaeospongoprnum imlayi* PESSAGNO, *Eucyrtidiellum pyramis* (AITA), *Pseudoeucyrtis reticularis* MATSUOKA & YAO, *Cinguloturris cylindra* KEMKIN & RUDENKO, *Parvingula mashitaensis* MIZUTANI, *Mirifusus mediodilatatus* (RÜST), *Ristola altissima* (RÜST), *Spongocapsula perampla* (RÜST),

Zhamoidellum ovum DUMITRICA, *Parvingula dhimenaensis* BAUMGARTNER, *Podbursa triancantha* (FISCHLI), *Podocapsa amphitreptera* FOREMAN, *Tricolocapsa funatoensis* (AITA).

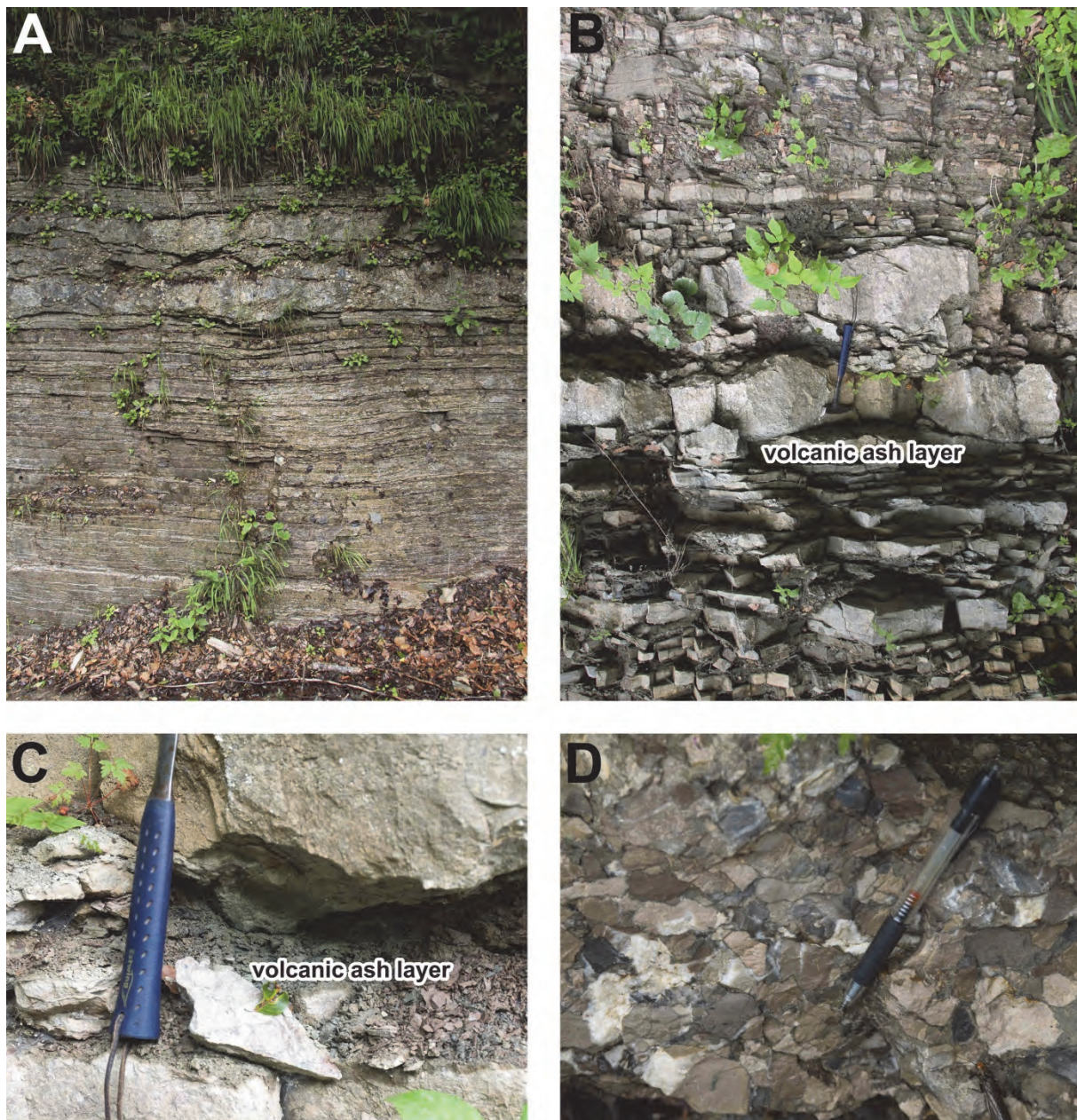


Fig. 8: Up to 20 cm thick breccia layers (slide flows) intercalated in the Early Oxfordian radiolarite sequence. Breccias cut slightly into the basal series (erosional contact), but more often they overlie the radiolarite sequence concordantly in a parallel manner. B and C) Details from the succession in A). Below the breccia, a green layer of volcanic ashes is preserved. These fine-grained ashes acted as slide horizon for the slide flows. D) Angular to subrounded (rare) components of the Early Oxfordian breccias along the Tauglboden road.

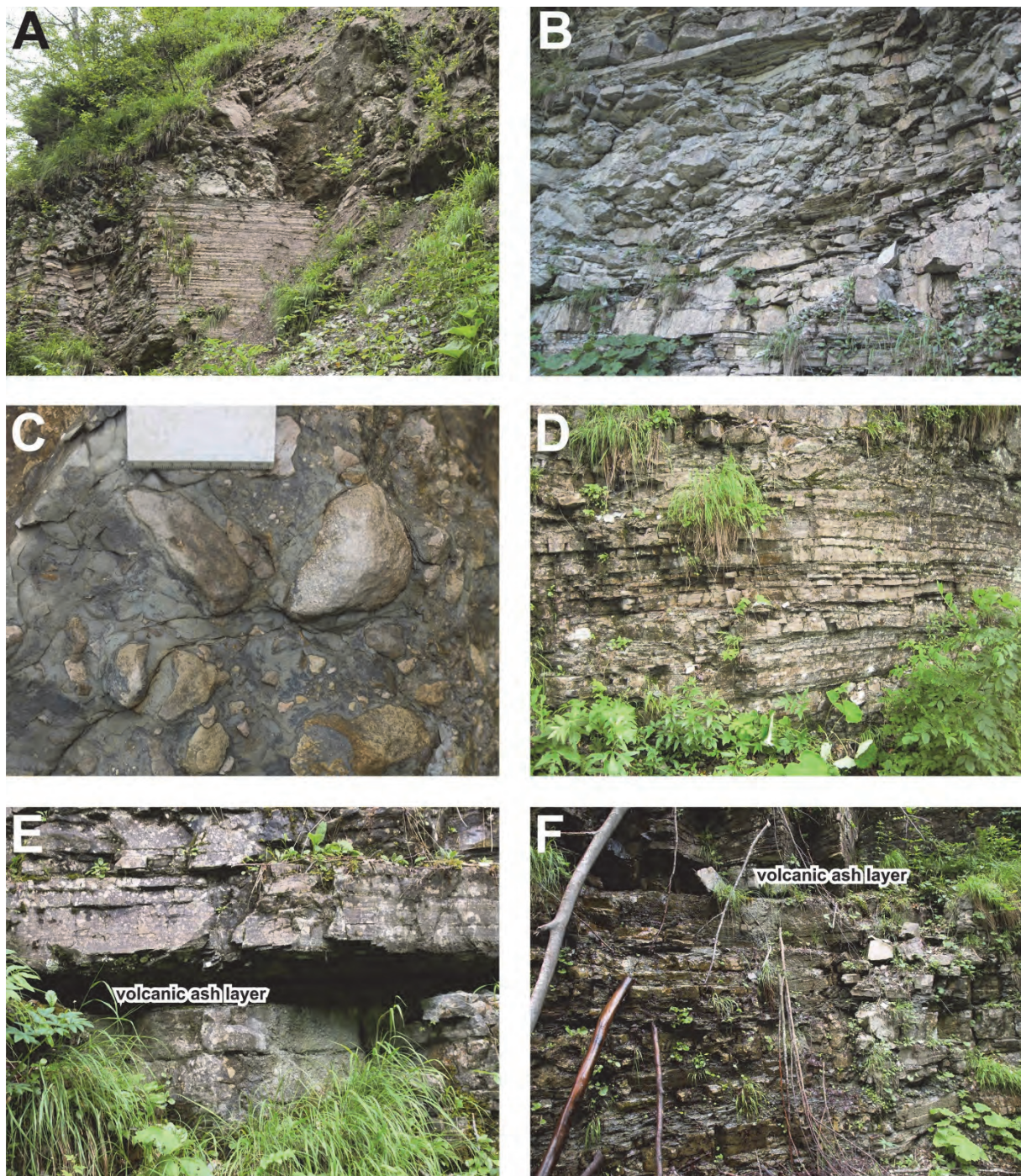


Fig. 9: Outcrops along the forest road Kesselstrasse. **A, B, C)** Early-Middle Oxfordian Tauglboden Formation. **A)** Well bedded and laminated marly radiolarites overlain by a slide flow with large boulders of Late Triassic lagoonal Dachstein Limestone. **B)** Channelized debris-flow. **C)** Mud-flow deposit. Subrounded clasts of the Early Rhaetian Kössen Formation, and Norian to Rhaetian lagoonal Dachstein Limestone. The matrix consists of marly clays without radiolarians. **D)** Kimmeridgian condensed radiolarite succession overlain by Early Tithonian debris-flow deposits. **E)** Lower volcanic ash layer of Early Tithonian age overlain by a slide flow. **F)** Higher volcanic ash layer of Early Tithonian age overlain by a slide flow.

This means, that the time span Latest Oxfordian to Kimmeridgian is characterized by a starved sequence. The volume of material shed into the basin decreased rapidly in the Late Oxfordian. The

Kimmeridgian is characterized by radiolarite sedimentation without deposition of resediments. In the Early Tithonian a new depositional cycle with mobilisation and redeposition of large volumes of rocks started, together with slump deposits mud and debris-flows. Whereas the older components in different chaotic deposits are similar to the Early to Middle Oxfordian sequence the content of Jurassic clasts is very low. Reworked Norian to Rhaetian clasts dominates the component spectrum. Radiolarites in this part of the succession are scarce, with silicified marls and silicified limestones being the matrix sediment. The preservation of the radiolarians in the matrix is generally very poor.

Waterfall

By reaching the waterfall we will see a several tens of metres thick sequence of dark-grey well bedded silicified marls and silicified limestones (Fig. 10). Slump deposits, mud flows, and debris flows are intercalated. The series is also characterized by intercalations of semi-consolidated volcanic ash layers.

Continuing the forest road along the waterfall Kesselstrasse, we reach the Late Tithonian sequence. The forest road provides several outcrops of different fine- und coarse-grained turbidites and mass transport deposits intercalated in grey silicified limestones. The components in these resediments consist of a mixture of older carbonate clasts (Norian to Rhaetian lagoonal and reefal Dachstein Limestone and Kössen Formation), as in the series below, and some shallow-water clasts from the Plassen Carbonate Platform to the south. The change from siliceous to calcareous sedimentation cannot be exactly dated, because of bad preservation stages of the organisms. The overlying silicified limestones with intercalated slope sediments (Barmstein Limestone) are of Late Tithonian to Early Berriasian age, palaeontological proven by radiolarians and calpionellids (e.g., STEIGER, 1981, 1992) as well as by shallow-water organisms (GAWLICK et al., 2005, 2009 for latest reviews).

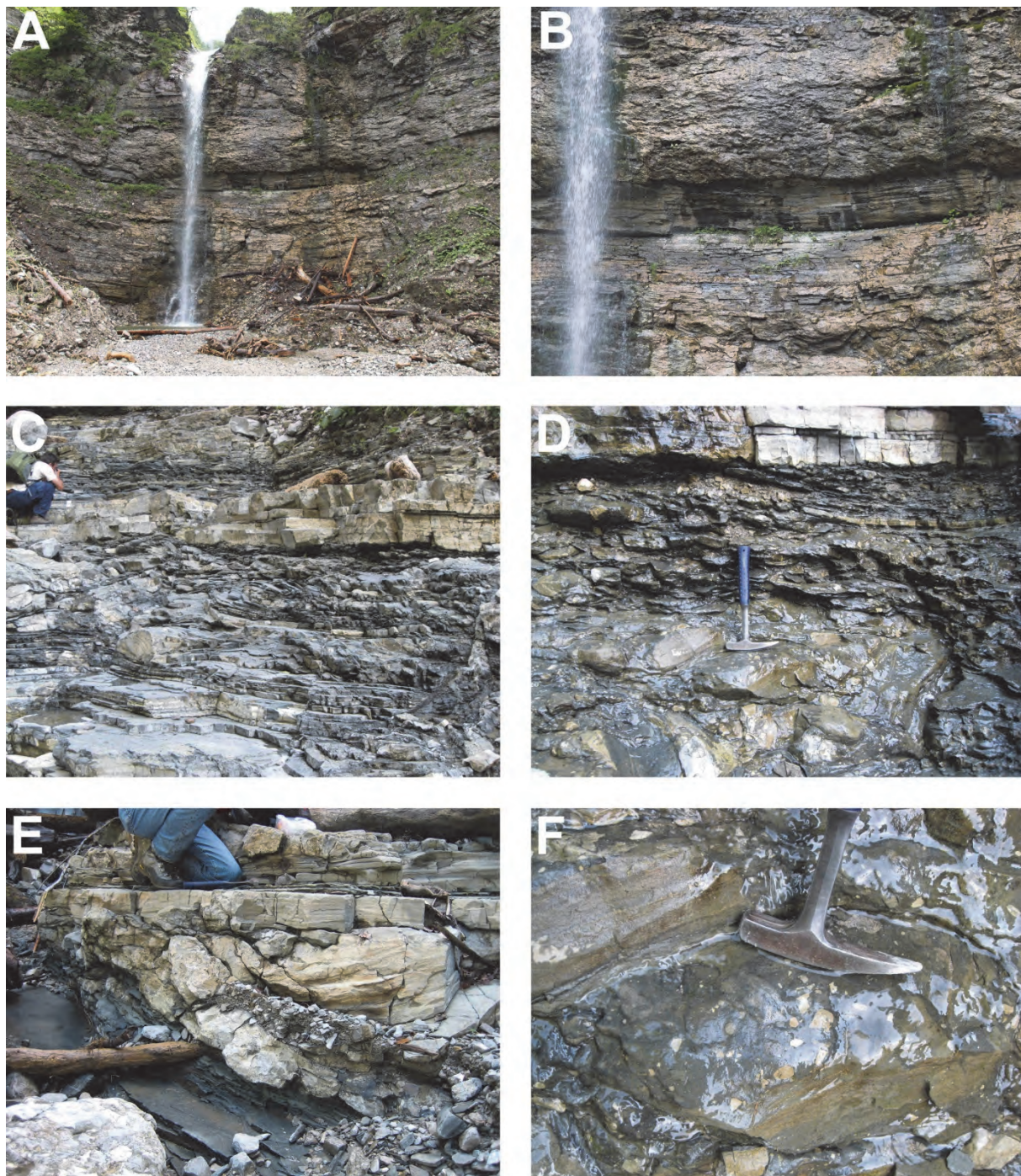


Fig. 10: Early Tithonian Tauglboden Formation of the waterfall Kesselstrasse section. A) Early Tithonian sedimentary succession with slump deposits, mud flows, and debris flows in a matrix of laminated silicified marls to limestones. B) Enlargement of A). Above a series of amalgamated debris flows a series of thin bedded and laminated calcareous radiolarites were deposited topped by a volcanic ash layer, followed by a slide flow. C) Slump deposit overlain by fine grained silicified carbonate turbidites. D) Mud flow deposit reworked in a slump deposit. E) Amalgamated series of silicified marls with breccia layers, overlain by parallel bedded laminated silicified limestones with marl intercalations. Intercalated breccia layers with erosive base. F) Enlargement of D) Late Triassic pebbles dominate the component spectrum.

3.2 Gaissau, Mörtlbach valley: Ruhpolding and Tauglboden Formations

Another Jurassic section, but in a more northernward position as the Taugl valley section, is the section Mörtlbach valley in the Osterhorn Block north of the village Gaissau, on the road to Gaissau/Krispl (parking place) (Figs. 3, 11). Following Jurassic strata developed above the Kössen Basin: the section starts with grey silicified limestones of Sinemurian to Early Pliensbachian age, whose sequence does not exceed a thickness of 5 metres. These grey limestones are overlain by reworked red nodular limestones forming a series of mass-flow deposits. This interval is rich in red marls making up the matrix of the different mass flows. The age of this interval is Late Pliensbachian to Toarcian. The lower Middle Jurassic (Aalenian) is preserved as very thin layer of *Bositra*-rich marly limestones (Böhm, 1992). On top of these Aalenian sedimentary rocks, a ferro-manganese horizon reflects a long lasting depositional gap (Bajocian to Bathonian). Directly above the ferro-manganese horizon deposited 2 cm thick red marls and a 3 cm thick layer of grey volcanic ash. According to X-ray diffraction this volcanic ash was transformed during shallow-burial diagenesis to a smectite-bentonite (following FISHER & SCHMINCKE, 1984). Above the bentonite deposited dm-bedded black radiolarites of ?Late Bathonian - Early Callovian age (Fig. 11), proven by following radiolarian faunas:

Sample GU 19/2001: *Archaeodictyomitra rigida* PESSAGNO, *Cinguloturris latiannulata* (GRILL & KOZUR), *Eucyrtidiellum semifactum* NAGAI & MIZUTANI, *Eucyrtidiellum unumaense* ssp. (YAO), *Eucyrtidiellum unumaense unumaense* (YAO), *Gongylothorax* aff. *favosus* DUMITRICA, *Hsum cf. hisuikyoense* ISOZAKI & MATSUDA, *Parahsuum longiconicum* SASHIDA, *Parvingula* cf. *dhimenaensis* BAUMGARTNER, *Praezhamoidellum yaoi* KOZUR, *Protunuma* cf. *quadriperforatus* O'DOGHERTY & GORICAN, *Protunuma* cf. *lanosus* OZVOLDOVA, *Theocapsomma medvednicensis* GORICAN, *Theocapsomma* sp. *Tricolocapsa* sp. A sensu OZVOLDOVA, *Tricolocapsa* sp., *Unuma* cf. *gorda* HULL, *Unuma* sp., *Williriedellum* sp. *Eucyrtidiellum semifactum*, *Hsum cf. hisuikyoense* and *Gongylothorax* aff. *favosus* are typical forms of the UA zone 7 according to BAUMGARTNER et al. (1995). *Protunuma* cf. *quadriperforatus* occur according to BAUMGARTNER et al. (1995) in the UA 5-6, but appear in the radiolarite sections of Northern Calcareous Alps also in younger levels and may reach the UA 8. *Cinguloturris latiannulata* should be a precursor form of *Cinguloturris carpathica* with the first FAD in the UA 7. *Zhamoidellum ovum* could not be detected in this sample. The age for this sample is therefore ?Late Bathonian to earliest Callovian.

Sample GU 20/2001: *Archaeodictyomitra* sp., *Gongylothorax* aff. *favosus* DUMITRICA, *Parvingula* sp. *Pseudodictyomitrella* sp. *Tricolocapsa conexa* MATSUOKA, *Tricolocapsa* aff. *fusiformis* YAO, *Tricolocapsa* cf. *parvipora* TAN, *Tricolocapsa* spp., *Williriedellum* cf. *dierschei* SUZUKI & GAWLICK, *Williriedellum* sp. This radiolarian association shows an age-range of Late Bathonian to Early Oxfordian. *Tricolocapsa* aff. *fusiformis* appear also in the section Fludergraben above the Callovian/Oxfordian boundary.

Sample Mörtl1//2001: *Archaeodictyomitra* cf. *amabilis* AITA, *Dictyomitrella* cf. *kamoensis* MIZUTANI & KIDO, *Eucyrtidiellum semifactum* NAGAI & MIZUTANI, *Eucyrtidiellum unumaense* ssp. (YAO), *Eucyrtidiellum unumaense unumaense* (YAO), *Gongylothorax* aff. *favosus* DUMITRICA, *Hsum* cf. *brevicostatum* (OZVOLDOVA), *Hsum* sp., *Parahsuum* sp., *Protunuma lanosus* OZVOLDOVA, *Protunuma* cf. *quadriperforatus* O'DOGHERTY & GORICAN, *Stichocapsa convexa* YAO, *Tricolocapsa* cf. *conexa* MATSUOKA, *Tricolocapsa tetragona* MATSUOKA, *Tricolocapsa* cf. *plicarum* YAO, *Tricolocapsa* sp., *Unuma* sp., *Williriedellum* *dierschei* SUZUKI & GAWLICK, *Williriedellum* *marcucciae* CORTESE, *Williriedellum* sp. *Gongylothorax* aff. *favosus*, *Archaeodictyomitra* cf. *amabilis*, *Dictyomitrella* cf. *kamoensis* and *Eucyrtidiellum semifactum* point to UA 7. In the Northern Calcareous Alps this radiolarian association is typical for the Early Callovian; but a Late Bathonian age cannot be excluded.

Sample GU14A/2001 from the transition black to red radiolarite: *Amphipyndax* sp., *Archaeodictyomitra mitra* DUMITRICA, *Archaeodictyomitra* sp., *Droltus galerus* SUZUKI, *Droltus* sp., *Eucyrtidiellum nodosum* WAKITA, *Eucyrtidiellum unumaense* ssp. (YAO), *Eucyrtidiellum unumaense* *unumaense* (YAO), *Eucyrtidiellum unumaense dentatum* BAUMGARTNER, *Eucyrtidiellum unumaense* *pustulatum* BAUMGARTNER, *Gongylothorax* aff. *favosus* DUMITRICA, *Hiscocapsa acuta* HULL, *Hsuum brevicostatum* (OZVOLDOVA), *Loopus* cf. *nudus* (SCHAAF), *Loopus* sp., *Praezhamoidellum bukkense* KOZUR, *Pseudodictyomitra* sp., *Stichomitra* sp. D sensu KIESSLING, *Tetracapsa* sp. A, *Tricolocapsa undulata* (HEITZER), *Tricolocapsa* sp. A sensu OZVOLDOVA, *Tricolocapsa* sp., *Triversus* spp., *Williriedellum carpathicum* DUMITRICA, *Williriedellum dierschei* SUZUKI & GAWLICK, *Williriedellum marcucciae* CORTESE, *Williriedellum* sp., *Zhamoidellum exquisita* HULL, *Zhamoidellum kozuri* (HULL), *Zhamoidellum* sp. The appearance of *Williriedellum carpathicum* indicates an age for the sample as Late Callovian to Early/Middle Oxfordian (*Williriedellum carpathicum* subzone of the *Zhamoidellum* zone; according to SUZUKI & GAWLICK, 2003a, updated in GAWLICK et al., 2009).

The thickness of the ?Late Bathonian to Middle Callovian black radiolarite is about 1 metre. Upsection graded the colour of the radiolarite to red. Between the black and the red radiolarite again a several cm-thick smectite-bentonite is proven (REITER, 2009).

The age of the less than 20 metres thick red radiolarite is Late Callovian to Oxfordian, most probably earliest Oxfordian according to in cases rich and well preserved radiolarian associations:

Sample GU1/2001: *Archaeodictyomitra patricki* KOCHER, *Archaeodictyomitra* sp., *Cinguloturris* cf. *carpatica* DUMITRICA, *Gongylothorax* sp., *Hiscocapsa* sp., *Parvingula* sp., *Protunuma* cf. *multicostatus* (HEITZER), *Stichomitra annibill* KOCHER, *Stichomitra* sp. D sensu KIESSLING, *Williriedellum* cf. *crystallinum* DUMITRICA, *Williriedellum* sp., *Zhamoidellum ovum* DUMITRICA. The age range of this sample is according to the radiolarian association Callovian to Kimmeridgian. On base of the fact that the underlying sample gives a Late Callovian to younger age, the lower age limit of this sample is Late Callovian.

Sample GU 3/2001: *Acanthocircus* cf. *suboblongus* (YAO), *Actinomma* cf. *siciliensis* KITO & DE EVER, *Archaeospongoprnum imlayi* PESSAGNO, *Archaeospongoprnum* cf. *tricostatum* STEIGER, *Archaeospongoprnum* spp., *Emiluvia chica* FOREMAN, *Emiluvia* sp., *Tritrabs* cf. *casmaliaensis* (PESSAGNO), *Archaeodictyomitra minoensis* (MIZUTANI), *Archaeodictyomitra* cf. *minoensis* (MIZUTANI), *Archaeodictyomitra rigida* PESSAGNO, *Archaeodictyomitra vulgaris* PESSAGNO, *Archaeodictyomitra* sp. B sensu WEGERER et al., *Archaeodictyomitra* spp., *Cinguloturris carpatica* DUMITRICA, *Cyrtocapsa* sp., *Droltus* sp., *Eucyrtidiellum ptyctum* (RIEDEL & SANFILIPPO), *Gongylothorax favosus* DUMITRICA, *Gongylothorax* aff. *favosus* DUMITRICA, *Hiscocapsa acuta* HULL, *Hiscocapsa* sp., *Hsuum brevicostatum* (OZVOLDOVA), *Lithocampium* sp., *Loopus doliolum* DUMITRICA, *Parahsuum carpathicum* WIDZ & DE EVER, *Parahsuum longiconicum* SASHIDA, *Parvingula dhimenaensis* BAUMGARTNER, *Parvingula* spp., *Pdobursa* sp., *Pseudodictyomitra* sp. D sensu MATSUOKA & YAO, *Stichomitra annibill* KOCHER, *Stichomitra* sp., *Syringocapsa* sp., *Tetracapsa* sp. A, *Tricolocampe* sp. B, *Tricolocapsa* cf. *leiostraca* (FOREMAN), *Tricolocapsa undulata* (HEITZER), *Tricolocapsium* sp. A, *Triversus hexagonatus* (HEITZER), *Triversus* spp., *Williriedellum carpathicum* DUMITRICA, *Wrangellium* aff. *hsui* (PESSAGNO), *Wrangellium* cf. *hsui* (Pessagno), *Wrangellium okamurae* (MIZUTANI), *Wrangellium* sp., *Zhamoidellum ovum* DUMITRICA. *Gongylothorax favosus* and *Gongylothorax* aff. *favosus* give UA 8 according to BAUMGARTNER et al. (1995). *Williriedellum carpathicum* has an FAD in the Late Callovian. Therefore the age of this sample is most probably Late Callovian to Early Oxfordian.

Sample GU 5/2001: *Tritrabs* sp., *Archaeodictyomitra minoensis* (MIZUTANI), *Archaeodictyomitra rigida* PESSAGNO, *Gongylothorax favosus* DUMITRICA, *Stichocapsa* sp., *Stichomitra tuscanica* (CHIARI, CORTESE & MARCUCCI), *Syringocapsa* sp., *Zhamoidellum* sp. The stratigraphic age is limited by the appearance of *Gongylothorax favosus*.

Sample GU 6/2001: *Acanthocircus* cf. *suboblongus* (YAO), *Acanthocircus* cf. *trizonalis* (RÜST), *Acanthocircus* sp., *Angulobracchia* sp. A, *Archaeospongoprnum* cf. *imlayi* PESSAGNO, *Archaeospongoprnum* spp., *Paronaella broennimanni* PESSAGNO, *Paronaella* cf. *mulleri* PESSAGNO, *Emiluvia* cf. *chica* FOREMAN, *Emiluvia premyogii* BAUMGARTNER, *Emiluvia* sp., *Spongostaurus* sp., *Triactoma* sp., *Tritrabs* cf. *exotica* (PESSAGNO), *Tritrabs* sp., *Acotripus* sp., *Archaeodictyomitra minoensis* (MIZUTANI), *Archaeodictyomitra mitra* DUMITRICA, *Archaeodictyomitra rigida* PESSAGNO, *Archaeodictyomitra sisi* YANG, *Archaeodictyomitra* cf. *sisi* YANG, *Archaeodictyomitra* spp., *Cinguloturris carpathica* DUMITRICA, *Cinguloturris* sp., *Dictyomitrella* sp., *Droltus galerus* SUZUKI, *Droltus* sp., *Eucyrtidiellum ptyctum* (RIEDEL & SANFILIPPO), *Eucyrtidiellum unumaense* (YAO), *Eucyrtidiellum* sp., *Gongylothorax favosus* DUMITRICA, *Hiscocapsa acuta* HULL, *Hiscocapsa* spp., *Hsuum brevicostatum* (OZVOLDOVA), *Hsuum* cf. *cuestaense* PESSAGNO, *Lithocampium* sp. A, *Lithocampium* sp., *Loopus* cf. *nudus* (SCHAAF), *Parahsuum carpathicum* WIDZ & DE EVER, *Parahsuum* sp. S sensu MATSUOKA, *Parahsuum* sp., *Parvingula dhimenaensis* BAUMGARTNER, *Parvingula spinata* (VINASSA), *Parvingula* spp., *Parvifavus* sp. A, *Pdobursa* sp., *Protunuma multicostatus* (HEITZER), *Pseudodictyomitra* cf. *primitiva* MATSUOKA & YAO, *Pseudodictyomitra* sp. D sensu MATSUOKA & YAO, *Pseudodictyomitra* sp. N sensu SUZUKI et al., *Solenotryma ichikawai* MATSUOKA & YAO, *Spongocapsula* sp., *Stichomitra annibill* KOCHER, *Stichomitra* sp., *Syringocapsa levis* (HORI), *Syringocapsa* sp. A sensu SUZUKI et al., *Syringocapsa* sp., *Tetracapsa* sp. A, *Tetracapsa* spp., *Thanarla* aff. *pulchra* (SQUINABOL), *Tricolocapsa* cf. *parvipora* TAN, *Tricolocapsa undulata* (HEITZER), *Tricolocapsium* sp. A, *Tricolocapsium* sp., *Triversus hexagonatus* (HEITZER), *Triversus* sp., *Williriedellum carpathicum* DUMITRICA, *Williriedellum crystallinum* DUMITRICA, *Wrangellium hsui* (PESSAGNO), *Wrangellium* aff. *hsui* (PESSAGNO), *Wrangellium* cf. *okamurai* (MIZUTANI), *Zhamoidellum ovum* DUMITRICA, *Zhamoidellum ventricosum* DUMITRICA, *Zhamoidellum* sp. From this rich and well preserved radiolarian association *Eucyrtidiellum unumaense*, *Gongylothorax favosus*, *Zhamoidellum ventricosum*, and *Williriedellum carpathicum* give an Late Callovian to Early Oxfordian age for this sample. *Loopus* cf. *nudus* and *Thanarla* aff. *pulchra* point to a younger age.

Sample GU 8/2001: *Archaeospongoprnum* sp. *Tritrabs* cf. *exotica* PESSAGNO, *Tritrabs* sp., *Archaeodictyomitra mitra* DUMITRICA, *Archaeodictyomitra* sp., *Gongylothorax favosus* DUMITRICA, *Gongylothorax* aff. *favosus* DUMITRICA, *Gongylothorax* sp., *Hiscocapsa* cf. *hexagona* (HORI), *Hiscocapsa* sp., *Loopus doliolum* DUMITRICA, *Protunuma japonicus* MATSUOKA & YAO, *Pseudodictyomitra primitiva* MATSUOKA & YAO, *Stichomitra tairai* AITA, *Stichomitra* sp., *Stylocapsa* cf. *oblongula* KOCHER, *Tricolocapsa* cf. *uesti* TAN, *Tricolocapsa* sp., *Triversus* sp., *Williriedellum crystallinum* DUMITRICA, *Wrangellium rudabanyaense* (GRILL & KOZUR), *Zhamoidellum ovum* DUMITRICA, *Zhamoidellum* sp. *Gongylothorax favosus*, *Gongylothorax* aff. *favosus*, and *Stylocapsa oblongula* give UA 8 according to BAUMGARTNER et al. (1995).

Sample GU 1/2002: *Acanthocircus* cf. *suboblongus minor* BAUMGARTNER, *Archaeospongoprnum* cf. *elegans* WU, *Archaeospongoprnum* sp., *Plegmosphaera* ? sp., *Spongotripus* sp., *Tritrabs* cf. *ewigi* (PESSAGNO), *Tritrabs exotica* (PESSAGNO), *Tritrabs* sp., *Archaeodictyomitra rigida* PESSAGNO, *Archaeodictyomitra* sp. B sensu WEGERER et al., *Archaeodictyomitra* sp., *Cinguloturris carpathica* DUMITRICA, *Eucyrtidiellum unumaense* (YAO), *Eucyrtidiellum unumaense pustulatum* BAUMGARTNER, *Gongylothorax favosus* Dumitrica, *Gongylothorax* aff. *favosus* DUMITRICA, *Gongylothorax* sp., *Hsuum*

brevicostatum (OZVOLDOVA), *Hsuum maxwelli* PESSAGNO, *Pseudodictyomitra primitiva* MATSUOKA & YAO, *Pseudodictyomitrella spinosa* GRILL & KOZUR, *Pseudodictyomitrella* sp., *Stichocapsa inflata* (BLOME), *Stichomitra annibill* KOCHER, *Tricolocampe* sp., *Triversus hexagonatus* (HEITZER), *Triversus* sp. The co-appearance of *Zhamoidellum ventricosum*, *Eucyrtidiellum unumaense*, *Gongylothorax favosus*, *Gongylothorax* aff. *favosus* and *Zhamoidellum ventricosum* point to UA 8.

In total, all radiolarian associations from the red radiolarite have an age range of Late Callovian to Early Oxfordian. A more exact biostratigraphic dating with radiolarian associations is yet not possible. Only the appearance of a few species give a hint for a slightly younger age, but age range and systematic order of these species is unproven at moment.

Rarely intercalated red clay layers, located in the middle part of the red radiolarite succession, consist also of smectite-bentonites (REITER, 2009). Still in the Early to Middle Oxfordian the red radiolarite passed into dark-grey radiolarites and cherty limestones. The radiolarite of this part in the section is laminated and contain the first fine-grained turbidites. The clasts are too small to be determined regarding their stratigraphic affiliation. Upsection the turbidites become coarse-grained with components consisting predominately of Late Triassic lagoonal Dachstein Limestone, whilst Early to Middle Jurassic clasts occur seldom. This component spectrum is identical to that of the Taugl valley resediments in the south.

To summarize, the age of the radiolarian-rich background sediment is Early to Middle Oxfordian according to the type-locality, even direct radiolarian biostratigraphic ages are not exact enough at moment (see above). In contrast to the thick succession in the Taugl valley, the thickness of the northern Tauglboden Basin succession does not exceed a few tens of metres (details in DIERSCHE 1980) with a maximal thickness of the intercalated mass flows of only 10-20 centimetres.

Radiolarian samples from the transitional part of the massive red radiolarite to laminated red-grey to grey calcareous radiolarites of the basal Tauglboden Formation yielded only moderate preserved radiolarian faunas. The radiolarian associations from this part of the succession gave a similar age as those from the red radiolarite below. A similar result was reached by the radiolarian associations from the Oxfordian boundary layer in the Urban valley (see above) and from the Fludergraben valley in the Salzkammergut region (SUZUKI et al., 2004), where first a red radiolarite and in turn the Tauglboden Formation overlie the Klaus Formation, dated in its upper parts by ammonites as deposited around the Callovian/Oxfordian boundary (MANDL, 1982).

Sample GU 9/2001: *Archaeodictyomitra sisi* YANG, *Eucyrtidiellum unumaense unumaense* (YAO), *Gongylothorax* sp., *Parvifavus* sp. A, *Stichocapsa* sp., *Zhamoidellum* cf. *ventricosum* DUMITRICA. This radiolarian association cannot be dated more precisely as UA 8 by the co-occurrence of *Eucyrtidiellum unumaense unumaense* and *Zhamoidellum* cf. *ventricosum*.

Sample GU 10/2001: *Eucyrtidiellum* cf. *unumaense* (YAO), *Eucyrtidiellum unumaense pustulatum* BAUMGARTNER, *Gongylothorax favosus* DUMITRICA, *Gongylothorax marmoris* KISSLING, *Hiscocapsa acuta* HULL, *Tricolocapsa matsuokai* SASHIDA, *Williriedellum* sp., *Zhamoidellum ovum* DUMITRICA, This radiolarian association cannot be dated more precisely as UA 8 by the co-occurrence of *Eucyrtidiellum* cf. *unumaense*, *Eucyrtidiellum unumaense pustulatum* and *Gongylothorax favosus*.

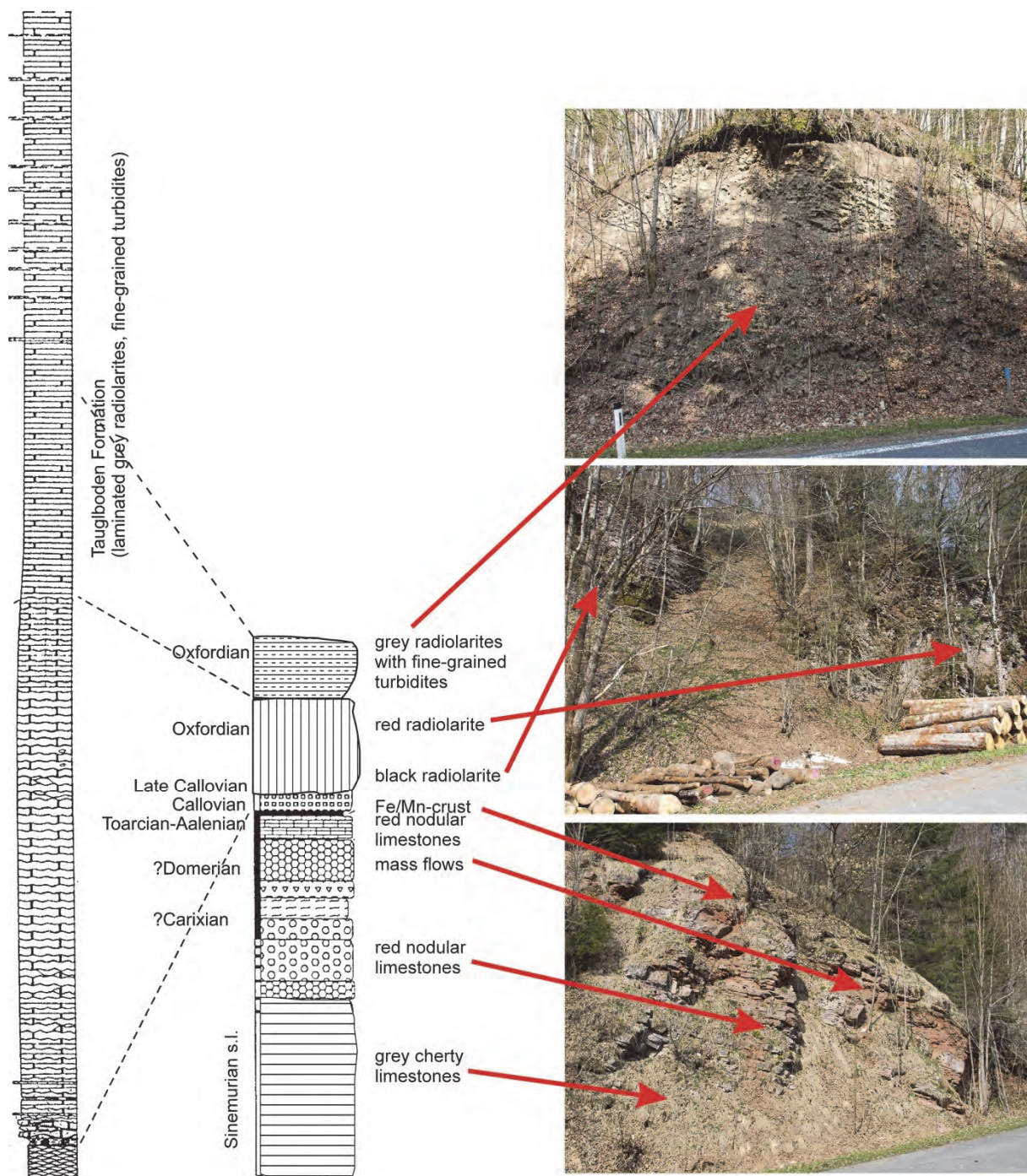


Fig. 11: Stratigraphy and facies of the Early to early Late Jurassic section along the road to the village Krispl in the Mörlbach valley (compare GAWLICK et al., 2012). Right section with photographs after BÖHM (1992), modified and completed for the Callovian-Oxfordian part. Left section from DIERSCHE (1980).

Sample GU 11/2001: *Archaeospongoprunum* sp., *Sphaerostylus lanceola* (PARONA), *Acotripos* cf. *sphaericus* OZVOLDOVA, *Archaeodictyomitra amabilis* AITA, *Archaeodictyomitra sisi* YANG, *Archaeodictyomitra* sp., *Droltus galerus* SUZUKI, *Eucyrtidiellum ptyctum* (RIEDEL & SANFILIPPO), *Gongylothorax favosus* DUMITRICA, *Hiscocapsa acuta* HULL, *Napora pyramidalis* BAUMGARTNER, *Parahsuum* sp., *Parvingula dhimenaensis* BAUMGARTNER, *Tetracapsa* sp. A, *Tetracapsa* sp., *Tricolocapsa undulata* (HEITZER), *Tricolocapsa* sp. A sensu OZVOLDOVA, *Williriedellum dierschei* SUZUKI & GAWLICK, *Zhamoidellum ovum* DUMITRICA. The occurrence of *Archaeodictyomitra amabilis* together with *Zhamoidellum ovum* points normally to the Early Callovian. Therefore the age range of *Archaeodictyomitra amabilis* has to be shifted at least to the Late Callovian - Early Oxfordian.

Sample GU 12/2001: *Archaeodictyomitra* cf. *mitra* DUMITRICA, *Archaeodictyomitra* cf. *sisi* YANG, *Archaeodictyomitra* sp., *Eucyrtidiellum unumaense* ssp. (YAO), *Eucyrtidiellum unumaense unumaense* (YAO), *Gongylothorax* aff. *favosus* DUMITRICA, *Gongylothorax oblongus* YAO, *Hsuum* sp., *Quarticella* cf. *ovalis* TAKEMURA, *Stichocapsa convexa* YAO, *Stylocapsa oblongula* KOCHER, *Theocapsomma* sp., *Tricolocapsa* cf. *conexa* MATSUOKA, *Tricolocapsa* cf. *plicarum* YAO, *Tricolocapsa* sp., *Unuma* sp., *Williriedellum dierschei* SUZUKI & GAWLICK. The biostratigraphic age of this radiolarian association is not very precise: UA 7 to 8. Important is the occurrence of *Gongylothorax oblongus* assigned by BAUMGARTNER et al. for the UA 4. A similar form was described by HULL (1997) as *Gongylothorax* aff. *oblongus* from North America in the time interval Late Oxfordian to Kimmeridgian. The stratigraphic range of *Gongylothorax oblongus* has to be extended at least to the Late Callovian - Early Oxfordian.

Sample GU 13/2001: *Tritrabs* sp., *Eucyrtidiellum unumaense* (YAO), *Eucyrtidiellum* sp., *Stichocapsa* cf. *japonica* YAO, *Stichomitra takanoensis* AITA, *Syringocapsa* sp., *Tricolocapsa* cf. *plicarum* YAO, *Tricolocapsa* sp., *Triversus* sp., *Zhamoidellum ovum* DUMITRICA. According to the co-occurrence of *Stichomitra takanoensis* and *Zhamoidellum ovum* this sample would be normally assigned to the UA 7 (Late Bathonian to Early Callovian). The position of the sample is in the Tauglboden Formation and above a lot of younger samples than UA 7. The age range of *Stichomitra takanoensis* has at least to be prolonged to the Late Callovian - Early Oxfordian.

3.3 Krispl: Oberalm Formation

Along the road to Krispl (Fig. 3) a Late Tithonian part of the Oberalm Formation can be studied (Fig. 12). Dm-bedded radiolarian wacke- to packstones intercalated by fine-grained resediments with shallow-water debris and greenish marl layers are the typical sedimentary rocks. Illite dominates the clay fraction from the greenish marls (VORTISCH, GAWLICK, unpublished data). In the calcareous turbidites two shedding directions are visible: some calcareous turbidites were shed from southern directions (Plassen Carbonate Platform s. str.), others came from the north (Wolfgangsee Carbonate Platform).

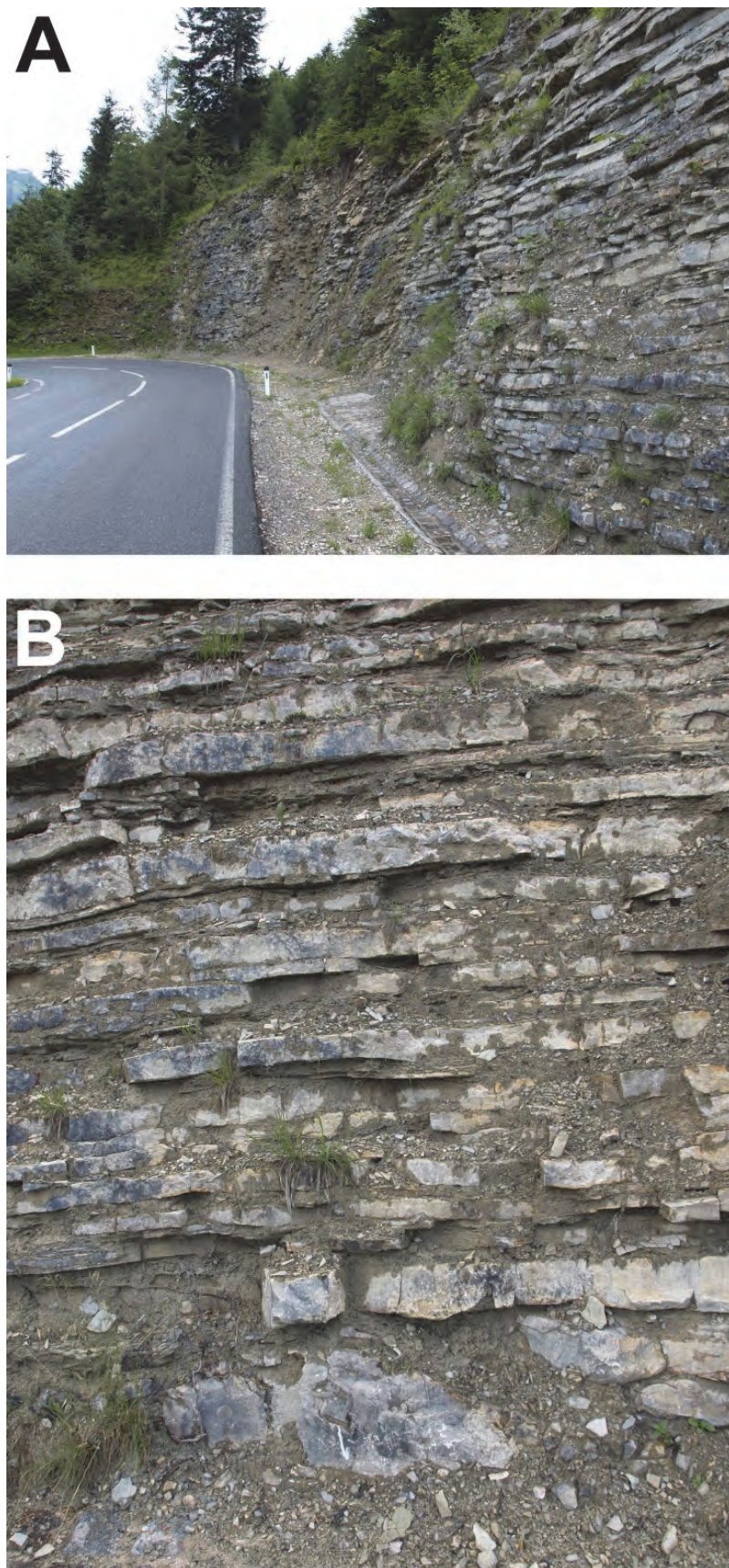


Fig. 12: Road cut with the Oberalm Formation along the road to Krispl. **A)** Outcrop situation before the fixation of metal nets. **B)** Dm-bedded limestone beds with intercalated green marls.

3.4 Mt. Barmsteine: Barmstein Limestone

Type-Locality: Resediments of the Plassen Carbonate Platform *s. str.* (Late Tithonian to Early Berriasian) intercalated in *Calpionella* Limestone.



Fig. 13: The Barmstein Limestone type-locality west of the township Hallein. **A)** Mt. Grosser Barmstein, view from the south. **B)** Coarse-grained Barmstein Limestone with chert nodules.

Detailed description of the type locality in GAWLICK et al. (2005). The cliffs of the Barmstein Limestones on the type locality (Fig. 13) consist of a roughly 160 m thick latest Tithonian to earliest Cretaceous succession - according to the final definition of the Jurassic/Cretaceous boundary based on the FAD of

the spherical variety of *Calpionella alpina* (Alpina subzone). In June 2016, the Berriasian Working Group voted by a large majority (76%) to adopt the *Crassicollaria/Calpionella* turnover as the primary marker for the base of the Berriasian (WIMBLEDON, 2017). But, the basal part of the succession has to be attributed to the highest part of the Tithonian (STEIGER, 1981, 1992; GAWLICK et al., 2005).

At the cliffs of the Barmstein Limestones, repeated shedding of mass transport deposits (olistostromes, debris and slide flows, and turbidites) resulted in a varying component spectrum, slightly varying dipping and variable grain size. In some Barmstein layers in the type area dominate (in cases slightly older) clasts of the inner lagoon of the Plassen Carbonate Platform, in other layers dominate reef-near clasts. In some channels older casts (e.g., dolomite, filament limestone, lagoonal limestones, *Saccocoma* limestone, radiolarite) can be found, which indicate deeper erosion in the provenance area. The component spectrum indicates an eroded sedimentary succession similar as found in the older Tauglboden Formation. Only the occurrence of Middle Triassic components in the Barmstein Limestones differs from the spectrum in the Tauglboden Formation. We suppose to see in these Triassic clasts erosion of deeper stratigraphic levels of the collapsed Trattberg Rise controlled by the formation of Late Tithonian escarpments.

In some flows appear clasts deriving from an evaporitic succession (STEIGER, 1981; PLÖCHINGER, 1974): pseudomorphs after gypsum, siltstones, and recrystallized dolomites with high porosity (most probably earliest Middle Triassic). A direct proof for the provenance from the Alpine Haselgebirge as in the “Tonflatschenbreccia” of the Leube quarry (PLÖCHINGER 1974, 1976) is not available for the Barmsteine type locality. A derivation from the Reichenhall Formation cannot be excluded. Together with the other Triassic-Jurassic components in the Barmstein layers, the Reichenhall Formation would complete the reworked Triassic succession from the Trattberg Rise (e.g., sedimentary sequence of the Berchtesgaden unit with Mt. Untersberg as frontal part). In addition, turbiditic grainstone layers occur intercalated in the *Calpionella* Limestone (Oberalm Formation). For the genesis of the Barmstein Limestones, tectonic control mechanisms as well as possible sequence stratigraphic cyclicity is discussed (GAWLICK et al., 2005, 2009). No Triassic Hallstatt Limestone clasts were found at the type locality.

References

- AUER, M., GAWLICK, H.-J., SUZUKI, H. & SCHLAGINTWEIT, F. (2009): Spatial and temporal development of siliceous basin and shallow-water carbonate sedimentation in Oxfordian Northern Calcareous Alps. - Facies, 55: 63-87, Berlin Heidelberg.
- BAUMGARTNER, P.O., BARTOLINI, A., CARTER, E.S., CONTI, M., CORTESE, G., DANIELIAN, T., DE WEVER, P., DUMITRICA, P., DUMITRICA-JUD, R., GORICAN, S., GUEX, J., HULL, D.M., KITO, N., MARCUCCI, M., MATSUOKA, A., MURCHEY, B., O'DOGHERTY, L., SAVARY, J., VISHNEVSKAYA, V., WIDZ, D. & YAO, A. (1995): Middle Jurassic to Early Cretaceous Radiolaria Biochronology of Tethys based on Unitary Associations. - Memoires de Geologie, 23: 1013-1048, Lausanne.
- BÖHM, F. (1992): Mikrofazies und Ablagerungsmilieu des Lias und Dogger der Nordöstlichen Kalkalpen. - Erlanger Geologische Abhandlungen, 121: 55-217, Erlangen.
- DIERSCHE, V. (1980): Die Radiolarite des Oberjura im Mittelabschnitt der Nördlichen Kalkalpen. - Geotektonische Forschungen, 58: 1-217, Stuttgart.
- FISCHER, A.G. (1965): Eine Lateralverschiebung in den Salzburger Kalkalpen. - Verhandlungen der Geologischen Bundesanstalt, 1965: 20-33, Wien.
- FISHER, R.V. & SCHMINCKE, H.-U. (1984): Pyroclastic rocks. - 1-472, Springer.

- FRANK, W. & SCHLAGER, W. (2006): Jurassic strike slip versus subduction in the Eastern Alps. - International Journal of Earth Sciences, 95: 431-450, Berlin Heidelberg.
- FRISCH, W. & GAWLICK, H.-J. (2003): The nappe structure of the central Northern Calcareous Alps and its disintegration during Miocene tectonic extrusion - a contribution to understanding the orogenic evolution of the Eastern Alps. - International Journal of Earth Sciences, 92: 712-727, Berlin Heidelberg.
- GARRISON, R.E. & FISCHER, A.G. (1969): Deep water Limestones and Radiolarites of the Alpine Jurassic. - SEPM Special Publication, 14: 20-56, Tulsa.
- GAWLICK, H.-J. (2000): Paläogeographie der Ober-Trias Karbonatplattform in den Nördlichen Kalkalpen. - Mitteilungen Gesellschaft Geologie- Bergbaustudenten Österreich, 44: 45-95, Wien.
- GAWLICK, H.-J. & FRISCH, W. (2003): The Middle to Late Jurassic carbonate clastic radiolaritic flysch sediments in the Northern Calcareous Alps: sedimentology, basin evolution and tectonics - an overview. - Neues Jahrbuch Geologie Paläontologie, Abhandlungen, 230: 163-213, Stuttgart.
- GAWLICK, H.-J. & HÖPFER, N. (1999): Stratigraphie, Fazies und Hochdruck-Mitteltemperatur-Metamorphose der Hallstätter Kalke der Pailwand (Nördliche Kalkalpen, Österreich). - Zeitschrift der Deutschen Geologischen Gesellschaft, 150: 641-671, Hannover.
- GAWLICK, H.-J. & SCHLAGINTWEIT, F. (2006): Berriaskan drowning of the Plassen carbonate platform at the type-locality and its bearing on the early Eoalpine orogenic dynamics in the Northern Calcareous Alps (Austria). - International Journal of Earth Sciences, 95: 451-462, Berlin Heidelberg.
- GAWLICK, H.-J., KRYSYNT, L. & LEIN, R. (1994): Conodont colour alteration indices: Paleotemperatures and metamorphism in the Northern Calcareous Alps - a general view. - Geologische Rundschau, 83: 660-664, Berlin Heidelberg.
- GAWLICK, H.-J., MISSONI, S., SCHLAGINTWEIT, F., SUZUKI, H., FRISCH, W., KRYSYNT, L., BLAU, J. & LEIN, R. (2009): Jurassic Tectonostratigraphy of the Austroalpine domain. - Journal of Alpine Geology, 50: 1-152, Wien.
- GAWLICK, H.-J., MISSONI, S., SCHLAGINTWEIT, F. & SUZUKI, H. (2012): Jurassic active continental margin deep-water basin and carbonate platform formation in the north-western Tethyan realm (Austria, Germany). - Journal of Alpine Geology, 54: 189-292, Wien.
- GAWLICK, H.-J., SCHLAGINTWEIT, F. & MISSONI, S. (2005): Die Barmsteinkalke der Typlokalität nordwestlich Hallein (hohes Tithonium bis tieferes Berriassium; Salzburger Kalkalpen) - Sedimentologie, Mikrofazies, Stratigraphie und Mikropaläontologie: neue Aspekte zur Interpretation der Entwicklungsgeschichte der Ober-Jura-Karbonatplattform und der tektonischen Interpretation der Hallstätter Zone von Hallein - Bad Dürrnberg. - Neues Jahrbuch Geologie Paläontologie Abhandlungen, 236: 351-421, Stuttgart.
- GAWLICK, H.-J., SCHLAGINTWEIT, F. & SUZUKI, H. (2007): Die Ober-Jura bis Unter-Kreide Schichtfolge des Gebietes Sandling-Höherstein (Salzkammergut, Österreich) - Implikationen zur Rekonstruktion des Block-Puzzles der zentralen Nördlichen Kalkalpen, der Gliederung der karbonatklastischen Radiolaritflyschbecken und der Entwicklung der Plassen-Karbonatplattform. - Neues Jahrbuch Geologie Paläontologie, Abhandlungen, 243: 1-70, Stuttgart.
- GAWLICK, H.-J., SUZUKI, H., VORTISCH, W. & WEGERER, E. (1999): Zur stratigraphischen Stellung der Tauglbodenschichten an der Typlokalität in der Osterhorngruppe (Nördliche Kalkalpen, Ober-Oxfordium - Unter-Tithonium). - Mitteilungen Gesellschaft Geologie- Bergbaustudenten Österreich, 42: 1-20, Wien.
- GORIČAN, Š., PAVŠIĆ, J. & ROŽIĆ, B. (2012): Bajocian to Tithonian age of radiolarian cherts in the Tolmin basin (NW Slovenia). - In: DANELIAN, T. & GORIČAN, Š. (Eds.): Radiolarian biochronology as key to tectono-stratigraphic reconstructions. - Bulletin de la Société géologique de France, 183: 369-382, Paris.
- GÜMBEL, C.W. von (1861): Geognostische Beschreibung des Bayrischen Alpengebirges und seines Vorlandes. I-XX. - 1-950, (Justus Perthes) Gotha.
- HAAS, J., KOVÁCS, S., KRYSYNT, L. & LEIN, R. (1995): Significance of Late Permian - Triassic facies zones in terrane reconstructions in the Alpine - North Pannonian domain. - Tectonophysics, 242: 19-40, Amsterdam.

- HAHN, F. (1913): Grundzüge des Baues der nördlichen Kalkalpen zwischen Inn und Enns. - Mitteilungen der Geologischen Gesellschaft in Wien, 6: 238-357 and 374-501, Wien.
- HAUG, E. (1906): Les nappes de charriage des Alpes calcaires septentrionales. - Bulletin de la Société Géologique de la France, 6: 359-422, Paris.
- HUCKRIEDE, R. (1971): Rhyncholithen-Anreicherung (Oxfordium) an der Basis des Älteren Radiolarits der Salzburger Kalkalpen. - *Geologica et Palaeontologica*, 5: 131-147, Marburg/Lahn.
- HULL, D.M. (1997): Upper Jurassic Tethyan and southern Boreal radiolarians from western North America. - *Micropaleontology*, 43 (Supplement 2): 1-202.
- KOBER, L. (1923): Bau und Entstehung der Alpen. - 1-289, (Bornträger) Berlin.
- KRISCHE, O., BUJTOR, L. & GAWLICK, H.-J. (2013): Calpionellid and ammonite biostratigraphy of uppermost Jurassic to Lower Cretaceous sedimentary rocks from the Leube quarry (Northern Calcareous Alps, Salzburg, Austria). - *Austrian Journal of Earth Sciences*, 101: 26-45, Wien.
- KRISCHE, O., GRABOWSKI, J., BUJTOR, L. & GAWLICK, H.-J. (2018, this volume): Early Cretaceous evolution of the central Northern Calcareous Alps. - Berichte der Geologischen Bundesanstalt
- LEBLING, C., HABER, G., HOFFMANN, N., KÜHNEL, J., WIRTH, E. (1935): Geologische Verhältnisse des Gebirges um den Königs-See, 20. - Abhandlungen Geologische Landesuntersuchung Bayerisches Oberbergamt: 1-46, München.
- LEIN, R. (1985): Das Mesozoikum der Nördlichen Kalkalpen als Beispiel eines gerichteten Sedimentationsverlaufes infolge fortschreitender Krustenausdünnung. - *Archiv für Lagerstättenforschung*, 6: 117-128, (Geologische Bundesanstalt) Wien.
- LEIN, R. (1987a): Evolution of the Northern Calcareous Alps During Triassic Times. - In: FLÜGEL, H.W. & FAUPL, P. (Eds.): *Geodynamics of the Eastern Alps*, 85-102, (Deuticke) Wien.
- LEIN, R. (1987b): Zur Verbreitung der Hallstätter Zone beiderseits des Pyhrn-Passes. - Oberösterreichische Geonachrichten, Folge 2: 21-37, Linz.
- LINZER, H.-G., RATSCHBACHER, L. & FRISCH, W. (1995): Transpressional collision structures in the upper crust: the fold-thrust belt of the Northern Calcareous Alps - *Tectonophysics*, 242: 41-61, Amsterdam.
- LIPOLD, M. v. (1854): Der Salzberg am Dürnberg nächst Hallein. - *Jahrbuch der kaiserlich-königlichen Geologischen Reichsanstalt*, 1854: 590-610, Wien.
- MANDL, G.W. (1982): Jurassische Gleittektonik im Bereich der Hallstätter Zone zwischen Bad Ischl und Bad Aussee (Salzkammergut, Österreich). - *Mitteilungen der Gesellschaft Geologie- Bergbaustudenten in Österreich*, 28: 55-76, Wien.
- MANDL, G.W., BRANDNER, R. & GRUBER, A. (2017): Zur Abgrenzung und Definition der Kalkalpinen Deckensysteme (Ostalpen, Österreich). - Tagungsband der Arbeitstagung der Geologischen Bundesanstalt, 2017: 254-255, Wien.
- MEDWENITSCH, W. (1962): Die Bedeutung der Grubenaufschlüsse des Halleiner Salzberges für die Geologie des Ostrandes der Berchtesgadener Schubmasse. - *Zeitschrift der Deutschen Geologischen Gesellschaft*, 113: 463-494, Hannover.
- MISSONI, S. & GAWLICK, H.-J. (2011a): Jurassic mountain building and Mesozoic-Cenozoic geodynamic evolution of the Northern Calcareous Alps as proven in the Berchtesgaden Alps (Germany). - *Facies*, 57: 137-186, (Springer).
- MISSONI, S. & GAWLICK, H.-J. (2011b): Evidence for Jurassic subduction from the Northern Calcareous Alps (Berchtesgaden; Austroalpine, Germany). - *International Journal of Earth Sciences* **100**: 1605-1631, (Springer).
- O'DOGHERTY, L., BILL, M., GORIČAN, Š., DUMITRICA, P. & MASSON, H. (2006): Bathonian radiolarians from an ophiolitic mélange of the Alpine Tethys (Gets Nappe, Swiss-French Alps). - *Micropaleontology*, 51: 425:485.
- O'DOGHERTY, L., CARTER, E.S., DUMITRICA, P., GORIČAN, Š., DE WEVER, P., HUNGERBÜHLER, A., BANDINI, A.N. & TAKEMURA, A. (2009): Catalogue of Mesozoic radiolarian genera. Part 1: Triassic. - *Geodiversitas*, 31: 213-270.

- O'DOGHERTY, L., GORIČAN, Š. & GAWLICK, H.-J. (2017): Middle and Late Jurassic radiolarians from the Neotethys suture in the Eastern Alps. - *Journal of Paleontology*, 109: 142-159.
- ORTNER, H., USTASZEWSKI, M. & RITTNER, M. (2008): Late Jurassic tectonics and sedimentation: breccias in the Unken syncline, central Northern Calcareous Alps. - *Swiss Journal Geosciences*, Supplement 1, 101: S55-S71, Basel.
- PLÖCHINGER, B. (1974): Gravativ transportiertes permisches Haselgebirge in den Oberalmer Schichten (Tithonium, Salzburg). - *Verhandlungen der Geologischen Bundesanstalt*, 1974: 71-88, Wien.
- PLÖCHINGER, B. (1976): Die Oberalmer Schichten und die Platznahme der Hallstätter Masse in der Zone Hallein-Berchtesgaden. - *Neues Jahrbuch Geologie und Paläontologie Abhandlungen*, 151: 304-324, Stuttgart.
- PLÖCHINGER, B. (1980): Die Nördlichen Kalkalpen. - In: OBERHAUSER, R. (Ed.): *Der geologische Aufbau Österreichs*, 217-264, (Springer) Wien New York.
- PLÖCHINGER, B. (1984): Zum Nachweis jurassisch-kretazischer Eingleitungen von Hallstätter Gesteinsmassen beiderseits des Salzach-Quertales (Salzburg). - *Geologische Rundschau*, 73: 293-306, Stuttgart.
- PUEYO, E. L., MAURITSCH, H. J., GAWLICK, H.-J., SCHOLGER, R. & FRISCH, W. (2007): New evidence for block and thrust sheet rotations in the central northern Calcareous Alps deduced from two pervasive remagnetization events. - *Tectonics* 26, TC5011.
- RATSBACHER, L., FRISCH, W., LINZER, H.G. & MERLE, O. (1991): Lateral extrusion in the Eastern Alps, Part 2: structural analysis. - *Tectonics*, 10: 257-271.
- REITER, W. (2009): Climate changes in the Middle and Late Jurassic: Isotope analysis of radiolarites from the Northern Calcareous Alps. - Unpublished Dipl. thesis, 1-56, Tübingen.
- SCHLAGER, M. (1956): Geologische Studien im Tauglboden. - *Mitteilungen der Naturwissenschaftlichen Arbeitsgemeinschaft am (vom) Haus der Natur in Salzburg*, 5: 31-44, Salzburg.
- SCHLAGER, M. & SCHLAGER, W. (1969): Über die Sedimentationsbedingungen der jurassischen Tauglbodenschichten (Osterhorngruppe, Salzburg). - *Anzeiger der Österreichischen Akademie der Wissenschaften. Mathematisch-naturwissenschaftlichen Klasse*, 106: 178-183, (Österreichische Akademie Wissenschaften) Wien.
- SCHLAGER, W. & SCHLAGER, M. (1973): Clastic sediments associated with radiolarites (Tauglbodenschichten, Upper Jurassic, Eastern Alps). - *Sedimentology*, 20: 65-89, (Blackwell) Oxford.
- SCHMID, S.M., FÜGENSCHUH, B., KISSLING, E. & SCHUSTER, R. (2004): Tectonic map and overall architecture of the Alpine orogen. - *Eclogae geologicae Helvetiae*, 97: 93-117, Basel.
- SPENGLER, E. (1951): Die nördlichen Kalkalpen, die Flyschzone und die Helvetische Zone. - In: SCHAFFER, F.X. (Ed.): *Geologie von Österreich*, 302-413, (Deuticke) Wien.
- SPÖTL, C., LONGSTAFFE, F.J., RAMSEYER, K., KUNKS, M.J. & WIESHEU, R. (1998): Fluid-rock reactions in an evaporitic mélange, Permian Haselgebirge, Austrian Alps. - *Sedimentology*, 45: 1019-1044, (Blackwell) Oxford.
- STEIGER, T. (1981): Kalkturbidite im Oberjura der Nördlichen Kalkalpen (Barmsteinkalke, Salzburg, Österreich). - *Facies*, 4: 215-348, Erlangen.
- STEIGER, T. (1992): Systematik, Stratigraphie und Palökologie der Radiolarien des Oberjura-Unterkreide-Grenzbereiches im Osterhorn-Tirolikum (Nördliche Kalkalpen, Salzburg und Bayern). - *Zitteliana (Abhandlungen Bayerischen Staatsammlung Paläontologie und historische Geologie)*, 19: 1-188, München.
- SUESS, E. & MOJSISCOVICS, E. v. (1868): Studien über die Gliederung der Trias- und Jurabildungen in den östlichen Alpen. Nr. II. Die Gebirgsgruppe des Osterhorns. - *Jahrbuch der k.k. geologischen Reichsanstalt*, 1868: 167-200, Wien.
- SUZUKI, H. & GAWLICK, H.-J. (2003a): Die jurassischen Radiolarienzonen der Nördlichen Kalkalpen. - (In: WEIDINGER, J.T., LOBITZER, H. & SPITZBART, I. (Eds.): Beiträge zur Geologie des Salzkammerguts. Gmundner Geo-Studien), 2: 115-122, Gmunden.

- SUZUKI, H. & GAWLICK, H.-J. (2003b): Biostratigraphie und Taxonomie der Radiolarien aus den Kieselsedimenten der Blaa Alm und nördlich des Loser (Nördliche Kalkalpen, Callovium-Oxfordium). - Mitteilungen Gesellschaft Geologie- Bergbaustudenten Österreich, 46: 137-228, Wien.
- SUZUKI, H. & GAWLICK, H.-J. (2009): Jurassic radiolarians from the base of the Hallstatt salt-mine (Northern Calcareous Alps, Austria). - Neues Jahrbuch Geologie Paläontologie, Abhandlungen, 251: 155-197, Stuttgart.
- SUZUKI, H., WEGERER, E. & GAWLICK, H.-J. (2001): Zur Radiolarienstratigraphie im unteren Callovium in den Nördlichen Kalkalpen - das Klauskogelbachprofil westlich von Hallstatt. - Zentralblatt Geologie Paläontologie, Teil 1, 2000: 167-184, Stuttgart.
- SUZUKI, H., WEGERER, E. & GAWLICK, H.-J. (2004): Radiolarians from the lower Oxfordian of Fludergraben (Austria, Northern Calcareous Alps). - 2004 Annual Meeting, Palaeontological Society of Japan, 126, Kitakyushu.
- TOLLMANN A. (1976a): Monographie der Nördlichen Kalkalpen. Teil II. Analyse des klassischen nordalpinen Mesozoikums. Stratigraphie, Fauna und Fazies der Nördlichen Kalkalpen. - 1-580, (Deuticke) Wien.
- TOLLMANN, A. (1976b): Der Bau der Nördlichen Kalkalpen. Orogenic Stellung und regionale Tektonik. - 1-449, (Deuticke) Wien.
- TOLLMANN, A. (1977): Geologie von Österreich, Band 1: Die Zentralalpen. - 1-766, (Deuticke) Wien.
- TOLLMANN, A. (1981): Oberjurassische Gleittektonik als Hauptformungsprozeß der Hallstätter Region und neue Daten zur Gesamttektonik der Nördlichen Kalkalpen in den Ostalpen. - Mitteilungen der Österreichischen Geologischen Gesellschaft, 74/75: 167-195, Wien.
- TOLLMANN, A. (1985): Geologie von Österreich, Band 2: Außerzentralalpiner Anteil. - 1-710, Wien (Deuticke).
- TOLLMANN, A. (1987): Late Jurassic/Neocomian Gravitational Tectonics in the Northern Calcareous Alps in Austria. - In: FLÜGEL, H.W. & FAUPL, P. (Eds.): Geodynamics of the Eastern Alps), 112-125, Wien (Deuticke).
- TRAUTH, F. (1950): Die fazielle Ausbildung und Gliederung des Oberjura in den nördlichen Ostalpen. - Verhandlungen der Geologischen Bundesanstalt, 1948: 145-218, Wien.
- VECSEI, A., FRISCH, W., PIRZER, M. & WETZEL, A. (1989): Origin and tectonic Significance of Radiolarian Chert in the Austroalpine Rifted Continental Margin. - In: HEIN, J. & OBRADOVIĆ, J. (Eds.): Siliceous Deposits of the Tethys and Pacific Regions), 65-80, (Springer) Berlin Heidelberg New York.
- WÄCHTER, J. (1987): Jurassische Massflow- und Internbreccien und ihr sedimentär-tektonisches Umfeld im mittleren Abschnitt der Nördlichen Kalkalpen. - Bochumer geologische geotechnische Arbeiten, 27: 1-239, Bochum.
- WEGERER, E., SUZUKI, H. & GAWLICK, H.-J. (2001): Zur stratigraphischen Einstufung von Kieselsedimenten im Bereich des Sandling (Nördliche Kalkalpen, Callovium-Oxfordium). - Mitteilungen Gesellschaft Geologie- Bergbaustudenten Österreich, 45: 67-85, Wien.
- WIMBLEDON, W.A.P. (2017): Developments with fixing a Tithonian/Berriasian (J/K) boundary. - Volumina Jurassica, XV: 181-186, Warszawa.

Field Trip Post-EX-3

Sediment-landform associations of major glaciations in the North Alpine Foreland



BERNHARD SALCHER¹, REINHARD STARNBERGER², JOACHIM GÖTZ³

¹ University of Salzburg, Department of Geography and Geology, Hellbrunner Strasse 34, 5020 Salzburg.
bernhard.salcher@sbg.ac.at

² Winham 10, 5121 Tarsdorf.

³ University of Graz, Department of Geography and Regional Science, Heinrichstraße 36, 8010 Graz.

Introduction

The Alpine Foreland gives a qualitative impression on the tremendous erosive and depositional impact of large Piedmont glaciers. Glaciers of this size and kind, warm-based, entering the foreland of an (active) mountain range are globally almost nonexistent during Interglacials.

One of the best modern examples is represented by the Malaspina Glacier/Alaska. Glaciers of similar size and dynamics entered the North Alpine Foreland during glacial maxima of at least the Middle Pleistocene where the global climate experienced an intensification of glacial cold periods (100 kyr world; e.g. Head and Gibbard, 2015). The tremendous impact of Quaternary glaciers on the Alpine Foreland was already discussed and summarized by Penck and Brückner (1909) providing the basis for interpreting complex stratigraphic glacial and glaciofluvial settings. The knowledge on the dynamics of major ice-lobes has recently largely expanded through progress in dating techniques and the increasing amount of comprehensive geodata, much reflecting anthropogenic activities within and along the Alpine range. A major outcome was for example to recognize that the full glacial expansion of each glacial maximum was much shorter than previously thought, covering few thousand years only (e.g. Wirsig et al., 2016). This view underlines the extreme dynamics driving landscape reorganization during these short periods.

The special setting of the North Alpine Foreland reflecting a slightly uplifted soft sedimentary basin (Alpine Molasse) provides ideal conditions for landform preservation and glacial modification. Non-glacial erosion is focused along few incised Danube tributaries leaving glacial and glaciofluvial sediments of several glacial maxima largely uneroded. Specifically, the slightly decreasing size of the Salzach Glacier Lobe with successive glacial maxima offers the opportunity to explore topographic and sedimentary features of glacial origin far exceeding the age of the LGM (Fig. 1).

This field excursion guides to some key features of the Salzach Glacier Lobe essential to understand glacial, glaciofluvial and associated postglacial processes associated with the impact of repeated foreland glaciations.

Stops are aligned to cover the temporal succession of processes, from ice built up to the period of maximum ice expansion and to ice wastage at the onset of global climate relaxation. Landforms and topographic features cover three glacial maxima. The excursion, finally, guides to sites of postglacial

landscape evolution reflecting the dynamics triggered by warm periods in subsequence to glacial maxima (Fig. 1).

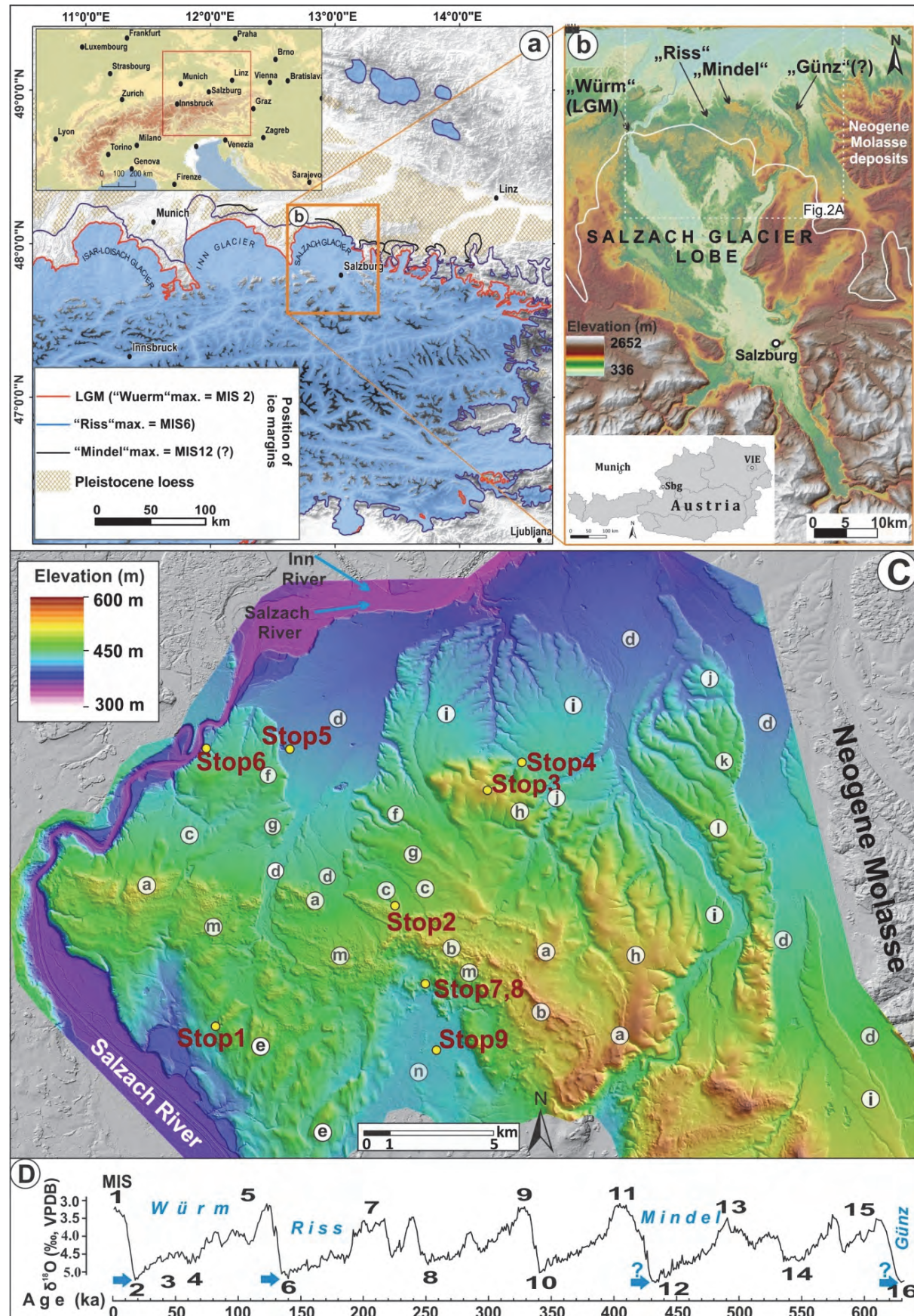


Fig. 1:

a) Extent of the Salzach Glacier Lobe (SGL) in the North Alpine Foreland during full-glacial periods of the last glacial maximum (LGM, "Würm", MIS 2), the penultimate glacial maximum ("Riss", MIS 6) and the antepenultimate maximum ("Mindel", MIS 12?).

b) Topography formerly covered by the SGL. Miocene Molasse preserved east of the major north alpine lobes. DEM bases on NASA's SRTM (90 m; for details see Farr and M. Kobrick, 2000). Modified from Salcher et al., 2015.

C) Topographic overview and locations of planned stops at this field trip. Abbreviations denote Quaternary landforms referring to the repeated glacial impact of this area. (a): LGM (Würm, MIS 2) terminal moraine 1 (max. extend); (b): LGM terminal moraine 2; (c): LGM, upper outwash "obere Niederterrasse" with sub-terrace levels; (d): LGM, lower outwash "untere Niederterrasse" with sub-terrace levels; (e): tunnel channels of subglacial drainage system (LGM); (f): Riss terminal moraine 1 (max. extend); (g): Riss terminal moraine 2; (h): Riss outwash, "Hochterrasse" (undifferentiated); (i) Mindel terminal moraine; (j): Mindel outwash "Jüngere Deckenschotter" (undifferentiated); (k): Günz terminal moraine, (l) Günz outwash "Ältere Deckenschotter" (undifferentiated); (m) LGM ice wastage deposits; (n) Peat bog (lbmer Moor)

DEM resolution is 10 m (resampled from airborne LiDAR).

D) $\delta^{18}\text{O}$ stack of Lisiecki and Raymo (2005) indicating Marine Isotope Stages (MIS) and tentative correlation with Alpine major glaciations (Würm, Riss, Mindel sensu Penck and Brückner, 1909; Raymo, 1997; van Husen and Reitner, 2011). Note that the periods of glacial foreland coverage were only a short fraction of a glacial, limited to maximum cold phases (i.e. MIS 2, 6, etc). The short periods of (suggested) ice expansion into the east Alpine foreland are marked with blue arrows.

Stop 1: Pit "Döstling", the advancing period of the Salzach Glacier Lobe

Gravel pit Döstling (Fig. 2) is situated at the eastern Salzach valley slope giving insights into the thick pile of glacial and glaciofluvial sediments. Well distinguishable units have a total thickness of 30 meters in the outcrop. The *upper* and the *lower unit* is built up by coarse-grained fluvial sediments and the *middle unit*, separating those two, comprises basal till. Deposition of coarse-grained fluvial sediments is interpreted to originate from a bedload dominated stream ("braided river") but regularly providing flow depths large enough for effective sorting (e.g. cross-bedded strata). The interfingering of the fluvial succession (*lower unit*) with the heavily consolidated basal till on top indicates that these sediments were deposited in the forefield of the advancing Salzach Glacier Lobe. Abundant sediments released by meltwaters of the advancing glacier largely filled the Salzach Valley and were subsequently overridden by the ice (till cap). Derived luminescence ages (Salcher et al., 2015) suggest that sediments of the *lower unit* (and thus including the interfingering basalt till) were already deposited during the penultimate glaciation (Riss, MIS 6) and left uneroded by the LGM glacier. Even though no absolute ages are available from the *upper unit*, a clearly younger age is suggested from the lower weathering intensity. Sediments are interpreted to represent the glacial outwash of the advancing stage of the subsequent glaciation (LGM). The LGM glaciation rather provided the modification of this thick glaciofluvial sediments of the penultimate (and older) sediments into streamlined bedforms (Fig. 2a; Salcher et al., 2010; Weinberger, 1952).

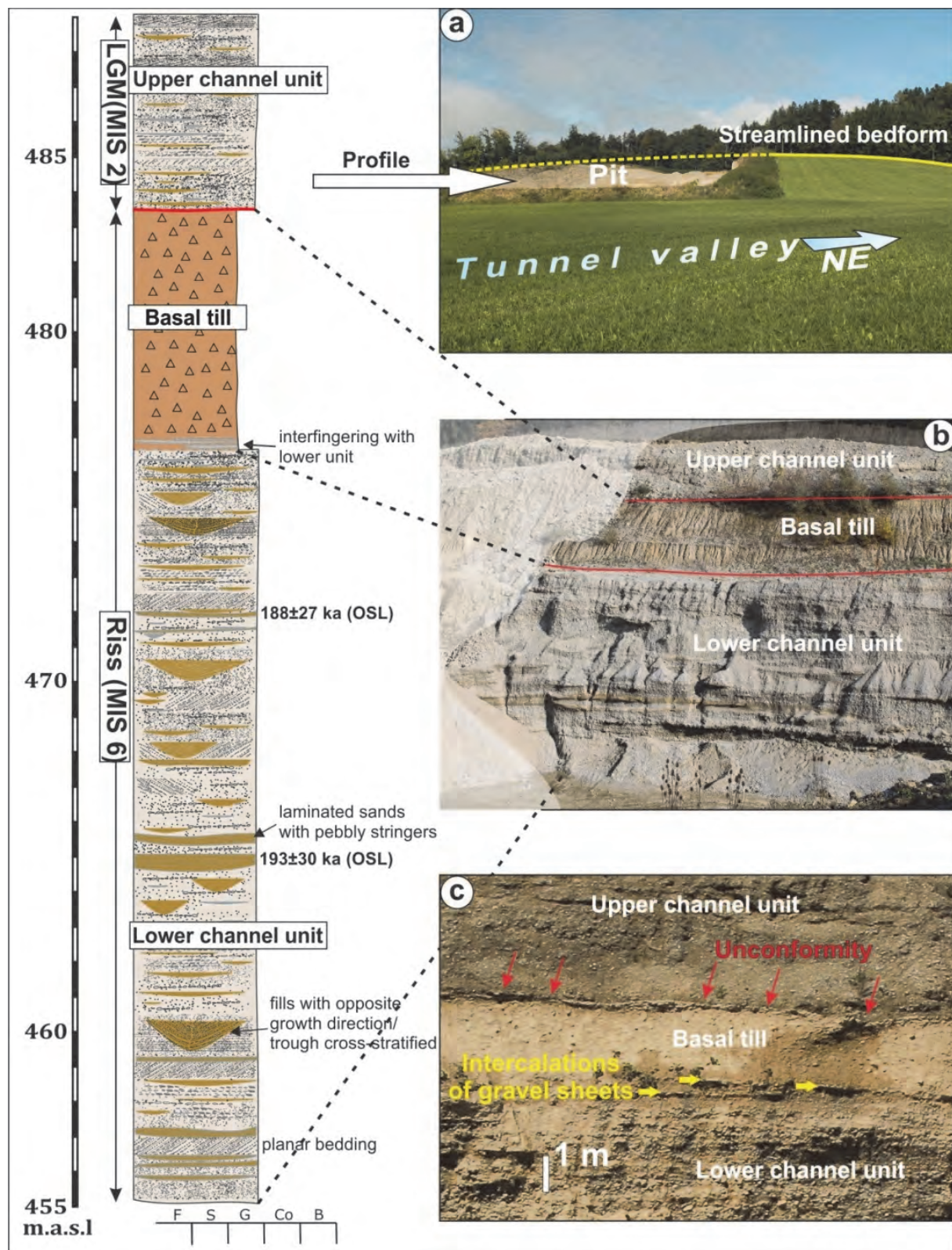


Fig. 2: Geological Profile (left) representing the advancing period of the Rissian (MIS 6) Salzach glacier. Glaciofluvial sediments are capped by basal till (b and c). Basal till is unconformably overlain by glaciofluvial gravels of the LGM (Upper channel unit, (b and c)). The outcrop is located in a streamlined bedform (a) referring to a postdepositional modification by glacial processes (potentially LGM).

Stop 2: Gravel pit “Pfaffinger”, Maximum position of the LGM glacier and evidence for the glacial series (Penck and Brückner, 1909)

We park just some hundreds of meters south of the gravel pit “Pfaffinger” and walk across the terminal moraine of the most extensive advance of the LGM Salzach Glacier Lobe to reach the outcrop (Fig. 3). The outcrop is situated within fluvial outwash associated with the terminal moraine representing the most extensive advance of the Salzach glacier during the LGM (Fig. 4). Glacial landforms of the penultimate glacial maximum (Riss/MIS 6) are situated directly north of it. The outcrop shows a succession of three coarse-grained, massive units all dominated by the sheetflood facies with only slight variations in structure.

The *lowest sheetflood* unit is separated from the *middle unit* by a ca. 3 to 4 m thick layer of *basal till*. While there is a clear unconformity between the *basal till* and the *middle sheetflood unit* above, the transition from the *lower sheetflood unit* to the *basal till* is indistinct and marked by gravel sheets intercalated into the till. Similar to the situation observed at the outcrop “Döstling”, this lower sheetflood unit is interpreted to reflect ice proximity and the subsequent overriding by the glacier leaving basal till. The rare occurrence of laminated fines on top of the basal till may point to uncoupling of the ice from the bed, giving rise to melt-out till formation. The stratigraphic context and luminescence ages suggests that these units represent the penultimate glaciation (Riss/MIS 6). If not eroded, the top decimetres of the *middle sheetflood* unit appears altered into a brownish to dark reddish paleosol. This paleosol may also form distinct wedge-shaped structures (up to ~3 m) referring to periglacial wedges (i.e. ice wedge casts). Just below paleosol formation, gravelly sediment often appears conglomerated. The *upper sheetflood unit* is separated by a sharp unconformity from the middle sheetflood unit. The absence of any weathering of the *upper sheetflood unit* well agrees with the derived LGM age. The clear decrease in thickness is related to the surface slope of the outwash. The intensively weathered paleosol can therefore be attributed to the Riss-Würm Interglacial period (Eemian), potentially also forming during later interstadials (e.g. MIS 3).

The three distinct sheetflood units are interpreted to reflect high-energy, supercritical sheetflows. These non-channelized horizontal bedload sheets are considered to represent deposits of shallow flash floods relating to the upper flow regime (Miall, 1977; Todd, 1989; Blair and McPherson, 1994). These supercritical sheetfloods are typical for building up slopes of alluvial fans (Nemec and Postma, 1993; Blair and McPherson, 1994) or similar features associated with a glacier, such as ice contact fans or ramps (Benn and Evans, 1998; Krzyszkowski and Zielinski, 2002).

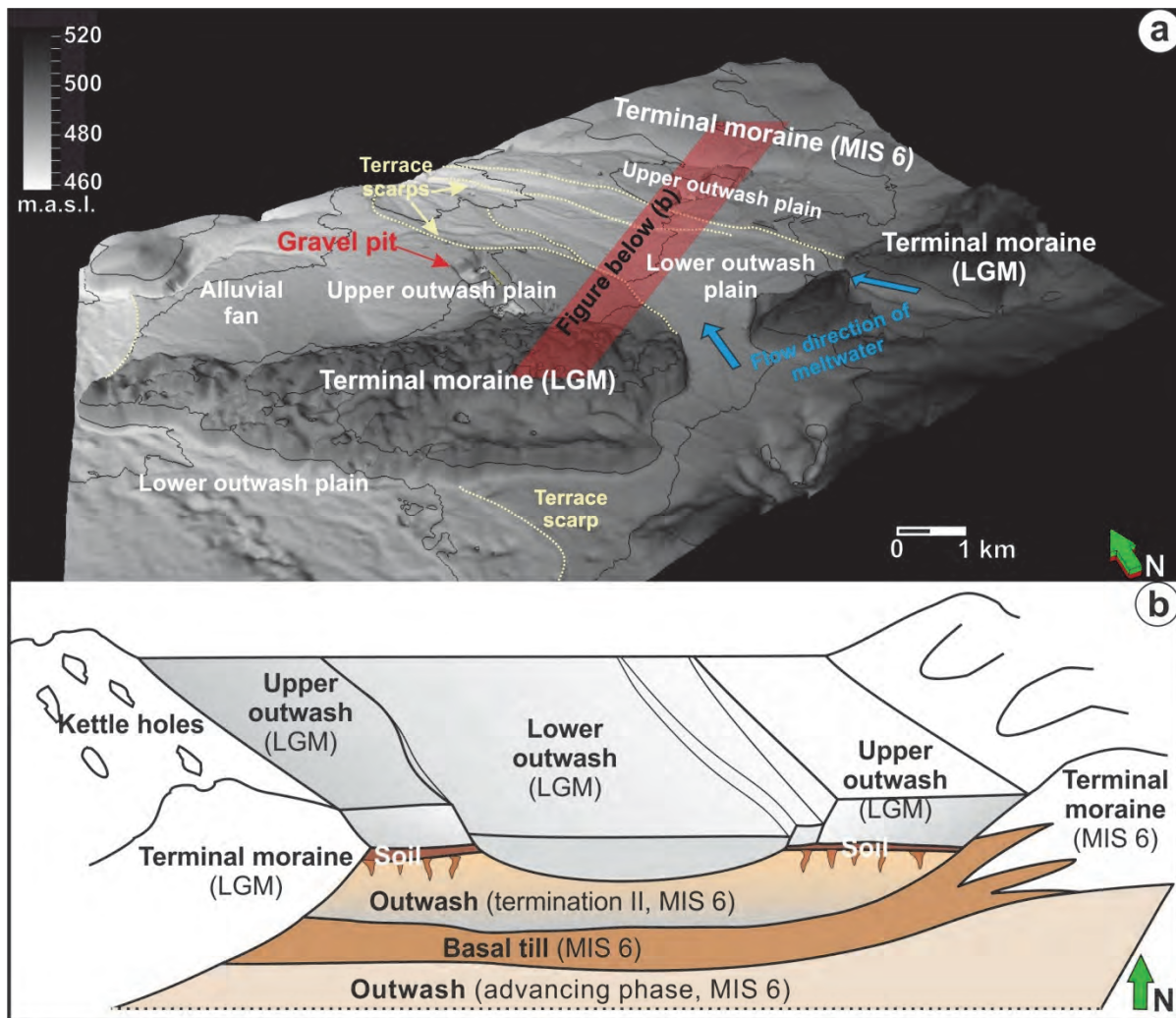


Fig. 3:

a) Topography near the terminus of the Salzach Glacier Lobe. The gravel pit ("Pfaffinger") is situated within outwash associated with the terminal moraine of the most extensive position of the LGM (terminal moraine 1; see also Fig. 2). The lower outwash plain is associated with the more proximal LGM terminal moraine. The red bar denotes the geological 3D profile shown in (b). DEM resolution is 1 m. DEM by courtesy of the Government of Upper Austria.

b) Sketch illustrating the stratigraphy of LGM/Würmian (MIS 2) and Rissian (MIS 6) deposits. Outwash gravel deposited during the advancing stage of the Riss period was later overridden by the glacier as indicated by the basal till. Later, during ice collapse at the end of the Riss period (termination II) outwash was deposited on top of the basal till. These sediments were subjected to intense soil forming processes (last interglacial) and occasionally covered by loess. The sketch is in well accordance with Penck and Brückner's (1909) glacial series model. Modified from Salcher et al., 2015.

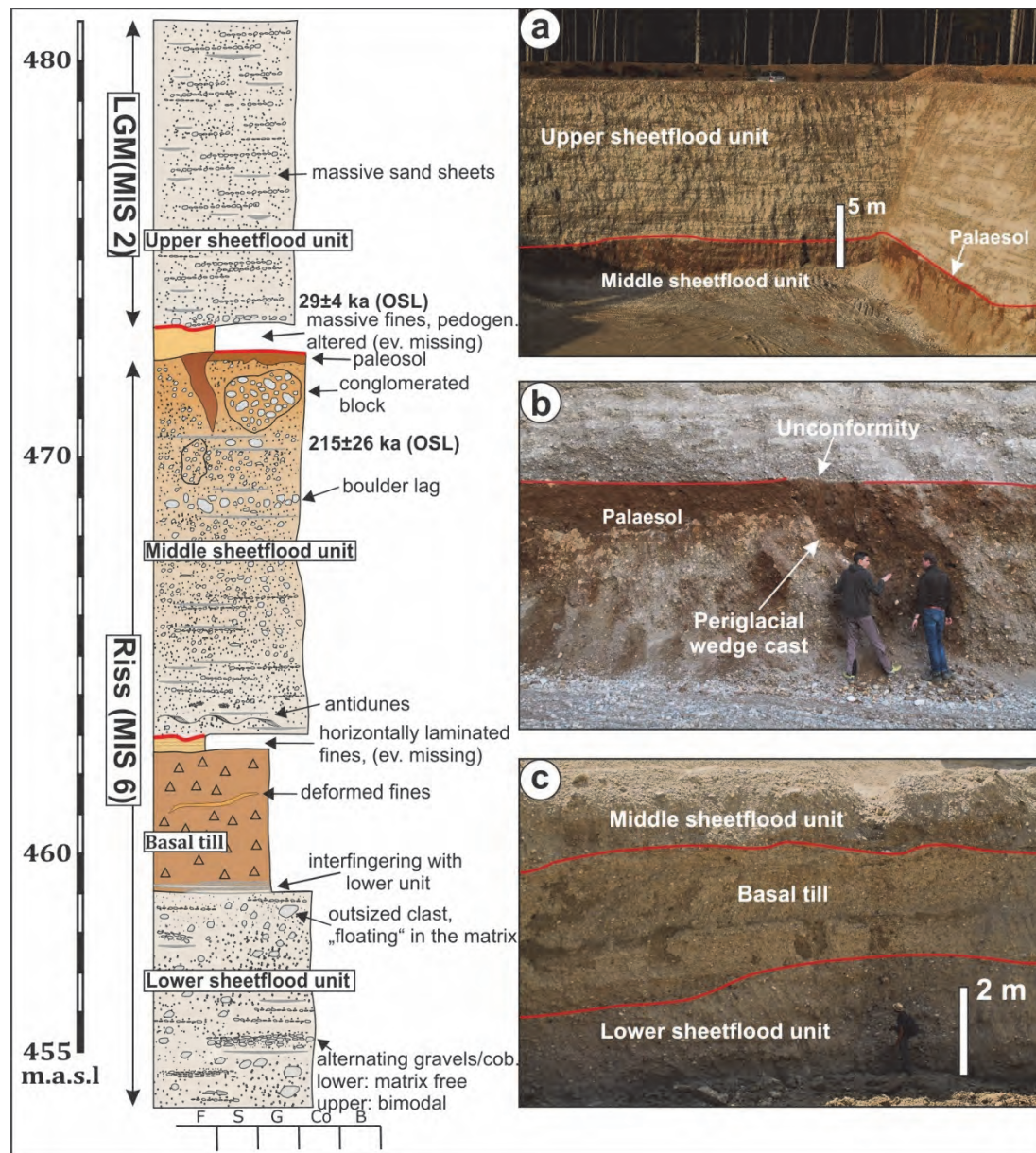


Fig. 4: Gravel pit "Paffinger" (see Figs. 1 and 3 for location and geological context). Profile shows the sequences development near the terminus of the Salzach Glacier. Glaciofluvial sediments deposited at the steep slopes of the former ice margin. They typically involve sheetflood sediments referring to shallow flash floods associated with the upper flow regime. Modified from Salcher et al., 2015.

Stop 3: Mindel terminal moraine

The Mindel glaciation (MIS 12 (?)) is considered to generally reflect the most extensive glaciation in the North Alpine Foreland of the Eastern Alps (e.g. van Husen, 2000). Only at some few spots some minor deposits might reflect an even earlier glaciation ("Günz"). However, if preserved, Mindel terminal moraines often appear very impressive exceeding the width and height of younger moraines (i.e. Riss and Würm) by far (Fig. 5a). So far there is still no clear absolute age constraint available from deposits related to the Mindel glaciation. Tentatively, deposits are considered to represent the MIS 12 (e.g. Raymo, 1997; van Husen, 2000). Note that the classical stratigraphy (i.e. Günz, Mindel, Riss, Würm) applied for Quaternary deposits of the East Alpine Foreland (Bavaria and Austria) is not applicable to deposits of the West Alpine foreland.

Stop 4: Glaciofluvial outwash of the Mindel glaciation (“Jüngere Deckenschotter”)

Glaciofluvial sediments relating to glacial deposits of the Mindel glaciation are referred to as “Jüngerer Deckenschotter” in the older literature. These glaciofluvial gravels commonly appear as erosional remnants with restricted spatial extend and typically characterized by a high degree of cementation (representing conglomerates). Pipe-like weathering structures (“Geologische Orgeln”) in between conglomerates are also typical (e.g. van Husen and Reitner, 2011) but not obvious in this outcrop (Fig. 5b). Both, the high degree of cementation and intense weathering are a function of time and also the relatively high content of carbonate clasts (potentially acting as source for dissolution and subsequent carbonate precipitation). Thick loess deposits on top, which may be intercalated by paleosols are also characteristic features on top of the Deckenschotters (here, landform gradient and degree of dissection prevents formation/preservation).

The outcrop (Fig. 5b) shows coarse-grained sediments including features of the upper flow regime (antidunes, plane beds). The sedimentary setting well reflects a dynamic ice marginal environment as already indicated by the topographic context in adjacency to the Mindel terminal moraine. The outcrop situated in a hollow seems at least to be partly natural. This is for example suggested by the occurrence of a cave (total length c. 20 m), recently discovered by mining activities in the gravel pit about 200 m to the west.



Fig. 5: Deposits relating to the Mindel glaciation.

- View from the Mindel terminal moraine (MIS 12?) towards south (Alps).
- Glaciofluvial gravels (“Höhere Deckenschotter”) associated with the Mindel stage moraine. Sediments are commonly intensively conglomerated. Ice proximity is underlined by features of the upper flow regime (c).

Stop 5: Sediments and topography along Salzach Glacier's main drainage

The gravel pit (Fig. 6a) is situated within the main meltwater route of the Salzach Glacier and represents thick glaciofluvial deposits of homogenous, horizontally bedded sandy gravels to cobbles. The outwash is associated with the LGM glacier, which was a bit less extensive than the one of the penultimate glaciation (Riss maximum, MIS 6; see also Figure 1 for differences in extent). As a consequence, Rissian deposits in the pathway of the LGM outwash were reworked (eroded). The erosional scarp slightly west of the outcrop marks the Rissian terrace ("Hochterrasse") which was left as erosional remnant.

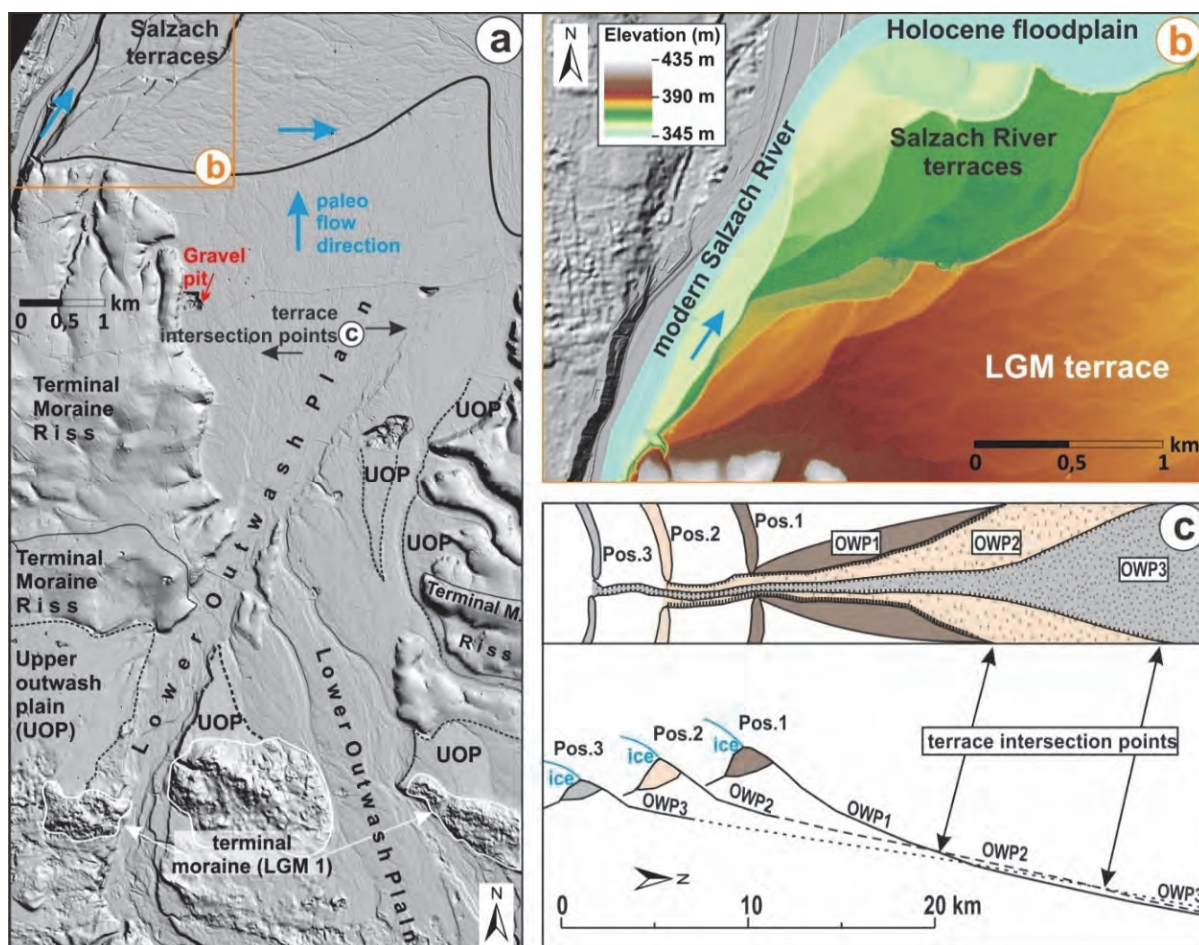


Fig. 6:

a) Fluvial outwash morphology along the Salzach Glacier's main drainage. Different terrace levels of a glacial period arise from glacier retreat and associated lowering of the glacier's drainage. Black arrows (a) mark the intersection points showing the transition from stream dissection (no accommodation space) to outwash formation (accommodation space): See c) for the conceptual model (modified from Troll, 1926 and Schreiner, 1997). Note the multiple sinks (kettle holes) in the terminal moraines (LGM 1) reflecting the incorporation of dead ice.

b) Terraces remnants distributed over an elevation range of c. 100 m demonstrate the dramatic incision of the Salzach River associated with glacial collapse. Note the change in river planform and flow direction from the top terrace level (braided, W-E directed) to lower levels (meandering, SW-NE). 0,5 m DEM by courtesy of the Government of Upper Austria.

Figures 6a and c highlight a typical, but rarely preserved (and detected) topographic feature of outwash related to different stages of glacier stabilization (Fig. 6c, Pos. 1, 2, 3). Drainage lowers with the slightly receding LGM glacier forming outwash of slightly different slopes. Outwash associated with the most extensive terminal moraine is the steepest, outwash associated with sediments from a more southern positions have a lower slope. This phenomenon leads to the apparent crossing of terraces (Troll, 1926) reflecting the change in accommodation space.

Stop 6: Ice collapse and fluvial incision

This Stop is located at Ach in the opposite to the Burghausen castle (Germany). Burghausen sits on glaciofluvial sediments of the LGM impressively showing the contrast in stream flow elevation and characteristics of the Salzach River between full glacial and present interglacial conditions (modern Salzach level). On the eastern river side numerous preserved terrace steps mark the successive incision of the river at the onset of deglaciation (Termination I, Fig. 6b). Glacier retreat was probably very rapid and glaciers were already at inner alpine positions at around 17–18 k.a. (e.g. Ivy-Ochs et al., 2004, Starnberger et al., 2011). Timing (and average rate) of fluvial incision into outwash (Fig. 6a) is however not fully clear but was likely not completed with the onset of the Holocene. The modern stream level is just above the Neogene bedrock suggesting that the incision of the cold stage sediments has largely ceased. Note the change in paleoflow direction and river planform. At the LGM outwash is N-S directed and shows a braided pattern (as already indicated by outcrop data). With full retreat of the glacier into the Salzach Valley, flow direction was W-E directed suggesting the strong influence of the Paleo-Inn River (modern confluence is few km to the north). Still, the stream appears bedload dominated (braided). Further, terraces suggest modern flow direction S-N to SSW-NNE and meandering planforms.

Stop 7: Ice wastage and associated landforms (Termination 1)

Ice collapse induces the formation of specific landforms such as kettle basins and hummocks (e.g. Eyles et al., 1999). The intensified melting process increases sediment release and promotes the local deposition of fluvial, gravitational and lacustrine sediments on or within the stagnant ice body. In accordance, landforms typically incorporate a large variety of sediments often associated with steep slopes and short topographic wavelengths (Fig. 7a). Kame-deltas of limited extend are common features proofing the existence of short-lived lakes (Figs. 7b, c). They formed between the ice margin and e.g. the terminal moraine incompletely filling some local basins. Importantly, the surface of the topset highlights the elevation of former lake levels at a given time of ice collapse. Kame deltas at multiple altitudes can therefore help to understand processes of ice collapse.

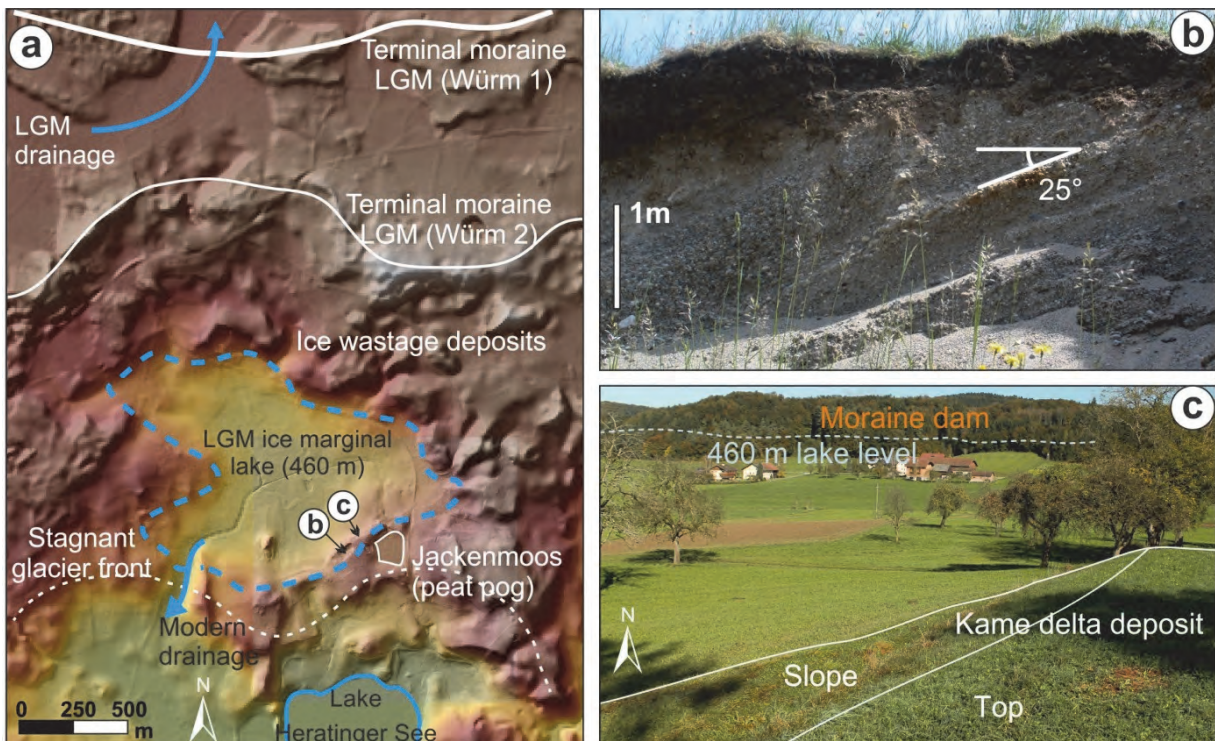


Fig. 7:

- a) Strongly undulating topography typical for an environment associated with the melting of a stagnant glacier. DEM by courtesy of the Government of Upper Austria.
- b) Foreset of a local kame delta deposit. See a) for location.
- c) The kame delta marks the elevation of a short-lived ice marginal lake, locally dammed by moraines. The presence of dead ice leads to the formation of kettles. These sinks may later turn in the tiny peat bogs (Jackenmoos, see Fig. 8). Modified from Götz et al., 2018.

Stop 8: The formation of kettle holes and its importance for postglacial processes. The Jackenmoos Kettle.

The full detachment of ice fragments from the glacier (“dead ice”) is a common process at a glacier’s terminal position. Naturally, the formation of dead ice is promoted when ice melting accelerates (ice collapse). If bodies of dead ice are incorporated into sediments, melt out of ice can result in characteristic topographic concave forms (“kettle-holes”). Kettle-holes or kettles are often appearing in larger fields with numerous kettles side by side. They are especially prevalent in terminal moraines (Fig. 6a) or associated with ice wastage (“kame and kettle topography”). In rare cases kettles can turn into (small) lakes, if there is e.g. some water inflow and the underlying material is suitable to prevent drainage (e.g. be provided by fine material through slope wash). Through lateral or vertical terrestrialisation these lakes can turn into kettle-hole mires (Fig. 8a). The given example shows a large kettle hole structure which has been completely horizontally grown by a floating peat mat (“floating mat terrestrialisation”). The result is the existence of an overgrown body of water. The contrast between the floating mat, the water body and the underlying material can also be beautifully discriminated by subsurface resistivity sections (Fig. 8b). The unusual high resistivity of the water body is a function of lower mineralization (i.e. surface water, with absence of mineralization through e.g. groundwater flow).

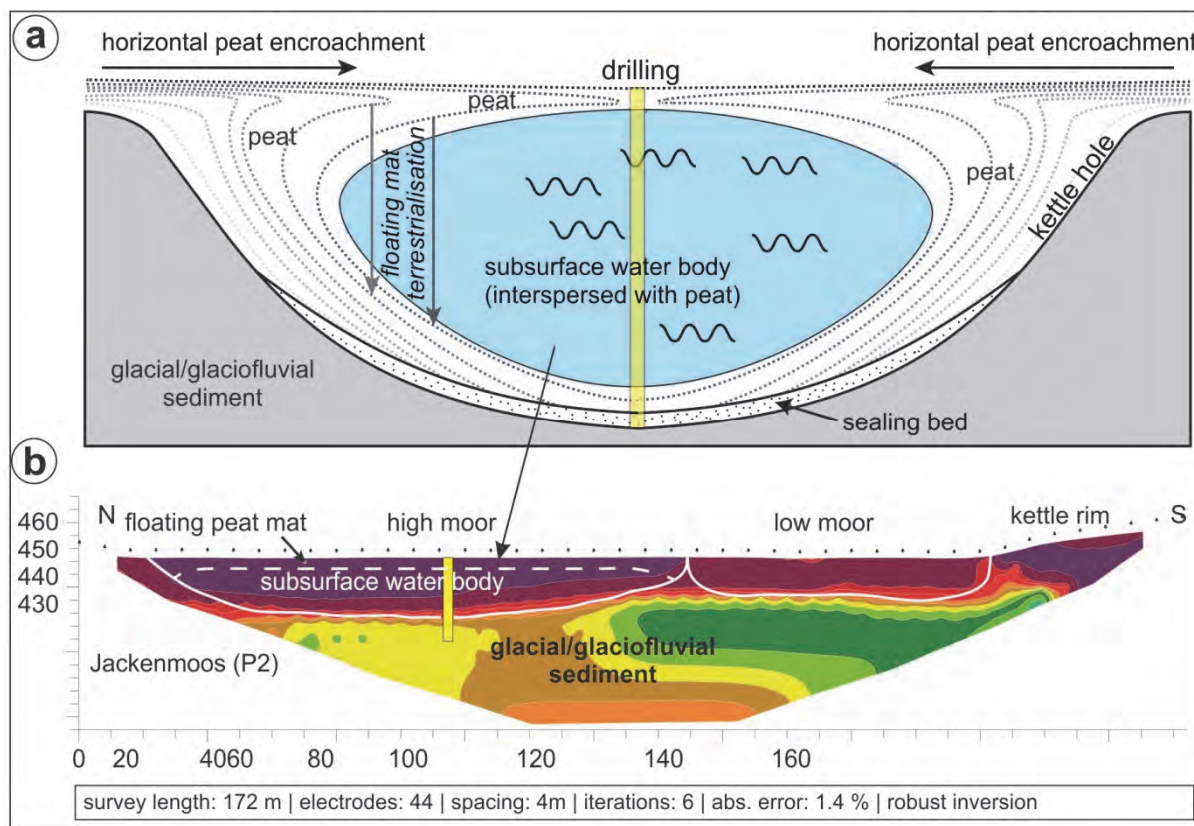


Fig. 8: Modified concept of peat formation in kettle-hole mires using results of the Jackenmoos peat bog.

- a) The model (i) modifies the concept of floating mat terrestrialisation after Gaudig et al. (2006). The location of the core drilling core is highlighted as yellow bar.
- b) Subsurface resistivities of ERT section crossing the Jackenmoos. Interpretation is indicated. Modified from Götz et al., 2018.

Stop 9: Peat bog “Ibmer Moor” – Natural trail

The “Ibmer Moor” is the largest peat bog area in Austria. The natural trail gives a quick overview on some relatively undisturbed parts of the largely destroyed peat bog. While the peat bog of the southern part (Salzburg area) was completely exploited (and thus destroyed) the northern part remained better preserved (Upper Austria; Fig. 9). Large parts of this northern part formed through Late Glacial to Holocene terrestrialisation of a lake left after deglaciation. The absence of significant drainage basins and minor water depth of few meters only promoted this process, which was largely completed at around 8000 yrs B.P. However, two smaller residual lakes remained resisting this terrestrialisation process (Lake Heratinger See and Leitensee, Fig. 9).

Very fine lake sediments reflect the absence of significant influx into the basin after deglaciation. Climate relaxation is indicated by lake marl deposition often present below the peat.

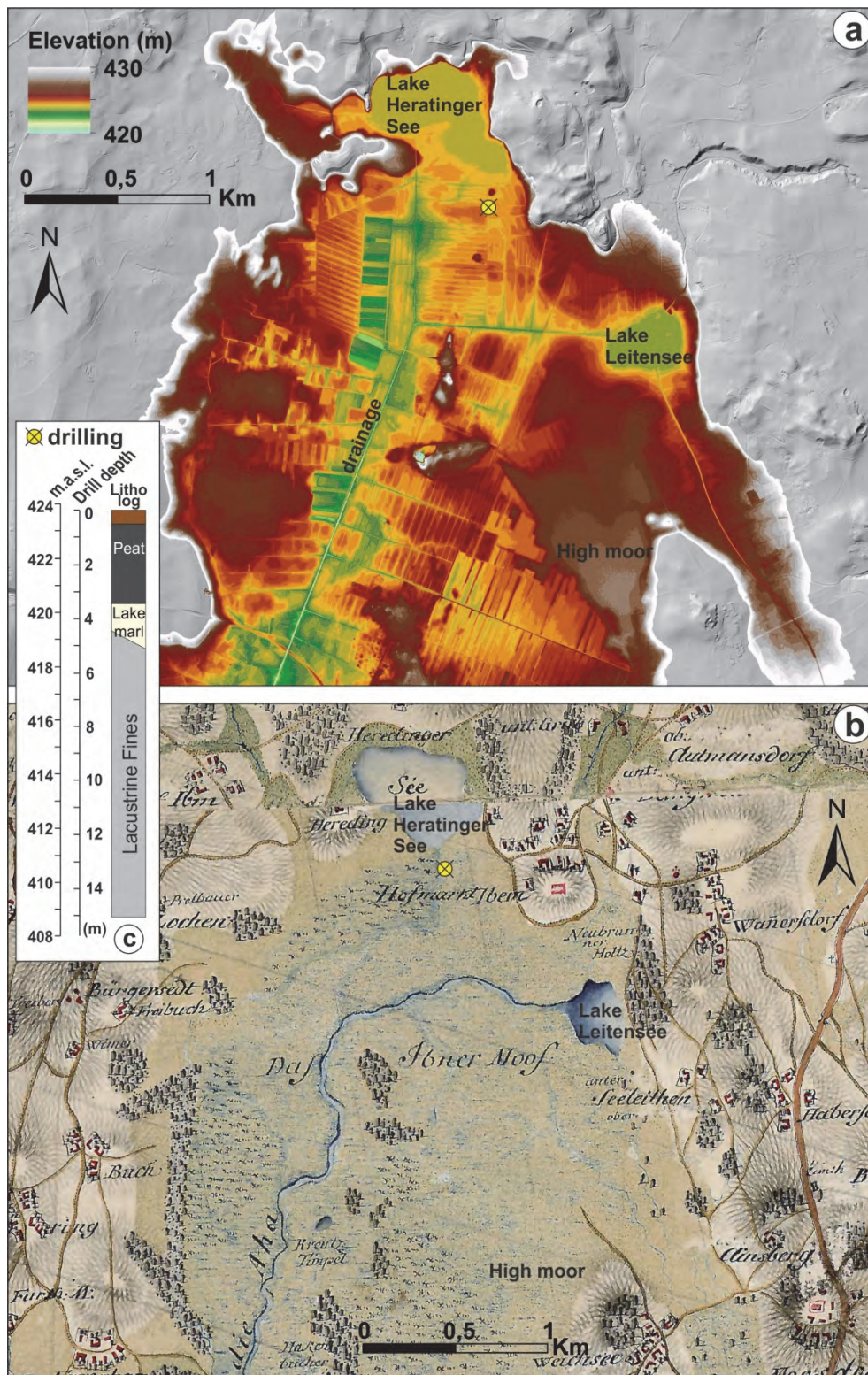


Fig. 9: Peat bog Ibmer Moor. a) DEM with 0.5 m ground resolution shows the major anthropogenic overprint through dewatering (long linear features from artificial lake drainages) and peat exploitation (rectangular features by peat cutting). 0.5 m DEM by courtesy of the Government of Upper Austria. B) First Military Survey (Josephinische Landesaufnahme; 1775–1777) showing approximately the same area as above (A) but with largely undisturbed environment. Note the natural drainage system and difference to A. Map is from <https://mapire.eu>. c) Drill log showing the Postglacial to Holocene stratigraphy just south of Lake Heratinger See (yellow circle in A and B).

Acknowledgements

Digital elevation provided by the Government of Upper Austria. We highly appreciated Ylvie Aranmanoth's field assistance.

References

- Benn, D.I. & Evans, D.J.A., 1998. Glaciers and Glaciations. Arnold, London.
- Blair, T.C. & Mcpherson, J.G., 1994. Alluvial fan processes and their natural distinction from rivers based on morphology, hydraulic processes, sedimentary processes, and facies s. *Journal of Sedimentary Research* 64A, 450-489.
- Eyles, N., Boyce, J.I. & Barendregt, R.W., 1999. Hummocky moraine: sedimentary record of stagnant Laurentide Ice Sheet lobes resting on soft beds. *Sedimentary Geology* 123, 163-174.
- Farr, T.G. & Kobrick, M., 2000. Shuttle Radar Topography Mission produces a wealth of data. *Eos, Transactions AGU* 81, 583-583.
- Gaudig G., Couwenberg J. & Joosten H., 2006. Peat accumulation in kettle holes: bottom up or top down? *Mires Peat*. 1:1-16.
- Götz, J., Salcher, B.C., Starnberger, R. & Krisai, R., 2018. Geophysical, topographic and stratigraphic analyses of perialpine kettles and implications for postglacial mire formation. *Geografiska Annaler: Series A, Physical Geography*, 100:3, 254-271.
- Head, M.J. & Gibbard, P.L., 2015. Early-Middle Pleistocene transitions: linking terrestrial and marine realms. *Quat. Int.* 389, 7-46.
- Ivy-Ochs, S., Schäfer, J., Kubik, P., Synal, H.-A. & Schlüchter, C., 2004. Timing of deglaciation on the northern Alpine foreland (Switzerland). *Eclogae Geologicae Helvetiae* 97, 47-55.
- Krzyszkowski, D. & Zielinski, T., 2002. The Pleistocene end moraine fans: controls on their sedimentation and location. *Sedimentary Geology* 149, 73-92.
- Lisiecki, L.E. & Raymo, M.E., 2005. A Pliocene-Pleistocene stack of 57 globally distributed benthic d₁₈O records. *Paleoceanography* 20, PA1003. <http://dx.doi.org/10.1029/2004PA001071>.
- Miall, A.D., 1977. A review of the braided river depositional environment. *Earth Science Reviews* 13, 1-62.
- Nemec, W. & Postma, G., 1993. Quaternary alluvial fans in southwestern Crete: sedimentation processes and geomorphic evolution. In: Marzo, M. & Puigdefabrigas, C. (Eds.), *Alluvial Sedimentation: International Association of Sedimentologists. Special Publication*.
- Penck, A. & Brückner, E., 1909. Die Alpen im Eiszeitalter. Tauchnitz, Leipzig.
- Raymo, M.E., 1997. The timing of major climatic terminations. *Paleoceanography* 12, 577-585.
- Salcher, B.C., Hinsch, R. & Wagreich, M., 2010. High-resolution mapping of glacial landforms in the North Alpine Foreland, Austria. *Geomorphology* 122, 283-293.
- Salcher, B.C., Starnberger, R. & Götz J., 2015: The last and penultimate glaciation in the North Alpine Foreland: New stratigraphical and chronological data from the Salzach glacier. *Quaternary International* 338, 218-231.
- Schreiner, A., 1997. Einführung in die Quartärgeologie. E. Schweizerbart'sche Verlagsbuchhandlung, Stuttgart.
- Starnberger, R., Rodnight, H. & Spötl, C. (2011). Chronology of the Last Glacial Maximum in the Salzach Palaeoglacier Area (Eastern Alps). – *Journal of Quaternary Science*, 26, 502-510.
- Todd, S.P., 1989. Stream-driven, high-density gravelly traction carpets: possible deposits in the Trabeg Conglomerate Formation, SW Ireland and some theoretical considerations of their origin. *Sedimentology* 36, 513.

- Troll, C., 1926. Die jungglazialen Schotterfluren im Umkreis der deutschen Alpen. *Forschung deutscher Landes- und Völkerkunde* 24, 157–256.
- van Husen, D., 2000. Geological processes during the Quaternary. *Mitteilungen der Österreichische Geologische Gesellschaft* 92, 135-156.
- van Husen, D. & Reitner, J.M., 2011. An outline of the quaternary stratigraphy of Austria. *Quat. Sci. J.* 60, 366-387.
- Weinberger, L., 1952. Ein Rinnensystem im Gebiete des Salzach-Gletschers. *Zeitschrift für Gletscherkunde und Glazialgeologie* 2.
- Wirsig, C., Zasadni, J., Christl, M., Akçar, N. & Ivy-Ochs, S., 2016. Dating the onset of LGM ice surface lowering in the High Alps. *Quat. Sci. Rev.* 143, 37-50.

